Introduction

Howdy!
My name is Ian Wilhite and I am a Senior in Robotics and Controls Engineering at Texas A&M! This portfolio contains a collection of reports and presentations from my engineering courses, project teams, programs, and competitions. The pdf content can be found on my github, and the start of each section leads with an overview of context, content, skills, and relevance. I would highly reccomend using the hyperlinks or ctrl-f to navigate this document. Thank you for taking the time to review my background, and I hope you get to meet a piece of me through my work!

Contents

Table of Contents **1**

1 Autonomous Aerospace Systems **2**

2 Dynamics and Vibrations **51**

3 Numerical Methods (4th Place in Final Competition) **77**

4 SEC Ignite Competition (3rd Place) **115**

5 Mechanical Modeling (Best Prototype Award) **132**

6 Mechanical Measurements **145**

7 Solid Mechanics **155**

8 Interdisciplinary Engineering ABET Requirements **183**

9 NASA L'SPACE Mission Concept Academy (MCA) **200**

Back to Contents

1. Autonomous Aerospace Systems

Summary

Autonomous Aerospace Systems (AERO 489) is a special topics course taught by Dr. John Valasek and Dr. Daniel Selva covering state space representation, uninformed and informed search, deterministic and stochastic world modeling, Reinforcement Learning (RL) models and training methods, and cumulated in a final project in which we modeled a dynamic game and trained an RL agent to play it.

- HW1: Uninformed and Informed Search in Deterministic and Non-Deterministic Environments
- HW2: First Order Logic (FOL) and Problem Structure
- HW3: Policy Comparison on Non-deterministic problems
- HW4: Q Learning - Foundations of Policy-Based RL
- HW5: Hyperparameter Tuning and Model Comparisons
- Final Project Presentation (Incomplete)
- Final Project Report (Complete)

Contributors: Ian Wilhite (Solo Course Project)

Key Skills: Autonomous Systems, Aerospace Engineering, Control Theory, Reinforcement Learning, Gymnasium, Stable Baselines, Python.

Relevance: The course highlighted the practical side of RL and ML implementation on real world systems based on system modeling, fundamental understandings, model selection, and implementation structure. The homeworks and projects provided an opporuntity to watch policies be developed.

Ian Wilhite

Aero 489 – Autonomous Systems

2/5/2025

Preliminary (10 points)

1) As a search problem, the state must contain the rovers location, the action must include rover traversal in all directions (and account for edge collision), and the search problem must also track the path cost in addition to the state. The world must contain cells with danger and a goal (science).
2) Because the environment is known, static, and fully observable, our rover begins the problem knowing all necessary information to search, the information it knows cannot change, and the information it knows is complete. Because it has all information it needs, and that information cannot change, it is not necessary to sense.

Basic Search (20 points)

1) Not all algorithms find the optimal solution: Depth-First Search (DFS) does not *always* find the optimal solution, because DFS will pick one potential path from its options and follow it to completion, and will return the first feasible solution it finds, which may or may not be the optimal solution, while other algorithms prioritize less costly solutions. BFS is less efficient than UCS because it must search all parallel paths but significantly outperforms DFS because it is more likely to find a *more* efficient solution in sweeping its options laterally. A* is the most efficient solution because it is the only informed search of the group and can rely on the Manhattan heuristic to approximate the goodness of a cell towards the optimal solution. For random problems, not all methods find the “correct”/optimal solution.
    a. Optimal Solution:

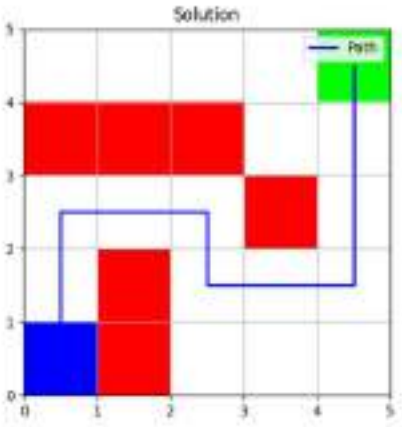

Fig. 1, sample problem with provided solution

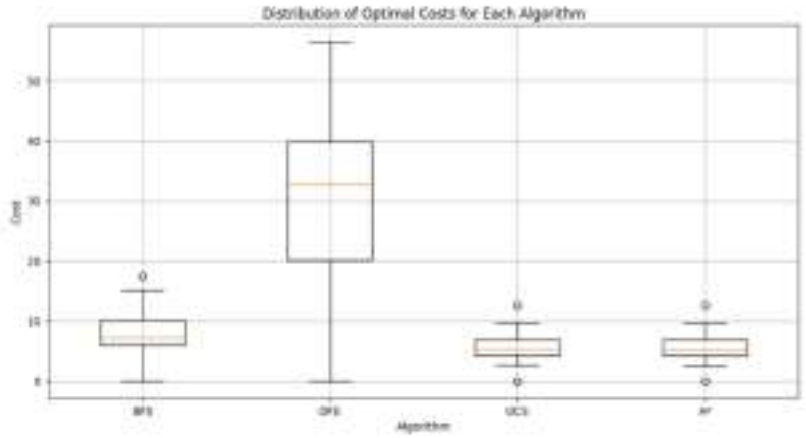

Fig. 2, Costs found by each algorithm

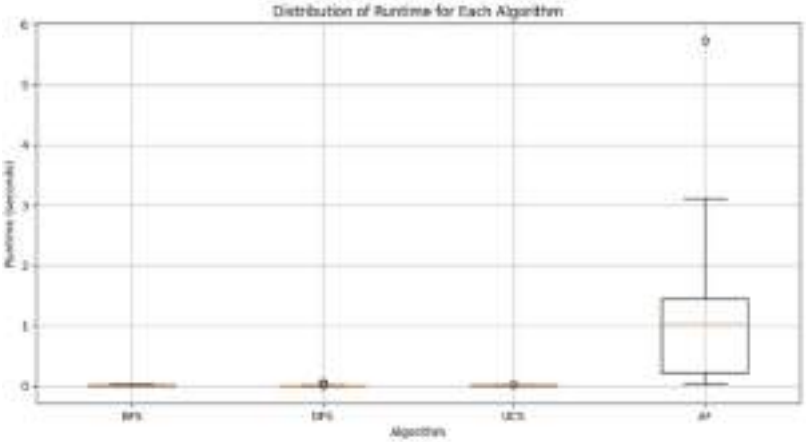

Fig. 3, Runtimes taken by each algorithm

2) In cost performance, the DFS did not find the optimal solution due to its tendency to burrow into an incorrect solution and return a local, suboptimal, solution. A* had a much larger runtime to find the solution. This means that the optimal search to use for this situation would be UCS.

```
Average Cost and Runtime for Each Algorithm:
BFS: Average Cost = 22.25, Average Runtime = 0.0032 seconds
DFS: Average Cost = 319.75, Average Runtime = 0.0032 seconds
UCS: Average Cost = 22.25, Average Runtime = 0.0035 seconds
A*: Average Cost = 22.25, Average Runtime = 0.7053 seconds
```

Fig. 4, Code output of search algorithms without Danger

3) By allowing the search to enter dangerous cells with a penalty, many of the less efficient algorithms average goes up by the increase of possible-but-less-optimal solutions, while A* can take the most advantage of the new opportunity and is the only algorithm to decrease its average cost. All algorithms required more runtime (about double) to search the larger pool of possible solutions.

```
Average Cost and Runtime for Each Algorithm:
BFS: Average Cost = 34.14, Average Runtime = 0.0073 seconds
DFS: Average Cost = 667.95, Average Runtime = 0.0039 seconds
UCS: Average Cost = 22.52, Average Runtime = 0.0104 seconds
A*: Average Cost = 21.29, Average Runtime = 1.3169 seconds
```

Fig. 5, Code output of search algorithms with Danger

Part 2:

Non-Deterministic World (30 points)

1) Changes:
    a. Creating transition_with_failure function that only moves the rover 75% of the time, and leaves the rover in its current state 25% of the time.
    b. Creating a transition_with_danger_and_failure function that is identical to the transition_with_danger except it calls the transition_with_failure for the base transition function then adds danger to the cost.
2) I believe that the solution will look similar to the optimal solution found by A*, only with nested conditions such that each step will fall into a conditional while loop where it will perform each action sequentially until the path is complete.

3) Yes, the algorithm completes the search, but no, it does not come close to other deterministic methods in terms of performance. It is not reasonable to compare

these, however, because the and-or search cannot assume that each function will work, it is extending additional effort to branch out along each potential option, and is also searching the cases in which the rover does not move, however this causes additional computation as it is simply in the same situation it previously was. It is worth noting that the And-Or search implemented returned solutions similar to those generated with a traditional Depth-First-Search.

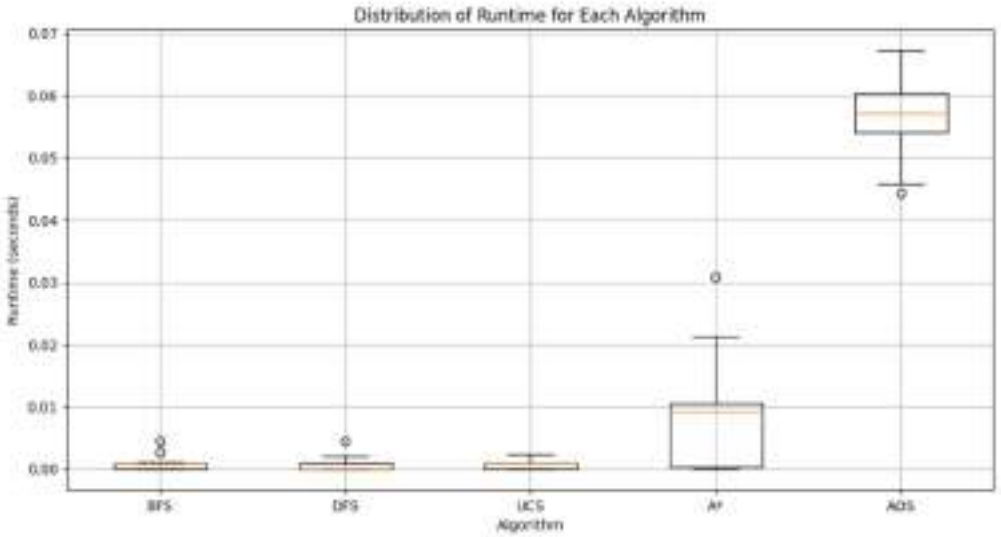

Fig. 6, Runtimes with Danger including AOS

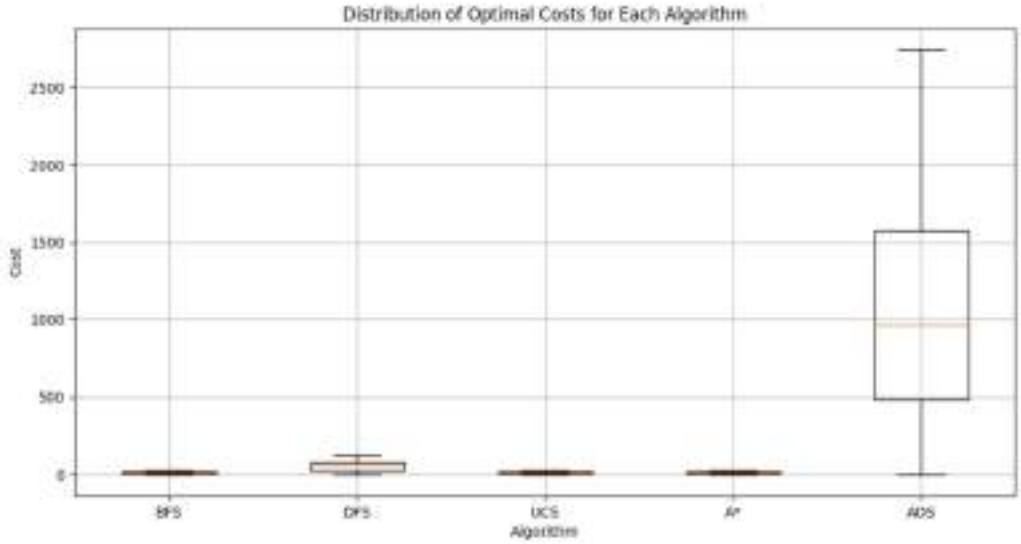

Fig. 7, Costs with Danger including AOS

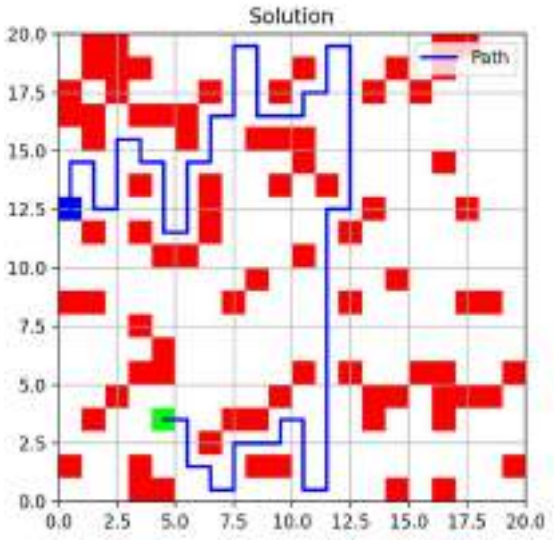

Fig. 8, 1st Sample AOS search solution

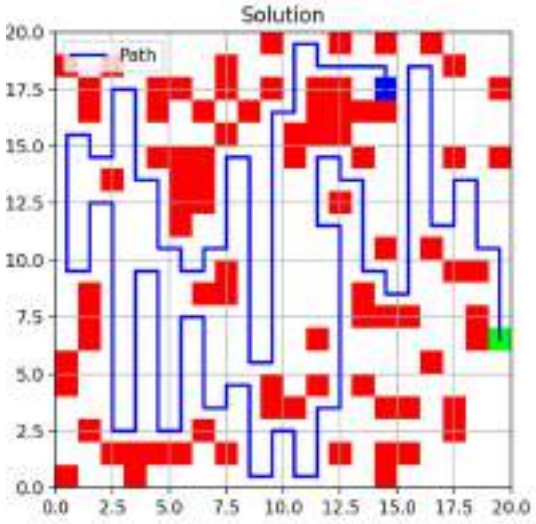

Fig. 9, 2nd Sample AOS search solution

4) Plots provided along with a sample of the path generated from the function.

```
Average Cost and Runtime for Each Algorithm:
BFS: Average Cost = 14.06, Average Runtime = 0.0009 seconds
DFS: Average Cost = 76.88, Average Runtime = 0.0005 seconds
UCS: Average Cost = 9.58, Average Runtime = 0.0012 seconds
A*: Average Cost = 9.29, Average Runtime = 0.0083 seconds
AOS: Average Cost = 164.13, Average Runtime = 0.0010 seconds
```

Fig. 10, Code output with Danger including AOS

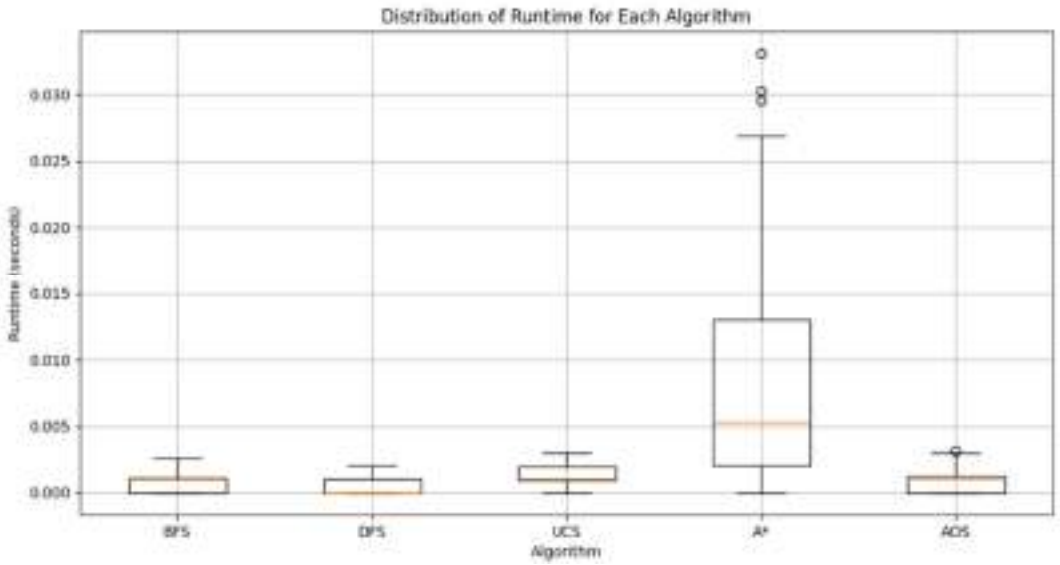

Fig. 11, Runtimes with Danger including AOS

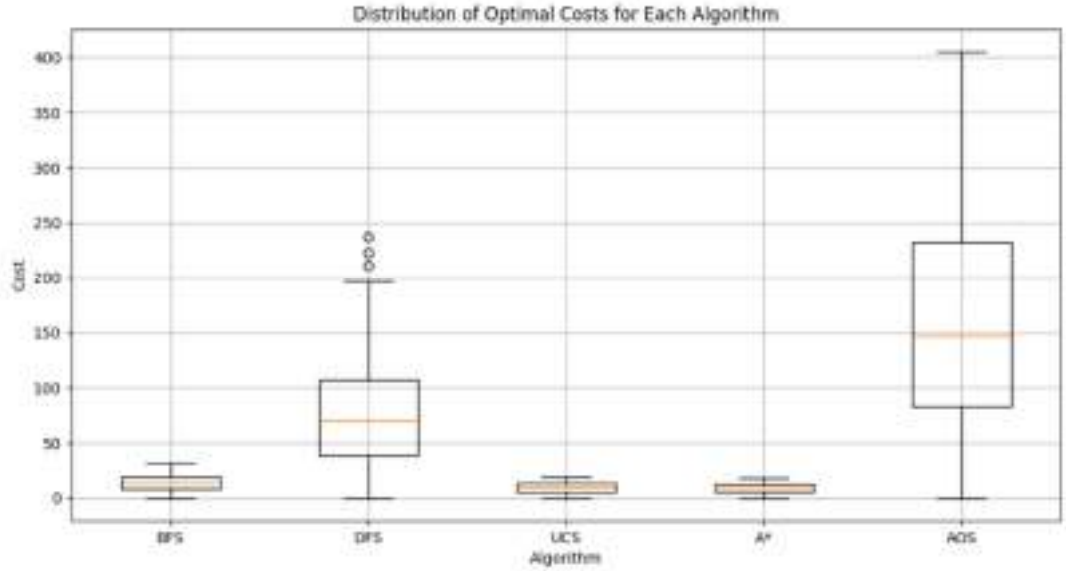

Fig. 12, Costs with Danger including AOS

Unknown World (10 points + 10 bonus)

1) To search the world without knowing the location of the alpha cell, a new heuristic would need to be developed for A*, involving the closeness using the spectrometer, given that the conditions for the search heuristic can be met. The noise must not break the admissibility of the heuristic, which a sensor would likely not so long as the majority of the noise comes from offset and proportional error, and that very little comes from randomness error.

AERO 489 – Selva
Ian Wilhite

2/24/2025

Short questions (10pts)

1) Syntax vs semantic
    a. Syntax is the structure of the notation for the problem. Semantics are the intended meaning of the problem.
    b. The difference between the two can arise when the syntax of the problem can "misunderstand" the intended result, like in the "everybody loves somebody" example in class that results in one "somebody" that everybody loves.
2) Predicate vs Function
    a. A predicate is a Boolean logical statement that evaluates to true or false. A function maps an input to an output and can return different data types. A predicate can be viewed as a type of function that only returns a Boolean.
    b. The IsEven(int num) returns [True, False] and would be considered a **predicate**, because the argument is a boolean.
    c. The SquareNum(int num) returns [int squaredNum], and would be considered a **function** because the return argument is not a boolean.
3) Action schema
    a. The action schema is the notation that describes the outcome of when a given action is applied to an object in a state.
4) Ground atomic sentence
    a. A ground atomic sentence is one that explains a particular relationship or fundamental existence of the world. Ie: Married(John, Jane)
5) Database vs standard FOL semantics
    a. Database semantics assume that information not explicitly given is false.
    b. FOL semantics will not assume anything about fact, and will claim that it could be either true or false.

Problem 1: FOL

a) Tell rules

b) Tell facts

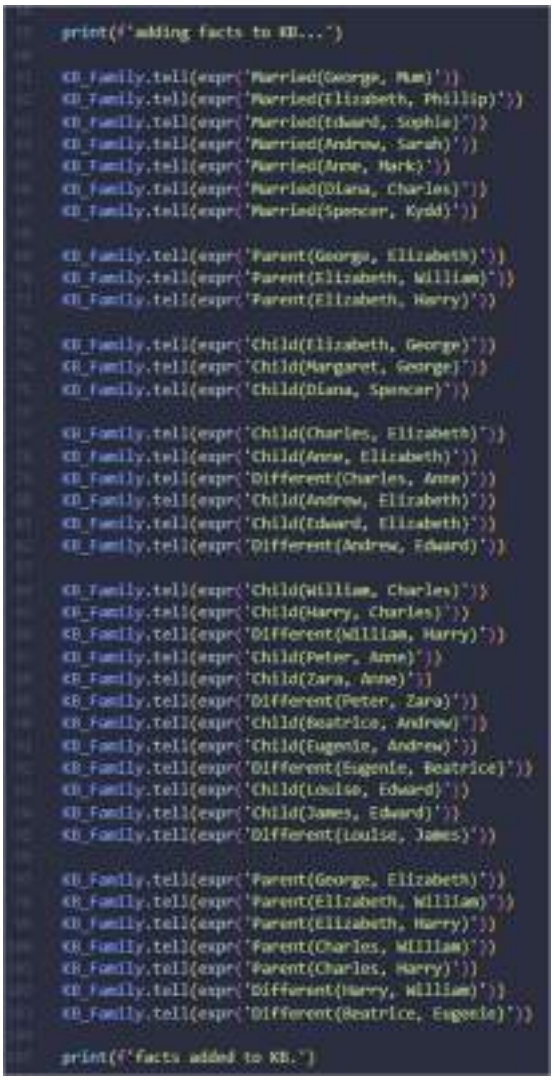

c) Ask
    a. Elizabeth's grandchildren
    b. Eugenie's siblings
    c. Zara's great-grandparents
    d. Eugenie's ancestors

Problem 2: Europa Rover

1) Domain:
    a. Requirements
        i. STRIPS is the most common basic notation that the PDDL system will use FOL to model the system.
    b. Predicates (variables to track)
        i. Rover location – the location of the rover on Europa (note: we do not need to track location alpha because it is static and does not move)
        ii. HasBiosample – whether or not the rover has obtained the sample
        iii. HasComponent – whether or not the rover has the component
        iv. BatteryCharged – whether or not the battery is charged

v. Drilled (based on location) – whether or not the current location has been drilled
vi. SoftwareUpdated – whether or not the rover software has been updated
vii. PreheatedDrill – whether or not the drilled has been preheated
viii. AnalysisCompleted – whether or not the analysis is complete
ix. ContactAvailible – whether or not transmission contact is available
x. DataTransmitted – whether or not the data has been transmitted (and the mission has been completed)

c. Actions
i. Charge
ii. Move
iii. Update software
iv. Retrieve components
v. Preheat drill
vi. Drill
vii. Analyze sample
viii. Transmit data

2) See attached files.

Ian Wilhite

AERO 489: Selva, Valasek

3/4/2025

Question 1: Formulate this problem as a Markov Decision Process. Specifically, provide the states, actions, rewards, and transition model.

State:

- The location of the rover within the world (x,y)
- The danger of the cells, as stored within the grid.

Actions:

- Move Up, (x,y) -> (x, y + 1)
- Move Right, (x,y) -> (x + 1, y)
- Move Down, (x,y) -> (x, y - 1)
- Move Left, (x,y) -> (x - 1, y)

Rewards:

- Move cost: -0.05 (included on unsuccessful moves)
- Goal reward: +1.00
- Crater cost: -1.00

Transition Model (for all actions):

- Move successfully -> 80%
- Stay in current cell -> 10%
- Slide towards center of grid -> 10%

Question 2: Write code in Python that implements the environment. This should include:

- A function to create a fixed test world (e.g., start cell in (1,1), goal in (5,5), danger cells in (1,4), (2,4), (2,2), (3,4), crater in (4,3)).

```
def create_test_problem_5x5(transition): # generates test
problem instance
    grid = np.empty((5, 5), dtype=object)
    for i in range(5):
        for j in range(5):
            science = 0
            danger = 0
            grid[i, j] = GridCell(science=science,
            danger=danger)
    grid[0][3].danger = 0.5
    grid[1][3].danger = 0.8
    grid[1][1].danger = 0.9
    grid[2][3].danger = 0.7
    grid[3][2].danger = 0.5
    grid[4][4].science = 1.0
    initial_state = RoverState(0, 0)
    return Problem(initial_state, goal_test, grid,
    transition_function=transition)
```

- A function to create a random world of this type

```
def generate_random_problem(transition): # generates random problem instance of size 8
    n = 8
    grid = np.empty((n, n), dtype=GridCell)
    n_unsafe = 0

    # Step 1: Initialize the grid with danger values
    for i in range(n):
        for j in range(n):
            if random.random() < percent_cells_with_danger:  # 10% chance of an unsafe cell
                danger = random.uniform(0.50001, 1)
                n_unsafe += 1
            else:  # Safe cell
                danger = random.uniform(0, 0.49999)

            grid[i, j] = GridCell(science=0, danger=danger)

    # Step 2: Set the goal cell among the safe cells (with danger < 0.5)
    goal_x, goal_y = np.floor(random.uniform(0, n-1)), np.floor(random.uniform(0, n-1))
    while (True): # keep find, but it's fine
        (start_x, start_y) = np.floor(random.uniform(0, n-1)), np.floor(random.uniform(0, n-1))
        if goal_x != start_x and goal_y != start_y:
            grid[goal_x, goal_y].science = 1.0
            grid[goal_x, goal_y].danger = 0.0
            break

    # Step 3: Find a random initial position that corresponds with a safe cell
    while True: # keep find, but it's fine
        initial_x, initial_y = random.randint(0, n-1), random.randint(0, n-1)
        if grid[initial_x, initial_y].danger <= 0.5:  # Only pick a safe cell
            initial_state = RoverState(initial_x, initial_y)
            break

    return Problem(initial_state, goal_test, grid, transition)
```

- Functions implementing the transition model and the reward function. Given a current state and action, they should return the next state and the reward respectively (or you can do this in the same function).

```
def transition_model(state, action, grid):
    """ Implements the stochastic movement model with 80% success, 10% stay, and 10% slide. """

    x, y = state.x, state.y
    # Define sliding move (towards the center of the grid)
    center_x, center_y = (N - 1) / 2, (N - 1) / 2 # 2, 2 for 5x5 grid

    # Apply probability
    rand_value = random.random()
    if rand_value < 0.8:  # 80% chance to move as intended
        new_x = x + action[0]
        new_y = y + action[1]
    elif rand_value < 0.9:  # 10% chance to stay in place
        new_x, new_y = x, y
    else:  # 10% chance to slide towards the center
        if x < center_x: new_x = x + 1
        elif x > center_x: new_x = x - 1
        if y < center_y: new_y = y + 1
        elif y > center_y: new_y = y - 1

    # Check if move is valid (not out of bounds)
    if 0 <= new_x < 5 and 0 <= new_y < 5:
        return RoverState(new_x, new_y)
    return state  # Stay in place if movement is invalid

def reward_function(state, grid):
    """ Returns the reward associated with the given state. """
    if grid[state.x][state.y].is_goal:
        return 1.00  # Goal reward
    if grid[state.x][state.y].danger >= 0.5:
        return -1.00  # Crater penalty
    return -0.05  # Move cost
```

Question 3: Write code for an agent that follows a given policy, specified as a look up table (state, action). Run an agent using a random policy (i.e., that moves randomly in this environment until reaching a terminal state) in the test problem 1000 times. Make a boxplot of the total undiscounted rewards collected by the agent.

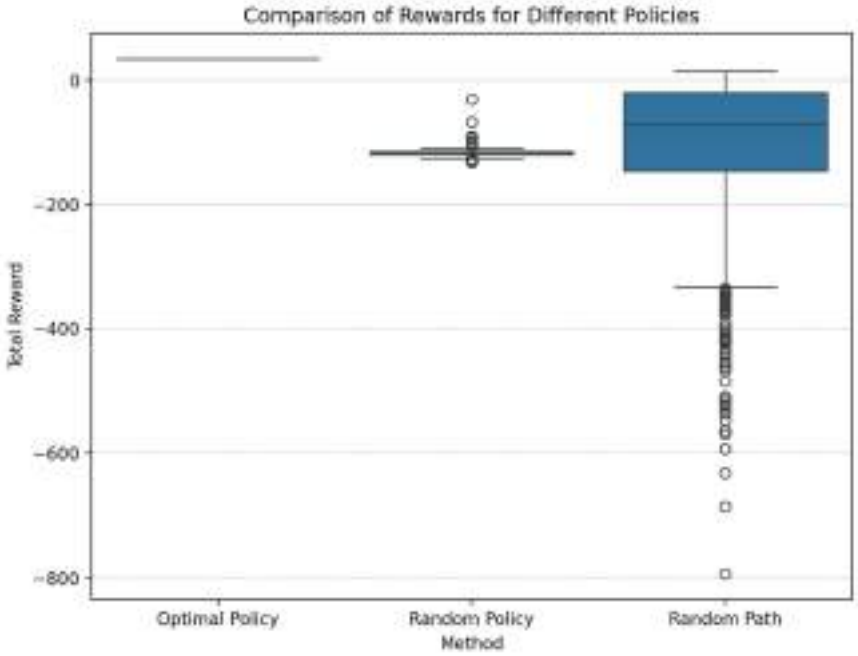

Random policy method represents that a policy was randomly generated then applied, if an infinite loop occurred then a penalty of -100 was applied and the episode terminated. The high cost in the random policy was often a result of the repeated high failure penalty. The random policy method has a cluster just below -100, because its failure is often due to the -100 failure penalty due to looping.

Random path indicates that a random move was applied at each possible situation, where the agent was allowed to cross back over the same location multiple times. The high cost in the random path was often due to the accumulation of the movement cost for 100+ moves to solve the problem. The random path is dispersed much more broadly as it has the chance to converge sooner, and a much lower spread as it allows for repeat cell visits.

The optimal policy agent only has a single value because there is no random element to the design process.

Question 4: Write an algorithm that implements value iteration. Compute the optimal value function and the optimal policy for the test problem using your algorithm (show the outputs visually). Evaluate an agent following the optimal policy and compare the total rewards obtained with those of the agent following a random policy

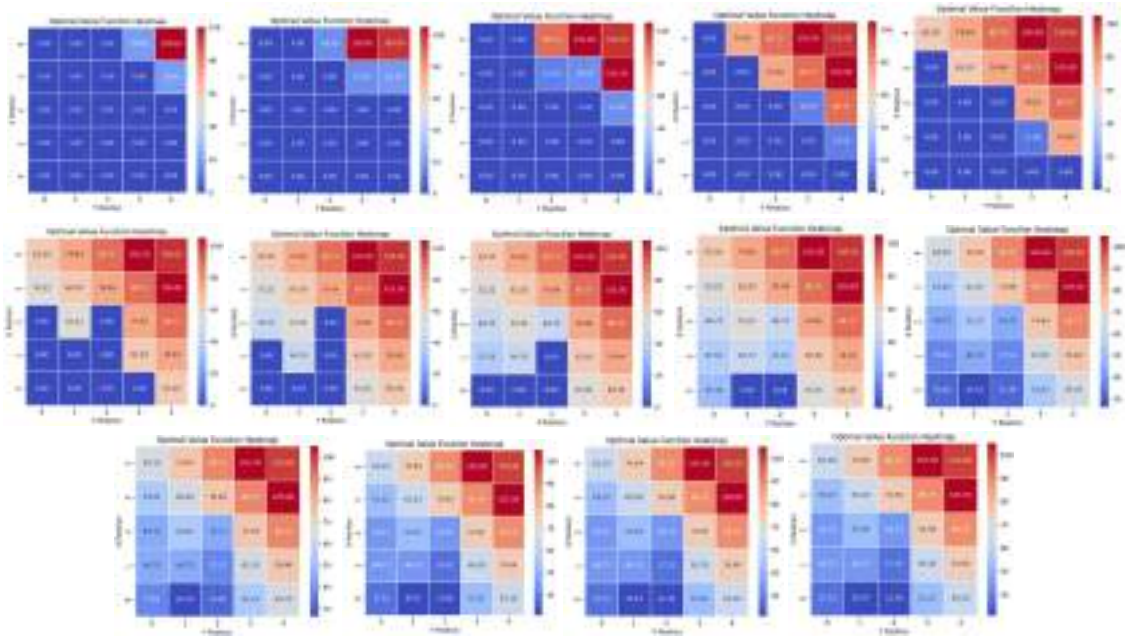

The optimal policy unsurprisingly performs much better than the other two random-based models at solving the problem and avoiding error. It is worth noting that there is an error in the policy generated in the top middle where the policy directs the agent to move left, when it should move right. This error might be caused by a discrepancy between the values being displayed and the combination of (reward + discount_factor * value[next_state]) which could be caused by the presence of a crater. This type of local maximum would result in an infinite loop in the policy as it would converge on a non-goal value.

```
[Running] python -u "c:\Users\iamwi\OneDrive\Documents\S4\AERO489\hw3.py"
Starting Random Policy Simulation...
Optimal Policy:
> > < > G
^ ^ > > ^
> > v > ^
v > > > ^
> > > > ^
Average Reward (Optimal Policy): 34.95
Average Reward (Random Policy): -116.26787
Average Reward (Random Path): -104.8485

[Done] exited with code=0 in 5.632 seconds
```

AERO 489

Valasek, Selva

4/3/2025

Ian Wilhite

HW4: Q Learning:

a) The reward matrix to represent the problem contains 100 utility for any move that results in being in the goal state (including staying in the goal state). In the first episode (1), we establish the impossible moves as -1, the successful moves into the goal state with a reward state of 100, and other possible moves as having 0 utility.

$$Q_{ep1} = \begin{bmatrix} 0 & -1 & -1 & -1 & 0 & -1 \\ -1 & 0 & -1 & 0 & -1 & 100 \\ -1 & -1 & 0 & 0 & -1 & -1 \\ -1 & 0 & 0 & 0 & 0 & -1 \\ 0 & -1 & -1 & 0 & 0 & 100 \\ -1 & 0 & -1 & -1 & 0 & 100 \end{bmatrix} \quad (1)$$

b) In the second episode (2), we iterate based on the potential utility of the options provided to the agent at any given time. We include staying in the current position as a valid option to allow the agent to save the utility of its current position, and to ease the extraction of the convergent utility of the entire system.

$$Q_{ep2} = \begin{bmatrix} 0 & -1 & -1 & -1 & 0 & -1 \\ -1 & 0 & -1 & 0 & -1 & 100 \\ -1 & -1 & 0 & 0 & -1 & -1 \\ -1 & 80 & 0 & 0 & 0 & -1 \\ 0 & -1 & -1 & 0 & 0 & 100 \\ -1 & 0 & -1 & -1 & 80 & 100 \end{bmatrix} \quad (2)$$

$$Q_{ep3} = \begin{bmatrix} 0 & -1 & -1 & -1 & 80 & -1 \\ -1 & 0 & -1 & 64 & -1 & 100 \\ -1 & -1 & 0 & 64 & -1 & -1 \\ -1 & 80 & 0 & 0 & 80 & -1 \\ 0 & -1 & -1 & 0 & 80 & 100 \\ -1 & 0 & -1 & -1 & 80 & 100 \end{bmatrix} \quad (3)$$

$$Q_{ep4} = \begin{bmatrix} 64 & -1 & -1 & -1 & 80 & -1 \\ -1 & 0 & -1 & 64 & -1 & 100 \\ -1 & -1 & 0 & 64 & -1 & -1 \\ -1 & 80 & 0 & 0 & 80 & -1 \\ 64 & -1 & -1 & 64 & 80 & 100 \\ -1 & 0 & -1 & -1 & 80 & 100 \end{bmatrix} \quad (4)$$

$$Q_{ep5} = \begin{bmatrix} 64 & -1 & -1 & -1 & 80 & -1 \\ -1 & 0 & -1 & 64 & -1 & 100 \\ -1 & -1 & 0 & 64 & -1 & -1 \\ -1 & 80 & 51.2 & 0 & 80 & -1 \\ 64 & -1 & -1 & 64 & 80 & 100 \\ -1 & 0 & -1 & -1 & 80 & 100 \end{bmatrix} \quad (5)$$

c) The final convergent matrix can be found by applying the process many times. After 1000 trials, the convergent matrix was found in (6). Some observations to note include that all columns contain either -1 or a constant. This represents that after converging, moving to that state from any other state will result in the same utility, or conversely, that the value of a given state is independent of the direction of approach. Recalling that the diagonal represents that utility of staying in a given state, combined that all columns contain the same value, the diagonal of the convergent matrix can be utilized to develop a common utility for each state.

$$Q_{conv.} = \begin{bmatrix} 64 & -1 & -1 & -1 & 80 & -1 \\ -1 & 80 & -1 & 64 & -1 & 100 \\ -1 & -1 & 51.2 & 64 & -1 & -1 \\ -1 & 80 & 51.2 & 64 & 80 & -1 \\ 64 & -1 & -1 & 64 & 80 & 100 \\ -1 & 80 & -1 & -1 & 80 & 100 \end{bmatrix} \quad (6)$$

By evaluating the diagonal, we can observe that the convergent Q matrix represents the intuition of the initial problem. The goal state is worth the full goal value of 100. States one and four that allow for one move to the goal state have value of the goal state multiplied by the discount factor, or 80. The subsequent states are each valued at their optimal move value multiplied by the discount factor, or valued at the goal state value multiplied by the discount factor to the power of the minimum number of moves to the goal state. This Q matrix would create an optimal policy to provide an appropriate optimal policy to exit the house.

AERO 489

Valasek, Selva

Ian Wilhite

4/13/2025

Acrobot-v1 Machine Learning Hyperparameter Study

Discussion:

1) Gymnasium Environment:
    a. Environment: Acrobot-v1
    b. It is a double pendulum driven from the joint between the arms [1]. The objective is to upright the assembly above the center pivot. This environment has a box observation space and a discrete action space with 3 options for the agent at a given timestep: apply positive torque, apply no torque, apply negative torque [1].
2) Three candidate algorithms:
    a. From the stable baselines compatibility table in Figure 1, we can identify that acrobot requires a discrete action space, meaning that Proximal Policy Optimization (PPO), Advantage Actor Critic (A2C), and Deep Q-Network (DQN) would work with the environment [2]. These algorithms were selected based on their popular usage for a variety of applications and Dr. Valasek's common mention of A2C.

Name					Multi Processing
ARS [3]	✔	✔	✘	✘	✔
A2C	✔	✔	✔	✔	✔
CrossQ [1]	✔	✘	✘	✘	✔
DDPG	✔	✘	✘	✘	✔
DQN	✘	✔	✘	✘	✔
HER	✔	✔	✘	✘	✔
PPO	✔	✔	✔	✔	✔
QR-DQN [1]	✘	✔	✘	✘	✔
RecurrentPPO [3]	✔	✔	✔	✔	✔
SAC	✔	✘	✘	✘	✔
TD3	✔	✘	✘	✘	✔
TQC [1]	✔	✘	✘	✘	✔
TRPO [1]	✔	✔	✔	✔	✔
MaskablePPO [1]	✘	✔	✔	✔	✔

Figure 1. Stable Baselines algorithm environment compatibility

3) Hyperparameter Study:
    a. The two hyperparameters I will evaluate are Learning Rate and the Discount Factor. I believe that the learning rate will affect the speed of convergence for the model, as well as the stability of the convergence achieved, whereas the discount factor will determine the performance and aggressiveness of the model in attempting to achieve high performance. An initial investigation can find a workable range for subsequent experiments. Using an average of three trials, a mean can be calculated and plotted in a heat map in Figure 2.

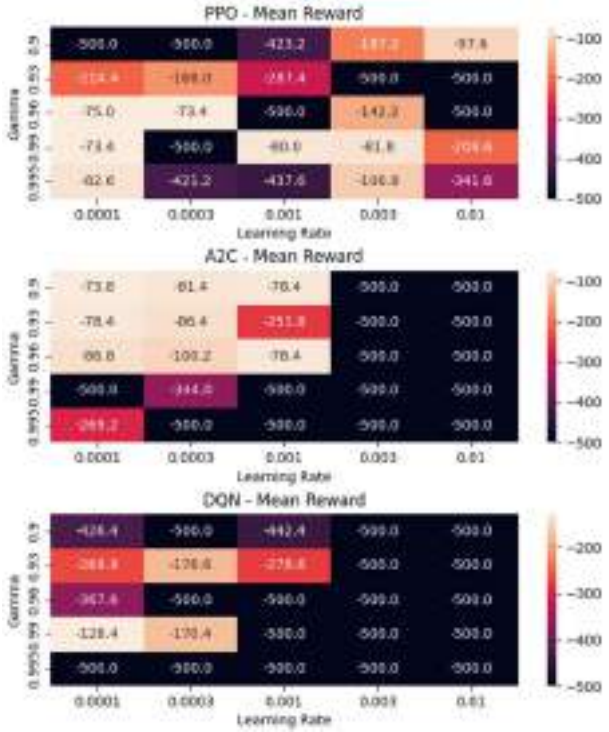

Figure 2. Hyperparameter study for 10,000 episodes

Many of the models simply did not converge, and therefore the training size needed to be increased, however the range seemed promising. It is worth noting that PPO succeeded with little trend, A2C showed a clear successful and unsuccessful region, and DQN showed little progress reinforcing the similar range to A2C.

With an increased timestep, the training curves for each model could be constructed with respect to the discount factor and learning rate. In Figure 4, it can be observed that with lower learning rates (the left columns) that the models converged slower or negligibly, whereas with higher learning rates (the right columns), the models demonstrated oscillation after convergence

or suffered failure altogether. The discount factor showed minimal impact, but broadly that a lower discount factor (top rows) created impatient models, that tended to be more aggressive in improving its rewards per episode, whereas a higher discount factor (bottom rows) created a more patient model that converged slower with fewer instances of decreasing rewards between episodes.

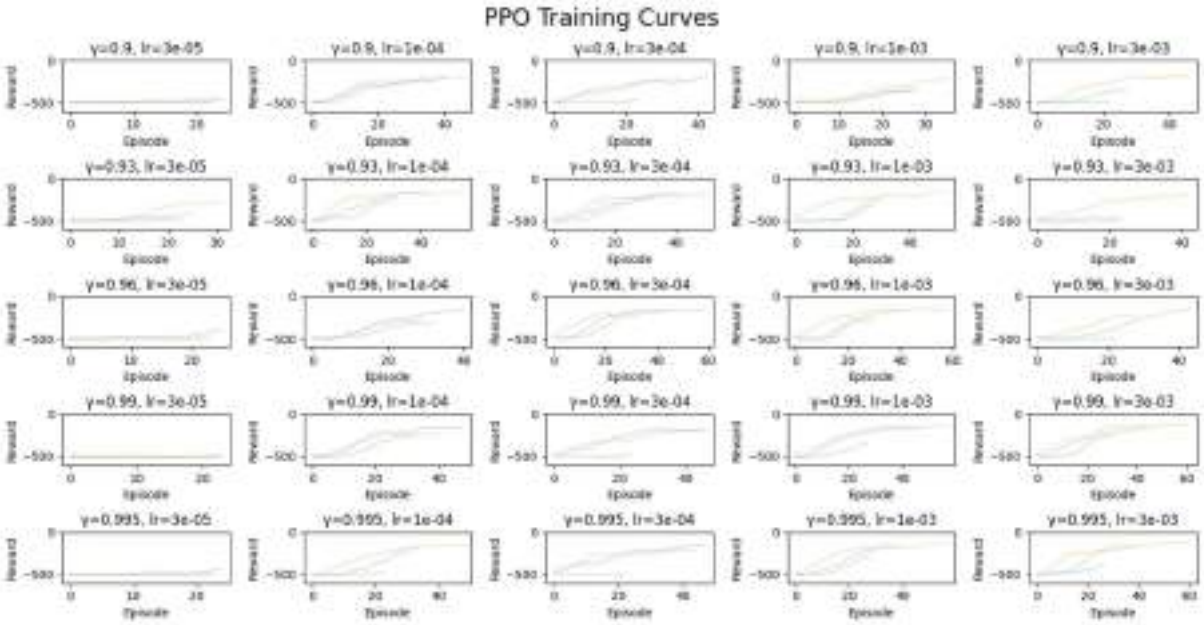

Figure 4. PPO Learning curves for 15,000 episodes w.r.t. discount factor and learning rate

For deep Q learning, all models across the board suffered from increased volatility in convergence. Notably, with very low learning rates they ended training sooner because they converged at negligible rewards.

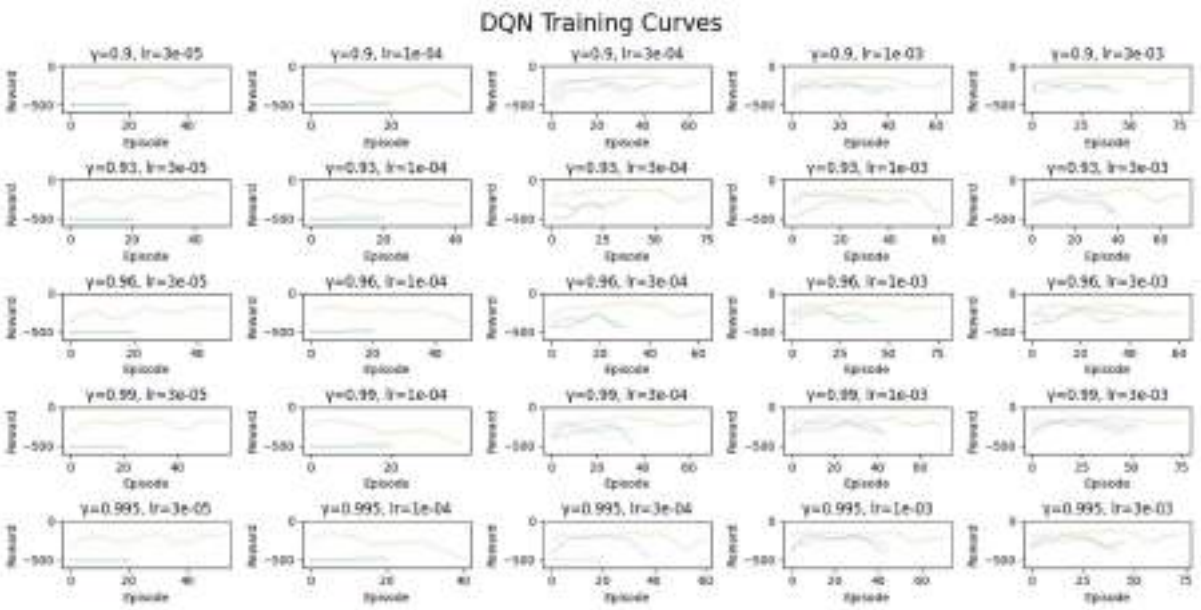

Figure 5. DQN Learning curves for 15,000 episodes w.r.t. discount factor and learning rate

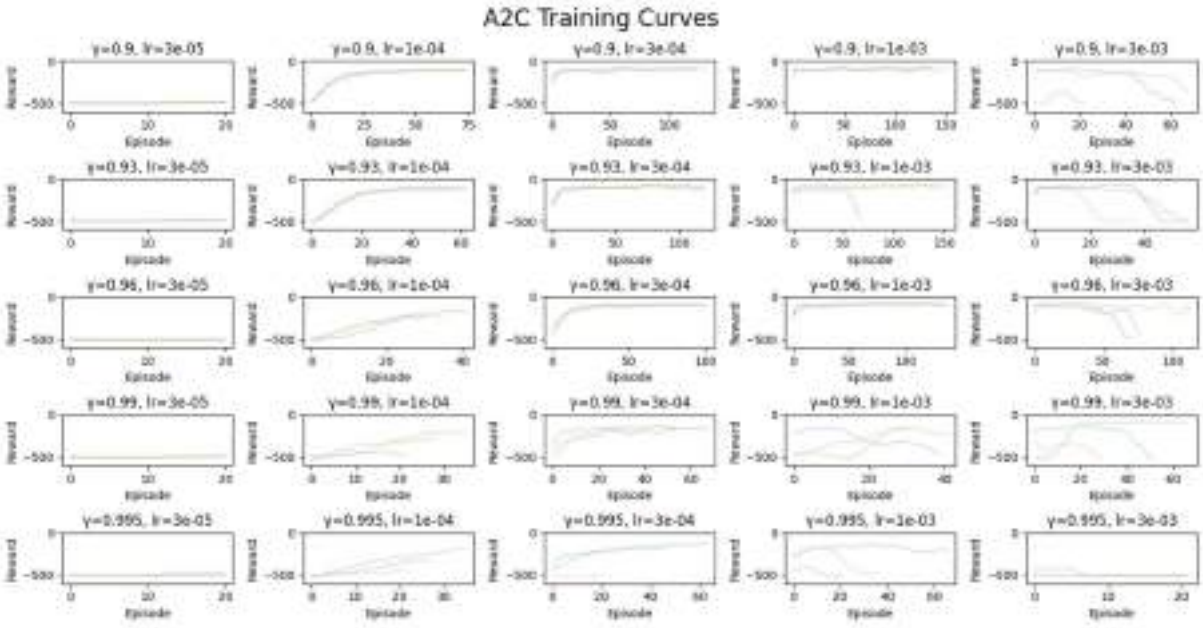

Figure 6. A2C Learning curves for 15,000 episodes w.r.t. discount factor and learning rate

A2C Learning clearly demonstrates the trends stated before, that as the discount factor decreases the model becomes impatient, particularly where the learning rate is effective to converge. When the learning rate is too high, the model does not converge, and when the learning rate is too low, it will not converge or will converge slowly.

4) Direct comparison

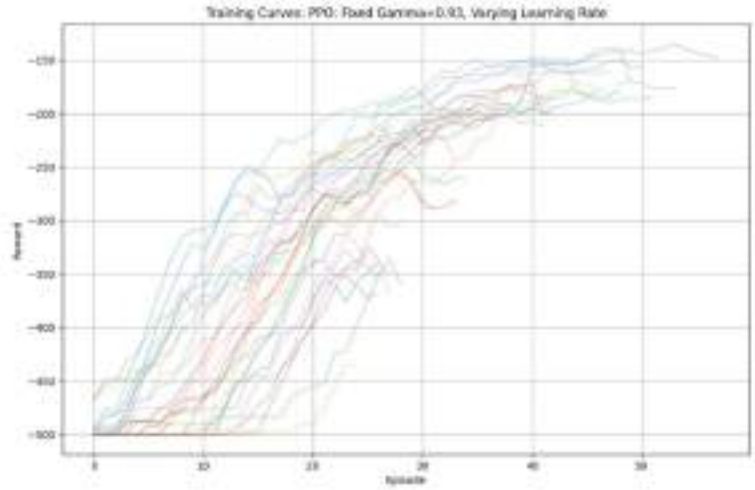

Figure 7. PPO Learning Curves while varying learning rate

Figure 8. PPO Learning Curves while varying discount factor

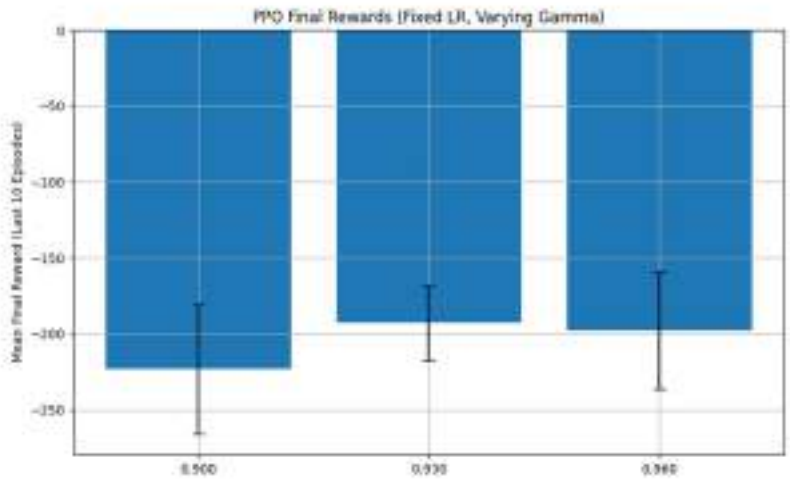

Figure 9. PPO rewards varying discount factor

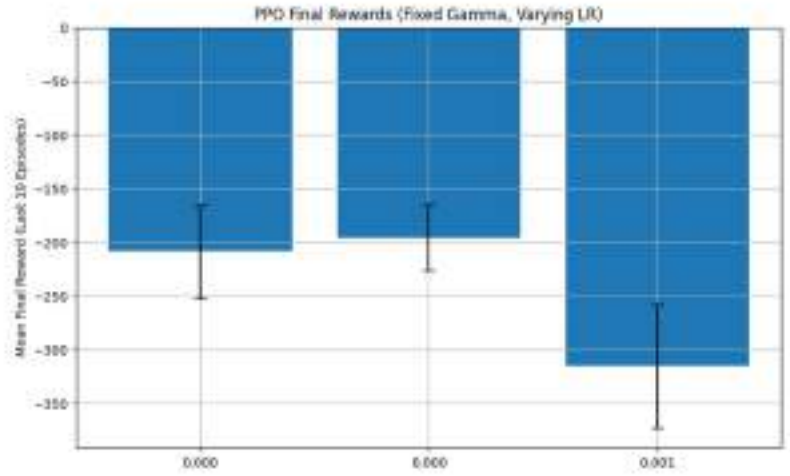

Figure 10. PPO rewards varying learning rate

PPO can be observed as converging consistently, and showing that the lower discount factors decrease the mean resulting reward. It should be noted that the ending rewards are not indicative of the peak rewards or the time to reach peak performance, only that after many iterations

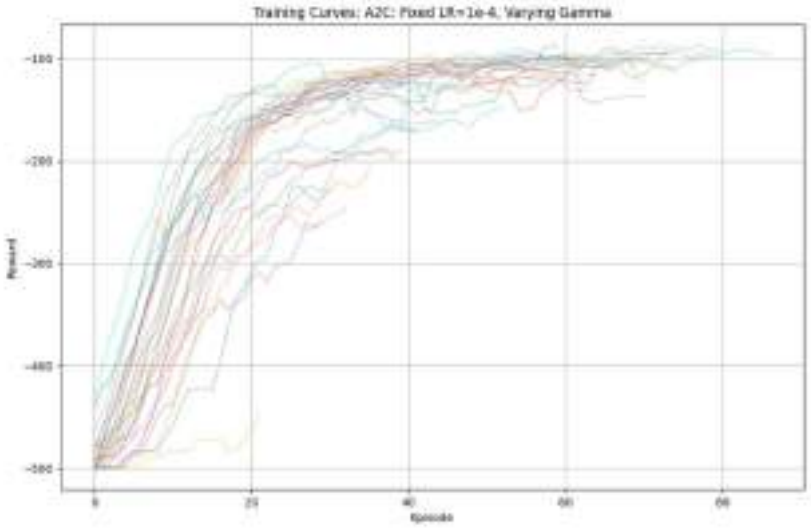

Figure 11. A2C Learning Curves while varying discount factor

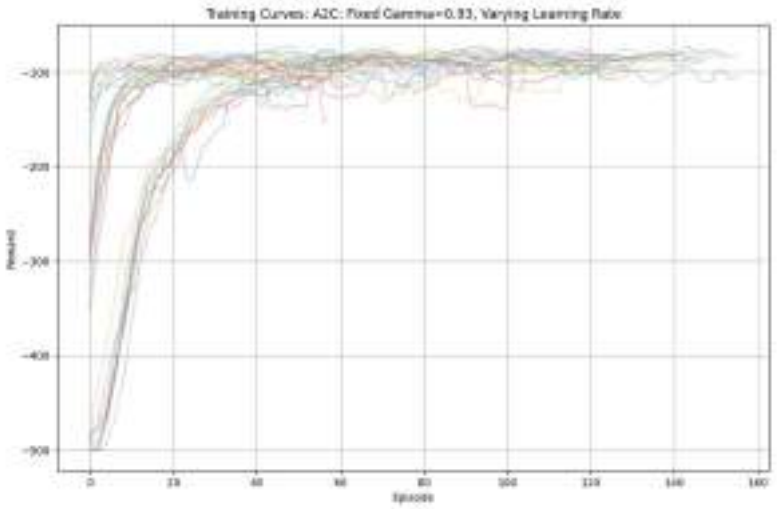

Figure 12. A2C Learning Curves while varying learning rate

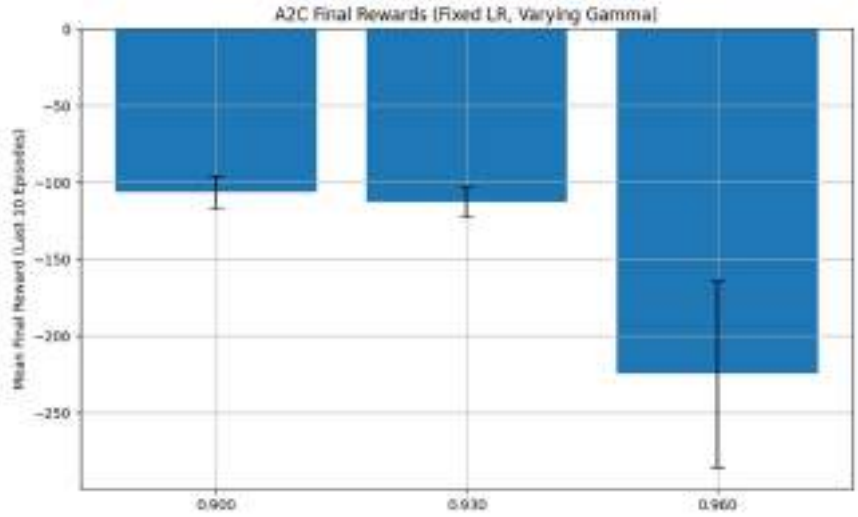

Figure 13. A2C rewards varying discount factor

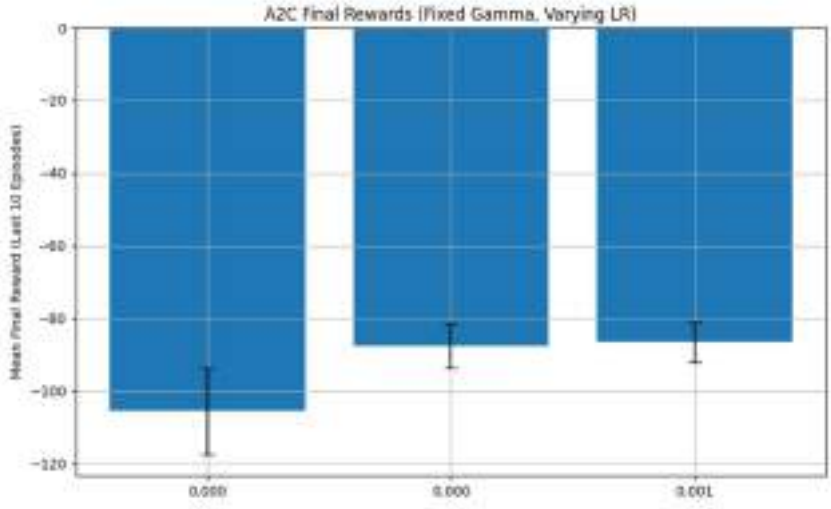

Figure 14. A2C rewards varying learning rate

A2C can be seen as noticeably continuing many of the otherwise observed trends with a lower uncertainty and consistency not only in the final results but also the learning curves path to convergence. The differing learning curves clearly show the paths that each factor takes to convergence. Noting the scale that nearly all of the A2C models outperform the PPO models on similar metrics.

Figure 15. DQN Learning Curves while varying discount

Figure 16. DQN Learning Curves while varying learning rate

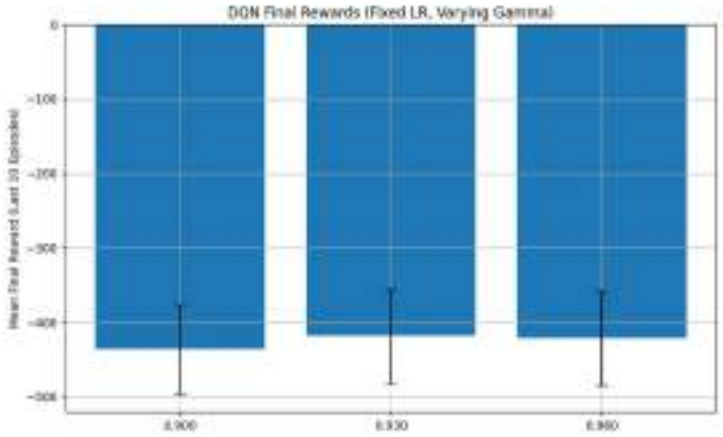

Figure 17. DQN rewards varying discount factor

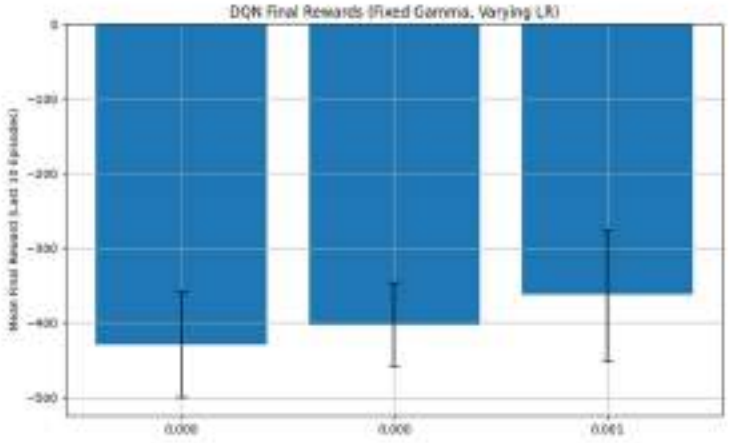

Figure 18. DQN rewards varying learning rate

While PPO demonstrated consistent convergence behavior, A2C outperformed it in both average final rewards and consistency across trials. DQN exhibited unstable learning and failed to converge in most settings, although a few isolated cases approached competitive performance.

5) Conclusion

This study evaluated the impact learning rate and discount factor on PPO, A2C, DQN algorithms using the Acrobot-v1 environment. Results showed that: Low learning rate led to non-convergence, whereas high learning rate led to oscillatory behavior; Low discount factor led to aggressive models that

converged quickly while high discount factors created more patient models that converged slower but rarely took any steps that decreased rewards.

a. A2C consistently outperformed PPO and DQN in similar ranges, however it is worth exploring a wider range of learning rates and discount factors as trends for optimality indicated that different models preferred different learning rates and discount factors. PPO could benefit from higher discount factors, A2C could benefit from lower discount factors, and DQN had little impact from discount factors. PPO could benefit from a lower learning rate, whereas A2C and DQN could benefit from a higher learning rate.
b. A2C was the easiest to train, followed by PPO, and I could not get DQN to reliably converge. A2C demonstrated the most consistent convergent given the same hyperparameters.
c. PPO seemed the easiest to tune in the sense that poor hyperparameters could be accounted for with additional training episodes. A2C had a very clear optimal region of performance with respect to its hyperparameters, meaning that although it was harder to find this optimal region of performance, inside there was consistent and rapidly converging high performance. DQN did not converge consistently across any region of hyperparameters and was consistently exiting training episodes, indicating a need for continued variance in the hyperparameters provided.
d. This is the most I have worked with machine learning models thus far, and I think it was an interesting way to better understand the role that hyperparameters can play in the training process for various models. I learned about the characteristics of PPO, A2C, and DQN, and the impacts that learning rate and discount factor have on the performance of various algorithms. I think that this has been one of the most beneficial assignments I have seen in the class so far with respect to applications of the concepts that we have been learning up to this point

Future work could include a broader range of learning rates and discount factors applied, increased trials to decrease uncertainty and determine trends more consistently, and optimization techniques applied to identify optimal parameters for different algorithms.

Appendix

[1] Farama Foundation. *Acrobot-v1 Environment Documentation*. Gymnasium Classic Control Environments. Available at: https://gymnasium.farama.org/environments/classic_control/acrobot/. Accessed April 13, 2025.

[2] Stable-Baselines3 Developers. *Algorithm Guide and Environment Compatibility*. Stable-Baselines3 Documentation. Available at: https://stable-baselines3.readthedocs.io/en/master/guide/algos.html. Accessed April 13, 2025.

Two Rope Ball Balancer

Ian Wilhite
5/1/2025

Modeling

RL setup

- State Space
  - Height
  - Height’
  - Angle
  - Angle’
- Action Space
  - Force on left rope (0, +50)
  - Force on right rope (0, +50)

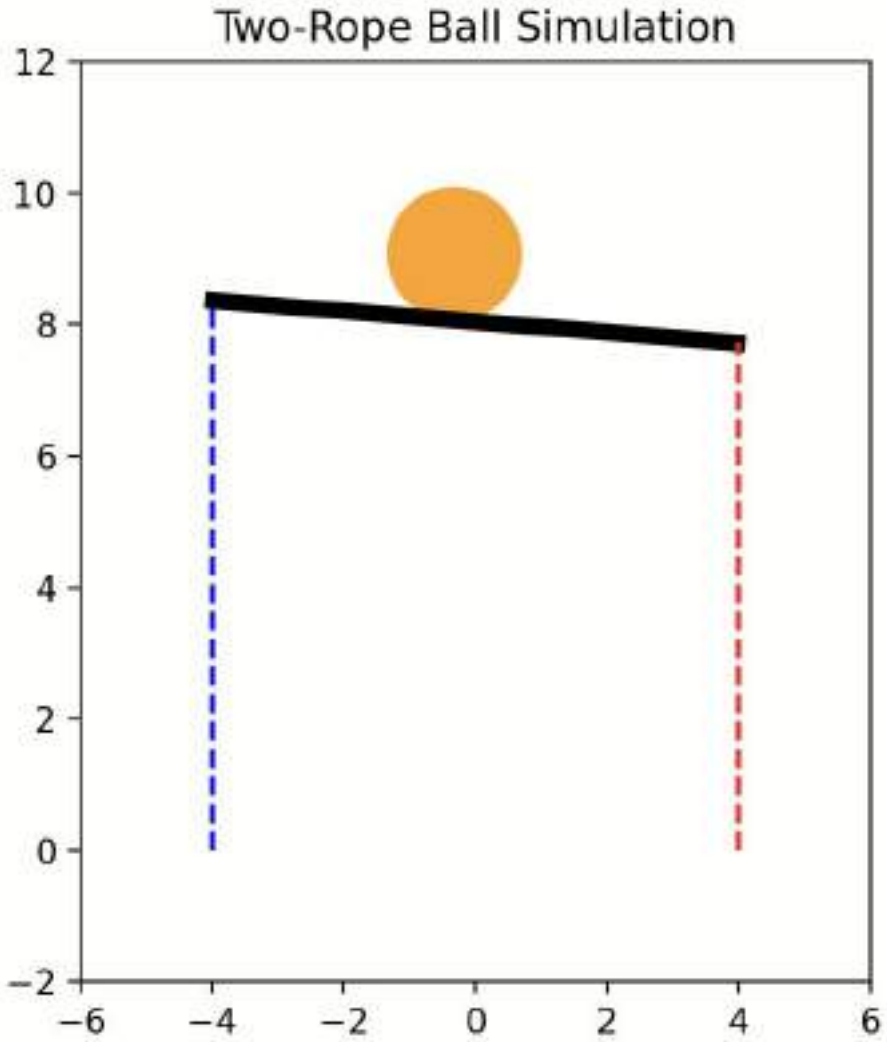

Two rope model

- matplotlib
- Physics work
- No time penalty (for now)

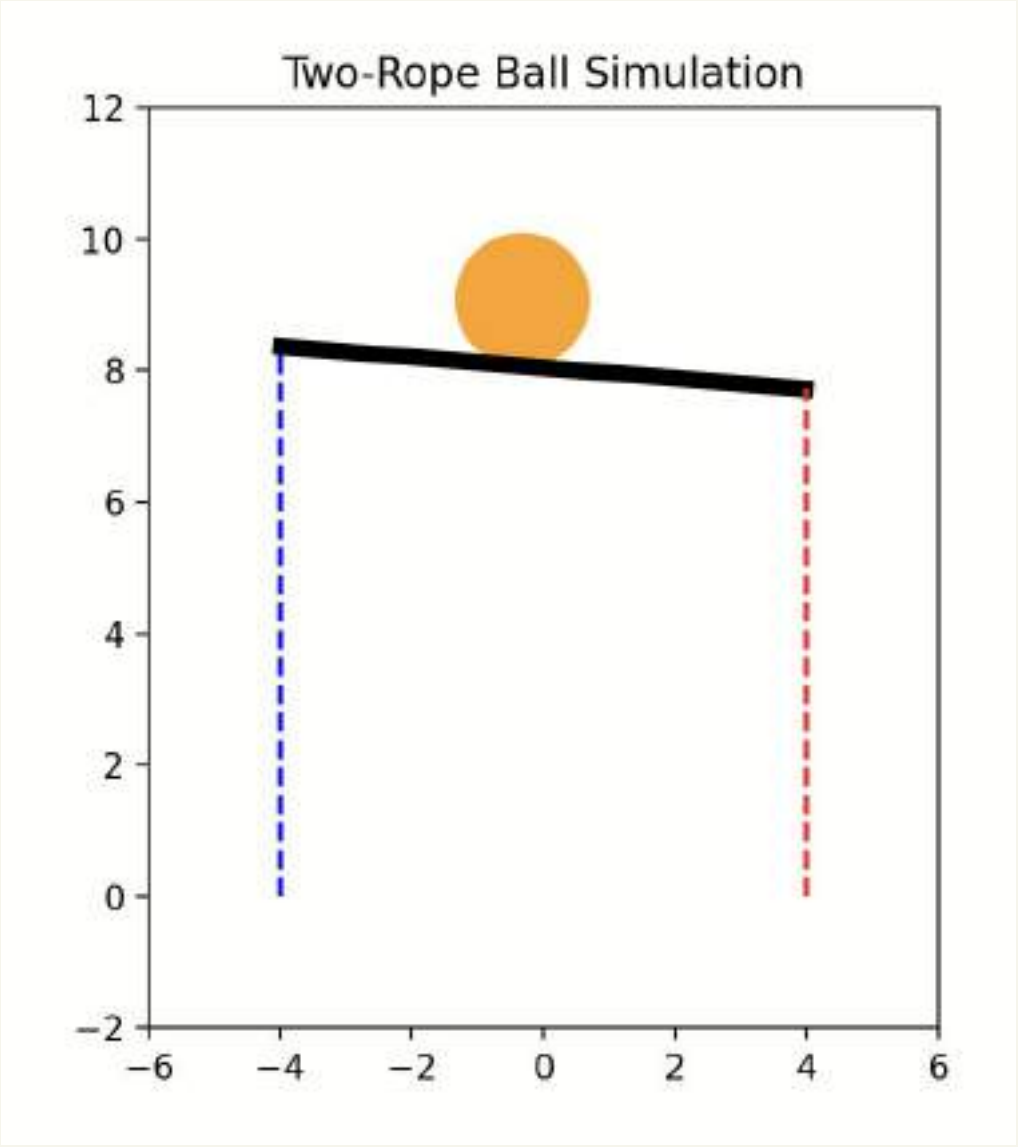

Training (pt 1)

PPO

- Chosen for robustness
- slow
- Worked!
  - High success rate

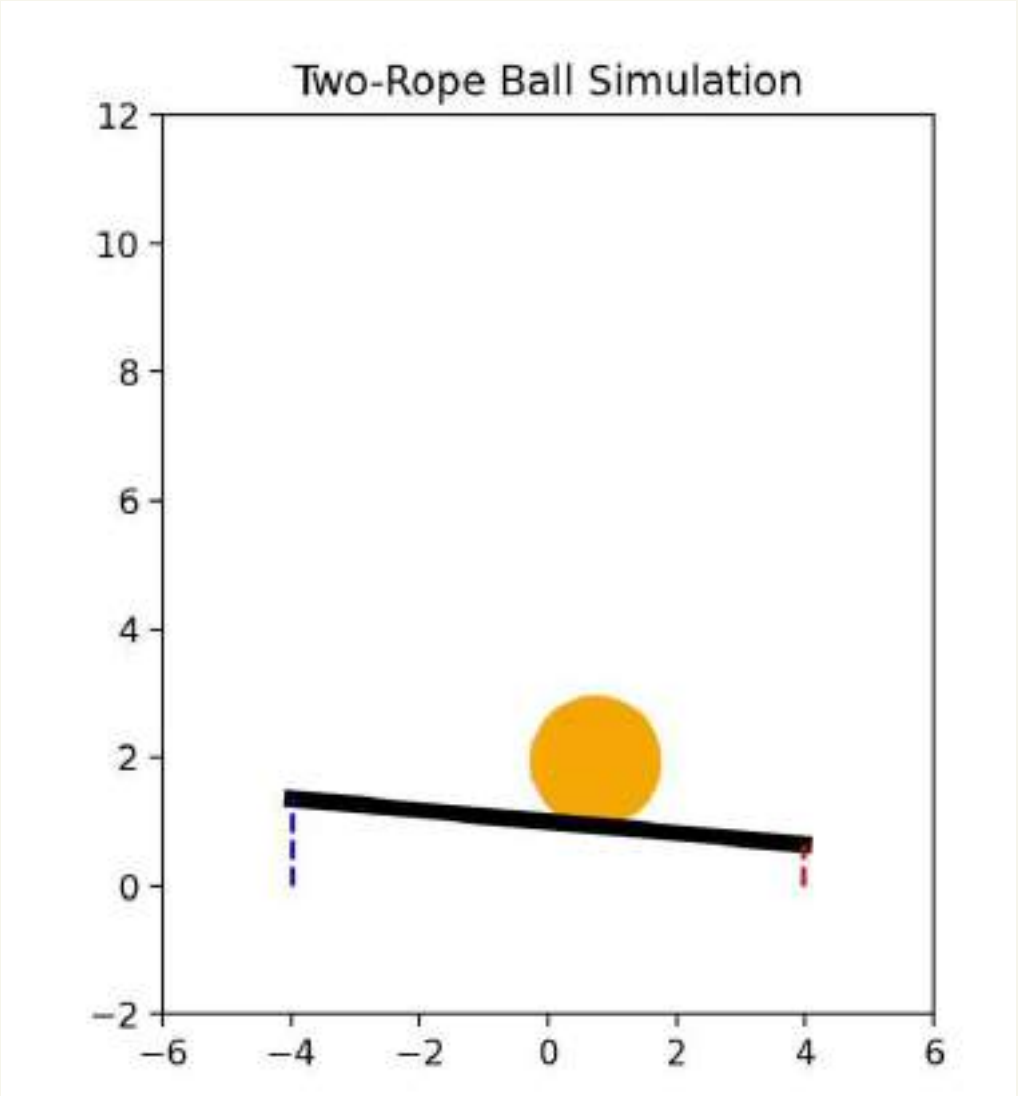

PPO-V1 learning curve

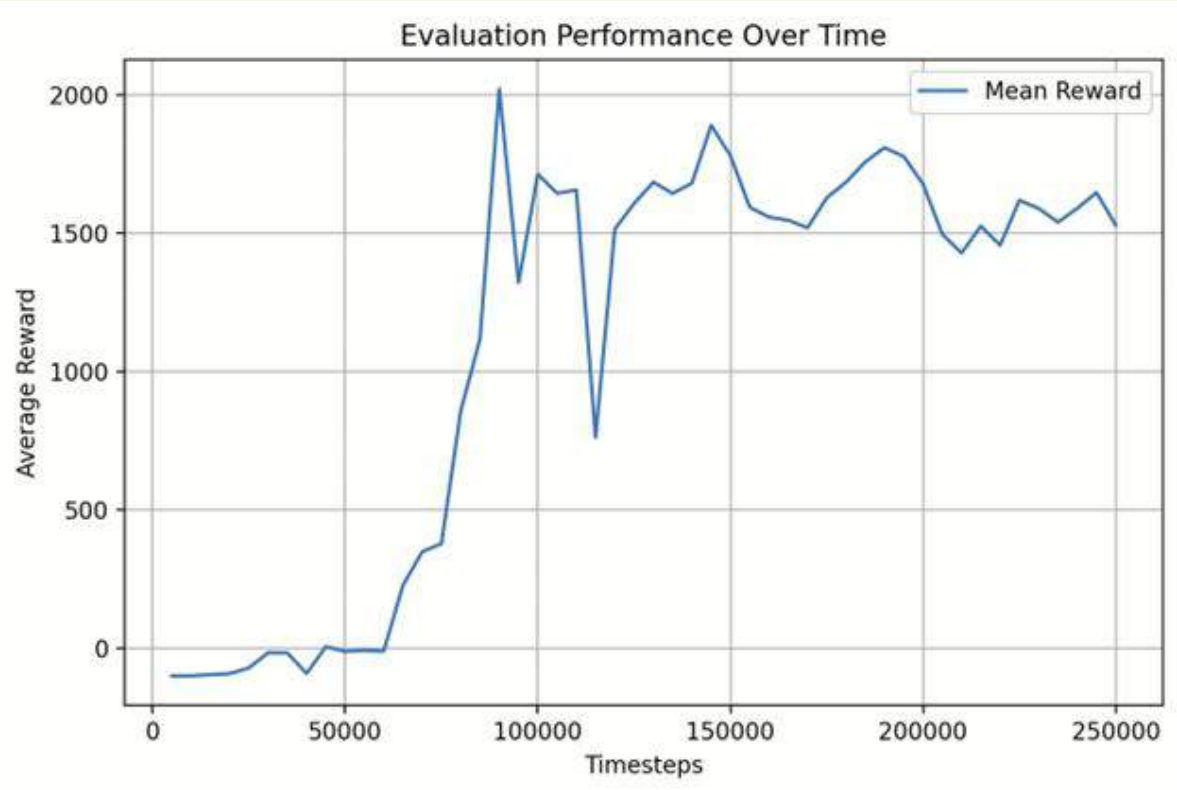

Training (pt 2)

PPO - w linear time penalty

- Lower success rate
- fast!
- worked!

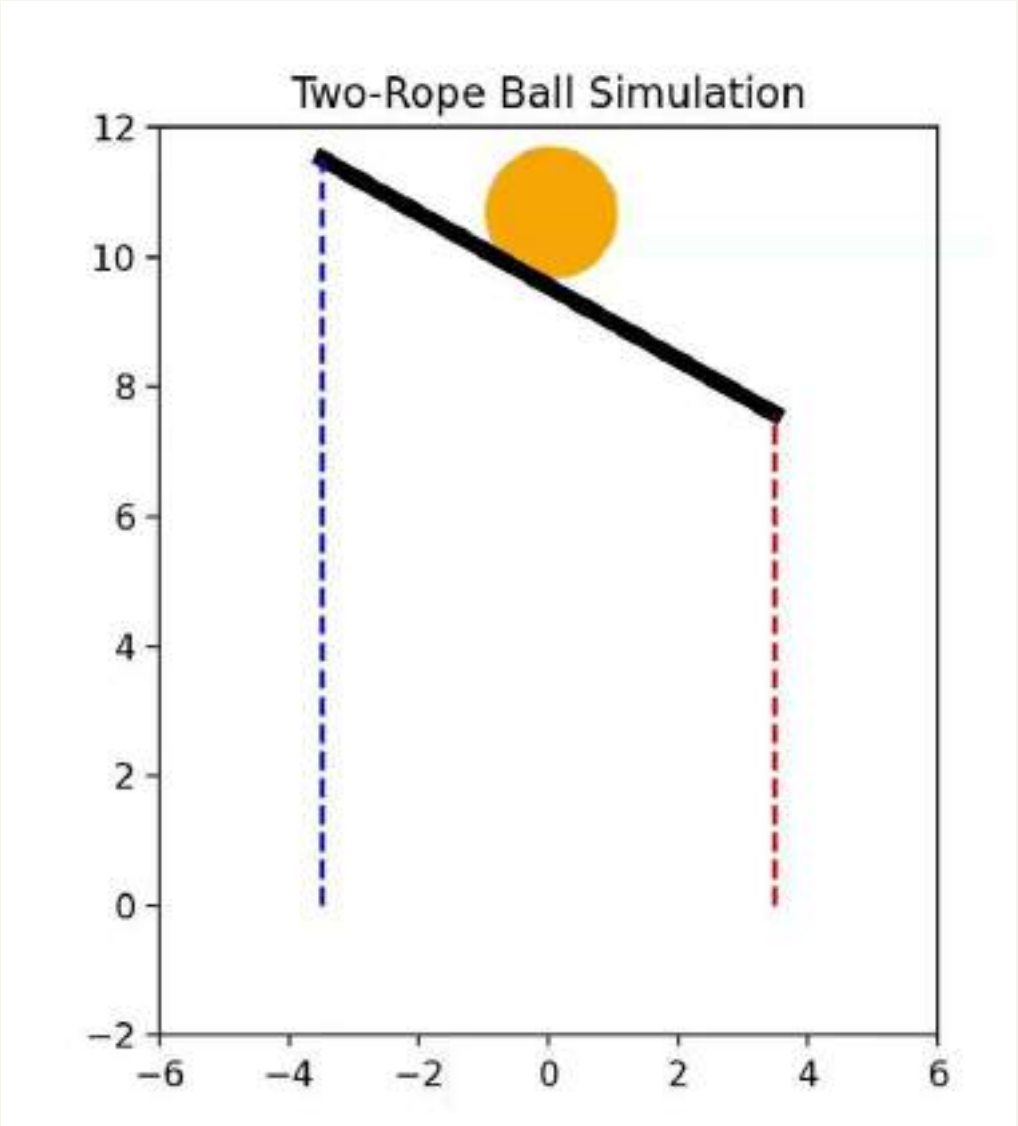

PPO-V2 learning curve

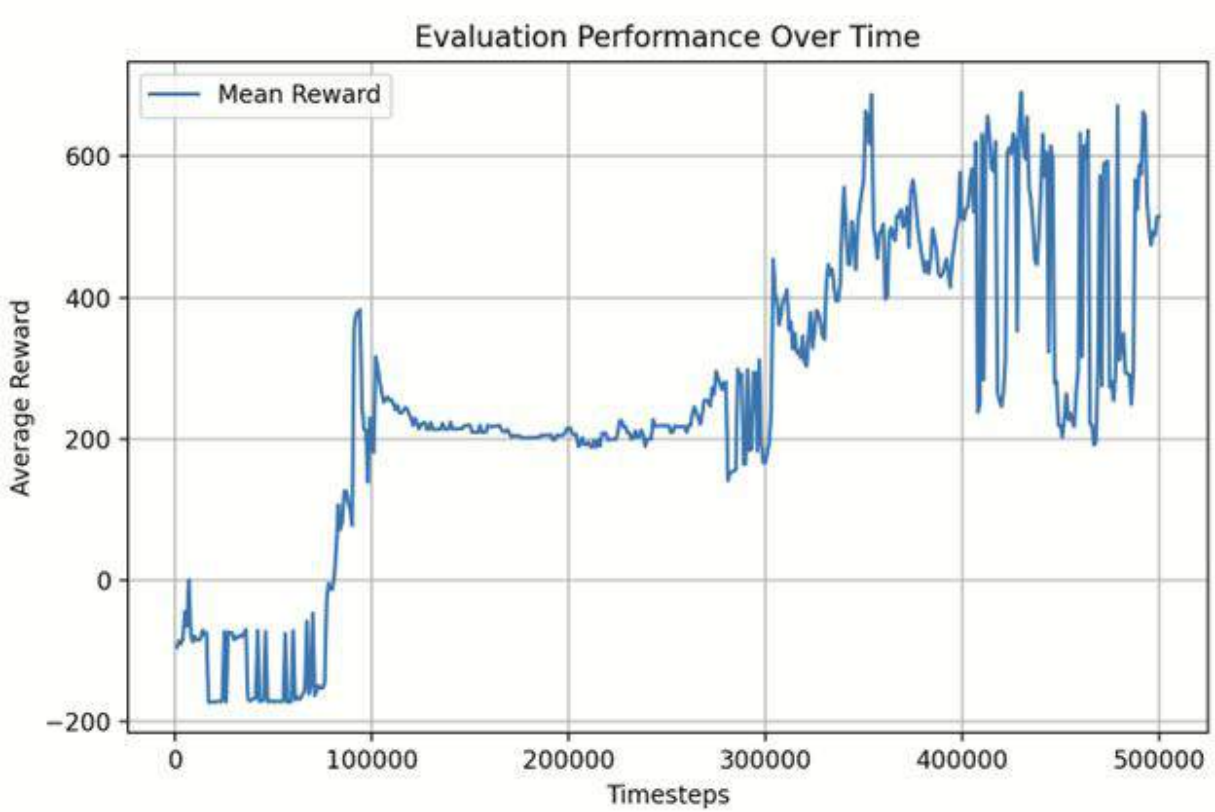

- Initially rewarded jerky movements
-

Success evaluation

Results!

```
[Running] python -u "c:\Users\ianwi\OneDrive\Docum
Gym RopeBall environment imported successfully!
Model reloaded successfully!
Success rate: 86.90%, sample size: 10000
Evaluation completed successfully!
```

- 86.9% Success Rate!
- There is definitely room for improvement
- worked!

Next Steps

Tuning:

- Hyperparameter study
- Implement A2C
- Replace heavy training with thoughtful training (hyperparameter tuning)

AERO 489
Project #2: Final
5/5/2025
Ian Wilhite

1) I chose to implement the 2-rope ball environment.
    a. The environment includes a random starting horizontal velocity, bar angle, angular frequency, and vertical velocity.
    b. The goal as stated was to raise the ball to a height of 10 without falling off the bar, and terminal conditions to ensure the model was meeting real-world constraints.
2) The reward structure and agent terminal conditions were structured to aide the agent to complete the assigned task and penalize suboptimalities in its completion of the task.
   Reward structure:
    a. Proportional height incentive – rewarding the agent for positive movement towards the goal condition.
    b. Proportional time disincentive – penalizing the agent proportionally for longer solutions.
    c. Nonlinear ball position penalty – minor penalty for small deviations from the middle of the ball, and higher penalties for allowing the ball to be closer to the edges of the bar.
    d. Minor maximum angle penalty – disincentivizing the agent from tilting the bar a large amount because of the time required to untilt the bar.

   Terminal condition structure:

    a. Checking the x position of the bar is not off the bar – if the ball has fallen off the edge of the bar the trial has ended.
    b. Checking the bar is upright – ending the trial if theta between negative and positive one-half pi.
    c. Checking the height is greater than negative 10 – this was added to prevent agent from falling into the void during training.
    d. Checking the height is greater than 10 – the success condition.

3) I chose to implement PPO because of its broad convergence in a variety of environments, and its notorious ease to train. During the training process, I varied

the ratio between the time and height proportional rewards, as well as the various minor penalties provided until the agent satisfactorily performed.

4) Short report:

This project allowed me to learn how to render real world scenarios and to apply the concepts of RL to real situations that I may face in industry. This project truly served to combine many of the skills of this course into a single relevant project relevant to the ways that these tools are currently being applied.

In designing the environment, a major aspect was determining which variables made a major impact on the state and would be required to fully describe any possible given state. Many variables excluded to decrease training time, and therefore the minimum number of variables possible were provided. The horizontal position of the bar and angle were added to represent the position of the system. Their derivatives were added to allow the agent to predict the motion of the system into the future. Their second derivatives were not added because the action the agent took would directly affect it, and therefore the agent did not need to know its own previous action, as it only needed to know what to do next. The height of the bar was intentionally not added to prevent the agent from learning to jerk the cables near the beginning or end, but rather to encourage the agent to act consistently throughout the trial.

The reward structure was revised continuously while the agent was being trained. The combination of linear, nonlinear, and weightings of rewards greatly changed the reaction of the agent to various states, and therefore how it responded to it. Reward shaping drastically affected nearly every aspect of the model's behavior and performance and eventually led to the success of the model. After pivoting to SAV, in tuning, I found that I needed to lower the learning rate to secure a more stable convergence, which finally secured a success rate of 79% in the randomly initialized environment.

I chose to implement Proximal Policy Optimization (PPO) initially because of its known simplicity in convergence as I was testing the environment, however, I chose to pivot to Soft Actor Critic (SAC) for its ability to perform well in environments with high entropy, making it more suitable for modeling a system of multiple variables and lower training times.

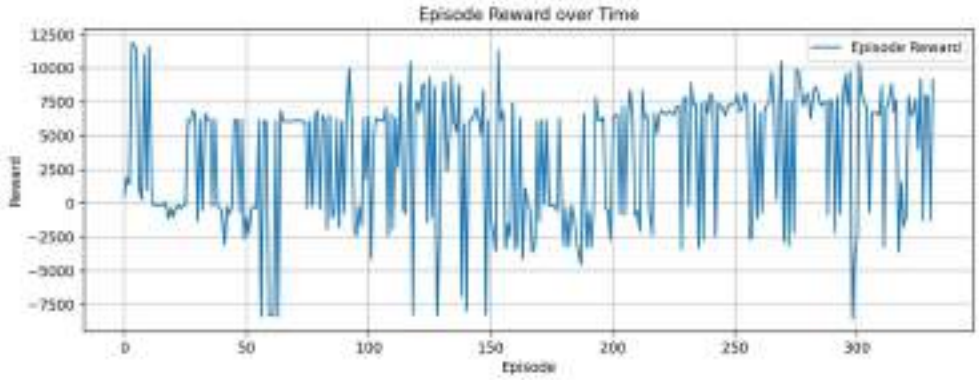

The reward over episode graph shows the improvement of the model, both initially and in stability as the frequency of success increases but could still allow for another decrease in the learning rate and additional trials to allow the model to succeed with higher frequency.

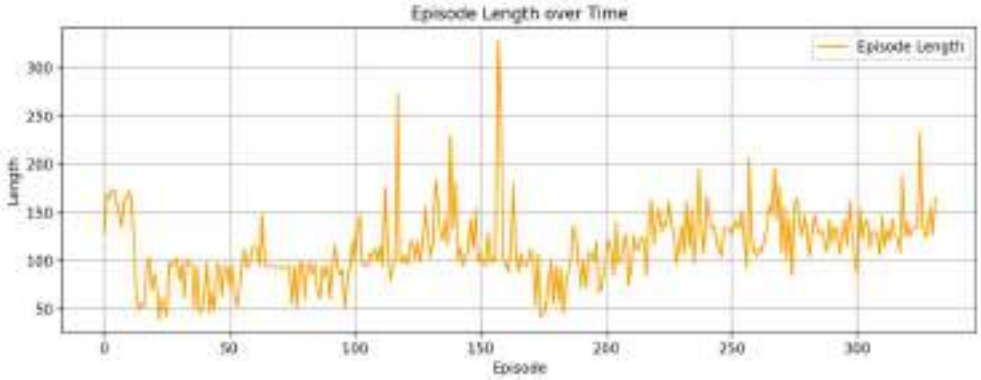

The episode length over time graph shows another perspective of the convergence strength. Initially, there is a sharp decrease in episode time as the model identifies the time penalty, and starts working around it as it learns to stabilize the ball. Around episode 200, the episode length started to rise alongside consistent episodic success, where the model was learning what tradeoffs were worth losing the time penalty points.

```
Training complete.
Model saved as 'sac_ropeball_trained'.
Loading the trained model...
Model loaded.
Testing the model over 100 episodes...
Success rate: 79.00%
```

To evaluate the model, 100 episodes with random initial angles, angular velocities, and ball speeds were performed, and the success rate for the trials were identified. The agent succeeded in 79 of the 100 episodes, for a success rate of 79% and securely meeting the established threshold of 70%.

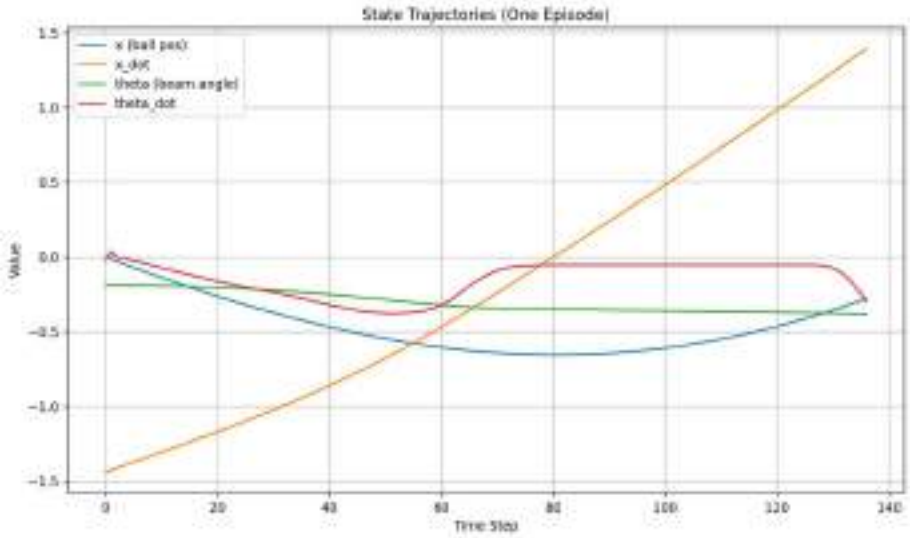

The state trajectories plot indicates the agent is able to observe the negative ball position and velocity, and apply a positive torque to counteract the balls motion. The agent is able to correct for and maintain the bars angle, and minimizes the bar's angular acceleration then maintains it.

The system can be observed balancing the ball initially until time step 60, then maximizing a consistent force to raise the bar to the desired height as quickly as possible. The agent can be observed near the end of the trial as accounting for the ball's position crossing the center of the bar and beginning to tilt the bar to correct for overshoot.

Overall, the agent has learned to stabilize and raise the bar to the desired position with satisfactory success. The modeling of the environment represents skills used in industry, while the learning and tuning process is a final application of the skills covered in the second half of the course. This has been certainly one of the most unique classes I have taken, and I truly believe that I have learned a lot from it.

Back to Contents

2. Dynamics and Vibrations

Summary

This section contains projects from an undergraduate dynamics course evaluating dynamic problems, modeling approaches, and foundational physical simulation.

- P1: Bungee Jumping
- P2: Piston Kinematics
- P3: Mixer Torques & Kinematics

Contributors: Tori Abell, Alois Campbell, Jake Smith, Eddy Silva, Ian Wilhite

Key Skills: Dynamics, Vibrations, System Modeling, Validation, and Technical Writing.

Relevance: The projects emphasize direct conclusions based on experimental results. In these works, I often worked to write the code for the simulations and generate the charts to represent the teams findings.

Computational Assignment 1 - Bungee Jumping

TO: Adolfo Delgado
FROM: Group 7 of MEEN 363 - 502 (Tori Abell, Alois Campbell, Eddy Silva, Ian Wilhite)
Subject: Assignment 1, Bungee Jumper
Date: 02/21/2025

EXECUTIVE SUMMARY

The objective is to analyze how the bungee cord's material properties affect the jumper's motion. The height of the jump, the weight of the person, the stiffness of the bungee cord material, the damping effect of the material, and the air resistance all affect the motion of the jumper. The equation of motion was derived by using Newton's second law and summing the forces in the vertical direction. Two main equations were formed, one considering the damping from the cord being stretched and the air drag and the other considering when the cord was not in tension, the person only experiencing damping from air resistance. Based on the general equation of motion, the natural frequency of the jumper depends on the cord stiffness (k), and the mass of the person. As expected, a higher stiffness, k, results in a higher natural frequency. A lower cord stiffness requires a higher initial jump height because it allows the cord to stretch more and the person to fall further. A higher cord stiffness would result in a smaller initial jump height required, but the person is more likely to experience injury from a higher acceleration and force acting on them.

METHOD

The first step in creating the equation of motion for the bungee jumper is to create a free-body diagram (FBD). As seen in **Figure 1**, there are three forces acting on the jumper throughout most of the fall; the jumper's weight, total damping, and the spring force in the cord. The result of Newton's Second Law equation from the FBD is **Equation 1**. Using the motion equation and the "solve_ivp" scipy function in Python, a second-order differential equation can be solved for position, velocity, and acceleration. To analyze the effect of the cord's stiffness on the motion of the jumper, 10 evenly spaced k values between 40 N/m and 240 N/m were used in the position, velocity, and acceleration equations and plotted as functions of time. Three plots were then made for the material loss factor (η), seen in **Equation 2**, with values ranging from 0.15 to 0.30. For clarity, the simulations assume an initial jump height of 100m with the cord considered taut at 82m from the ground (x=0m).

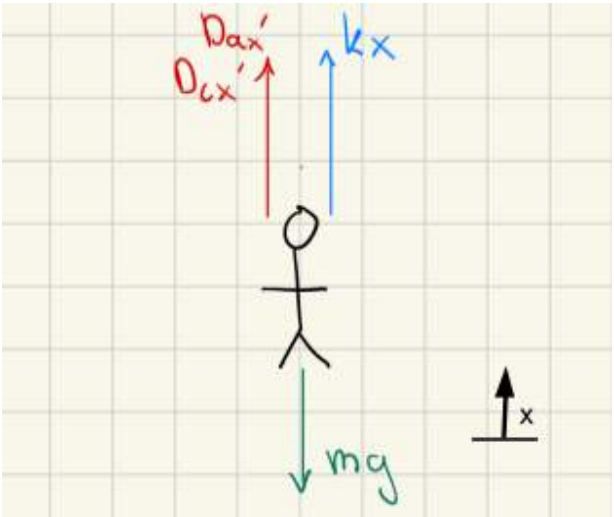

Figure 1: Free Body Diagram of Bungee Jumper

An important factor to consider with this problem is that the damping and spring force caused by the cord are inactive if the jumper is within 18 meters of the platform. 18 meters is the length of the cord so it will only be in tension after that distance. This means in **Equation 2**, D is equal to D_a within 18 meters.

Equations:
Motion Equation:

$$\Sigma F = mx'' = -mg + k(x_0 - l - x) + Dx' \quad \text{Equation 1}$$

- x_0: Initial Position (m)
- x: Position (m)
- x': Velocity (m/s)
- x'': Acceleration (m/s^2)
- l: Length of Bungee Cord
- m: Mass (kg)
- k: Cord Stiffness (N/m)
- D: Total Damping Coefficient (Ns/m)

Total Damping Coefficient:

$$D = D_C + D_a = \frac{k\eta}{\omega_n} + D_a \quad \text{Equation 2}$$

- D_C: Viscous Damping Coefficient (Ns/m)
- D_a: Air Resistance Equivalent Damping (8 Ns/m)

To better understand and analyze the jumper's motion, **Equation 3** showcases the natural frequency in terms of the equivalent cord stiffness and mass in the system. Meanwhile, **Equation 4** describes the cord's spring constant in terms of its material and physical properties.

Natural Frequency:

$$\omega_n = \sqrt{\frac{k}{m}} \quad \text{Equation 3}$$

Cord Stiffness:

$$k = \frac{EA}{l} \quad \text{Equation 4}$$

- E: Elastic Modulus (MPa)
- A: Cross-sectional area of Bungee Cord (m^2)
- l: Length of Bungee Cord (m)

PROCEDURE

A model was constructed to simulate the motion of the bungee jumper using the initial value problem (IVP) solver built into the Python Scipy library. First, a set of constants and initial values were set such that the simulation could use some values as constants and vary others over a provided range and step. Arrays were constructed to contain the values for each combination of the spring constant and loss factor. Each simulation was run and the arrays were propagated using the solution found with the IVP solver. A free fall curve was plotted to show motion without elastic force or damping resistance. A horizontal line representing the point of zero elastic deflection was plotted. The stored values were then printed to the console and stored as a CSV for

processing.

The equilibrium points approach the point of zero elastic deflection (the rope length from the jump height) as the k value of the spring increases. This phenomenon follows the understanding that stiffer springs will deflect less under equal loading conditions.

In the reported times of maximum acceleration, the third reported value aligning with k=40 and η=0.30 shows the maximum acceleration at t=0. This discrepancy can be attributed to the increasing η value which led to the first oscillation having a lower maximum magnitude of acceleration than the free fall region. The reported time value represents the initial acceleration due to gravity, the point of minimum velocity, and before the bungee cord is engaged. This is to be expected because, during the first oscillation, the peak remains below the equilibrium point of the spring. Therefore, the body remains in damped harmonic motion after the initial free fall. As seen in the free fall region of the acceleration chart of **Figure A**, the acceleration begins only due to gravity; however, as the body falls and accelerates, the air resistance increases proportionally to the velocity, leading to an exponential decrease in the magnitude of the acceleration as the downward velocity of the jumper leads to a positive force on the body.

This implies several things: that the acceleration is at a maximum in the free fall region, that once the body enters the damped harmonic motion region it can never re-enter the free fall region, and that within the initial free fall region, the acceleration is at its maximum at the initial state. Therefore, the reported time value for the acceleration must be correct.

For reported values, both parameters were varied simultaneously, but to aid in visualizing trends, each was plotted while the other was fixed, as depicted in **Figures 2 and 3**. The simulations were run for 20 seconds as these would allow for quicker computing times, and the jumper would be considered to be moving slow enough to be recovered safely.

RESULTS and DISCUSSION

With the equations of motion, velocity, and acceleration solved using Python's matplotlib library, **Figures 2 and 3** show the position of the jumper as a function of time with varying K and η values. As per the assumptions, these figures include a "free fall" for the first 18m of descent from an initial position of 100m from the ground (x=0m), as well as a sample "free fall" with no bungee cord for reference. The 18m when the cord begins to act on the jumper are also marked by a dotted line in both graphs.

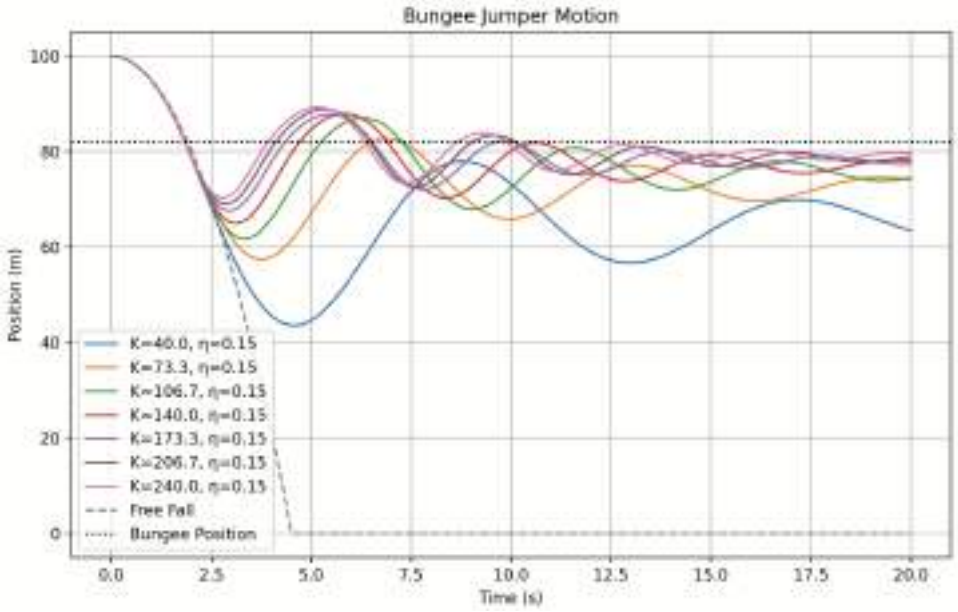

Figure 2: Bungee Jumper position as a function of time with varying K values

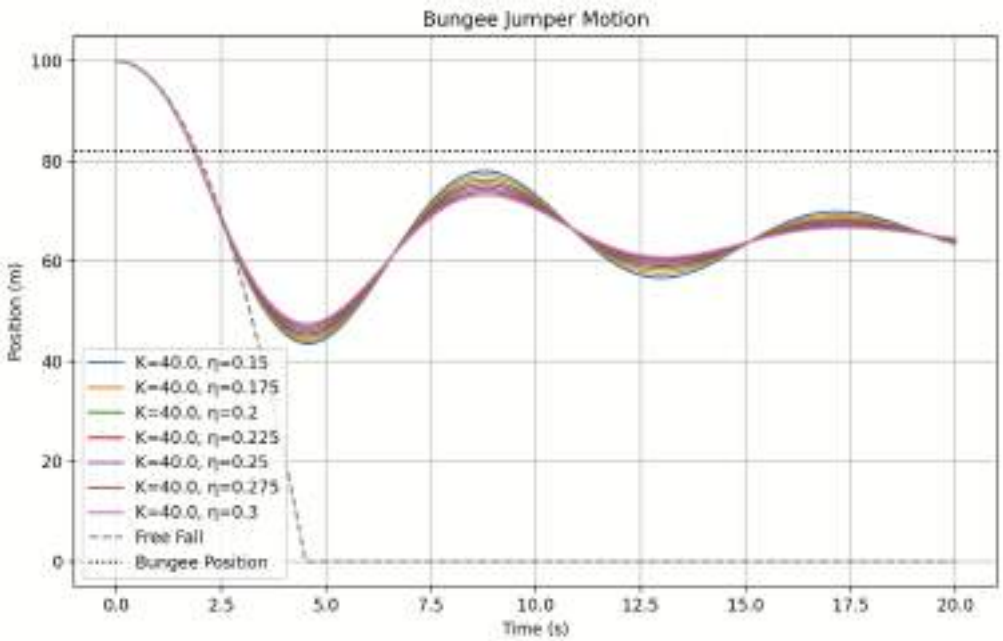

Figure 3: Bungee Jumper position as a function of time with varying η values

From **Figure 2**, it can be seen that there is a lot of variation in both the amplitude and period of the oscillatory motion of the jumper. As these values of k are bounded between 40N/m and 240N/m and η between 0.15 and 0.30, a minimum fall position, maximum velocity, and maximum acceleration can all be identified using **Table A** and interpreting **Figures 2, 3, and A**. At k=40N/m and η = 0.15, the absolute lowest point the jumper reaches is 45.8m from the ground after 4.8s, his maximum acceleration of 11.4m/s^2 is obtained after 4.4s and his maximum absolute velocity is 18.7m/s at 2.5s. In terms of his position, this would mean that maximum acceleration is when he is being pulled up before the first bungee recoil and maximum speed is at the end of the freefall. Furthermore, all of these maxima emerge from the first ½ period of motion, further insinuating the importance of the cord's stretching abilities to dictate the subsequent oscillations. Additionally, from varying k and η coefficients, k was noticed to have a larger impact on the behavior of the jump following a trend of lower maximum acceleration and bigger fall height as k decreased. From **Table A**, this is seen by the k=240N/m value resulting in a maximum acceleration of 27.1m/s^2 and a minimum tower height of 28.2m, which are significantly more dangerous than the previously seen k=40N/m values. Following this line of reasoning, it would be reasonable to assume that is the reason why jumpers can fall without sustaining serious injury from a high tower. The force experienced at any moment in time by the jumper is slowly being "lost" in the cord the more it stretches and results in a less violent jolt when it comes time to reverse the direction of their trajectory. Meanwhile, maximum velocity remained more or less constant throughout all trials (around -18m/s) at the tail end of the freefall.

As such, the simulation showed that an increasing K coefficient would lead to a higher maximum acceleration, making k=40N/m the "safest" option while still allowing for the jumper to experience the longest fall. This is consistent, as k depends on the elastic modulus, cross-sectional area, and the original length of the cable. The original cable length is given as 18m. Natural rubber or other elastomers are typically used for the core of the cable. The cable is typically covered by a woven synthetic material such as nylon to protect the rubber from heat/sunlight. Based on these two considerations, the material selection for the core is narrowed down to natural rubber, which has an elastic modulus in the range of 3.45Mpa to 24.1Mpa [1].

Another important consideration is the possibility of stress relaxation and hysteresis of the bungee cable, which would result in permanent deformation and weakening of the cable and safety concerns. "Hysteretic" would refer to the uneven forces being exerted on the person between falling downward and upward. It also is dependent on the uneven compression and tension rope friction properties (i.e. the rope can compress easier than stretch or vice-versa). Since cord manufacturing affects η and K, the mechanical properties of the rope affect the

studied displacement, velocity, and acceleration. Therefore, the manufacturing process of the rubber should involve vulcanization of the rubber to reduce the possibility of stress relaxation. Vulcanization introduces cross-links between the polymer chains, strengthening the material. Research proves that more crosslinks produced during the vulcanization process result in the material being capable of withstanding more stress without permanent deformation[2]. Vulcanization also leads to higher elasticity (E=1.5Mpa [3]), and consequently, a lower stiffness(k). Furthermore, vulcanization improves the cable's ability to withstand hysteresis, because the cable will also be stronger under compression after vulcanization[2]. In particular, carbon-containing cross-links are proven to increase the lifespan of vulcanizates[2] compared to other materials typically used to vulcanize natural rubber. Assuming the diameter of the cord is around 2.5cm, the resulting stiffness value for a fixed cord length of 18m, using **Equation 4**, is 41 N/m. The k value corresponds to the lowest k value from previous evaluations, indicating that it will meet the vertical distance constraints too. Based on the figures, the k value of 40 N/m results in enjoyable conditions for the jumper, and the jumper will experience minimal amounts of upward acceleration. The maximum acceleration the jumper will reach is just under $15m/s^2$, or less than 1.5g, which is less than a person will experience on a typical roller coaster[4], but still more than they experience on a daily basis. They would also experience only around 3 ups/downs within 20 seconds, the assumed time it takes for their velocity to be low enough to be safely recoverable. Thus, the jumper will have fun without putting their safety at risk.

Finally, ride expectations also affect the model in unaccounted-for ways. They have to do with the behavior of the person dropping. As this is a person, they can flail their arms in/out to decrease/expand their surface area in contact with the air. This could make the assumed constant damping coefficient of the air (Da=8) change at a moment's notice - impacting the simulation by slowing or quickening descent.

CONCLUSIONS

In conclusion, the jumper can complete the jump without sustaining injury by observing the parameters that influence maximum acceleration and velocity. Such parameters include the cord stiffness (k), the cord length, the jumper's vertical starting position, the cord's loss factor, and the manufacturing and mechanical properties of the cord. Ultimately, a lower K value and higher η value would mean that the jumper experiences less maximum acceleration while also coming to the equilibrium position as quickly as possible. This would ensure the jumper has a smoother experience that also comes to an end quicker as opposed to violently being pulled back and suspended in oscillation for longer. Overall, taking into account the safety and enjoyment of the person jumping, it is most ideal to choose a vulcanized natural rubber cord with a stiffness of around 40N/m, and for the jumper to start at an absolute minimum height of 55 meters. Then, the jumper will not be injured due to acceleration or due to hitting the ground.

APPENDIX

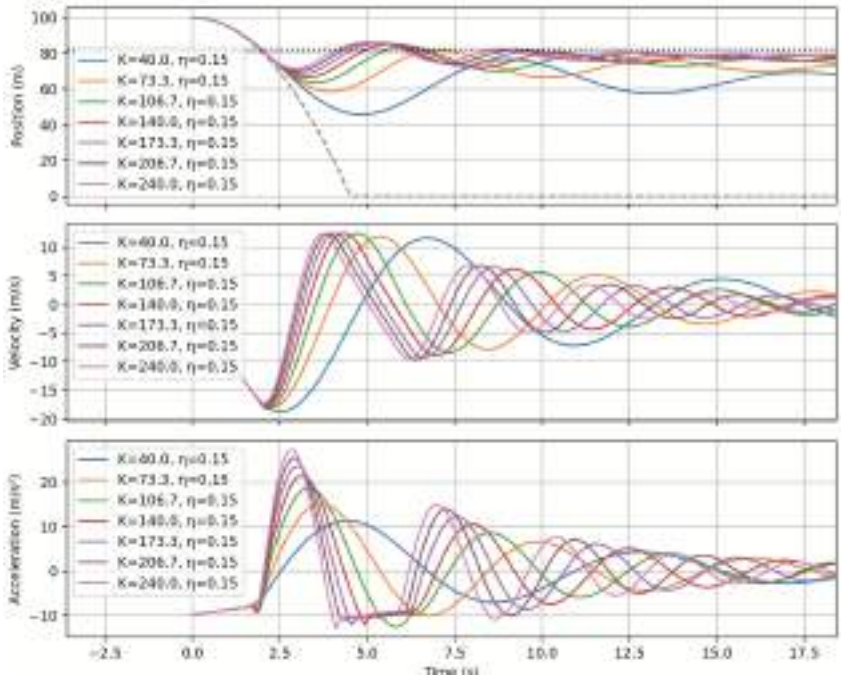

Figure A: Modeled Equations of Motion, Velocity, and Acceleration using varied K and η values.

Table A: Numerical values of select cases in the simulation with accompanying maximum acceleration, velocity, and deflection

Eta	*K (N/m)*	*Max_acc (m/s^2)*	*Max_acc _time (s)*	*Max_vel (m/s)*	*Max_vel_ time (s)*	*Min_pos (m)*	*Min_pos_ time (s)*	Minimum Tower Height req. (m)	Cord Stretched Length (m)
0.150	*40.0*	*11.4*	*4.4*	*18.7*	*2.5*	*45.8*	*4.8*	54.2	36.2
0.225	*40.0*	*10.5*	*4.3*	*18.1*	*2.5*	*47.8*	*4.8*	52.2	34.2
0.300	*40.0*	*9.8*	*0.0*	*17.6*	*2.4*	*49.5*	*4.8*	50.5	32.5
0.150	*68.6*	*14.7*	*3.7*	*18.0*	*2.3*	*57.5*	*4.0*	42.5	24.5
0.300	*68.6*	*12.5*	*3.6*	*16.8*	*2.2*	*60.3*	*4.0*	39.7	21.7
0.150	*97.1*	*18.0*	*3.4*	*18.3*	*2.2*	*62.4*	*3.6*	37.6	19.6
0.300	*97.1*	*15.9*	*3.2*	*17.8*	*2.1*	*64.3*	*3.6*	35.7	17.7
0.150	*240.0*	*27.4*	*2.8*	*17.3*	*2.0*	*71.3*	*2.9*	28.7	10.7
0.300	*240.0*	*27.1*	*2.7*	*18.0*	*2.1*	*71.8*	*2.9*	28.2	10.2

REFERENCES

[1] “NR- Natural Rubber,” Rahco-Rubber, https://rahco-rubber.com/materials/nr-natural-rubber/.
[2]”Natural Rubber, Vulcanized (NR, IR, Polyisoprene),” Matweb, https://www.matweb.com/search/datasheet_print.aspx?matguid=6588439546ac4492965c894ddff3f5da.
[3] S Baxter, M.A.A Wilson, 1963, “Stress relaxation of vulcanized rubbers III — Experimental study, Polymer,” Volume 4, Pages 163-173, ISSN 0032-3861, https://doi.org/10.1016/0032-3861(63)90023-5.
[4] “How a Coaster Moves,” Coaster Force, https://coasterforce.com/physics/.

Computational Assignment 2 - Kinematics of Crankshaft and Rod

TO: Adolfo Delgado
FROM: Group 7 of MEEN 363 - 502 (Tori Abell, Alois Campbell, Jake Smith, Eddy Silva, Ian Wilhite)
Subject: Assignment 2, Crankshaft and Rod
Date: 04/02/2025

EXECUTIVE SUMMARY

The objective is to derive and analyze the displacement, velocity, and acceleration of the slider (point B) and the center of mass of the connecting rod (point G) as functions of the crank angle (θ). Using a constant crank angular velocity of 300 rpm, kinematic equations for point B and point G were derived using the geometric method to describe the motion of the system. The analysis was performed for three different crank-to-rod length ratios: P = 0.1, 0.3, 0.5. Computational simulations generated time-based plots of position, velocity, and acceleration for both point B and point G over two full revolutions of the crank. The results show significant variation in position, velocity, and acceleration of points B and G depending on the value of P. As P increases, the magnitude and variation of the slider's velocity and acceleration increase, reflecting stronger dynamic effects. This analysis confirms the importance of geometric ratios in crank-slider mechanisms and supports using Newton's Second Law to identify force trends acting on the system components.

METHOD

To obtain kinematic equations for point B, a geometric approach was used. It consisted of adding the horizontal lengths of the members and setting that equal to the i vector position of B (x_B) at any given time. The vertical distance with respect to B (y_B) was set to 0 as there is no vertical translation at that point. Nevertheless, a kinematic constraint was determined by setting the bar heights equal to each other. The results are the **Equations (1) and (2)** for position below. Taking the derivative of these equations results in the equations for velocity and acceleration - **Equations 3, 4, 5, and 6**. The position, velocity, and acceleration of point G were then evaluated using vector properties based on the given position of G (center of rod l_2).

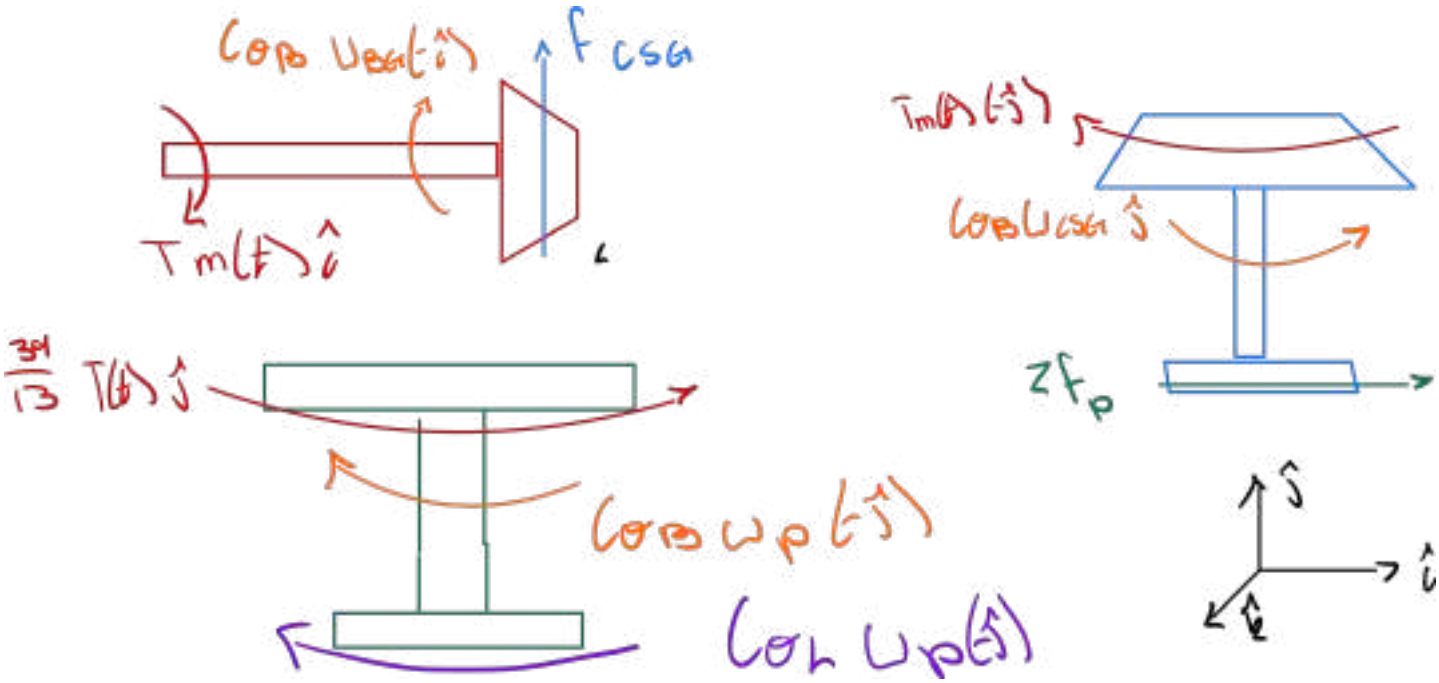

Figure 1: Diagram of Bodies

Geometrical derivation of equations of motion for point B:

Given:

$P = \frac{l_1}{l_2}$, θ'=ω=300 rpm, $l_T = 7ft$, $l_T = l_1 + l_2$

Position (X, Y Components)

$$l_1 cos(\theta) + l_2 cos(\phi) = x_B \quad (1)$$

$$l_1 sin(\theta) = l_2 sin(\phi) \quad (2)$$

Velocity (X, Y Components)

$$-l_1 sin(\theta) * \theta' = l_2 sin(\phi) * \phi' + \dot{x}_B \quad (3)$$

$$l_1 cos(\theta) * \theta' = l_2 cos(\phi) * \phi' \quad (4)$$

Acceleration (X, Y Components)

$$-l_1 sin(\theta) * \theta'' - l_1 cos(\theta) * \theta'^2 - l_2 cos(\phi) * \phi'^2 = l_2 sin(\phi) * \phi'' + \ddot{x}_B \quad (5)$$

$$l_2 cos(\phi) * \phi'' = l_2 sin(\phi) * \phi'^2 + l_1 cos(\theta) * \theta'' - l_1 sin(\theta) * \theta'^2 \quad (6)$$

θ'' term goes to 0 due to constant velocity, zero acceleration condition given

The vector equation properties to find the position, velocity, and acceleration of point G from the EOM derived for point B:

$$r_{OG} = r_{OB} + r_{BG} = x_B(i) + \frac{l_2}{2} * (cos(\phi)(-i) + sin(\phi)j) \quad (7)$$

$$v_G = v_B + \omega_{BG} \times r_{BG} = \dot{x}_B(-i) + \phi'(-k) \times \frac{l_2}{2} * (cos(\phi)(-i) + sin(\phi)j) \quad (8)$$

$$a_G = a_B + \omega_{BG}' \times r_{BG} + \omega_{BG} \times \omega_{BG} \times r_{BG}$$

$$a_G = \ddot{x}_B(-i) + \phi''(-k) \times (\frac{l_2}{2} * (cos(\phi)(-i) + sin(\phi)j)) + \phi'^2(\frac{l_2}{2})(cos(\phi)(i) - sin(\phi)j) \quad (9)$$

Cramer's Rule

To analytically solve for the variables in the equations above, Cramer's Rule was used. Below is an example using the angular velocities.

$$\begin{bmatrix} -l_1 sin(\theta) & -l_2 sin(\phi) \\ l_1 cos(\theta) & l_2 cos(\phi) \end{bmatrix} \begin{bmatrix} \theta' \\ \phi' \end{bmatrix} = \begin{bmatrix} \dot{x}_B \\ 0 \end{bmatrix}$$

$$\theta' = \begin{vmatrix} \dot{x}_B & -l_2 sin\phi \\ 0 & l_2 cos\phi \end{vmatrix} \div \begin{vmatrix} -l_1 sin(\theta) & -l_2 sin(\phi) \\ l_1 cos(\theta) & l_2 cos(\phi) \end{vmatrix}$$

$$\phi' = \begin{vmatrix} -l_1 sin(\theta) & \dot{x}_B \\ l_1 cos(\theta) & 0 \end{vmatrix} \div \begin{vmatrix} -l_1 sin(\theta) & -l_2 sin(\phi) \\ l_1 cos(\theta) & l_2 cos(\phi) \end{vmatrix}$$

After finding a general solution for position, velocity, and acceleration about points B and G, Python was used to create a data set spanning 2 periods using time as the x-axis and the solved terms in the y (seen in the figures below).

PROCEDURE

Using the derived kinematic equations (**Equations 1-6**) for point B, the numpy library in Python was used to construct the model and plot the results. The plots were constructed in terms of P, which is the ratio between l_1 and l_2, to observe the effect of varying the ratio between l_1 and l_2. These figures were compiled to create three subplots in **Figure 2**.

A similar approach was taken for the kinematic equations of point G (**Equations 7-9**) in **Figures 3, 4, 5, 6, and 7**. To ensure no mistakes were made, the kinematic equations of point A were derived geometrically and averaged with B to determine an alternate expression of G (**Appendix Equations**). Since the AB bar is symmetric, the center of mass must be equally positioned between points A and B, rendering this alternate version acceptable for the simulation. In other words, the X position of G is the average of A and B, and the Y position of point G is found by dividing the Y position of A by two. Since this latter approach was significantly easier to code, it was the approach used in the final simulation.

Once these equations and parameters were set, the given constant velocity of θ' (=300 rpm) and θ'' (=0) were used to solve for the rest of the unknowns using the built-in numpy solver, ultimately rendering all the tables and figures discussed.

RESULTS and DISCUSSION

Figure 2 shows the horizontal position, velocity, and acceleration of point B with varying ratios between l_1 and l_2 (P). When P equals 0.1, for example, l_1 is 10% of l_2. The length of l_1 plus l_2 is given as 7ft, therefore when P=0.1, l_1=0.7ft and l_2 =6.3ft. When point A moves below y=0 in the positive x-axis, point A and point B begin moving in the -x direction, until link OA and link AB are both horizontal and lying along the x-axis at y=0. At this position, the horizontal location of points B and A will be at their minimum. Point A will be at x = -0.7ft and point B will be at x = 6.3 ft. **Figure 2** displays this expected result when the position of B is at its minimum, at 6.3ft. The same logic applies to all values of P. Furthermore, the graph displays three points at which the horizontal location of B is 7ft. At these points, links OA and AB are both horizontal along the x-axis, and the horizontal location of A is positive. The first time this occurs is when θ and ϕ are zero. Later occurrences occur at the end of each rotation until reaching the max angle simulated (2π radians).

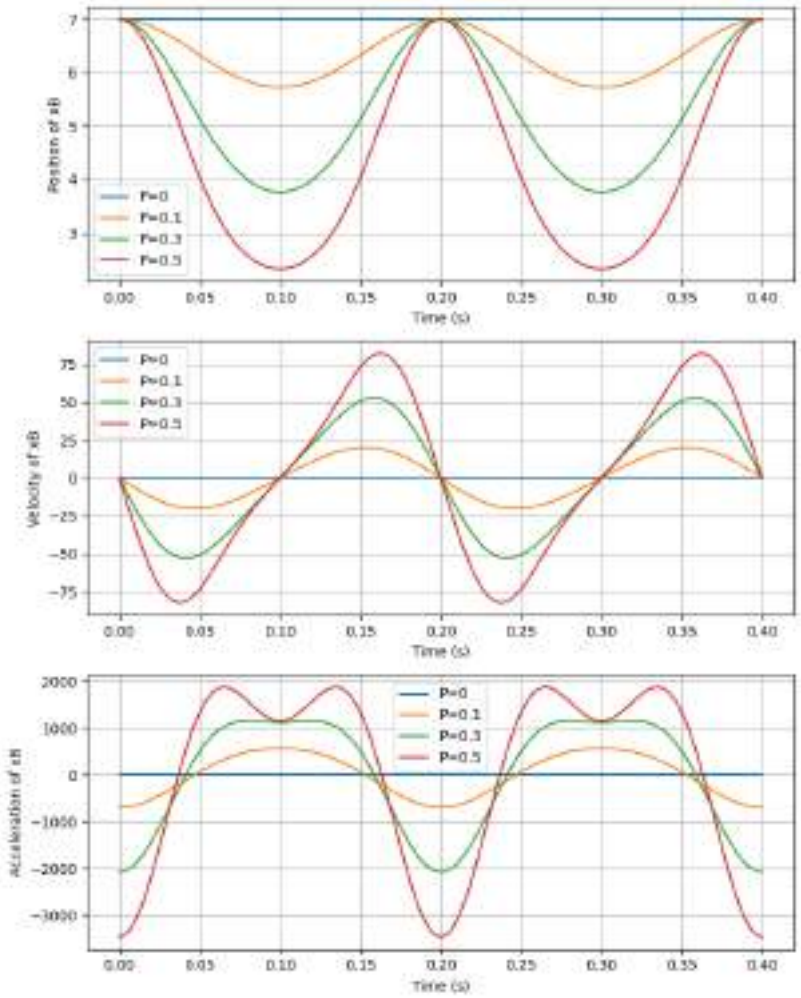

Figure 2: Plot of point B horizontal position, velocity, and acceleration as a function of time with varying P values.

Additionally, the maximum and minimum velocities of point B and the time they occur are displayed in **Figure 2** and recorded in **Table 1** in the appendix. The maximum and minimum acceleration for point B and the time they occur are recorded in **Table 2** in the appendix. The maximum/minimum velocity magnitude is approximately 82.3 ft/s. The magnitude of the minimum acceleration is 3454 ft/s^2, and the magnitude of the maximum acceleration is approximately 1150 ft/s^2. Both the maximum and minimum velocities and acceleration occur when P =0.5, right before and after point A is on the y-axis. The positive maximum acceleration (expanding crankshaft) and by extension the maximum force takes place right before and after the two bars are horizontal to each other, with point A being in the negative x direction. These accelerations also result in accompanying maximum magnitudes of velocity, which come about from these abrupt acceleration local maxima. In the inverse case, where point A is located in the positive x-axis at y=0, the acceleration is at its absolute maximum with the rod fully extended and preparing to contract/expand fully, depending on the cycle direction.

Figure 3 displays the varying vertical position of point G and the corresponding horizontal position. Point G's motion is a combination of a circular motion from the crank rotation, θ, and the back and forth translations of point B. Due to the combined effects, point G's motion is oblong/"egg-shaped", becoming thicker at the bottom of the stroke than the top. This asymmetrical motion begins to appear differently as L_1/L_2 decreases, looking more like a symmetrical oval. This is because when L_1 is small compared to L_2, the motion of L_2 acts more like a linear

translation, as the circular motion is less prevalent. This leads to the motion of G being thinner and more symmetrical.

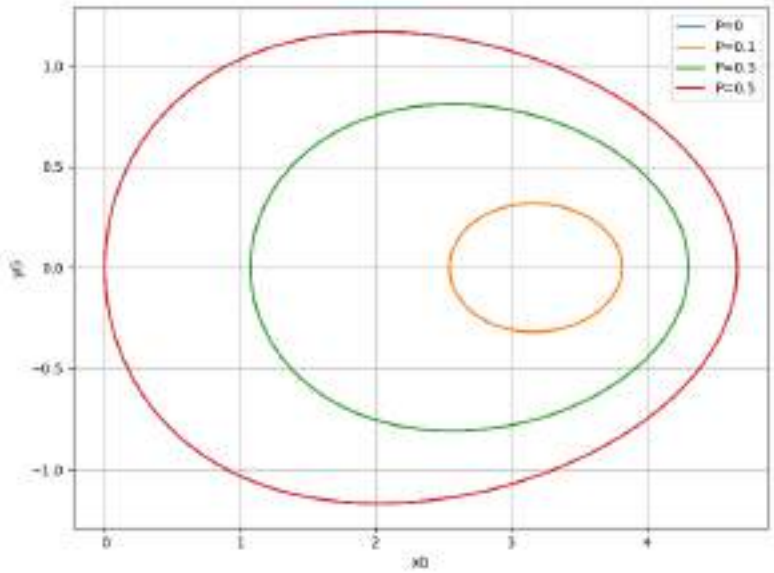

Figure 3: Plot of the motion of point G vertical position vs horizontal position ($Y_G$vs X_G).

For the P=0 case, there is only one fixed geometry solution available. Therefore, it does not show on the graph as there is no variation in position observable. This same logic applies to all other figures for the position, the velocity, and acceleration of points B and G. Since there is no change in geometry due to the constraints, there is no motion and no observable changes, creating a flat slope at 0.

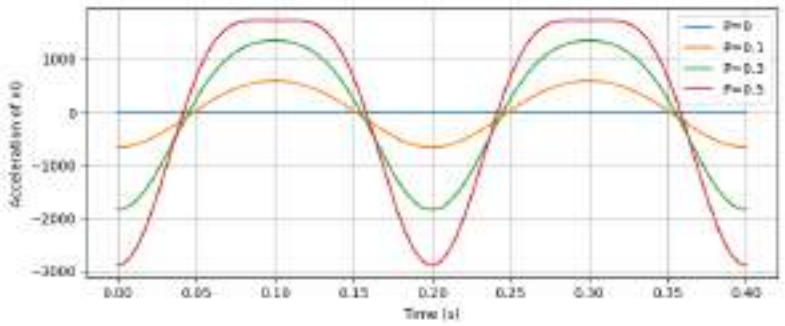

Figure 4: Plot of point G horizontal acceleration as a function of time with varying P values.

Newton's second law can be applied to the problem based on the acceleration. Since force is mass times acceleration, point G and point B experience the greatest force in the x direction, where the magnitude of the acceleration is the greatest, at times indicated by the solution. **Figures 4 and 5** indicate that the acceleration of point G in the horizontal direction has the greatest magnitude where the links reach their maximum or minimum x position (see **Figure 6** in the appendix for the plot of the position and velocity of point G). Therefore, link AB experiences the greatest force at its center of gravity when it changes directions along the x-axis.

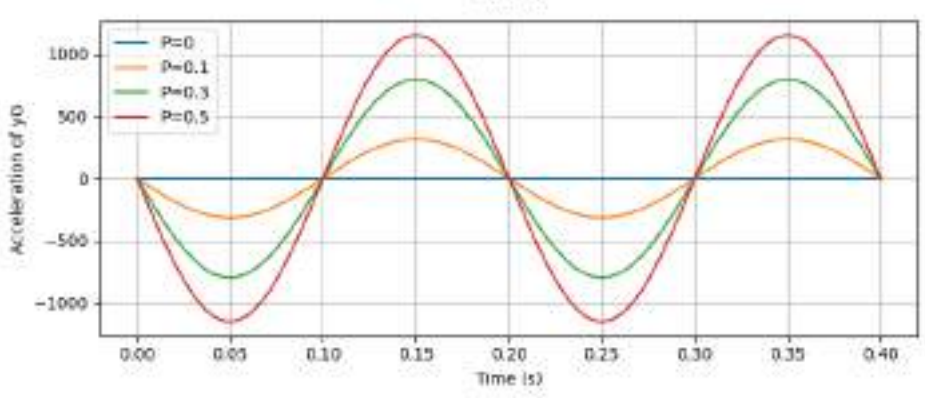

Figure 5: Plot of point G vertical acceleration as a function of time with varying P values.

Figure 5 illustrates the vertical acceleration of point G over time for varying P values. The vertical position in **Figure 7** in the appendix exhibits a sinusoidal pattern that reflects the crank's rotational motion, while the velocity and acceleration curves show how rapidly this vertical motion changes throughout the stroke. As P increases, the vertical velocity and acceleration both grow in magnitude, indicating a stronger vertical influence from the crank's rotation. The peaks in acceleration occur near the midpoints of each stroke, where the vertical direction reverses and inertial forces peak. This vertical dynamic is particularly important in applications like internal combustion engines, where vertical forces translate into vibrations and stresses that impact structural design and operational smoothness.

CONCLUSIONS

In conclusion, the kinematic analysis of the crank-slider mechanism reveals significant dependence on the crank-to-rod length ratio (P). As P increases, the dynamic effects on both point B and point G become more pronounced, with greater velocity and acceleration magnitudes. These findings have direct implications for the design and performance of reciprocating systems, where balancing force transmission and inertial effects is crucial. Newton's Second Law reinforces that maximum force corresponds to maximum acceleration, which occurs at predictable angular positions (fully expanded or contracted). This analysis provides valuable insight into optimizing component dimensions to reduce wear, minimize vibrations, and ensure efficient mechanical performance. Ultimately, this makes the mechanism ideal for the use case given of the crankshaft two-stroke engine.

APPENDIX

Point B Maximum and Minimum Velocities	
Time (s)	**Velocity (ft/s)**
0.0376	-82.3
0.163	82.3
0.237	-82.3
0.362	82.3

Table 1: Maximum and minimum velocity of point B and the time it occurs.

Point B Maximum and Minimum Acceleration	
Time (s)	**Acceleration (ft/s^2)**
0	-3454
0.119	1150
0.080	1150
0.200	-3454
.280	1150
0.319	1150
0.400	-3454

Table 2: Maximum and minimum acceleration of point B and the time they occur.

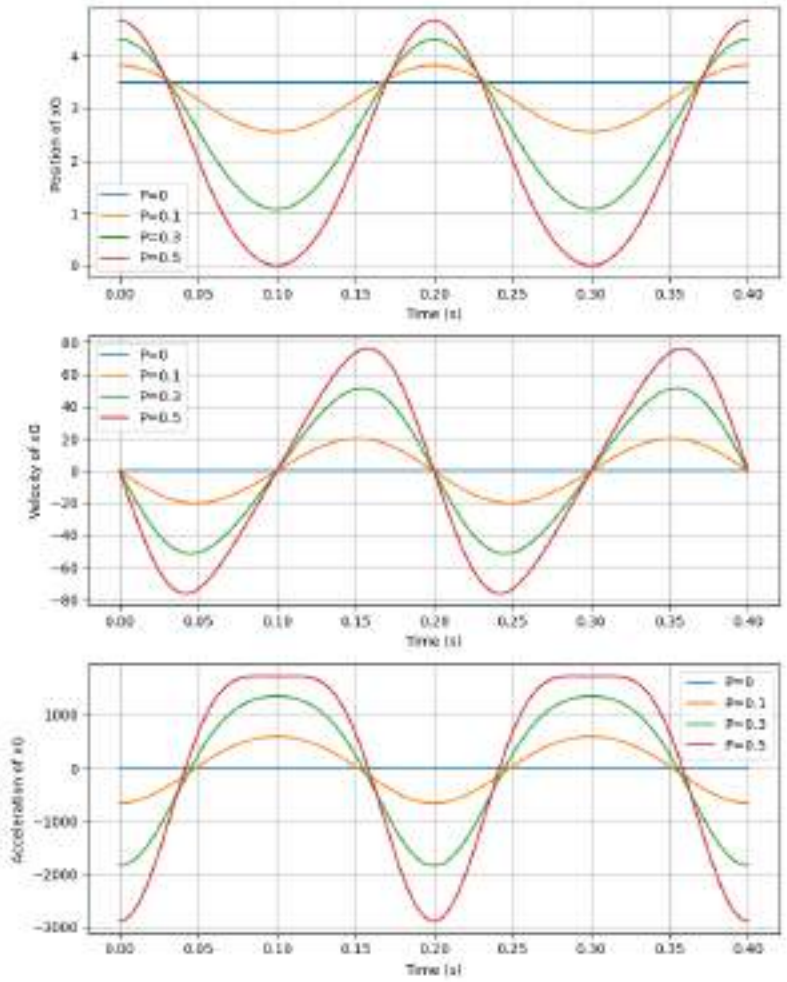

Figure 6: Plot of point G horizontal acceleration as a function of time with varying P values.

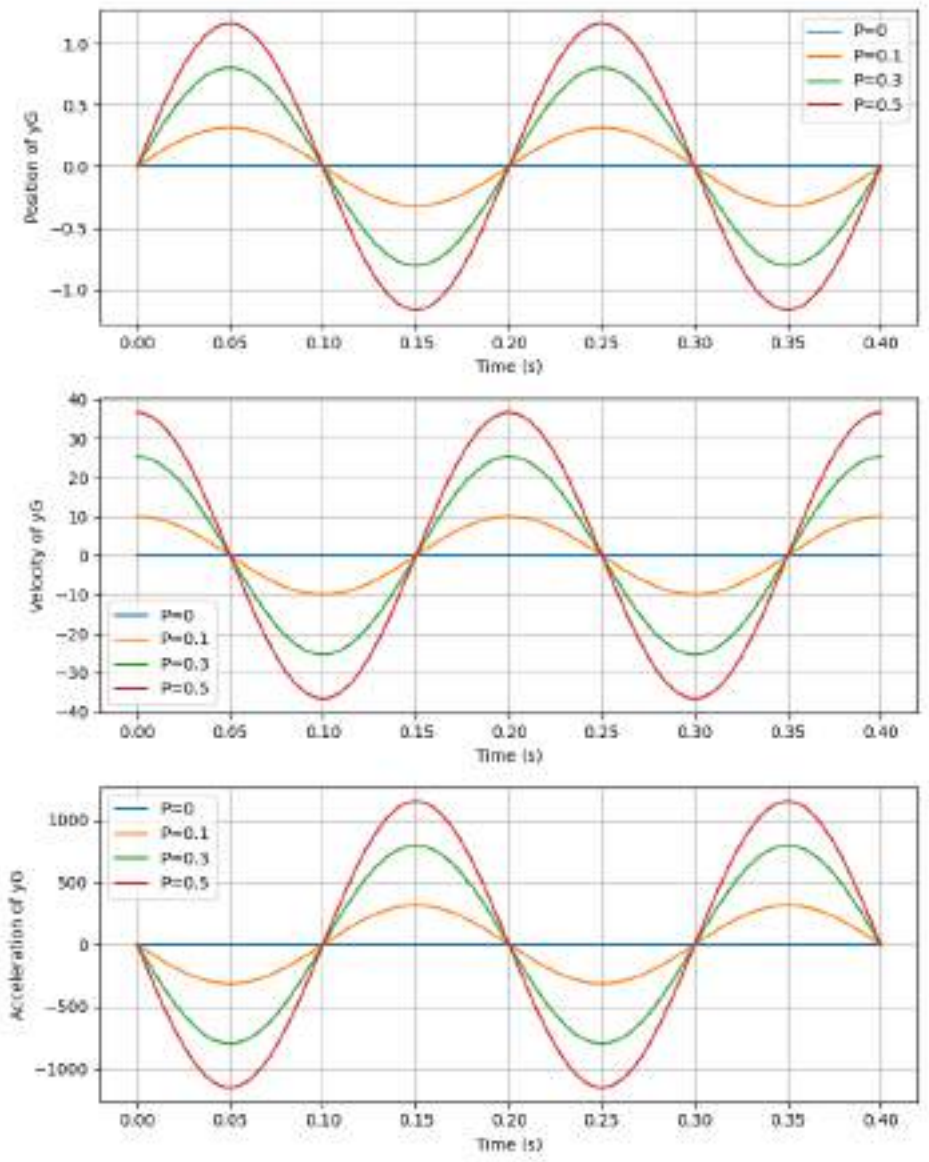

Figure 7: Plot of point G vertical position, velocity, and acceleration as a function of time with varying P values.

Alternative proof for point G, used to verify equations, and the simulation used:
For point G, an average between points A and B was taken:

Point A:
Position (X, Y Components)

$$l_1 cos(\theta) = x_A \quad \text{(A.1)}$$

$$l_1 sin(\theta) = y_A \quad \text{(A.2)}$$

Velocity (X, Y Components)

$$-l_1 sin(\theta) * \theta' = \dot{x}_A \quad \text{(A.3)}$$

$$l_1 cos(\theta) * \theta' = \dot{y}_A \quad \text{(A.4)}$$

Acceleration (X, Y Components)

$$-l_1 sin(\theta) * \theta'' - l_1 cos(\theta) * \theta'^2 = \ddot{x}_A \quad \text{(A.5)}$$

$$l_1 cos(\theta) * \theta'' - l_1 sin(\theta) * \theta'^2 = \ddot{y}_A \quad \text{(A.5)}$$

Average of points A and B, for point G:

Position

$$\frac{x_A + x_B}{2} = x_G = (l_1 cos(\theta) + \frac{1}{2} l_2 cos(\phi)) \quad \text{(A.6)}$$

$$\frac{y_A}{2} = y_G = \frac{1}{2} * l_1 sin(\theta) \quad \text{(A.7)}$$

Velocity

$$\frac{\dot{x}_A + \dot{x}_B}{2} = \dot{x}_G \quad \text{(A.8)}$$

$$\frac{\dot{y}_A}{2} = \dot{y}_G = \frac{1}{2} * l_1 cos(\theta) * \omega \quad \text{(A.9)}$$

Acceleration

$$\frac{\ddot{x}_A + \ddot{x}_B}{2} = \ddot{x}_G \quad \text{(A.10)}$$

$$\frac{\ddot{y}_A}{2} = \ddot{y}_G = \frac{1}{2} (l_1 cos(\theta) * \theta'' - l_1 sin(\theta) * \omega^2) \quad \text{(A.11)}$$

θ'' term goes to 0 due to constant velocity, zero acceleration condition given

REFERENCES

[1] Dynamics in Engineering Practice, 11th Ed (only), D.W. Childs & Ap. Conkey, CRC Pubs https://www.crcpress.com/Dynamics-in-Engineering-Practice-Eleventh-Edition/Childs-Conkey/9781482250251

Computational Assignment 3 - Modeling a Mechanical System

TO: Adolfo Delgado
FROM: Group 7 of MEEN 363 - 502 (Tori Abell, Alois Campbell, Jake Smith, Eddy Silva, Ian Wilhite)
Subject: Assignment 3, Modeling a Mechanical System
Date: 04/28/2025

EXECUTIVE SUMMARY

The objective is to derive equations of motion and find the total energy and dissipative power of the system. The equation of motion can be found through two methods. First, an equation of motion for the system is established by summing forces and moments for the five components and implementing the kinematic constraints of the system. The second method for finding the equation of motion is by analyzing the potential, kinetic, and dissipated energy of the system and using the concept of conservation of mechanical energy. Additionally, given specific damping coefficients and the motor speed, the motor torque and paddle speed are calculated. They will require a minimum of 323 newton meters of torque to drive the system, and will take 3.27 seconds from beginning at rest to reach 99% of operating speed. Due to power losses in the system, such as in the bearings, the efficiency of the system is 84%, and it costs $438 per day, $75 of which was lost due to friction.

METHOD

The mixer system presented had many moving parts. Under further inspection, they can be broken up into five distinct free bodies:

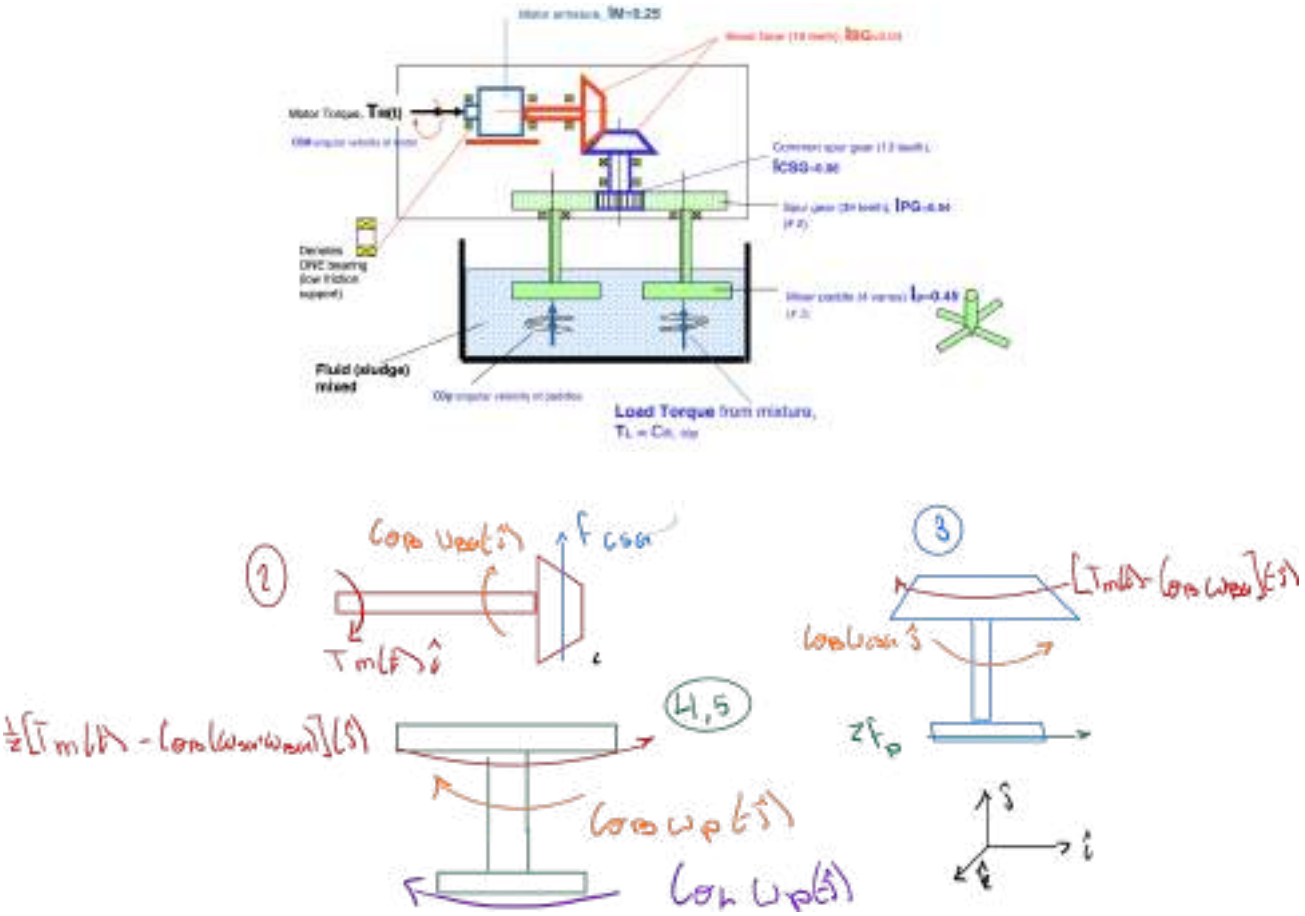

Figure 1: Free Body Diagrams for Components

Using this approach, the system can be described using 5 equations - one for each of the bodies:

$$I_M\theta_1'' = T_M - T_{12} - \theta_1' C_{\theta B} \quad (1)$$

$$I_{BG}\theta_2'' = T_{12} - T_{23} - 2\theta_2' C_{\theta B} \quad (2)$$

$$I_{BG}\theta_3'' = T_{23} - T_{34} - 2\theta_3' C_{\theta B} \quad (3)$$

$$I_{PG}\theta_4'' = T_{34} - T_{45} \quad (4)$$

$$I_P\theta_5'' = T_{45} - T_L = T_{45} - C_{\theta L}\omega_P - \theta_5' C_{\theta B} \quad (5)$$

Furthermore, some kinematic constraints are used to simplify these equations. The defined gear ratios and relationships between the bodies were used to explain how the motor's input torque is converted into output torque at the paddles.

$$\theta_1 = \theta_2 = \theta_3 = \theta_M \quad (6)$$

$$\theta_4 = \theta_5 = \theta_P \quad (7)$$

$$3\theta_M = \theta_P,\ 3\theta_M' = \theta_P',\ 3\theta_M'' = \theta_P'' \quad (8)$$

The five motion equations can be simplified to two, where θ_M is the angle of the motor, θ_P is the angle of the paddle, T_{CSG} is the torque of the center spur gear, T_{SG} is the torque of the additional spur gears, and the relationship of the torques are applied:

$$\theta_M''[I_M + 2I_{BG} + I_{CSG}] = T_M - 5\theta_M' C_{\theta B} - T_{CSG} \quad (9)$$

$$T_{CSG} = \frac{13}{39} T_{SG} \quad (10)$$

$$\theta_P''[2(I_{PG} + I_P)] = T_{SG} - 2C_{\theta B}\theta_P' - 2C_{\theta L}\omega_P \quad (11)$$

After this step, the equations are simplified even further, into a single equation.

$$\Rightarrow 9\theta_P''[I_M + 2I_{BG} + I_{CSG}] + \theta_P''[2(I_{PG} + I_P)] = 3T_M - 15\theta_P' C_{\theta B} - 2C_{\theta B}\theta_P' - 2C_{\theta L}\omega_P$$

$$\Rightarrow [9(I_M + 2I_{BG} + I_{CSG}) + 2(I_{PG} + I_P)]\theta_P'' = 3T_M + [-47C_{\theta B} - 2C_{\theta L}]\theta_P'$$

$$\Rightarrow 3T_M = \theta_P''[9(I_M + 2I_{BG} + I_{CSG}) + 2(I_{PG} + I_P)] + [47C_{\theta B} + 2C_{\theta L}]\theta_P' \quad (12)$$

Therefore,

$$I_{eq} = 9(I_M + 2I_{BG} + I_{CSG}) + 2(I_{PG} + I_P) \quad (13)$$

$$C_{eq} = 47C_{\theta B} + 2C_{\theta L} \quad (14)$$

Using the conservation of mechanical energy equation, P_{diss} (dissipative power) and P_{drive} (external drive power) can be used to describe the non-conservative forces in the system (from the damping and driving torque):

$\frac{d}{dt}(E_k + E_p) + P_{diss} = P_{drive}$, where E_k is the kinetic energy and E_p is the potential energy. (15)

$$\frac{d}{dt}E_k = [9(I_M + 2I_{BG} + I_{CSG}) + 2(I_P + I_{PG})]\theta_P'' * \theta_P' \quad (16)$$

$$P_{diss} = C_{\theta B}(\frac{d}{dt}\theta_1)^2 + 2C_{\theta B}(\frac{d}{dt}\theta_2)^2 + 2C_{\theta B}(\frac{d}{dt}\theta_3)^2 + 2C_{\theta B}(\frac{d}{dt}\theta_5)^2 + 2C_{\theta L}(\frac{d}{dt}\theta_5)^2 \quad (17)$$

$$P_{diss} = [47C_{\theta B} + 2C_{\theta L}](\frac{d}{dt}\theta_P)^2 = [47C_{\theta B} + 2C_{\theta L}](\theta_P') * (\theta_P') \quad (18)$$

$$P_{drive} = (T_M) * 3\theta_P' \quad (19)$$

The simplified energy equation is as follows, using (16), (18), and (19):

$$[9(I_M + 2I_{BG} + I_{CSG}) + 2(I_P + I_{PG})]\theta_P'' + [47C_{\theta B} + 2C_{\theta L}](\theta_P') = 3(T_M) \quad (20)$$

Therefore, the same I_{eq} and C_{eq} were determined as in the Newtonian approach:

$$I_{eq} = 9(I_M + 2I_{BG} + I_{CSG}) + 2(I_{PG} + I_P) \quad (13)$$

$$C_{eq} = 47C_{\theta B} + 2C_{\theta L} \quad (14)$$

PROCEDURE

Using the results obtained from the kinematic constraints, free body diagrams, and equations of motion, the mixer can be analyzed under steady state and transient conditions. Using the values that were provided, this is the current state of the system:

- Motor torque T_M for a <u>constant</u> motor speed of 60 Hz (377 rad/s):
  - $T_M * 3 = \theta_P''[9(I_M + 2I_{BG} + I_{CSG}) + 2(I_{PG} + I_P)] + [47C_{\theta B} + 2C_{\theta L}]\theta_P'$
  - $= 0 + [47(0.028) + 2(3.2)](125.66)$
  - $T_M = 323.2$ Nm

- Power from the motor:
  - $P = T * \omega$
  - $P = 323.2 * 377$
  - $P = 121.8\,\text{kW}$
- Power lost from bearings:
  - $\omega_{CSG} = \omega_M = 377\,rad/s$
  - $\omega_P = \omega_M * \frac{N_{CSG}}{N_{PG}} = 377 * \frac{1}{3} = 126\,rad/s$
  - $P_{diss} = [47C_{\theta B}](\theta_P')^2 = [47(0.028)](126)^2$
  - Total Power Lost, $P = 20.8kW$
- Power from the load:
  - $P_L = T_L * \omega = C_{\theta L} * \omega^2$
  - $P_L = 2 * 3.2 * 126^2$
  - $P_L = 101.1kW$
- Mechanical efficiency:
  - $\eta = \frac{P_L}{P_M} * 100 = \frac{102}{122} * 100$
  - $\eta = 84\%$
- Cost to operate:
  - $C = 0.15\frac{\$}{kW*h}$
  - $Energy = Power * t = 121.8 * 24 = 2923\,kW * h$
  - $Cost\ Per\ Day = E * C$
  - $Cost\ Per\ Day = \$438$
- Money lost:
  - $Energy\ Lost = Bearing\ Power * t = 20.8 * 24 = 499\,kW * h$
  - $Cost\ Per\ Day = Energy\ Lost * C$
  - $Money\ Lost = \$75$
- System time constant:
  - $I_{eq} = 9(I_M + 2I_{BG} + I_{CSG}) + 2(I_{PG} + I_P)$
  - $= 9(0.25 + 2(0.04) + 0.06) + 2(0.54 + 0.45)$
  - $= 5.49\,kg * m^2$
  - $C_{eq} = 17C_{\theta B} + 2C_{\theta L} = 47(0.028) + 2(3.2) = 7.72\frac{Nm}{rad/s}$
  - $\tau = \frac{I_{eq}}{C_{eq}} = \frac{5.49}{7.72}$
  - $\tau = 0.711\,s$
- Time Response:
  - $\omega_p = \omega_{steady}(1 - e^{-t/\tau})$
  - $\omega_p = 126(1 - e^{-t/0.711})$
- Time to reach operating speed:
  - $124.74 = 126(1 - e^{-t/0.711})$
    - 124.74 is 99% of the operating speed. This value is used because ln(0) does not exist.

- $0.99 = 1 - e^{-t/0.711}$
- $ln(0.01) = -t/0.711$
- $t = 3.27s$

RESULTS and DISCUSSION

The gear ratios are a significant part of the system and are used to simplify the equations. By applying the gear ratio kinematic constraints and using the Newtonian method, the system is modeled in **Equation 12**. The equations of motion are found by summing forces and torques between the gears, as indicated by the free-body diagrams in **Figure 1**. The system's equivalent inertia and viscous damping coefficient are noted in **Equations 13** and **14**.

Additionally, the energy method is applied to the system to verify the first approach. The two main components in the energy equations are the power lost from the bearings and load, the torque from the motor, and the power due to kinetic energy. The energy method also uses the gear ratio kinematic constraints to simplify the result, and the final equation (**Equation 20**) results in the same equation of motion as the Newtonian method, as expected. The system's equivalent inertia and viscous damping coefficients are equivalent to those calculated using the Newtonian method, which verifies the results of both methods.

Considering the given values, several key quantities from the system are calculated in the procedure, and recorded in **Table 1**. It is important to note that the power in the motor can be calculated from the torque of the system and verified by summing both the dissipated power and the power of the load.

Table 1: Key values from the system.

T_{Motor}	323Nm
P_{Motor}	121.8kW
P_{diss}	20.8kW
P_{Load}	101.1kW
η	84%
$Cost\ Per\ Day$	$438
$Money\ Lost$	$75
τ	0.711s
$Time\ to\ reach\ \ operating\ speed$	3.27s

The money lost is due to the power losses in the system. To reduce the money lost each day, the frictional losses in the bearings should be reduced by implementing a maintenance routine on the system and applying lubricant to ensure smoother bearings. Furthermore, the paddles could be designed to be more efficient. If the losses are reduced, the efficiency of the system would be improved.

$$126(1 - e^{-t/0.724}) \quad (21)$$

Equation 21 is the equation for the mixer speed as a function of time. **Figure 2** displays a graphical representation of the speed. The time constant, τ, is the value at which the system reaches 63% of its operational speed. **Figure 2** visually confirms the time constant of 0.724 seconds, showing that the speed reaches approximately 63% of its steady-state value. By observation of **Figure 2**, the time at which the system reaches its operating speed is around 3 seconds, validating prior calculations recorded in **Table 1**.

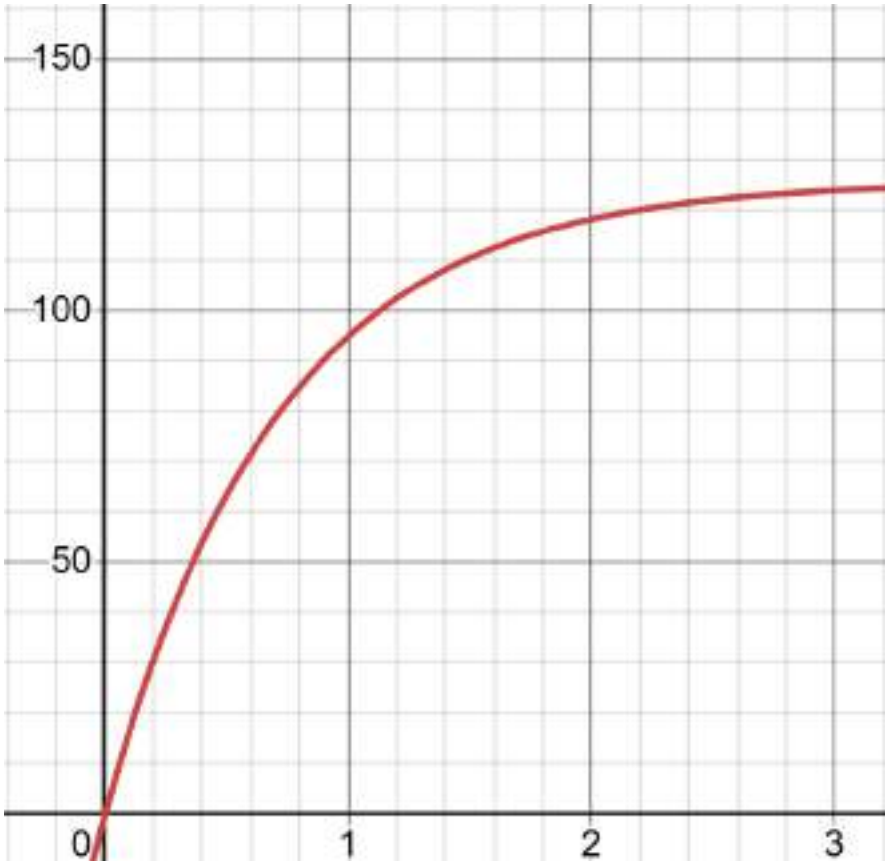

Figure 2. Mixer Speed (rad/s) as a Function of Time (s)

CONCLUSIONS

The mechanical system for the mixer was modeled successfully by applying principles of dynamics and energy conservation. The equivalent inertia and viscous damping parameters were determined consistently through independent approaches. Steady-state performance calculations established the required motor torque, operating speeds, and mechanical power losses within the system. The startup response analysis determined the system time constant and characterized the transient behavior of the paddles. As such, due to its mode of operation, this mixer can probably be classified as a “Paddle industrial mixer” [2]. To further improve its performance, an optimal angle can be set for the viscous fluid being mixed. From certain sources, it can be determined that a 45-degree angle [3] would provide the least amount of resistive torque from the fluid. The modeling effort clearly demonstrates the importance of accounting for mechanical inefficiencies, especially bearing and load damping, to accurately predict system performance. Overall, the work validates the modeling approach and highlights the need for precise dynamic characterization in the design and operation of mechanical systems.

APPENDIX

Detailed steps regarding the derivation of the EOM of the system using the power equation:

From (15) to (16), using the kinematic constraints to simplify:

$$\frac{d}{dt}E_k + 0 = (9I_M\theta_M'' + 2 * 9I_{BG}\theta_M'' + 9I_{CSG}\theta_M'' + 2I_{PG}\theta_P'' + 2I_P\theta_P'') * \theta_P'$$

To determine the left side of (15) in (16):

$$E_k = \frac{1}{2}I_M\theta_1'^2 + \frac{1}{2}I_{BG}\theta_2'^2 + \frac{1}{2}(I_{BG} + I_{CSG})\theta_3'^2 + 2\frac{1}{2}I_{PG}\theta_4'^2 + 2\frac{1}{2}I_P\theta_5'^2$$

$$E_p = 0$$

Using the kinematic constraints to simplify (17) to (18):

$$P_{diss} = C_{\theta B}(\frac{d}{dt}\theta_M)^2 + 2C_{\theta B}(\frac{d}{dt}\theta_M)^2 + 2C_{\theta B}(\frac{d}{dt}\theta_M)^2 + 2C_{\theta B}(\frac{d}{dt}\theta_P)^2 + 2C_{\theta L}(\frac{d}{dt}\theta_P)^2$$

$$P_{diss} = C_{\theta B}9(\frac{d}{dt}\theta_P)^2 + 2C_{\theta B}9(\frac{d}{dt}\theta_P)^2 + 2C_{\theta B}9(\frac{d}{dt}\theta_P)^2 + 2C_{\theta B}(\frac{d}{dt}\theta_P)^2 + 2C_{\theta L}(\frac{d}{dt}\theta_P)^2$$

To find the final EOM using energy in (20) from the previous equations:

$$\frac{d}{dt}(E_k + E_p) + P_{diss} = P_{drive}$$

$$[9(I_M + 2I_{BG} + I_{CSG}) + 2(I_P + I_{PG})]\theta_P'' * (\theta_P') + [47C_{\theta B} + 2C_{\theta L}](\theta_P') * (\theta_P') = (T_M) * \theta_M'$$

$$[9(I_M + 2I_{BG} + I_{CSG}) + 2(I_P + I_{PG})]\theta_P'' * (\theta_P') + [47C_{\theta B} + 2C_{\theta L}](\theta_P') * (\theta_P') = \frac{1}{3}(T_M) * \theta_p'$$

(Notice how the θ_P'/ω values cancel out to get a familiar equation of motion.)

REFERENCES

[1] Dynamics in Engineering Practice, 11th Ed (only), D.W. Childs & Ap. Conkey, CRC Pubs https://www.crcpress.com/Dynamics-in-Engineering-Practice-Eleventh-Edition/Childs-Conkey/9781482250251

[2] Anderson Process. 2022. "It's in the Mix: Industrial Mixers Defined, Types and Applications." Anderson Process. December 15. https://www.andersonprocess.com/its-in-the-mix-industrial-mixers-defined-types-and-applications/.

[3] Liu, Y., and Zhang, X. 2024. "Design and Analysis of a Novel Hybrid Energy Harvester for Smart Wearable Devices." Advances in Mechanical Engineering. https://doi.org/10.1177/16878132241269238.

Back to Contents

3. Numerical Methods (4th Place in Final Competition)

Summary

This section includes four project phases from the Numerical Methods course (MEEN 357), in which we placed 4th of 20 teams.

- Phase 1: Foundations & Subfunctions
- Phase 2: System Verification & Analysis
- Phase 3: Parameter Validation & Strategic Approach
- Phase 4: Final Competition Submission (Document)

Contributors: Jacob Hargreaves, Ian Wilhite, David Guess

Key Skills: Numerical Methods, Computational Analysis, Algorithm Development, Software Development, and Convex Optimization.

Relevance: This work demonstrates the development and management of large codebases, iterative verification and validation, and system design struture.

MEEN 357 - 501
Authors: Jacob Hargreaves, David Guess, Ian Wilhite

6.1 Coding

Question 1: We had you define the acceleration due to gravity as a field in a structure that you had to pass as an input argument to several functions. Instead, we could have had you type the value for the constant, 3.72 m/s2 , directly in those functions. Do you believe there is an advantage to how we had you do it? Explain. Would you have done it differently? Explain why or why not.

We believe that there are advantages to the way we define acceleration in this project. Because we did not code the gravity constant to simply be the value on Mars, we can update the gravity constant easily if we want to analyze the rover on other planets or moons. If we wanted to change the gravity constant, we could simply alter its structure in one place rather than having to change its value in every single function. It is for these reasons that we would not have done anything differently regarding the acceleration due to gravity.

Question 2: What happens if you try to call F_gravity using a terrain slope of 110 degrees? Is this desirable behavior? Explain why you think this.

When we try to call F_gravity using a terrain slope above 90 degrees, such as a slope of 110 degrees, F_gravity returns a force greater than the force of gravity in free fall. This is because the equation used in this function is $F_{gravity} = -\ m_{rover} * g * sin(\alpha)$ and when α (the angle of inclination) is above 90 degrees, the sin() value is greater than 1. This is not desirable behavior because the rover would never feel a force of gravity greater than the free fall force.

6.2 Motor and Speed Reducer Behavior

Question 3: What is the maximum power output by a single rover motor? At what motor shaft speed does this occur? Provide graphs or other data to support your answer.

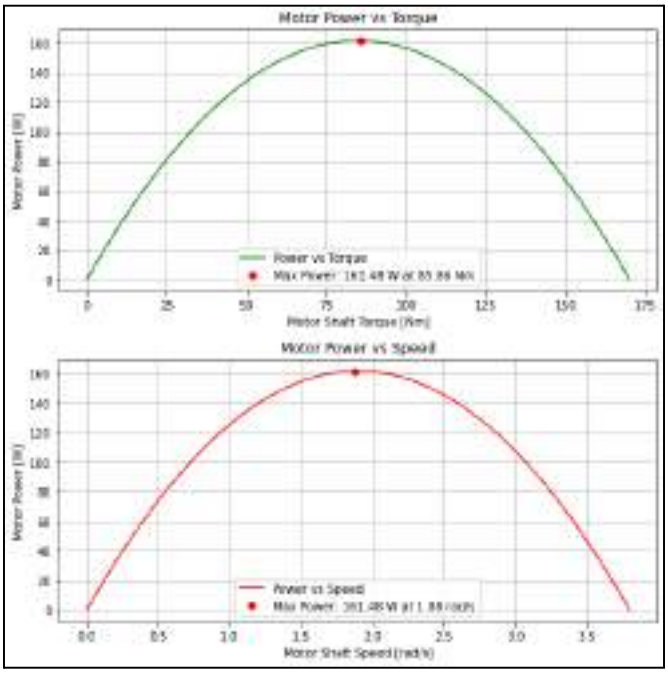

As shown in the graph above, the maximum power output by a single rover motor is about 161.48 Watts and occurs at a motor shaft speed of 1.88 rad/s.

Question 4: What impact does the speed reducer have on the power output of the drive system? Again, provide any graphs or supporting data.

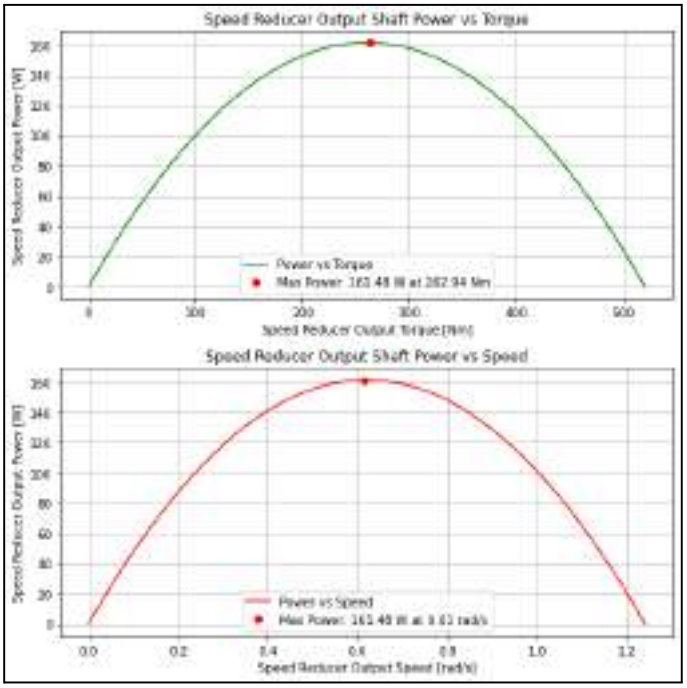

The speed reducer causes the maximum power output of the drive system to occur at a much lower motor shaft speed of 0.61 rad/s, as seen above. The speed reducer does this in order to help the rover overcome resistance such as rough terrain. The rover can better overcome this resistance as it has more torque at a lower speed. The speed reducer allows for more torque overall as compared to the figures in question #3.

6.3 Rover Behavior

Question 5: Examine the graph you generated using analysis_terrain_slope.py. (Provide the graph in your response for reference.) Explain the trend you observe. Does it make sense physically? Why or why not? Please be precise. For example, if the graph appears linear or non-linear, can you explain why it should be the way you observed? Refer back to the rover model and how slope impacts rover behavior.

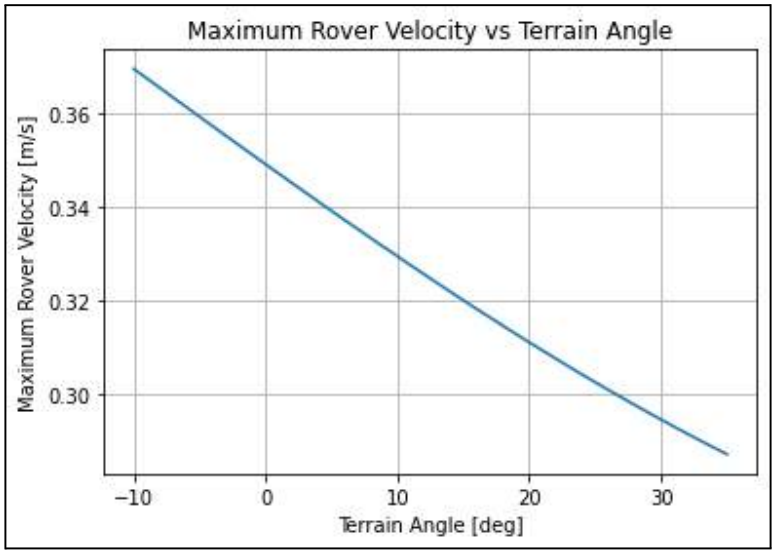

This trend from the graph above makes perfect sense. On downhill motion (Negative Terrain Angle) the rover experiences additional acceleration from gravity. Therefore, a higher maximum velocity is obtained. On flat and uphill motion (Positive Terrain Angle), the maximum velocity of the rover steadily decreases. This is because the rover has to overcome both gravity and rolling resistance pulling it backward.

Additionally, the graph appears approximately linear, which suggests that the impact of slope on the rover's speed is proportional, which aligns with the rover model where gravitational forces and resistive forces change linearly with increasing slope.

Question 6: Examine the graph you generated using analysis_rolling_resistance.py. (Provide the graph in your response for reference.) Explain the trend you observe. Does it make sense physically? Why or why not? Please be precise. For example, if the graph appears linear or non-linear, can you explain why it should be the way you observed? Refer back to the rover model and how the coefficient of rolling resistance impacts rover behavior.

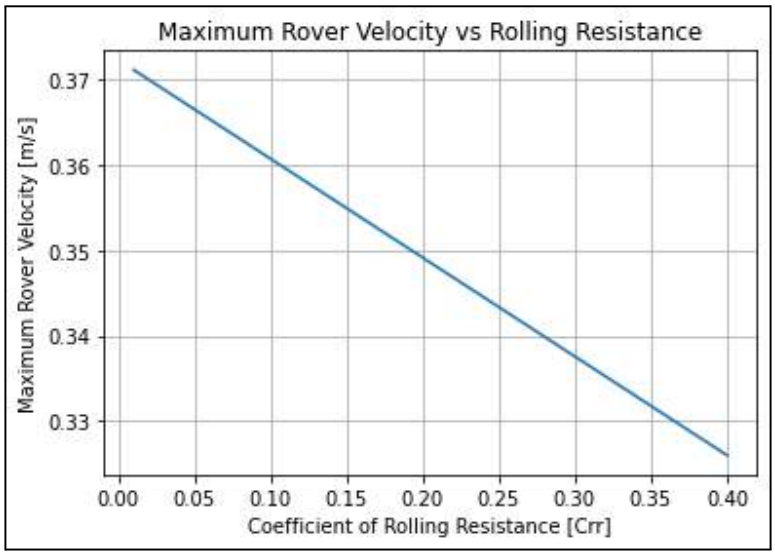

This graph shows a linear decrease in maximum rover velocity as the coefficient of rolling resistance (Crr) increases. This makes sense because rolling resistance is a force that opposes the rover's motion. As Crr increases, the motor has to exert more energy to overcome this resistance. Since the rolling resistance is directly proportional to Crr, the decrease in velocity follows a linear trend. This means that as Crr rises, the rover's maximum achievable speed steadily decreases. This is also consistent with the energy required to counteract the increasing resistance.

Question 7: Examine the surface plot you generated using analysis_combined_terrain.py. (Provide the graph in your response for reference.) What does this graph tell you about the physical conditions under which it is appropriate to operate the rover? Based on what you observe, which factor, terrain slope or coefficient of rolling resistance, is the dominant consideration in how fast the rover can travel? Please explain your reasoning.

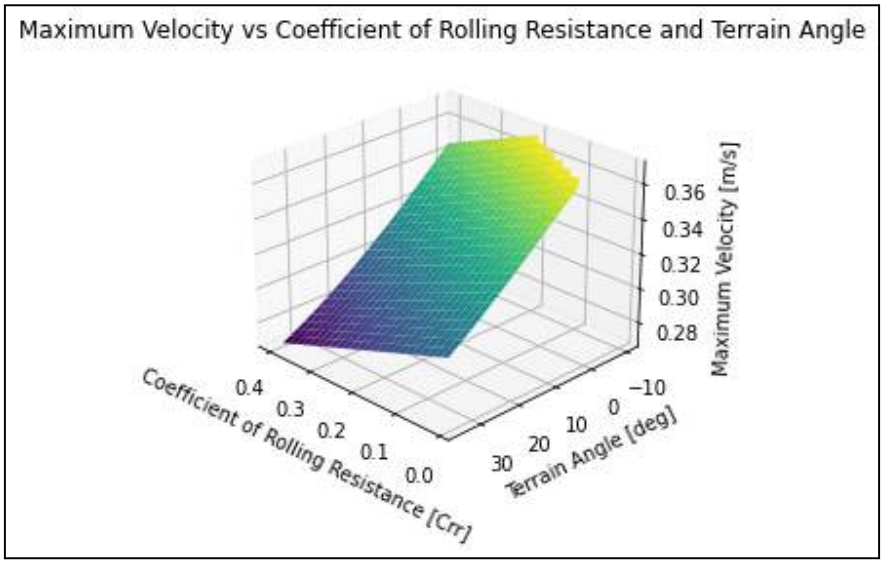

The 3D-surface plot shows that both the terrain slope and the coefficient of rolling resistance (Crr) have a significant impact on the maximum velocity of the rover. As the terrain slope increases, the rover's maximum velocity decreases, and as the Crr increases, the velocity also decreases. However, the graph shows that terrain slope has a more noticeable effect on the rover's speed compared to the rolling resistance. This is evident from the steep gradient along the terrain angle axis, meaning that changes in slope result in larger variations in speed. Therefore, terrain angle is the dominant factor. This is because steeper angles significantly reduce the rover's maximum velocity while rolling resistance primarily adds resistance.

Task 2:

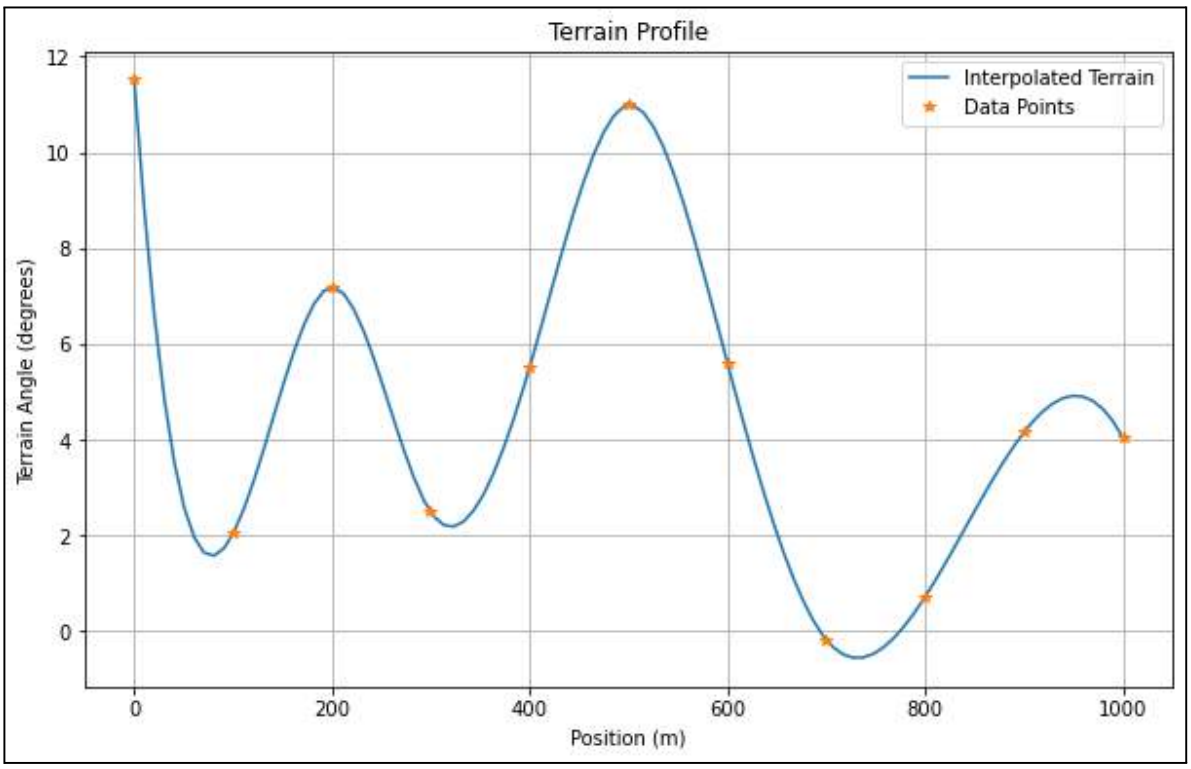

Experiment_Visualization Curve

The terrain profile generated through cubic spline interpolation exhibits smooth characteristics throughout the entire path. The graph shows that the blue interpolated line transitions naturally between the data points (marked by orange stars) without any jarring changes or breaks. This smoothness is from using cubic polynomials between points, which ensures continuous slopes and curvatures at the transitions. Additionally, the curve maintains accuracy to our input data, as evidenced by the interpolated line passing exactly through each orange star marker. This smooth behavior makes sense for modeling real-world terrain since actual landscapes typically don't have abrupt elevation changes.

Task 5:

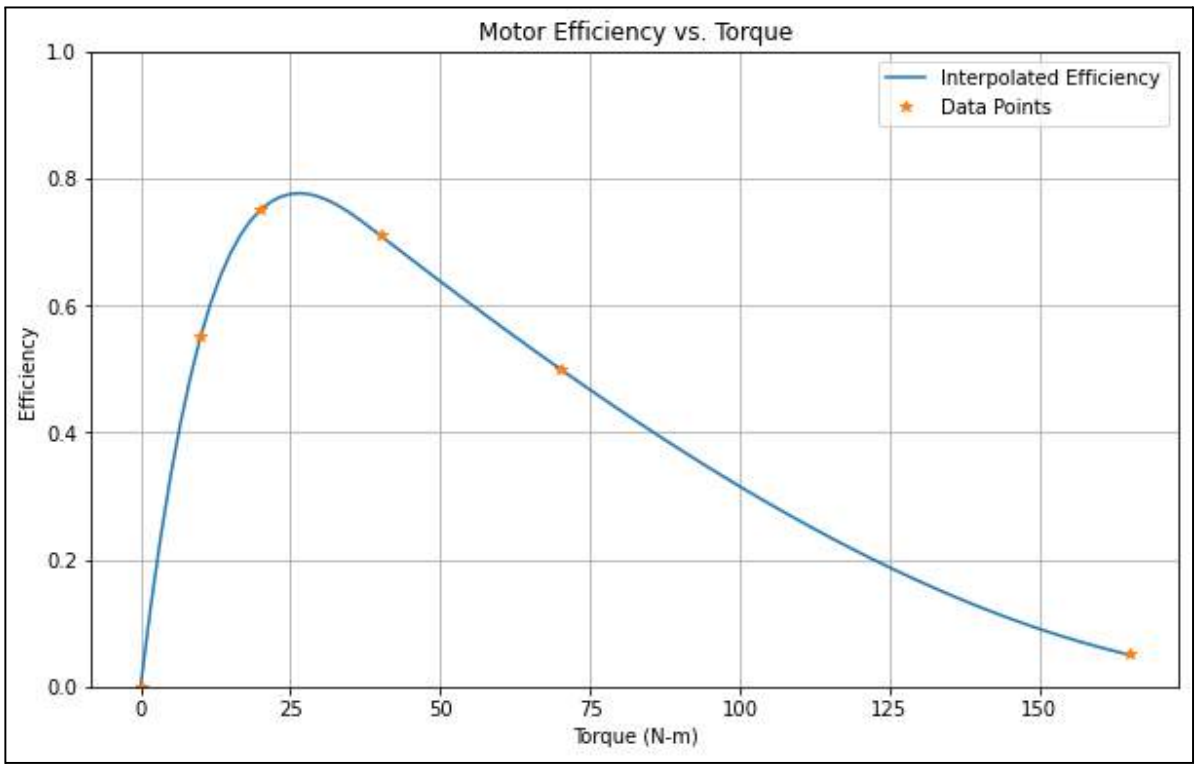

Efficiency_Visualization Curve

This motor efficiency curve shares a similar overall shape with Figure 2 from the handout - starting at zero, rising to a peak, then declining - though it operates at a much higher torque range. The curve is smooth throughout due to the cubic spline interpolation used to connect the data points. The interpolated line passes exactly through all six data points (marked with stars), which is a key property of cubic spline interpolation.

Task 8:

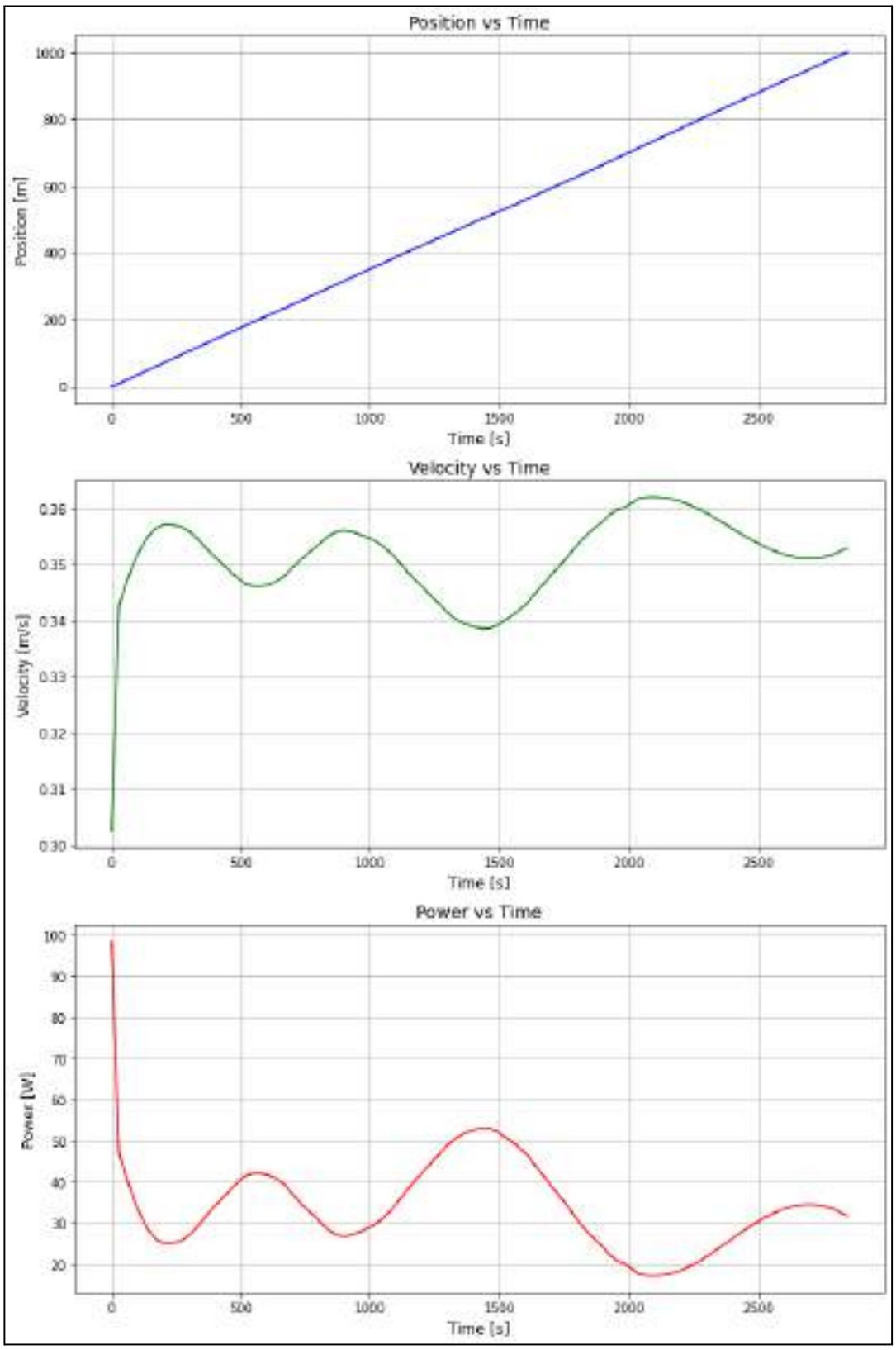
Position vs Time
Position [m]
Time [s]
Velocity vs Time
Velocity [m/s]
Time [s]
Power vs Time
Power [W]
Time [s]

(a) Position vs Time: The position-time graph shows a slightly non-linear relationship. While there is an overall upward trend, the slope (which represents velocity) varies over time rather than being constant. This nonlinearity occurs because the rover's velocity changes as it encounters different terrain angles, requiring different amounts of power and resulting in varying speeds across the trajectory.

(b) Velocity-Power Relationship: Looking at the velocity and power plots, there's a clear correlation - when the rover requires more power (shown by spikes in the power graph), there are corresponding changes in velocity. The relationship appears inverse in many cases - when the rover encounters situations requiring more power (likely uphill sections), the velocity tends to decrease slightly. This makes physical sense as the rover needs to expend more energy to maintain motion against gravity on inclines, resulting in slightly reduced velocity.

(c) Velocity Profile and Terrain: The velocity shows periodic variations between approximately 0.34-0.36 m/s, which likely corresponds to changes in terrain elevation. The dips in velocity (around t=1500s) suggest encounters with uphill sections where the rover must work harder against gravity, while slight increases in velocity may correspond to downhill or level sections where less power is required to maintain motion.

(d) Velocity Smoothness: The velocity graph shows smooth transitions rather than abrupt changes. This smoothness is due to two factors:
1. The terrain profile was interpolated using cubic splines, creating smooth transitions between terrain points
2. The rover's inertia and motor characteristics prevent instantaneous velocity changes, leading to gradual transitions as terrain conditions change

Rover Telemetry Data

Variable	**Value**
completion_time	2842.92 s
distance_traveled	1000 m
max_velocity	0.36 m/s
average_velocity	0.35 m/s
battery_energy	1094725.05 J
batt_energy_per_distance	1094.725 J/m

Task 9:

During Experiment 1, the battery energy used is 1,094.725 kJ. This is greater than the energy provided by the Lithium Iron Phosphate battery pack, as this batter only provides 907.2 kJ. Therefore, no, the rover can not complete the case defined by Experiment 1 with the 0.9072e6 J Lithium Iron Phosphate battery pack. There is not sufficient energy capacity to handle the demands shown in the simulation. We arrived at this conclusion by analyzing the output of Experiment 1.

Phase 3 Report

Jacob Hargreaves
David Guess
Ian Wilhite

Task 1:

define_mission_events.py

mission_events			
Field Name	***Value***	***Units***	***Description***
alt_heatshield_eject	8000	Meters	The altitude where the heat shield ejects
alt_parachute_eject	900	Meters	The altitude where the parachute ejects
alt_rockets_on	1800	Meters	The altitude where the rockets turn on
alt_skycrane_on	7.6	Meters	The altitude where the sky crane turns on

define_planet.py

high_altitude			
Field Name	***Value***	***Units***	***Description***
temperature	-38.94 @ 7000 m	Celsius	The temperature based on altitude above 7000 meters
pressure	0.000646 @ 7000 m	KPa	The temperature based on altitude above 7000 meters

low_altitude			
Field Name	***Value***	***Units***	***Description***
temperature	-31 @ 0 m	Celsius	The temperature based on altitude below 7000 meters

pressure	0.669 @ 0 m	KPa	The temperature based on altitude below 7000 meters

mars			
Field Name	***Value***	***Units***	***Description***
g	-3.72	m/s^2	The value of gravity on Mars
altitude_threshold	7000	KPa	The temperature based on altitude below 7000 meters
low_altitude	-	-	The dictionary low_altitude
high_altitude	-	-	The dictionary high_altitude
density	-	-	The dictionary density

define_rovers.py

wheel, rover 1			
Field Name	***Default Value***	***Units***	***Description***
radius	0.30	Meters	Radius of the wheel
mass	1	kilograms	Mass of wheel

wheel, rover 2			
Field Name	***Default Value***	***Units***	***Description***
radius	0.30	Meters	Radius of the wheel
mass	2	kilograms	Mass of wheel

wheel, rover 3			
Field Name	***Default Value***	***Units***	***Description***
radius	0.30	Meters	Radius of the wheel
mass	2	kilograms	Mass of wheel

wheel, rover 4			
Field Name	***Default Value***	***Units***	***Description***
radius	0.20	Meters	Radius of the wheel
mass	2	kilograms	Mass of wheel

speed_reducer, rover 1			
Field Name	***Default Value***	***Units***	***Description***
type	reverted	-	Radius of the wheel
diam_pinion	.04	Meters	Diameter of the pinion
diam_gear	.07	Meters	Diameter of the gear
mass	1.5	kilograms	Mass of speed reducer

speed_reducer, rover 2, 3, & 4			
Field Name	***Default Value***	***Units***	***Description***
type	reverted	-	Radius of the wheel
diam_pinion	.04	Meters	Diameter of the pinion
diam_gear	.06	Meters	Diameter of the gear
mass	1.5	kilograms	Mass of speed reducer

motor, rover 1			
Field Name	***Default Value***	***Units***	***Description***
torque_stall	170	-	Torque of the motor while stalling
torque_noload	0	N*m	Torque of the motor with no load
speed_noload	3.80	Rad/s	Angular speed of the motor with no load
mass	5.0	kilograms	Mass of the motor

motor, rover 2 & 3			
Field Name	***Default Value***	***Units***	***Description***
torque_stall	180	-	Torque of the motor while stalling
torque_noload	0	N*m	Torque of the motor with no load

speed_noload	3.70	Rad/s	Angular speed of the motor with no load
mass	5.0	kilograms	Mass of the motor

motor, rover 4			
Field Name	***Default Value***	***Units***	***Description***
torque_stall	165	-	Torque of the motor while stalling
torque_noload	0	N*m	Torque of the motor with no load
speed_noload	3.85	Rad/s	Angular speed of the motor with no load
mass	5.0	kilograms	Mass of the motor

chassis, rover 1, 2, & 3			
Field Name	***Default Value***	***Units***	***Description***
mass	659	kilograms	Mass of chassis

chassis, rover 4			
Field Name	***Default Value***	***Units***	***Description***
mass	674	kilograms	Mass of chassis

science_payload, rover 1, 2, & 3			
Field Name	***Default Value***	***Units***	***Description***
mass	75	kilograms	Mass of science payload

science_payload, rover 4			
Field Name	***Default Value***	***Units***	***Description***
mass	80	kilograms	Mass of science payload

power_subsys, rover 1, 2, & 3			
Field Name	***Default Value***	***Units***	***Description***
mass	90	kilograms	Mass of power subsystem

power_subsys, rover 4			
Field Name	***Default Value***	***Units***	***Description***
mass	100	kilograms	Mass of power subsystem

rover			
Field Name	***Default Value***	***Units***	***Description***
wheel	wheel	-	Dictionary of the wheel
speed_reducer	speed_reducer	-	Dictionary of the speed_reducer
motor	motor	-	Dictionary of the motor

planet			
Field Name	***Default Value***	***Units***	***Description***
g	3.72	m/s^2	Gravity value on the planet (Mars)

define_edl_system.py

parachute			
Field Name	***Value***	***Units***	***Description***
deployed	True	-	True means it has been deployed but not ejected
ejected	False	-	True means the parachute is no longer attached to the system

diameter	16.25	m	Diameter of the parachute
Cd	0.615	-	Coefficient of drag on the parachute
mass	185.0	kg	Mass of the parachute

rocket			
Field Name	***Value***	***Units***	***Description***
on	False	-	Indicates if the rocket is currently on.
structure_mass	8.0	kg	Mass of the rocket structure excluding fuel.
initial_fuel_mass	230.0	kg	Initial mass of fuel.
fuel_mass	230.0	kg	Current fuel mass (less than or equal to initial_fuel_mass).
effective_exhaust_velocity	4500.0	m/s	Effective exhaust velocity of the rocket.
max_thrust	3100.0	N	Maximum thrust generated by the rocket.
min_thrust	40.0	N	Minimum thrust generated by the rocket.

speed_control			
Field Name	***Value***	***Units***	***Description***
on	False	-	Indicates if the speed control mode is activated.
Kp	2000	-	Proportional gain term for speed control.
Kd	20	-	Derivative gain term for speed control.
Ki	50	-	Integral gain term for speed control.
target_velocity	-3.0	m/s	Desired descent speed.

position_control			
Field Name	***Value***	***Units***	***Description***
on	False	-	Indicates if the position control mode is activated.
Kp	2000	-	Proportional gain term for position control.
Kd	1000	-	Derivative gain term for position control.
Ki	50	-	Integral gain term for position control.
target_altitude	7.6	m	Target altitude, reflecting the sky crane cable length.

sky_crane			
Field Name	***Value***	***Units***	***Description***
on	False	-	Indicates if the sky crane is lowering the rover.
danger_altitude	4.5	m	Altitude considered too low for safe rover touchdown.
danger_speed	-1.0	m/s	Speed below which the rover would impact too hard on the surface.
mass	35.0	kg	Mass of the sky crane.
area	16.0	m^2	Frontal area used for drag calculations.
Cd	0.9	-	Coefficient of drag for the sky crane.
max_cable	7.6	m	Maximum length of cable for lowering the rover.
velocity	-0.1	m/s	Speed at which the sky crane lowers the rover.

heat_shield			
Field Name	***Value***	***Units***	***Description***
ejected	False	-	True if the heat shield has been ejected from the system.
mass	225.0	kg	Mass of the heat shield.

diameter	4.5	m	Diameter of the heat shield.
Cd	0.35	-	Drag coefficient of the heat shield.

edl_system			
Field Name	***Value***	***Units***	***Description***
altitude	NaN	m	Current altitude of the system, updated throughout the simulation.
velocity	NaN	m/s	Current velocity of the system, updated throughout the simulation.
num_rockets	8	-	Total number of rockets in the system.
volume	150	m^3	Volume of the system.
parachute	parachute	-	Parachute dictionary with deployment and drag properties.
heat_shield	heat_shield	-	Heat shield dictionary with mass and drag properties.
rocket	rocket	-	Rocket dictionary with thrust and fuel properties.
speed_control	speed_control	-	Speed control dictionary for descent speed management.
position_control	position_control	-	Position control dictionary for altitude management.

sky_crane	sky_crane	-	Sky crane dictionary for rover lowering.
rover	rover	-	Rover dictionary (defined in another file).

Task 2:

get_mass_rover			
Calling Syntax	***Description***	***Input Arguments***	***Output Arguments***
get_mass_rover(edl_system)	Computes the total mass of the rover based on the specifications in the edl_system dictionary, as per Phase 1 requirements.	edl_system: dictionary containing rover components and their respective masses	m: total mass of the rover (float)

get_mass_rockets			
Calling Syntax	***Description***	***Input Arguments***	***Output Arguments***
get_mass_rockets(edl_system)	Returns the current total mass of all rockets on the EDL system.	edl_system: dictionary containing the number of rockets and the masses of the rocket components	m: total mass of all rockets (float)

get_mass_edl			
Calling Syntax	***Description***	***Input Arguments***	***Output Arguments***

get_mass_edl(edl_system)	Returns the total current mass of the entire EDL system, accounting for any ejected components.	edl_system: dictionary containing the masses of the EDL system's components, including parachute, heat shield, rockets, sky crane, and rover	m: total current mass of the EDL system (float)

get_local_atm_properties			
Calling Syntax	***Description***	***Input Arguments***	***Output Arguments***
get_local_atm_properties(planet, altitude)	Returns local atmospheric properties—density, temperature, and pressure—at a given altitude.	planet: dictionary with atmospheric properties and calculation functions for density, temperature, and pressure based on altitude; altitude: altitude above the planet's surface (meters)	density: atmospheric density (kg/m³); temperature: local temperature (°C); pressure: local pressure (kPa)

F_buoyancy_descent			
Calling Syntax	***Description***	***Input Arguments***	***Output Arguments***
F_buoyancy_descent(edl_system, planet, altitude)	Computes the net buoyancy force acting on the EDL system during descent.	edl_system: dictionary containing volume of the EDL system; planet: dictionary with gravity and atmospheric functions; altitude: altitude above the planet's surface (meters)	F: net buoyancy force (float)

F_drag_descent			
Calling Syntax	***Description***	***Input Arguments***	***Output Arguments***

F_drag_descent(edl_system, planet, altitude, velocity)	Computes the net drag force acting on the EDL system during descent.	edl_system: dictionary containing the components of the EDL system; planet: dictionary with atmospheric properties; altitude: altitude above the planet's surface (meters); velocity: current descent velocity (m/s)	F: net drag force (float)

F_gravity_descent			
Calling Syntax	***Description***	***Input Arguments***	***Output Arguments***
F_gravity_descent(edl_system, planet)	Computes the gravitational force acting on the EDL system.	edl_system: dictionary with the mass of the EDL system; planet: dictionary with gravity parameter	F: gravitational force (float)

v2M_Mars			
Calling Syntax	***Description***	***Input Arguments***	***Output Arguments***
v2M_Mars(v, a)	Converts descent speed to Mach number on Mars as a function of altitude.	v: descent speed (m/s); a: altitude (m)	M: Mach number (float)

thrust_controller			
Calling Syntax	***Description***	***Input Arguments***	***Output Arguments***
thrust_controller(edl_system, planet)	Implements a PID Controller for the EDL system to adjust thrust based on errors in velocity control.	edl_system: dictionary containing the control parameters, telemetry, and rocket specifications; planet: dictionary with gravity information	edl_system: modified dictionary with updated thrust and telemetry data

edl_events			
Calling Syntax	***Description***	***Input Arguments***	***Output Arguments***
edl_events(edl_system, mission_events)	Defines events occurring in EDL System simulation	edl_system: EDL system state, mission_events: mission-specific event altitude/speed values	events: List of event functions for EDL conditions

edl_dynamics			
Calling Syntax	***Description***	***Input Arguments***	***Output Arguments***
edl_dynamics(t, y, edl_system, planet)	Calculates EDL dynamics as it descends to the Mars surface	t: Time, y: State vector, edl_system: EDL system details, planet: Planet details affecting EDL	dydt: Array of rates of change in state vector variables

update_edl_state			
Calling Syntax	***Description***	***Input Arguments***	***Output Arguments***
update_edl_state(edl_system, TE, YE, Y, ITER_INFO)	Updates the status of the EDL system based on simulation events, like ejection, activation, and landing conditions.	edl_system (dict): EDL system state, TE (list): Event times, YE (list): State at event times, Y (array): States, ITER_INFO (bool): Logging flag	edl_system (dict): Updated system, y0 (array): New initial conditions, TERMINATE_SIM (bool): Simulation termination flag

simulate_edl			
Calling Syntax	***Description***	***Input Arguments***	***Output Arguments***

simulate_edl(edl_system, planet, mission_events, tmax, ITER_INFO)	Runs the simulation of the EDL system through iterative time steps until termination based on events or time limit	edl_system (dict): System parameters, planet (dict): Planetary constants, mission_events (dict): Event conditions, tmax (float): Max time, ITER_INFO (bool): Logging flag	T (array): Simulation time steps, Y (array): State vectors, edl_system (dict): Final system state

Task 3:

IVP Solver
The while loop in simulate_edl uses solve_ivp with the DOP853 method, an 8th-order Runge-Kutta method that provides higher accuracy compared to other methods like RK45. This higher precision is essential due to the specific event criteria we are monitoring, requiring close alignment with actual values to correctly detect each event.

solve_ivp is called with the following parameters:

- fun: A lambda function representing the system's dynamics, edl_dynamics(t, y, edl_system, planet).
- tspan: A tuple defining the simulation time span, (0, tmax).
- y0: An array of initial state variables, including initial velocity, altitude, fuel mass, and other state indicators.
- method: Set to "DOP853" to ensure high accuracy for Martian descent simulation.
- events: A set of conditions to trigger specific events, as defined by edl_events(edl_system, mission_events).
- max_step: The maximum step size for the solver, set to 0.1 for finer granularity.

Each iteration of solve_ivp simulates until one of the defined events occurs. When an event triggers, the solver captures t (time) and y (state variables like altitude, fuel, etc.), which are then updated within the update_edl_state function.

Updating the EDL System
The update_edl_state function is crucial for this loop, as it processes the event results from solve_ivp and updates edl_system accordingly. This function also sets up the initial conditions y0 for the next loop iteration and checks if the simulation should terminate by updating the TERMINATE_SIM flag.

Key events handled by update_edl_state include:
1. Heat Shield Ejection: Heat shield is detached when a certain altitude is reached.
2. Parachute Ejection: Parachute is released based on altitude criteria.
3. Rockets Activation: Rockets are ignited for descent control at specific altitude.
4. Sky Crane Activation: Sky crane system is engaged to lower the rover.
5. Out of Rocket Fuel: Fuel depletion triggers a termination condition if descent is not complete.
6. Sky Crane Safety Failure: The rover crashes if descent control or sky crane fails.
7. Speed Controller Activation: Engages to maintain a target descent speed.
8. Altitude Controller Activation: Altitude controller engages as the sky crane takes over, disabling speed control.
9. Rover Grounded: Reaches the surface (altitude of zero), ending the simulation.

Explanation of the Loop
The while loop in simulate_edl repeats until TERMINATE_SIM is set to True. Termination occurs when time runs out, the rover safely lands, fuel depletes, or a crash is detected.

The process within each loop iteration is as follows:
1. A lambda function for the system dynamics (fun) is passed to solve_ivp.
2. solve_ivp runs the simulation until one of the specified events occurs, producing arrays of t (time) and y (state variables) for the event.
3. update_edl_state then adjusts edl_system, sets y0 for the next pass, and updates TERMINATE_SIM if an exit condition is reached.
4. The loop appends time (T) and state variables (Y) for further analysis, updating tspan with new bounds for the next simulation pass.

This iterative simulation loop accurately models different operational phases of the EDL sequence: parachute deployment, rocket firing, sky crane descent, and finally, rover touchdown.

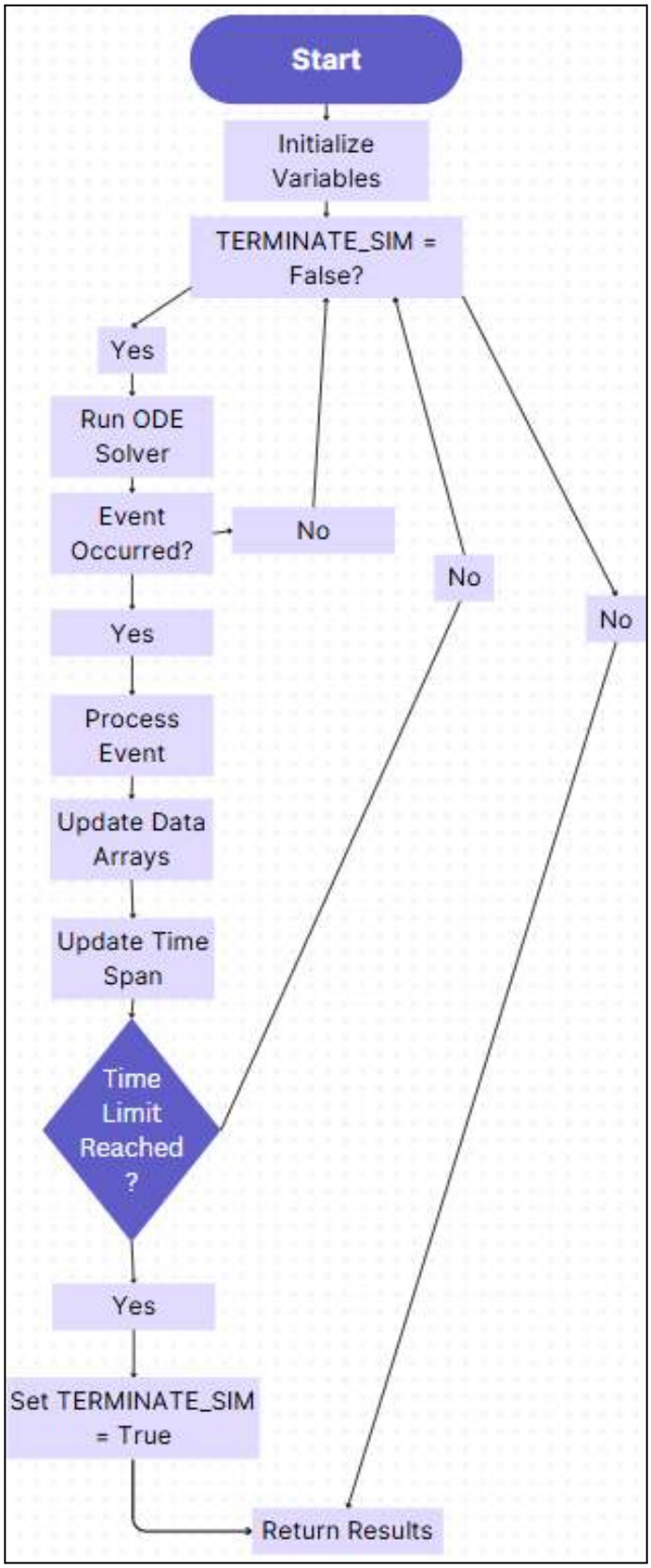
Start
Initialize Variables
TERMINATE_SIM = False?
Yes
Run ODE Solver
Event Occurred?
No
Yes
Process Event
Update Data Arrays
Update Time Span
Time Limit Reached ?
No
Yes
Set TERMINATE_SIM = True
No
Return Results

Task 4:

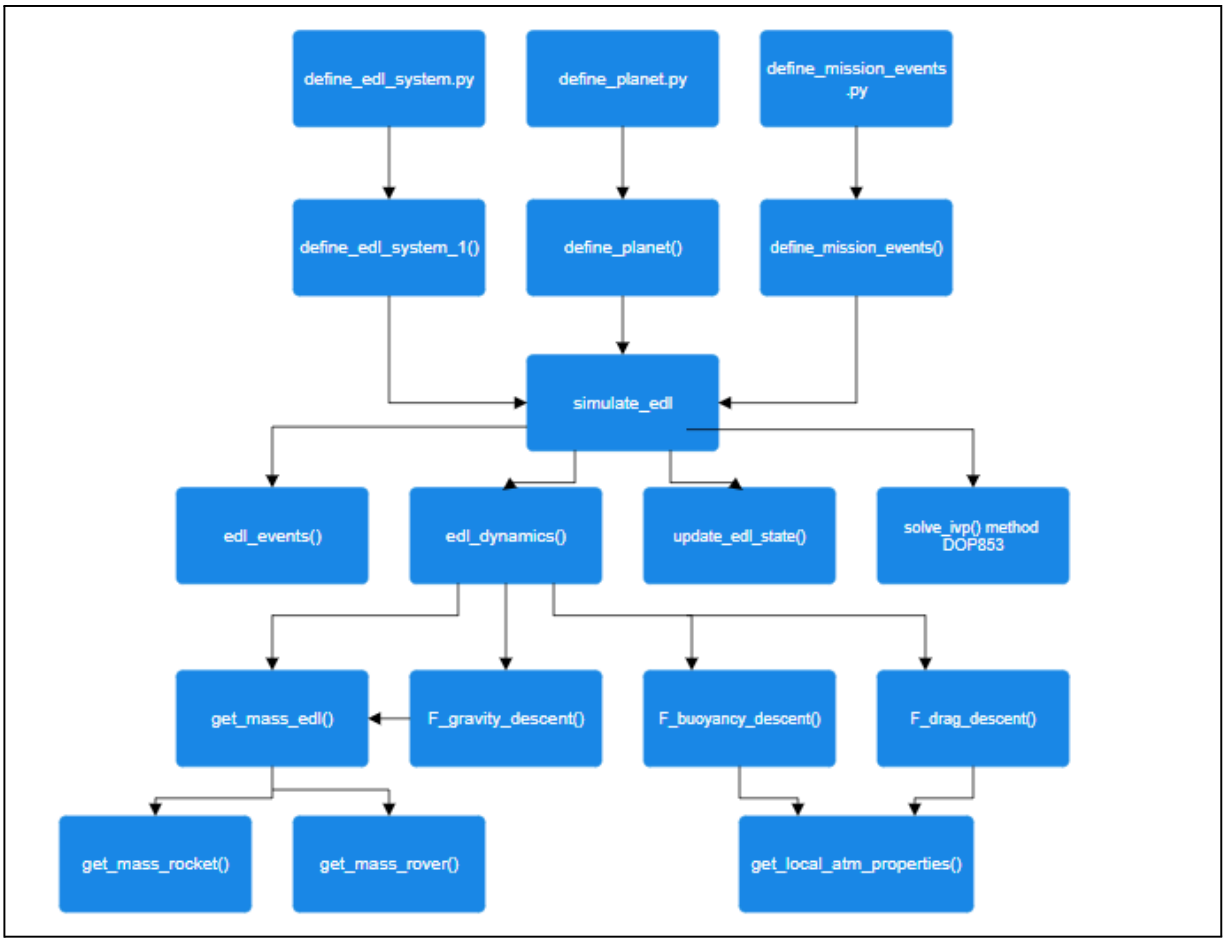

This flowchart begins with the imported files, followed by the loading of key dictionaries. These dictionaries help establish variables that are then passed into simulate_edl. Inside simulate_edl, we track each function call: the flow splits to cover edl_events, update_edl_state, and the solve_ivp function. From solve_ivp, we see the call to edl_dynamics, which itself branches out to get_mass_edl, F_gravity_descent, F_buoyancy_descent, and F_drag_descent. In turn, F_gravity_descent calls get_mass_edl again, which then leads to two final functions, concluding this branch. Meanwhile, both F_buoyancy_descent and F_drag_descent further call get_local_atm_properties, completing the flow.

Task 5:

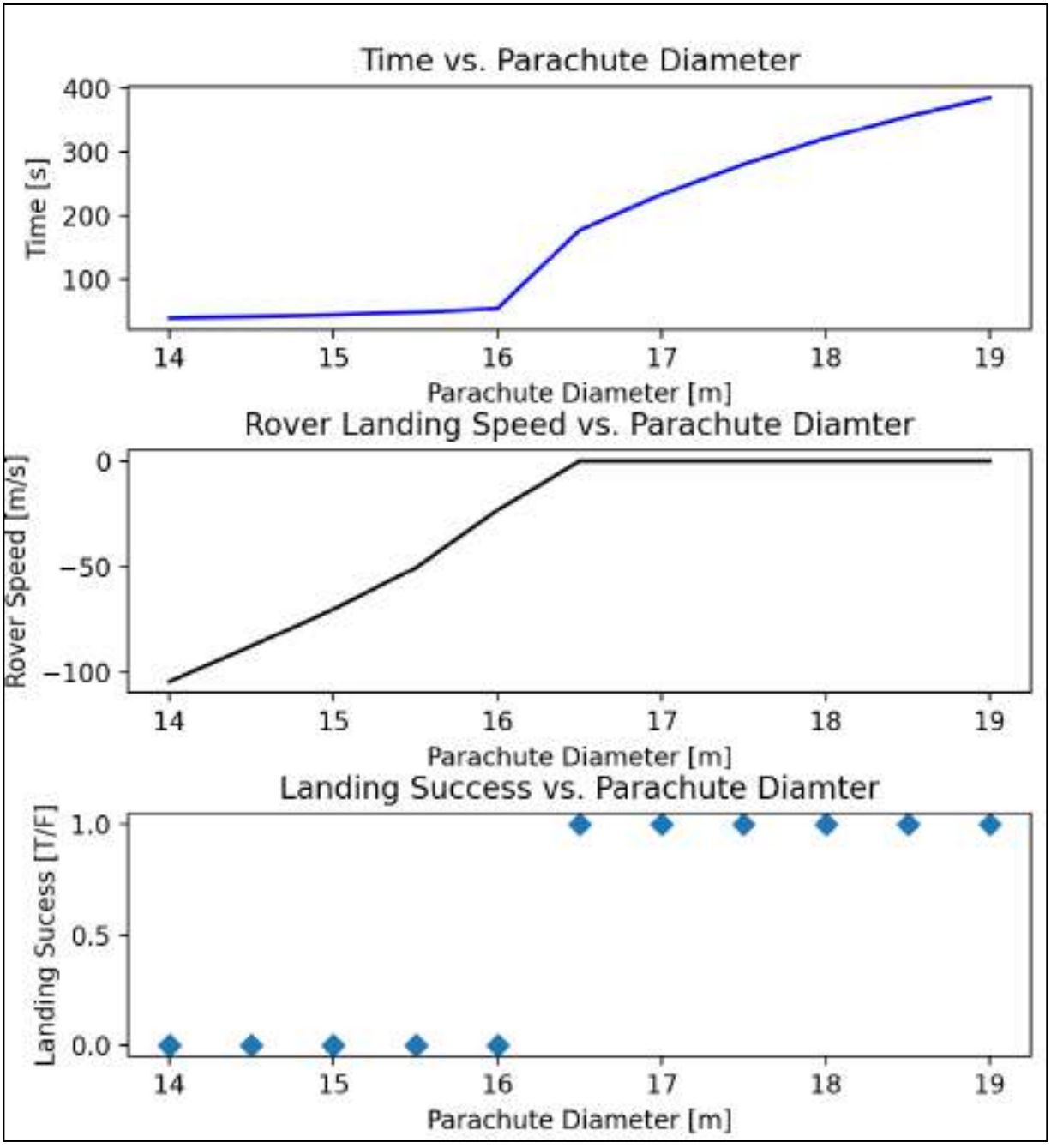

The results in Figure 1 show the effects of parachute diameter on simulation time, rover landing speed, and landing success. To ensure a successful landing, only parachutes with diameters between 16.5 and 19 m are viable, as smaller sizes led to failed landings. Among these, minimizing landing time is preferred, and the first graph confirms that larger diameters increase descent time. Therefore, we recommend a 16.5 m parachute, which provides a safe landing in the shortest time.

Task 6:

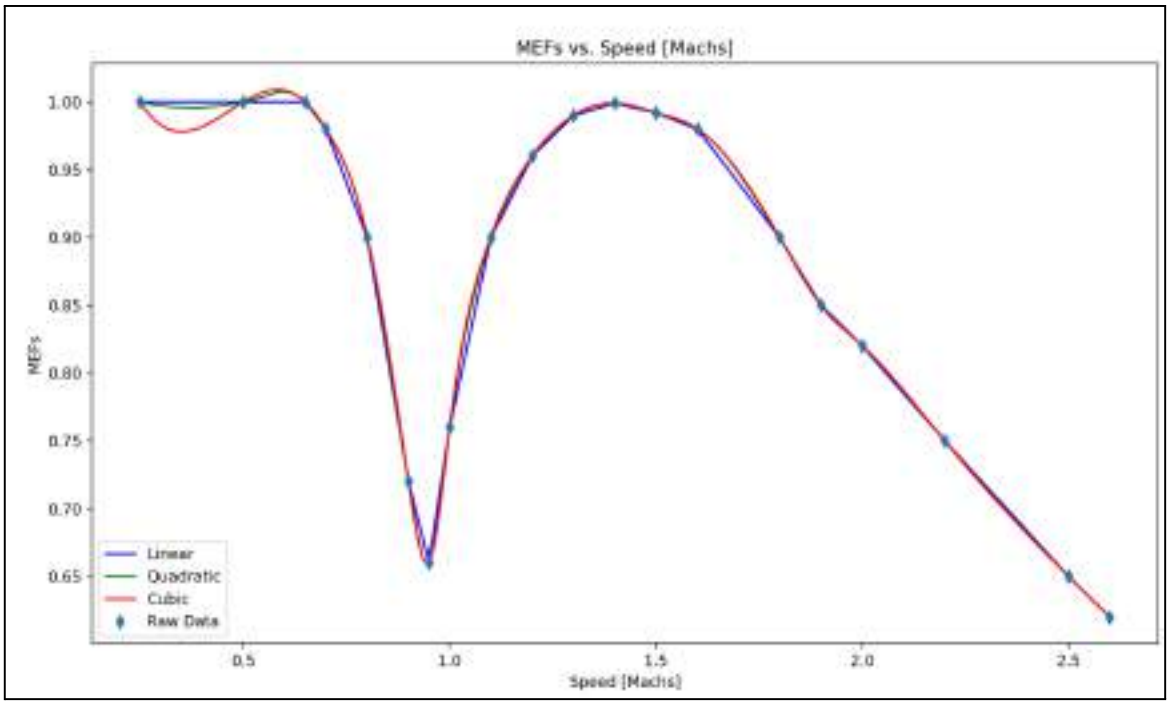

6.1)

The continuous model was created by interpolating the data provided. This data came from simulation, meaning that the error is negligible and there is no need for a regression. We chose to use the quadratic interpolation as a representation of the data provided, because it would best extrapolate the data to the range outside the data provided. To generate this plot, we

6.2)

After incorporating the function into the parachute drag model, we re-evaluated our parachute diameter recommendations. By updating the drag coefficient and re-running our analysis, we observed a shift in the recommended parachute diameter range. Our previous recommendation of 16.5 m no longer guaranteed a successful landing, as the range shifted to [17, 19] m. Consequently, we now recommend a 17 m parachute diameter for optimal landing performance within the updated model.

PROJECT PHASE 4:

Optimization Challenge Report

Prepared for

MEEN 357 - Section 501

Team #10

By

Jacob Hargreaves

Ian Wilhite

David Guess

November 29, 2024

Aggie Honor Code: *"On my honor, as an Aggie, I have neither given nor received unauthorized aid on this academic work."*

"None of the members of the team communicated in any way with other teams with regards to specific coding issues with this project."

Signature:	*Jacob Hargreaves*	Date:	*11/29/2024*
	David Guess	Date:	*11/29/2024*
	Ian Wilhite	Date:	*11/29/2024*

Table of Contents

Table of Contents..... 2
Introduction..... 3
Formulation of the Design Problem..... 3
Considered Design Solutions..... 3
Final Design Selection..... 4
Numerical Methods Used..... 4
Description of Final Design..... 5
Performance Data..... 6

Introduction

The design of an Entry, Descent, and Landing (EDL) system and a rover for a Martian mission is a challenging problem that requires careful consideration of multiple factors.
The goal is to create a system that can safely land on Mars and allow the rover to travel at least 1 kilometer on a single battery charge. This involves optimizing key parameters like landing velocity, rover speed, and energy usage while staying under the $7.2 million budget. To meet these requirements, we had to choose the best combination of components, such as parachutes, motors, batteries, and chassis materials, while making trade-offs between cost, performance, and weight. This project highlights the complexity of designing systems for real-world space exploration missions.

Formulation of the Design Problem

We aim to design an Entry, Descent, and Landing (EDL) system coupled with a rover capable of traversing at least 1 km on a single battery charge over a predefined Martian terrain. The design must balance key performance metrics: speed, cost, and battery efficiency, while adhering to specific constraints. Among these, speed is prioritized, followed by cost considerations. The design solution should:

- **Maximize rover speed** to reduce the total mission duration.
- **Minimize total cost**, ensuring it stays within the $7.2 million budget.
- Optimize battery capacity to achieve sufficient energy per meter (J/m) without excessive weight or cost.

Ensure the system satisfies constraints such as:

- Landing velocity below 1 m/s.
- Rover chassis strength exceeding 40,000 units.
- Mass and geometry limits for all components.

Key decision variables include:

- Parachute diameter, fuel mass, wheel radius, and gear diameter (continuous variables).
- Motor type, battery type, number of modules, and chassis material (discrete variables).

Considered Design Solutions

To address the rover's design requirements, we examined multiple options for key components and materials, considering performance and cost.

1) **Motor Selection**: The six available motor types were evaluated, focusing on their efficiency, torque, and speed capabilities. High-efficiency motors offered a balance of performance and reasonable cost increases. Both torque_he and speed_he motors stood

out as superior options, with the speed_he motor chosen for its ability to maximize rover speed, a primary objective.

2) **Chassis Material**: The three chassis material options—steel, magnesium, and carbon fiber—were compared for cost, strength, and weight. While carbon fiber exceeded budget constraints due to its high cost, magnesium emerged as the optimal choice. Its high specific strength allowed for a lighter chassis, aligning with the weight limits, while maintaining structural integrity and meeting strength requirements.
3) **Battery Configuration**: Various battery types and configurations were analyzed for energy efficiency and cost. PbAcid-1 batteries provided a good energy-to-cost ratio, making them a favorable option. Initial testing started with 10 modules to evaluate performance before editing the configuration.

Final Design Selection

We developed a Python program called value_sweep.py designed to comprehensively analyze the EDL process by systematically compiling and evaluating constraint values across multiple iterations. Our approach involved collecting data for each constraint, sorting iterations by time, and strategically eliminating scenarios that did not work.

Unlike traditional methods that focus on optimizing a single parameter, our approach allowed for simultaneous multi-constraint analysis. This methodology provided a more holistic and nuanced optimization strategy, enabling us to maximize overall performance in ways that would have been impossible with a narrow, single-constraint approach. By examining the complex interplay between different constraints, we gained deeper insights into the system's potential.

The effectiveness of this strategy was evident in the progressive evolution of our value_sweep.py outputs. The data range from our initial analysis to the final iterations demonstrated significant improvements in our understanding and optimization of the EDL process, validating the power of our comprehensive analytical approach.

We used this approach to optimize our design and choose the best one, given the constraints and the parameters we wanted to emphasize.

Numerical Methods Used

Our Python script employs several numerical optimization methods for maximizing objectives and solving constraints. These methods are from the scipy.optimize library and include:

1. **Trust-Region Constrained Algorithm (trust-constr)**:

    - This method solves the optimization problem with constraints and bounds defined using a Nonlinear Constraint object. It iteratively updates the solution while respecting constraints like strength, cost, and battery energy limits.
2. **Sequential Least Squares Programming (SLSQP)**:
    - This method minimizes the objective function with equality and inequality constraints defined via the ineq_cons dictionary. It is also bound-aware.
3. **Differential Evolution**:
    - A global optimization algorithm that explores the search space more thoroughly compared to local optimizers. It handles constraints through a nonlinear constraint and allows population-based exploration.
4. **Constrained Optimization BY Linear Approximations (COBYLA)**:
    - It deals with constraints by linear approximations and can handle inequality constraints without requiring explicit gradient definitions.

Additionally, grid search is employed in the loops to systematically explore the parameter space before optimization, providing initial guesses (x0) for the optimization algorithms. This enhances the likelihood of finding a global maximum.

Description of Final Design

We arrived at our final design by optimizing key aspects of our rover in order to minimize the time while staying within the parameters. The following are key parameters found when designing our rover:

- **Parachute:** We found that minimizing the parachute diameter to 14 m allowed our rover to descend the quickest.
- **Wheel Radius:** Our wheel radius is maximized at almost 0.7 m in order to allow the rover to move the furthest that it can in the least amount of rotations.
- **Speed Reducer (d2):** Additionally, the speed reducer is the smallest that it can be at 0.05 m in order to maximize the number of rotations that the wheel has.
- **Fuel and Chassis Mass:** Our fuel mass and chassis mass are both a bit on the heavier side but light enough to allow the rover to land safely and quickly.

We found that the budget constraint was not one of the key factors to create tough decisions in our design. This is shown in our total cost as we are about $1.25 million under the $7 million budget.

Table 1: Final Optimized Rover Parameters

Parameter	Value	Units
Optimized Parachute Diameter	14.00	m
Optimized Fuel Mass	200.304121	kg
Time to complete EDL Mission	128.786949	s
Rover Velocity at Landing	-0.100512	m/s
Optimized Wheel Radius	0.699995	m
Optimized d2	0.05	m
Optimized Chassis Mass	375.299577	kg
Time to Complete Rover Mission	395.625	s
Time to Complete Mission	524.412	s
Average Velocity	2.436	m/s
Distance Traveled	1000.00	m
Battery Energy per Meter	541.524	J/m
Total Cost	5751017.33	$

Performance Data

The final rover design, optimized by using the COBYLA method, meets all mission requirements while achieving high performance in the Entry, Decent, Landing, and traversal phases. Below is a detailed summary of the performance results.

- **Motor**: The high-efficiency speed_he motor was selected to maximize the rover's speed without significantly increasing energy consumption.
- **Chassis Material**: Magnesium was chosen for its lightweight and high strength-to-weight ratio. The cost was also a very big consideration for this choice
- **Battery**: PbAcid-1 batteries were selected for their reliability and cost efficiency. A configuration of 5 battery modules was used to achieve the necessary energy storage.

Table 2: Chosen Rover Specifications

Parameter	Chosen Specification
Motor	*speed_he*
Chassis Material	Magnesium
Battery	PbAcid-1
Number of battery Modules	5
Optimization Method	COBYLA

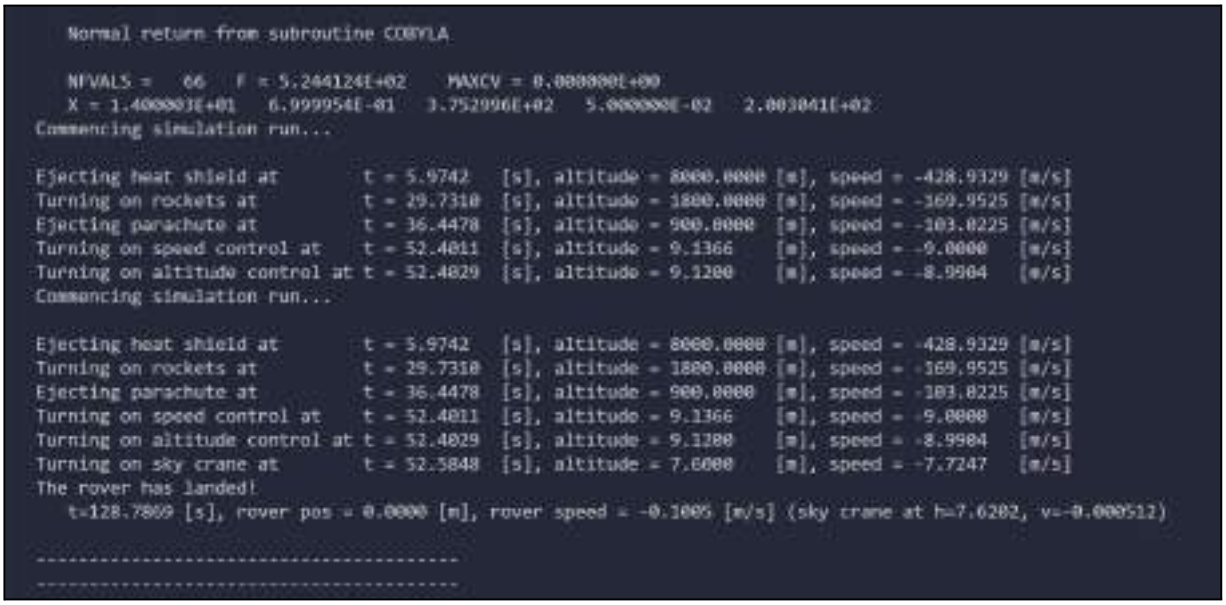

Figure 1: Rover Mission Timesheet

These results demonstrate the efficacy of the chosen design approach and optimization method. The design success highlights its capability to meet the heavy constraints of the Mars Mission.

Back to Contents

4. SEC Ignite Competition (3rd Place)

Summary

Our team competed in the Students Engineering Council's Ignite competiton Aerospace-Mechanical Track to develop a simulation of a landing rocket, where my team achieved 3rd place of 50+ teams. I worked to develop our control system simulation and organize much of the team collaberation.

Contributors: Eduardo Burciaga-Ichikawa, Kalen Jaroszewski, Julia Sopala, and Ian Wilhite

Key Skills: Computational Fluid Dynamics (CFD), Finite Element Analysis (FEA), Model Predictive Control (MPC), Numerical Methods, Simulation, Technical Writing, Team Collaboration, Project Management.

Relevance: This project showcases the ability to apply advanced engineering principles in a competitive environment, demonstrating skills in simulation, control system design, and technical communication.

Final Report:

Development of a Rocket Landing Simulation Using a Gimbal and Landing Gear

Eduardo Burciaga-Ichikawa, Kalen Jaroszewski, Julia Sopala and Ian Wilhite

Ignite Design Challenge

November 23, 2024

Table of Contents

Introduction **3**
Problem **4**
Background 4
Purpose 4
Design Criteria 5
Solution **6**
Overview 6
Material Selection 6
Gimbal 6
Landing Gear 8
Nose Cone 9
Landing Controls 10
Conclusion **14**
References **16**

Introduction

This paper explores the development of a rocket landing simulation that aims to enhance the landing efficiency and stability of the rocket landing vertically. Designing efficient and reliable landing systems for rockets remains a crucial challenge to safely and consistently land a rocket. The rocket explored in this paper has been modified to reduce mission costs and play a significant role in advancing reusable space technology. The design implemented gimbals for thrust vector control and robust landing gear systems, along with a redesign of the nose cone to realistically model the rocket that would go through both launching and landing. The design leverages gimbal systems to dynamically adjust thrust direction, ensuring precise control of the rocket's orientation during descent. Additionally, including landing gear improves stability upon touchdown, mitigating the risk of tip-over or damage. This solution addresses two fundamental challenges in rocket landings: maintaining attitude control during descent and ensuring structural integrity upon contact with the ground. By tackling these issues, the design enhances the reliability and efficiency of rocket recovery systems, paving the way for advancements in reusable rocket technology.

Problem

Background

The challenge of landing a rocket upright is both a technical and operational problem central to modern aerospace engineering. Traditional expendable launch systems discard hardware after a single use, driving up costs and limiting the efficiency of space exploration and transportation. In contrast, successful vertical landings of reusable rockets can drastically reduce costs and environmental impact. In industry, notable companies like SpaceX and Blue Origin have pioneered reusable rocket technology by implementing advanced systems such as thrust vector control (TVC) and deployable landing gear **[1]**. These technologies enable rockets to correct their attitude during descent and safely absorb impact upon touchdown. Thrust vector control, often achieved through gimbaled engines, allows for fine-tuned adjustments to the rocket's trajectory. Additionally, landing gear equipped with damping mechanisms ensures stability during landing, even on uneven surfaces.

Research highlights the complexities of balancing stability, accuracy, and robustness. For example, Reuben Ferrante illustrates how gimbal systems contribute to minimizing drift during descent while investigating computational methods for simulating controlled landings **[1]**. A second project that influenced the use of gimbals and a redesign of the nose cone is a launch report from the AIAA Regional Student Conferences which tested the launch of a rocket by replacing the fins with a gimbal **[2]**. These advancements inspire our approach to integrating gimbals and landing gear into a simulation that accurately models the dynamics of a rocket landing while implementing a better thrust-to-weight ratio **[3]**.

Purpose

Landing a rocket upright is a valuable problem to solve due to its implications for cost efficiency, safety, and the feasibility of sustainable space exploration. The difficulty lies in maintaining stability during descent and ensuring a secure touchdown on varying terrains. Without reliable control mechanisms, rockets risk instability, which can lead to mission failure, loss of valuable hardware, and environmental hazards.

This problem affects industries and organizations striving to make space travel more accessible. Reusable rockets can significantly reduce the cost of payload delivery, increasing accessibility to orbital applications for research institutions, private companies, and governments.

Design Criteria

To address the problem quantitatively, our team established the following design criteria:

1. **Stability During Descent:** The rocket must maintain an upright orientation with minimal angular drift, measured as the deviation from vertical (in degrees).

2. **Landing Controls:** The code for the rocket simulation must result in a zero velocity when altitude approaches zero, while maintaining stability to disturbances that can occur during landing.
3. **Impact Absorption:** The landing gear should effectively dampen forces upon touchdown to prevent structural damage, quantified by measuring landing impact forces (in Newtons).
4. **Minimized Mass:** No amount of material should be carried needlessly. All parts should be designed to perform their purpose with the minimum amount of additional material, and of the lightest possible material.

Solution

Overview

Our solution to the problem of landing a rocket upright integrates three key mechanical components: gimbal implementation, landing gear addition, and a nose cone redesign. The material these parts are manufactured from also plays an important role and has been considered carefully. Finally, vertical landing requires robust controllers in both the vertical axis and in the gimbal that can accommodate disturbances introduced from a variety of sources.

Together, these elements address the critical challenges of stability, precision, and impact absorption, as defined in our design criteria. Each component has been developed with an emphasis on efficiency, reliability, and adaptability to ensure successful landings under various conditions.

Topic 1: Material Selection

AISI 321 Annealed Stainless Steel SS

Property	Value	Units
Elastic Modulus	1968040.273	kgf/cm^2
Poisson's Ratio	0.27	N/A
Tensile Strength	6322.201972	kgf/cm^2
Yield Strength	2390.422007	kgf/cm^2
Tangent Modulus		kgf/cm^2
Thermal Expansion Coefficient	1.7e-05	/°C
Mass Density	0.0080000001	kg/cm^3
Hardening Factor	0.85	N/A

Figure 1: Material Properties of AISI 321

Stainless steel was selected for numerous reasons. The most significant factor is the ability to maintain a high yield strength at increasing temperatures. Compared to 6061 Aluminum, AISI 321 stainless steel is significantly heavier and more expensive. The thrust from the engines was adequate to compensate for the additional mass, while the ability to withstand higher temperatures accounted for the additional price. The need to withstand high temperatures is very important as the rocket will travel above the speed of sound. The choice of stainless steel for large rockets has been proven with the most notable example being SpaceX Starship.

Topic 2: Gimbal Implementation

Gimbal systems are crucial for thrust vector control, enabling the rocket to adjust its trajectory during descent. By tilting the engine's thrust direction relative to the rocket's center of mass, gimbals allow for fine-tuned corrections to stabilize orientation and counteract disturbances such as wind or uneven terrain below.

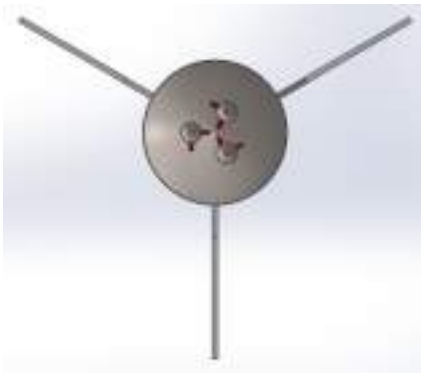

Figure 2: Bottom and side view of the gimbal engines at the base of the rocket

Design Approach

The design incorporates three thrusters mounted on gimbals, which adjust the orientation of each thruster to dynamically control the thrust vector based on real-time feedback from onboard sensors. A proportional-integral-derivative (PID) controller processes data from gyroscopes and accelerometers to maintain vertical alignment, minimizing angular drift even under external disturbances. Stability is further enhanced by strategically positioning the fins, as seen in **Figure 3**, and ensuring the center of pressure is located behind the center of gravity, promoting aerodynamic balance throughout descent. The three engines are designed around the specifications of Raptor V3 with a slightly heavier gimbal. The red linkages are hydraulic actuators for thrust vector control. The first of the orthogonal actuators is for the x position, while the other is for the y position. Three engines are used as this would allow for finer control in series with the gimbal to increase the precision of control.

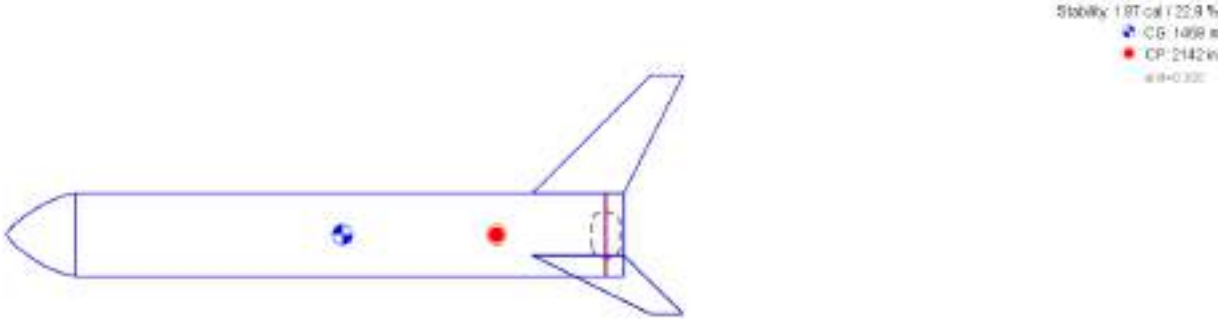

Figure 3: OpenRocket Simulator modeled rocket.

Topic 3: Landing Gear Addition and Topology Optimization

Landing gear provides critical support to absorb impact forces and stabilize the rocket upon touchdown. The design incorporates collapsible legs with shock-absorbing mechanisms to prevent tipping or structural damage.

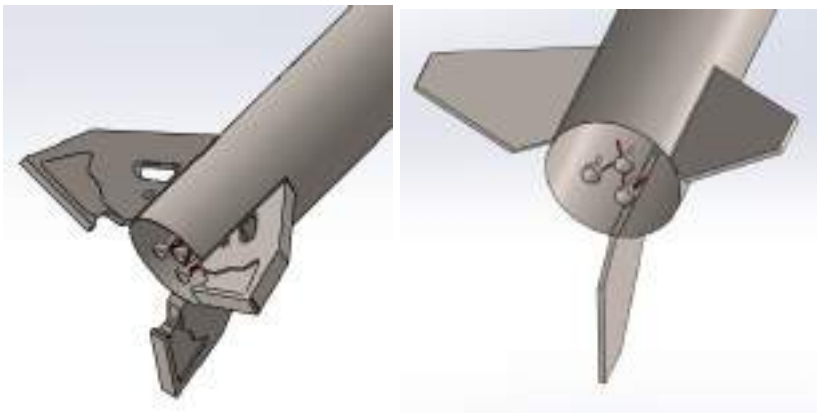

Figure 4: Isometric view of the original landing gear/fins vs final design

Design Approach

The landing gear consists of stainless steel fins equipped with pneumatic dampers that compress upon impact to dissipate energy. The legs are arranged around the rocket's base to maximize stability and are foldable to minimize drag during ascent. In the future, the system should also include footpads designed to distribute forces evenly, even on uneven terrain.

Implementation and Results

Using SolidWorks Topology Optimization, the design space was iteratively refined to remove unnecessary material while retaining the structural integrity required to support the calculated loading weight. The final design achieves a 28% weight reduction with respect to the base mold while meeting all performance criteria for impact absorption validated through FEA with a Factor of Safety of 8.3, as seen in **Figure 5**.

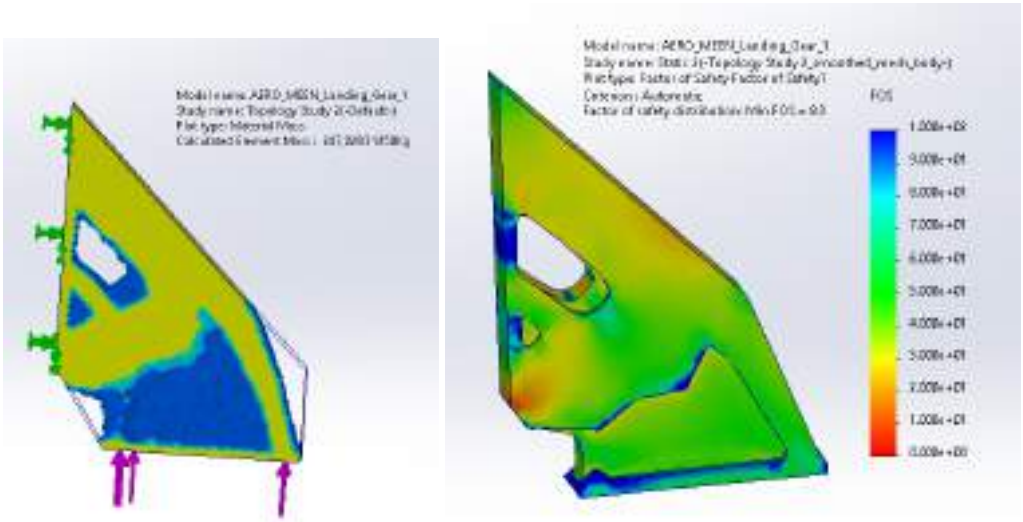

Figure 5: Landing gear topology and FEA analysis

Topic 4: Nose Cone Re-design and Computational Fluid Dynamics (CFD)

The nose cone plays an essential role in aerodynamics during ascent and stability during descent. By optimizing its shape and material properties, we improved its performance in both phases of flight.

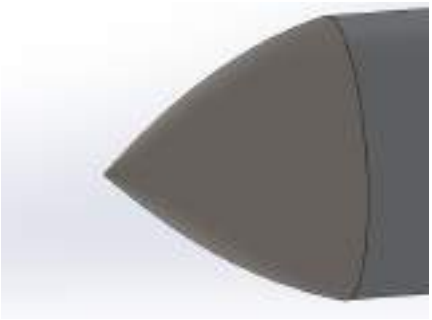

Figure 6: 3/4 Parabolic nose cone design, side view

Design Approach

The redesigned nose cone (**Figure 6**) features a 3/4 parabolic shape that minimizes drag during ascent and promotes aerodynamic stability during descent. The 3/4 parabolic shape is one of the most efficient shapes at supersonic speeds [7]. The nose cone also houses sensors that work in conjunction with the gimbal system to monitor wind patterns and atmospheric conditions.

Implementation and Results

Using SolidWorks' Flow Simulation, the nose cone design was tested at standard flight conditions during the ascent stage (500 m/s). Compared to the cone design, the new nose cone

resulted in a 12.5% reduction in drag forces and a lower distribution of pressures at the nose cone caused by the supersonic flows, as seen in **Figure 7**.

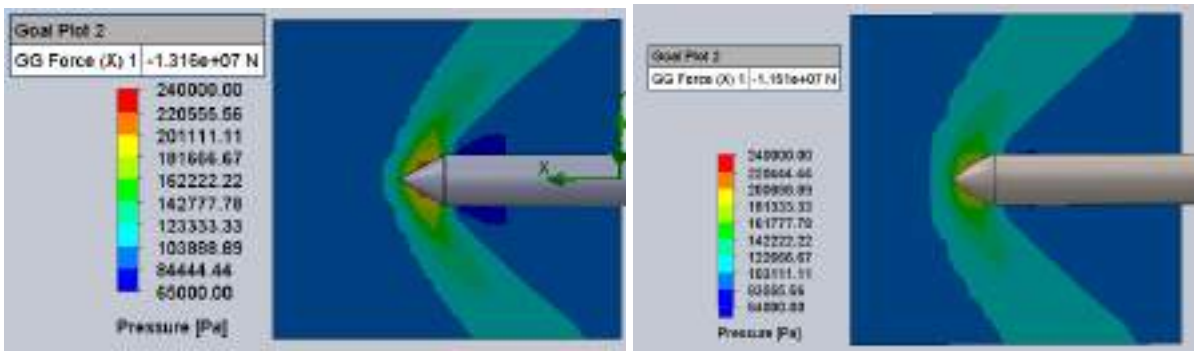

Figure 7: Nose cone CFD analysis of old vs final design at supersonic speeds

Additionally using CFD, the coefficient of drag was calculated from the model by using the coefficient of drag equation and the drag forces. The flow was directed upward from the bottom of the rocket to simulate the downward movement upon descent at 50 m/s. This resulted in a coefficient of drag of 1.427 (**Figure 8**), which was used for the trajectory simulations.

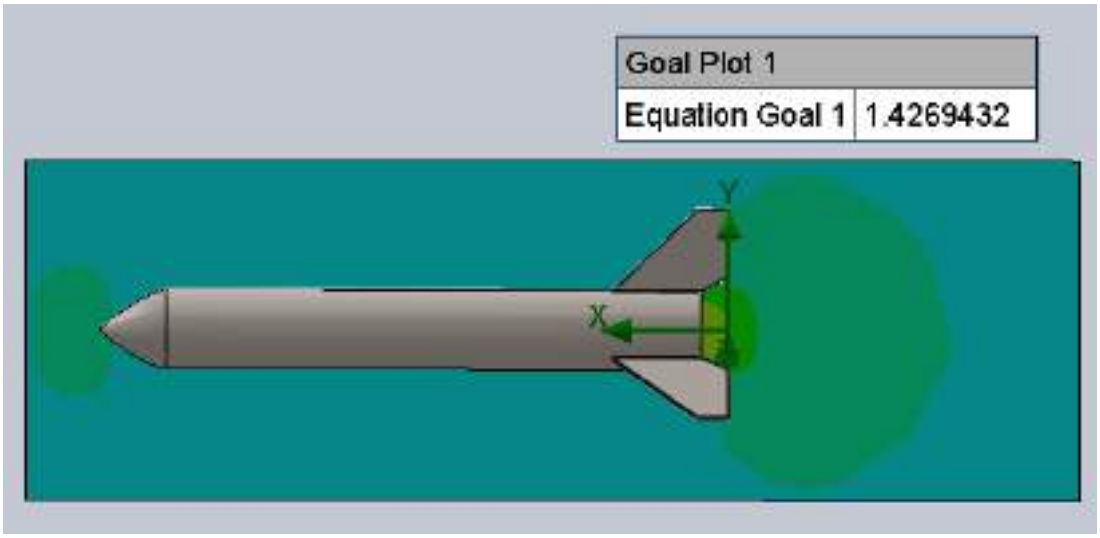

Figure 8: CFD of the rocket in descent & drag coefficient

Topic 5: Landing Controls

The control algorithm for the descent and landing process is a crucial element of the success of a rocket's performance. The descent must be controlled, feasible, and minimize the normal force of landing applied to the rocket as it touches down. There are many factors that could be considered, including but not limited to fuel efficiency, landing time, peak force minimization, thruster performance accommodations or acceleration constraints. Regardless, a solution

focusing on optimization would require an in-depth cost function analysis of these parameters. Solving for an optimal solution to this very complex problem **[6]**; however, for the scope of this report, only feasibility and force minimization will be considered.

```
# --- Constants Section ---
g = 9.81  # Acceleration due to gravity in m/s^2
mass = 685000 # mass in kg
Cd = 1.427  # Drag coefficient from CFD simulation
rho = 1.225  # Air density at sea level in kg/m^3
A = 0.5 # Cross-sectional area of the rocket in square meters
engine_thrust = 3.2*1000000 # thurst per engine
num_engines = 3 # number of engines
```

Figure 9: Rocket landing forces script inputs

```
Rocket Landing Forces:
Time to touchdown: 36.60 [s]
Touchdown Velocity: 0.190 [m/s]
Deceleration during landing: 0.018 [m/s^2]
Impact Force: 6.732 [MN]
Normal Force at landing: 13.452 [MN]
Net Power Applied 75.744 [GW]
```

Figure 10: Rocket landing forces script output

Design Approach

The landing controls system ensures the rocket maintains stability and lands upright by processing real-time sensor data to dynamically adjust thrust and orientation. This system combines a model representing a stable hover with an error-driven controller that integrates feedback from onboard sensors with control algorithms, enabling precise adjustments to gimbals and thrusters during descent. This system demonstrates effective landing in reasonable conditions with a minimal touchdown velocity **[Figure 10]**.

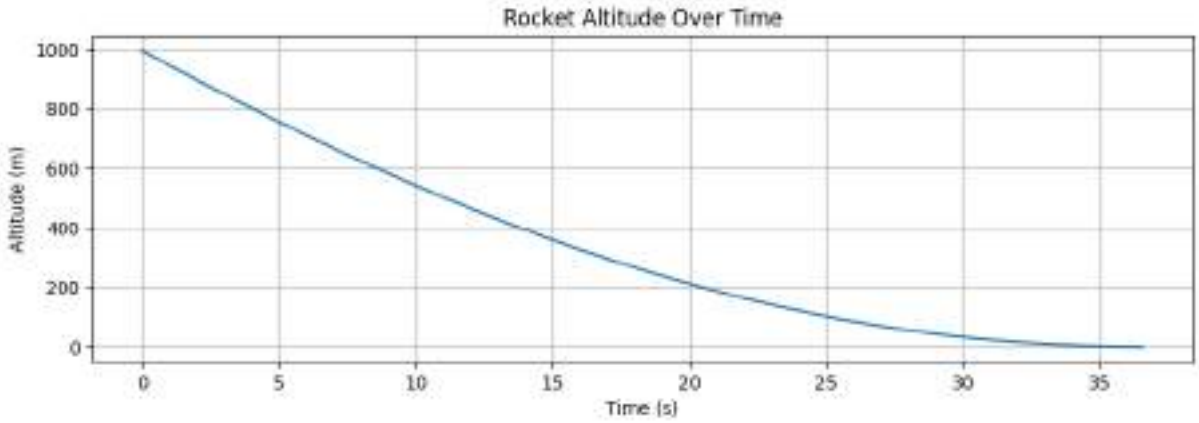

Figure 11: Simulated rocket altitude while landing

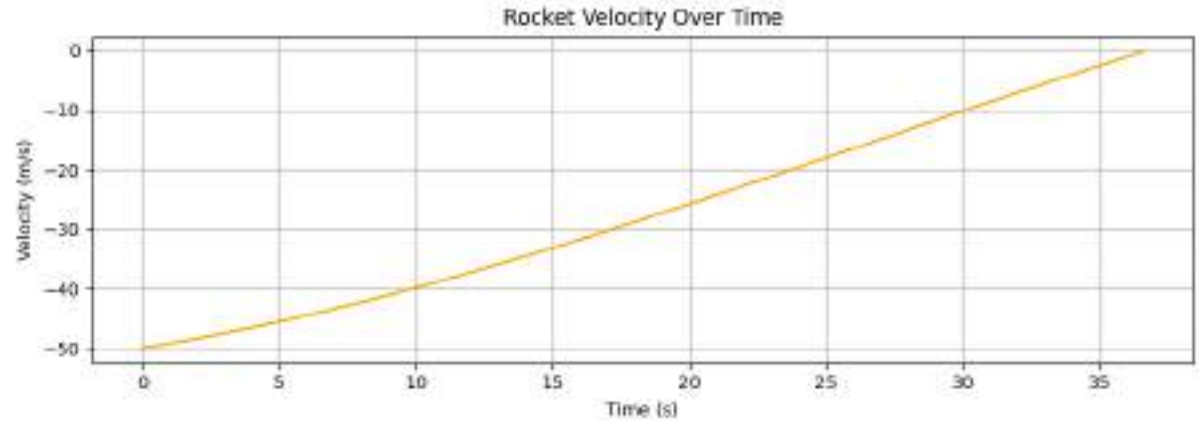

Figure 12: Simulated rocket velocity while landing

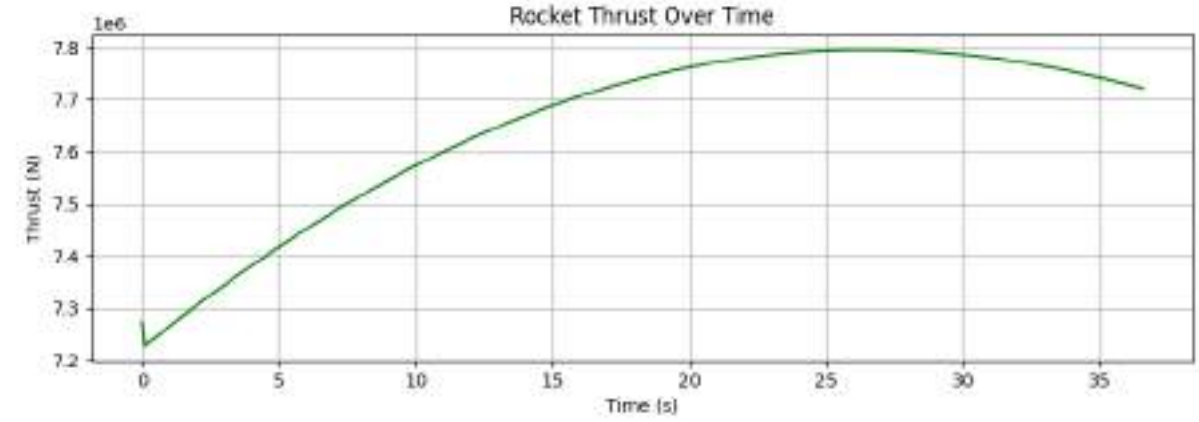

Figure 13: Simulated rocket thrust while landing

Altitude Control Algorithm Design

The control system is based on a Hybrid Controller or Model Predictive Controller (MPC) containing both a model term and an error-driven term. The model term is based on precalculated values known about the object being controlled and its current position, whereas the error-driven Proportional-Integral-Derivative (PID) controller element processes data from accelerometers, tachometers, and altimeters to correct the actual differences between setpoints and real-time measured outputs **[Figure 9]**, **[Figure 10]**. The model calculates the thrust required to maintain the current velocity by accounting for the weight and drag forces known, and the PID algorithm calculates the necessary adjustments to the thrust output to account for all variance from equilibrium. This system has advantages over purely Model Driven approaches as it can account for disturbances during flight to ensure that disturbances cannot accumulate into large errors. This system has advantages over purely error-driven approaches as the model accounts for a majority of the thrust required, and the PID controller can be more narrowly refined to account exclusively for the adjustments to the model **[Figure 11], [Figure 12], [Figure 13]**. This system will likely have a marginally slower refresh rate as compared to either of the previously discussed approaches, however, the increased reliability and performance would consistently outperform the alternatives **[4]**.

The starter code provided the foundations for solving the dynamics problem while leaving the controller open-ended, with a bias towards an open-loop controller with no feedback **[9]**. The solution implemented has the advantage of resilience towards disturbances.

Gimbal Control Algorithm Design

The gimbal control system would be based purely on an error-driven PID controller, which processes data from gyroscopes, accelerometers, magnetometers and an Internal Measurement Unit (IMU) to minimize the error between the current state of the rocket and the neutral vertical position. The PID algorithm calculates the necessary adjustments to the gimbals to maintain vertical alignment and counteract external forces such as wind or drift. This system does not require a model driven element in the current application as it is meant to purely maintain the stability of the flight. If a model were to be implemented in this system, it would be based on a two-dimensional inverted pendulum, for which each axis could be solved independently **[5]**. This kind of extended functionality would allow for horizontal displacement correction, allowing for precise control over the location of landing.

Conclusion

The challenge of safely and efficiently landing a rocket upright is pivotal in advancing reusable spaceflight technology. Our solution integrates three key innovations: gimbal implementation for thrust vector control, landing gear to absorb impact forces and maintain stability, and a redesigned nose cone for improved aerodynamics and sensor integration. Together, these components address the critical design criteria of stability during descent, precision of landing, and effective impact absorption, demonstrating a holistic approach to solving this complex engineering problem.

Challenges and Lessons Learned

Throughout the project, the team faced several challenges, including balancing lightweight designs to durability, ease of simulation and accuracy, and accurately simulating real-world conditions. The team also had to work on parallel development and understanding how one layer of analysis affected the others. For example, as we were performing the Computation Fluid Dynamics, we realized that an error meant that there was a slightly different drag coefficient, and we needed to retune the PID controller for this new value. Many times in industry, this kind of thing will happen, and this experience demonstrates the need for organized planning and coordination for dependent processes.

Overall, these challenges highlighted the fundamentally interdisciplinary nature of many classically-disciplined engineering challenges that occur in industry and research, while underscoring the importance of iterative testing, collaborative development and project planning.

From this experience, we learned to approach engineering problems systematically, breaking them into manageable components and validating each step through simulations. Additionally, we gained insights into how theoretical knowledge translates into practical design considerations.

Contributions

- **Ian Wilhite**: Designed the control algorithms for the landing, ensuring stable descent.
- **Eduardo Burciaga-Ichikawa**: Led the development of the landing gear, including material selection and impact testing, along with running topology and CFD analysis.
- **Kalen Jaroszewski**: Designed and tested the aerodynamic properties of the nose cone, integrating sensors for enhanced feedback.
- **Julia Sopala**: Consolidated data, and ensured alignment of all components with the design criteria and reporting it.

Room for Growth

Looking forward, next steps for the project could include a more in depth comparison of materials and consideration of design for manufacturing of parts, testing the design under more

variable environmental conditions, and prototyping scaled physical models for validation. The controllers could be expanded to utilize the varied power between the three thrusters, or to include drag manipulators like flaps. Testing could include further validity testing with the current altitude controller, and implementation of the gimbal controller and full system simulations. In implementing the ideas discussed, this system could become a reliable method for assisting rocket landing accuracy and improving affordability of space missions.

References

[1] R. Ferrante, "A robust control approach for rocket landing," *Theses Univ. Edinburgh,* 2017.

[2] C. Fang *et al.*, "Gru & Vector Gimbal Rocket Design and Launch Report," in *2024 Regional Student Conferences*, 2024, p. 85702.

[3] C. Trom, "Development of a vertically landed rocket design challenge for expanding the pipeline and enhancing education of students pursuing careers in space," University of Illinois at Urbana-Champaign, 2022.

[4] Z. Hou and Z. Wang, "From model-based control to data-driven control: Survey, classification and perspective," *Information Sciences*, vol. 235, pp. 3–35, 2013, doi: 10.1016/j.ins.2012.07.014.

[5] İ. Yiğit, "Model free sliding mode stabilizing control of a real rotary inverted pendulum," *International Journal of Control, Automation and Systems*, vol. 23, no. 10, 2015, doi: 10.1177/1077546315598031.

[6] C. Wang and Z. Song, "Trajectory optimization for reusable rocket landing," in *2018 IEEE CSAA Guidance, Navigation and Control Conference (CGNCC)*, Xiamen, China, 2018, pp. 1-6, doi: 10.1109/GNCC42960.2018.9019105.

[7] V. K. Shah, "Determination of the optimum nose cone geometrical shape for supersonic missile," Aerospace Science and Technology, vol. 133, 2023, doi: 10.1016/j.ast.2022.106774.

[8] A. Aboelhassan, M. Abdelgeliel, E. E. Zakzouk, and M. Galea, "Design and implementation of model predictive control based PID controller for industrial applications," *Energies*, vol. 13, no. 24, p. 6594, 2020, doi: 10.3390/en13246594.

[9] B. Borovic, A. Q. Liu, D. Popa, H. Cai, and F. L. Lewis, "Open-loop versus closed-loop control of MEMS devices: choices and issues," *Journal of Micromechanics and Microengineering*, vol. 15, no. 10, p. 1917, 2005, doi: 10.1088/0960-1317/15/10/018.

Back to Contents

5. Mechanical Modeling (Best Prototype Award)

Summary

The need was a toy for the elderly which could help preserve dexterity. Our team recieved the "Best Prototype" award out of 80 students.

- meen-210-Final_Project.pdf

Contributors: Astrid Garcia, Mckenzie McCain, Ryan Welty, Ian Wilhite

Key Skills: Mechanical Design, Computer Aided Design (CAD), SolidWorks, Finite Element Analysis (FEA), 3D Modeling, Technical Documentation.

Relevance: This project showcases the ability to design, model, and analyze mechanical components and assemblies using industry-standard software. It reflects a strong understanding of mechanical design principles.

FIDGET FUN

GROUP 13: MEEN 210-505
FALL '24 PROJECT

By Ryan Welty, Mckenzie McCain, Ian Wilhite and Astrid Garcia

THE TEAM

MEEN 210-505 FALL SEMESTER

IAN WILHITE

RYAN WELTY

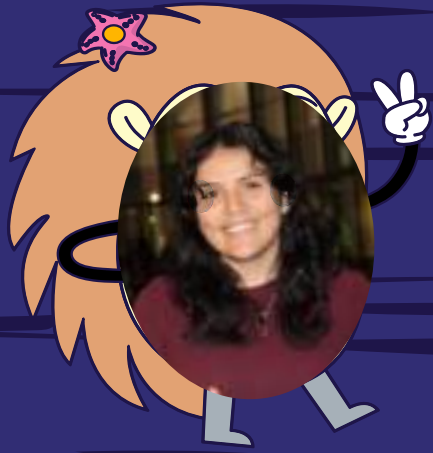

ASTRID GARCIA

MCKENZIE MCCAIN

VIDEO ADVERTISEMENT

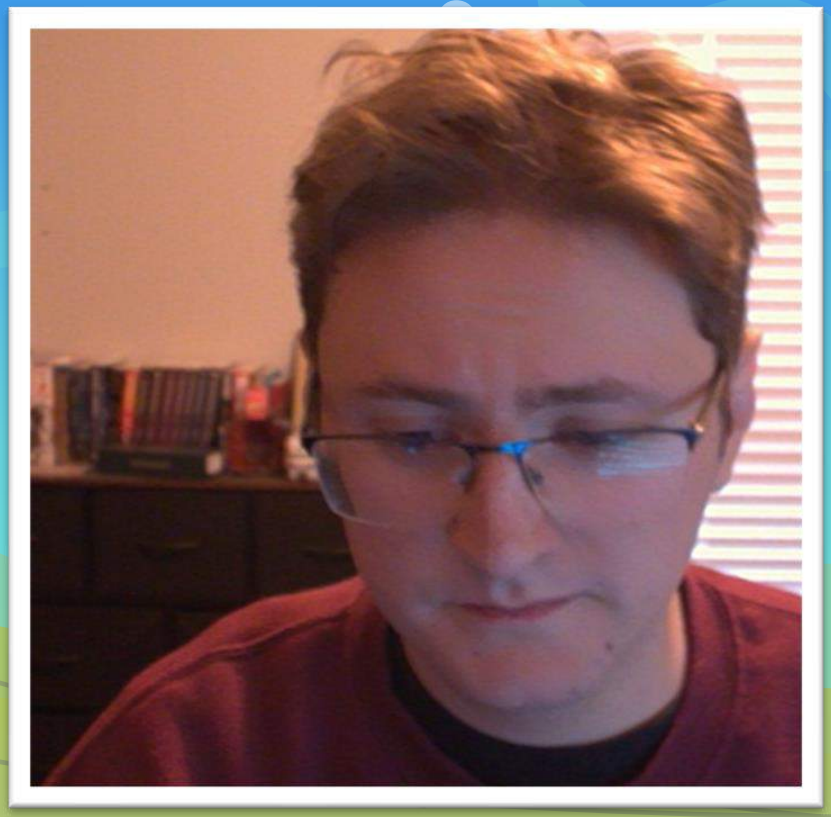

WHAT IS FIDGET FUN

A customizable, modular fidget toy that transforms into endless puzzle track configurations! Simply snap the pieces together, and let the magic unfold as a smooth ball glides along the creative paths you design.

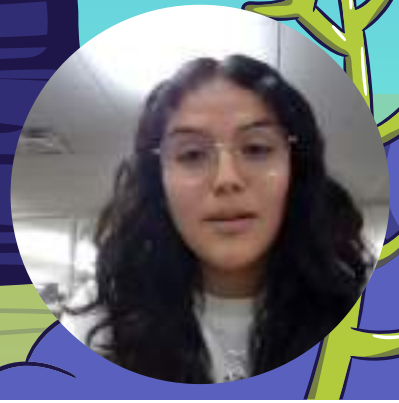

CONCEPTS

Elderly Toy Concept Design

Tuesday, September 17, 2024 6:51 PM

Topics: Maze + Geometry

1. marble game
2. bingo-related?
3. puzzle / puzzle box
4. magnet fishing
5. jigsaw
6. matching game
7. forming game

Requirements:

- ≥ ¼ non-trivial parts
- ≥ 1 3d printed part
- ≥ 1 moving parts

* can be powered by hand or motor

Moving Part Ideas

- spring-loaded mechanism
- rotating disk

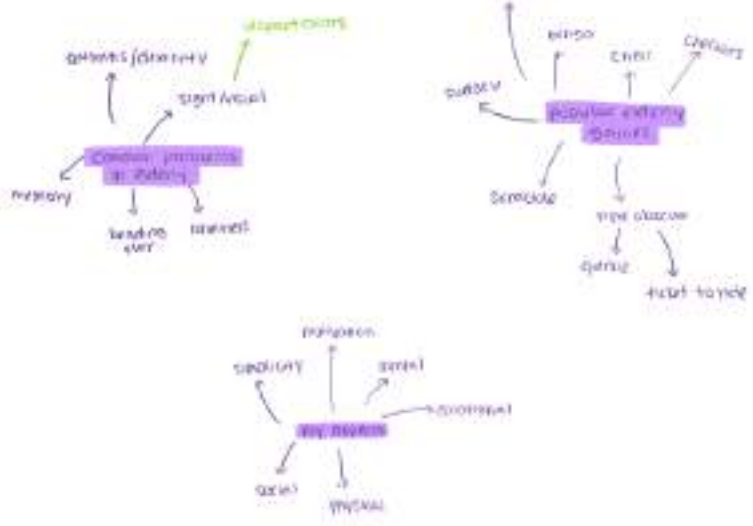

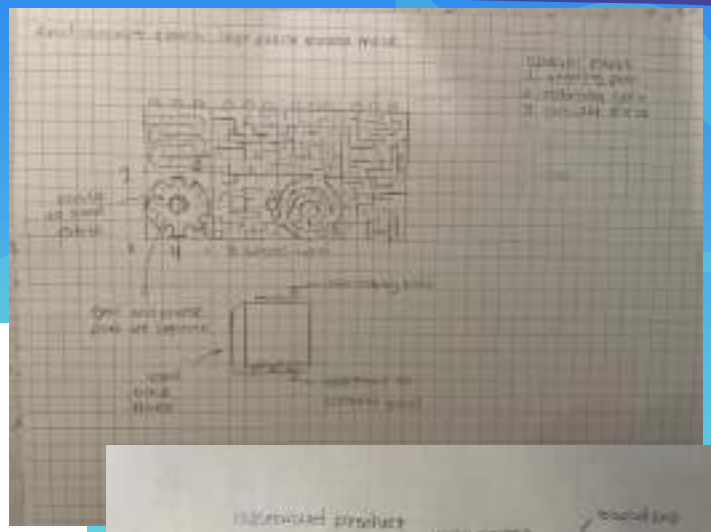

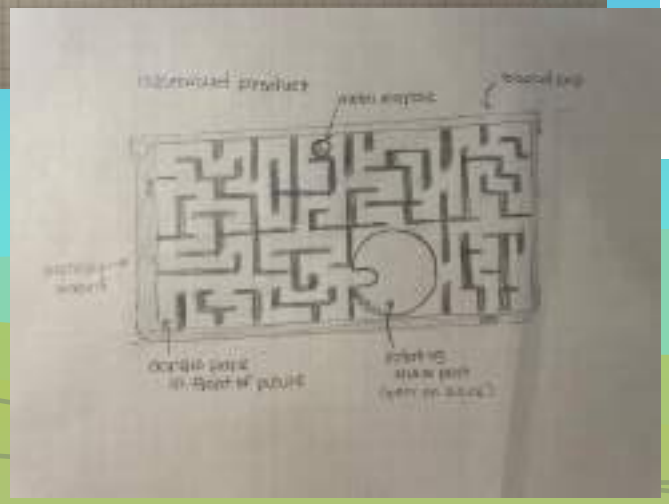

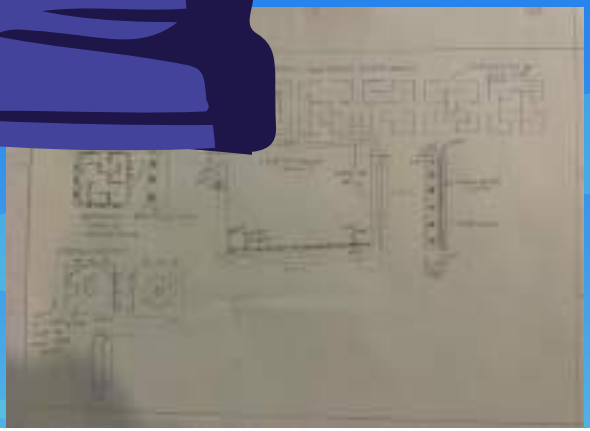

Elderly Toy Concept Design

Tuesday, September 17, 2024 6:51 PM

Topics: Maze + Geometry

1. marble game
2. bingo-related?
3. puzzle / puzzle box
4. magnet fishing
5. jigsaw
6. matching game
7. forming game

Requirements:

- ≥ ¼ non-trivial parts
- ≥ 1 3d printed part
- ≥ 1 moving parts

* can be powered by hand or motor

Moving Part Ideas

- spring-loaded mechanism
- rotating disk

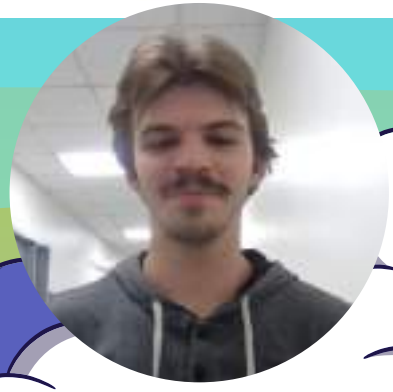

THE PRODUCT

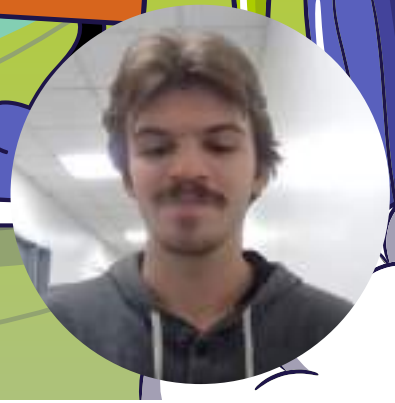

PROBLEM & NEEDS

"My grandma loves gardening, reading, and solving puzzles. Recently, she has started noticing changes. Her hands feel stiff when she tries to grab plates from the cabinets or even when she goes to grab her favorite book. She has also noticed that she often forgets where she places her keys and has found it hard to concentrate for long periods of time. This has begun to make her sad and frustrated because her body doesn't work the way it used to. She needs something that will engage her mind and helps her feel calm and in control"

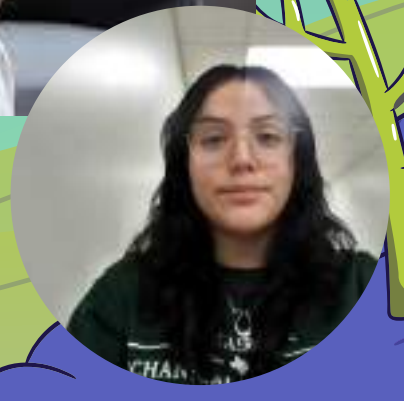

PROBLEM & NEEDS

Target Audience

- Intended for anyone in the elderly age range group, someone 65 years or older. Although it is not restricted to just this age group. This product is also intended for people suffering from medical conditions such as Alzheimer's or dexterity /mobility issues.

Why & How would they use your product?

- Why: Fun, colorful, and easy to use!
- How: Just snap the pieces together and watch the ball glide through the path

Needs Statement

•Engaging mental stimulation
•Price-conscious
•The key aspects should include topics: social, physical, mental, or emotional
•Accommodating to elderly individuals
•Intuitive gameplay mechanics

•Based off the project outlines from milestone 0, we were able to produce our needs statement

ENGINEERING REQUIREMENTS

Design Components:

- Block Width
- Block Thickness
- Ball Diameter (from stock ball bearing)
- Tolerance around ball
- Length of pegs
- Depth of path

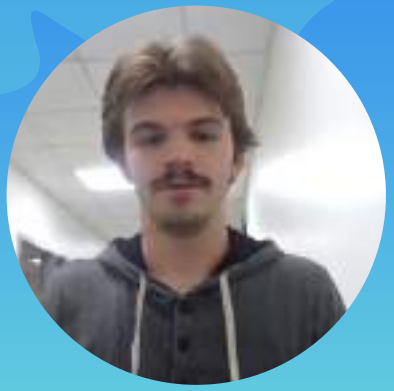

Name	Value / Equation
Global Variables	
"block_width"	= 100mm
"block_thickness"	= 15mm
"ball_dia"	= 0.25in
"ball_tol"	= 2mm
"peg_dia"	= 6mm
"peg_tol"	= 1mm
"patt_offset"	= 3mm
"peg_len"	= 10mm

MODELING

Animated Exploded View of Fidget Fun Assembly

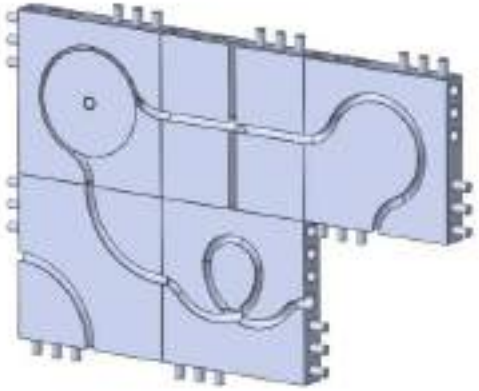

FABRICATION PROCESS

MACHINE USED: Creality K1 3D printer
MATERIAL: Smooth PLA
Washer & Screw
23 hr print time, 310.96 grams
Same scale print
Conformity :

- The washer and screw
- The tolerance
- Size of ball bearing
- Scratched board design
- Orientation of the plates

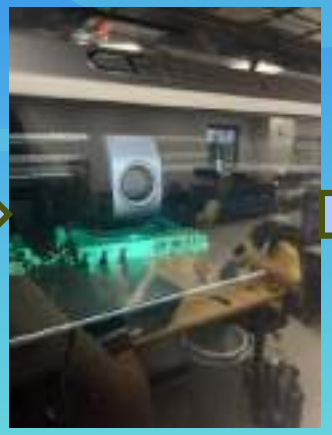


THANKS AND GIG EM'

Back to Contents

6. Mechanical Measurements

Summary

This section includes a technical memorandum from the Mechanical Measurements course (MEEN 260).

- meen-260-memo.pdf

Contributors: Ian Wilhite (Solo Project)

Key Skills: Data Acquisition, Instrumentation, Sensors, LabVIEW, Signal Processing, Technical Writing, Experimental Analysis.

Relevance: This document demonstrates hands-on experience with experimental setups, data acquisition systems, and the analysis and presentation of experimental results in a professional format.

MEEN 260-908

3/23/2025 **To:** Dr. Heather Lewis

From: Ian Wilhite, *ICW*

Subject: Experimental natural frequency analysis

Abstract

In many mechanical systems that undergo typical harmonic excitation, vibrations are inevitable. Engines, buildings, and generators all undergo some type of vibration and oscillation and must determine the extent that harmonic excitation may impact a system, and therefore engineers need a robust methodology to numerically determine and experimentally verify the natural frequency of their system. In this experiment we seek to predict and experimentally verify the natural frequency of vibration for the mechanical systems provided. The beam's dimensions were measured, and the Virtual Instrument (VI) in LabVIEW captured displacement traces under different loads [1]. Calculated damping ratios, logarithmic decrements, and natural frequencies were compared against theoretical values derived from beam theory. Experimental natural frequencies for both deflection magnitudes averaged 93.79 rad/s, while the theoretical value was 167.95 rad/s. A 95% confidence interval and two-sample t-test confirmed consistency across both trials. Furthermore, linear regression was used to calibrate strain measurements and predict an unknown weight, validating the effectiveness of the calibration process. Sources of error in the collected values of the traces include calibration uncertainty, temperature fluctuations, and sensor noise. Results deviated from theoretical predictions, likely due to accumulation of sources of error in measured values and sensor calibration for experimental values. This reiterates the importance of analysis on the vibrations of harmonically excited mechanical systems and the impacts that those vibrations can have on the performance and life cycle of those systems. Future work could include additional trials to mitigate the impact of inconsistencies in trials and analysis on additional peaks pending on the noise in the sensors used to measure amplitude.

Introduction

The experiment performed is designed to analyze the effects of the vibrations in a cantilevered beam. These vibrations, if not properly accounted for, can lead to fatigue, noise, inefficiency, or catastrophic failure in components ranging from engine mounts and turbine blades to bridges and aerospace structures. Understanding the methodologies to predict the natural frequency is essential to many oscillating systems which receive harmonic excitation including engines, heavy machinery, and large structures [3]. In this experiment, the cantilever beam's dimensions were measured to calculate the equivalent

system mass and area moment of inertia across the axis of deflection. These processes rely on the generated trend between collected datapoints, which

The Virtual Instrument (VI) in LabVIEW was utilized to capture the displacement of the beam under loading conditions [1]. The experimentally found traces were used to calculate the logarithmic decrement, damping ratio, and natural frequency for the vibrations under small and large deflection. The theoretical natural frequency was determined using beam theory and compared to the experimental values obtained from the displacement traces. A 95% confidence interval was constructed to find the bounds of the natural frequency. Similarly, various masses were applied, and the deflection of the beam was determined. Then a trendline was created and used to predict an unknown mass. This process highlights the validity of the sensors and data collection processes, and their ability to verify the calibration and determine the predictive value in the data collected.

Procedure

First the properties of the beam should be found including length, width, and thickness of the cantilever beam. The material should be noted so that the material properties can be referenced later.

$$M_e[kg] = 0.23 * M_{beam}[kg] + m_{applied}[kg] \quad (1)$$

The equivalent mass can be found using Equation (1), which requires the mass of the beam and the mass applied to the end of the beam. The area moment of inertia for the beam can be found applying Equation (2) using the base width of the beam and the height of the beam.

$$I_{area}[m^4] = \frac{1}{12} b[m] * (h[m])^3 \quad (2)$$

Using the known properties of the beam, we can apply beam theory to determine the natural frequency of oscillation using Equation (3).

$$\omega_n \left[\frac{rad}{sec}\right] = \sqrt{\frac{3EI}{M_e l^3}} \left[\frac{rad}{sec}\right] \quad (3)$$

Where omega is the undamped natural frequency of the beam in unit radians per second, E is Young's modulus of the beam material in unit pascal, I is the area moment of inertia of the beam cross-section in unit meter to the fourth, Me is the equivalent system mass in kilograms, which accounts for the effective mass of the cantilever beam in vibration, and l is the length of the bar in meters.

Using the known masses, the gauge can be calibrated to accurately measure the displacement of the beam. For the first trial, we displaced the beam a small amount and recorded the displacement over time for the vibration until the displacement amplitude decayed to equilibrium. For the second trial, we displaced the beam a large amount and similarly recorded the displacement over time for the vibration of the beam. From the data, we extracted the peak amplitudes and the time at which they occurred, then applied Equation (4) to determine the logarithmic decrement of the system.

$$\delta = \frac{1}{n}\ln\left(\frac{x_n}{x_{n-1}}\right) \tag{4}$$

The damping ratio could then be calculated using the logarithmic decrement between each pair of peaks using Equation (5).

$$\xi = \frac{\delta}{\sqrt{4\pi^2 + \delta^2}} \tag{5}$$

In order to construct a confidence interval for each parameter, the t-score must be identified for the scenario. To construct a 95% confidence interval, we identify that for six measured peaks, there are five found logarithmic decrement values, five damping ratios, and five natural frequencies calculated, therefore, to construct a confidence interval, we identify that there are four degrees of freedom and an alpha value of 0.05. We can then use Equation (6) to determine the confidence intervals for the natural frequency of the small and large excitations.

$$CI = \bar{x} \pm t\frac{s}{\sqrt{n}} \tag{6}$$

Using the damped natural frequency and the known eta value, the natural frequency can be experimentally determined for each of the trials known. The relationship between damped and undamped natural frequency is given traditionally by Equation (7).

$$\omega_d = \omega_n\sqrt{1-\xi^2} \tag{7}$$

Which can be rearranged into a form more useful for analysis as seen in Equation (8).

$$\omega_n = \frac{\omega_d}{\sqrt{1-\xi^2}} \tag{8}$$

Using the relationship provided for the natural frequency in Equation (8), the propagation of uncertainty can be applied to determine the uncertainty of the experimental natural frequency using Equation (9) [2][4].

$$\delta\omega_n = \sqrt{\left(\delta\omega_d * \frac{\partial\omega_n}{\partial\omega_d}\right)^2 + \left(\delta\xi\frac{\partial\omega_n}{\partial\xi}\right)^2} = \sqrt{\left(\delta\omega_d * \frac{1}{\sqrt{1-\xi^2}}\right)^2 + \left(\delta\xi * \omega_d\frac{-\xi}{(1-\xi^2)^{-\frac{3}{2}}}\right)^2} \tag{9}$$

In the second part of the experiment, strain measurements were taken as known weights were incrementally applied to the cantilever beam. Using the "Lab04-PartB.vi" file in LabVIEW, the strain (in Ohms) was recorded for masses of 0g, 50g, 100g, 120g, 150g, and 200g. After all known weights were measured, an unknown mass was applied and its strain recorded. These data points were used to perform a linear regression in Excel, enabling the prediction of the unknown weight.

Results and Discussion

The primary goal of the first part of this experiment was to determine the natural frequency of a cantilever beam and compare theoretical predictions with experimental

measurements. The data obtained from small and large displacement traces were utilized to calculate logarithmic decrement, damping ratio, and natural frequency.

Table 1: Material properties for the cantilever beam.

Characteristic	**Value**	**Unit**
Material	Steel	n/a
Width	51.17	mm
Thickness	1.56	mm
Length	22.3	cm
Moment of Inertia	1.619*10^-11	m^4
Density	7.85	g/cm^3
Youngs Modulus	207*10^9	Pa
Mass	139.7	g

As shown in Table 1, the beam was made of steel with a width of 51.2 mm, a thickness of 1.56 mm, and a length of 22.3 cm. Using beam theory and Equation (3), the theoretical natural frequency was calculated as167.95 rad/s.

Table 2 and Table 3 summarize the extracted peak amplitudes, time intervals, and calculated parameters from the vibration traces.

Using the experimentally determined damped frequency and damping ratio, the natural frequency can be experimentally determined for each trial, which is displayed in Table 2.

Table 2: Trace natural frequencies and confidence intervals

Trace	**Natural Frequency (rad/s)**	**Uncertainty (rad/s)**	**Confidence Interval**
Small displacement	93.79	1.229	(92.56, 95.02)
Large displacement	93.79	1.229	(92.56, 95.02)

From Table 1, the mean natural frequency for the small displacement trace was 93.79 rad/s with a standard deviation of 0.99 rad/s. The mean damping ratio was calculated as 0.0035, and the logarithmic decrement was found to be 0.0193.

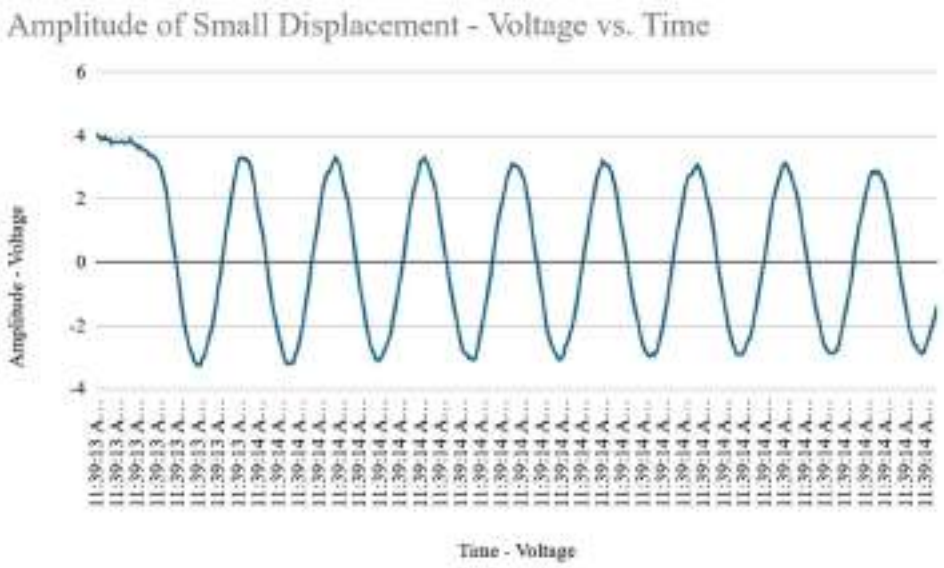

Figure 1: Amplitude of small excitation

For the large displacement trace, the mean natural frequency remained 93.79 rad/sec with a standard deviation of 0.99 rad/sec. The damping ratio and logarithmic decrement were calculated to be 0.0031 and 0.0193, respectively.

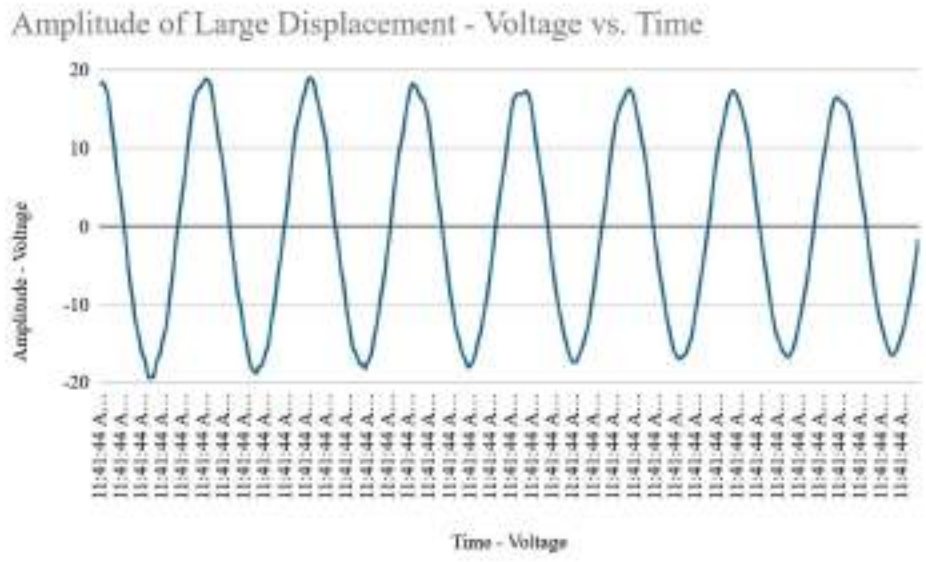

Figure 2: Amplitude of large excitation

A two-sample t-test was performed to determine whether the natural frequencies obtained from the small and large displacement traces were statistically different. The test yielded a t-value of 0.0595, which was less than the critical value of 2.306 for a 95% confidence level and 8 degrees of freedom. Therefore, we fail to reject the null hypothesis, indicating that the two frequencies are statistically equivalent.

The theoretical natural frequency of 167.95 rad/sec deviated significantly from the experimentally determined value of 93.79 rad/sec for both small and large displacements. This difference indicates many sources of error.

After applying the masses to the beam, the resistance values were determined for various masses applied and presented in Table.

Table 3: Summary of found values.

Mass (grams)	Resistivity (Ohms)
0	-0.00370511
50	-0.00367987
100	-0.00365754
120	-0.00365266
150	-0.00363531
200	-0.00361276

The collected data from Table 3 was then plotted in Figure 3 and a trendline plotted.

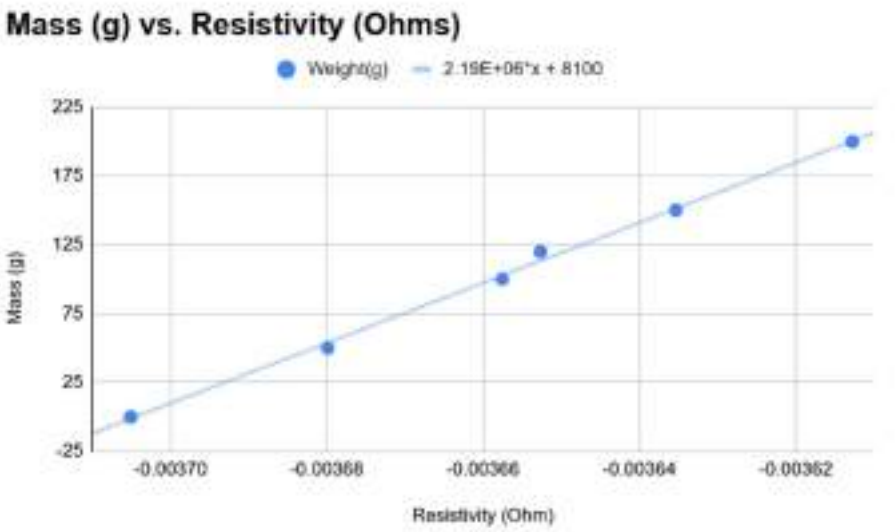

Figure 3: Plotted experimental mass over resistivity

The strain measurements under known weights produced a highly linear relationship (R^2 = 0.996) shown in Equation (10), validating the strain gauge's consistency in the static loading scenario. Using the linear regression model, the unknown mass was predicted with high accuracy, demonstrating the practical utility of the gauge system in low-frequency or static load measurements.

$$W[g] = 2.19 * 10^6 * R + 8100 \quad (10)$$

The unknown strain measurement of -0.00357253 ohms was input into the regression equation, yielding a predicted mass of 276.2 grams.

There were likely errors in the calibration of the strain gauge, which could have introduced a small offset to the measurements or a linear scaling factor into the amplitude

but likely not a major effect on the time of the peaks. Minor error could be attributed to temperature fluctuations, material defects, or beam bending asymmetry. Sensor noise during the measurement of the amplitudes likely played a significant role in the noise of the logarithmic decrement which propagated into the damping ratio and the calculated undamped natural frequency. The sensor noise could be identified in the "capping" of the peaks of the displacement graph as well as the general increase in noise at the maximum displacement due to hysteretic effects potentially acting to smooth the amplitude data while the beam was in motion. These effects can be observed in Figures 1 and 2.

Other sources of error could include material defects or other vibrations in the testing assembly supporting the beam being analyzed.

A 95% confidence interval was constructed for both displacement traces to assess the variability in natural frequency. Using Equation (5), the confidence interval was determined and presented in Equations (6), and (7).

Conclusion/Summary

After performing a two-sample t-test, it can be concluded that there is a statistically significant difference between the damped natural frequency and the undamped natural frequency.

The objective of this experiment was to analyze the vibrational behavior of a cantilever beam and compare the theoretical and experimental natural frequencies. Using beam theory, the theoretical natural frequency was calculated to be 167.95 rad/sec, while the experimentally determined values for small and large displacement traces were approximately 93.79 rad/sec. The results demonstrated a significant deviation between theoretical and experimental frequencies. These results indicate major sources of error in the experimental procedure applied or the methodologies presented.

A 95% confidence interval was constructed for both traces, indicating that the experimental results were consistent across different displacement magnitudes. Additionally, a two-sample t-test confirmed that there was no statistically significant difference between the small and large displacement traces, reinforcing the reliability of the measured values.

The second half of the experiment demonstrated the practical use of strain gauge calibration through linear regression. The unknown mass was predicted with high accuracy, validating the reliability of the calibration procedure and the strain gauge system. Together, these two experimental methods showcase the importance of both frequency analysis and accurate calibration in mechanical measurement systems.

Despite the discrepancies observed, the experiment provided valuable insights into the importance of accounting for measurement errors and environmental factors when analyzing vibrational systems [3]. Future works could include minimizing sensor noise, or refining calibration methods. Overall, this experiment emphasized the need for additional work in understanding and predicting the natural frequencies of mechanical systems.

References

[1] Gilman, J., and Glasofer, J., 2003, "Introduction into LabVIEW Programming, MEEN 260 Laboratory Manual," Texas A&M University.

[2] Beckwith, T. G., Marangoni, R. D., and Lienhard, J. H., 2007, *Mechanical Measurements*, 6th ed., Pearson Prentice Hall, Upper Saddle River, NJ.

[3] Rao, S. S., 2011, *Mechanical Vibrations*, 5th ed., Pearson, Upper Saddle River, NJ.

[4] Clough, R. W., and Penzien, J., 2003, *Dynamics of Structures*, 3rd ed., McGraw-Hill, New York.

Appendix

$$\omega_n \left[\frac{rad}{sec}\right] = \sqrt{\frac{3EI}{M_e l^3}} \left[\frac{rad}{sec}\right] = \sqrt{\frac{3(207 * 10^9[Pa])(1.619 * 10^{-11}[m^4])}{(0.23 * 0.140[kg])(0.223[m])^3}} = 167.95 \left[\frac{rad}{sec}\right] \quad (11)$$

Table 4: Cantilever beam free vibration trace with *small* displacement.

Time	x_i (Peak amplitude)	T_d	δ (log decrement)	ξ (damping ratio)	ω_n (natural frequency)
(sec)	(Volts)	(sec)	-	-	(rad/s)
t_1 =0.998	x_1 =3.2318	T_{d1} =0.068	0.0420	0.0067	92.40
t_2 =1.066	x_2 =3.0988	T_{d2} =0.066	0.0010	0.0002	95.20
t_3 =1.132	x_3 =3.0957	T_{d3} =0.067	0.0363	0.0058	93.78
t_4 =1.199	x_4 =2.9854	T_{d4} =0.067	-0.0173	-0.0028	93.78
t_5 =1.266	x_5 =3.0376	T_{d5} =0.067	0.0478	0.0076	93.78
t_6 =1.333	x_6 =2.8957	-	-	-	-
	Mean:	0.0670	0.0193	0.0035	93.79
	Std deviation:	0.00071	0.0102	0.0045	0.99

Table 5: Cantilever beam free vibration trace with *large* displacement.

Time	x_i (Peak amplitude)	T_d	δ (log decrement)	ξ (damping ratio)	ω_n (natural frequency)
(sec)	(Volts)	(sec)	-	-	(rad/s)
t_1 =0.556	x_1 =18.2464	T_{d1} =0.066	0.0097	0.0015	95.20
t_2 =0.622	x_2 =18.0709	T_{d2} =0.067	0.0354	0.0056	93.78
t_3 =0.689	x_3 =17.4425	T_{d3} =0.067	0.0231	0.0037	93.78
t_4 =0.756	x_4 =17.0434	T_{d4} =0.068	0.0142	0.0023	92.40
t_5 =0.824	x_5 =16.8022	T_{d5} =0.067	0.0142	0.0023	93.78
t_6 =0.891	x_6 =16.5645	-	-	-	-
	Mean:	0.0670	0.0193	0.0031	93.79
	Std deviation:	0.00071	0.0102	0.0016	0.99

Table 6: Summary of found values.

Value	Units	$Small$	$Large$
ω_n	rad/sec	93.8	93.8
$\delta\omega_n$	rad/sec	1.2	1.2
ξ	n/a	0.0035	0.0031
$\delta\xi$	n/a	0.0056	0.0020
ω_d	rad/sec	93.8	93.8
$\delta\omega_d$	rad/sec	1.2	1.2

Back to Contents

7. Solid Mechanics

Summary

This section contains two projects from the Solid Mechanics course (MEEN 305).

- Project 1: Hollow-Tube Truss Analysis
- Project 2: Solar Flower Frame Analysis

Contributors: Nick Licon, Andres Pinzon, Ian Wilhite, and David Wood

Key Skills: Solid Mechanics, Stress Analysis, Strain Analysis, Material Behavior, Finite Element Analysis (FEA), Structural Analysis.

Relevance: These projects demonstrate a solid understanding of the principles of solid mechanics and their application to the analysis of structural components under various loading conditions.

Design and Analysis of a 2D Truss

MEEN 305-500 – Project 1

By Ian Wilhite, David Wood, Nick Licon, and Andres Pinzon

Introduction

In this project, we designed and analyzed a two-dimensional truss structure to determine an optimal layout with optimal cross-sectional geometry for each truss member to carry multiple point loads. To simplify our design process and analysis, we (1) generated truss designs with point loads applied exactly at joint locations, (2) assumed the weight of truss members to be negligible, and (3) assumed “smooth pins” at all truss member joints so that bending moments are neglected. These assumptions allowed us to treat each truss member as two-force members, either in tension or compression. Therefore, the only factors to consider when testing the structural integrity are the yield strength and critical buckling load.

The two-dimensional truss was required to fulfill the following specifications:

- Span a distance of 20 ft.
- Be made of A-36 steel.
- Support a 15-kip load at its center, a 10-kip load located 4 ft from one side, and a 5-kip load 4 ft from the other.
- Contain a minimum safety factor of 1.5 for all truss members under any potential failure mechanism (either yielding or buckling)
- For all truss members to have circular cross-sections

The first part of our design process was to brainstorm potential truss models. Each team member generated at least one unique truss design based on their analysis as seen in **Figures 1-5**. We then determined the minimal amount of mass required to satisfy the design constraints listed above for each truss design, accounting for failure due to either yielding or buckling. The design with the least amount of mass required to satisfy the design requirements was selected as the best model. Finally, we verified our results by calculating the individual factor of safety for each member of our final design, ensuring that they were all at least 1.5.

Truss Model

Individual Models:

As a part of the collaborative brainstorming process, multiple proposals were generated. They intended to take vastly different approaches to the problem to ensure a wide variety of possible solutions were considered. A common analysis process was then generated as a method to effectively determine the best model.

Method 1: Square Frame - Ian Wilhite

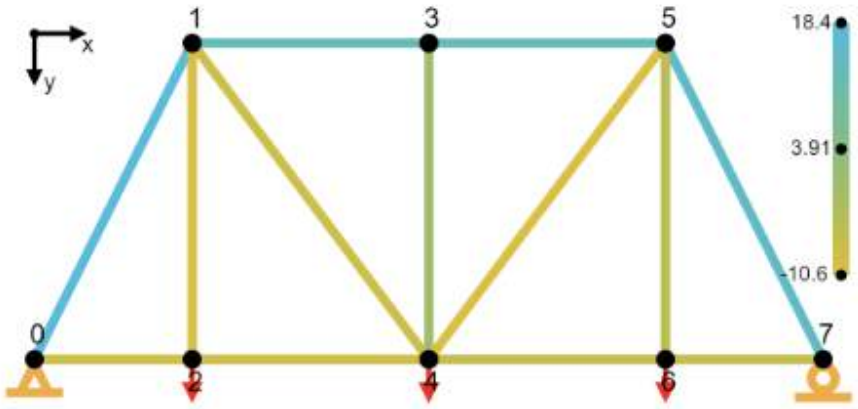

Figure 1. Visual analysis for square frame truss.

This method was intended to take inspiration from many train bridges across the country, and their very square or rectangular appearance by creating parallel beams and adding cross branches to support each segment. The segment widths were modified to allow for loading at the correct increments for analysis.

Method 2: Webbed Frame - David Wood

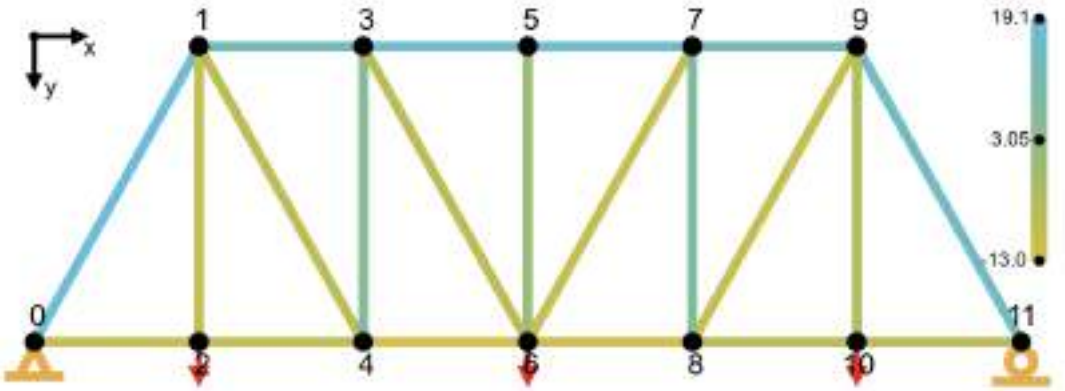

Figure 2. Visual analysis for webbed frame truss.

This model explored whether it would be worth increasing the number of webs in the truss to reduce the overall load for each truss member. While more webs correspond to more

needed material, making the bridge heavier, it also contains members significantly shorter in length. This makes them much more resilient to buckling or bending. However, the actual tensile/compressive stress exerted per member remained approximately the same, compared to this same bridge above with 1 web.

Method 3: Parabolic-inspired Frame - Nicholas Licon

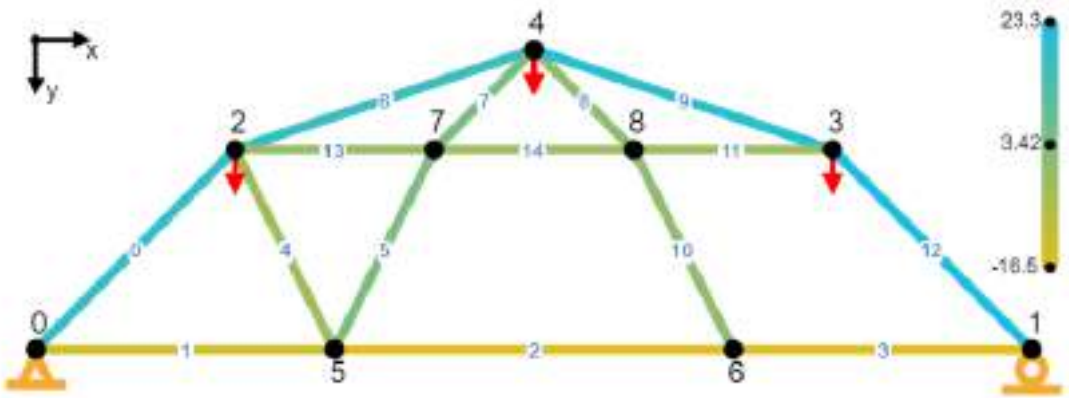

Figure 3. Visual analysis for the Parabolic-inspired Frame.

This shaped truss came from the idea that forces applied to a curved structure are often stronger than others. The shape of a “parabolic” structure distributes the load along the curve of the structure creating members of compression spaced out along the curve as shown with the blue two force members.

Method 4: Pentagonal Frame - Andres Pinzon

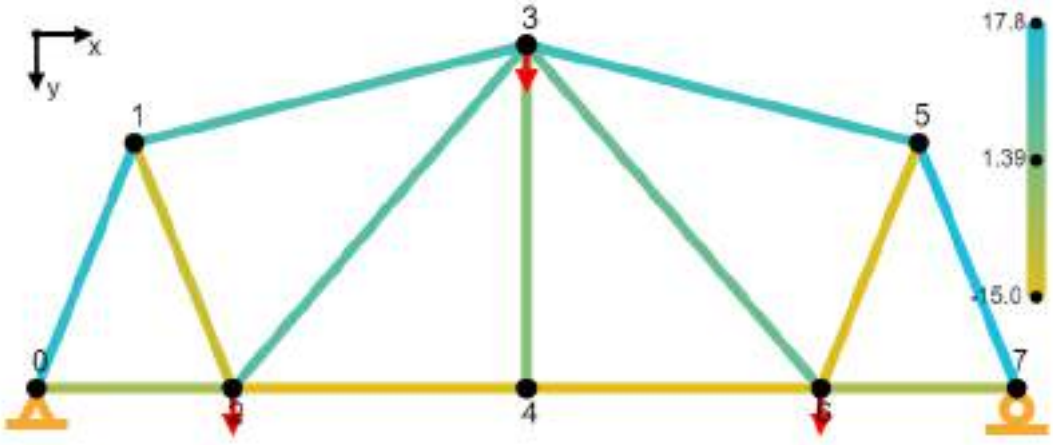

Figure 4. Visual analysis for pentagonal frame truss.

This model was created based on modifications to an already existing warren bridge. The main change is increasing the main member's height. This created a more pentagonal look

to the frame and it was noticeably stronger than a simple warren bridge model. The axial force each member sustained was minimized to keep each member's area from growing too much.

Method 5: Triangular Frame - Ian Wilhite

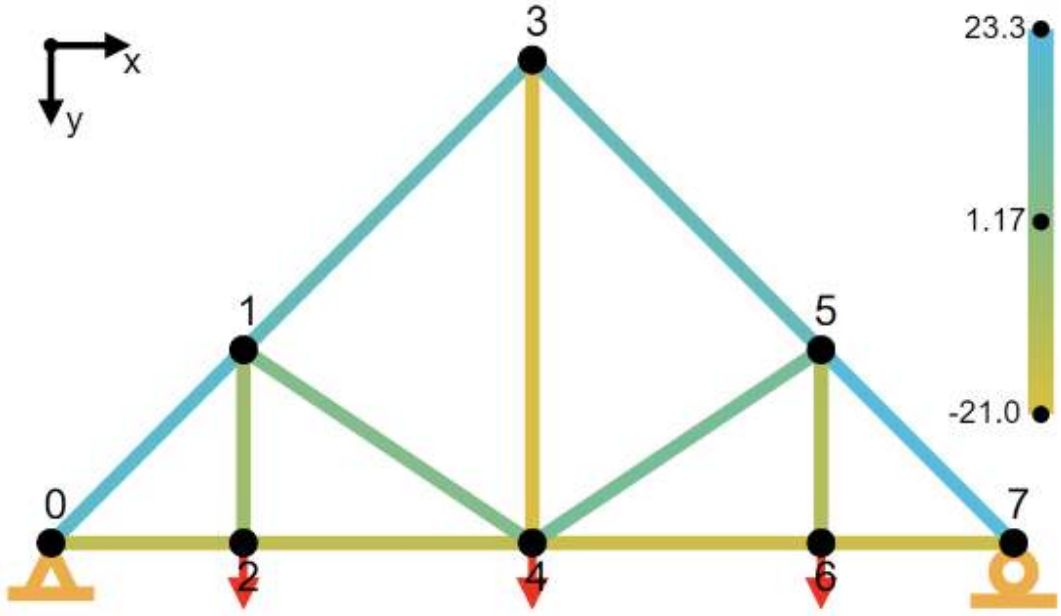

Figure 5. Visual analysis for triangular truss.

This model was meant to remain as simple as possible to theoretically take advantage of the roundup error in frames with many small beams all being rounded up to the nearest quarter inch. This resulted in a substantially weaker truss because the fewer members resulted in less optimal placement of each.

Chosen Model: Parabolic Inspired - Nicholas Licon

This model reduced the total volume of material needed to support the weight. This model leverages a proper balance between linkage placement and roundup radii to generate a truss that can effectively support the loading provided.

Justification of Choice

Each truss was analyzed to determine the total volume of material it would require. The total volume of each truss was then compared to determine the optimal design for the loading conditions.

#	Name	Designer	Volume Required (in^3)	Weight Required (lb)
1	Square Frame	Ian Wilhite	2444.240	694.164
2	Webbed Frame	David Wood	1596.073	453.284
3	Parabolic Inspired	Nicholas Licon	1227.537	348.621
4	Pentagonal Frame	Andres Pinzon	2204.261	626.010
5	Triangular Frame	Ian Wilhite	3690.243	1048.029

Table 1. Comparison of bridge designs.

Analysis Process

Each truss presented was analyzed initially using an online calculator which performed the node forces for each truss and presented the forces per member given the loading conditions. These results were imported into a spreadsheet in which each truss could be compared to intake the force, safety factor, and failure stress, to output the total volume and weight of the truss.

Geometric Properties

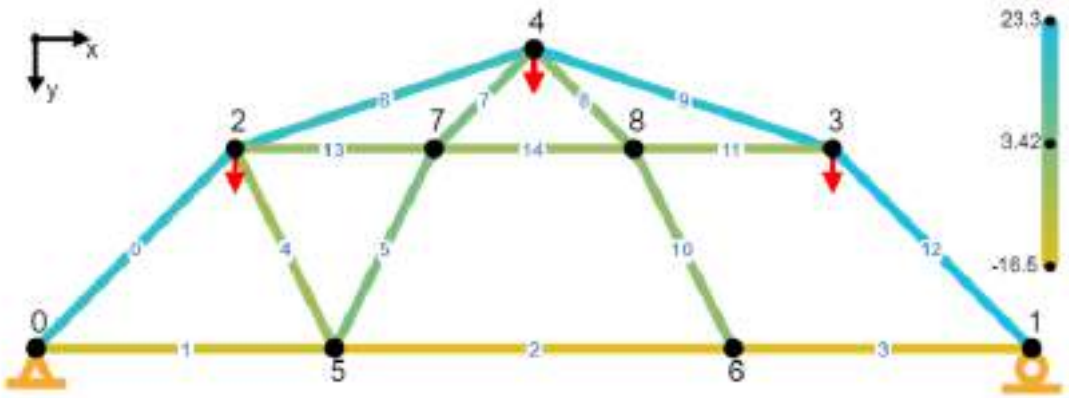

Density of A-36 steel = 0.284 lb/in^3

RED = Compression	BLUE = Tension

Member	Length (in)	Area (in^2)	Volume (in^3)	Weight (lbs)	FOS
0	67.884	1.767	119.961	34.069	2.555
1	72	0.785	56.545	16.060	2.0943
2	96	0.785	75.398	21.413	1.714
3	72	0.785	56.549	16.060	1.714
4	53.664	0.196	10.537	2.992	2.108
5	53.664	1.227	65.856	18.703	3.551
6	75.9	3.142	238.447	67.719	2.244
7	33.936	0.785	26.653	7.570	2.875
8	33.936	0.0491	1.666	0.473	N/A
9	75.9	3.142	238.447	67.719	1.899
10	53.664	0.0491	2.634	0.748	N/A
11	48	0.196	9.425	2.677	2.356
12	67.884	2.405	163.280	46.372	2.091
13	48	0.196	9.425	2.677	4.712
14	48	0.196	9.425	2.677	2.356

Table 2. Analysis of parabolic inspired truss.

TOTAL VOLUME, TOTAL WEIGHT: **1227.537 in^3**, **348.621 lbs**

Tasks and Responsibilities

Each member was expected to participate in group brainstorming, generate one truss design, and a brief description of their approach and inspiration for their truss. There was also a strong collaborative effort in gaining a fundamental understanding of the equations, simulation tools, and theory behind what constitutes a good truss.

Ian Wilhite - Ian was responsible for creating the spreadsheet to analyze the trusses, the framework of the report, the chosen model, and Tasks and Responsibilities.

Nicholas Licon - Nicholas was responsible for the Introduction.

Andres Pinzon Diaz - Andres was responsible for the geometric properties, excel appendix.

David Wood - David was responsible for the Introduction, and the generation of Geometric Properties for the selected truss.

Appendix

Matlab code for solving forces:

```
% Number of nodes and members
n_nodes = 9;
n_members = 15;

% Node coordinates (x, y)
nodes = [0, 0; 20, 0; 4, 4; 16, 4; 10, 6; 6, 0; 14, 0; 8, 4; 12, 4];
% External forces (Fx, Fy) at each node
forces = [0, 0; 0, 0; 0, -5; 0, -10; 0, -15; 0, 0; 0, 0; 0, 0; 0, 0];
% Connectivity matrix (start node, end node)
members = [0, 2; 0, 5; 5, 6; 6, 1; 2, 5; 7, 5; 2, 4; 4, 7; 4, 8; 4, 3; 6, 8; 3,
8; 3, 1; 2, 7; 7, 8] + 1;

% Initialize system of equations
n_eqs = 2 * n_nodes; % 2 equations (Fx and Fy) per node
A = zeros(n_eqs, n_members + 3); % Matrix of coefficients
b = zeros(n_eqs, 1);             % Vector of constants
% Reaction forces (supports at nodes 0 and 1)
% Loop through each member and define equations based on equilibrium
for member_id = 1:n_members
    n1 = members(member_id, 1);
    n2 = members(member_id, 2);

    % Calculate direction cosines (l, m)
    dx = nodes(n2, 1) - nodes(n1, 1);
    dy = nodes(n2, 2) - nodes(n1, 2);
    L = sqrt(dx^2 + dy^2);
    l = dx / L;
    m = dy / L;

    % For node n1 (Fx and Fy)
    A(2*n1-1, member_id) = l;  % Fx equation for node n1
    A(2*n1, member_id) = m;    % Fy equation for node n1
```

```
    % For node n2 (Fx and Fy)
    A(2*n2-1, member_id) = -l; % Fx equation for node n2
    A(2*n2, member_id) = -m;   % Fy equation for node n2
end
A(1, n_members+1) = 1; A(2, n_members+2) = 1;
A(4, n_members+3) = 1;
for i = 1:n_nodes
    b(2*i-1) = forces(i, 1); % Fx
    b(2*i) = forces(i, 2);   % Fy
end
% Solve for forces in each member and support reactions
disp(A);
disp(b);
x = A \ b;
% Display the results
forces_in_members = x(1:n_members);
reaction_forces = x(n_members+1:end);
disp('Forces in members (kips):');
disp(forces_in_members);
disp('Reaction forces (kips):');
disp(reaction_forces);
```

Output of MatLab code:

```
Forces in members (kips):
   19.0919
  -13.5000
  -16.5000
  -16.5000
   -3.3541
    3.3541
   17.3925
    4.2426
    0.0000
   20.5548
    0.0000
   -3.0000
   23.3345
   -1.5000
   -3.0000

Reaction forces (kips):
    0.0000
  -13.5000
  -16.5000
```

Truss visualization:

trussanalysis.com

Excel sheets used to calculate geometric properties:

	Young's Modulk A-36	Yield Strength		Factor of Safety
	29000	36000		1.5
		36		

	A	B	C	D	E	F	H	I	J
7	Member ID	Start -> End Nod	Length (ft)	Axial Force (kips)	force * FoS	Area (in^2)	Radius - yield (in)	Moment of Inertia, I (in	Radius - gyration (in)
8	0	0 → 2	5.657	19.99	29.985	0.7564189997	0.50	0.79	0.88
9	1	0 → 5	6	-13.5	-20.25	0.5625	0.42	0.05	0.00
10	2	5 → 6	8	-16.5	-24.75	0.6875	0.47	0.05	0.00
11	3	6 → 1	6	-16.5	-24.75	0.6875	0.47	0.05	0.00
12	4	2 → 5	4.472	-3.354	-5.031	0.13975	0.21	0.00	0.00
13	5	7 → 5	4.472	3.354	5.031	0.13975	0.21	0.12	0.50
14	6	2 → 4	6.325	17.24	25.865	0.7245833333	0.48	0.79	0.90
15	7	4 → 7	2.828	4.243	6.3645	0.1767916667	0.24	0.05	0.42
16	8	4 → 6	2.828	0	0	0	0.00	0.00	0.00
17	9	4 → 3	6.325	20.55	30.825	0.85625	0.52	0.79	0.94
18	10	6 → 8	4.472	0	0	0	0.00	0.00	0.00
19	11	3 → 8	4	-3	-4.5	0.125	0.20	0.00	0.00
20	12	3 → 1	5.657	23.33	34.995	0.9720833333	0.56	0.79	0.82
21	13	2 → 7	4	-1.5	-2.25	0.0625	0.14	0.00	0.00
22	14	7 → 8	4	-3	-4.5	0.125	0.20	0.00	0.00

			Total Vol (in ^3)	Total Mass (lb)
			1227.537	348.621

	K	L	M	N	O	P	Q	R	X
7	Radius - Failure (	Radius to 1/8th (in)	Area(in^2)	Volume (in^3)	Weight (lb)	FOS t	Pcr	FOS c	FOS Consolidated
8	0.88	1.00	3.14	213.26	60.57	0.92	49.76	2.56	**2.56**
9	0.42	0.50	0.79	56.55	16.06	-2.09	2.71	0.00	**2.09**
10	0.47	0.50	0.79	75.40	21.41	-1.71	1.52	0.00	**1.71**
11	0.47	0.50	0.79	56.55	16.06	-1.71	2.71	0.00	**1.71**
12	0.21	0.25	0.20	10.54	2.99	-2.11	0.30	0.00	**2.11**
13	0.50	0.63	1.23	65.86	18.70	13.17	11.91	3.55	**3.55**
14	0.90	1.00	3.14	238.45	67.72	6.50	39.02	2.24	**2.24**
15	0.42	0.50	0.79	26.65	7.57	6.66	12.20	2.88	**2.88**
16	0.00	0.13	0.05	1.67	0.47	N/A	0.05	0.00	**0.00**
17	0.94	1.00	3.14	238.45	67.72	6.50	39.02	1.90	**1.90**
18	0.00	0.13	0.05	2.63	0.75	N/A	0.02	0.00	**0.00**
19	0.20	0.25	0.20	9.42	2.68	-2.36	0.38	0.00	**2.36**
20	0.92	1.00	3.14	213.26	60.57	4.85	49.76	2.09	**2.09**
21	0.14	0.25	0.20	9.42	2.68	-4.71	0.38	0.00	**4.71**
22	0.20	0.25	0.20	9.42	2.68	-2.36	0.38	0.00	**2.36**

Equations for Excel Columns:

Column	**A**	**B**	**C**
Equation	Member ID	Member Start->End	Length

Column	**D**	**E**	**F**
Equation	Axial Force (kips)	=D8*$E$3	=abs(E8*1000/$C$3)

Column	**H**	**I**	**J**
Equation	=sqrt(F8 / PI())	=PI()/4*L8^4	=if(D8>0, (E8*1000*C8*C8*12^2/(PI()^3*$B$3*1000*0.25))^(1/4),0)

Column	**K**	**L**	**M**
Equation	=max(J8,H8)	=floor(K8, 1/8) + 0.125	=pi()*L8^2

Column	**N**	**O**	**P**
Equation	=C8*pi()*L8^2*12	=N8*0.284	=$C$4/(D8/M8)

Column	**Q**	**R**	**X**
Equation	=(PI()^2 * 29000*I8) / (C8*12)^2	=if(D8>0,Q8/D8,0)	=if(P8<0,-P8,R8)

Meen 305 Project 2: Flower Petal Loadings

By David Wood, Nick Licon, Andres Pinzon, and Ian Wilhite

Section 1: Problem Summary

The client has a flower solar panel of 8 blades. The task provided was to design a truss and column structure that could support the mass of the blades and their loading during usage. The objective of this design is to minimize the mass of the column and truss with a given deflection while keeping reasonable factors of safety.

Section 2: Design Process

The column must not fail due to yielding/fracturing due to stresses, buckling due to applied load, or laterally deflect more than 0.3 in.

To get a radius that would create a maximum deflection of 0.3 in, Equations () were used. Then, the maximum stresses at critical points were calculated on either side of the column to make sure the column would not yield under the load. Additionally, the critical buckling load was calculated so that we could ensure the column would not buckle, since oftentimes a column will buckle before it yields under a compressive load.

There were a number of design constraints applied to ensure valid :

- Lateral deflection not to exceed 0.3 inches.
- Factor of safety on all calculated values of at least 2.
- Constant thickness of the column vertically (as opposed to varied thickness as a function of height) for ease of manufacturing and ability to use existing commercial products.
- Column may be hollow to allow for more efficient use of material.
- All column measurements must be in increments of ¼ inch for ease of manufacturing.

Failure due to Yielding:

The first thing we noticed for the column was the column would experience maximal stress when the solar panels were in the vertical (90°) position. This is because the sum of the panel components acts as a concentrated load 1 ft away from the column's central axis, generating a bending stress. Furthermore, the wind force, which is also modeled as concentrated load, is also highest when the panels are in the vertical position. If the wind force acts in the direction so that it hits the back of the panels, it will generate an additional bending moment and stress in the same direction. To illustrate this, three free body diagrams with different configurations are provided below to display our thought process and logically lead to the highest failure scenario for the column.

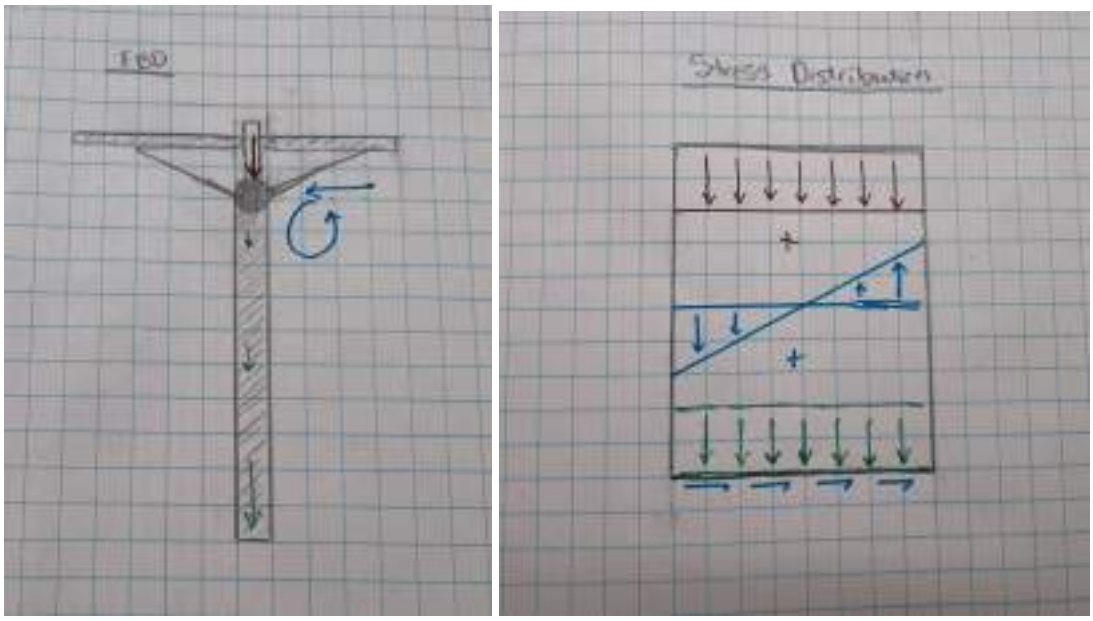

Figure 1. Force/Moment Diagram and Stress Distribution for Flat Position

In this configuration, there is no bending stress generated by the solar panels. Furthermore, the bending stress generated by the wind is smaller because the wind force data is provided and approximated at a lower value of 40 lbs. The column should not be designed to avoid failure under this scenario because there are other configurations that can generate much higher stresses. The same logic applied for the angled (45°) position. There is some bending stress generated by the weight of the solar panels, and the bending stress generated by the wind is also higher too (wind force modeled at 85 lbs), but they are both not as great as the vertical position.

A moment is calculated by multiplying the magnitude of a force and its perpendicular distance from an axis by which it revolves. In the case of the bending stress generated by the solar panels, the *radius* is maximal in the vertical position. For the bending stress generated by the wind, the *force* is maximal in the vertical position. Therefore, we decided to not design the column based on an angled configuration because, logically, there are other configurations that generate higher stresses.

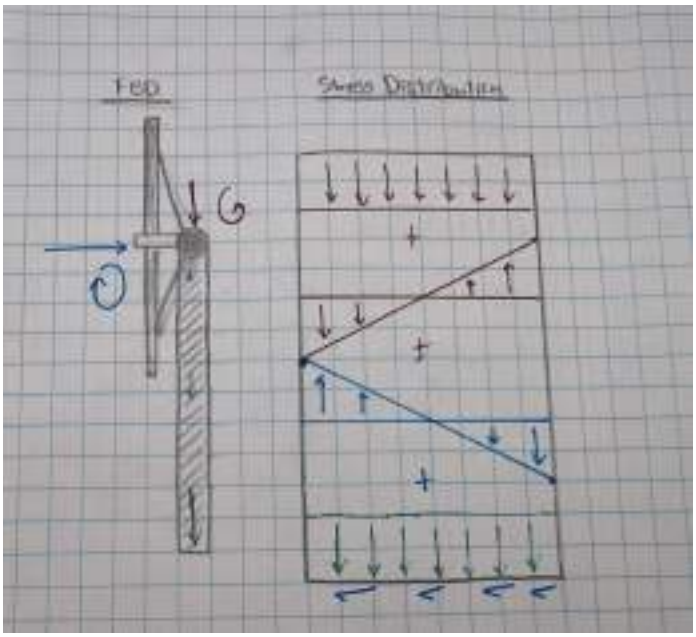

Figure 2. Force/Moment Diagram and Stress Distribution for Oncoming Wind

In this configuration, the bending moments generated by the weight of the solar panels and the wind partially offset each other because they are acting opposite in direction. As seen in **Figure 2**, on the left side of the column, the solar panels generate a maximum compressive stress, while the wind force generates a maximum tensile stress. On the right side of the column, the solar panels generate a tensile stress and the wind force generates a compressive stress. Regardless of where, the bending stresses are always cancelling each other out to some degree.

The last consideration is where the force is applied on the back side of the panels. This would generate much higher stresses because the bending moments would be acting in the same direction, with maximum compression on the left side and maximum tension on the right, as you can see below:

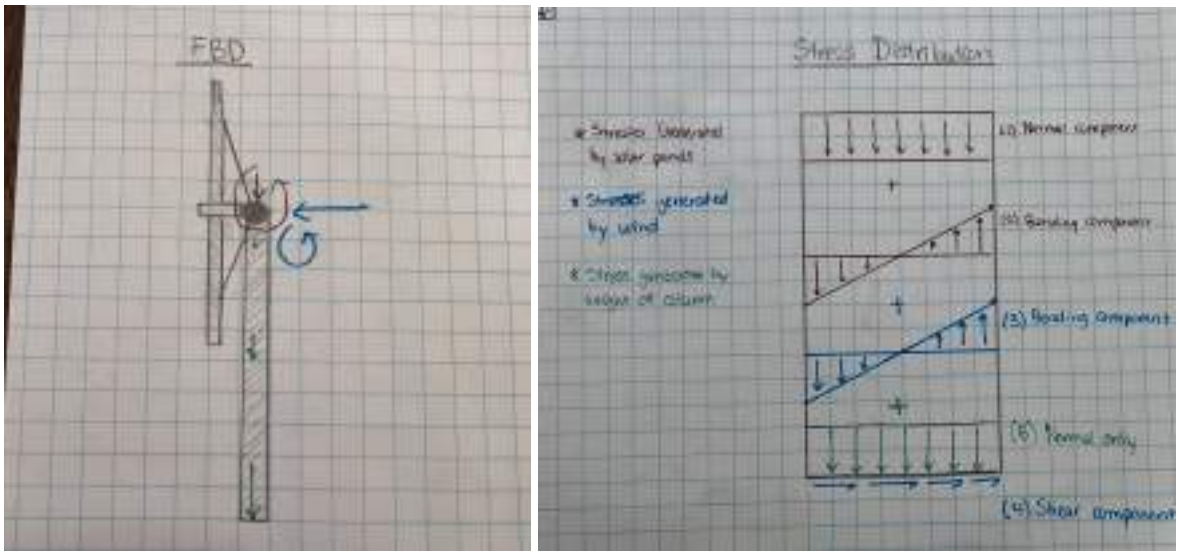

Figure 3. Force/Moment Diagram and Stress Distribution of Highest Failure Scenario

This is the configuration for the column by which the most stress is generated, and the one we need to design around. As you can see, the weight of the solar panels generates a stress that has both normal and bending components, while the wind force generates a stress that has shear and bending components. The weight of the column itself generates stress too, but unlike the other stresses, it varies with the length of the column. The normal stress due to the weight of the column is maximal at the bottom and zero at the top of the column.

The normal stress components have a uniform distribution, meaning that the magnitude and direction of the stress is constant at any individual location within the column's cross-section. Bending stresses, on the other hand, have a linear distribution based on the distance it is from the central axis of the column. The magnitude of this stress is the same in either direction from the center but opposite in direction, depending on whether you are closer or further away from where the moment-inducing force is being applied. On the left side, it generates a maximum compressive stress, while on the right it generates a maximum tensile stress.

The formulas used to calculate all stresses exerted on the column are summarized below:

Normal Stress	Shear Stress	Bending Stress	Torsional Stress
$\sigma = \frac{P}{A}$	$\tau = \frac{VQ}{It}$	$\sigma = -\frac{My}{I}$	$\tau = \frac{T\rho}{J}$

Brittle Materials

Brittle materials have different strengths in the tensile and compressive directions, being much stronger in compression than tension. This rules out our ability to use the **maximum normal stress theory**, which is derived based on the assumption that the material is equally

strong in compressive/tensile directions. Instead, we will find the locations in the column where stress is maximum in either compressive or tensile directions, and compare them to the compressive/tensile stresses provided for each material.

We determined that there are two locations on the beam where failure is most likely to occur. Referencing the two-dimensional stress distribution layout in **Figure 3**, these points would be the lower left-hand corner and the upper-right hand corner. As the lower left location, the column is under **maximal compressive stress.** The compressive stresses add upon each other, and, due to the nature of each distribution, they accumulate to a maximum at this location. In the upper right location, the column is potentially under **maximal tensile stress**.

NOTE: The word “potentially” is used because the downward normal components acting on the right side of the column may be greater in magnitude than the upward components due to bending, but this is highly unlikely.

Ductile Materials

There is no data given on compressive/tensile strengths for the ductile materials. This is likely because yielding in ductile materials is dominated by shear mechanisms, and they are not super direction-dependent. Therefore, we will assume that the ductile materials are equally strong in compressive/tensile directions and use the **maximum shear stress theory** (or Tresca criterion) to determine if it will yield under compressive loads. Note that the magnitude of maximum compression at a location will be greater than the maximum tension at another. The yield strength is estimated based on the formula:

$$\tau_{\substack{abs \\ max}} = \frac{\sigma_1 - \sigma_2}{2} = \frac{\sigma_y}{2}$$

The shear stress generated by the wind is neglected because it is relatively small (see **Appendix B.3**), so there is no need to determine the principal stresses. The maximum stress will simply be the lower-left corner (see **Figure 3)** where it is under maximum compression.

Failure Due to Buckling

Buckling also had to be taken into consideration as the weight of the column could cause it to fail on itself. This occurs when the forces acting on the column overcome its ability to resist bending, and this depends on its stiffness (bending rigidity, EI), how it's supported, and its length. In this case, with a fixed-free setup, the column's weight itself can create enough stress to make it buckle when it reaches a critical value. It's like a battle between the column's rigidity and the load trying to push it into instability.

$$W_c = 7.84\frac{EI}{L^2}$$

This critical weight required to maintain the integrity of the column did not make much of an impact in the end. Since we were minimizing the weight of the column, our results yielded values that were much lower. Nonetheless, these calculations are important to make as they ensure this specific part of the design is secure and it adds an extra layer of credibility to our final design.

Minimizing Lateral Deflection to less than 0.3 inches

To make sure the column did not deflect more than 0.3 inches there were two scenarios that had to be considered. First we were tasked with finding the most suitable design without any wind forces, so the only thing causing the column to deflect was the bending moment caused by the blades.

Figure 4. Deflection due to bending stress

Due to this bending effect, the lateral deflection of the column was found using the equation seen in **Figure 4**. A design was then optimized to have a FOS that was less than 2.

Once wind was taken into consideration, another deflection was required to be calculated. This time the column was going to be deflected due to a force that pushes sideways and would make the column bow out over its length.

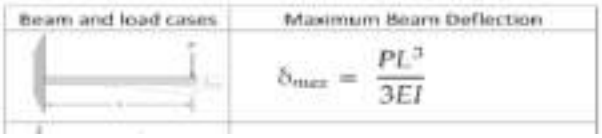

Figure 5. Deflection due to Force

With a new input causing a deflection on the column by the amount seen in the equation in **Figure 5**, our FOS changed from our minimum of 2 down to less than 1 for our chosen model. This would mean that the column would deflect more than the expected 3 inches. A new inner and outer radius were constructed to make sure that the sum of the deflections caused by both the wind and the bending would not exceed 3 inches.

Column Conclusions

For the column, it was clear that limiting the deflection to 0.3 inches was the primary limiting factor for design optimization. Calculations of failure due to buckling or yielding/fracturing did not even come close to their determined limits.

Section 2.2 Design Considerations for Truss:

The Truss must not fail due to buckling or normal stress under the load of the panel and must pass with a factor of safety greater than 2. The analysis of the truss problem is a statically indeterminate problem. Connected to a rigid wall there are 3 unknowns due to the cantilever beam-like properties it will have. Additionally, the force of the truss acts upward three feet from the wall. This means that we must use analysis of beam deflection to determine the fourth equation to solve for all four unknowns. To solve the beam deflection problem we will assume the compatibility to be no deflection at the end of the panel meaning that at what the truss is supporting the weight the displacement is 0 (L=3, v = 0).

Once the force acting on the truss is found a test for both brittle materials and ductile materials will be performed as well as for what the radius of the cylindrical solid truss should be.

Position one of the flowers allows us to ignore the truss in that position due to the compatibility of the orientation and the bar. With the weight going straight down the only compatibility for the panel that we know is that the displacement of the bar in the x direction is zero, meaning that the trust can exert any force upon the panel in that position leading no force to be placed on the truss in this position.

Volume = Area * length
Density(lbs/in^3) = Density(lbs/ft^3) / (12^3)

Material	Minimum radius	Volume	Weight
Gray cast iron 30	0.220in	5.7699in^3	1.402lbs
Gray cast iron 60	0.205in	5.01in^3	1.450lbs
Stainless steel 304	0.189in	4.258in^3	0.4189lbs
Aluminum Alloy	0.243in	7.0395in^3	0.387lbs

Table 1. Evaluation of Truss

Aluminum Alloy gives the same amount of support as the others for the minimized weight of the truss making it the best material to use for our given case.

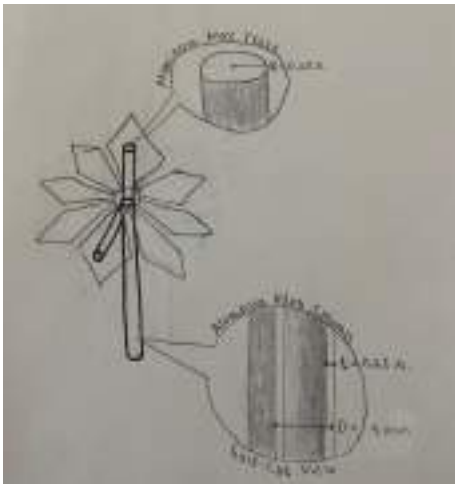

Figure 6. Sketch of Truss6

Section 3: Results

Section 3.1 Calculated Values

Parameter	Value
Maximum Lateral Deflection	0.3 [in]
Flower Weight	40 [lbs]
Column Height	10 [ft]
Number of Flowers	8
Minimum Factor of Safety	2
End condition factor	0.25

Table 2. Assumed parameters

Material	Material Type	Inner Radius (in)	Outer Radius (in)	Density (lb/ft^3)	Mass (lb)	FOS
Cast Iron 30	Brittle	3.75	4	420	177.5	2.127
Cast Iron 60	Brittle	3.5	3.75	500	197.7	2.322
Stainless steel 304	Ductile	3.00	3.25	170	58.0	2.047
Aluminum Alloy	Ductile	4.25	4.50	95	45.3	2.071

Table 3. Evaluation of Column

Section 3.1 Final Recommendations

Section	Material	Mass (lb)
Truss	Aluminum	0.387
Column	Aluminum	45.3
Total		45.7

Table 4. Chosen Masses

To minimize weight, both parts should be made of the aluminum alloy option, and the total structure will have a total weight of 45.7 lbs.

Conclusion

For the column, it was clear that limiting the deflection was the primary limiting factor for design optimization. Calculations of failure due to buckling or yielding/fracturing did not even come close to their determined limits. It could be inferred that in future analysis, this limit could be revisited as a design constraint. For the truss, the main limiting design factor was critical buckling load. The designs proposed meet the specified design constraints, and would perform as expected if constructed. Next steps for the project could include verification of calculated values via simulation, or scale tests to ensure the assumptions provided hold true. The design implemented effectively minimizes the weight of the material of the structure, minimizing the error from excluding their weight while calculating stresses.

Section 4: Member Contributions

The following is a summary of the contributions each member provided to the generation of the design and report presented:

- David Wood: David worked on developing the calculator for the column, specifically for the brittle materials. He also evaluated the columns compressive and tensile strength, and took the lead on debugging the calculator.
- Nick Licon: Nick developed the calculator for the truss for both ductile and brittle materials. He also introduced many of the analysis techniques that were crucial to evaluating the column.
- Andres Pinzon Diaz: Andres primarily worked on understanding the column buckling equations and their applications, then their implementation in the column.
- Ian Wilhite: Ian worked on developing the calculator for the column, specifically for the ductile materials. He also worked on preliminary reporting and approach structure.

Appendix

A. Tables

Table 1 Material Properties

Material	Density (lb/ft^3)	Elastic Modulus (ksi)	Tensile Yield Stress (ksi)	Tensile Ultimate Stress (ksi)	Compressive Ultimate Stress (ksi)	Shear Yield or Ultimate Stress (ksi)
Gray cast iron 30	420	15000		30	100	15
Gray cast iron 60	500	20000		60	180	30
Stainless steel 304	170	27500	40			20
Aluminum Alloy	95	10150	43			20

B. Calculations

B.1 Column Stress Analysis and Dimensional Optimization of Brittle Material Options

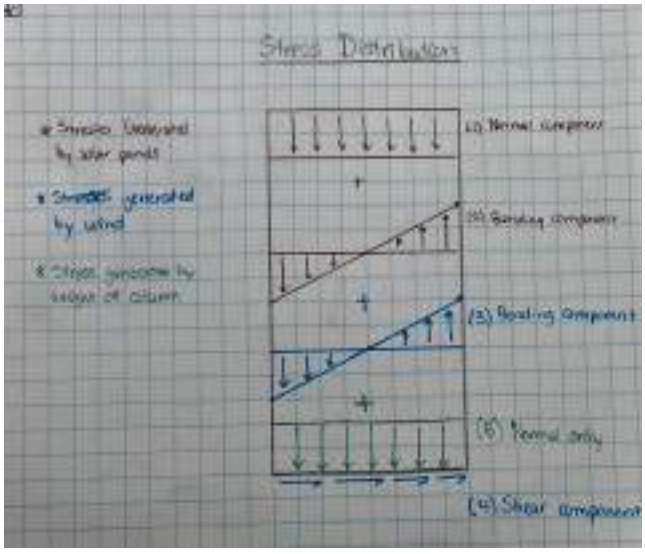

- Max compressive stress (lower left corner) = $\sigma_{panels,\ normal} + \sigma_{panels,\ bending} + \sigma_{wind,\ bending} + \sigma_{column\ weight}$
- Max Tensile Stress (upper right corner) = $\sigma_{panels,\ normal} + \sigma_{panels,\ bending} + \sigma_{wind,\ bending}$

SIGN CONVENTION: Negative sign is used for compression; positive sign is used for tension. So stresses must be greater than the maximum (negative) compressive stress, and less than the maximum (positive) tensile stress

$$\sigma_{max,\ compression} = -\frac{(320\ lbs)}{\pi\left(r_o^2 - r_i^2\right)} - \frac{(320\ ft{\cdot}lbs)\cdot r_o}{\frac{\pi}{4}\left(r_o^4 - r_i^4\right)} - \frac{(120lbs \cdot 120in)\cdot r_0}{\frac{\pi}{4}\left(r_o^4 - r_i^4\right)} - \frac{\rho{\cdot}\pi\left(r_o^2 - r_i^2\right)(120in){\cdot}g}{\pi\left(r_o^2 - r_i^2\right)}$$

$$\sigma_{max,\ tension} = -\frac{(320\ lbs)}{\pi\left(r_o^2 - r_i^2\right)} + \frac{(320\ ft{\cdot}lbs)\cdot r_o}{\frac{\pi}{4}\left(r_o^4 - r_i^4\right)} + \frac{(120lbs \cdot 120in)\cdot r_0}{\frac{\pi}{4}\left(r_o^4 - r_i^4\right)}$$

Gray Cast Iron 30: r_0 = 4.0 in, r_i = 3.75 in

$$\sigma_{max,\ compression} = -\frac{(320\ lbs)}{\pi\left(4^2 - 3.75^2\right)} - \frac{(320\ ft{\cdot}lbs)\cdot 4}{\frac{\pi}{4}\left(4^4 - 3.75^4\right)} - \frac{(120lbs \cdot 120in)\cdot 4}{\frac{\pi}{4}\left(4^4 - 3.75^4\right)} - \frac{0.243{\cdot}\pi\left(4^2 - 3.75^2\right)(120in){\cdot}32.2}{\pi\left(4^2 - 3.75^2\right)}$$

= -2.586619605 ksi > -100 ksi; well within failure limit

**The density was converted to lbs/in^3*

$$\sigma_{max,\,tension} = -\frac{(320\ lbs)}{\pi\left(4^2-3.75^2\right)} + \frac{(320\ ft{\cdot}lbs)\cdot 4}{\frac{\pi}{4}\left(4^4-3.75^4\right)} + \frac{(120lbs\cdot 120in)\cdot 4}{\frac{\pi}{4}\left(4^4-3.75^4\right)}$$

= 1.542307995 ksi < 30 ksi; well within failure limit

Gray Cast Iron 60: r_0 = 3.75in, r_i = 3.50 in

$$\sigma_{max,\,compression} = -\frac{(320\ lbs)}{\pi\left(3.75^2-3.5^2\right)} - \frac{(320\ ft{\cdot}lbs)\cdot 3.75}{\frac{\pi}{4}\left(3.75^4-3.5^4\right)} - \frac{(120lbs\cdot 120in)\cdot 3.75}{\frac{\pi}{4}\left(3.75^4-3.5^4\right)} - \frac{0.289\cdot\pi\left(3.75^2-3.5^2\right)(120in)\cdot 32.2}{\pi\left(3.75^2-3.5^2\right)}$$

= -3.000360171 ksi > -180 ksi; well within failure limit

$$\sigma_{max,\,tension} = -\frac{(320\ lbs)}{\pi\left(4^2-3.75^2\right)} + \frac{(320\ ft{\cdot}lbs)\cdot 4}{\frac{\pi}{4}\left(4^4-3.75^4\right)} + \frac{(120lbs\cdot 120in)\cdot 4}{\frac{\pi}{4}\left(4^4-3.75^4\right)}$$

= 1.769908297 ksi < 60 ksi; well within failure limit

B.2 Column Stress Analysis and Dimensional Optimization of Ductile Material Options

- Stress, is any direction, must be less than $\sigma_{yield} = 2*\tau_{ultimate}$, per Tresca criterion. σ_{yield} = 2 * 20ksi (for both ductile materials) = **40 ksi.**
- The maximum stress in compression will always be greater than the maximum stress in tension, so there is no need to calculate maximum tension.

Stainless Steel 304: r_0 = 3.25 in, r_i = 3.0 in

$$\sigma_{max,\,compression} = -\frac{(320\ lbs)}{\pi\left(3.25^2-3^2\right)} - \frac{(320\ ft{\cdot}lbs)\cdot 3.25}{\frac{\pi}{4}\left(3.25^4-3^4\right)} - \frac{(120lbs\cdot 120in)\cdot 3.25}{\frac{\pi}{4}\left(3.25^4-3^4\right)} - \frac{0.0984\cdot\pi\left(3.25^2-3^2\right)(120in)\cdot 32.2}{\pi\left(3.25^2-3^2\right)}$$

= -2.914629187 ksi > -40 ksi; well within failure limit

**The density was converted to lbs/in^3*

Aluminum Alloy: r_0 = 4.5 in, r_i = 4.25 in

$$\sigma_{max,\,compression} = -\frac{(320\ lbs)}{\pi\left(4.5^2-4.25^2\right)} - \frac{(320\ ft{\cdot}lbs)\cdot 4.5}{\frac{\pi}{4}\left(4.5^4-4.25^4\right)} - \frac{(120lbs\cdot 120in)\cdot 4.5}{\frac{\pi}{4}\left(4.5^4-4.25^4\right)} - \frac{0.0549\cdot\pi\left(4.5^2-4.25^2\right)(120in)\cdot 32.2}{\pi\left(4.5^2-4.25^2\right)}$$

= -1.505973093 > -40 ksi; well within failure limit

**The density was converted to lbs/in^3*

B.3 Calculations for Shear Stress in Column (why it's neglected)

The shear stress for the cast iron 30 was determined using the formula:

$$\tau_{wind} = \frac{V_{wind}\cdot Q}{It} = \frac{120lbs\cdot\frac{2}{3}\left(r_o^3-r_i^3\right)}{\frac{\pi}{4}\left(r_o^4-r_i^4\right)\cdot 2r_o} = \textbf{0.001939119528 ksi.}$$

Since it was so small, we decided to exempt it in our stress analysis for simplicity.

B.4 Calculations for deflection

$M = n * w * 1ft * sin\theta$

Where n is the number of petals, w is the weight of each, and theta is the angle it makes with the x axis

M_{90° = 3840 lbm*in

$\boldsymbol{\delta}_{max} = \frac{ML^2}{2EI}$

$\boldsymbol{\delta}_{max} = \frac{PL^3}{3EI}$

Gray Cast Iron 30: r_0 = 4.0 in, r_i = 3.75 in

$\boldsymbol{\delta}_{max} = \frac{3840*120^2}{2*15000*45.74} = 0.0403\ in$

\+ wind

$\boldsymbol{\delta}_{max} = \frac{120*120^3}{3*15000*45.74} = 0.101$ in

= 0.141in

Gray Cast Iron 60: r_0 = 3.75 in, r_i = 3.5 in

$\boldsymbol{\delta}_{max} = \frac{3840*120^2}{2*20000*37.46} = 0.0369\ in$

\+ wind

$\boldsymbol{\delta}_{max} = \frac{120*120^3}{3*20000*37.46} = 0.0922$ in

= 0.129in

Stainless Steel 304: r_0 = 3.25 in, r_i = 3.0 in

$\boldsymbol{\delta}_{max} = \frac{3840*120^2}{2*27500*24.01} = 0.0419\ in$

\+ wind

$\boldsymbol{\delta}_{max} = \frac{120*120^3}{3*27500*24.01} = 0.105$ in

= 0.147in

Aluminum Alloy: r_0 = 4.5 in, r_i = 4.25 in

$\boldsymbol{\delta}_{max} = \frac{3840*120^2}{2*10150*65.82} = 0.0413\ in$

\+ wind

$\boldsymbol{\delta}_{max} = \frac{120*120^3}{3*10150*85.82} = 0.103$ in

= 0.145in

*All below the max deflection that would give us a FOS of 2 (0.15in)

B.5 Calculations for buckling

$W_c = 7.84\frac{EI}{L^2}$

Gray Cast Iron 30: r_0 = 4.0 in, r_i = 3.75 in

$W_c = 7.84\frac{15000*45.7}{120^2}$

= 373217 lb

Gray Cast Iron 60: r_0 = 4.0 in, r_i = 3.75 in

$W_c = 7.84\frac{20000*37.46}{120^2}$

= 407898 lb

Stainless Steel 304: r_0 = 3.25 in, r_i = 3.0 in

$W_c = 7.84\frac{27500*24.01}{120^2}$

= 359483 lb

Aluminum Alloy: r_0 = 4.5 in, r_i = 4.25 in

$W_c = 7.84\frac{10150*65.82}{120^2}$

= 363729 lb

B.6 Truss Calculations

Use superposition to derive an expression for displacement of the cantilever beam.

Total deflection

| |

Weight of the bar

$$v = \frac{-PL^2}{48EI}(6x - L) \quad L/2 \le x \le L$$

+

Force of the truss acting upward

$$y = \frac{Px^2}{6EI}(3a - x) \text{ for } 0 < x < a$$

L = 60 in, x = 36in, a = 36in

Find highest force on truss in all three positions:

Ideal position:

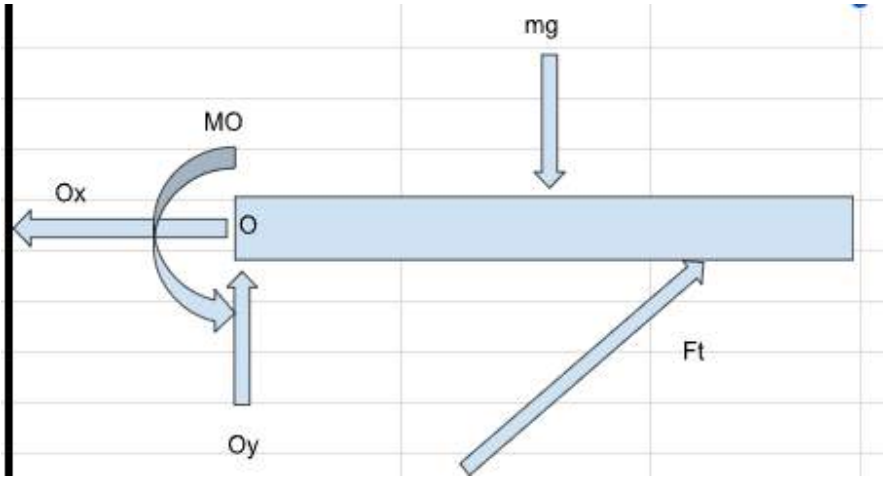

Knowns: mg = 40lbs, EI = 145000 kip/in^2

Unknowns: Ox, Oy, Mo, Ft

Compatibility: At x = 36 ; v = 0 (where the truss connects)

$\Sigma Fx = 0 = Ox + Ft\,cos(18.434)$

$\Sigma Fy = 0 = Oy + Ft\,sin(18.434) - mg$

$\Sigma Mo = 0 = Mo + Ft\,sin(18.434) \cdot 36in - mg \cdot 30in$

$$v = \frac{1}{EI}\left(\frac{mg\cdot(60in)^2}{48}(6\cdot 36in - 60in) - \frac{Ftsin(18.434)\cdot(36in)^2}{6}(3\cdot 36in - 36in)\right)$$

Find Ft with v = 0

$$0 = \left(\frac{(40)\cdot(60in)^2}{48}(6\cdot 36in - 60in) - \frac{Ftsin(18.434)\cdot(36in)^2}{6}(3\cdot 36in - 36in)\right)$$

$$Ft = \frac{\frac{(40)\cdot(60in)^2}{48}(6\cdot 36in - 60in)}{\frac{sin(18.434)\cdot(36in)^2}{6}(3\cdot 36in - 36in)} = 95.161lbs$$

Top side of position 2:

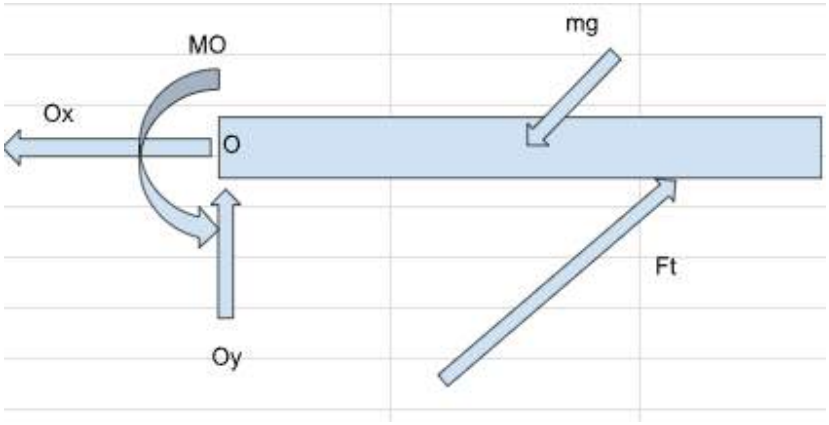

Knowns: mg = 40lbs, EI = 145000 kip/in^2
Unknowns : Ox, Oy, Mo, Ft
Compatibility: At x = 36 ; v = 0 (where the truss connects)

$\Sigma Fx = 0 = Ox + Ft\,cos(18.434) - mgcos(45)$

$\Sigma Fy = 0 = Oy + Ft\,sin(18.434) - mgsin(45)$

$\Sigma Mo = 0 = Mo + Ft\,sin(18.434)\cdot 36in - mgsin(45)\cdot 30in$

$$v = \frac{1}{EI}\left(\frac{mgsin(45)\cdot(60in)^2}{48}(6\cdot 36in - 60in) - \frac{Ftsin(18.434)\cdot(3in)6^2}{6}(3\cdot 36in - 36in)\right)$$

Bottom side of position 2

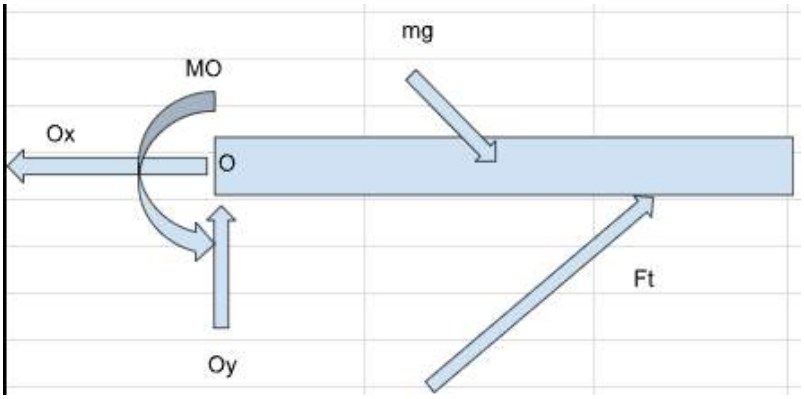

Knowns: mg = 40lbs, EI = 145000 kip/in^2
Unknowns : Ox, Oy, Mo, Ft
Compatibility: At x = 36 ; v = 0 (where the truss connects)

$\Sigma Fx = 0 = Ox + Ft\,cos(18.434) + mgcos(45)$

$\Sigma Fy = 0 = Oy + Ft\,sin(18.434) - mgsin(45)$

$\Sigma Mo = 0 = Mo + Ft\,sin(18.434) \cdot 36in - mgsin(45) \cdot 30in$

$v = \frac{1}{EI}\left(\frac{mgsin(45)\cdot(6in)0^2}{48}(6 \cdot 36in - 60in) - \frac{Ftsin(18.434)\cdot(3in)6^2}{6}(3 \cdot 36in - 36in)\right)$

V equation same for both to find Ft
Find Ft with v = 0

$0 = \left(\frac{(40sin(45))\cdot(60in)^2}{48}(6 \cdot 36in - 60in) - \frac{Ftsin(18.434)\cdot(3in)6^2}{6}(3 \cdot 36in - 36in)\right)$

$Ft = \frac{\frac{(40sin(45))\cdot(60in)^2}{48}(6\cdot 36in - 60in)}{\frac{sin(18.434)\cdot(3in)6^2}{6}(3\cdot 36in - 36in)} = 67.289lbs$

Vertical position

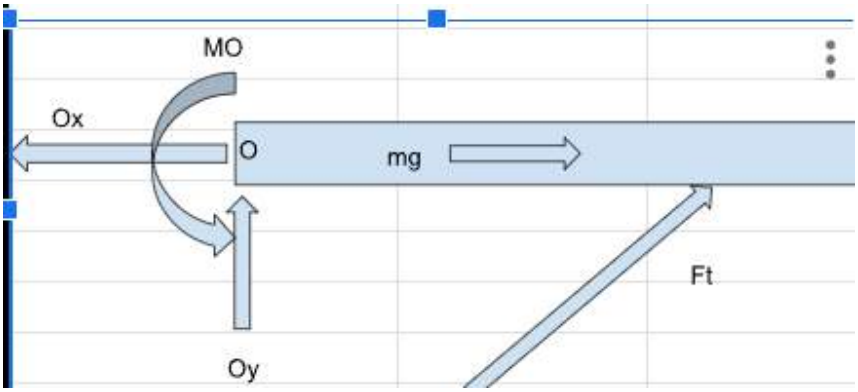

Knowns: mg = 40lbs, EI = 145000 kip/in^2
Unknowns: Ox, Oy, Mo, Ft
Compatibility: At x = 36in ; v = 0 (where the truss connects)

$\Sigma Fx = 0 = Ox + Ft\,cos(18.434) + mg$

$\Sigma Fy = 0 = Oy + Ft\,sin(18.434)$

$\Sigma Mo = 0 = Mo + Ft\,sin(18.434) \cdot 36\,in$

$v = \frac{1}{EI}\left(-\frac{Ftsin(18.434)\cdot(3in)6^2}{6}(3 \cdot 36in - 36in)\right)$

When v = 0

$0 = \frac{1}{EI}\left(-\frac{Ftsin(18.434)\cdot 36^2}{6}(3 \cdot 36 - 36)\right)$

Ft must be 0

Since position 3 has the most force on it it will fail first so we will test materials and design in that orientation

Ft = 95.161lbs

Calculate radius of the truss for the force applied with all 4 materials

$P_{cr} = \frac{\pi^2 EI}{L^2}$

$\sigma = \frac{P}{A}$

$A = \pi r^2$

$L = 3.162ft = 37.947in$

$Pcr = F * F.O.S$

$Pcr = \frac{\pi \cdot (EI)}{(L)^2}$

$I = \frac{\pi r^4}{4}$

Brittle:

<u>Gray cast iron 30</u>

EI = 15000 ksi

$I = \frac{\pi r^4}{4}$

σult = 100 ksi

$\sigma allow$ = 50 ksi

$\sigma allow = F/\pi r^2$

$r = \sqrt{\frac{95.161lbs}{50000\ lbs/in^2 \cdot \pi}} = 0.0246in$

$Pcr = F * F.O.S = 190.322lbs$

$Pcr = \frac{\pi \cdot (EI)}{(L)^2}$

$Pcr = \frac{\pi \cdot (15000000\ lbs/in^2 \cdot \frac{\pi r^4}{4})}{(37.947in)^2}$

$r = \sqrt[4]{\frac{4 \cdot (37.947in)^2 \cdot 190.322lbs}{\pi^3 \cdot 15000000\ lbs/in^2}} = 0.220in$

<u>Gray cast iron 60</u>

EI = 20000 ksi

σult = 180 ksi

$\sigma allow$ = 90 ksi

$\sigma allow = F/\pi r^2$

$r = \sqrt{\frac{95.161lbs}{90000\ lbs/in^2 \cdot \pi}} = 0.0183in$

$Pcr = F * F.O.S = 190.322lbs$

$Pcr = \frac{\pi \cdot (EI)}{(L)^2}$

$Pcr = \frac{\pi \cdot (20000000\ lbs/in^2 \cdot \frac{\pi r^4}{4})}{(37.947in)^2}$

$r = \sqrt[4]{\frac{4 \cdot (37.947in)^2 \cdot 190.322lbs}{\pi^3 \cdot 20000000\ lbs/in^2}} = 0.205in$

Ductile:

Stainless steel 304

EI = 27500 ksi

$\sigma yield$ = 40 ksi

$\sigma allow$ = 20 ksi

$\sigma allow = F/\pi r^2$

$r = \sqrt{\frac{95.161lbs}{20000\ lbs/in^2 \cdot \pi}} = 0.0389in$

$Pcr = F * F.O.S = 190.322lbs$

$Pcr = \frac{\pi \cdot (EI)}{(L)^2}$

$Pcr = \frac{\pi \cdot (27500000\ lbs/in^2 \cdot \frac{\pi r^4}{4})}{(37.947in)^2}$

$r = \sqrt[4]{\frac{4 \cdot (37.947in)^2 \cdot 190.322lbs}{\pi^3 \cdot 27500000\ lbs/in^2}} = 0.189in$

Aluminum Alloy

EI = 10150 ksi

$\sigma yield$ = 43ksi

$\sigma allow$ = 21.5ksi

$\sigma allow = F/\pi r^2$

$r = \sqrt{\frac{95.161lbs}{21500\ lbs/in^2 \cdot \pi}} = 0.375in$

$Pcr = F * F.O.S = 190.322lbs$

$Pcr = \frac{\pi \cdot (EI)}{(L)^2}$

$Pcr = \frac{\pi \cdot (10150000\ lbs/in^2 \cdot \frac{\pi r^4}{4})}{(37.947in)^2}$

$r = \sqrt[4]{\frac{4 \cdot (37.947in)^2 \cdot 190.322lbs}{\pi^3 \cdot 10150000\ lbs/in^2}} = 0.243in$

Back to Contents

8. Interdisciplinary Engineering ABET Requirements

Summary

This section includes documents fulfilling the ABET requirements for the Interdisciplinary Engineering program (ITDE 201).

- Personal Statement (PS)
- Degree Plan (DP)
- Professional Development Plan (PDP)
- Ethical Code Statement (ECS)

Contributors: Ian Wilhite (Solo Project)

Key Skills: Professional Development, Career Planning, Engineering Ethics, ABET Accreditation, Lifelong Learning.

Relevance: These documents showcase a commitment to professional growth and an understanding of the ethical and professional responsibilities of an engineer, as outlined by ABET.

ITDE Design Your Own Degree (DYOD) degree planner and Personal Statement

**Students pursuing a pre-defined tracks do NOT need to complete this planner.*

Please be very thorough in your responses for #1, 4, 5. The Review Committee expect well thought out responses that align with your choosen curriculum. Do not feel you need to restrict yourself in the length of your narrative.

Last Name	First Name	UIN
Wilhite	Ian	333008004

The Personal Statement and Degree Plan (DP) needs to be completed and submitted by Midterm week in your first full term in ITDE. A Registration Hold will be put on your if degree plan is not submitted by this time.

1) Why do you want to major Interdisciplinary Engineering?

Many courses that would be helpful in pursuit of a graduate degree in Robotics and Controls Engineering have been scattererd across the undergraduate diciplines: complex analysis, DSA, Modelling of mechancial systems, and digital signals. The goal in creating and executing a degree in Interdiciplinary engineering is to leverage the many relevant courses across multiple departments into a single consolidated program.

2) What are the multiple disciplines you intend to study for your Interdisciplinary Engineering degree?

they have all had to learn outside of their origional degree program: controls theory (Meen), robotoic software development with ROS and understanding Data Structures and Algorithms (DSA) for optimization (CSEN), fundamental digital systems design and I/O functionality (ECEN) on mainstream microcontrollers (Pis, arduino, pikhawk, etc), and complex analysis and a working understanding of linear algebra for computational needs (MATH).

3) What is the common thread through the courses you've chosen from different disciplines to make this a specialized study of engineering?

science, the applications from electrical and the abstract theory from math - all are essential to robotic development and I've heard time and time again in industry, research, and private R&D that most people end up getting a degree in one then having to go back and learn the others. The advantage that this degree program provides is the opportunity to cherrypick the exact relevant coursework to a controls application.

4) What are your plans immediately upon graduation with your BS in Interdisciplinary Engineering?

A) entering a gradaute program for higher level controls research to further my knowledge and network in the robotics sector; potentially taking a fellowship at Nasa, SWRI, LANL, or ORNL. The goal after finishing a higher degree would to be working in Research and Development either in the military or privately. Nasa is notorious for their robotics R&D and I believe requires no introduction. The Southwest Research Institute in San Antonio has been making large strides in their UAS and Autonomous systems research, as well as their dynamics in zero gravity environments. Los Alamos is admittedly the least applicable of the four but through ancillary projects will always have a home in the mountains for a controls engineer. Oak Ridge has been working heavily in the manufacturing automation space and was recently recruiting experts in UAS and UAV development for some upstarting projects - and I believe they will continue to in the future.

B) Joining the workforce as an Automation, Controls, or Robotics Engineer, likely in the industrial sector working on manufacturing robotics or the R&D sector of a major manufacturing company

C) joining the workforce in the military sector applying controls theory in the military or a defense contractor like Lockheed, Northup Gruman, Boeing, or Raytheon. In my work on a club project, I have already met with Lockheed Skunkworks engineers for autonomous UAV design.

5) What are your long term career goals?

industry that changes lives; Factory automation and power amp alleviates the labor for employees; military applications save soldiers; textbook controls applications are used everywhere from thermostats to autonomous vehicles. I want to make an impact with my work, and know that the things I create are going on to do more good long after I've left.

NAME: Ian Wilhite **UIN:** 333008004

***A complete and thorough Degree Plan (DP) is due by the end of the 5th week of your first full term in ITDE. A Registration Hold will be put on your if degree plan is not submitted by this time.*

DEGREE PLAN INSTRUCTIONS

Below are the ITDE Degree Requirements for your degree plan. There are two main areas: Core UCC/ITDE requirements (70 credits) and Technical Electives (58 credits).

Use the degree requirements and rules to build your degree plan starting in Semester #1. Directions to build your plan are below in 1-7.

1. In Cell I31, please start with your First Semester at TAMU for Semester #1:

a. Enter Term and Year (i.e. Fall 2023) in the blue boxes below.

b. Enter the Courses; Credits per course; and Grades received in courses.

c. Enter any dual credit or AP credit (only those that apply toward your ITDE degree) in Semester #1.

2. Continue to enter the same information in the following semesters until you reach your Current Semester.

3. In your Current Semester:

a. Enter the current Term and Year.

a. Enter current Coures; Course Names; their Pre-/Co-Requisites; and their Credits.

b. Enter IP (for In Progress) for your current grades.

4. Using the ITDE Degree Requirements rules for the Core UCC/ITDE(Area #1) and Technical Electives(Area #2):

a. Using the TAMU catalog (catalog.tamu.edu) in the Course Descriptions area along with the disciplines identified in #2 on the PS tab, start identifying the courses you which to take to apply as Techncial Electives in Area #2.

b. Enter the Courses; Credits; and Pre-/Co-reqs in Area #2 - Technical Electives. A good starting point is looking at the 400-level courses and then work backworks for what is required for pre-/co-reqs.

c. Be mindful of the rules in Areas #2 and #5 for the Techncial Electives!

d. Once you have at least 58 credits of technical electives, start building your degree plan at the right. **BE WARY OF PRE-/CO-REQS!**

e. Do not include those courses not applying toward ITDE degree.

5. In Area #4:

a. Indicate any minors or certificates and their coursework you are pursuing and these courses are in your degree plan.

b. These courses can also count towards your techncial electives in Area#2.

c. BE WARY OF PRE-/CO-REQS!

6. Make sure you triple-check the right-side of this sheet (semester-by-semester schedule) and the left-side (DP rules) agree and there are no pre-/co-req violations.

7. A letter grade of at least a C is required for all courses in the degree plan!!!

ITDE DEGREE REQUIREMENTS

1. Core UCC/ITDE - 70 total credits

Courses	Credits	Pre-requisites/Notes	DP Semester	Suggested Semester
Following 27 credits constitute the Common First Year Engineering curriculum				

CHEM 107 or CHEM 120 (4 credits)	3		S2	S1
CHEM 117	1	CHEM 107 or concurrent	S2	S1
ENGL 103 or ENGL 104	3		AP	AP
ENGR 102	2	Math 150/151 or concurrent	S1	S1
ENGR/PHYS 216	2	C or better in ENGR 102; C or better in Math 151; C or better in PHYS 206 or concurrent enrollment	S2	S2
ENGR/PHYS 217	2	C or better in ENGR/PHYS 216; C or better in MATH 152; C or better in PHYS 207 or concurrent enrollment	S5	S3
MATH 151	4	Math 150	AP	AP
MATH 152	4	Math 151 or equivalent	AP	AP
PHYS 206	3	C or better in MATH 151	AP	AP
PHYS 207	3	C or better in PHYS 206; C or better in Math 152	AP	AP
Communication Elective: COMM 203, COMM 205, COMM 243, ENGL 203, or ENGL 210	3	ENGL 203	AP	AP
ITDE 401 *(W course)*	3	Senior classification and approval of instructor	S5	Fall term of final year
ITDE 402	2	ITDE 401	S6	Spring term of final year
ITDE 201 *(C course)*	1		S3	1st fall term in ITDE
ITDE 301	1		S5	2nd fall term in ITDE
ITDE 399 - High Impact Experience	0		S5	Any term starting in 2nd year
ITDE 499 - Degree Plan Approval	0		S6	In your final term
MATH 251 or 253	3	Math 251	S1	S1
MATH 308	3	Math 308	S2	S2
MATH 304, MATH 323, MATH 311 or MATH 4(	3	Math 304	S1	S1
Math/Science Elective	3	*Math 407*	S6	Any term
Creative Arts UCC*	3	*perf 301/phil 482*	S5	Any term
American History UCC*	3	*hist 105*	AP	AP
American History UCC*	3	*hist 106*	AP	AP
POLS 206	3		AP	AP
POLS 207	3		S1	S1
Language, Philosophy, Culture UCC*	3	*hist 104*	AP	AP
Social and Behavioral Science UCC*	3	*phil 107*	AP	AP
Total Credits	**70**		**ABET Math/Sciences:**	**32**

See core.tamu.edu for options. At least 1 course needs to be ICD and at least one course needs to be CD.

***Please HIGHLIGHT IN RED ICD and CD courses on your Degree Plan (DP).*

2. Technical Electives - 58 total credits

a. No more than 30 credit hours from a single engineering department (please use RED font)

b. At least 24 credits of the technical electives must be composed of 300- and 400-level courses taken at TAMU.

HIGHLIGHT THESE COURSE NAMES/# IN YELLOW.

c. At least 34 credits of **engineering topics** in technical electives (see Area #5 below).

HIGHLIGHT THESE CREDITS IN ORANGE.

Courses	Credits	Pre-requisites/Notes	DP Semester
Meen 408	3	meen 364	S6
Meen 431	3	meen 364	S6
Meen 364	3	260, 363, ecen 215	S5
Meen 363	3	meen 357, meen 305*	S4
Meen 260	3	meen 315	S4
Meen 305	3	meen 225 & *meen 210*	S3
meen 357	3		S3
meen 221	3		S2
meen 210	2		S3
Meen 315	3		S4
Ecen 215	3		S3
stat 211	3		S2
econ 202	3		AP
csce 110	4		AP
csce 221	4	120, co 222	S4
ecen 222	3		S4
csce 411	3	221, 222	S6
csce 120	3		S3
ecen 248	4		S5
engr 462	1		S2
Total Credits	**60**	*Must add up to at least 58 cre*	

3. Degree plan must total at least 128 credits

	Credits	
Total # of credits in DP	**130**	(Sum of areas #1 and #2)

4. Minors and/or Certificates

List minor/certificate name and courses.

Course	Course Name	Credits
Control of Mechanical Systems		
Meen 363		3
Meen 364		3
Meen 408		3
Meen 431		3
Meen 433		3
	Total Credits	15

Course	Course Name	Credits
Math		
Math 152	Calc 2	4
Math 251	Calc 3	3
Math 308	Differential Equations	3
Math 304	Linear Algebra	3
Math 407	Complex Variables	3
	Total Credits	16

5. ABET Criteria

a. A total of at least 45 credits of engineering topics must be included. The UCC/ITDE Core includes 11 credits (marked with orange boxes below). Technical electives must include another 34 credits from Area#2 above.

b. Add engineering topics courses highlighted in ORANGE from your technical electives in Area #2 to the table below.

Note: **The following courses MAY NOT be included in the engineering topics category (they may be included in the DP elsewhere):**

Any course offered under CLEN, IDIS, ITSV, ESET, MARE, MARR, MART, MMET, or MXET prefixes

Any of ENGR 101, 251, 260, 262, 270, 281

Any of ENGR/MTDE 301, 311, 312, 313, 350, 351, 360, 421, 450, 451, 461, 462, 470

Any of ENGR/MTDE Engineering Entrepreneurship courses

Courses	Credits	DP Semester
Core UCC/ITDE		
ENGR 102	2	S1
ENGR/PHYS 216*	1	S2
ENGR/PHYS 217*	1	S3
ITDE 401 *(W course)*	3	S8
ITDE 402	2	S9
ITDE 201 *(C course)*	1	S3
ITDE 301	1	S5
ITDE 399 - High Impact Experience	0	S7
ITDE 499 Degree Plan Approval	0	S9
Technical Electives		
Meen 408	3	S6
Meen 431	3	S6
Meen 365	3	S5
Meen 364	3	S5

* ENGR/PHYS 216 and 217 each include 1 credit of engineering topics (the 1 credit of math/science in each course is not included here).

Meen 363	3	S4
Meen 260	3	S4
Meen 315	3	S4
Ecen 215	3	S3
Meen 305	3	S3
meen 357	3	S4
Csce 452	3	S6
Csce 431	3	S6
Csce 331	3	S5
csce 313	3	S5
csce 350	3	S4
csce 221	3	S4
	59	

Semester #1: First term at TAMU (*Include HS dual/AP credit that meet ITDE requirements*)

Term Year	***Fall 2023***	***please include summer tems in plan***		
Course	**Course Name**	**Pre-requisites**	**Credits**	**Grade**

Chem 119	Gen Chem 1		4	A
ENGR 102	engineering computation		2	A
POLS 207	State and local gov		3	B
MATH 251	Multi		3	B
Math 304	Linear		3	B
Math 151		AP	4	
Math 152		AP	4	
Phys 206		AP	3	
Phys 207		AP	3	
engl 104		AP	3	
engl 203		AP	3	
hist 104 - 106		AP	9	
pbsi 107		AP	3	
pols 206		AP	3	
csce 110		AP	4	
econ 202		AP	3	
			57	

idiot chec
#REF!

Semester #2

Term Year	**Spring 2024**			
Course	**Course Name**	**Pre-requisites**	**Credits**	**Grade**
Meen 221	statics		3	B
Math 308	Diff eq		3	B
Phys 216			2	A
Chem 120			4	C
Stat 211	stats 1		3	C
engr 462			1	A

	16

Semester #3

Term Year	Fall 2024		15		
Course	**Course Name**	**Pre-requisites**	**Credits**	**Grade**	
csce 120	**Program Design and Concepts**		**3**	**4**	12
Meen 357	Engienering Analysis		3	**4**	12
ecen 215	Principles of Electrical Engineering		3	**4**	12
itde 201	Foundations of Interdiciplinary Engineering		1	**4**	4
meen 305	Solid Mechanics		3	**2**	6
Meen 210	Geometric Modeling for Mechanical Design		2	**4**	8
					3.6

Semester #4

Term Year	Spring 2025		18	
Course	**Course Name**	**Pre-requisites**	**Credits**	**Grade**
meen 363	Dynamics and Vibrations		3	
meen 260	Mechanical Measurements		3	
AGCJ 404	Science Influnecers Program		3	
Math 407	Complex analysis		3	
Meen 315	Thermo		3	
AERO 489	autonomous aerospace systems		3	

Semester #5

Term Year	Summer 2025		6	
Course	**Course Name**	**Pre-requisites**	**Credits**	**Grade**
Creative Arts UCC*	Performance in World Cultures		3	
CSCE 222	Discrete Structures for Computing		3	

Semester #5

Term Year	Fall 2025		16	
Course	**Course Name**	**Pre-requisites**	**Credits**	
csce 221	Data Structures and Algorithms		4	
ecen 314	signals and systems		3	
ITDE 301	experimentation in itde		1	
ITDE 399 - High Imp	High Impact Experience		0	
ITDE 401 (W course	ITDE Capstone 1		3	
Meen 364	Dynamic Systems and Controls		3	**Grade**
phys 217	Experimental Physics and Engineering lab III - Electricity and Mag		2	

Semester #6

Term Year	Fall 2025		14	
Course	**Course Name**	**Pre-requisites**	**Credits**	
CSCE 411	Design of analytical algorithms		3	
itde 402	ITDE Capstone 2		2	
meen 408	Mechanics of Robotic Manipulators		3	
meen 431	Advanced System Dynamics and Controls		3	
ecen 420			3	
ITDE 499	degree plan approval		0	**Grade**

Personal Development Plan:

By Ian Wilhite

Vision Statement:

My vision is to lead and innovate in the field of robotics and control engineering, developing cutting-edge solutions that enhance the intersection between technology and humanity. I aim to create systems that not only drive efficiency and precision in industrial applications but also improve safety and accessibility in critical areas such as healthcare, disaster response, and sustainable infrastructure. By fostering collaboration, engaging in continuous learning, and adhering to the highest ethical standards, I strive to bridge the gap between emerging technologies and the needs of society, ensuring that the advancements in robotics serve as a force for good in the world.

Note: struck through items were placed on the plan as a part of an earlier revision and have been accomplished since being initially added.

Development Themes

- Learning
    1) 2025-2026: I will obtain relevant certificates in the immediate future to demonstrate to employers and institutions of higher education proof of my tangible skills.
        a) ~~Study for the Certified SolidWorks Associate certification (CSWA) and sit for the exam by December 2024 (free in the Zach FEDC)~~
        b) Utilize online certificates to learn and recognize skills that I wish to learn such as:
            i) ~~2024: Matlab Onramps Certification~~
            ii) 2025: Linkedin Learning Github Essentials
    2) 2026-2028: I will obtain degree(s) to demonstrate my knowledge to employers.
        a) 2026-2028: Maintain efforts in coursework and monitor degree plans to ensure meeting appropriate requirements. I will maintain a semesterly GPA above a 3.5.
        b) 2026: I will graduate in May of 2026 with a Bachelors in Interdisciplinary Engineering.
        c) 2027-2028: I will either graduate from an A&M Masters program in May of 2027, or a reputable non-A&M Masters program in May of 2028.
    3) 2029-2031: I will obtain professional licenses to certify the quality of my work.
        a) Take the FE exam in 2026/2027 and begin the working hours to qualify for the PE exam.
        b) Prepare for and take the PE exam in 2030/2031 (>4 years after FE)

    c) Begin hours for Project Management Professional (PMP) Certification in 2027 (Only if relevant, PE/PhD is plenty, and although another certificate would help, it would not be particularly relevant)
    d) Prepare for and take the PMP exam in 2030/2031 (>3 years of work)
- Networking
    1) 2025-2027: I will be actively involved in a student chapter of a professional society in school to find connections to my peers as well as internships and full time employment.
        a) 2024: I will uphold my office as an executive, and continue to plan and execute events for the remainder of the 2024-2025 academic year.
        b) 2025: I will run for president and use the opportunity to advocate for structural changes to our events calendar to better engage new members.
        c) 2025-2026: I will remain involved in the organization by remaining engaged in leadership, and being engaged in the big/little program.
        d) 2024-2026: I will attend the SEC and ASME career fairs and industry nights to learn about and network with companies that hire Controls, Automation, and Systems Engineers.
    2) 2026-2029: I will engage with professional societies for conferences, networking events, and professional growth opportunities.
        ~~a) NERC - UMASS 9/2024~~
        b) IEEE conferences: ICRA 5/2025
        c) TEROS 4/30/24 @UT
        d) Ubiquitous Robotics (UR) Conference 6/2/2025 @ TAMU
    3) 2027-2029: I will find ways to support student chapters of professional organizations through mentorship, networking with recruiters, and technical consulting
        a) I will be engaged in professional networks through the TAMU Industry Advisory Council; ASME national mentorship programs; any company specific mentorship programs
    4) 2024-2030: I will develop a respectable online presence through the use of social media platforms to make myself visible to employers and
        a) 2024: Upkeep Linkedin, maintain a positive image on Instagram.
        b) 2025: establish personal projects Instagram/Youtube account.
        c) 2026: Github personal academic website.
        d) 2027-2028: I will maintain a consistent image and watch for new emerging popular technologies.
- Experience
    1) 2025-2026: I will participate in interdisciplinary collaborative projects to apply my skills early in my career
        a) 2024: set project objectives and tasks for DRON project with TURTLE
        b) 2025: find additional personal projects relevant to robotic employers, potentially with publishable content
        c) 2026: find an undergraduate role in a research lab where I can collaborate in robotic projects with a novel purpose

    d) 2025-2026: identify persons for a robotics-related senior design project
    e) 2026: successfully deliver a senior design project.
2) 2025-2027: I will find early career opportunities that allow me to learn a variety of skills, ideally in a rotational program
    a) 2025: I will find and complete an internship or research fellowship that allows me to work professionally in the robotics field.
    b) 2026: I will find and complete a research oriented program that supports research for graduate programs.
    c) 2027: I will find summer programs that support masters programs by bringing varied skills, ideally through travel or rotational programs.
3) 2027-2030: I would like to find roles where I can learn in a hands-on manner by applying lessons learned to tangible projects - ideally in a research or a private R&D environment
    a) 2027-2030: find work post-masters either in industry working in R&D or academia in a PhD program

- Leadership
    1) 2025-2026: I will look to student organizations for leadership opportunities in *social* and professional development roles
        a) 2025: continue to serve as ASME Secretary; support the goals and ambitions of my officers; ensure to utilize events as opportunities to meet new people.
        b) 2026: look for additional roles to network within electrical, mechatronic, and interdisciplinary groups.
        c) 2025-2026: look for leadership positions within professional organizations in robotics-related groups.
    2) 2026: I will look to student organizations for leadership opportunities in *technical* and project management style roles
        a) 2025: I will continue as a project lead in TURTLE and effectively coordinate my subteams to grow my skills in technical leadership, my understanding of autonomous systems, and help develop the skills of others.

Last Updated: December 2024.

Ian Wilhite
ECS developed for ITDE 201

PREAMBLE:
The field of Robotics and Controls is dedicated to designing and implementing systems that enhance efficiency, safety, and precision across a wide range of applications, from industrial automation to critical healthcare devices. As these systems increasingly interact with humans and impact essential societal functions, the need for a robust ethical framework becomes paramount. A clear code of ethics ensures that engineers prioritize public welfare, maintain professional integrity, and navigate the complex challenges of this rapidly evolving discipline responsibly. This code serves as a guiding document to uphold trust, accountability, and excellence in all endeavors within Robotics and Controls engineering.

EXPLANATION OF HOW THIS CODE WAS WRITTEN:
This code was developed by referencing existing professional ethical guidelines, including the National Society of Professional Engineers (NSPE) Code of Ethics, the American Society of Mechanical Engineers (ASME), and the Institute of Electrical and Electronics Engineers (IEEE) Code of Ethics. These codes provide foundational principles that were adapted to reflect the unique nature of Robotics and Controls engineering.

CANONS AND REFLECTIONS:

1. Robotics and Controls Engineers shall hold paramount the safety, health, and welfare of the public.
   Reflections - Robotics and Controls engineers often work in industrial applications, and in doing so are creating systems to work alongside humans, and the results of a malfunction could be catastrophic. This canon emphasizes that public safety shall always be prioritized over efficiency or cost reduction. Robotics and Controls engineers must ensure machines are operating in a safe manner around humans.
2. Robotics and Controls Engineers shall issue public statements only in an objective and truthful manner.
   Reflections - Robotics is a growing field with questions constantly being raised on safe practices, reliability, and new developments. Robotics and Controls engineers shall issue statements only with proper research, knowledge, and relevance. Transparency is crucial for any communications, along with potential downsides and dangers to new methodologies.
3. Robotics and Controls Engineers shall perform services only in the areas of their competence.
   Reflections - Robotics and Controls engineering spans a vast range of specialties, from artificial intelligence to biomechanical systems. Engineers in this field must recognize and respect the boundaries of their expertise, seeking further education or consulting specialists when necessary. This ensures that projects are approached with adequate knowledge and skill, reducing the risk of errors that could jeopardize safety or functionality. Competence also involves staying updated with advances in technology

and ethical standards, as a lack of proficiency can lead to unintended harm or diminished trust in the profession.

4. Robotics and Controls Engineers shall act for each employer or client as faithful agents or trustees.
   Reflections - The Robotics and Controls industry is still emerging, making trust between clients, employers, and the public critical to its success. Engineers must prioritize honesty, integrity, and quality in their work to uphold this trust. By acting as dependable agents, they strengthen the field's credibility and lay a reliable foundation for future innovations. This trustworthiness is not only vital for current projects but also reinforces the profession's reputation, encouraging wider acceptance and investment in the field.
5. Robotics and Controls engineers shall ensure reliability in accountability measures.
   Reflections - As automation grows in scale and applicability, there is an increasingly prevalent need for redundant safety measures. As automation becomes more commonplace, the public will trust it more, and will act with less caution around potentially dangerous machinery, requiring more robust safety measures and control systems.
6. Robotics and Controls Engineers shall uphold and enhance the honor, integrity, and dignity of the growing profession.
   Reflections - As pioneers of a new space, the public perception of the discipline is very malleable, bringing all the more importance to the upholding ethical standard to protect the public. When one bridge collapses, it is a tragedy, but people don’t lose faith in every bridge ever built; if one robot kills someone, then the entire industry is brought to a standstill. Without trust, there is no future for this industry, the American nuclear engineering sector can demonstrate that much; while this field is still growing and defining its role, it is incredibly important that the public perception be upheld.

Back to Contents

9. NASA L'SPACE Mission Concept Academy (MCA)

Summary

Through the NASA Lucy Student Pipeline Accelerator and Competency Enabler (L'SPACE) Mission Concept Academy (MCA) I have had the incredible privelige to serve as the Project Manager (PM) and lead a group of 20 scientists, engineers, and programmatics specialists across the country to develop a NASA Discovery-Class mission from scratch. We propose PHOENIX, an unmanned rover mission to Mars to support future human exploration. The PDR document is included below, as it contains all relevant details of the other documents.

- Mission Concept Review (MCR)
- System Requirements Review (SRR)
- Mission Design Review (MDR)
- Preliminary Design Review (PDR)

Contributors: Mission Concept Academy Summer 2025 Team 01

Key Skills: Systems Engineering, Mission Design, NASA Project Lifecycle, System Requirements, Technical Writing, Team Collaboration.

Relevance: This experience provides direct insight into NASA's mission development process, how scientific needs drive system design, how programmatics enable their conduction. In addition to serving as the Project Manager, I also worked heavily on the Command and Data Handling (CDH) Engineering Subsystem.

L’SPACE MCA

Planetary Habitat Operations & Exploration Investigation eXpedition

PRELIMINARY DESIGN REVIEW

TEAM 1 - P.H.O.E.N.I.X

Submission date - 8/18/2025

P.H.O.E.N.I.X

To mars and beyond

Table of Contents

Table of Contents **2**
Table of Figures **7**
Table of Acronyms **10**
1.0 Mission Overview **13**
1.1 Mission Statement 13
1.2 Science Traceability Matrix 15
Figure 1.2.1: Science Traceability Matrix 18
1.3 Summary of Mission Location 19
1.4 Mission Requirements 22
Figure 1.4.1: Requirements Table 25
1.5 Concept of Operations (ConOps) 26
Figure 1.5.1: Concept of Operations 28
1.6 Vehicle Design Summary 29
Figure 1.6.1: Complete Rover Design 30
Figure 1.6.2: Complete Rover Design Top View 31
Figure 1.6.3: Complete Rover Design Bottom View 32
Figure 1.6.4: Internal Rover Design View 32
1.7 Science Instrumentation Summary 34
1.8 Programmatic Summary 35
1.8.1 Team Introduction 35
Ian Wilhite – Project Manager (PM) 35
Aidan Piper – Deputy Project Manager of Resources (DPMR) 35
Danyal Khan – Lead Systems Engineer (LSE) 35
Alanis Cubi Negron – Chief Scientist (CS) 35
Ibrahim Jaber – Program Analyst (PA) 36
Gabi Zabiegaj – Mechanical Engineer (ME) 36
Pablo Pena – Mechanical Engineer (ME) 36
Fatima “Flynn” Mendoza - Thermal Engineer (TE) 36
Andy Lien – Thermal Engineer (TE) 37
Adrian Raj – Command & Data Handling Engineer (CDHE) 37
Conor Foley – Command & Data Handling Engineer (CDHE) 37
Asherr Ralph – Electrical Engineer (EE) 37
Audrey Sorenmann – Electrical Engineer (EE) 38
Lucia Piedra – Scientist / Astrobiologist 38
Anna Hulett – Scientist / Astrobiologist 38
Matthew Lawrence – Scientist / Planetary Geologist 38
Katelyn Czarnowski – Scientist / Planetary Geologist 39
1.8.2 Team Management Overview 40
Figure 1.8.2.1: Organizational Chart 40

1.8.3 Schedule Overview 42
Table 1.8.3.1: Phase Milestones Table 42
1.8.4 Cost Overview 44
Figure 1.8.4.1: P.H.O.E.N.I.X Budget Breakdown Chart 44
Figure 1.8.4.2: P.H.O.E.N.I.X Budget Breakdown Table 45
2.0 Overall Vehicle and System Design 46
2.1 Spacecraft Overview 46
Figure 2.1.1: Engineering SubSystem Table 47
Figure 2.1.2: System Requirements Table 53
2.1.1 Mechanical Subsystem Overview 54
2.1.1.1 Mechanical Subsystem Requirements 56
Figure 2.1.1.1.1: Mechanical Requirements Table 57
2.1.1.2 Mechanical Sub-Assembly Overview 58
2.1.1.3 Mechanical Subsystem Recovery and Redundancy Plans 63
2.1.1.4 Mechanical Subsystem Manufacturing and Procurement Plans 64
2.1.1.5 Mechanical Subsystem Verification Plans 66
Figure 2.1.1.5.1: Mechanical Verification Plan Table 66
2.1.2 Power Subsystem Overview 68
2.1.2.1 Power Subsystem Requirements 71
Figure 2.1.2.1.1: Power Requirements Table 73
2.1.2.2 Power Sub-Assembly Overview 74
2.1.2.3 Power Subsystem Recovery and Redundancy Plans 78
2.1.2.4 Power Subsystem Manufacturing and Procurement Plans 80
2.1.2.5 Power Subsystem Verification Plans 82
2.1.3 CDH Subsystem Overview 84
Figure 2.1.3.1: Software Architecture Flowchart 85
2.1.3.1 CDH Subsystem Requirements 87
Figure 2.1.3.1.1: CDH Requirements Table 89
2.1.3.2 CDH Sub-Assembly Overview 90
2.1.3.3 CDH Subsystem Recovery and Redundancy Plans 95
2.1.3.4 CDH Subsystem Manufacturing and Procurement Plans 96
2.1.3.5 CDH Subsystem Verification Plans 98
Figure 2.1.3.5.1: CDH Verification Plan Table 99
2.1.4 Thermal Control Subsystem Overview 102
Figure 2.1.4.1: RIMFAX casing radiation 103
Figure 2.1.4.2 Hot Case Heat Flow Map 103
Figure 2.1.4.3: Cold Case Heat Flow Map 104
2.1.4.1 Thermal Control Subsystem Requirements 105
Figure 2.1.4.1.1: Thermal Requirements Table 106
2.1.4.2 Thermal Control Sub-Assembly Overview 107
2.1.4.3 Thermal Control Subsystem Recovery and Redundancy Plans 111

2.1.4.4 Thermal Control Subsystem Manufacturing and Procurement Plans 112
2.1.4.5 Thermal Control Subsystem Verification Plans 114
Figure 2.1.4.5.1: Thermal Verification Plan Table 114
2.1.5 Payload Subsystem Overview 116
2.1.5.1 Science Instrumentation Requirements 120
Figure 2.1.5.1.1: Payload Requirements Table 121
2.1.5.2 Payload Subsystem Recovery and Redundancy Plans 123
Figure 2.1.5.2.1: Instrument Redundancy Matrix 124
2.1.5.3 Payload Subsystem Manufacturing and Procurement Plans 126
2.1.5.4 Payload Subsystem Verification Plans 129
Figure 2.1.5.4.1: Payload Verification Plan Table 130
2.2 Interface Control 132
Figure 2.2.1: System Block Diagram 136
Figure 2.2.2: Robotic Arm Design 138
Figure 2.2.3: N^2 System Interfaces Chart 140
3.0 Science Mission Plan 141
3.1 Science Objectives 141
3.2 Experimental Logic, Approach, and Method of Investigation 142
3.3 Payload Success Criteria 145
Figure 3.3.1: Instrument Success Criteria 146
3.4 Testing and Calibration Measurements 147
3.5 Precision and Accuracy of Instrumentation 149
1 µSv/h–10 Sv/h3.6 Expected Data & Analysis 151
Figure 3.6.1: Raman spectra of a mineral under vacuum and CO_2 conditions 151
Figure 3.6.2: Raman spectra of a mineral showing shifts due to changes in temperature and pressure 151
Figure 3.6.3: Raman spectra of minerals collected by a Mars rover in laboratory and simulated Martian conditions 151
Figure 3.6.4: Transmission Data Graph Example 152
Figure 3.6.5: Comparative Transmission Spectra Example 153
Figure 3.6.6: RIMFAX Example Data 154
Figure 3.6.7: Gamma Neutron Example Data 155
4.0 Mission Risk Management 156
4.1 Safety and Hazard Overview 156
4.1.1 Risk Analysis 157
Figure 4.1.1.1 Advanced Risk log 164
4.1.2 Failure Mode and Effect Analysis (FMEA) 165
Figure 4.1.2.1: FMEA Table 170
4.1.3 Personnel Hazards and Mitigations 171
5.0 Activity Plan 173
5.1 Project Management Approach 173

Figure 5.1.1: Teamwide Organizational Chart 173
5.2 Mission Schedule 176
5.2.1 Schedule Basis of Estimate 176
5.2.2 Mission Schedule 179
Figure 5.2.2.1: Gantt Chart for Phase C1 182
Figure 5.2.2.2: Gantt Chart for Phase C2 183
Figure 5.2.2.3: Gantt Chart for Phase D1 184
Figure 5.2.2.4: Gantt Chart for Phase D2 185
Figure 5.2.2.5: Gantt Chart for Phase D3 186
Figure 5.2.2.6: Gantt Chart for Phase D4 187
Figure 5.2.2.7: Gantt Chart for Phase E1 187
Figure 5.2.2.8: Gantt Chart for Phase E2 188
Figure 5.2.2.9: Gantt Chart for Phase F1 189
Figure 5.2.2.10: Gantt Chart for Phase F2 189
5.3 Budget 190
5.3.1 Budget Basis of Estimate 190
5.3.2 Total Mission Cost 192
Figure 5.3.2.1: P.H.O.E.N.I.X Full Budget Table 193
5.3.3 Personnel Budget 194
Figure 5.3.3.1: Personnel Phase Allotment Table 195
Figure 5.3.3.2: P.H.O.E.N.I.X Personnel Budget 196
5.3.4 Travel Budget 197
Figure 5.3.4.1: Trip Estimate Breakdown 197
Figure 5.3.4.2: Travel Cost Breakdown Table 198
5.3.5 Outreach Budget 199
Table 5.3.5.1: Outreach Budget Table 200
5.3.6 Direct Costs 201
Table 5.3.6.1: Direct Costs Table 205
5.4 Scope Management 206
5.4.1 Change Control Management 206
Figure 5.4.1.1: Change Log 208
5.4.2 Scope Control Management 209
5.5 Outreach Summary 211
6.0 Conclusion **213**
Bibliography/References 214
Declaration of Generative AI Usage 232
Appendices 233
Figure A.1: (TBD/TBR Table) 233
Figure A.2 (Mission Change Log) 233
Figure A.3 (Heat Transfer Equations) 234
Figure A.4: (Submersible Gamma Neutron Probe with Rotary and Linear motion Sensors

CAD) 234
Figure A.5: (Submersible Gamma Neutron Probe with Rotary and Linear motion Sensors CAD Drawing) 235
Figure A.6: (Tire CAD) 236
Figure A.7: (Tire CAD Drawing) 237
Figure A.8: (Spokes CAD) 238
Figure A.10: (Front Rocker Bogie Arm CAD Drawing) 240
Figure A.11: (Front Rocker Bogie Arm CAD) 241
Figure A.12: (Back Rocker Bogie Arm CAD) 242
Figure A.13: (Back Rocker Bogie Arm CAD Drawing) 243
Figure A.14: (Robotic Arm Base CAD) 244
Figure A.15: (Robotic Arm Base CAD Drawing) 245
Figure A.16: (Robotic Arm Connector CAD) 246
Figure A.17: (Robotic Arm Connector CAD Drawing) 247
Figure A.18: (Robotic Arm Bottom Joint CAD) 248
Figure A.19: (Robotic Arm Bottom Joint CAD Drawing) 249
Figure A.18: (Robotic Arm Top Joint CAD) 249
Figure A.20: (Robotic Arm Top Joint CAD Drawing) 250
Figure A.21: (Robotic Arm Back Swivel CAD) 251
Figure A.22: (Robotic Arm Back Swivel CAD Drawing) 252
Figure A.23: (Robotic Arm Front Swivel CAD) 253
Figure A.24: (Robotic Arm Front Swivel CAD Drawing) 254
Figure A.25: (Robotic Arm Gripper CAD) 255
Figure A.26: (Robotic Arm Gripper CAD Drawing) 256
Figure A.27: (Chassis Differential CAD) 257
Figure A.28: (Chassis Differential CAD Drawing) 258
Figure A.29: (Chassis CAD) 259
Figure A.30: (Chassis CAD Drawing) 260
Figure A.31: (Mechanical Subsystem MCCET) 261
Figure A.32: (SER for Mini-TLS) 261
Figure A.33: (SER for Rimfax) 261
Figure A.34: (SER for Gamma Neutron Probe) 261
Figure A.35: (SER for Spectrometer) 261
Figure A.36: (Thermal Subsystem MCCET) 262
Figure A.37: (Software MCCET) 263
Figure A.38: (Electronics MCCET) 264

Table of Figures

Figure 1.2.1: Science Traceability Matrix 18
Figure 1.4.1: Requirements Table 25
Figure 1.5.1: Concept of Operations 28
Figure 1.6.1: Complete Rover Design 30
Figure 1.6.2: Complete Rover Design Top View 31
Figure 1.6.3: Complete Rover Design Bottom View 32
Figure 1.6.4: Internal Rover Design View 32
Figure 1.8.2.1: Organizational Chart 40
Table 1.8.3.1: Phase Milestones Table 42
Figure 1.8.4.1: P.H.O.E.N.I.X Budget Breakdown Chart 44
Figure 1.8.4.2: P.H.O.E.N.I.X Budget Breakdown Table 45
Figure 2.1.1: Engineering SubSystem Table 47
Figure 2.1.2: System Requirements Table 53
Figure 2.1.1.1.1: Mechanical Requirements Table 57
Figure 2.1.1.5.1: Mechanical Verification Plan Table 66
Figure 2.1.2.1.1: Power Requirements Table 73
Figure 2.1.3.1: Software Architecture Flowchart 85
Figure 2.1.3.1.1: CDH Requirements Table 89
Figure 2.1.3.5.1: CDH Verification Plan Table 99
Figure 2.1.4.1: RIMFAX casing radiation 103
Figure 2.1.4.2 Hot Case Heat Flow Map 103
Figure 2.1.4.3: Cold Case Heat Flow Map 104
Figure 2.1.4.1.1: Thermal Requirements Table 106
Figure 2.1.4.5.1: Thermal Verification Plan Table 114
Figure 2.1.5.1.1: Payload Requirements Table 121
Figure 2.1.5.2.1: Instrument Redundancy Matrix 124
Figure 2.1.5.4.1: Payload Verification Plan Table 130
Figure 2.2.1: System Block Diagram 136
Figure 2.2.2: Robotic Arm Design 138
Figure 2.2.3: N^2 System Interfaces Chart 140
Figure 3.3.1: Instrument Success Criteria 146
Figure 3.6.1: Raman spectra of a mineral under vacuum and CO_2 conditions 151
Figure 3.6.2: Raman spectra of a mineral showing shifts due to changes in temperature and pressure 151
Figure 3.6.3: Raman spectra of minerals collected by a Mars rover in laboratory and simulated Martian conditions 151
Figure 3.6.4: Transmission Data Graph Example 152
Figure 3.6.5: Comparative Transmission Spectra Example 153
Figure 3.6.6: RIMFAX Example Data 154

Figure 3.6.7: Gamma Neutron Example Data 155
Figure 4.1.1.1 Advanced Risk log 164
Figure 4.1.2.1: FMEA Table 170
Figure 5.1.1: Teamwide Organizational Chart 173
Figure 5.2.2.1: Gantt Chart for Phase C1 182
Figure 5.2.2.2: Gantt Chart for Phase C2 183
Figure 5.2.2.3: Gantt Chart for Phase D1 184
Figure 5.2.2.4: Gantt Chart for Phase D2 185
Figure 5.2.2.5: Gantt Chart for Phase D3 186
Figure 5.2.2.6: Gantt Chart for Phase D4 187
Figure 5.2.2.7: Gantt Chart for Phase E1 187
Figure 5.2.2.8: Gantt Chart for Phase E2 188
Figure 5.2.2.9: Gantt Chart for Phase F1 189
Figure 5.2.2.10: Gantt Chart for Phase F2 189
Figure 5.3.2.1: P.H.O.E.N.I.X Full Budget Table 193
Figure 5.3.3.1: Personnel Phase Allotment Table 195
Figure 5.3.3.2: P.H.O.E.N.I.X Personnel Budget 196
Figure 5.3.4.1: Trip Estimate Breakdown 197
Figure 5.3.4.2: Travel Cost Breakdown Table 198
Table 5.3.5.1: Outreach Budget Table 200
Table 5.3.6.1: Direct Costs Table 205
Figure 5.4.1.1: Change Log 208
Figure A.1: (TBD/TBR Table) 233
Figure A.2 (Mission Change Log) 233
Figure A.3 (Heat Transfer Equations) 234
Figure A.4: (Submersible Gamma Neutron Probe with Rotary and Linear motion Sensors CAD) 234
Figure A.5: (Submersible Gamma Neutron Probe with Rotary and Linear motion Sensors CAD Drawing) 235
Figure A.6: (Tire CAD) 236
Figure A.7: (Tire CAD Drawing) 237
Figure A.8: (Spokes CAD) 238
Figure A.10: (Front Rocker Bogie Arm CAD Drawing) 240
Figure A.11: (Front Rocker Bogie Arm CAD) 241
Figure A.12: (Back Rocker Bogie Arm CAD) 242
Figure A.13: (Back Rocker Bogie Arm CAD Drawing) 243
Figure A.14: (Robotic Arm Base CAD) 244
Figure A.15: (Robotic Arm Base CAD Drawing) 245
Figure A.16: (Robotic Arm Connector CAD) 246
Figure A.17: (Robotic Arm Connector CAD Drawing) 247
Figure A.18: (Robotic Arm Bottom Joint CAD) 248

Figure A.19: (Robotic Arm Bottom Joint CAD Drawing) 249
Figure A.18: (Robotic Arm Top Joint CAD) 249
Figure A.20: (Robotic Arm Top Joint CAD Drawing) 250
Figure A.21: (Robotic Arm Back Swivel CAD) 251
Figure A.22: (Robotic Arm Back Swivel CAD Drawing) 252
Figure A.23: (Robotic Arm Front Swivel CAD) 253
Figure A.24: (Robotic Arm Front Swivel CAD Drawing) 254
Figure A.25: (Robotic Arm Gripper CAD) 255
Figure A.26: (Robotic Arm Gripper CAD Drawing) 256
Figure A.27: (Chassis Differential CAD) 257
Figure A.28: (Chassis Differential CAD Drawing) 258
Figure A.29: (Chassis CAD) 259
Figure A.30: (Chassis CAD Drawing) 260
Figure A.31: (Mechanical Subsystem MCCET) 261
Figure A.32: (SER for Mini-TLS) 261
Figure A.33: (SER for Rimfax) 261
Figure A.34: (SER for Gamma Neutron Probe) 261
Figure A.35: (SER for Spectrometer) 261
Figure A.36: (Thermal Subsystem MCCET) 262
Figure A.37: (Software MCCET) 263
Figure A.38: (Electronics MCCET) 264

Table of Acronyms

Abbreviation	Definition
ADV	Action/Decision Vector
AI	Artificial Intelligence
AZUR	AZUR Space Solar Power GmbH
CCB	Change Control Board
CCHP	Constant Conductance Heat Pipe
CDH	Command and Data Handling
CDR	Critical Design Review
CER	Cost Estimating Relationships
ConOps	Concept of Operations
COTS	Commercial Off-The-Shelf
CP-MU	Critical Protection - Monitoring Unit
DC	Direct Current
DMU	Data Management Unit
ECC	Error-Correcting Code
EMI	Electromagnetic Interference
EOL	End Of Life
ESDMD	Exploration Systems Development Mission Directorate
FEA	Finite Element Analysis

Abbreviation	Definition
FMEA	Failure Modes and Effects Analysis
FPS	Fluid Protection System
HBS	Human Biology System
IMU	Inertial Measurement Unit
ISRU	In-Situ Resource Utilization
JMARS	Java Mission Planning and Analysis for Remote Sensing
JPL	Jet Propulsion Laboratory
L’SPACE MCA	L’SPACE Mission Concept Academy
L’SPACE NPWEE	L’SPACE NASA Proposal Writing and Evaluation Experience
MCCET	Mission Concept Cost Estimate Tool
MCR	Mission Concept Review
MG	Mission Goal
Mini-TLS	Miniature Tunable Laser Spectrometer
MLI	Multi-Layered Insulation
MRO	Mars Reconnaissance Orbiter
MDR	Mission Definition Review
MPPT(s)	Maximum Power Point Tracker(s)
NASA NCAS	NASA Community College Aerospace Scholars
PDR	Preliminary Design Review

Abbreviation	Definition
PWR	Power
RAD	Radiation Assessment Detector
RIMFAX	Radar Imager for Mars’ Subsurface Experiment
RLS	Raman Laser Spectrometer
ROI	Region of Interest
ROSA	Roll-Out Solar Array
RTG	Radioisotope Thermoelectric Generator
SMD	Science Mission Directorate
SRB	Systems Review Board
SRR	System Requirements Review
STM	Science Traceability Matrix
SYS	System
TCS	Thermal Control System
TBD	To Be Determined
TBR	To Be Resolved
TLS	Tunable Laser Spectrometer
TRL	Technology Readiness Level
UHF	Ultra High Frequency

1.0 Mission Overview

1.1 Mission Statement

P.H.O.E.N.I.X (Planetary Habitat Operations & Exploration InvestigatioN eXpedition) is an unmanned rover mission to Mars. The basic mission design is derived from the goal of investigating subsurface ice reservoirs to characterize environmental hazards, and better understand them in order to support future human exploration. Determining this data will give valuable insight into which areas of Mars are suitable for habitation, traversal, and future exploration. As with NASA's Discovery-class missions, the rover will land in the northern mid-latitudinal region of Mars where there is high potential for shallow ice beneath the surface, allowing high-value science to be performed on Mars in a favorable location for future flights and high science data return. This location is also favorable due to high solar solar access, and traversable terrain for the rover to collect data on. The mission aligns with the NASA Science Mission Directorate (SMD) and Exploration Systems Development Mission Directorate (ESDMD) by targeting in-situ resource utilization (ISRU), minimizing risks and hazards, and driving habitability research.

Science goals are derived from NASA's HBS-1LM Moon to Mars Objective and the Origins, Worlds, and Life Decadal Strategy goal Q10.3b: Understand the effects of short-and long-duration exposure to the environments of the Moon, Mars, and deep space on biological systems and health, using humans, model organisms, systems of human physiology, and plants [69].

The mission is guided by four key objectives. The first encompasses assessing the effects of radiation on a pressurized liquid sample using a neutron probe, informing ISRU and life support safety based on the results. Secondarily, analysis of subsurface stratigraphy and dielectric properties via radar to evaluate ice accessibility and potential for potable water. Third, determining the ratio of certain hydrogen atoms available in samples of hydrated volcanic rock with a laser spectrometer to trace water source evolution. Finally, to identify the crystal structure of asteroid-impact minerals using a Raman Laser Spectrometer to study endogenic and exogenic processes affecting water distribution.

To accomplish these objectives, the rover is engineered for long-duration autonomous operation in harsh Martian conditions. Its mechanical subsystem utilizes a heritage rocker-bogie suspension, titanium fittings, and an aluminum chassis for resilient mobility across more than 10km of variable terrain. The power subsystem includes ROSA-style solar panels, a 4300 Wh lithium-ion battery, and a smart distribution unit for efficient, fault-tolerant energy management. The CDH system

features radiation-hardened processing and redundant communication pathways. Thermal control maintains internal temperatures from -120°C to +30°C using multilayer insulation and active heating using electric heaters. All subsystems meet planetary protection guidelines and mission constraints on mass, volume, cost and schedule.

By locating accessible water ice, monitoring radiation exposure, and expanding understanding of Martian water cycles, the rover delivers critical data to guide astronaut landing site selection and surface system design. The mission represents a significant step toward enabling a sustainable human presence on Mars, aiding in the future of space exploration by providing valuable data for years to come.

1.2 Science Traceability Matrix

The Science Traceability Matrix (STM) holds the primary focus of four objectives derived from the *Human Exploration goal HBS-1LM* and the *Science Exploration goal Q10.3b* [69].

Human Exploration goal HBS-1LM objectives:

Direct contributions to the *HBS-1LM* goal are made by increasing knowledge of planetary science, planetary geology, and materials engineering innovation that is vital to understanding the Martian environment, sustaining long-duration manned missions, and protecting the health of astronauts. Mission constraints are met within the instruments' 15kg allocated mass, volume, and resolution requirements.

1. Investigate potential Martian environmental exposure impacts on a custom-engineered, pressurized, and rover-attached Fluid Protection System (FPS) that internally houses the CP-MU DMU-100 Submersible Gamma Neutron Probe and an earth water sample. The probe shall use its passive ionization chamber to monitor for, document, and transmit gamma radiation level (µSv/h) fluctuations in weekly intervals for a minimum of one year. The planetary science data collected from this objective shall drive Materials Engineering innovation to uncover and eliminate planetary hazards that threaten the integrity of mission-critical fluids (life support, rocket propellant, agricultural fluids containing minerals for successful plant cultivation, and drinking water) in transportation, storage and recycling on the Martian surface during future long-duration manned missions. This research is essential for preventing fluid contamination, depressurization and explosion hazards, and unstable thermal regulation across the extreme temperature variations of the Martian environment.

2. Investigate how subsurface stratigraphy, dielectric properties, and dust layer thickness influence the accessibility and long-term stability of near-surface ice. The Radar Imager for Mars' Subsurface Experiment (RIMFAX) shall use a ground-penetrating radar to analyze signal delays and reflection strength, allowing identification of subsurface layer boundaries, material transitions, and dielectric properties indicative of dust and possible ice-rich zones [53]. From these observables, dielectric permittivity and radar wave velocity can be estimated to derive subsurface material properties such as layer thickness, composition variation, and porosity across a 10 km traverse [53].

Science Exploration goal Q10.3b objectives:

These objectives below shall contribute directly to goal Q10.3b by exploring the geological history of the Martian subsurface and the environmental impact on the endogenic and exogenic controls on the presence of liquid water. The stakeholder's experiment constraints of 185 kg mass, under 5 grams of radioactive materials, and $450 million budget for the system and its instruments are met within these

requirements. Under the prohibited materials constraint the Radioisotope Thermoelectric Generator (RTG) is prohibited and not used.

1. Determine the Deuterium to Hydrogen (D/H) ratio in hydrated volcanic rock on the Martian surface for understanding the history of water presence through insights into the sources, losses, and recycling of water. The Miniature Tunable Laser Spectrometer (TLS) shall collect absorbance spectra in the 2500–25,000 nm range of H in hydrated volcanic rock samples in order to define the relative abundance of protium and deuterium, demonstrate an understanding of the long-term controls that have influenced the availability of liquid water on Mars through both endogenic, such as internal volcanic and geologic processes, and exogenic, such as surface-atmospheric interactions.

2. Determine the crystal structure of minerals formed by asteroid impacts that interact with exposed subsurface ice within 0-1m depth for understanding the long-term endogenic and exogenic controls on the presence of Martian liquid water. The Raman Laser Spectrometer shall operate within ±10% mineral identification accuracy, 10 cm^{-1} spectral resolution and a 6–8 cm^{-1} peak separation capability allowing for precise and accurate identification of hydroxyl groups and raman spectra collection in Olivine in asteroid rocks surface sites. This investigation explores Martian geological history, its evolution to the present state through the past Martian dynamic force interactions, and how time has affected the subsurface.

Science Goals	Science Objectives	Science Measurement Requirements		Instrument Performance Requirements		Predicted Instrument Performance	Instrument	Mission Requirements
		Physical Parameters	Observables					
"*HBS-1LM: Understand the effects of short- and long-duration exposure to the environments of the Moon, Mars, and deep space on biological systems and health, using humans, model organisms, systems of human physiology, and plants*." — Moon to Mars Objectives, NASA	Investigate the long duration Martian environmental impacts on a protected and pressurized earth-fluid sample for unknown hazards that may threaten the integrity of future mission-critical life support, rocket propellant, and agricultural fluids.	Periodically monitor the Earth fluid sample for risks, hazards, and contamination that may bypass the custom-engineered Fluid Protection System's protective layers and document via data generation.	Use a passive ionization chamber to monitor gamma radiation levels in µSv/h, recording data at weekly intervals over a one-year period for transmission back to Earth.	Range	1 µSv/h to 10Sv/h	1 µSv/h to 10Sv/h	CP-MU DMU-100 Submersible Gamma Neutron Probe	The instrument must survive fluid submersion for a minimum of one year while measuring for potential radiation contamination within the fluid protection system.
				Operating Temperature	30°C to +57°C	30°C to +57°C		
				Accuracy	±5%	±10%		
				Time Constant	12 seconds slow	2 seconds fast, 12 seconds slow		The instrument must study the difference in permittivity to identify insulating dust layers and potential ice-rich zones
	Investigate how subsurface stratigraphy, dielectric properties, and dust layer thickness affect the accessibility and long-term stability of near-surface water ice, in support of in-situ resource utilization and environmental risk	Estimate dielectric permittivity and radar wave velocity to characterize subsurface material properties, including layer thickness, composition changes, and porosity variations across	Analyze radar signal delay and reflection strength to determine layer boundaries, depth to subsurface features, and dielectric (Ɛ) contrasts indicative of dust deposits and possible ice-rich zones.	Penetration Depth	≥ 10 km	≥ 10 m	Radar Imager for Mars' Subsurface Experiment (RIMFAX)	
				Frequency Range	100-1200 MHz	150-1200 MHz		
				Permittivity Range	$\Delta\varepsilon_r \leq 0.1$	$\Delta\varepsilon_r \leq 2$		The instrument must detect the subsurface layering to a depth of at least 10 m to assess ice stability underneath dust and regolith
				Vertical Resolution	≥ 15 cm	15 cm - 30 cm		

	reduction for future human exploration.	a 10 km traverse.						
"Q10.3b: What are the long-term endogenic and exogenic controls on the presence of liquid water on terrestrial planets?"—Origins, Worlds, and Life: A Decadal Strategy for Planetary Science and Astrobiology 2023–2032	Determine the Deuterium to Hydrogen (D/H) ratio in hydrated volcanic rock on Mars' surface.	Define the relative abundance of protium and deuterium within samples of hydrogen from hydrated volcanic rock.	Collect absorbance spectra in the 2500–25,000 nm range of H in selected hydrated volcanic rock samples at multiple surface sites.	Wavenumber Range	3593.3-3594.3 cm^-1	3593.3-3594.3 cm^-1	Miniature Tunable Laser Spectrometer (Mini-TLS)	System must navigate to and collect samples of hydrated volcanic rock.
				Spectral Resolution	0.0001 cm^-1	0.0001 cm^-1		
				Sensitivity	<80 ppb	10 ppb		
				Integration Time	1 s	2.4 s		System must have the ability to heat volcanic rock to 935 K to study structural water released as gas.
	Determine the crystal structure of minerals formed by asteroid impacts interacting with exposed subsurface ice.	Identify chemical structure, crystal structure, and bond structure of Olivine from asteroids.	Collect raman spectra in the 11,111–33,333 nm range of Olivine in selected asteroid rocks at multiple surface sites.	Mineral Identification Accuracy	±10%	≥ 90%	Raman Laser Spectrometer (RLS)	
				Detection Sensitivity	≤ ~100 ppm	6–8 cm^{-1} peak separation		
				Power Consumption	20 - 30W	Between 20 - 30 watts		System must operate in the Martian Temperature range of 293.15° K to 120.15° K
				Spectral Resolution	10 cm^{-1}	10 cm^{-1}		

Figure 1.2.1: Science Traceability Matrix

1.3 Summary of Mission Location

The location selected for the P.H.O.E.N.I.X mission is the Erebus Montes region of Arcadia Planitia. Erebus Montes is located within 60° latitude North or South, the Potential High Priority Radar Targeting Zone (PHPRTZ), and a region containing excess subsurface ice within the upper meter of the regolith.

Erebus Montes has ample regions of scientific interest to complete the objectives located within the STM. Of these objectives, only the two for the science exploration goal require specific geological features. These features are the presence of hydrated volcanic rock and asteroid impacts which exposed subsurface ice. The region is situated between two Amazonian lava flows and contains exposed terrain from the older Noachian-Hesperian era [115]. This access to both new and old geological terrain with glacial processes offers the ability to categorize the way water ice has interacted with Martian geological and climate changes [115].

The TES dust index in Figure 1.3.2 shows the region is moderately dusty, posing challenges to the systems operation and communication. However, this lends the advantage of the subsurface ice being more cold and therefore more stable [115]. There is a flat pocket of less dust in the Northwestern corner of the ROI where the rover will land to avoid communication issues during deployment.

The P.H.O.E.N.I.X ROI is a 60 km wide, 17 km long ellipse at 39° N, 191.1° E. The ROI sits on a region of Noachian-Hesperian transition terrain in the Northeastern region of Erebus Montes [115]. In the Northwest corner of the ROI there is a concentric crater fill (CCF). CCFs form through asteroids contacting ice-rich regions with subsequent glacial movement carving the crater walls [6]. This introduces the asteroid minerals to interactions with ice, interactions which are important to understand the way water can change crystal structures important for studying the fourth objective. Evidence points towards asteroids bringing life-sustaining elements (C, H, P) to Mars [96]; many studies hypothesize that organics may be preserved in ice-rich environments [28].

There are multiple ice rich lobate debris aprons (LDA) in the Southern region of the ROI [115]. LDAs are formed when rock debris piles up next to escarpments. The ROI LDAs consist of the Noachian-Hesperian crust, a period with mass volcanic activity [125]. The Noachian-Hesperian terrains that feed into LDAs have been found to contain hydrated minerals suggesting the LDAs would make hydrated volcanic rock easily accessible for studying the third objective [28]. This makes Erebus Montes’ LDAs a compelling target for collecting preserved, hydrated volcanic material.

Figure 1.3.1: ROI Overlaid with PHPRTZ

This figure displays the region of interest within the contractors requirements. Additionally the small pink and yellow squares show the confirmed locations of CCFs and LDAs respectively. There are other locations which are likely to have these features.

Figure 1.3.2: ROI TES Dust Index

Erebus Montes is dusty, but in the Northwest corner of the ROI there is a regions where the rover can avoid dust while the spacecraft lands and the deployment process begins

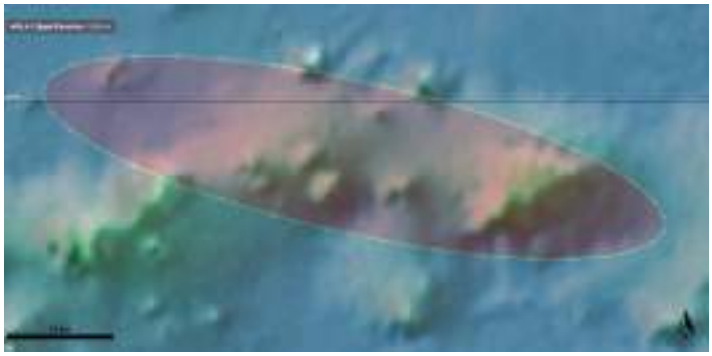

Figure 1.3.3: ROI Elevation Map

The region has large cliffs where the LDAs are present. To navigate to the Southeast corner of the ROI, the rover will use a pass through the North and South mountains in the middle of the ROI. The Mountain at the East end has a high possibility for LDAs but must be traversed around.

1.4 Mission Requirements

In order to ensure traceability and alignment between the science objectives and the engineering design, P.H.O.E.N.I.X mission is developed within a clear hierarchy that flows from the mission goal down to mission requirements to system requirements that then flow down to subsystem requirements. At the highest level, the mission goal is to advance NASA's pursuit of sustainable exploration on Mars by demonstrating a cost-effective Discovery-class mission that can traverse the Martian terrain and return critical scientific data back to Earth. This goal then drives the mission requirements, which are captured in NASA's stated constraints concerning mass,volume,budget and schedule. These mission requirements then cascade into system requirements, setting the functional demands of the spacecraft system such as having a mobility system, a power system and a deployable structure in a stowed configuration. Furthermore, they flow into the subsystem requirements that define the specific performance parameters of the spacecraft, such as thermal requirements to ensure the spacecraft is able to survive the harsh environment on the Martian surface, to the mechanical requirements where it is able to traverse the Martian surface, to the power requirements that ensure the spacecraft is operational at all times and is able to function all systems and finally, to the CDH requirements that define data storage, processing and transmission.

Customer constraints are a key driver of mission architecture, which determines the high-level requirements concerning mass, volume, and budget. The team seeks to meet the system constraints presented by NASA, serving as the funding agency for the Mission Concept Academy's Discovery-class mission.

The spacecraft shall not exceed a mass of 200 kg. In a stored configuration, the spacecraft shall not exceed the dimensions of 2.5 m x 2.5 m x 2.5 m. This volume will house all the electronics, instruments, and payload suite. The spacecraft shall maintain the stored configuration for the entirety of the launch, transit, and entry into the Martian atmosphere. In an expanded form, there is no volume or mass constraint placed on the spacecraft. The spacecraft shall demonstrate resistance to temperatures consistent with atmospheric entry and descent. The spacecraft shall incorporate a landing attenuation system capable of withstanding surface impact.

After deployment on the landing site selected, the spacecraft shall traverse the terrain effectively to travel a minimum of 10 km. The spacecraft shall demonstrate an ability to traverse various Martian terrains, including sandy regions, icy regions, and small, medium, and large-sized rocks. The spacecraft shall demonstrate the ability to endure fluctuations in Martian atmospheric conditions, including dust storms, diurnal temperature variations, and reduced atmospheric pressure.

The spacecraft shall carry a scientific payload containing all instrumentation to complete science objectives. The volume of the scientific payload shall not exceed a cube of dimensions 0.5 m x 0.5 m x 0.5 m, nor a mass of 15 kg. This is to ensure the mission satisfies the human exploration goal and gets samples from the Martian surface that can be transmitted back to Earth for research. Furthermore, this research will contribute a great deal to the future of sustainability on Mars and future manned missions.

P.H.O.E.N.I.X is a discovery mission and not a flagship mission; hence, the budget allocated to this mission is 450 million USD and shall be used effectively for the manufacturing of the spacecraft, its components, employee-related expenses (ERE), and testing of the spacecraft. The Spacecraft system shall not have a Radioisotope Thermoelectric Generator (RTG) or any similar power generation system. Furthermore, any radioactive material is allowed for use on other spacecraft subsystems, but cannot exceed a cumulative mass of 5g of radioactive material on all subsystems. The spacecraft must be ready for integration with the other systems by October 1st, 2029, and must be ready for launch on December 1st, 2029. The launch site shall be in Cape Canaveral in Florida.

Req #	Requirement	Rationale	Parent Req.	Child Req.	Verification Method	Req. met?
MG 0.1	The system shall survive the martian environment for a minimum of one year.	The system must be able to survive the martian environment to fulfill its purpose and send data back to earth ground station and potentially return martian samples	Customer	SYS.01 SYS.02 SYS.05 SYS.06 MECH.01 PAYL.02	Demonstration	Met
MG 0.2	Shall investigate the presence of ice glaciers on Mars for future missions and sustainability	Foundational science driver for the mission: Human habitation requires large volumes of drinkable water, water for propellant and agricultural use for long term sustainability missions on Mars	Customer	SYS.03 SYS.07 SYS.08	Demonstration	Met
SYS.01	The system shall have sufficient power to carry out the objectives for the duration of its mission	System needs power to operate, communicate back to earth and carry out its objectives	MG 0.1	PWR.01	Test	Met
SYS.02	System shall maintain operating temperatures and survive the harsh thermal environment ranging from on the martian surface	The system and it's scientific instrumentation must be kept in operating temperature ranges in order to function properly	MG 0.1	TCS.01	Test	Met
SYS.03	System shall traverse the martian surface smoothly and reach the required science points of interest	Points of interest are marked across potential high priority Radar targeting zones on Mars that are defined by the thickness of the atmosphere to allow for easy landing and research point.	MG 0.2	MECH.02 MECH.03 MECH.04	Test	Met
SYS.04	System shall not exceed a total mass of 200kg	Constraints provided by NASA for the mission	Customer		Inspection	Met
SYS.05	System shall have a backup that is always ready to take over if a failure occurs	In the case of failure, if a component of the main system fails, the backup can takeover and still carry out the mission to some capacity	MG 0.1	PWR.04 PWR.05	Analysis	Met
SYS.06	System must withstand the solar winds for the duration of its mission	All components on the rover must be strong enough to withstand the strong solar winds on mars	MG 0.1	PWR.02 PWR.03	Test	Met

SYS.07	System shall send and receive data collected with the science instrumentation back to the earth ground station	Data sent back to the earth ground station about Mars will be essential to future scientific research for sustainability on mars	MG 0.2	CDH.03 CDH.04	Analysis	Met
SYS.08	System shall comply with all applicable planetary protocol regulations	NPR 8020.12D *Planetary Protection Provisions for Robotic Extraterrestrial Missions*	MG 0.2		Analysis	Met
SYS.09	Radioactive material used for any subsystem shall not exceed a total mass of 5g. If material is necessary for the power subsystem shall not utilize radioactive material of total mass more than 5g.	Constraints provided by NASA for the mission	Customer		Inspection	Met
SYS.10	System shall not make use of a Radioisotope Thermoelectric Generator (RTG) or any derivative thereof for power generation	Constraints provided by NASA for the mission	Customer		Inspection	Met
SYS.11	System shall not exceed the dimensions of 2.5 m x 2.5 m x 2.5 m while in its stored configuration	Constraints provided by NASA for the mission	Customer		Inspection	Met
SYS.12	System shall not exceed a cost of $450M	Constraints provided by NASA for the mission	Customer		Inspection	Met

Figure 1.4.1: Requirements Table

1.5 Concept of Operations (ConOps)

P.H.O.E.N.I.X shall be a semi-autonomous exploration rover, designed to contribute to the goals of the NASA Science Mission Directorate (SMD) and Exploration Systems Development Mission Directorate (ESDMD). This mission was designed to fill a gap in knowledge regarding the landing zone wherein the rover shall operate for the duration of the mission. The Concept of Operations (ConOps) encompasses the operational steps involved in landing, all activities on the Martian surface, and decommissioning. The purpose of the experiment is to investigate subsurface ice reservoirs, characterize environmental hazards, and better understand them in order to support future human exploration.

The rover shall begin surface deployment procedure upon T-1 sol, Martian day, of landing at the designated chosen landing site. It shall begin activation of the system operational instruments. The power systems shall first be stabilized. Upon power stabilization, the scientific instruments shall be deployed and brought online, and initial communication and telemetry tests shall be conducted. Thermal control systems shall be activated to maintain the appropriate daylight temperature, which includes using heaters to ensure the electronics operate within their designated temperature range. The rover shall then calibrate the scientific instruments and await initial command from ground operations located at Kennedy Space Center.

As seen on the ConOps graphic, the mission is divided into 5 major operational phases: Rover Touchdown (T+1 days), Traversal to Target Site (T+2-44 days), Science Mode (T+45 days), Repeat Sites #2-#3 (T+46-135 days), and End of Life (T+135-365 days). Rover Touchdown (T+1 days) consists of verification of Instrument Calibration, System Start-up, Data Link, and Signal Verification, as well as the initial command execution from MRO. Traversal to Target Site (T+2-44 days) contains a Day and Night Mode to better allocate available power during the autonomous travel period. Day mode has the rover traveling as 0.08 km/h with a Heartbeat telemetry transmitted at 10 hz, while Night mode aids in power conservation by having the rover traveling 0.05 km/h with a reduced Heartbeat telemetry transmitted at 5 hz, with the addition of the electric heaters powered on and solar panels retracted back into the rover. In all modes, power will be focused on thermal control systems and maintaining appropriate temperatures throughout the system. The transition from day mode to night mode shall repeat throughout the Martian sol cycle during the autonomous travel period to the designated science site. Science Mode (T+45 days) utilizes a Gamma Ray Neutron probe to detect radiation, while RIMFAX sends radio-frequency electromagnetic waves. The surface Mini TLS heats up rocks and collects gas to measure the D/H ratio. The RLS emits a laser beam and gets a spectroscopic reading. All data is stored and transmitted to MRO. Repeat Sites #2-#3 (T+46-135 days) have the rover traveling to complete

additional mission locations. End of Life (T+135-365 days) has final data transmission, and the system finally shuts down.

After verification of all systems, the rover shall begin autonomous travel to the designated science site at 0.08 km/h by the design of the rover and the environment, which shall occur at T+2 sol after surface deployment procedure and instrumental calibration.

Upon arrival at the science site, a switch will occur from either day or night mode to science mode. Once switched to science mode the system will deploy its science instrumentation for use similarly to that of Mars 2020 Perseverance [82]. Once science instrumentation is deployed the system shall begin calibration of science instruments and ready systems for data collection. Instrument calibration occurs during Rover Touchdown (T+1 days), where scientific instruments undergo initial system checks to confirm functionality.

Once science instruments have been successfully deployed and calibrated data and sample collection of ice on the Martian surface will begin. The rover shall relay all collected data during its time in science mode to the Mars Reconnaissance Orbiter, which shall relay stored data to Earth for scientific research on the future of sustainability on Mars.

Upon completion of the data collection objectives at the designated travel site, the rover shall travel to the next site and repeat travel mode and science mode procedures until completion of the mission objective.

Towards the end of the mission, the rover shall transmit all scientific stored data to the MRO and conduct standard shutdown procedures and proceed into a dormant state. This will be implemented by a command executed by the OBC once all of the scientific objectives have been achieved, the scientific data required has been acquired and the rover is not able to further continue to traverse or it full-fills the mission timeline decided by the team.

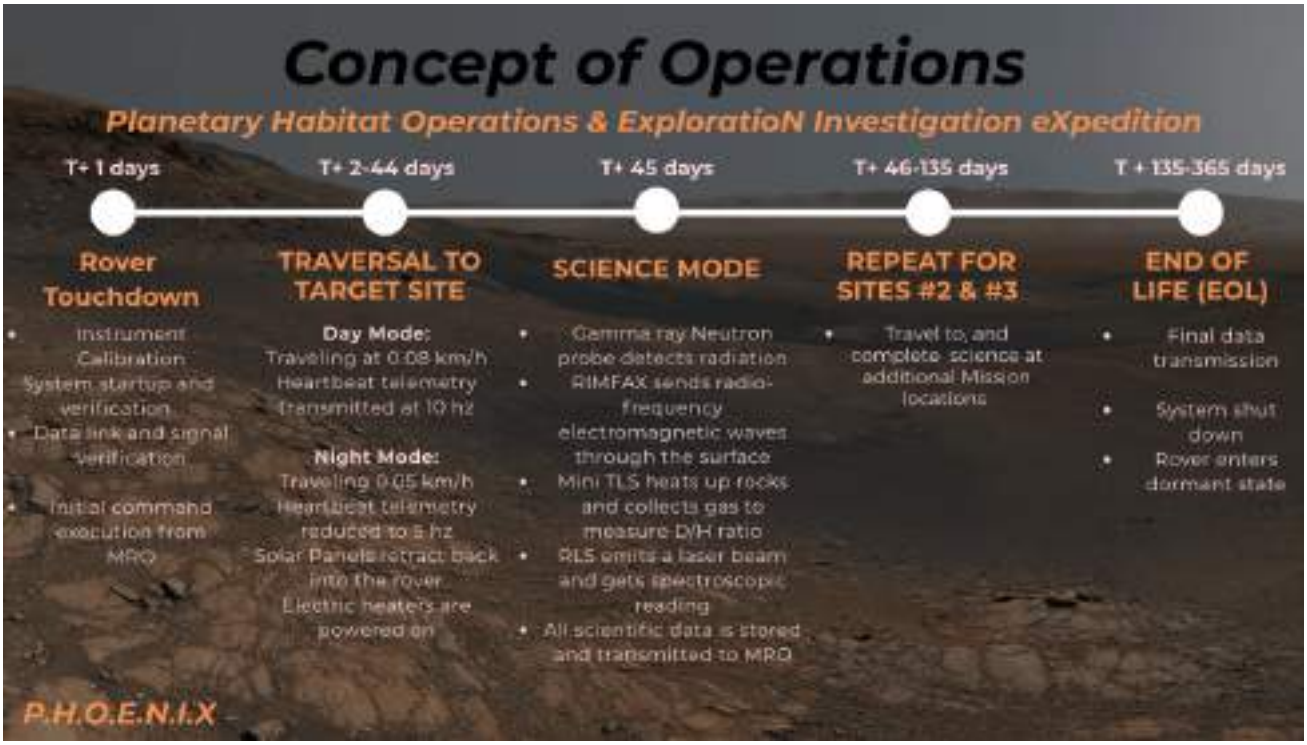

Figure 1.5.1: Concept of Operations

1.6 Vehicle Design Summary

The following section covers the final design the team decided on after reviewing a variety of designs for the rover. Taking inspiration from successful Mars rover reconnaissance missions such as Curiosity and perseverance, the team decided to go with a similar design. This was mainly due to strong structural integrity of most parts of the rovers that had been used on those missions as well as having flight heritage which saved a lot of design and conceptualization time and prioritized testing and simulation for the rover.

Overall dimensions of the rover in a stored configuration includes a 0.35 cubic meter box that will be about 10 inches from the ground, and will be connected to 4 legs that will be connected to 6 wheels. The rover weighs in at approximately 175 kg and consumes 900 watts of power through a daytime cycle conducting science. In accordance with the science objectives of this mission, there will be 4 scientific instruments mounted on the rover at different locations on the chassis as shown in figure 1.6.1 with each scientific instrument having its own distinct purpose as it pertains to the scientific objectives of the mission.

For mobility, the system decided by the mechanical engineers was the rocker bogie system that has been used on missions like the Perseverance rover which allows for greater shock absorption and smooth terrain travel, considering the rough terrain of Mars, it will be essential in keeping the rover balanced and keeping the suspension at an appropriate level and this is where the rocker bogie system functions best [100].

Part of the basic rover design consists of four instruments and an oven. These four instruments shall be mounted at different locations on the rover. As shown in figure 1.6.1.1, one of the instruments RIMFAX is mounted below the rover, the mini TLS is mounted on top of the chassis and the RLS mounted inside the rover. Each location was decided on after a meeting with the science team to ensure proper instrument positioning for accurate data collection from each instrument.

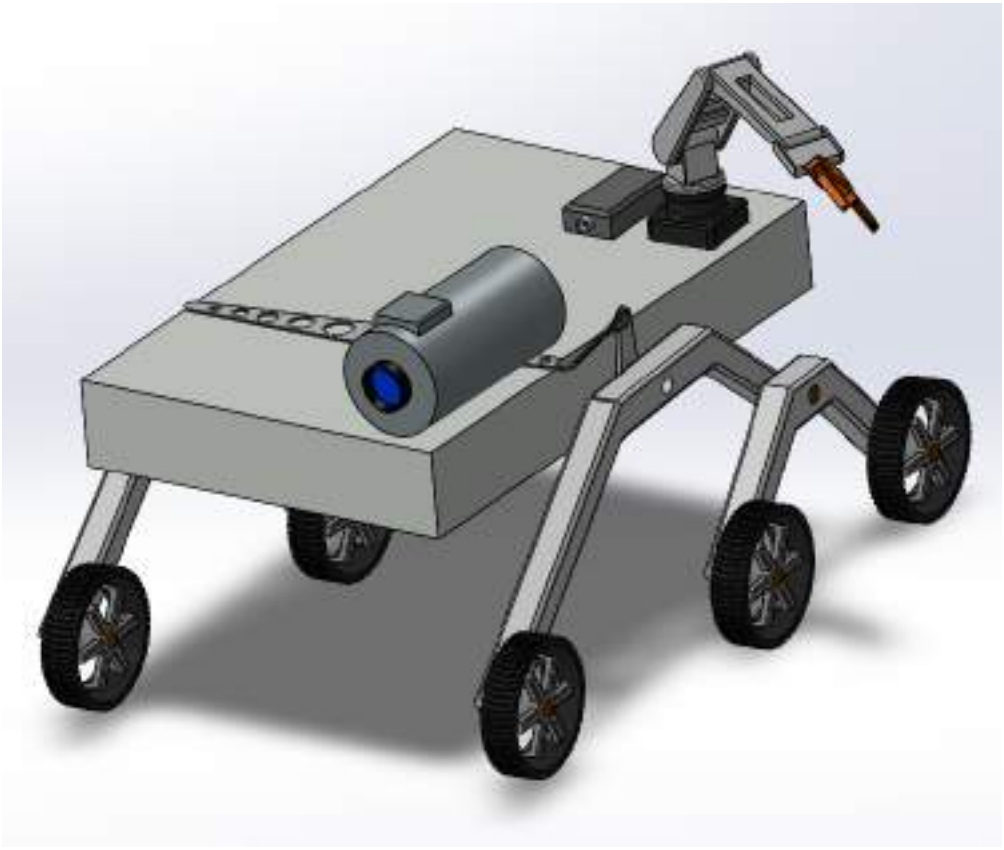

Figure 1.6.1: Complete Rover Design

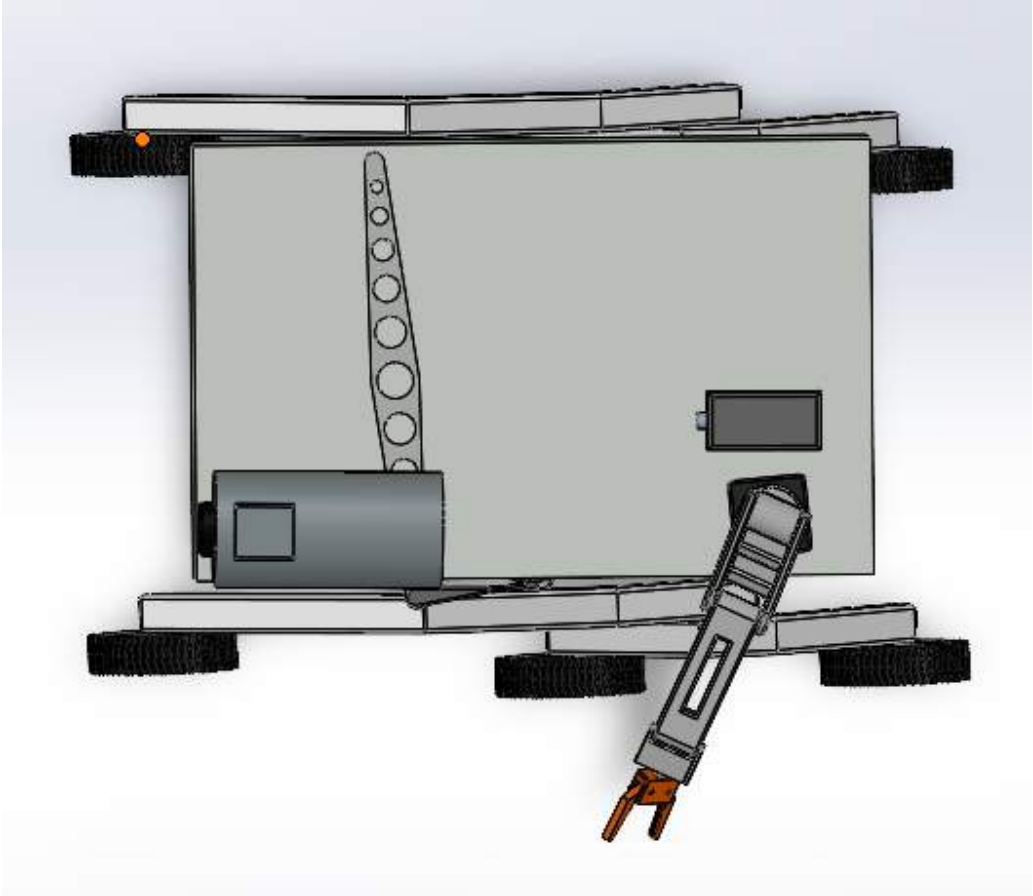

Figure 1.6.2: Complete Rover Design Top View

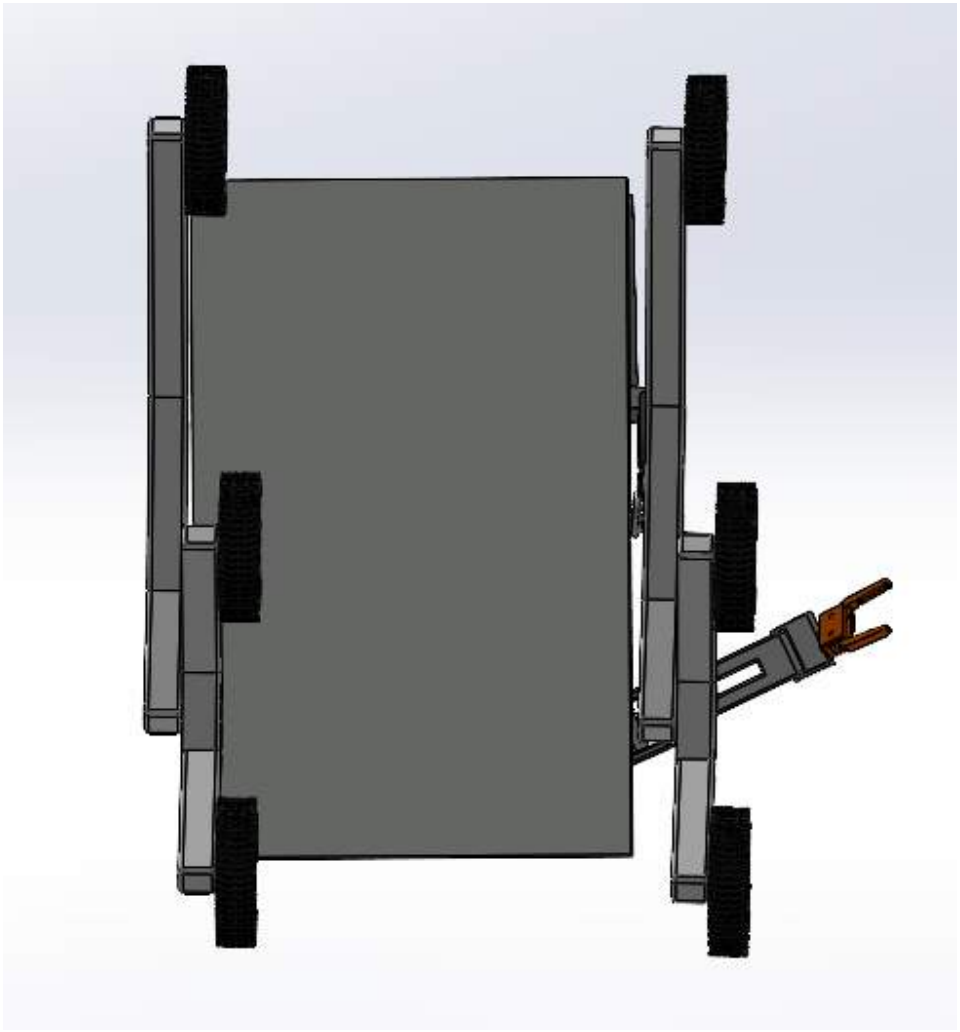

Figure 1.6.3: Complete Rover Design Bottom View

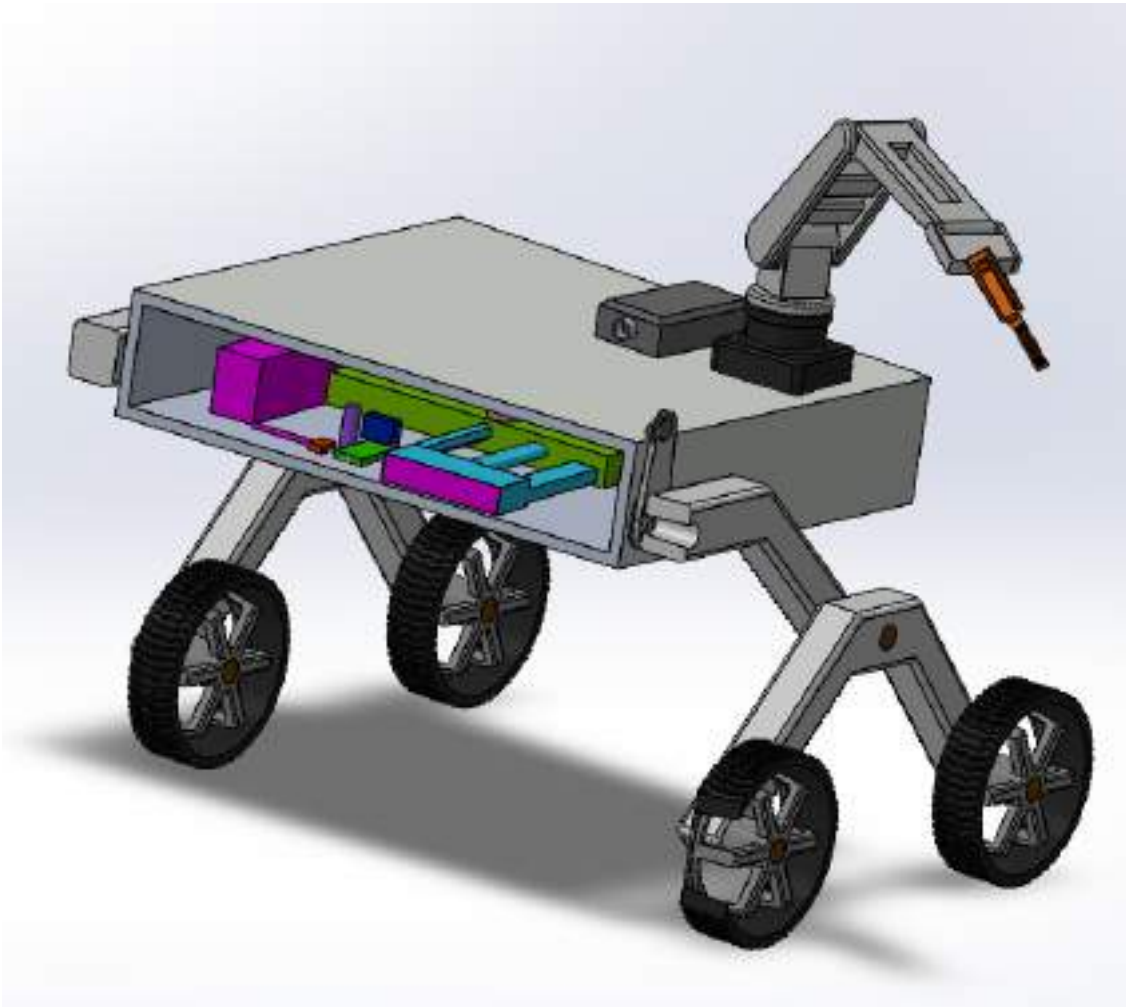

Figure 1.6.4: Internal Rover Design View

1.7 Science Instrumentation Summary

In support of Human Exploration Goal HBS-1LM, the first objective utilizes the CP-MU DMU-100 submersible Gamma Neutron probe, which will investigate the Martian environmental impacts of Gamma radiation on a protected and pressurized earth-water sample, leading to the collection of environmental risk data for driving material science innovation in protecting mission-critical fluids. The probe detects gamma radiation using a gas-filled chamber where an electric field is applied. When gamma rays enter the chamber, they ionize the gas, creating charged particles, and are then collected by an electrode. The end result produces a measurable current in which is amplified and converted then sent to the OBC for data analysis.

The second objective, utilizing the Radar Imager for Mars Subsurface Experiment (RIMFAX), will investigate how subsurface stratigraphy, dielectric properties, and dust layer thickness affect the accessibility and long-term stability of near-surface ice in support of ISRU and environmental risk reduction. It will image shallow subsurfaces beneath the rover and provide information regarding regolith and composition, transmitting ground-penetrating radio signals with an operating frequency range of 150 - 1200Mhz. The radio waves bounce off of different underground layers and objects, causing variation in signal behavior which bounce back, collecting the returned signals and the return times. Then the data is processed and transmitted to enable data analysis and identify areas with high potential of in-situ resource access.

In support of Science Exploration Goal Q10.3b, the first objective uses the Miniature Tunable Laser Spectrometer (Mini-TLS) to study the D/H ratio of volcanic martian rock to reveal how past sources of water on Mars were geologically altered over time. An oven implemented within the rover, heats the collected sample of rocks to release volatile gases which will be directed into the instrument’s gas cell, where a tuned laser beam passes through them. The gases will absorb light at certain wavelengths, allowing the instrument to identify their compounds. The recorded absorption patterns are then processed and sent to the onboard computer for analysis.

In the second objective, the Raman Laser Spectrometer (RLS) will investigate Martian regolith for molecular identification of organic and minerals, leading to further understanding of the geochemical history of Mars. It studies the minerals within rock and soil samples by shining a laser through a special window made of fused quartz onto the sample. Afterwards, the minerals within the sample start to scatter light at certain wavelengths where the spectrometer analyzes the scattered light to determine which minerals are in the sample as well as their chemical structures. It is connected to the rover’s robotic arm, allowing it to precisely aim at the target samples and the data collected is sent to the rover’s computer.

1.8 Programmatic Summary

1.8.1 Team Introduction

Ian Wilhite – Project Manager (PM)

Ian is a senior in Robotics and Controls Engineering at Texas A&M – College Station from Fort Worth, Texas. Ian serves as President of the American Society of Mechanical Engineers, Project Lead for the Disaster Response Observation Network in TURTLE Robotics, and works in the Human Empowering Robotics and Controls Lab. Ian currently works at the Army Research Laboratory as an Aerial Autonomy intern and plans to apply to graduate schools for Fall of 2026.

Aidan Piper – Deputy Project Manager of Resources (DPMR)

Aidan Piper is a junior at the University of Illinois Urbana Champaign majoring in Aerospace Engineering, overseeing mission risks alongside schedule and budget as DPMR. Aidan has held leadership roles in both sides of the aerospace field through project manager in LSPACE's NPWEE and leading an international team of 5 in a case study for Brazilian company Azul Airlines. Combining these positions and their transferable skills along with teaming experience in larger groups through student organizations and classwork, Aidan is well equipped to lead the programmatic subteam. Aidan also has STEM outreach experience through serving as a tour guide for the Grainger College of Engineering and a counselor for high school-based programs run by the college and aerospace department.

Danyal Khan – Lead Systems Engineer (LSE)

Danyal is a junior studying Aerospace Engineering at the University of Michigan Ann Arbor. Danyal is currently the recovery bay lead for Michigan's rocketry team Michigan Aeronautical Science Association (MASA) directly responsible for the recovery of the team's rocket and holds the position of Vice President of Operations for Michigan Aviators, a social club for students interested in aviation/aerospace at Umich. Danyal plans to do a masters in aerospace/mechanical engineering after graduation.

Alanis Cubi Negron – Chief Scientist (CS)

Alanis is a senior studying Computer Science at the Polytechnic University of Puerto Rico. Alanis participated in NASA's LSPACE Proposal Writing and Evaluation Experience (NPWEE) as a Chief Scientist, where she collaborated with a multidisciplinary team to develop competitive mission proposals and evaluate technical feasibility aligned with NASA's strategic goals. Alanis's background also includes

participation in competitive robotics, earning awards in technology and programming, and collaborating on STEM initiatives with NASA and the Puerto Rico Institute of Robotics. Alanis will continue to pursue a Master's Degree in Systems Engineering.

Ibrahim Jaber – Program Analyst (PA)

Ibrahim is a senior studying Mechanical Engineering at the University of Minnesota – Twin Cities in Minneapolis, Minnesota. He currently serves as the Front Wing Design Lead for the University of Minnesota's Formula SAE Vehicle Team, where he is responsible for designing, manufacturing, and testing the front wing, as well as leading the development of new brake ducts for the car. Professionally, Ibrahim works as a Mechanical Engineering Intern at Reell Precision Manufacturing, where he designs overload tooling to support product development. After completing his degree, Ibrahim plans to pursue his Professional Engineering license to further his career in mechanical engineering.

Gabi Zabiegaj – Mechanical Engineer (ME)

Gabi is an incoming junior studying Aerospace Engineering and minoring in Computer Science and Material Sciences and Engineering at the University of Illinois Urbana-Champaign in Champaign-Urbana, Illinois. She is a member of the Illinois Space Society's Micro-g NExT team, where she designs and manufactures astronaut tools, even testing the team's tool at NASA's Neutral Buoyancy Lab in Houston, Texas. Gabi is also involved in undergraduate research, and she is developing a 3D-printable filament created from plastic waste to be used on agricultural drones. After graduating with her bachelor's, Gabi plans on pursuing further work in sustainable aerospace materials research.

Pablo Pena – Mechanical Engineer (ME)

Pablo is a sophomore in Mechanical Engineering at The University of Texas at Austin from Houston, Texas. Pablo is a member of the Design Build Fly team and Student Engineers Educating Kids at UT Austin and is pursuing projects in CAD design, robotics, and autonomous systems. He plans to apply to graduate schools and continue developing expertise in robotics, aerospace, and computational engineering.

Fatima "Flynn" Mendoza - Thermal Engineer (TE)

Flynn is a rising junior at Texas Tech University in Lubbock, Texas, studying Mechanical Engineering with a minor in Mathematics and Anthropology. At TTU, Flynn is the Vice President of the Tech SSA branch, and is pledging the service fraternity Alpha Phi Omega. Flynn was a Europa ICONS intern last summer, where Flynn wrote python scripts to analyze data on the European surface and automate aspects of the

research. Flynn participated in the SUBSEA Tieback Student Design Competition, gaining experience with extremely tight margins. After graduating with a Bachelor’s in Mechanical Engineering, Flynn plans to get certified as a professional engineer.

Andy Lien – Thermal Engineer (TE)

Andy is a sophomore in Moraine Valley Community College in Palos Hills, Illinois, and a member of Phi Theta Kappa Honors Society. Andy is also a NASA Community College of Aerospace Scholars (NCAS) scholar, completing all 3 missions of NCAS with one of them being working on a conceptual integration of disability accommodation into the Beta ALIA-250 eVTOL air taxi that aligns with NASA’s Advance Air Mobility goal as a Risk and Safety Modeling Lead. Andy plans on transferring to a four-year institution ideally the University of Illinois Urbana-Champaign to pursue a Bachelor’s in Aerospace Engineering, and ultimately pursue a Master’s in Systems Engineering.

Adrian Raj – Command & Data Handling Engineer (CDHE)

Adrian is a sophomore studying Aerospace Engineering at The University of Texas at Austin in Austin, Texas. Adrian currently serves as the Webmaster of the American Institute of Aeronautics and Astronautics (AIAA), an Engineering Representative of Student Government (UTSG), a Student Mentor with Student Engineers Educating Kids (SEEK), and an Undergraduate Research Assistant at the University of North Texas (UNT) under the Testing & Machine Learning for Context-Driven Systems (TaMaLe) NSF REU site project. Adrian plans to apply for the Master’s or Ph.D. in Aerospace Engineering program at The University of Texas at Austin for the Fall 2028 semester.

Conor Foley – Command & Data Handling Engineer (CDHE)

Conor is a sophomore studying Aerospace Engineering at The Georgia Institute of Technology in Atlanta, Georgia. Conor is currently a Controls Engineer on the Ramblin’ Rocket Club GNC Project Team designing and testing state estimation and controls algorithms for a Jet-Vanes rocket. Conor will begin conducting nonlinear dynamics research on the MODAL research team at Georgia Tech in the upcoming semester. Conor plans to graduate with a Bachelor’s in Aerospace Engineering in 2027 and continue at Georgia Tech to earn a Masters through the BS/MS program.

Asherr Ralph – Electrical Engineer (EE)

Asherr is a sophomore studying Electrical Engineering at Michigan State University in East Lansing, Michigan. He serves on MSU Rocketry’s Electronics & PCB team, integrating sensors into flight computers, and is active in the Imagine Software Club, developing full-stack projects and participating in hackathons. He previously

worked at Schweitzer Engineering Laboratories assembling and calibrating electrical protection devices. Asherr has earned the Provost’s Scholarship, Dean’s List honors, and leadership certifications. He plans to transfer to another four-year university and graduate in May 2028.

Audrey Sorenmann – Electrical Engineer (EE)

Audrey is a sophomore at Century College in White Bear Lake, Minnesota, studying Aerospace Engineering. Audrey currently serves as the Assistant Project Manager at the University of Minnesota’s Small Satellite Research Laboratory, a UNP and AFRL-funded undergraduate research lab. At Century College, Audrey serves as the President of the Engineering Club and Rocketry Club, and is a member of both the Student Senate and the Phi Theta Kappa Honors Society. After graduating with her A.S. degree in the spring of 2026, Audrey plans to transfer to a 4-year university to complete her Bachelor’s of Aerospace Engineering, and ultimately earn a Master’s and Ph.D. in order to deepen her understanding and professional knowledge within the field.

Lucia Piedra – Scientist / Astrobiologist

Lucia is a sophomore in the Texas A&M Engineering Academy at the Spring Branch Houston Community College campus located in Houston, Texas, studying general engineering, and is soon to major in aerospace or electrical engineering. Entering the MCA, Lucia contributes with her previous robotics experience from participating in the BEST, VEX, and FIRST Robotics competitions, which introduced her to team collaboration and mechanical design. Following the completion of her bachelor's degree in 2028, Lucia will pursue higher education for a Master's degree within the STEM field to deepen her expertise and knowledge to contribute to science exploration.

Anna Hulett – Scientist / Astrobiologist

Anna is a rising sophomore at Southwestern University in Georgetown, Texas, pursuing a Bachelor of Science degree in biology. Anna has earned Dean’s List honors in both semesters and was inducted into the Beta Beta Beta biology honor society, reflecting academic excellence and dedication to the biological sciences. She plans to pursue a Master’s and Ph.D. specializing in astrobiology and planetary geology to advance space exploration research.

Matthew Lawrence – Scientist / Planetary Geologist

Matthew is a sophomore at Blinn College in Bryan, Texas, a member of Phi Theta Kappa Honors Society, a NASA Community College Aerospace Scholars (NCAS) alumnus, and a Student Analyst for Texas A&M University System Cyber Operations. In

2026, Matthew will transfer to a four-year university to achieve a B.S. in Physics with aspirations of graduate school to pursue and contribute to STEM research.

Katelyn Czarnowski – Scientist / Planetary Geologist

Katelyn is a rising sophomore at the University of Illinois at Urbana-Champaign, pursuing a B.S. in systems engineering. Some personal achievements include Eagle Scout and James Scholar. This past year, Katelyn served as EdOut Logistics Lead for the Illinois Space Society, Applied Engineering Education Lead for IISE, and Treasurer of the UIUC Book Lovers. During the L’Space NPWEE Academy, Katelyn served as Lead Systems Engineer. She currently supports the NSF-funded POETS-ERC as a research assistant, leads planning for Illinois Space Day, and will teach a Siemens NX workshop this fall. Katelyn plans to pursue a Master’s degree after graduation.

1.8.2 Team Management Overview

Figure 1.8.2.1: Organizational Chart

Current workload distribution follows a similar structure to past deliverables where the deliverable is split into broad sections which are then assigned to subteams by the project manager. Subteam leads then assign individual tasks and sections to individuals or small groups on their subteam. By tracking progress with a shared spreadsheet, the team reinforces mutual accountability while setting a clear pace for the completion of the deliverable.

Team organization has shifted slightly since the SRR to accommodate personnel turnover within the programmatic subteam. An updated organizational chart, seen in Figure 1.8.2.1, reflects the departure of dedicated mission assurance specialists. In response to changes in personnel, all team members are now expected to document and mitigate risks as they perform their expressly assigned tasks while the DPMR coordinates high-level tracking and communication regarding risks.

The decision-making methodology of the team remains largely unchanged from its original iteration, focusing on input from the entire team before the leadership makes a decision. This process proved effective following the addition of a separate science experiment payload and the subsequently associated descope. As the decision was not time-sensitive, the team was able to discuss the options regarding how to incorporate

the addon and the benefits and drawbacks of each approach. By taking in feedback from all members, this approach led to success in a real-world environment. After considering the feedback, team leads and the project manager selected an external mounting option. While this approach is preferred when time allows, the team can still exercise the option to consult the relevant subteam members, team lead, and project manager when time is of the essence.

Moving forward, there are a few areas where the team can improve. Firstly, by implementing an unobtrusive system of informal progress check-ins, whether it be at the beginning of each subteam's weekly meeting or through some asynchronous upload of a research summary, trade study, or section drafts, the team reduces procrastination without overburdening members. Secondly, reinforcing active usage of the task tracker will ensure everyone can get a status update on the team's progress at just a glance.

In recent weeks, the team has faced some challenges ranging from personnel turnover to the sudden announcement of a third-party payload being integrated into the spacecraft. The team also recently had to adjust to the withdrawal of the two dedicated mission assurance specialists. Not only did this loss in personnel impact the programmatics subteam, but also the team as a whole given the role's dedicated focus on identifying, documenting, and mitigating risks. As noted above, the team distributed the responsibility of mission assurance across the entire team with the DPMR overseeing. Aside from personnel issues, the team had to adjust and rescope following the addition of a third-party science payload. Key impacts were identified across all three subteams and a cohesive plan to move forward within the new design constraints and considerations was devised.

1.8.3 Schedule Overview

Table 1.8.3.1 provides a high level overview of mission phases focusing on the duration and major milestones. Milestones in bold require going before a standing review board (SRB) per protocol outlined in NPR 7120.5 [77]. Respective times for each milestone can be seen in Table 1.8.3.2.

Phases C and D, which focus on fabrication, testing, and assembly regarding subsystems and the rover as a whole, consume the mission's time prior to rover handoff by October 1, 2029 and the non-negotiable launch window for Mars starting December 1, 2029. Phase E begins with cruise to Mars before transitioning to year-long surface activities outlined in Figure CONOPS. Closeout, or phase F, which is planned to start a year after landing on Mars, is split between data recovery & decommission for 2 months before ending with the archiving of mission data & lessons alongside a final debrief, scheduled to occur by the end of December.

Phase	**Duration**	**Milestones**
C1	9/28/25 - 11/30/26	KDP C, **Critical Design Review** (CDR)
C2	12/1/26 - 3/31/28	**System Integration Review** (SIR)
D1	4/1/28 - 12/1/28	KDP D, System Acceptance Review (SAR), Mission Readiness Review (MRR)
D2	1/1/29 - 6/30/29	**Operational Readiness Review** (ORR)
D3	7/1/29 - 10/1/29	Rover Handoff
D4	10/2/29 - 12/1/29	Flight Readiness Review (FRR), KDP E, Launch
E1	12/2/29 - 9/1/30	Cruise, Post Launch Assessment Review, Critical Event Readiness Review, EDL, & Surface Activation
E2	9/1/30 - 9/1/31	Surface Activities, End of Mission, Decommissioning Review (DR)
F1	9/1/31 - 11/1/31	KDP F, Disposal Readiness Review (DRR), Rover Decommission & Asset Return
F2	11/1/31 - 12/31/31	Data Archiving and Mission Debrief

Table 1.8.3.1: Phase Milestones Table

SRB Milestones	Date
CDR	11/27/26
SIR	3/29/28
ORR	6/28/29

Table 1.8.3.2: Mandatory SRB Milestone Dates

1.8.4 Cost Overview

The total estimated cost for P.H.O.E.N.I.X is approximately $435 million which is below the mission allowed maximum of $450 million. The mission cost is summarized in the Figure 1.8.4.1 below. This cost encompasses the full scope of the mission and includes personnel, travel, outreach, facilities, and other direct costs. These categories are developed using a combination of parametric modeling and known rates derived from the NASA cost estimating handbook and other sourced public data as sourced for each respective section.

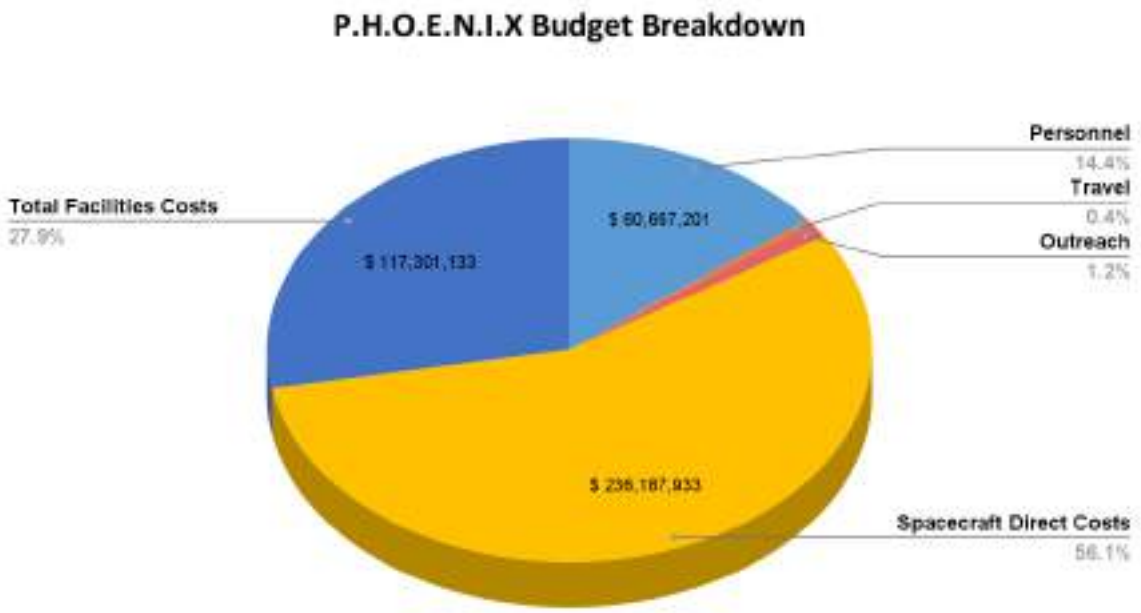

Figure 1.8.4.1: P.H.O.E.N.I.X Budget Breakdown Chart

The budget is organized into four primary categories: Personnel, Travel, Outreach, and Direct Costs as reflected in Figure 1.8.4.2. Personnel include all personnel costs except for outreach personnel which are included in the Outreach category. To account for uncertainties, a cost margin has been applied across each category. These margins provide risk mitigation and flexibility against unexpected issues or scope changes.

P.H.O.E.N.I.X Budget Breakdown	
Personnel	$ 60,667,201
Travel	$ 1,592,186
Outreach	$ 4,847,876
Spacecraft Direct Costs	$ 236,187,933
Total Facilities Costs	$ 117,301,133
Total Mission Cost	$ 439,009,301
Total Mission Cost Limit	$450,000,000
Total Mission Cost Delta	-$10,990,699

Figure 1.8.4.2: P.H.O.E.N.I.X Budget Breakdown Table

2.0 Overall Vehicle and System Design

2.1 Spacecraft Overview

Subsystem	Mass (kg)	Dimensions (mm)	Max Power Draw (W)
Mechanical	104.58	Chassis 700 x 450 x 100 Tire 150 x 150 x 40 Spokes 135 x 135 x 35 Front Rocker 215 x 147.9 x 40 Back Rocker 363.2 x 190.9 x 40 Differential 455 x 10 x 2	140
Power	43.29	Power Storage Battery: 640 x 225 x 220 PDCU: 360 x 475 x 275 Solar Panels (Deployed): 325 x 325 x 4 Thermal Buffering and Heat Pipes: 430 x 400 x 75 Converter for External Unit: 80 x 40 x 10	120Wh/sol, 4380W stored power
CDH	8.82	RAD5545 160 x 233.35 x 22.86 RH3440 160 x 100 x 22.86 Twisted Pair Cable 1.8 mm diameter 6100 linear mm RS-422 5.1 x 4.5 x 1.05 UHF Radio ~100 x 100 x 50 Antenna ~150 mm diameter, 200 mm height	50
Thermal		KHLVA 102/5 ~50.80mm x 25.40mm Diameter 0.25mm Thermal Louvers ~531.1 mm x 397mm x 63 mm MISER ~216 mm x 216 mm x 1.9 mm	380

Instrument	8.61	RLS: 80 × 95.5 × 125 mm^3 Mini-TLS: 23.5 × 16.3 × 15.5 cm RIMFAX: 0.196 m x 0.120 m x 0.066 CP-MU DMU-100 Submersible Gamma Neutron Probe: 16.51 × 8.89 × 22.86 cm	120

Figure 2.1.1: Engineering SubSystem Table

The rover is a low-cost Mars rover designed to investigate near-surface water ice and assess environmental risks to support future human exploration. The system architecture integrates six core subsystems: Mechanical, Power, Command & Data Handling (CDH), Thermal, Payload and Comms.

The Mechanical Subsystem comprises the chassis, rocker-bogie suspension, and wheels, this subsystem provides structural integrity and terrain adaptability. It shall withstand static loads up to 1500 N, vibrational frequencies up to 2000 Hz, shock loads up to 6000 N, and maintain ≥95% actuation performance throughout the mission (MECH.01–MECH.05). The Power Subsystem comprises ROSA-based solar panels, a 4380Wh lithium-ion battery, and a redundant power distribution unit. The subsystem must generate at least 200 Wh of power per sol to handle basic operations and active science time, handle 120 W peak loads, and maintain safe operation from -30°C to +50°C (PWR.01–PWR.05). The Command and Data Handling Subsystem comprises onboard processing and communication between systems and Earth. Requirements include a 1 GHz processor, 1 Mbps uplink, and 16 Kbps downlink, with sufficient bandwidth to handle telemetry and science data (CDH.01–CDH.02). The Thermal Subsystem regulates temperature-sensitive components using passive insulation and active heating. It maintains the system within 303–313 K and instrument-specific thermal ranges (TCS.01). The Payload Subsystem includes a total of four scientific instruments. The RIMFAX shall detect radar signal changes in subsurface layers down to 10 meters depth for identifying ice-rich zones defined by a permittivity difference of less than or equal to 0.1 (PAYL.01). The CP-MU Submersible Gamma Neutron Probe will measure and record radiation dosage from 1 µSv/h to 10 Sv/h inside of a (FPTS) Fluid Protection and Testing System (PAYL.02). The Miniature Tunable Laser Spectrometer shall collect data within a 1-second integration time from hydrated volcanic rock to determine the Deuterium to Hydrogen (D/H) ratio. The (PAYL.03) Raman Laser Spectrometer shall collect Olivine Raman spectra in the 11,111–33,333 nm range to identify the chemical, crystal, and bond structure of Olivine from asteroids (PAYL.04).

All subsystems are designed within a maximum stored configuration of 2.5 m x 2.5 m x 2.5 m, a mass cap of 200 kg, and a cost ceiling of $450M, with readiness milestones targeted for integration by October 2029 and launch by December 2029.

Req #	Requirement	Rationale	Parent Req.	Child Req.	Verification Method	Req. met?
MG 0.1	System shall survive the martian environment for a minimum of one year.	The system must be able to survive the martian environment to fulfill its purpose and send data back to earth ground station and potentially return martian samples	Customer	SYS.01 SYS.02 SYS.05 SYS.06 MECH.01 PAYL.02	Demonstration	Met
MG 0.2	Shall investigate the presence of ice glaciers on Mars for future missions and sustainability	Foundational science driver for the mission: Human habitation requires large volumes of drinkable water, water for propellant and agricultural use for long term sustainability missions on Mars	Customer	SYS.03 SYS.07 SYS.08	Demonstration	Met
SYS.01	The system shall have sufficient power to carry out the objectives for the duration of its mission	System needs power to operate, communicate back to earth and carry out its objectives	MG 0.1	PWR.01	Test	Met
SYS.02	System shall maintain operating temperatures and survive the harsh thermal environment ranging from on the martian surface	The system and its scientific instrumentation must be kept in operating temperature ranges in order to function properly	MG 0.1	TCS.01	Test	Met
SYS.03	System shall traverse the martian surface smoothly and reach the required science points of interest	Points of interest are marked across potential high priority Radar targeting zones on Mars that are defined by the thickness of the atmosphere to allow for easy landing and research point.	MG 0.2	MECH.02 MECH.03 MECH.04	Test	Met
SYS.04	System shall not exceed a total mass of 200kg	Constraints provided by NASA for the mission	Customer		Inspection	Met
SYS.05	System shall have a backup that is always ready to take over	In the case of failure, if the main system fails, the backup can takeover and still carry out the mission	MG 0.1	PWR.04 PWR.05	Analysis	Met

SYS.06	System must withstand the solar winds for the duration of its mission	All components on the rover must be strong enough to withstand the strong solar winds on mars	MG 0.1	PWR.02 PWR.03	Test	Met
SYS.07	System shall send and receive data collected with the science instrumentation back to the earth ground station	Data sent back to the earth ground station about Mars will be essential to future scientific research for sustainability on mars	MG 0.2	CDH.03 CDH.04	Analysis	Met
SYS.08	System shall comply with all applicable planetary protocol regulations	NPR 8020.12D *Planetary Protection Provisions for Robotic Extraterrestrial Missions*	MG 0.2		Analysis	Met
SYS.09	Radioactive material used for any subsystem excluding the power subsystem shall not exceed a total mass of 5g	Constraints provided by NASA for the mission	Customer		Inspection	Met
SYS.10	System shall not make use of a Radioisotope Thermoelectric Generator (RTG) or any derivative thereof for power generation	Constraints provided by NASA for the mission	Customer		Inspection	Met
SYS.11	System shall not exceed the dimensions of 2.5 m x 2.5 m x 2.5 m while in its stored configuration	Constraints provided by NASA for the mission	Customer		Inspection	Met
SYS.12	System shall not exceed a cost of $450M	Constraints provided by NASA for the mission	Customer		Inspection	Met
CDH.01	The Command and Data Handling (CDH) system shall have a minimum uplink rate of 1 Mbps and a minimum downlink rate of 16 Kbps.	The system must be able to send scientific and telemetric data to and from Earth.	SYS.07	CDH.02	Analysis	Met
CDH.02	The CDH system shall have a minimum processing rate of 1 GHz.	The system must be able to process the scientific and telemetric data it receives from both Earth and instrumentation/sensors.	CDH.01	CDH.03 CDH.04	Test	Met

CDH.03	The CDH system shall have a minimum memory of 8 GB of RAM.	Provides working memory for executing flight software, processing sensor data, running algorithms, and sending commands.	SYS.07		Inspection	Met
CDH.04	The CDH system shall have a minimum storage of 10 TB.	Due to incoming datastreams and intermittent opportunities for uplink, large onboard data storage helps limit data loss and data can be stored for the duration of the mission.	SYS.07		Inspection	Met
CDH.05	The CDH system shall maintain operation of critical components between -30°C to +50°C.	The system must be able to withstand Martian temperature swings.	SYS.02		Test	Met
CDH.06	The CDH system shall withstand radiation up to 10 krad(Si).	The system must be radiation-hardened to maintain operation in the Martian environment.	SYS.02		Test	Met
CDH.07	The CDH system must be able to communicate 550 km.	The system must be able to send and receive critical information.	SYS.07		Demonstration	Met
CDH.08	The CDH system must be able to communicate with and check on instrumentation and other subsystems.	The system controls the whole rover and collects all the data from the instrumentation. The system needs to know when other subsystems fail to initiate recovery or redundant components.	MG.02		Test	Met
MECH.01	The chassis shall tolerate a static load up to 1500 N.	The system must not risk fracture or fatigue that would result in complete structural failure and inability to carry out the mission.	MG.01		Analysis	Met
MECH.02	Mechanical subsystems shall tolerate vibrations up to 2000 Hz.	The system must be able to tolerate vibrations from travel.	SYS.03		Analysis	Met
MECH.03	Suspension subassembly shall tolerate shock loads up to 6000 N.	The system must be able to tolerate shock loads from travel.	SYS.03		Analysis	Met
MECH.04	Suspension subassembly shall withstand a 45 degree tilt in any direction.	The system must be able to tolerate tilts from travel.	SYS.03		Demonstration	Met

PWR.01	The system shall generate at least 200 Wh per sol under average Martian insolation and withstand peak power draws of 120 W for a minimum of 30 minutes up to 3 times per Sol.	Supports nominal rover operation, mobility, communication and science payloads	SYS.01		Analysis	Met
PWR.02	Solar panels shall deploy autonomously and tolerate up to 20 m/s wind.	Ensures survivability under common Martian conditions	SYS.06		Test	Met
PWR.03	The system shall maintain operation of critical components between -30°C to +50°C.	Ensures battery and electronics functionality	SYS.06		Test	Met
PWR.04	The system shall minimize integration risk using EMI shielding to absorb shockwaves and modular connectors to divert signals from critical components.	Reduces failure during integration and operations	SYS.05	TCS.02 TCS.03	Test	Met
PWR.05	Provide redundant power paths for critical systems via RCE's and power and analogue modules	Enhances fault tolerance by dividing power distribution and handling between two computers, helping to reduce uptime	SYS.05		Test	Met
TCS.01	The Thermal Control System (TCS) shall help maintain the system at the allowable temperature range of 303K to 313K.	This ensures the TCS keeps components within safe temperature limits to prevent failure from Mars' extreme thermal conditions.	SYS.02	TCS.02 TCS.03 PAYL.04	Test	Met
TCS.02	The Multilayer Insulation(MLI) shall aid in thermally housing the rover system within the temperature range of 303K to	Ensures that the rover system within is protected from the harsh Martian temperatures and conditions as well as aid in maintaining the operable temperatures.	TCS.01		Test	Met

	313K					
TCS.03	The electrical heater units shall provide a heating temperature range of 303K to 313K.	Ensures that the rover system is in the operable temperature range but provides heat throughout the system.	TCS.01		Test	Met
PAYL.01	RIMFAX shall detect radar signal changes in subsurface layers down to 10 meters depth.	Fulfills Human Exploration science objective #2 by identifying ice-rich zones defined by a permittivity difference of less than or equal to 0.1.	MG.02		Test	Met
PAYL.02	CP-MU Submersible Gamma Neutron Probe shall measure and record radiation dosage measurements ranging from 1 µSv/h to 10 Sv/h.	Fulfills Human Exploration science objective #1 by recording Martian environmental radiation impact data in the transported Fluid Protection System over a minimum one year duration period.	MG 0.1		Test	Met
PAYL.03	Miniature Tunable Laser Spectrometer shall collect and receive data from hydrated volcanic rock within a 1-second integration time.	Fulfills Science Exploration science objective #2 by determining the Deuterium to Hydrogen (D/H) ratio.	SYS 0.7		Test	Met

Figure 2.1.2: System Requirements Table

2.1.1 Mechanical Subsystem Overview

The mechanical subsystem forms the structural backbone of the rover and is responsible for integrating all subassemblies, protecting inner components from the Martian atmosphere, and mobilizing the rover. Mechanical subsystems include the chassis, suspension system, and drive system. The mechanical subsystem prioritizes reliability, safety, and efficiency in order to best serve the overall rover.

The chassis is made of aluminum 6061, a light-weight yet high strength alloy, that allows for adherence to the mass requirement without compromising its structural integrity. By offering a rigid housing for inner components, it provides protection against the Martian environment, minimizing the impact of radiation and dust. With the absence of a ductile-to-brittle transition temperature, aluminum 6061 remains ductile at extremely low temperatures, -250°C [45], which far exceeds the expected cold case for this rover, making it a good selection for extreme Martian temperatures.

The suspension system utilizes the rocker-bogie mechanism, a mechanism used on all Martian rover missions. Attached to the chassis with a differential, the rocker-bogie linkage allows for independent motion of its arms, which allows the rover to maintain constant contact with the ground while evenly distributing loads among the wheels. Since the rocker-bogie mechanism does not use springs or active damping, rover oscillations are minimized, which is favorable for fragile science instruments that need stability in order to take accurate, precise measurements. In addition to minimizing oscillations, the rocker-bogie mechanism is able to climb obstacles up to twice the wheel diameter, allowing for smooth maneuvering over the rugged Martian terrain. Made of titanium, the suspension system can endure repeated mechanical stresses, thermal cycling, and intense environmental conditions without deformation or fatigue. Titanium’s high density allows the rover to have a low center of mass, offering added stability to the design.

The drive assembly consists of the wheels, motors, and guidance, navigation, and control hardware. Responsible for mobilizing the system, the drive assembly is designed for reliability and precision. The drive assembly consists of six independently powered wheels and associated guidance, navigation, and control (GNC) hardware. The rover is equipped with six motors for driving, and four motors for steering the corner wheels. Each motor is connected to an encoder for precise velocity and position control. This configuration enables both six-wheel drive and four-wheel steering, providing high maneuverability and built-in redundancy. By independently controlling and powering each wheel, failures can be isolated without compromising the rover’s overall movement capability, ensuring that a single-point failure in the wheel assembly does not cause a full failure for the entire rover. The drive assembly allows for slow and deliberate rover

movement, which are essential for navigating Martian terrain safely and allowing scientific instruments to operate accurately.

The subassemblies within the mechanical subsystem provide a reliable and stable foundation for the rover, while continuously supporting the rover’s scientific capabilities.

2.1.1.1 Mechanical Subsystem Requirements

The mechanical subsystem contains the chassis, suspension subassembly, and drive assembly, and must ensure structural integrity, terrain adaptability, and environmental resilience throughout the mission.

The chassis and suspension subassemblies are responsible for safely housing and transporting all components. Therefore they must be designed to handle the harsh Martian environment consisting of dust storms, ragged terrain, intense thermal cycling, high radiation threat, and reactive atmosphere. Materials for the mechanical subsystem that had the lowest risk of failure in such a harsh environment were chosen. To reduce risks of mission failure due to structural failure, requirements were defined based on expected static loads, shock loads, and vibrational frequencies. The chassis shall tolerate a static load up to 1500 N. With the maximum mass requirement of the rover being 250 kg and Mars' gravitational acceleration being 3.7 m/s^2, the rover's maximum possible weight would be approximately 750 N, and for a safety factor of 2, the rover would have to tolerate a static load of 1500 N. Typical space random vibration tests reach up to 2000 Hz [35], so the mechanical subsystems shall be designed to tolerate vibrations up to 2000 Hz. To tolerate shock loads greater than the rover's static load for added safety, the suspension system shall tolerate four times its safety static load of 1500 N, or 6000 N.

In addition to tolerating forces encountered during travel, the mechanical subsystem must travel smoothly over any encountered obstacles, such as rocks or small craters. The mechanical subsystem shall withstand a 45 degree tilt in any direction, eliminating the potential of flipping or falling over and ensuring all fragile housed components and instrumentation are kept safe.

Req #	Requirement	Rationale	Parent Req.	Child Req.	Verification Method
MECH.01	The chassis shall tolerate a static load up to 1500 N.	The system must not risk fracture or fatigue that would result in complete structural failure and inability to carry out the mission.	MG.01		Analysis
MECH.02	Mechanical subsystems shall tolerate vibrations up to 2000 Hz.	The system must be able to tolerate vibrations from travel.	SYS.03		Analysis
MECH.03	Suspension subassembly shall tolerate shock loads up to 6000 N.	The system must be able to tolerate shock loads from travel.	SYS.03		Analysis
MECH.04	Suspension subassembly shall withstand a 45 degree tilt in any direction.	The system must be able to tolerate tilts from travel.	SYS.03		Demonstration

Figure 2.1.1.1.1: Mechanical Requirements Table

2.1.1.2 Mechanical Sub-Assembly Overview

Each subassembly within the mechanical subsystem has been designed with emphasis on safe traveling ability, reliable performance in Martian conditions, and integration of subassemblies. The challenges that influenced such decisions include traversing rugged terrain, exposure to extreme temperatures, and strict mass criterion [54]. The rover will encounter rocky obstacles, thermal cycling, and various loads, and the mechanical subsystem was designed with these challenges in mind.

The chassis is the structural backbone of the rover, holding all subsystems together. For a durable and lightweight frame, the chassis will be made of aluminum 6061. The chassis will offer protection to scientific instruments and other subassemblies from dust and radiation exposure. The chassis will feature thicker aluminum walls with a tantalum coating, which is proven to significantly reduce radiation [46]. The chassis will connect to the suspension system with a differential through titanium fittings, which will allow the chassis and its inner components to remain at the average position of the suspension system for increased stability.

The inner dimensions of the chassis are 943.65 x 1143.65 x 318 mm, allowing room for two OBCs, two battery packs, mini-TLS, oven, RAMAN Laser Spectrometer, GNC components, and necessary wiring and thermal components.

The most prominent environmental factors the chassis must withstand are dust and thermal cycling. To address these factors, the chassis material, aluminum 6061, was selected. Due to aluminum 6061’s high shear strength, the chassis will avoid risk of material fatigue throughout the mission lifetime and ensure the chassis can comfortably tolerate all loads. Aluminum 6061’s high fracture toughness lessens the risk of cracks propagating in the material as the dust scratches the surface. Aluminum 6061’s low thermal expansion coefficient of 23.5 µm/m·°C [46] will lessen the impact of thermal cycling on the chassis material throughout a Martian sol.

The rover will implement a rocker-bogie suspension system. Featured on all NASA Martian rover missions, this suspension system has demonstrated its ability to consistently and safely traverse the ragged Martian surface and was therefore chosen for this mission [68]. This suspension system consists of six wheels connected through a pivoting linkage system that allows each wheel to move independently and climb over obstacles twice the diameter of the wheels.

The rocker refers to the longer pivoting arms, which connect to the front wheels and the bogies. The bogie refers to the ‘responding’ arms attached to the rockers that connect to the middle and rear wheels. As the rover encounters obstacles, the rockers and bogies pivot independently at the joints to maintain constant contact with the ground. The chassis remains at the average pitch angle of the two rockers, which are

connected to each other and the chassis through a differential. The differential tilts as obstacles are encountered to maintain at least one rocker wheel on the ground at all times for stability.

The rocker and bogie bars will be made of titanium tubing, like past rovers. The rocker is L-shaped, with one end attached to a drive wheel and the other attached to the bogie through a pivot point. The bogie is similarly L-shaped, with one end attached to a drive wheel and the other attached to an idle wheel used for balance. The bars will connect to the wheel mounts through titanium fittings, allowing for each wheel to have independent motion. The rockers connect to the bogies through a pivot joint, and the rockers connect to each other and the chassis through a differential. The differential connects the rockers to the chassis through similar titanium fittings as those used on the wheel mounts, which allows for the rockers to pivot independently and the chassis to remain at its average position. This system distributes the rover’s weight equally among the six wheels, allowing for balanced loads. Furthermore, this will avoid one wheel or leg joint wearing faster than another, which is an added benefit of the rocker-bogie system along with excellent obstacle handling.

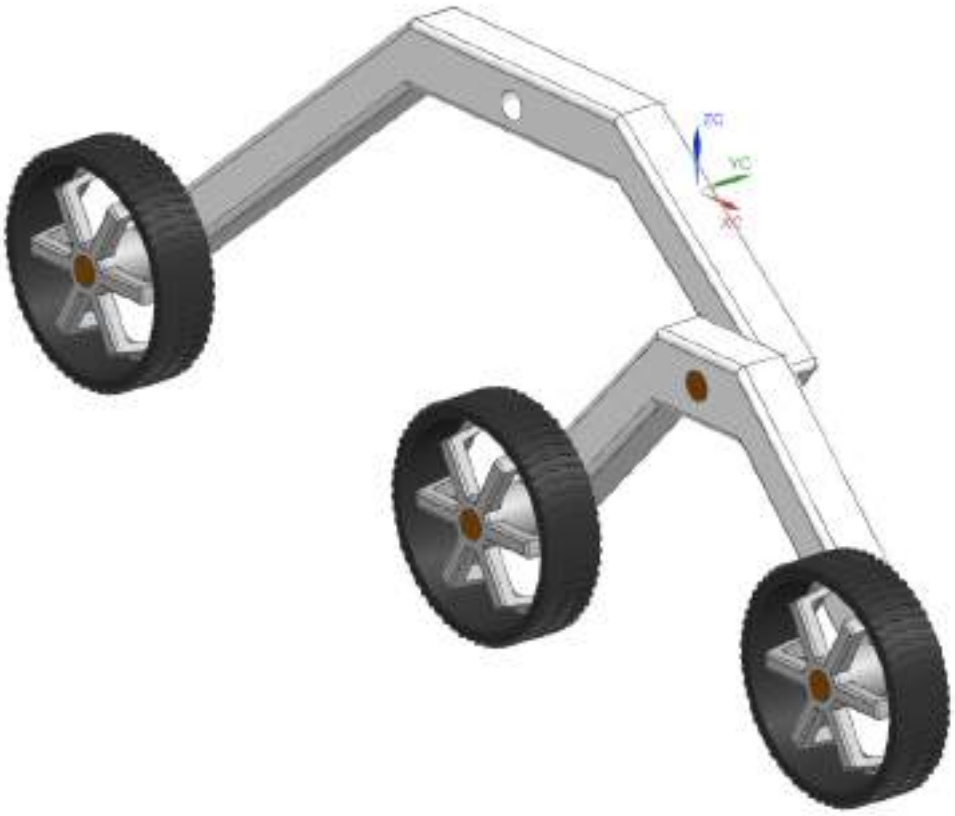

Figure 2.1.1.2: The Rocker Bogie Subsystem

The most common operational and environmental challenges the legs must withstand are shock loads, dust, and thermal cycling. To properly handle these factors, the leg material, titanium, was selected. To address shock loads and dust presence, titanium's high fracture toughness of 100 MPa·m½ [14] will provide shock absorption and dust tolerance by reducing the risk of cracks propagating in the material. To avoid warping or wearing during thermal cycling, titanium has a low thermal expansion coefficient of 8.6 µm/m·°C [14]. The material selection will allow the legs to withstand the environment.

The wheel design affects the rover's ability to handle varying terrain conditions, resist wear over time, and remain operationally reliable through repeated usage. The wheels are manufactured from Aluminum 6061, a material with high fracture toughness and low thermal expansion coefficient, which will allow the wheels to withstand the Martian environment.

Figure 2.1.1.2.1: The Wheel Subsystem

Each of the rover's six wheels will be equipped with an individual drive motor, providing fully independent movement and increased control across uneven, rugged terrain. In addition to the drive motors, the four corner wheels will each include a steering motor, enabling the rover to turn and maneuver around obstacles. This configuration allows for precise movements such as tight-radius turns, pivoting in place, and crab-walking. To ensure precise control and feedback, every motor, both drive and steering, will be paired with an encoder that shall provide measurements of motor position and speed.

The Guidance, Navigation, and Control (GNC) subassembly consists of the state estimator, controller, and planner. The state estimator will return a complete pose estimate by fusing incoming positional, velocity, and acceleration data from accelerometer, gyroscope, and intermittent GNSS positional data from the Mars reconnaissance orbiter (MRO). The controller will implement a closed loop position controller to smoothly dampen perturbations from the intended path and convert the Command and Control (C&C) input into the action space of motor currents, actuators, and steering angles. The planning module will serve as the root of the autonomy stack such that when the rover enters radio silent areas it is capable of continuing to utilize its location estimate to follow an optimal path towards its destination enabling prolonged

periods of operation without RF input. The state estimator, control system, and path planner will be implemented by a subcontractor and incorporated into the main system.

Similar aluminum chassis have been flown on past NASA Martian rovers, but not in the intended environment. Similarly, the rocker-bogie system has been implemented on every NASA Martian rover. The fundamental concept is flight proven, but hardware for P.H.O.E.N.I.X will not be exactly similar to those flown on previous missions. Since geometries and specific component designs will be modified to fit P.H.O.E.N.I.X's design, the chassis and suspension systems will have a TRL of 7.

2.1.1.3 Mechanical Subsystem Recovery and Redundancy Plans

The mechanical subsystem shall implement as many recovery and redundancy strategies as possible in order to ensure the rover's constant operation in the harsh Martian environment. Likely mechanical risks associated with the mission include motor failures, material fractures, and dust-clogged joints.

Certain subassemblies cannot implement redundancies. The rover chassis and legs are too large and massive to feasibly include redundant components. Due to mass and volume restrictions, it is not possible to have a second chassis as this would double the size of the rover, exceeding given volume constraints. Similarly due to mass restrictions, the legs cannot be designed with redundancy as the mechanical subsystem's mass budget would be exceeded. The likeliest risk for the chassis and legs are material fractures, and since redundancy is not possible, the material selection criteria shall focus on being failure resistant and strong. Careful material selection and extensive verification methods that demonstrate low risks of material failure in expected conditions will compensate for the absence of redundancy in the chassis and legs.

In the instance of mobility issues - motor failure, wheel fracture, or dust clogging a joint - redundancy can be implemented in the rover's design. The rover features six wheels connected to the rocker-bogie suspension system instead of four. There is enough redundancy built into having six wheels to allow for two wheels to break and the rover to retain the ability to stay upright. The wheels' motors move independently of each other, so the loss of one wheel will not affect the others.

Recovery is possible with independent wheel movement that allows motors to fail in isolation. Each wheel in the rover's mobility system is driven and steered independently, which allows for failures to be isolated without compromising the rover's overall movement capability. This recovery design ensures that a single-point failure in the wheel assembly does not cause a full failure for the entire system.

2.1.1.4 Mechanical Subsystem Manufacturing and Procurement Plans

For the mechanical subsystem, including the spoke hub, wheels, rocker-bogie mechanism, and chassis, Xometry's CNC machining lead time calculator was utilized as a baseline. Xometry was selected as a method of lead time estimate because of its proven capabilities in precision CNC machining and ability to handle aerospace-grade metals such as Aluminum and Titanium.

For the wheel spokes, which are made from Aluminum 6061, Xometry estimated a lead time of 11 business days. To account for logistics, possible rework, and quality assurance, a 35% margin of error was created, yielding an estimated total lead time of 15 business days.

The rocker-bogie arms were split into two parts to improve maneuverability: the front rocker and the back rocker, which are made of Titanium Grade 2. Both components will be processed via CNC machining. According to Xometry's lead times, the front and rocker have estimated lead times of 11 business days each. Utilizing the 35% margin of error, this results in an estimated total lead time of 15 business days.

The differential in the rocker-bogie mechanism was split into three parts - two mounts, two pivoting links, and one bar that attaches to the chassis. Each component is made of Titanium Grade 2 and will be manufactured through CNC machining. Xometry estimated lead times of 11 days, 7 days, and 11 days for the three differential parts respectively. Adding the 35% margin of error, the estimated total lead times for the differential components are 10 to 15 business days.

The final component of the mechanical subsystem is the chassis. Made from Aluminum 6061, the chassis is split into two parts for simple assembly and integration. Xometry estimated lead times of 11 business days each to manufacture the chassis via CNC machining, and with the error margin, each component of the chassis will have an estimated lead time of 15 business days.

The GNC subsystem will be entirely subcontracted by Lockheed Martin. The lead time is estimated to be approximately 2 months, and with a margin of error of 1 month, the GNC subsystem's lead time is estimated to be 3 months. All mechanical components besides the GNC subassembly were chosen to be manufactured in-house via CNC machining for a number of reasons. The mechanical subsystem's ability to integrate other subsystems is of utmost importance, and design revisions will likely be necessary during integration of other subsystems. In-house manufacturing eliminates the time needed to contact contractors with the changes that will inevitably occur, allowing for smoother integration. In addition, all mechanical components, most notably the chassis and rocker-bogie legs, will undergo structural testing, meaning that multiple iterations will be necessary as tests shall be conducted to component failure.

Manufacturing in-house allows for more rapid prototyping and iteration, which will be very necessary for the mechanical subsystem. Relying on external contractors to manufacture mechanical components would increase the lead times by introducing delays in iteration. Communication between NASA engineers and the contractor would be inherently slower and more formal than in-house collaboration. Any issues discovered during testing or assembly would be discovered after waiting for the parts to arrive from the supplier, and only then could changes be submitted to the contractor which would add even more time. The use of alternate suppliers will slow the iteration severely, resulting in a great loss of valuable time that could be spent testing or assembling, and in-house manufacturing shall therefore be used.

2.1.1.5 Mechanical Subsystem Verification Plans

Req #	Requirement Summary	Verification Method	Rationale for Method	Preliminary Verification Plan
MECH.01	The chassis shall tolerate a static load up to 1500 N.	Analysis	To ensure the chassis can tolerate the expected static load with a safety margin and prevent the risk of mission failure due to material fatigue	Finite element analysis will be used to simulate static loads of 1500 N and the chassis's response will be analyzed
MECH.02	Mechanical subsystems shall tolerate vibrations up to 2000 Hz.	Analysis	To ensure the mechanical subsystems can tolerate vibrations encountered during launch and prevent the risk of mission failure due to material fatigue	Finite element analysis will be used to simulate vibrations of 2000 Hz and the rover's response will be analyzed
MECH.03	Suspension subassembly shall tolerate shock loads up to 6000 N.	Analysis	To ensure the suspension system can tolerate shock loads encountered during travel on Martian terrain and prevent the risk of mission failure due to material fatigue	Finite element analysis will be used to simulate shock loads of 6000 N and the suspension subassembly's response will be analyzed
MECH.04	Suspension subassembly shall withstand a 45 degree tilt in any direction.	Demonstration	To ensure the rover can safely maneuver over obstacles encountered during travel on Martian terrain and prevent the risk of mission failure from tipping over	The CAD assembly will maneuver over a 45 degree slope and continuous ground contact with at least 4 wheels will be demonstrated

Figure 2.1.1.5.1: Mechanical Verification Plan Table

The majority of mechanical subsystem requirements will be verified using finite element analysis (FEA). MECH.01, MECH.02, and MECH.03 define specific loads and vibrations the rover must tolerate. Verifying that each of these specific loads and vibrations are tolerable by the mechanical subsystem significantly lowers the possibility of component or material failure, and therefore also lowers the risk of mission failure. Analysis through FEA was chosen as the verification method for these requirements due to its ability to validate the design’s integrity by demonstrating its behavior under realistic conditions, identifying potential failure points, and simulating a variety of loads.

MECH.04, the requirement to withstand a 45 degree tilt in any direction, ensures the rover’s ability to avoid tipping or falling over while encountering likely Martian

obstacles. To verify the rover’s ability to safely maneuver obstacles, the motion will be simulated in the CAD assembly by moving the rover over a steep obstacle and demonstrating constant four-wheel contact.

2.1.2 Power Subsystem Overview

The P.H.O.E.N.I.X rover's Electrical Power Subsystem (EPS) is engineered to provide efficient and long-term survivable energy across all mission phases on the Martian surface, supporting both critical vehicle systems and high-value science instruments.

For power generation, deployable AZUR Space 4G32C quadruple-junction GaAs panels provide 1.3 m² of collection area. Under clear Martian conditions at beginning-of-life (BOL), the arrays deliver ~200–220 W peak at local noon and ~950–1,000 Wh per sol of electrical energy. Nominal planning with the electrostatic dust shield (EDS) assumes ~750 Wh/sol (typical range 600–900 Wh/sol depending on season and pointing). During dusty periods the EDS helps sustain output in the ~450–650 Wh/sol band; severe dust events are budgeted at ~300–400 Wh/sol. External bypass diodes across every 5–8 cells mitigate localized shading/dust patches. Array output is routed via space-grade cabling to dual Packet Digital MPPT-6SBB buck-boost controllers (94–98% efficient), which maximize energy harvest under changing incidence angles and dust conditions [89]. The MPPTs are mounted within the Warm Electronics Box (WEB) and regulate a 24 V DC main bus.

Energy storage is handled by a flight-proven EaglePicher SAR-10211 battery pack which are placed in a 4S6P configuration, have a capacity of 500 Wh capacity, and designed for 2,000 cycles [90]. The battery resides in a Phase Change Material (PCM) enclosure that maintains 10–30 °C cell temperatures; survival heaters cover extended nights and dust storms. A smart BMS manages state-of-charge, thermal limits, and telemetry to CDH. The pack is sized to buffer ~300 W short-duration peaks and to sustain overnight survival loads.

The PDCU provides conditioned distribution with current-limited smart FET switching, EMI filtering, and microcontroller-based load prioritization. Loads are grouped as survival (thermal heaters, CDH, minimal comms), mission-critical (mobility/arm, primary science), and auxiliary (secondary payloads, non-essential heaters). In power-limited scenarios (dust accumulation, low sun angles), the PDU sheds lower-priority loads while preserving survival functions. Sensitive payloads receive isolated DC-DC power (regulated 28 V, >90% efficiency, high isolation) to minimize conducted noise.

Parameter	**Value (Nominal with EDS)**
Array Peak (noon)	200-220 W
Daily energy (BOL)	950-1000 Wh/sol

Nominal energy	~750 Wh/sol (600-900 band)
Dusty contingency	450-650 Wh/sol
Severe dust event	300-400 Wh/sol
Battery Capacity	500 Wh usable, 4380W stored
Night survival load	114 W avg (30% duty on 380 W)
Traverse load	100-120 W avg (day)
Science mode load	70-120 W range
Data Relay/CDH peak	143 W (conservative)
Design Margin	≥25% daily
Bus & Voltages	24 V DC main, 28 V DC-DC isolated

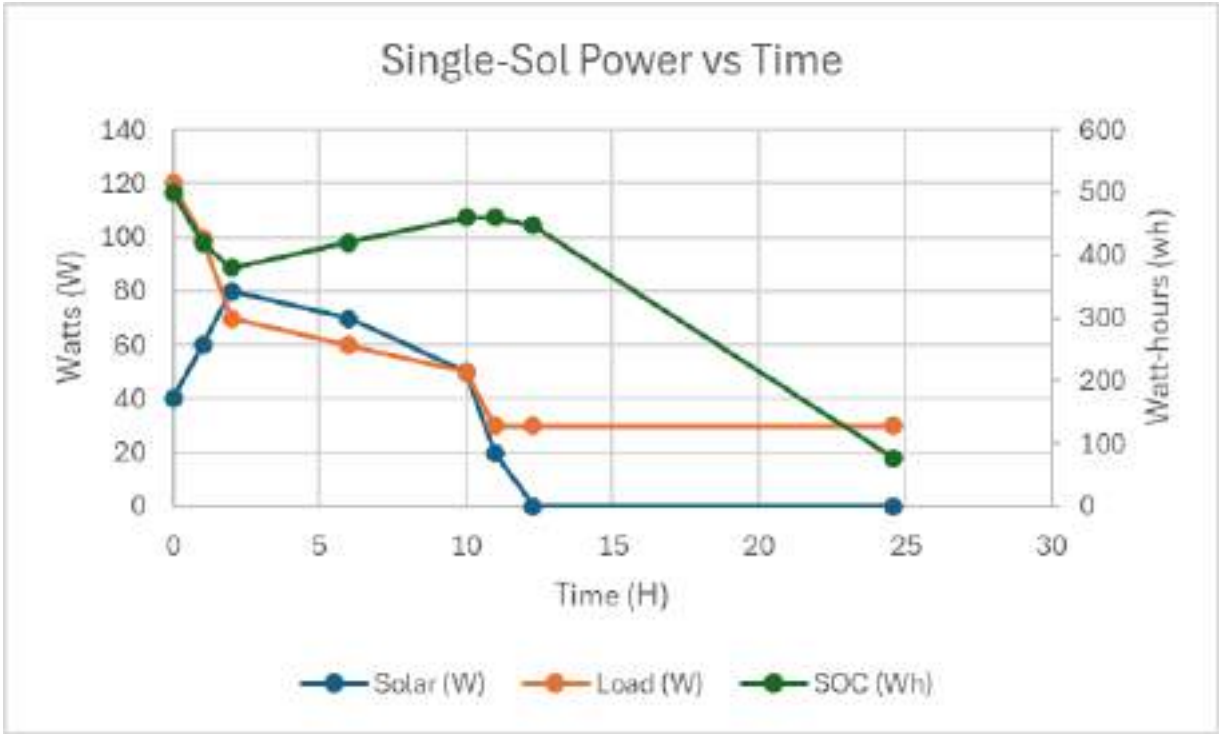

Figure 2.1.2.1

Figure 2.1.2.1 presents a representative single-sol power profile for the P.H.O.E.N.I.X rover, illustrating solar generation, power consumption, and battery state of charge (SOC) across a typical Martian day (sol). The plot is derived from detailed phase-based

data that aligns closely with operational activities described in the mission's Concept of Operations (ConOps).
The mission phases are mapped to specific time intervals within the sol, reflecting key operational steps:

- Landing & Boot-up (0–1 hr): Solar power starts modestly at 40 W while power demand peaks at 120 W due to system initialization and instrumentation startup. This results in a net battery draw of approximately 80 Wh, decreasing SOC from full capacity.
- Instrument Deploy and Calibration (1–2 hr): Average solar input rises to 60 W with load slightly lower at 100 W as instruments stabilize, reducing battery draw but still net negative.
- Traverse Mode (2–6 hr): Solar generation increases to around 80 W, while load averages 70 W due to intermittent driving and navigation. Surplus energy during this phase recharges the battery, reflected by an increase in SOC.
- Science Operations (6–10 hr): Solar power remains near 70 W, with loads around 60 W as primary science instruments collect data. The battery continues to recharge, supporting sustained science mode activity.
- Data Relay Window (10–11 hr): Solar input and load both average near 50 W, balancing energy consumption for high-powered communication bursts.
- Idle and Recharge (11–12.3 hr): Solar production drops to around 20 W while loads remain at about 30 W, slightly reducing net energy and causing a small SOC decline.
- Night Survival (12.3–24.6 hr): Solar generation ceases while loads average 30 W primarily for survival heaters and avionics. Battery power sustains these loads, leading to a significant SOC decline overnight.

Integrating these phases yields a total solar energy input of approximately 776 Wh and total load consumption of about 1,198 Wh over the full 24.6-hour sol. The negative net energy (-422 Wh) underscores the vital role of the battery in covering the gap between generation and consumption, especially during high-load and nighttime phases. The SOC curve plotted on the figure corresponds with this dynamic, showing battery discharge during energy deficits and recharge during surplus periods.

This phase-based power analysis and corresponding single-sol plot provide a clear visualization of the rover's daily energy management strategy. By representing the ConOps phases within a single sol, the plot captures the cyclic nature of Mars surface operations; where daily solar availability, load variability, and battery buffering interplay to maintain continuous rover functionality.

2.1.2.1 Power Subsystem Requirements

The Electrical Power Subsystem (EPS) must provide reliable and survivable energy for the rover throughout all phases of the mission, from landing and initial activation through traversal, science operations, contingency survival, and eventual decommissioning. To achieve this, the EPS has been designed around a set of requirements that balance daily operational needs, environmental survivability, and system safety margins, ensuring mission objectives can be met under both nominal and degraded Martian conditions.

At the core of the design, the EPS shall generate a minimum of 200 watt-hours per sol while supporting peak power draws up to 120 watts for at least 30 minutes at a time, repeating up to three times per sol. This requirement ensures that the system can close the daily power loop by simultaneously covering mobility activities, science instrument operation, communications relays, and thermal survival functions. To better frame the system demand, the spacecraft structure is expected to consume 10–20 W, science payloads require 70–120 W, command and data handling draws 30–50 W, communications typically use 50 W but can peak at 143 W during high-power transmissions, navigation averages 100–120 W, and thermal control averages 114 W, with a night survival duty cycle requiring 30% operation of a 380 W peak load. By anchoring the daily energy balance to these expected loads and incorporating margin, the rover maintains sufficient capacity to survive periods of reduced insolation and fluctuating demand. Verification will be achieved through analysis of power budgets and simulations of load profiles, since these energy flows can be effectively validated using modeled Martian insolation and subsystem duty cycles.

For reliable power generation, the solar arrays shall be capable of autonomous deployment and survivability in Martian wind conditions up to 20 m/s. These structural requirements ensure the EPS can withstand dynamic entry, descent, and landing disturbances as well as routine surface winds, preventing catastrophic loss of energy production due to deployment failure or structural damage during mission operations. Furthermore, the inclusion of an electrodynamic dust shield provides additional resiliency against particulate accumulation, preserving solar efficiency over long-duration surface activities. Verification will rely on physical deployment and wind-load tests, as mechanical survivability is best demonstrated through direct testing rather than analysis alone.

The EPS must also guarantee functionality across the harsh Martian thermal regime. Critical electrical and electrochemical components, including the battery and power conversion electronics, shall maintain operability between –30 °C and +50 °C. This temperature envelope was derived from expected diurnal swings inside the Warm

Electronics Box (WEB) and provides adequate margin to ensure chemistry stability in the battery and reliability in sensitive avionics. While non-critical components may tolerate wider ranges, adherence to this requirement ensures that survival loads and mission-critical functions remain intact even under environmental stress. Verification will be accomplished through thermal vacuum chamber testing, the standard method to validate operation under simulated Martian hot and cold extremes.

To reduce integration risk and protect sensitive payloads, the EPS shall employ electromagnetic interference (EMI) shielding and modular connectors. The shielding ensures that any stray electromagnetic fields are safely grounded, limiting interference with high-sensitivity science payloads and avionics. The use of modular connectors reduces the chance of integration errors, simplifies subsystem interfacing, and diverts harmful transient signals away from critical components. Verification will be carried out through EMI/EMC compliance testing and inspection, since actual interference effects and grounding behavior cannot be fully captured with modeling alone.

Finally, to meet fault-tolerance expectations, the EPS shall provide redundant power paths to all critical systems via the redundant control electronics (RCEs) and power distribution modules. This redundancy ensures that no single point of failure can disable essential rover functions. Even in the event of a partial system failure, high-priority survival and science loads would remain powered, enabling graceful degradation and continued mission functionality. Verification will combine subsystem-level analysis with targeted fault-injection testing, which together ensure not only that redundant pathways exist on paper but also that they engage correctly under hardware failure conditions.

Req #	Requirement	Rationale	Parent Req.	Child Req.	Verification Method
PWR.01	The system shall generate at least 200 Wh per sol under average Martian insolation and withstand peak power draws of 120 W for a minimum of 30 minutes up to 3 times per Sol.	Supports nominal rover operation, mobility, communication and science payloads	SYS.01		Analysis
PWR.02	Solar panels shall deploy autonomously and tolerate up to 20 m/s wind.	Ensures survivability under common Martian conditions	SYS.06		Test

PWR.03	The system shall maintain operation of critical components between -30°C to +50°C.	Ensures battery and electronics functionality	SYS.06		Test
PWR.04	The system shall minimize integration risk using EMI shielding to absorb shockwaves and modular connectors to divert signals from critical components.	Reduces failure during integration and operations	SYS.05		Test
PWR.05	The system shall provide redundant power paths for critical systems via RCE’s and power and analogue modules	Enhances fault tolerance by dividing power distribution and handling between two computers, helping to reduce uptime	SYS.05		Test

Figure 2.1.2.1.1: Power Requirements Table

2.1.2.2 Power Sub-Assembly Overview

The Electrical Power Subsystem of the rover is engineered in order to provide consistent, reliable energy during all mission phases, and ensure the continuous operation of both critical rover systems. Additionally, the high-value scientific instruments shall receive adequate power from the EPS, and continuously operate when planned during the mission on the Martian surface. The subsystem integrates power generation in the use of a battery and solar panels, storage, and distribution functions in a hybrid bus architecture that is resistant to single-point failures. Overall, the EPS is designed to accommodate the environmental variability on the surface of Mars, and mitigate risks including dust accumulation, low solar angles, temperature extremes, and energy cycling. The most important requirement of the EPS is to guarantee uninterrupted power for surface operations, data collection to achieve scientific goals, temperature regulation, communications to and from Earth, and thermal control of all subsystems. In doing so, the EPS shall embed sufficient margins in all operations and function autonomously to mitigate failures. In contrast to prior missions, where dust storms and component degradation could significantly compromise operations, P.H.O.E.N.I.X 's EPS incorporates a combination of active management, intelligent load prioritization, and fault-tolerant design to ensure long-duration survivability and operational efficiency [111]. All aspects of the subsystem have been designed as a unified system. Each component interfaces with the others to support mission objectives under all conditions.

The primary power source for the rover comes from the solar panels. Utilizing deployable AZUR Space 4G32C quadruple-junction gallium-arsenide solar arrays shall provide a total collection area of approximately 1.3 square meters. This array was chosen for its high efficiency, prior flight heritage, and resilience under Martian insolation conditions. At the beginning of the cell’s life, the arrays can deliver peak power levels of approximately 200 to 220 watts under peak conditions, corresponding to roughly 950 to 1,000 watt-hours per Martian sol. To address the constant challenge of dust accumulation, the P.H.E.O.N.I.X rover’s system integrates an electrostatic dust shield, which maintains a nominal energy output of approximately 750 watt-hours per sol during operations. During moderate dust conditions, energy generation is projected to remain within 450 to 650 watt-hours per sol, while severe dust storms are budgeted to provide 300 to 400 watt-hours per sol. These estimates are critical for prioritizing rover activities and integrating modes of operation based on weather events. The solar arrays are equipped with external bypass diodes every five to eight cells, preventing shading or dust coverage from reducing overall efficiency. By allowing currents to bypass potentially affected cells, the diodes are able to maintain the overall energy output. This protects individual cells from damage, and ensures consistent power delivery, even when a portion of the solar array might be compromised.

Energy harvested from the solar arrays is routed via space-grade cabling to dual Packet Digital MPPT-6SBB maximum power point tracking controllers (MMPTs) to different parts of the rover. These MMPTs are housed within a separate area within the rover that is thermally controlled for electronics that have higher operating temperatures. These controllers operate around 95% efficiency, and shall dynamically operate to shed load resistance. This maximizes energy extraction under variable weather conditions. The MPPTs regulate the 24-volt DC main bus, providing a stable voltage reference for the distribution and storage subsystems. The close integration of the MPPTs with the solar arrays and battery system allows the rover to maintain a continuous energy flow, even under partial shading or array degradation. The MPPT controllers continuously monitor voltage, current, and temperature, providing real-time telemetry to the rover's Command and Data Handling system and adjusting operation to optimize power harvest while preserving component longevity.

Energy storage is provided by a flight-proven EaglePicher SAR-10211 lithium-ion battery pack, configured in a 4S6P architecture with a usable capacity of 500 watt-hours. This pack is designed for over two thousand cycles, providing sufficient longevity to support the planned mission duration. The battery resides within a Phase Change Material thermal enclosure that passively buffers against extreme temperature fluctuations, maintaining cell temperatures between 10 and 30 degrees Celsius. Survival heaters supplement this passive system during extended nights or dust-induced energy shortages, ensuring that the battery maintains optimal operational temperatures. The battery management system continuously monitors state-of-charge, cell temperatures, and overall health, communicating critical telemetry to the CDH system and enabling autonomous energy allocation. The pack is sized to buffer short-duration peak loads of approximately 300 watts [27], such as high-demand robotic arm movements or instrument deployment, while sustaining overnight survival loads averaging 114 watts, accounting for intermittent operation of thermal heaters. This architecture ensures that essential systems remain functional during periods of low energy availability, including extended dust storms or low sun-angle periods.

The power distribution unit (PDU) manages and conditions electrical power from the generation and storage subsystems. The PDU employs solid-state switches, current-limiting circuitry, and electromagnetic interference filtering. These components work together to deliver safe, conditioned energy to all other rover subsystems. Electrical loads are categorized into survival, mission-critical, and other groups,helping to enable dynamic load shedding and prioritization during low-energy times. Survival loads include thermal heaters, avionics, and minimum communications and telemetry, while mission-critical loads cover mobility actuators, the robotic arm, and primary science instruments. Auxiliary loads include secondary payloads and non-essential heating elements, which can be shed to preserve energy for survival and critical

operations. Sensitive payloads receive isolated 28-volt DC-DC power conversion with greater than 90 percent efficiency, minimizing conducted noise and ensuring measurement fidelity. The PDU's microcontroller-based logic continuously evaluates bus voltages, current demands, and battery state-of-charge, executing autonomous load shedding and restoration sequences without ground intervention, thereby enhancing the rover's ability to survive unforeseen energy-limited conditions.

Thermal management and environmental resilience are deeply integrated into the EPS design. The Warm Electronics Box provides a controlled environment for the MPPT controllers and PDU electronics, mitigating the impacts of Martian temperature swings that range from -80°C at night to +20°C during midday [55]. The battery's PCM enclosure extends survivability by storing thermal energy during warmer periods and releasing it during the night, reducing the duty cycle required from survival heaters. This combination of active and passive thermal strategies allows the system to maintain critical energy and thermal functions even in the event of heater failure or prolonged low insolation. Solar panel deployment mechanisms are designed to tolerate wind speeds of up to 20 meters per second, ensuring that panels can autonomously unfold and orient correctly without mechanical compromise. These environmental considerations reflect an integrated design philosophy that prioritizes both energy efficiency and component longevity in the Martian context.

Redundancy and fault tolerance are central to the EPS's operational limits. The dual MPPTs controller architecture allows continuous energy extraction even if one controller experiences partial degradation. Cross-strapped battery strings help ensure that essential loads shall be supported by either string independently. The PDU integrates redundant DC-DC converters for critical buses, operating in parallel under nominal conditions and providing automatic failover if one unit experiences degradation. Solid-state power controllers within the PDU are capable of isolating faulted circuits and executing preprogrammed load-shedding sequences to protect remaining systems. Autonomous monitoring algorithms track all electrical parameters, enabling real-time response to transient faults, such as short circuits, overcurrent events, or bus voltage sags, without requiring intervention from ground control. This layered redundancy ensures that essential systems, including thermal survival heaters, avionics, and communications, remain powered, while non-essential instruments can be temporarily disconnected until system stability is restored.

The EPS has been sized to provide sufficient energy margins to support all mission scenarios, including traverse operations averaging 100 to 120 watts, science mode operations ranging from 70 to 120 watts, and data relay peaks conservatively estimated at 143 watts. Nominal daily energy generation under the EDS system is approximately 750 watt-hours, with a design margin exceeding 25 percent to

accommodate seasonal solar variability, dust deposition, and array aging. Energy budgets are carefully coordinated with operational planning, enabling the rover to autonomously schedule high-demand activities during periods of peak solar availability while conserving energy during low-insolation periods. In combination with the intelligent load prioritization, this ensures that critical functions remain supported even under extended dust storms or other adverse environmental conditions.

Subsystem integration has been approached with modularity and interoperability as guiding principles. Electrical and mechanical decoupling of solar arrays, MPPT controllers, battery packs, and distribution units reduces single-point failure risk while facilitating independent verification, testing, and replacement if necessary. Cabling and connectors conform to NASA Class K space-grade standards, ensuring durability through launch, landing, and prolonged exposure to Martian dust and thermal cycling. The design ensures that every component, from energy generation to distribution and storage, operates as part of an interconnected, resilient system. The integration of thermal management, EMI shielding, and autonomous load management further enhances reliability and guarantees that the rover can meet mission objectives over extended operational periods.

Overall, the Electrical Power Subassembly embodies a comprehensive approach to energy management on Mars. By combining high-efficiency solar arrays, robust and thermally protected lithium-ion batteries, intelligent distribution with prioritized load management, and layered redundancy, the subsystem ensures continuous support for critical rover operations. The design accommodates environmental variability, anticipates component degradation, and embeds autonomous recovery strategies, enabling the rover to sustain science, mobility, and communications functions throughout the mission. The EPS demonstrates a careful balance of efficiency, reliability, and survivability, providing a high-confidence energy solution capable of supporting long-duration surface exploration while mitigating the risks inherent to operating in a harsh and remote extraterrestrial environment. Through this integrated and resilient architecture, the rover is equipped to achieve its scientific and exploratory objectives, maintaining operational integrity and ensuring mission success even under the most challenging Martian conditions.

2.1.2.3 Power Subsystem Recovery and Redundancy Plans

The Electrical Power Subsystem shall include a layered recovery and redundancy strategy. This design helps ensure that no single failure may compromise the continued operation of the mission. Utilizing this approach builds on outlined NASA principles that strive to eliminate single-point failures within critical systems [82]. This approach also draws from lessons learned on prior Exploration Rover missions, where power anomalies caused significant operational consequences. Therefore, using a layered architecture with load-shedding capabilities and fault detection systems allows for redundancy across systems for power generation, storage, and distribution, and allows the rover to recover from potential anomalies.

Solar arrays have been divided into dual strings with independent regulation, which are responsible for primary power generation.These panels are independently regulated. Allowing for partial array degradation with dual string architectures means that power availability shall not be reduced below survival thresholds if arrays do not continue to operate at their peak capacity. The same is true for the power regulation system. Storage redundancy is achieved through two parallel battery banks, either of which can support essential mission functions independently. Cross-strapping between banks allows the system to reconfigure in response to anomalies, balancing charge cycles and ensuring continued operation even in the event of partial cell failure.

Providing redundancy for the power distribution unit is achieved via paired DC-DC converters for the critical buses. These converters operate parallelly under normal conditions, and induce automatic failover should a single unit degrade. In addition to these, the rover has solid-state power controllers, which are able to provide fault isolation within circuits. Should failure occur, the system shall rapidly isolate the fault, protect remaining loads, and initiate preprogrammed load shedding sequences. Essential systems including thermal survival heaters, avionics, and communications shall constantly remain powered, while non-essential instruments are disconnected until stability is restored.

Recovery strategies include both autonomous and ground-commanded procedures. Should power availability fall below safe levels, such as during extended dust storms, the electrical power system transitions into low-power survival mode, shutting down all but essential thermal and communication functions back to Earth. This approach is modeled after the Mars Exploration Rovers’ recovery from the 2007 global dust storm, when autonomous power reduction ensured vehicle survival despite minimal solar input [29]. Once power levels return to acceptable thresholds, the electrical power system shall autonomously resume recharging and shall return to normal functionality, addressing power needs of non-critical systems in a staged sequence.

Thermal resilience is an additional element of redundancy. Batteries shall be maintained within safe temperature ranges through passive buffering and heaters. Passive buffering systems utilize phase-changing materials that extend survivability of components during heater failure or extended low-power operations. This combination of active and passive measures reduces dependence on any single thermal control element and protects against catastrophic failure.

The electrical power subsystem Redundancy and Recovery framework ensures that mission-critical functions are protected under degraded conditions, or long-term operations beyond initial mission timeframe. By embedding redundancy at every level, integrating fault detection and isolation, and ensuring survival through autonomous recovery modes, the subsystem provides high confidence in sustained operation. Even in the event of major anomalies, the rover can continue to maintain communications, protect its thermal state, and eventually return to full operations, ensuring the mission continues to meet its science and exploration objectives.

2.1.2.4 Power Subsystem Manufacturing and Procurement Plans

In alignment with NASA procurement policy NPD 1370.1, the Power Subsystem will be procured entirely through commercial suppliers, with each critical component carefully selected based on flight heritage, technical readiness, and reliability. To mitigate schedule risk, lead times have been estimated using analogous data from vendor listings, NASA smallsat programs, and heritage missions, including Mars rover procurement, with margins added for export clearance, customization, and qualification testing.

For primary power generation, the team shall procure AZUR SPACE 4G32C Advanced quad-junction solar cells. These high-efficiency GaAs cells were chosen for their proven performance and extensive use on ESA and commercial deep-space missions. Because AZUR SPACE provides bare cells, array integration will be outsourced to an experienced U.S. contractor, such as MMA Design or Deployable Space Systems. MMA has strong heritage in CubeSat deployable arrays, while DSS has fabricated large NASA arrays including Psyche, so the final contractor will be determined by scaling requirements and cost optimization. Based on analogous European mission data and commercial procurement reports [91], we estimate 6–8 months for cell delivery and an additional 4–6 months for panel integration and testing. With a 25% margin, the total timeline is 12–16 months. As a contingency, SolAero Technologies (Rocket Lab) is identified as a backup supplier. While SolAero's triple-junction cells have slightly lower efficiency, they offer fully U.S.-based production and integration, reducing export delays. SolAero's published mission experience, including Mars InSight and Cygnus spacecraft arrays, supports an estimated lead time of 8–12 months. To remain on schedule for the October 2029 spacecraft integration milestone, procurement of solar cells and panel fabrication will be initiated by March 2028.

For power conditioning, the team selected the VPT SVRFL2800S-series isolated DC-DC converter as the primary component. This Class K, space-qualified power module is radiation-tolerant, has strong flight heritage, and is a trusted component in NASA missions [92]. Procurement will be conducted directly through VPT or via authorized aerospace distributors. Comparable procurement timelines from NASA smallsat reports and EEE-INST-002 guidelines [92] suggest a lead time of 12–16 weeks; with an added 25% schedule margin, 14–20 weeks are assumed. As a contingency, Texas Instruments space-qualified DC-DC converters were identified based on their widespread use in spaceflight electronics, including Mars rover avionics boards[. Lead times for TI converters are estimated at 16–20 weeks, with additional time required for electrical interface modifications and qualification screening. Procurement of this component will occur no later than mid-2029 to align with payload integration.

To optimize energy harvest from the solar array, the team has selected Packet Digital MPPT-6SBB buck-boost controllers. Packet Digital has delivered these controllers on multiple NASA smallsat programs with proven performance in maintaining optimal photovoltaic efficiency under variable solar input. The procurement timeline for these devices is estimated at 20–24 weeks, and with a 25% margin, 25–30 weeks are assumed for integration. As a contingency supplier, AAC Clyde Space was identified, offering standalone MPPT units with extensive CubeSat and microsatellite heritage. Procurement timelines for Clyde MPPTs are estimated at 18–24 weeks, yielding 22–28 weeks with a margin. While comparable in availability, the trade-off is slightly lower efficiency relative to Packet Digital's specialized designs, along with higher export complexity since primary manufacturing is based in the UK. MPPT orders must be placed no later than late 2028 to support electrical system integration.

Energy storage will be provided by the EaglePicher SAR-10211 lithium-ion battery. This custom pack was selected for its established spaceflight heritage as EaglePicher batteries have flown on numerous NASA spacecraft, including the Mars Phoenix Lander. They were chosen also for its ability to operate across the mission's environmental range. Due to its specialized design, procurement lead time is longer, with industry reports indicating 24–32 weeks; with a 10% buffer for screening, 26–35 weeks are assumed [27]. To maintain schedule flexibility, procurement must begin in mid-2028 for readiness prior to environmental testing in 2029. The estimate for the cost of this component ranges from $35,000-$40,000, based on estimates from the NCIM Concept Cost calculator provided by NASA, along with testing methods and level of craftsmanship required to create a custom battery for this mission. This procurement time is supported by similar suppliers, but could be lessened if tests prove to be nondestructive. As a backup, the team identified ChargeX and Mobile Power Solutions, both of which have experience producing ITAR-compliant aerospace-grade batteries [86] These suppliers could deliver comparable batteries in 20–28 weeks based on their smallsat program heritage, which equates to 22–31 weeks with margin. While slightly faster, they would likely incur higher qualification costs and require additional screening.

2.1.2.5 Power Subsystem Verification Plans

Verifying the Electrical Power Subsystem is essential to ensuring that design assumptions, performance margins, and redundancy strategies shall operate within in-situ conditions. The verification plan was created via thorough discussion, including aspects of analysis, inspection, demonstration, and testing for all components, aligning with NASA standards for subsystem verification and validation. Verification will occur progressively, beginning at the component level and culminating in system-level tests that confirm readiness for integration and flight. By adopting a phased approach, the project minimizes risk, validates redundancy features, and ensures that performance requirements are met before progressing to later development stages.

At the component level, verification begins with acceptance testing of solar cells, batteries, converters, and controllers. For solar arrays, verification includes functional testing under simulated solar flux and angular variation, alongside accelerated degradation testing to replicate Martian dust and radiation conditions. Coating performance is validated through environmental chamber tests that simulate dust accumulation cycles and thermal cycling across extreme temperature ranges. Battery verification focuses on charge-discharge cycling to validate the expected capacity of 100 ampere-hours, thermal performance testing across –40°C to +50°C, and radiation tolerance assessments. Each battery bank undergoes vibration and shock testing to confirm survivability through launch and landing, as well as pressure testing for safety under potential venting scenarios.

For power electronics, including DC-DC converters and solid-state power controllers, verification involves both electrical and radiation testing. Efficiency and load regulation are validated through laboratory load cycling at varying demand levels. Radiation testing evaluates performance under total ionizing dose and single-event effects, confirming that the components meet mission duration requirements without significant degradation. Solid state power converters undergo short-circuit and overload testing to confirm their ability to isolate faults quickly without compromising system stability.

Subsystem-level verification involves integration testing of generation, storage, and distribution units. These tests confirm that the solar arrays and batteries interface properly with the power conversion and distribution unit and that redundancy features perform as intended. For example, controlled fault injection will be used to validate cross-strapping of battery banks, failover functionality of paired converters, and isolation of faulted lines by solid state power controllers. Load shedding protocols will be tested by simulating bus overloads and monitoring system prioritization of thermal and communications loads. These tests provide direct evidence that recovery and redundancy strategies function as expected under realistic scenarios.

System-level verification includes end-to-end power testing during integrated spacecraft environmental testing. This phase validates the Electrical Power System under simulated launch vibration, thermal vacuum, and electromagnetic compatibility conditions. During these tests, the spacecraft will undergo operational scenarios including cruise, entry-descent-landing, and surface night operations. Power demand profiles for each mission phase will be simulated, and Electrical Power System response will be evaluated against subsystem requirements. The tests also verify that telemetry data from the Electrical Power System provides accurate and timely fault information to both autonomous control systems and ground operators.

In addition to lab and system testing, verification includes analytical modeling. Power budgets are validated through simulations that model environmental conditions, including dust storms and sunlight variations on the Martian surface. Thermal-electrical coupled models predict the impact of heater demand on battery charge retention, and fault tree analyses verify that no single-point failure can compromise critical mission survival. These analytical methods provide coverage for on-surface scenarios that cannot be reproduced on the ground.

The Electrical Power System verification plan encompasses several formal reviews, such as the CDR, FIR, and ORR. At each milestone, verification data is reviewed against requirements to confirm compliance and identify any new or outstanding risks. This process ensures that by launch, the Electrical Power System will have been demonstrated to support all mission phases with the margins of power production, redundancy, and recovery capabilities. Through testing, modeling, and review, the verification plan provides high confidence that the Electrical Power System will perform as intended throughout the mission lifecycle, safeguarding the success of the science and exploration objectives.

2.1.3 CDH Subsystem Overview

The Command and Data Handling (CDH) Subsystem serves as the brains of the rover, managing data processing, storage, communication, and coordination across all subsystems. It integrates four key subassemblies: the Onboard Computer (OBC), Data Storage, Data Interfaces, and Telecommunications.

The Onboard Computer (OBC) is responsible for executing commands, processing storage, and managing control loops. During traverse phases the OBC uses sensor and state data from the GNC system to guide the rover. When the rover transitions into science mode, the OBC diverts power towards instrument operation, executes measurement commands, and collects data.

The Data Storage subassembly stores data from science instruments, sensors, as well as relevant environmental and geographical data for safe traverses. The science operations and sensors collect huge amounts of data which cannot all be processed immediately. The OBC will determine important data and tag data by its priority for transmission to Earth. During periods of high demand, telemetry will be prioritized ahead of science data to ensure the rover’s safety.

The Data Interface provides the electrical and logical pathways between instruments, subsystems, and the OBC. These will be physical links including transceivers and wires that have low-latency and are radiation protected against loss of information. This allows telemetry collection, science data collection, and command distribution.

The Telecommunications subassembly is responsible for the transfer of data between the rover and Earth. This operation will occur through a relay with the Mars Reconnaissance Orbiter (MRO) through an Ultra High Frequency (UHF) radio [41]**.** During traverse phases, the rover will transmit periodic heartbeat telemetry to confirm its health and position. In science phases, the large amount of data will be compressed and stored until scheduled relay windows during night mode when less demand exists for the radio.

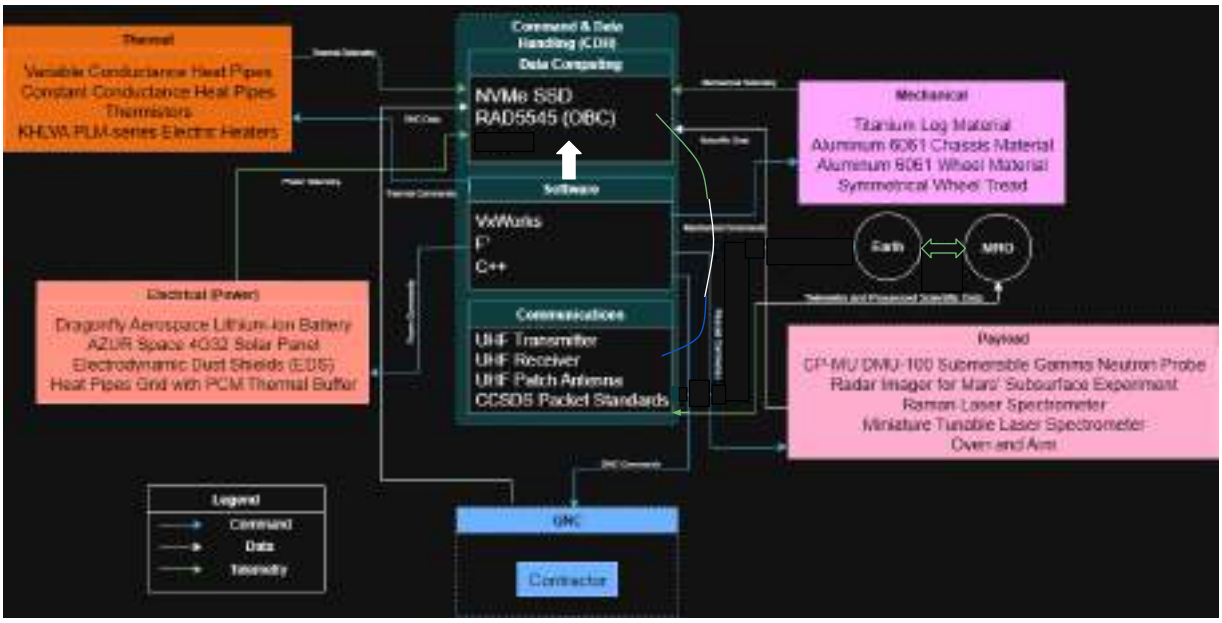

Figure 2.1.3.1: Software Architecture Flowchart

The CDH subsystem is structured around three functional blocks: Data Computing, Software Execution, and Communications. These blocks together manage the collection, processing, prioritization, and transmission of data. The software runs on the data computing structure, and executes all CDH actions from commands to data handling. Through the data computing system the software can give or receive communications including data, commands, and telemetry. A software architecture diagram illustrates how the CDH interfaces with other rover systems, using RS-422 for physical connections and standardized software protocols for message handling and execution.

The Electrical Power System (EPS), which includes lithium-ion batteries and deployable solar panels with electrodynamic dust shields, is tightly integrated with the CDH system. The CDH receives real-time telemetry data from the EPS including battery voltage, current draw, charge status, and internal temperature and compares this data against expected operating profiles. When deviations are detected, CDH commands can modify EPS behavior: enabling/disabling charging, deploying solar arrays, or redistributing power across subsystems. Power modes such as science mode, sleep mode, and emergency mode are also managed via CDH logic based on power and mission conditions.

Thermal regulation is another key interface. The thermal control system includes passive elements such as multi-layer insulation (MLI) and active elements like electric heater [56]. Thermistors throughout the rover provide temperature data to the CDH,

which responds by activating or deactivating heaters or adjusting heat pipe flow [77]. For colder Martian nights, the CDH can initiate power-conserving overnight heating cycles and shut down non-essential systems to preserve critical functionality. All thermal telemetry is logged and used to refine thermal response strategies and plan future power availability.

Although the GNC subsystem is provided by an external contractor, the CDH subsystem is responsible for processing the GNC data onboard. The OBC receives measurements from the IMU, including accelerometer and gyroscope data, and fuses them with wheel odometry and actuator feedback through an Extended Kalman Filter [49]. This provides an accurate real-time state estimate of the rover's position, velocity, and orientation, which is essential for localization and path planning. CDH software then uses this information to calculate error between the current and target state, sending corrective commands to the mobility subsystem to close the loop [103].

The CDH software is written in C++ due to its performance efficiency and suitability for real-time embedded systems. C++ is consistently used by NASA missions and most recently on Mars on Perseverance. Software development shall be done through Visual Studio Code inside Docker containers for embedded portability, and managed using Git version control [93]. The modular software architecture separates drivers, control routines, and communication layers to reduce risk and enhance reliability. Safety-critical logic is incorporated to maintain spacecraft operability even under adverse conditions.

The flight software runs on VxWorks, a proven real-time operating system (RTOS) with extensive flight heritage, including Spirit, Opportunity, Curiosity, and Perseverance [93]. The ROTS provides deterministic scheduling, task management, and hardware abstraction which ensures real-time updates for CDH operations. In this system, VxWorks will handle task scheduling, I/O, and support communication with C++ controlling higher-level logic.

For the framework, JPL's F' has been chosen as a proven framework from 2014 on, with applications within many cubesats and several Mars missions. It is built specifically for lighter weight missions and has modularity to support the development of this mission [43]. It provides infrastructure for commands, telemetry, event reporting, and fault detection and can be used with both C++ and VxWorks.

Commands from Earth are prepared by mission control and sent during scheduled DSN communication windows. These messages are relayed via the MRO to the rover's UHF radio. Following CCSDS standards, these commands include instructions to activate instruments, update configurations, modify science plans, or adjust mobility parameters [42]. The CDH system checks message integrity and routes

commands to the appropriate subsystems. Priority execution ensures that time-sensitive commands (e.g., fault recovery or power reallocation) are handled immediately, while others are queued and executed as bandwidth and system state allow [42].

All data generated on the rover telemetry, health logs, science measurements is collected and processed by the CDH subsystem before transmission. The data is compressed, timestamped, compressed into packets, and assigned priority. Critical telemetry such as power levels, internal faults, and system temperatures are prioritized over less urgent science data. These packets are transmitted via UHF to MRO during scheduled overpass windows and subsequently sent to Earth. The CDH system ensures redundant transmission of urgent data and manages lower-priority data buffering for delayed downlink opportunities.

2.1.3.1 CDH Subsystem Requirements

The CDH (Command & Data Handling) Subsystem consists of the Onboard Computer (OBC) subassembly, Data Storage subassembly, Data Interfaces subassembly, and Telecommunications subassembly. In order to meet all of the mission requirements, the subsystem must be able to navigate and analyze its surroundings and goals for mission success.

The Command and Data Handling (CDH) Subsystem enables spacecraft coordination, autonomy, and communication. It integrates four key subassemblies: Onboard Computer (OBC), Data Storage, Data Interfaces, and Telecommunications; each of which supports critical mission functions. The OBC executes flight software and manages autonomy routines. Its performance, memory, and radiation tolerance are vital for maintaining control and system integrity in the harsh Martian environment. Data Storage ensures scientific and telemetry data are logged reliably and accessibly, necessitating sufficient capacity, fast write speeds, and resilience to environmental degradation. Data Interfaces serve as the internal communication backbone, linking the OBC to instruments, actuators, and sensors with reliable timing and low signal noise key for coordinated subsystem execution and fault response [5, 6]. Telecommunications handles the uplink and downlink of mission data between the rover and Earth via orbital relays. Efficient encoding, low power draw, and fault-tolerant transmission are essential to maintaining operational awareness and ensuring scientific return. Each subassembly is interdependent, and failure in any one of them risks total mission loss.

In order to determine the values for each quantified requirement, analogous missions were used as a guide. The Perseverance and Curiosity rovers are the two most applicable as they are the two most recent NASA rovers on Mars. The general computing specifications for the uplink/downlink rates, processing speed, memory, and storage were all chosen based on Curiosity and Perseverance. Although those rovers

are larger, electronics have improved since they were designed meaning the same specifications can be expected out of smaller form factors [49]. The CDH system will be within the rover; the Thermal Subsystem will keep the rover at a range of +30°C to +40°C. To account for any failure in the thermal control an operation range of -30°C to +50°C is required with a larger bottom bound because Mars does not tend to get much hotter than the range but gets much colder [125]**.** The radiation requirement is a conservative number based on the protection of subassemblies of the CDH subsystem on Perseverance [127]**.** This requirement of 10 krad can afford to be conservative for the same reason the temperature can, the CDH subassemblies are completely contained within the rover. The rover will communicate to Earth via the MRO, this means it must have the range to reach the MRO. At maximum the MRO is about 316 km from Mars and accounting for the MRO not being directly above the rover, a range of 550 km is required [104].

Constant verification and testing of subcomponents is needed to ensure the CDH subsystem can reach maximum performance. Methods would include demonstrations of the technological capabilities in the CDH Subsystem in a safe space, computer analysis, using effective programming for debugging, and early software testing.

Req #	Requirement	Rationale	Parent Req.	Child Req.	Verification Method
CDH.01	The Command and Data Handling (CDH) system shall have a minimum uplink rate of 256 kbps and a minimum downlink rate of 16 Kbps.	The system must be able to send scientific and telemetric data to and from Earth.	SYS.07	CDH.02	Analysis
CDH.02	The CDH system shall have a minimum processing rate of 120 MHz.	The system must be able to process the scientific and telemetric data it receives from both Earth and instrumentation/sensors.	CDH.01	CDH.03 CDH.04	Test
CDH.03	The CDH system shall have a minimum memory of 256 MB of RAM.	Provides working memory for executing flight software, processing sensor data, running algorithms, and sending commands.	CDH.02		Inspection
CDH.04	The CDH system shall have a minimum storage of 400 GB.	Due to incoming datastreams and intermittent opportunities for uplink, large onboard data storage helps limit data loss and data can be stored for the duration of the mission.	SYS.07		Inspection

CDH.05	The CDH system shall maintain operation of critical components between -30°C to +50°C.	The system must be able to withstand Martian temperature swings.	SYS.02		Test
CDH.06	The CDH system shall withstand radiation up to 10 krad(Si).	The system must be radiation-hardened to maintain operation in the Martian environment.	SYS.02		Test
CDH.07	The CDH system must be able to communicate 550 km.	The system must be able to send and receive critical information.	SYS.07		Demonstration
CDH.08	The CDH system must be able to communicate with and check on instrumentation and other subsystems.	The system controls the whole rover and collects all the data from the instrumentation. The system needs to know when other subsystems fail to initiate recovery or redundant components.	MG.02		Test

Figure 2.1.3.1.1: CDH Requirements Table

2.1.3.2 CDH Sub-Assembly Overview

The CDH subsystem is split into four subassemblies: onboard computer, data storage, data interfaces, and telecommunications. These four subassemblies make the CDH subsystem the central brain of the whole rover. They ensure the science objectives can be achieved and the rover can adapt to any changes in health. The overall TRL of the subsystem is 7.

Onboard Computer

The OBC is the central nervous system for all rover functions. It hosts the F' software framework with C++ running on the VxWorks RTOS. The OBC is the BAE Systems RAD5545 [45]**.** It offers ~5.6 GOPS performance with four RAD5500 coats, high speed SerDes I/O including RapidIO, and 12 SpaceWire links. The RAD5545 is a radiation-hardened design with system-level shielding, located in a low-dose bay, ECC-protected memory and F' will provide fault management. It can handle a total ionizing dose of 100 Krad (Si) and single event upsets of 1e-3 upsets/card-day. It also supports thermal extremes with its operation temperatures at -55 to 125 degrees Celsius.

The OBC manages all flight modes and timelines. It has the ability to switch between the night, traverse, science, and day modes. To do so it has to independently control the power and thermal system to ensure safe operating temperature and correct power distribution for the rover's subsystems. In the case that the rover or its subsystems are not operating correctly the OBC is able to control fault detection, isolation, and recovery (FDIR).

It collects health telemetry from every subsystem. These SVC::Health pings must be responded to. Missed pings trigger a strike counter and crossing a threshold raises an event. This triggers a safe policy which can include restarting a component, a full restart process, or a OBC warm reset [59]. Every critical task the rover executes has VxWorks watchdogs and a constant top-level watchdog is run. If either stops being services, a recovery routine is fired such as log and orderly app reset or makes the board-level watchdog reset the RAD 5545 [98, 99].

VxWorks BSP initializes the RAD5545 on boot and then launches F''s Active Rate Groups with determinism [64]. After boot, F' provides typed ports for commands, telemetry, and events. It also provides CmdSequencer for time-tagged command scripts [65]. This simplifies the integration testing and supports in-the-loop fault injection. The time synchronization comes from the telecommunications subassembly, is distributed to the F' time base, and the time-tagged data can then align with orbit-relay windows determined by the OBC.

The OBC subassembly has a TRL 7. The RAD5545 is in a line of BAE RAD55xx devices with strong heritage and this version stems from the RAD750, a OBC used on Curiosity, Perseverance, and more [65]. Both VxWorks and F' are flight-proven as discussed in the software architecture narrative and earn a TRL 7. This gives the subassembly as a whole a TRL 7.

Data Storage

The Data Storage subassembly provides capture and retention of instrument, telemetry, and navigation data between UHF relays. The system will have EDAC wear management, integrity checks, and data deletion control. F''s BufferManager will be used to allocate memory.

The chosen device is the Mercury RH3440. It is a radiation-tolerant, 3U VPX solid-state data recorder (SSDR) with 440 GB of flash memory. The SSDR is designed for harsh, radiation intense environments with the ability to withstand a total ionizing dose (TID) >100 krad and operating/storage temperature ranges of 40°C to 72°C/-55°C to 105°C [66]. It boasts strong ECC and defect mitigation, allowing for operation under long traverse periods. The peak write/read speeds are in the 1GB/s area.

The recorder's ECC and F''s integrity layers including checksums on files and periodic scrubs help reduce latent errors. Additionally, the rover has two RH3440s allowing for backup storage as well as mirrored data on each card. The recorder sits on a conduction-cooled VPX rail with temperature sensors to be fed to the OBC and the thermal control system can be adjusted if temperatures are at risk of data loss.

The OBC will track unsafe write windows where power is used at capacity and there is risk of abrupt power interruption. Files will be isolated and partitioned with F''s storage manager with four partitions: health logs, imagery, telemetry, science. In the situation where data is corrupted, checksums are recomputed during each read operation and after this corruption the system can correct using the redundant copy or mark it as corrupted and purely switch to using the redundant data. The most critical files will be the ones on both storage devices including command sequences, health logs, and navigation data.

The Data Storage has a TRL 7 due to the RH3440's space tested past but lack of use in past rover missions.

Data Interfaces

The data interfaces subassembly handles communication between all internal parts of the rover. It connects the OBC, instruments, sensors, actuators, controllers,

SSDRs, and radio. This is done using RS-422 transceivers and twisted-pair cabling.

Its responsibility is to offer a path for data transfer without corruption of this data during transfer. The Texas Instruments SN65C1168E-SEP (Space Enhanced Plastic) dual RS-422 driver/receiver along with the Gore DXN2605 will be used to achieve this. The RS-422 meets TIA/EIA-422-B standards and provides radiation performance including immunity to 43 MeV-cm²/mg at 125 °C, ELDRS-free to 30 krad, and TID rated/lot-tested to 20 krad [68] [69]. The Gore cabling is a shielded twisted pair cable with a 100 ohm differential impedance. It can operate at temperatures from −55 °C to +200 °C and the small diameter allows for easy connection to all important systems [72].

The Data Interfaces subassembly has a TRL 7 due to the RS-422 and shielded twisted pair cable flight heritage.

Telecommunications

The telecommunication subassembly is the channel between the rover and Earth through the MRO. It communicates in the UHF bandwidth, with the MRO having 16 channels for this link ranging from 390 MHz to 450 MHz [57].

Science and telemetry data is downlinked on each overpass of the MRO. The rover transmits the stored data based on the priority assigned in each 8-15 minute window. The uplink brings new command sequences, clock corrections, configuration files, and any software updates. The link implements CCSDS Proximity-1 Space Link Protocol providing short-duration two-way relay links [58].

The L3Harris C/TT-510 Electra-Lite Transceiver will be the radio used. It is designed for Mars relay operations. The radio supports a 2.048 Mb/s transfer rate and has an agile frequency range to communicate to the MRO [59]. The antenna is UC-3004-531R Quadrifilar Helix (QFH) selected for its low-profile form factor and almost omnidirectional pattern that supports a moving MRO. The antenna is placed away from any interfering systems.

The telecommunications subassembly is assessed at TRL 6. The radio has a TRL 8 for its use in cubesats and other space applications, but the antennas' lack of use in deep space operations limits the system.

End-to-End Operation

1. Boot
    a. Power comes on from power system
    b. RAD5545 loads VxWorks
    c. Bootloader checks integrity of RH3440 storage

    d. System enters safe mode until all initial health checks complete for all systems
2. Initialization
    a. Onboard clock synced with last known time
    b. Hardware buses (RS-422, controllers, power interfaces) initialized
    c. All subassemblies pinged to confirm responsiveness
    d. Collect baseline health telemetry including voltage, current, temperatures, etc.
    e. Startup health report saved to SSDR
3. Normal Mode
    a. Switch from safe mode to idle mode
    b. Enable scheduled tasks from ConOps
    c. Load navigation plan from SSDR
4. CDH
    a. Receive ground commands through UHF radio
    b. Prioritize safety commands
    c. Validate command with checksum
5. GNC
    a. Receive sensor data from IMU, other measurement sensors
    b. Store raw measurements
    c. Pass sensor data to state estimator (EKF)
    d. Send sensor data to controller
6. Science Operations
    a. Activate instruments according to timeline
    b. Collect and timestamp science data
    c. Store data in science partition
7. Data Management
    a. Periodic verify file checksums
    b. If corruption detected, restore from redundant copy
    c. Manifest of all stored files
    d. Queue new files for downlink according to priority
8. Communications
    a. Configure Transceiver (frequency, data transfer rate)
    b. Perform pre transmission checks for power availability
    c. Begin downlink starting with health and nav data, then science
    d. Accept uplinked commands and data
9. FDIR
    a. Periodic health checks
    b. If unresponsive, isolate the component, switch to safe configuration
    c. If watchdog not kicked on schedule, trigger a system reset

    d. If files are becoming corrupted in partition, separate that partition
    e. Under communication loss enter safe mode and wait for ground intervention
10. Night mode
    a. Power down nonessential subsystems
    b. Only OBC + telecommunications active
    c. Resume operations when power level sufficient
11. Shutdown
    a. Flush logs and telemetry to SSDR
    b. Power down instruments and subsystems
    c. Power off

Conclusion

The CDH subsystem has a TRL 6 with the individual TRLs of 7, 8, 7, and 6 for OBC, Data Storage, Data Interface, and Telecommunications respectively. The CDH subsystem and its subassemblies are the operation backbone on the rover. Every action the rover takes is decided by the CDH system and all faults must be identified and mitigated by this system.

2.1.3.3 CDH Subsystem Recovery and Redundancy Plans

The rover will store its own local world map, and is capable of using its elevation relative to its surroundings as a heuristic for signal propagation effectiveness, and therefore if the rover loses contact with the MRO, or earth ground station it will be able to autonomously search for acceptable command signals. Due to the lightweight nature and incredible importance of the OBC and data storage devices, failure mitigation can be implemented through duplicate OBCs and data storage such that [there will be two of each]. Larger subassemblies including the antenna, however, do not justify complete redundancy due to their large mass and volumetric constraints. Antenna failure follows grateful degradation and therefore is unlikely to become completely inoperative.

The team will use two OBCs and two SSDs for the mission (as stated earlier), which will lead to a higher amount of memory and storage, but also a larger mass and volume, which can affect the trajectory of the spacecraft. However, since the OBC is initially lighter than the other components of the spacecraft, it is safe to say that it should not have a major impact and can achieve its purpose in the time allotted for the mission.

The UHF Antenna is a crucial component of the spacecraft, but is a major risk for the mission due to its size and vulnerability to damage and malfunctioning. Despite the power and importance of the antenna, it plays a major role in the mass of the spacecraft, and is prone to damage from space debris. If the antenna manages to become damaged, atmospheric communication with the spacecraft to Earth will be interrupted and no longer feasible, rendering the spacecraft ineffective.

In terms of software, programming issues are likely during the duration of the mission. Therefore, the implementation of a recovery procedure such as safe mode is required and essential for the spacecraft to continue its mission. This also includes coding bugs that can affect the spacecraft’s trajectory and timeline, meaning the team must be able to have a safety plan already in place in case such a situation arises during the mission.

Overall, the various CDH components of the spacecraft have also been tested, verified, and applicable in the spacecraft’s mission for Mars exploration and research. Therefore, there is a low chance of risk if we have recovery plans and constant testing and verification of our components.

2.1.3.4 CDH Subsystem Manufacturing and Procurement Plans

For the Command and Data Handling subsystem, various components must be identified and sourced with satisfactory cost estimates and lead times. As NASA is required not to compete with the commercial sector, many of these specialized parts are rare but commercially available and therefore must be procured from these suppliers.

The onboard computer (OBC) selected is the RAD5545 by BAE Systems with a lead time of 12 months [44]. A margin of one month will be built in to account for any issues with manufacturing. BAE Systems is the sole contractor for the RAD5545 computer and has an extensive history of supplying NASA with OBCs in the past including on perseverance and the MRO. The RAD5545 is radiation tolerant up to a 100 Krad ionizing dose and can withstand a range of -55 to 125 degrees Celsius. The processing power offers 5.6 giga-operations per second/3.7 giga-floating-point operations per second [40]. The backup option, also supplied by BAE Systems, is its predecessor, the RAD750 which still meets the mission requirements although not preferred due to its slower performance and memory capacity. The RAD5545 has a processing power 10 times greater than the 750. The RAD750 would also have a lead time of 12 months from BAE Systems with a margin of 1 month.

The UHF Transceiver selected is the L3Harris C/TT-510 Electra-lite Transceiver (ELT) [39, 40]. Lead times for the transceiver are not publicly available but based on similar technology the lead time is estimated to be 18 months based on similarly complex technology. To account for the use of an estimate, a longer, four month margin will be applied to this lead time. The procurement costs are not directly available, however based on similar technology, other transceivers cost between $200-400k. The L3Harris ELT has been used on Curiosity, Perseverance, and MRO relays, and from those missions a reasonable estimate is $250K. L3Harris has supplied the UHF radio for the past three Mars rovers and has been a reliable radio in each. The radio can supply data rates up to 2 Mbit/s and operates within the Mars UHF bandwidth. Additionally, its lightweight and small design is specifically catered to Mars missions. The backup supplier is JPL with its ELT. JPL has historically developed the technology that allowed Electra-lite to be possible [40]. This is a backup because JPL has not had to manufacture a similar radio since 2009, but JPL has continued to consistently supply NASA with outstanding technology. The estimated lead time for JPL is 24 months due to the lack of recent development of an Electra-lite radio with a margin of 6 months to account for this need for new development. The necessity for a light weight UHF radio limits the choices making JPL the backup supplier despite rules against competing with the industry.

The Data Storage selected is the Mercury RH3440 Solid-State Data Recorder [95]. The SSD has 440gb of flash memory and can support write speeds of 1160 MB/s

and read speeds of 1040 MB/s. Additionally, it is low power, 14w max, and light weight, <620g. The SSD is designed for space and is currently in use on the ISS and a L3Harris space project. It can survive in the temperature ranges of Mars with its range of -55°C to 105°C, and it is radiation hardened to a dose of 100 krad. The lead time is 12 months based on similar radiation hardened storage devices with a margin of 2 months. The backup is the RH3480 from Mercury [62]. This SSD is very similar to the 3340 with more storage and faster speeds. However, this is accompanied by higher weight and power draw. This is still in the acceptable range, just not as fit to the mission as the 3340. It has a similar lead time.

The RS-422 Transceiver selected is the Texas Instruments SN65C1168EMPWSEP supplied by Mouser with a published lead time of 2 weeks and a margin of 2 extra weeks [97]. Using a COTS supplier for transceivers is advantageous due to the large amount of stock they contain, which means the margin can be small. Because multiple transceivers will be needed, and will be purchased potentially more than once, the short lead time will not deter progress. The backup supplier is also Mouser which has Texas Instruments THVD9491DTSEP with an 18 week lead time and a built in margin of 4 weeks if they have to purchase more stock to cover the 20 total needed [98]. The benefits of COTS are less abundant here with a longer lead time and only 15 currently in stock. Mouser has worked with and supplied NASA in the past and Texas Instruments is consistently one of the largest government contracted companies and has a long history working with NASA even supplying switches for ground stations [11, [120] [121].

The Data Interface cable is the WireMasters supplied Gore DXN2605, 30 AWG Twisted Pair [31]. Wiremasters publish a lead time of 5 weeks for orders. Because it is currently in stock the margin is 2 weeks. The backup product shall be the DXN2604, also supplied by WireMasters with similar lead time [32]. Both cables have an impedance of 100 ohms and high temperature ranges of −55 °C to +200 °C. The DXN2605 is chosen over the 2604 because of its lighter weight and smaller size. This cable is for data transfer, not power, so a high-profile cable is unneeded. COTS was chosen because the product is readily available, custom cable would increase lead times and prices, and the cable will be thermally and radiation protected by the rover.

The UHF antenna shall be the UC-3004-531R (Quadrifilar Helix), as sourced by Antennas.us [46]. The antenna is primarily used in military satellites, but is tuned for the correct bandwidth and has omnidirectional gain allowing it to be used on Mars Rovers. Antennas US publishes a lead time of 10-12 weeks. To build in margin an extra 4 weeks will be added to allow for any slowdowns in production. The backup supplier and product shall be the Anywaves QFH. This antenna may be the better option, but costs and lead times are unavailable due to the custom nature of the antenna. Anywaves has

made antennas for cubesats and small rovers in the past and each antenna is custom made to meet the specifications of the system [25].

2.1.3.5 CDH Subsystem Verification Plans

Req #	Requirement Summary	Verification Method	Rationale for Method	Preliminary Verification Plan
CDH.01	The Command and Data Handling (CDH) system shall have a minimum uplink rate of 256 kbps and a minimum downlink rate of 16 Kbps.	Analysis	The system must be able to send scientific and telemetric data to and from Earth.	Uplink and downlink rates must be analyzed for maximum efficiency and accuracy through examining their technological capabilities (256 kbps for uplink and 16 Kbps for downlink).
CDH.02	The CDH system shall have a minimum processing rate of 120 MHz.	Test	The system must be able to process the scientific and telemetric data it receives from both Earth and instrumentation/sensors.	Processing rate must be tested in a scientific setting for determination of its effectiveness at 120 MHz.
CDH.03	The CDH system shall have a minimum memory of 256 MB of RAM.	Inspection	Provides working memory for executing flight software, processing sensor data, running algorithms, and sending commands.	Memory must be reviewed for future spacecraft mission applications to ensure its productivity at 256 MB of RAM.
CDH.04	The CDH system shall have a minimum storage of 400 GB.	Inspection	Due to incoming datastreams and intermittent opportunities for uplink, large onboard data storage helps limit data loss and data can be stored for the duration of the mission.	Storage must be reviewed for future spacecraft mission applications to ensure its productivity at 400 GB.
CDH.05	The CDH system shall maintain operation of critical components between -30°C to +50°C.	Test	The system must be able to withstand Martian temperature swings.	Temperature must be tested in a scientific setting to demonstrate its ability to withstand -30°C to +50°C.

CDH.06	The CDH system shall withstand radiation up to 10 krad(Si).	Test	The system must be radiation-hardened to maintain operation in the Martian environment.	Radiation must be tested in a scientific setting to demonstrate its ability to withstand at most 10 krad.
CDH.07	The CDH system must be able to communicate 550 km.	Demonstration	The system must be able to send and receive critical information.	Communication must be demonstrated in a way that can communicate at least 550 km.
CDH.08	The CDH system must be able to communicate with and check on instrumentation and other subsystems.	Test	The system controls the whole rover and collects all the data from the instrumentation. The system needs to know when other subsystems fail to initiate recovery or redundant components.	CDH system must be tested to collaborate and interact with other components of the other systems through communication and verification methods.

Figure 2.1.3.5.1: CDH Verification Plan Table

CDH.01 describes the uplink and downlink rates being 256 kbps and 16 Kbps, respectively. This requirement is for the system to receive telemetric data from and relay back to Earth. Since this is in the analysis stage, the team will need to examine its efficiency and accuracy in order to achieve mission success. For this requirement, the UHF (Ultra-High Frequency) Antenna used will be the model, UC-3004-531R (Quadrifilar Helix) by Antennas.us. After extensive research, the team concluded that this antenna was the best for the mission, due to its industry-wide use and reliability. In the case of any delays or obstacles within the mission timeline, the backup supplier will be Anywaves QFH, which is well-known for the creation of cubesats and small rovers.

CDH.02 describes the processing rate being at least 120 MHz. This requirement is for the system to process scientific and telemetric data from both Earth and the spacecraft instrumentation. Since this is in the test stage, the team will need to test the processing rate in a scientific setting to determine its effectiveness in order to achieve mission success. For this requirement, the UHF (Ultra-High Frequency) Antenna used will also be the model, UC-3004-531R (Quadrifilar Helix) by Antennas.us. After extensive research, the team concluded that this antenna was the best for the mission, due to its industry-wide use and reliability. In the case of any delays or obstacles within the mission timeline, the backup supplier will also be Anywaves QFH.

CDH.03 describes the memory capacity being at least 256 MB of RAM. This

requirement is for the system to provide working memory for executing flight software, processing sensor data, running algorithms, and sending commands. Since this is in the inspection stage, the team will need to review the memory capacity for future spacecraft mission applications to ensure its productivity in order to achieve mission success. For this requirement, the OBC (Onboard Computer) used will be the RAD5545 by BAE Systems. After extensive research, the team concluded that this OBC was the best for the mission, due to its industry-wide use and reliability. In the case of any delays or obstacles within the mission timeline, the backup supplier will also be BAE Systems with a different version, the RAD750, with slower performance and lower memory capacity.

CDH.04 describes the data storage being at least 400 GB. This requirement is for the system to limit data loss and retain more data throughout the mission timeline. Since this is in the inspection stage, the team will need to review the data storage for future spacecraft mission applications to ensure its productivity in order to achieve mission success. For this requirement, the SSD (Solid-State Drive) used will be the RH3440 Solid-State Data Recorder by Mercury. After extensive research, the team concluded that this SSD was the best for the mission, due to its industry-wide use and reliability. In the case of any delays or obstacles within the mission timeline, the backup supplier will also be Mercury with a different version, the RH3480, with greater weight and higher power draw.

CDH.05 describes the Martian temperature withstanding being within -30°C to +50°C. This requirement is for the system to endure extreme temperature swings during the mission timeline. Since this is in the test stage, the team will need to test the temperature range in a scientific setting in order to demonstrate its ability to withstand Martian temperature range. For this requirement, all technological components of the CDH subsystem have to endure the Martian temperature range in order to achieve mission success. After extensive research, the team concluded that all of our technological components meet this requirement and are able to be launched with the spacecraft. In the case of any delays or obstacles within the mission timeline, the backup suppliers will also meet this requirement with their different versions, therefore, there should be little delay with the timeline.

CDH.06 describes the radiation tolerance withstanding up to 10 krad. This requirement is for the system to endure extreme radiation during the mission timeline. Since this is in the demonstration stage, the team will need to test the radiation tolerance in a scientific setting in order to demonstrate its ability to withstand high amounts of radiation. For this requirement, the OBC (Onboard Computer) used will be the RAD5545 by BAE Systems. After extensive research, the team concluded that this OBC was the best for the mission, due to its industry-wide use and reliability. In the case of any delays or obstacles within the

mission timeline, the backup supplier will also be BAE Systems with a different version, the RAD750, with lower radiation tolerance.

CDH.07 describes the communication range to be at least 550 km. This requirement is for the system to send and receive critical information throughout the mission. Since this is in the demonstration stage, the team will need to apply the communication range in a scientific setting in order to demonstrate its ability to properly communicate back and forth between the spacecraft and Earth. For this requirement, the radio used will be the C/TT-510 Electra-Lite Transceiver by L3Harris while the UHF (Ultra-High Frequency) Antenna used will be the model, UC-3004-531R (Quadrifilar Helix) by Antennas.us. After extensive research, the team concluded that this radio and antenna were the best for the mission, due to its industry-wide use and reliability. In the case of any delays or obstacles within the mission timeline, the backup supplier for the antenna will also be BAE Systems with a different version, the RAD750, with a lower communication range.

CDH.08 describes the communication between the CDH subsystem and all other subsystems and spacecraft instrumentation. This requirement is for the system to work together with other subsystems in order for the spacecraft to properly function. Since this is in the test stage, the team will need to test the subsystem communication in a scientific setting to ensure that all subsystems can function properly throughout the mission timeline. For this requirement, all subsystem components have been proven to collaborate with each other effectively and accurately. After extensive research, the team picked out the best components not only for the spacecraft, but also for the ability to work with other components in the spacecraft. In the case of any delays or obstacles within the mission timeline, all backup suppliers have been proven to collaborate with each other effectively and accurately, too.

2.1.4 Thermal Control Subsystem Overview

The thermal control system (TCS) will function to maintain the system within the appropriate operational temperature range. The main component will be thermal insulation in the form of MLI made from double sided mylar and beta cloth. These have emissivity and absorptivity values of .03 and .00006, and .8 and .45 respectively. The number .00006 was chosen as an arbitrary ‘near zero’ value since the absorptivity of double sided aluminized mylar was listed as ‘near zero’ in sources. Excess heat will be rejected via a combination of thermal radiators and passive thermal Louvers. The passive thermal Louvers will react to the system temperature, adjusting how much heat they reject.

In addition to the insulation and radiators, the TCS will utilize a constant conductance heat pipe (CCHP) to distribute heat away from high temperature instruments like the oven to instruments that need higher temperatures like the RIMFAX. There will also be a number of electric heaters attached with every payload, controlled by the CDH system. They will activate when indicated, based on the temperature sensed at each location. This will be facilitated by thermal sensor monitoring if the heaters need to be on and how much heat needs to be directed to an area.

The operating temperature for most of the science instruments fall into the 303 to 313 degrees Kelvin range. The Gamma Neutron Probe has an operational temperature of 30 C to 57 C, or 303K to 330K [77]. The RIMFAX instrument has an operational temperature of 228K to 333K [32] and the Raman Laser Spectrometer has an operational range from 228K to 313K [52]. These three will function at a system range of 303K to 313K. However the Mini TLS has a lower operational temperature range of 263K to 293K [128].

Other payloads include the batteries, which have an operational temperature of 10 to 30 degrees celsius or 283 to 303 degrees Kelvin. The MPPT has an operational range of 253K to 318K and the DC to DC converters have a range of 218K to 398K. The latter two will be comfortable in the system range of 303K to 313K, however the batteries will need to be kept at cooler temperatures.

The CDH payloads have broad operational temperature ranges. The Rad 5545 can operate between 218K and 398K, the L3Harris Electralite survives between 228K and 345K, the RH 3440 between 233K and 345K, the RS-422 from 218K to 398K, and the Antenna from 233K to 358K. All of which can survive in the system’s target range of 303K-313K.

When calculating the heat flow map and wattage load many variables had to be considered- such as the protruding casing for the RIMFAX. This protruding casing

made the shape of the rover more complex, and necessitated additional calculations for paneling that was too small to include in the diagram for the heat flow map. Below, Figure 2.1.3.1 displays the heat radiated from this protrusion to the surface and atmosphere. This small amount of radiation was added to the total surface/atmosphere radiation in Figures 2.1.3.2 and 2.1.3.3.

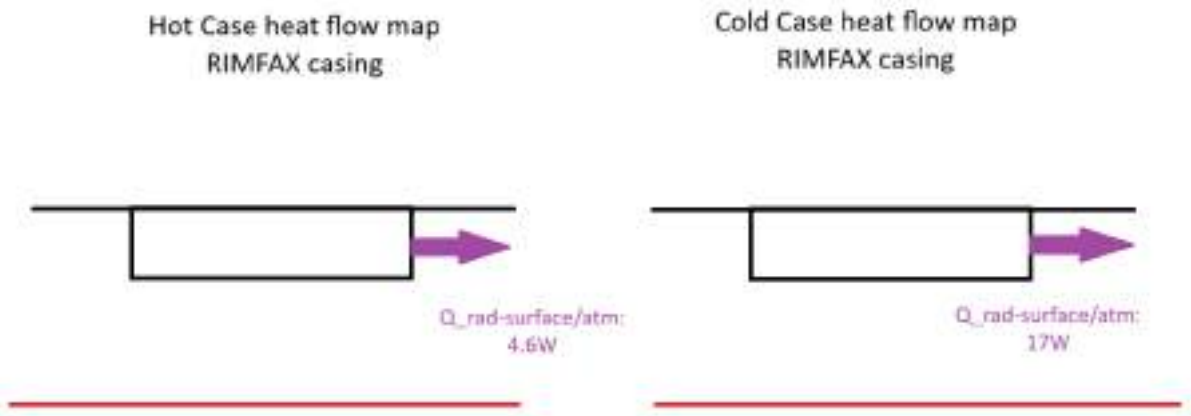

Figure 2.1.4.1: RIMFAX casing radiation

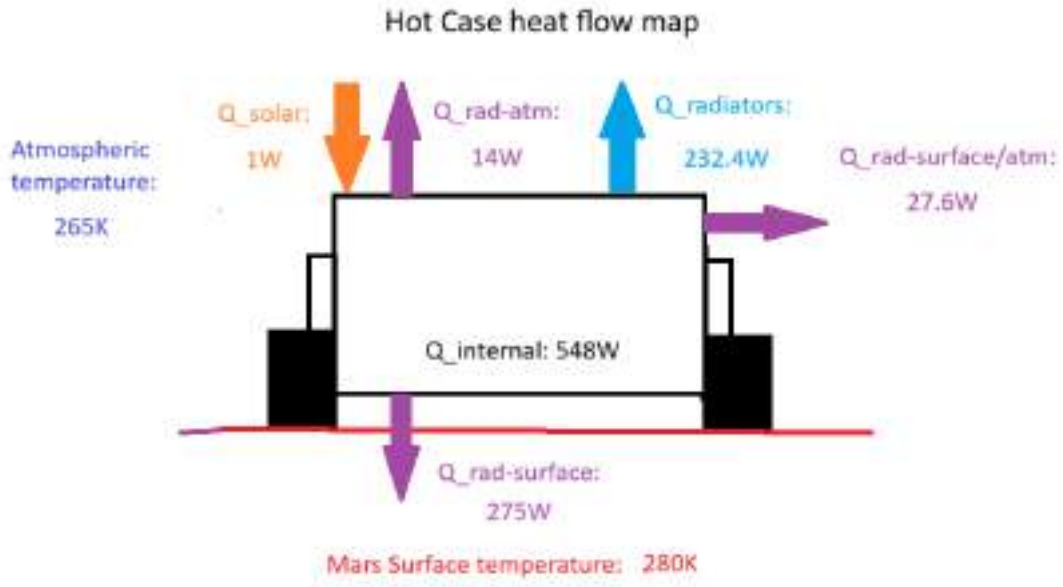

Figure 2.1.4.2 Hot Case Heat Flow Map

Included in figures 2.1.3.3, the radiation lost through the thermal louvres is included, since they cannot retain the same heat if that area were otherwise taken up the double sided mylar MLI.

Both cases have loads of Q_net = 0W, meaning the system temperature is sustainable and unchanging. For the hot case, Q_in would be [548W + 1W] and Q_out would be [275W + 27.6W + 232.4W + 14W]. Which are both equal to 549W, making Q_net = Q_in - Q_out = 0W. For the cold case, Q_in is equal to [548W + 383W] and Q_out is equal to [30W + 48W +71W + 782W]. Both equal 931W, meaning Q_net = Q_in - Q_out = 0W.

Observing both figures 2.1.3.2 and 2.1.3.3. It is salient that the bottom of the rover radiates much more heat, this is because it was decided that the belly of the rover would be made of beta cloth, which radiates and absorbs much more heat than the non-reactive and insulating double sided mylar covering the rest of the rover.

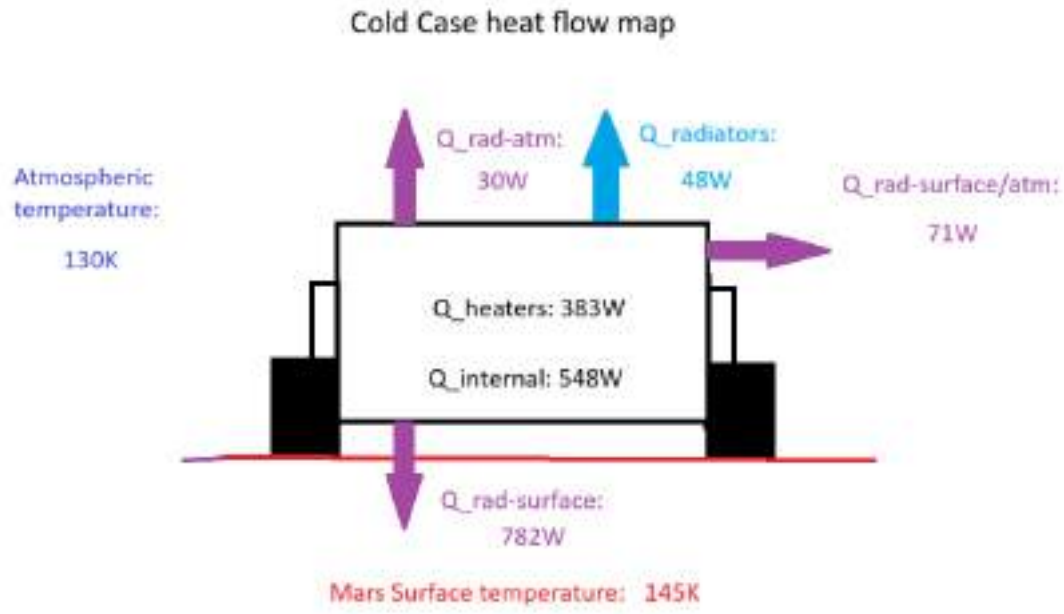

Figure 2.1.4.3: Cold Case Heat Flow Map

2.1.4.1 Thermal Control Subsystem Requirements

The thermal control system must protect the designated instrumentation and power system to ensure no failure that will result in the mission being compromised. To achieve this the TCS shall keep the system between 303K and 313K, and keep each component within its operational temperature. The Mini TLS shall be kept at a lower temperature of 280 to 290 degrees Kelvin.

Components used to achieve this include MLI coatings, which shall aid in thermally isolating the system to maintain its operational temperature range. This MLI will consist of Double Sided Mylar for the majority of the coating, with the belly of the rover having MLI made of beta cloth. The MLI design includes an outer cover layer, which is key to protecting the under layers and rover hardware from the outer environment, radiation, and micrometeoroids. It also consists of levels of reflective layers underneath the outer cover, as well as minimizing thermal conduction from the exterior to the interior. The MLI shall also have an innermost layer called the inner cover, which faces the interior hardware. This layer must generate a minimal amount of particulate contaminants, aid in reducing stress for the interior reflective layers, and not be aluminized to reduce the risk of an electrical short, which is a fire hazard. These layers shall be separated by a form of netting in the design to minimize thermal conductivity within the layers. The design shall also implement a form of ventilation within the MLI with the inclusion of perforations in areas of the MLI to aid in outgassing to minimize pressurization within the MLI.

To ensure the rover system is able to function properly without freezing in the Martian environment in adherence to the system's requirements, an active TCS is necessary to tackle this challenge. One such active TCS is an electrical heater, the electric heater draws power to electrically produce heat from the electrical source and transfer this heat elsewhere.To control the heating, heat pipe designs shall be implemented and integrated into the system to equally distribute heat around the system. Radiators shall be used for excessive heat dissipation. These design measures shall help in meeting the system requirements.

In order for the TCS to meet the system requirements, methods of verification and validation must be conducted to ensure each component meets the requirements. These methods include CAD thermal modeling of the subassemblies. After acquiring results, the components shall be tested in a thermal vacuum chamber at one of NASA’s research facilities to validate the thermal modeling analysis on CAD. The components shall then be tested with other subsystems in a mission simulation testing area to ensure all thermal subsystems comply with the mission system requirements.

Req #	Requirement	Rationale	Parent Req.	Child Req.	Verification Method
TCS.01	The Thermal Control System (TCS) shall help maintain the system at the allowable temperature range of 303K to 313K.	This ensures the TCS keeps components within safe temperature limits to prevent failure from Mars' extreme thermal conditions.	SYS.02	TCS.02 TCS.03	Test
TCS.02	The Multilayer Insulation(MLI) shall aid in thermally housing the rover system within the temperature range of 303K to 313K	Ensures that the rover system within is protected from the harsh Martian temperatures and conditions as well as aid in maintaining the operable temperatures.	TCS.01	-	Test
TCS.03	The electrical heater units shall provide a heating temperature range of 303K to 313K.	Ensures that the rover system is in the operable temperature range but provides heat throughout the system.	TCS.01	-	Test

Figure 2.1.4.1.1: Thermal Requirements Table

2.1.4.2 Thermal Control Sub-Assembly Overview

The thermal control system shall be made up of several subassemblies, including the MLI, the radiators, the heat pipes, and the electric heaters.

For the MLI, double sided mylar will be used for the top and sides of the rover, due to its extreme insulating properties. This will prevent too much heat from radiating to the atmosphere of mars. However, for the belly of the rover beta cloth will be used, allowing more heat to radiate to the surface, which will have a less severe temperature difference from the rover than the atmosphere. This decision was made after a python simulation of 8 cases, using different MLI materials and different material combinations. Every case except two had a difference of over 1000W between the hot and cold case, with 3 having a difference of over 2000W. A coating made from all double sided mylar was the only other one that had a difference of under 1000W, but it conserved too much heat. It required 434 W of heat to be dispersed even in the cold case. This posed a major overheating risk were any radiators to fail. And were the MLI to fail it would be a single point failure since minimal additional or backup heating would be available due to the constant overheating risk. Instead, by using a beta cloth on the bottom of the rover, the system only needs 318W of heating in the cold case and 237W of heat dissipated in the hot case, or a range of 571W.

This analysis was done with a simplified model for the rover, without the RIMFAX casing protrusion. Taking into account the externally mounted RIMFAX and its beta cloth casing, 335W of heating is needed and 232.4W of heat needs to be dissipated.

This works because the double sided mylar is overly insulating, while the beta cloth is insulating but allows for heat to escape. The TRL of double sided mylar is 5 since it has been successfully used before, under different circumstances. The beta cloth has a TRL of 6, having been used on the Columbia space shuttle[82].

In order to radiate the needed heat, 4 20-bladed thermal Louvres will be used. These have a TRL of 6, since they have a lot of mission heritage and have been tested in space[100], but have not been to mars specifically. Each will radiate a minimum of 12W fully closed and 62W fully open, with an emissivity value of .14 when the blades are closed and an emissivity value of .74 when the blades are fully open[101]. In total they will radiate 248W fully open and 48W fully closed. They will be set to start opening at 232K, since according to analysis via python modeling this is the temperature at which the system stops losing heat and starts needing to dissipate it where no thermal controls were present.

However, considering the emissivity of the closed thermal louvres, each louvre will radiate 12W, taking up a space that would otherwise radiate 2.5W. Between the 4 of them, in the cold case they will radiate 48W over an area that would otherwise radiate

10W. This brings the heating needed for the cold case up to 373W.

The 248W they radiate is 11W more than the hot case’s needed 253W of heat radiated out, however for redundancy one small MISER radiators will be utilized, expelling an additional 12W [100]. This allows for 23W of extra heat that could be radiated were an unexpectedly hot situation to arise, or were dust accumulation to cause unexpected insulation. One will be attached to the top of the rover, directly over the mini-TLS, to assist in keeping it at a lower operational temperature. The MISER radiator has a TRL of 6, since the entire system has been tested in a relevant environment, but does not have much mission heritage.

Several constant conductance heat pipes (CCHP) will be utilized, The TRL of constant conductance heat pipes is 8, being a very commonly used instrument for space travel in many relevant environments. One moving heat from the oven to other parts of the rover, namely the RIMFAX and Raman laser spectrometer. This will provide a degree of passive heating while the oven is running. The evaporator will be placed near the oven as the heat source, go down the front of the rover, and then towards the back along the bottom. Ending between the RIMFAX and ramen spectrometer, which is where the condenser will be located.

Another heat pipe will run along the inside of the roof of the rover, up to the gamma neutron probe from the oven, using the same principles. Once again, providing passive heating while the oven is on.

There will also be a small heat pipe running from the battery powering the mechanical arm to the Louvre behind the arm, making it possible to keep the battery at a reduced temperature since it has a lower operational temperature range. The condenser will use the thermal Louvre as a heat sink instead of the MISER because the MISER has a limited capacity and can only radiate 12W.

A CCHP will run from the batteries to the same spot where the first CCHP has its heat sink, between the RIMFAX and spectrometer. The batteries have a low operational temperature whereas these 2 instruments have higher operational temperatures. Moreover since the RIMFAX is mounted beneath the rover, it radiates more than it would if it were inside the rover. Because of its small size, the radiation leaving through the sides of its casing would only be 16.9 W in the cold case and 4.6W in the hot case. The passive heating from the batteries would be useful in heating this instrument, especially since the batteries are reliably on more than the oven. This would reduce the strain on the electric heaters.

Finally, a CCHP will run from the center of the rover as the heat sink to the thermal louvres, This will function as to mitigate uneven temperature distribution in the center as opposed to the edges and along the face.

In order to provide the remaining 373W of heating, a minimum of 38 Dwyeromega KHLVA-102/5 Electrical Heaters need to be used. For redundancy 50 heaters will be used, each providing 10W of heating[100]. These heaters have a TRL of 5, since they have not been on relevant missions. The decision to use 12 extra heaters stems from preventing any single point failures for the system nor any individual instrument. Specifically, 20W of redundant heating will be allocated to the RIMFAX, RLS, and battery. This is because the RIMFAX and RLS have higher operating temperatures than most of the payloads in the system- making them a top priority in the case of a failure. They need to both be able to generate more heat than anticipated in the case of unexpectedly cool temperatures and in the case of a failure in one of the heaters. The batteries on the other hand, have a very narrow operational temperature range and will have extra redundancy to account for the higher degree of control necessary in the case of a failure. The mini TLS and CDH system will each receive 10W of redundant heating. The additional 40W of redundant heating will each be placed evenly throughout the rover, one in each quadrant. This is to keep the system as a whole within its desired temperature range.

The 38 heaters will be distributed as such: two dedicated to each science instrument, 2 dedicated to the battery, an additional 2 for the CDH system, and another 2 for the oven and mechanical arm. The remaining 24 will be distributed evenly across the rover in order to maintain the system’s desired temperature range. These will be controlled electronically through software that interfaces with the thermal sensors.

As the final component of the TCS, there will be a number of thermal sensors monitoring each instrument and major component. These sensors will be thermosisters specifically, because of their high sensitivity and ability to sense small temperature changes. These have a TRL of 6, with some flight heritage but not in similar configurations or on Mars. This was deemed important because the system’s desired temperature range is relatively narrow.

2 will be mounted to each instrument, battery, and CDH system; for redundancy. In case of a failure in one. They will not be running concurrently, to avoid burning both out or wearing both down. The second one will regularly be turned on to cross check the measured temperature against each other, as a method for verifying the original is still operational and accurate. This way the second sensor functions as both a backup sensor and a verification method.

Each sensor will send its information back to the computer system, which will check the measured temperature against the desired temperature range for the system, and each instrument if it requires cooler temperatures. If the measured temperature is close to dropping below the desired temperature range, it will signal for the heaters to kick on; if the measured temperature is near the upper limit it will signal for the heaters

to turn off. Depending on how much the discrepancy is and what the system’s overall temperature is (measured by other sensors), the amount of heat directed to the sensors will be adjusted.

One environmental concern relevant to the TCS is Mars's variable temperatures. Due to the thin atmosphere, temperatures are so variable that the surface temperature can be up to 24 degrees celsius hotter than the atmospheric temperature, less than two meters from the surface[72]. This has been accounted for in the atmospheric and surface temperatures used for the calculations. With a difference of 15 degrees kelvin used for the hot and cold case.

Another risk to the mission is the dust storms[34], which can coat the rover in dust and insulate the system [53]. To mitigate, the TCS can radiate more than would be required assuming no dust.

Another hazard previously addressed is Mar’s temperatures themselves[3]. We chose a region where the lowest expected temperature is -130C or 145K. This nears the coldest considered case for the low temperatures of mars. This has been thoroughly mitigated through analysis, where it has been ensured that the P.H.O.E.N.I.X rover retains enough heat and has enough heaters to withstand those temperatures. Moreover, it has been ensured that each instrument and system will stay within their operational temperature ranges.

2.1.4.3 Thermal Control Subsystem Recovery and Redundancy Plans

The Thermal Control System (TCS) shall implement contingent redundant and recovery plans in the scenario that a component of the TCS fails and jeopardizes the mission. The TCS subassembly's redundancy shall focus on the heat pipes, thermistor thermal sensors, and electrical heaters. The recovery shall be focused solely on the thermistor thermal sensors and their ability to relay information to the command data handling.

In order to monitor the temperature status of the overall rover system, thermistors shall be implemented. In the case of thermistor failure, there shall also be multiple thermal sensors per instrument to ensure cross-verification of the measurement of the instrumentation temperature. This also ensures that in the event of failure, the other will be able to monitor the instrumentation and keep the TCS intact. In the scenario where the heat pipe fails, redundant heat pipes shall be implemented under the risk strategy the system shall also begin relying on redundant electrical heaters. In the scenario of overheating from the heatpipes, the heat shall be redirected to the Miser Radiators and Thermal Louver Radiators to maintain operating temperatures. As mentioned, redundant electrical heaters will be implemented not only in case the heat pipe fails, but also to ensure that if one heater fails, the others will work in its place to ensure the system is thermally isolated from the Martian environment. This will allow the rover to continue the mission without jeopardizing the science goals and objectives. For the MLI redundancy in the case of MLI degradation, multiple layers of reflective layers shall be implemented, even if the outer cover, such as the double-sided mylar and beta cloth, degrades. Once that begins to not function, then power must be redistributed to the closest electrical heater under the command of the thermistor through software command to maintain the ambient temperature near the compromised region of the MLI.

A recovery implementation is crucial when it comes to the thermal control system of the rover. The only recovery concern for the TCS will be for the thermistor thermal sensor as it is the only software link to the rest of the TCS. There shall be a recovery software implementation/command from the CDH subsystem where if the system overheats or cools down to levels of extreme cold, a fail-switch sensor such as the thermistor sends the signal to command the TCS, primarily the electrical heater to power down non-critical components of the rover and funnel power into the TCS to guide the rover back to operating temperatures if that's not feasible a second command would be given to the TCS to commence a re-startup sequence.

2.1.4.4 Thermal Control Subsystem Manufacturing and Procurement Plans

The companies for the thermal subsystem, such as Dwyeromega, Sierra Space, Advanced Cooling Technologies, NI Solutions, Dunlap, Dunmore Aerospace, Sheldahl, and Skygeek, were selected due to their past and ongoing affiliations with NASA through contracts and other partnerships. Dwyeromega was chosen for their past affiliations with NASA, such as the Apollo 11 Mobile Quarantine. Dwyeromega specializes in electrical heater units, which are part of the TCS [25]. The backup supplier for the heaters would be McMaster-Carr with their ultra-thin heaters. Currently, McMaster-Carr does not have any affiliation with NASA but provides a NASA-level of aerospace products. Sierra Space aids in the production of thermal louver radiators for heat dissipation and retention [6]. Sierra Space was chosen as it is a key NASA partner or contractor, especially under the Space Act Agreement with NASA. McMaster-Carr would also be the backup for thermal louvers [42]. Advanced Cooling Technologies specializes in various types of heat pipes, especially the Constant Conductance Heat Pipes. Advanced Cooling Technologies was chosen as it is a NASA contractor and has collaborated with NASA, especially for NASA's VIPER mission to the Lunar south pole [54]. Backups for the Constance Conductance Heat Pipe (CCHP) would be Pure World Energy Inc. for their Constance Conductance Heat Pipe (CCHP) design solution. NI Solutions specializes in thermal sensors such as the thermistor, which will be a part of the rover system to monitor any thermal irregularities. NI Solutions was chosen due to its being a NASA contractor and its utilization of LABVIEW FPGA for the James Webb Space Telescope from NI Solutions. The backup supplier for the thermistors would be TE Connectivity, and their NASA-qualified thermistors would also be used. Jaco Aerospace shall serve as the main supplier of VT-295E nylon threads for sewing the MLI together. Jaco Aerospace was chosen as it is one of NASA's vendors when it comes to supplying aerospace-grade materials. The backup would be A&E Gutterman with their specialized nylon threads. A&E Gutterman has met US industry governmental requirements and provides thermally resistant and resilient threads. Both Dunmore Aerospace and Sheldahl specialize in MLI blanket films as well as adhesive tapes; both of these companies will be backup suppliers for one another in case the other does not have the necessities. Dunmore Aerospace and Sheldahl are NASA contractors and provide MLI films and sheets especially for CubeSat satellites, and more. SkyGeek worked with aerospace companies and helped in the production and distribution of adhesives for the MLI, such as EPON 815C, which is used to bond fasteners to the overall structure. The backup supplier for this particular adhesive is Ellsworth, which also has EPON 815C for aerospace applications. The team's choice for COTS, especially for the electrical heaters, thermistors, nylon, and MLI adhesives, was based on its low complexity, cost, and reliability. The team has gone ahead and chosen these companies due to their past and current affiliations by providing high TRL of material and more for NASA.

Lead times for these products vary by the complexity of the design, testing, approval, and shipment. Dwyeromega provided their lead time of 6 weeks if not in stock, but a 2-week margin should be given in case of any unforeseen occurrence, therefore around 8 weeks [26]. For the backup supplier, lead time for McMaster-Carr would be around 6 weeks as well with a 2-week margin [6]. For the Sierra Space Thermal Louver Radiators, lead times should be around 12 weeks for manufacturing approval and delivery, according to similar manufacturers like Kelair Dampers, with a 2-week margin for any unforeseen circumstances [43]. Advanced Cooling Technologies' lead times for the CCHP vary, as the CCHP must be designed per the mission requirements and therefore shall be placed at around 14 weeks due to the complexity of the design, as well as manufacturers that make similar heating solutions plus testing with a 2-week margin to account for any uncertainty. The backup supplier Pure World Energy, would also be around 14 weeks with a 2-week margin. NI Solutions' thermistor lead time would be around 26 weeks, according to manufacturers such as AvNet, which makes similar products [5]; a 2-week margin would also be implemented to account for uncertainties as well. The team's backup thermistor would also come from McMaster-Carr, which has the same lead time as the electrical heater one, and would be around 6 weeks with a 2-week margin. Dunmore Aerospace MLI film lead times would be between 1-3 months, as these numbers come from the SatCatalog [11]; however, taking the upper bound being 3 months, a 1-month margin would be put in place to account for any errors for Dunmore, as well as noting the backup supplier Sheldalh. Jaco Aerospace's nylon thread lead time would be around 6-7 weeks; however, a 2-week margin shall be put in place as well [104]. This lead time plus margin also applies to the backup supplier, Jaco Aerospace. Skygeek lead times would be 4 weeks as they provided their lead time on the catalog, and shall be given a 2-week margin as well for any uncertainty [106]. The same lead time applies to the backup supplier, Miller-Stephenson, with a 2-week margin set in place for it. These procurement times should adhere to the scheduling of the development of the P.H.O.E.N.I.X rover and will allow it to meet its science mission objectives.

2.1.4.5 Thermal Control Subsystem Verification Plans

Req #	Requirement Summary	Verification Method	Rationale for Method	Preliminary Verification Plan
TCS.02	The Multilayer Insulation(MLI) shall aid in thermally housing the rover system within the temperature range of 303K to 313K.	Test	Ensures that the rover is safe from harsh Martian conditions and helps maintain proper operating temperatures.	Conduct thermal vacuum (TVAC) testing with the rover system encased in MLI, exposing it to simulated Martian temperatures. Use thermistors to monitor the temperatures.
TCS.03	The electric heater units shall provide a heating temperature range of 303K to 313K.	Test	Ensure that the rover is within operable temperatures through heat distribution throughout the system.	Conduct system-level testing through TVAC testing with all systems integrated and online. Activate electric heaters to an operable temperature of 303K to 313K. Use thermistors to monitor the temperatures.

Figure 2.1.4.5.1: Thermal Verification Plan Table

In order to ensure that the thermal subsystem is functioning per the requirements, the team has proposed 2 specific crucial verification methods for the TCS. Each targets the crucial components that make up the TCS, the electric heaters, and the multilayer insulation components. TCS.02 on the requirements table specifically covers the MLI, the double-sided mylar and beta cloth of the outer cover, the goldized kapton of the reflective layers, and the aluminized kapton of the inner cover, all of which are provided by Dunmore Aerospace and Sheldahl for the aluminized kapton. TCS. 02 explicitly states that the MLI shall aid in thermally housing the rover system within the operational temperature range of 303K to 313K. In order to ensure that this requirement is met, the team’s verification method proposal is to test the MLI. This test is to ensure that the MLI secures the rover and allows it to operate while in harsh Martian conditions, and also helps maintain proper operating temperatures. For the MLI, the team has decided to conduct thermal vacuum testing(TVAC) for the verification plan. For this test, the rover system will be encased in the MLI, exposing it to simulated Martian-like temperatures while simulating the mission. The goal of this test is to ensure that the rover system is thermally isolated from the Martian-like temperatures. The temperature reading for the system under the casing must read between 303K to 313K for the verification to be successful. The thermal sensors already in place to conduct the temperature readings are the thermistors within the P.H.O.E.N.I.X rover provided by NI Solutions. TVAC would allow the components to go through cycles of hot and cold temperatures

for analysis of verification.

TCS.03 on the requirements table covers a crucial active component of the TCS, the electric heaters. TCS.03 explicitly states that the electric heater units provided by Dwyeromega, specifically the KHLVA-102/5 Electrical Heaters, shall provide an operating temperature range of 303K to 313K. Fifty units of the KHLVA-102/5, as stated, shall be integrated into the rover system to provide heating for the system. To ensure that this requirement is met, the team formulated that a system-wide test shall be conducted as well to ensure proper function of the electric heater. This test must be conducted to ensure that the P.H.O.E.N.I.X rover system is provided with sufficient heat to be within the desirable operational temperature range. This test must be conducted on a systems-level with all systems integrated and online, also simulating the mission as well. Thermistors, as mentioned before, have been set in place and shall monitor the data of temperatures to ensure the success of verification. The goal of this test is to ensure that the rover system is provided just enough heat to reach 303K to 313K in order to be successful and to make sure it doesn't overheat or leave cold regions. These TVAC tests will allow the team to verify that the TCS works as intended. This way, it’ll ensure that the mission won’t be jeopardized due to a faulty TCS.

2.1.5 Payload Subsystem Overview

The first objective will be fulfilled by the CP-MU DMU-100 Submersible Gamma Neutron Probe. Waterproof and made to withstand high heat applications, it is durable, and built to last as a tried-and-true TRL level-4 scientific safety instrumentation actively utilized by first responders, nuclear facilities, and hazmat teams in extreme environments, proving its worth through a history of reading Gamma radiation dosage in multiple sources such as water, nuclear reactor cores, and fuels. It will now extend its earth legacy to a multi-planetary one, operating inside of the team's custom-engineered, aluminum-based, cylinder shaped Fluid Protection System (FPS) mounted to the top of the rover. The probe will monitor a protected earth fluid sample for Martian environmental impacts and contamination in weekly intervals over a one-year minimum duration. This recorded data will provide a strong contribution to materials science and engineering breakthroughs, uncover unknown threats to mission-critical fluids, and aid in the engineering of the next generation fluid storage systems that are necessary for astronaut safety and sustaining of long-duration missions on Mars.

The probe features an ionizing gas chamber that measures ion pairs formed from interaction within the gas, creating an electric field that produces a measurable current with a dosage range of 1 µSv/h to 10 Sv/h. The collected data will be monitored for, recorded, and transmitted using a 12 seconds slow time constant (response time) for precise, accurate, and stable radiation detection across subtle to extreme Gamma radiation level increases. The collected data will be stored on the Communication and Data Handling system's RAD5545 onboard computer using a NVMe solid-state drive. Transmission will then occur via UHF to the Mars Reconnaissance Orbiter and on to Earth for weekly monitoring of Gamma radiation environmental levels within the FPS. The instrument was originally designed by the manufacturer for mobile operation using batteries, but the team has implemented a hardwire power method via rover where it will use an estimated maximum power of 270 mW. The instrument is designed to be compact, maintaining a lightweight mass of 1.3 kg and a total volume of 3362 cm^3, fitting well within the 15kg total mass and 0.5 m x 0.5m x 0.5m total volume constraints for the human exploration mission goal.

There are potential environmental risks such as the fluid freezing during the Martian night, but this is mitigated in three ways. The first being thermal regulation via internal earth-like pressurization within the FPS. The second will have a CDH controlled electric heater that activates depending on the region's sensed temperature. The third would be to run probe testing during the night which could provide benefits of heating up the inside of the FPS's aluminum housing from probe's generated heat. Given that the FPS is mounted to the top of the rover, the risk of de-pressurization is greatly reduced

by avoiding obstacles, balancing weight on the rover, and benefits from being located in direct line of sight for solar rays to be monitored.

For the second mission objective, the payload centers on a single, highly capable instrument, the Radar Imager for Mars' Subsurface Experiment (RIMFAX). This ground-penetrating radar was chosen because it can give a clear look beneath the Martian surface by mapping layers, detecting material changes, and identifying areas that may hold ice. It works across a wide frequency range, from 150 to 1200 MHz, which lets it pick up both fine details and deeper structures. Under ideal conditions, it can resolve layers just 15 centimeters apart and sense features buried up to ten meters down. Mounted under the rover, the folded dipole antenna points toward the ground so that it can continuously send radar pulses into the subsurface and collect reflections as the rover drives. From those reflections, it can determine properties like dielectric permittivity and radar wave velocity, which in turn tell us about porosity, composition changes, and how the ground is layered which are critical for evaluating how accessible and stable any near-surface ice might be.

It is designed for reliability as the entire system weighs around three kilograms, draws only five to ten watts of power, and has no moving parts to wear down over time. Its technology has already been proven on NASA's Perseverance rover, given the instrument is not being modified and solely being used for a different scientific objective, it is measured at a TRL 7, as a retest will later determine the system to be finalized and later considered flight qualified. That track record, along with its compact size and efficiency, makes it a perfect fit for the mission's constraints without compromising the science to accomplish. It draws steady power from the rover's power system and relies on the thermal control subsystem to keep its electronics within a safe operating range despite the extreme swings in Martian temperature which can plunge to –153°C at night and rise to around 21°C during the day in equatorial regions. Data from RIMFAX passes through the rover's Communication and Data Handling system, which uses a radiation-hardened RAD5545 onboard computer to process and store information on a high-capacity NVMe solid-state drive before transmitting it via UHF to the Mars Reconnaissance Orbiter and on to Earth. Navigation data, along with terrain mapping from JMARS, helps guide the rover along safe, scientifically valuable paths for RIMFAX to scan. In addition, surface composition readings from spectrometers add another layer of context, helping confirm if radar-identified features actually contain hydrated minerals or other promising signs.

Considering the environmental hazards identified in our Mission Concept Review, RIMFAX's electronics are sealed to prevent contamination from fine, abrasive dust that can infiltrate sensitive systems. The same dust, whipped up in storms that can stretch across the planet, can also block sunlight and affect temperatures, so the radar's design

avoids reliance on optical sensors for its core functions. Radiation exposure is another concern, mitigated by hardened components and shielding. The Martian terrain itself, with its slopes, craters, and unexpected rock formations, poses a constant challenge, but integration with the rover's mobility systems ensures radar scanning happens only where it's safe to traverse and pause.

Once the rover touches down in a low-dust region of Erebus Montes, RIMFAX will be calibrated to set a baseline before operations begin. As the rover moves toward key sites like concentric crater fill formations and ice-rich lobate debris aprons, the radar will collect profiles at roughly every ten centimeters, creating a continuous subsurface map. When the rover reaches a high-priority location, the scanning density will increase to every five centimeters, capturing the fine-scale details we need for deeper analysis. All of this data will be processed, compressed, and sent back to Earth, where it can be integrated with other instrument results to pinpoint the best areas for future in-situ resource utilization.

The Miniature Tunable Laser Spectrometer was selected to analyze the hydrogen gases in collected samples of volcanic rocks to detect the possible presence of water on the Martian planet. The selection of this instrument was dependent on multiple factors aimed at understanding the long-term internal and external factors that have influenced the presence of water, while aligning with the direct constraints from stakeholders who wish to expand science exploration.

In a previous deliverable, such as the Systems Requirements Review (SRR), trade studies were conducted to properly select this instrument based on the criteria that will allow for an instrument that meets mission science goals and operates reliably within the environmental constraints of Mars. The consideration of mass, volume, precision, reliability, and power consumption led to the selection of this instrument, which is understood to determine the type of gas present based on its reaction of absorptivity to light. As this instrument is a successor to the tunable laser spectrometer, it is more compact and lightweight, offering a superior option to minimize payload mass while still providing precise measurements of isotopes (forms of elements with different neutron numbers), which is essential for studies of habitability on Mars. Location and purpose of the Mini-TLS (Miniature Tunable Laser Spectrometer) instrument are similar to the full-size TLS instrument used in the SAM (Sample Analysis at Mars) Suite of the Curiosity rover [77]. These compare in that they were meant to study the environment of planet Mars, specifically to analyze the gases that the soil may contain and release to produce water.

This spectrometer is to function once a sample of martian rock is collected by the robotic arm and is then placed into the oven to reach a temperature that will allow the gases that are trapped within the sample to be released to be analyzed by the

instrument. Analysis occurs when the spectrometer's laser light is introduced to gases within the chamber, and the distinct types of gases start to absorb the light in a differentiating manner. The collected data by the detector is then sent to the RAD5546 onboard computer to process, and this data is then stored in the NVMe SSD.

To support the functions of this instrument, other components within the rover maintain the instrument at a stable temperature, such as the double-sided mylar MLI on the exterior, goldized kapton MLI on the interior, variable conductive ammonia heat pipes, and KHLVA PLM-series electrical heaters, which work together with thermistor thermal sensors to prevent temperature fluctuations that could affect measurement accuracy.

The selected instrumentation to achieve the science exploration goal and its last objective includes the Raman Laser Spectrometer (RLS) which is designed to analyze and detect what materials from Mars are made of based on its reactive reflection to laser light. It is designed to function by analyzing the crystal, chemical, and bond structure on a sample of Martian rock fragments and asteroid olivine that has been altered by geophysical and environmental forces to determine what elements may be within those samples. The RLS operates by emitting a laser with a maximum distance of 4.8 cm to the sample that causes molecular vibrations to produce scattered light where it passes back through the window and into the spectrometer detector, which records the Raman spectra. The rover’s onboard computer then processes the raw spectra to reduce noise and highlight key spectral features where the processed data is transmitted to Earth via a rover to orbiter communication system then to a relay orbiter, which forwards them through a deep space communication link to Earth based ground stations. The scientific goal of investigating how the dynamic forces on planet Mars have altered the existence of water in its liquid form is pursued through the direct analysis of the surface and subsurface chemical composition. The RLS cannot operate independently. Spacecraft subsystems that support the RLS are the rover’s robotic arm, thermal control, power, CDH, communications, and environmental protection subsystems to perform accurate Raman spectroscopy under Martian conditions.The instrument conforms to the mission's rover with a mass of 2.4 kg and a volume of approximately $81 \times 98 \times 125\ mm^3$ [24]. It has a power consumption of 20 to 30 watts that varies with the temperature and operation mode along with performance metrics that ensure evident mineral detection as well as detection of trace components. This instrument will collect Raman spectra with a range between 11,111 to 33,333 nanometers of olivine within the selected location of Erebus Montes. The TRL of the RLS instrument is at a 7 based on environmental testing and system level integration [24]. It begins to function when a laser beam is directed into a held sample in its analysis chamber. As the laser interacts with the molecules in the sample, it provokes the Raman effect which is where a small portion of the light is inelastically scattered.

This scattering results from changes in the vibrational energy levels of the molecules, producing unique shifts in light energy. These shifts correspond to specific vibrational modes, which it detects and converts into spectral peaks. This collection of data creates a Raman spectrum that reveals the sample's molecular and mineral composition to better understand Martian geology [14].

2.1.5.1 Science Instrumentation Requirements

The four science instruments selected each have a requirement derived from its scientific function, expected performance under Martian conditions, and its interface with other subsystems such as thermal control, command and data handling, and mechanical mounting.

Req #	Requirement	Rationale	Parent Req	Child Req	Verification method
PAYL 0.1	The selected RIMFAX instrument shall detect radar signal changes in Martian subsurface layers from the surface down to 10 meters depth to identify ice-rich zones defined by a permittivity difference of less than or equal to 0.1	At a depth of 10 meters in the Martian regolith, ice is expected to be found, and a permittivity difference of 0.1 allows radar signals to differ between ice and soil for the use of future astronauts.	MG 0.2		Test
PAYL 0.2	The Submersible Gamma Neutron Probe instrument shall operate reliably in the Martian environment for at least one year and measure radiation levels ranging from 1 µSv/h to 10 Sv/h to detect potential radiation contamination.	The instrument must operate reliably throughout the mission duration to detect a wide range of radiation levels and confirm contamination risks early in a timely manner that investigates the exposure of Martian surface environments.	MG 0.1		Test
PAYL 0.3	The Miniature Tunable Laser Spectrometer instrument shall collect and receive data from hydrated volcanic rock within a 1-second integration time to enable accurate and precise determination of the	The Miniature Tunable Laser Spectrometer instrument shall collect and receive data from hydrated volcanic rock within a 1-second integration time to enable accurate and precise	SYS 0.7		Test

	Deuterium to Hydrogen (D/H) ratio on Mars.	determination of the Deuterium to Hydrogen (D/H) ratio on Mars.			
PAYL 0.4	The Raman Laser Spectrometer instrument shall collect Raman spectra in the 11,111–33,333 nm range from Olivine at multiple surface sites while operating within the TCS-controlled temperature range of 228 K to 313 K.	The RLS is to function properly based on temperature conditions that allow for sufficient data to be collected to accurately identify mineral compositions such as Olivine at various surface sites.	TCS.05		Test

Figure 2.1.5.1.1: Payload Requirements Table

The Radar Imager for Mars' Subsurface Experiment (RIMFAX) supports the goal of identifying accessible water ice deposits. It must detect dielectric differences down to a depth of 10 meters with a permittivity sensitivity ≤ 0.1. To meet this requirement, the instrument must be mounted on a stable platform with minimal electromagnetic interference and sufficient power and data bandwidth [52]. It must also interface with the mobility subsystem to maintain ground coupling while traversing varied terrain.

The Submersible Gamma Neutron Probe (SGNP) addresses the objective of monitoring radiation hazards to mission-critical fluids. It shall operate continuously for at least one Martian year, detecting gamma and neutron radiation levels between 1 µSv/h and 10 Sv/h. To support long-duration performance, the instrument requires thermal stability within operational bounds and mechanical integration within a sealed fluid testbed. The probe must be electrically and thermally isolated while still interfacing with CDH for periodic data collection and transmission.

The Miniature Tunable Laser Spectrometer (Mini-TLS) enables analysis of the Deuterium-to-Hydrogen (D/H) ratio in hydrated volcanic rock. It must collect absorbance spectra with a sensitivity better than 80 ppb and an integration time of ≤1 second. The spectrometer must be mounted on a mobility-accessible arm or stable surface to acquire accurate samples, with localized thermal control and vibration damping to maintain optical calibration. Integration with CDH is required for both real-time command and high-resolution data logging.

The Raman Laser Spectrometer (RLS) is used to analyze the crystal structure of Olivine and other minerals formed via ice-impact interactions. It must collect spectra in the 11,111–33,333 nm range and resolve features with at least 10 cm^{-1} spectral resolution. This instrument operates effectively only within a thermal envelope of 228 K to 313 K, requiring close coordination with the thermal control system (TCS). In addition,

the RLS must be positioned to access mineral targets and avoid shadowing or dust contamination.

Each instrument's performance is subject to verification through functional testing under simulated Martian conditions (temperature, radiation, and mechanical stresses). Requirements also include placement, power draw, signal conditioning, and structural mounting interfaces, which will be fully specified in the Interface Control Document (ICD).Together, these instruments ensure the P.H.O.E.N.I.X payload can deliver high-resolution, high-value science within the constraints of volume, mass (≤15 kg), and energy budget allocated to the payload subsystem.

2.1.5.2 Payload Subsystem Recovery and Redundancy Plans

Science Measurement Requirements		Baseline Performance Requirements		Instrument			
Physical Parameters	Observables			CP-MUDMU-100 Submersible Gamma Neutron Probe	RIMFAX	Mini TLS Spectrometer	Raman Laser Spectrometer
Periodically monitor the Earth fluid sample for risks, hazards, and contamination that may bypass the custom-engineered Fluid Protection System's protective layers and document via data generation.	Use a passive ionization chamber to monitor gamma radiation levels in µSv/h, recording data at weekly intervals over a one-year period for transmission back to Earth.	Range	1 µSv/h to 10Sv/h	●	○	◔	◔
		Operating Temperature	30°C to +57°C				
		Accuracy	±5%				
		Time Constant	12 seconds slow				
Estimate dielectric permittivity and radar wave velocity to characterize subsurface material properties, including layer thickness, composition changes, and porosity variations across a 10 km traverse.	Analyze radar signal delay and reflection strength to determine layer boundaries, depth to subsurface features, and dielectric (Ɛ) contrasts indicative of dust deposits and possible ice-rich zones.	Penetration Depth	≥ 10 km	○	●	◔	◔
		Frequency Range	100-1200 MHz				
		Permittivity Range	ΔƐr ≤ 0.1				
		Vertical Resolution	≥ 15 cm				
Define the relative abundance of	Collect absorbance spectra in the 2500–25,000 nm	Wavenumber Range	3593.3-3594.3 cm^-1	○	◔	●	◑
		Spectral	0.0001 cm^-1				

protium and deuterium within samples of hydrogen from hydrated volcanic rock.	range of H in selected hydrated volcanic rock samples at multiple surface sites.	Resolution					
		Sensitivity	<80 ppb				
		Integration Time	1 s				
Determine the crystal structure of minerals formed by asteroid impacts interacting with exposed subsurface ice.	Identify chemical structure, crystal structure, and bond structure of Olivine from asteroids.	Mineral Identification Accuracy	±10%	○	◔	◔	●
		Detection Sensitivity	≤ ~100 ppm				
		Power Consumption	20 - 30W				
		Spectral Resolution	10 cm^{-1}				
Legend							
○	Does not contribute to objectives						
◔	Does not meet baseline						
◑	Partial contribution to objectives						
●	Instrument can fully meet objectives						

Figure 2.1.5.2.1: Instrument Redundancy Matrix

The payload subsystem will address recovery and redundancy for each instrumentation in the event of issues arising with their function or performance. CP-MU DMU-100 has a freeze risk that will be addressed by running testing during the night to heat up the internal housing fluid environment as the instrument operates at a minimum of 30°C which is warm. On Mars, clays and ice-dust layers can tamper RIMFAX's radar pulses and disrupt its depth, to confront this, the instrument will stick to the low end of its 150–1200 MHz band, limit the soundings to 2–4 m, and stack multiple passes for a clear return. For the Raman spectrometer, a quick calibration check will be made before and after every run and only trust fully quantitative data when the sample sits at the controlled 935 K, outside those windows spectra is treated as qualitative data. With the Mini-TLS, rather than investing in extra cooling gear, measurements will be conducted at night, when Martian temperatures reliably stay between –10 °C and 20 °C, keeping the laser and optics within requirements.

The payload ensures that the failure of a single instrument does not disrupt the overall mission progress, as other instruments are capable of compensating for any deficiencies. The main focus of the first Human Exploration Goal objective, detecting

contamination in stored terrestrial fluid samples, is determined by the DMU-100 Submersible Gamma Neutron Probe, which is capable of measuring radiation levels ranging from 1 μSv/h to 10 Sv/h with a minimum accuracy of ±5%. If that probe were to fail, the Mini-TLS Spectrometer and Raman Laser Spectrometer could still provide guiding data by detecting chemical or mineral changes and volatile signatures, which might indicate contamination even without direct gamma readings. For the second objective, aiming to map subsurface layers and locate potential ice-rich zones, RIMFAX will deliver detailed dielectric profiles down to 10 km with a vertical resolution of 15 cm. In the event of system downtime, surface spectroscopy conducted by the Mini-TLS and Raman systems remains capable of discerning hydrated mineralogy and modifications in lithochemical properties, providing partial yet significant understandings into subsurface geochemical conditions. In isotopic abundance analyses of hydrogen and deuterium, the Mini-TLS is chosen as the main instrument, however, the Raman Laser Spectrometer is adept at complementing this function by identifying hydration states and detecting spectral shifts associated with isotopic variations. When it comes to analyzing the crystal structure of minerals formed by asteroid impacts, the Raman Laser Spectrometer provides full mineral identification, while the Mini-TLS can add supporting data by targeting specific spectral ranges associated with impact-related bonds or volatiles. This ensures that even with a partial system failure, critical data can still be collected, maintaining the mission’s science goals.

2.1.5.3 Payload Subsystem Manufacturing and Procurement Plans

The most appropriate contractor for delivering the CP-MU DMU-100 Submersible Gamma Neutron Probe is Technical Associates, the manufacturer and developer of the original DMU-100 system, which is designed for high-resolution gamma and neutron monitoring in harsh environments such as nuclear waste storage and deep geological repositories. The DMU-100 utilizes a passive ionization chamber for long-term gamma radiation monitoring and has been tested for reliability in highly pressurized and submerged conditions which are characteristics essential to its deployment within a custom-engineered, pressurized Fluid Protection System attached to a Martian rover. In this case, the protection system will internally house both the DMU-100 and an Earth water sample to simulate and monitor radiation impacts on mission-critical fluids. The probe will transmit gamma dose rate data (in µSv/h) on a weekly cadence over a full Martian year to evaluate material shielding performance and radiological degradation risk, directly supporting Materials Engineering advancements for fluid transport, recycling, and protection on Mars. While the DMU-100 was not originally built for planetary applications, its compact cylindrical form (94 cm length, 4.5 cm diameter), sealed pressurized body, and low-power passive sensing make it a strong candidate for Martian adaptation, provided the FPS handles external environmental exposure. Technical Associates has not published lead times for space applications, but based on comparable ruggedized radiation probes and historical shipment cycles for geological monitoring systems, a conservative fabrication and modification lead time of 10–14 months is estimated. With a 25% margin, the final lead time projection is 12.5–17.5 months, assuming integration of Martian-specific housing and thermal protection. [12]

The best primary contractor for Radar Imager for Mars’ Subsurface Experiment (RIMFAX) is the Norwegian Defence Research Establishment (FFI), which originally developed and delivered the flight model for NASA’s Perseverance rover. With direct experience designing ground penetrating radar systems tailored for extreme planetary environments, making them the most reliable and flight proven option for any mission requiring subsurface imaging or ice detection. RIMFAX demonstrated its capability to detect dielectric contrasts and resolve subsurface layers down to 10 meters with depth resolution from 10 - 40 cm depending on material permittivity. If FFI is unavailable, a strong alternative is Mala GeoScience, a commercial leader in modular radar systems.While they lack direct spaceflight heritage, their field tested hardware has potential for adaptation, provided design for justification and address thermal/radiation constraints. Research shows the instrument was developed between 2014 - 2019, with the flight model delivered in early 2019, suggesting a conservative lead time estimate of 12 - 18 months for a mission-adapted system. Including a 25% margin for integration and testing, the final expected lead time is 15 - 22.5 months, based on historical milestones and integration pacing from NASA and FFI [103].

Thales Alenia Space is the best primary contractor for the Raman Laser Spectrometer for missions focusing on life detection on Mars due to their direct experience, mission-specific design, and successful development of the ExoMars RLS, the only Raman system made for biosignature detection on Mars. Should Thales Alenia Space be unavailable, Teledyne Princeton Instruments (TPI) is the recommended backup for the Raman Laser Spectrometer. Their specialization in deep cooled detectors and customizable spectrometers have been used in NASA missions such as Europa Clipper and Lunar Trailblazer. Furthermore, they also provide radiation tolerant, thermally stable, and compact Raman systems, making them a good alternative to Thales Alenia Space. Detailed manufacturing and delivery timelines for the Raman Laser Spectrometer are not publicly disclosed. However, publicly documented delivery or upgrade milestones can be used as indirect indicators. Using publicly available sources, the flight model of the Raman instrument control unit (RLS) was delivered to Thales Alenia Space Italia in Turin from IRAP on June 25, 2024 and it is estimated that it will be integrated into the full system in 2025, giving a 6-10 month lead time estimate but with a 25% margin of error, the total lead time estimate increases approximately to 8-15 months.

The primary supplier selected for the Mini-TLS instrument is the Southwest Research Institute (SwRI), as this organization is known for its successful contribution to missions with spectrometers and gas analyzing instrumentation, such as the MAss Spectrometer for Planetary EXploration (MASPEX) and the Magnetic Anomaly Plasma Spectrometer (MAPS) [59]. As stated by the Southwest Research Institute’s Department of Space Operations, their specialties include particle radiation detection and spectroscopy, which is imperative to achieve the scientific goals and objectives within this mission. SwRI is a flight-proven contractor that is able to deliver time leads with accuracy and quality which will ensure the mini-TLS instrument performs reliably to meet mission requirements [128].

As a backup supplier, Ball Aerospace is chosen for its strong flight heritage and proven experience in developing spectrometry instruments. Ball's instrumentation includes systems designed for a full spectrum of electromagnetic observations, such as in missions like the Ozone Mapping and Profiler Suite (OMPS) and the Green Propellant Infusion Mission (GPIM), as both served to test environmental sensors, which are vital to the payload of P.H.O.E.N.I.X [93]. Ball Aerospace is also considered because this company values the importance of compact and lightweight instrumentation, critical within the payload subsystem to meet requirements and criteria, as the mini-TLS was decided [97]. Overall, it optimizes the mass and volume constraints, which increases the level of precision.

The decision to use a COTS was based on the considerations of time, cost, risk, and reliability. Choosing a part that is already designed, tested, and manufactured

allows for efficient use of time and budget, which increases predictability in performance outcomes, along with lowering technical risks. SwRI and Ball Aerospace are able to contribute to the performance that the mini-TLS must meet to be successful within the P.H.O.E.N.I.X mission with their extensive experience and reliable performance.

2.1.5.4 Payload Subsystem Verification Plans

Req #	Requirement Summary	Verification Method	Rationale for Method	Preliminary Verification Plan
PAYL 0.1	The Submersible Gamma Neutron Probe Instrument shall operate reliably in the Martian environment for at least one year and measure radiation levels ranging from 1 µSv/h to 10 Sv/h to detect potential radiation contamination.	Test	The instrument must operate reliably throughout the mission duration to detect a wide range of radiation levels and confirm contamination risks early in a timely manner that investigates the exposure of Martian surface environments.	Verify neutron performance readings using 12 second time constant in a pressurized environment.
PAYL 0.2	The selected RIMFAX instrument shall detect radar signal changes in Martian subsurface layers from the surface down to 10 meters depth to identify ice-rich zones defined by a permittivity difference of less than or equal to 0.1	Test	At a depth of 10 meters in the Martian regolith, ice is expected to be found, and a permittivity difference of 0.1 allows radar signals to differ between ice and soil for the use of future astronauts.	Bench-calibrate the radar and antenna; verify timing, bandwidth, and transmit power. Analysis: use radar link budget to validate detectability at 10 m under expected regolith loss tangent; correlate with test data. Environmental: TVAC functional sweeps + EMI/EMC to confirm no degradation in performance.
PAYL 0.3	The Miniature Tunable Laser Spectrometer instrument shall collect and receive data from hydrated volcanic rock within a 1-second integration time to enable accurate and precise determination of the Deuterium to Hydrogen (D/H) ratio on Mars.	Test	The Miniature Tunable Laser Spectrometer instrument shall collect and receive data from hydrated volcanic rock within a 1-second integration time to enable accurate and precise determination of the Deuterium to Hydrogen (D/H) ratio on Mars.	Functional timing: command acquisitions; verify per-spectrum integration time ≤1.0 s • rock interaction: use hydrated analog samples; confirm signal strength and lack of interfering lines. • TVAC: run spectra across 228–313 K chamber; verify calibration stability. • EMI/EMC: verify no susceptibility to rover radios/actuators; no emissions exceeding limits.

PAYL 0.4	The Raman Laser Spectrometer instrument shall collect Raman spectra in the 11,111–33,333 nm range from Olivine at multiple surface sites while operating within the TCS-controlled temperature range of 228 K to 313 K.	Test	The RLS is to function properly based on temperature conditions that allow for sufficient data to be collected to accurately identify mineral compositions such as Olivine at various surface sites.	Spectral performance: acquire spectra from NIST/ASTM standards and olivine; verify peak positions and identification confidence vs thresholds. • TVAC: run thermal cycles 228–313 K under vacuum with periodic spectral checks; verify no calibration drift beyond budget. • Vibration & shock: sine/random vibe and shock per launch environment; post-test functional check. • EMI/EMC: susceptibility/emissions testing while rover subsystems operate.

Figure 2.1.5.4.1: Payload Verification Plan Table

RIMFAX (Test + Analysis):

Bench-calibrate timing, bandwidth, and transmit power using the flight antenna. Success = recovery of known interfaces at correct depths and ~15 cm near-surface vertical resolution. Use full-wave EM modeling and a radar link budget to map bench results to flight conditions, demonstrating ~10 m detectability under expected loss. Qualify with sine/random vibration, thermal-vacuum (with functional sweeps), and EMI/EMC with rover comms active to confirm performance and interfaces remain within spec after launch- and ops-like stress.

Mini-TLS (Test + Analysis):

Verify timing and isotope-ratio fidelity. End-to-end runs confirm per-spectrum integration time ≤ 1.0 s. Quantify D/H accuracy and precision with standards spanning the Martian range. Control matrix effects by measuring hydrated basalt analogs to confirm adequate signal and absence of interfering lines. Assess stability in thermal-vacuum across ≈ 228–313 K with calibration checks at each setpoint, and run EMI/EMC to verify immunity to rover emissions and compatibility with co-located electronics.

RLS (Test):

Lead with spectral performance and environmental robustness. Using calibration standards and olivine, verify wavenumber accuracy against thresholds needed for

reliable mineral identification. Check focus and spot-size at temperature extremes to ensure optical stability. Perform thermal-vacuum cycling from 228 K to 313 K with periodic spectral checks to hold calibration. Validate launch survivability via sine/random vibration and shock, followed by post-test functional checks. EMI/EMC with the powered rover stack confirms susceptibility margins and emissions compliance.

2.2 Interface Control

The system interface diagram shows the relationship between each subsystem and how each subsystem interfaces with the other. These subsystems include the following: structures, payload, data handling, comms, navigation, thermal and power. Each of the subsystems play a distinct role and are crucial to the success of this mission. By mapping out the interfaces, failure modes can be identified and mitigated early on in the design process of the rover.

Each subsystem is configured to have its own specific function but it all comes down to system integration, hence the N^2 chart is a visual representation of how all subsystems will have to work together in sync, ultimately supporting the spacecraft's goals and ensuring operational integrity.

The spacecraft structure is the foundational subsystem, it consists of the chassis, wheels, motors, actuators and all mechanical components that are physically present on the rover. This subsystem is positioned at the highest level on the interface chart because it serves as the primary housing and structural support for all the other subsystems. The key functions of this subsystem include providing support and physical protection to all internal and external subsystems ensuring structural solidity of the spacecraft.

The main system interfaces the structure subsystem receives outputs from is the power and thermal control subsystem. The structure is reliant on the power subsystem to supply electrical energy to the mechanical components, such as the motors on the wheels or any actuators the rover will have. This reinforces the rover's mobility and the operation of any deployable or moving parts, such as a deployable radiator used by the thermal control subsystem or deployable solar cells used for generating electrical power.Adequate power supply is essential for maintaining the rover's navigation, scientific experimentation and data collection capabilities.

Furthermore, the chart also illustrates the most vital output to the spacecraft structure which is heat dissipation through the structure from the TCS subsystem. TCS is a critical system that keeps the spacecraft structure, any components and electronics within nominal temperature ranges considering the harsh thermal environment on Mars with temperatures that go as low as 146 Kelvin to as high as 278 Kelvin. Despite these extreme temperature fluctuations, it is important to keep the structural elements of the spacecraft and any mounted subsystems operational.

The spacecraft structure is essential to the integration of all subsystems which highlight the unidirectional flow of power and thermal management into the spacecraft structure, emphasizing its dependence on these subsystems for flight readiness.

The payload subsystem, which is the instrument module, houses all of the scientific instrumentation that is designed to achieve both the scientific and human exploration goals provided by NASA that is the customer. This suite of instrumentation is an integral part of the mission, as it enables collection and transmission of valuable scientific data that pertains to future sustainability and manned missions on Mars.

The instrument module consists of distinct and unique instruments, each having its own functionality but working towards achieving the desired science objectives.

This subsystem solely sends inputs to the CDH subsystem but receives outputs from CDH, TCS and the power subsystem. The payload sends an instrument status signal to the CDH subsystem which includes an onboard computer that processes that signal and decides if the instrumentation is currently offline, if that is true, the CDH subsystem outputs an experiment activation command signal to the payload subsystem, where the instrumentation begins data collection. Once the data has been collected and the instruments have performed their operation at the research point, the scientific data is then inputted into the CDH subsystem which then sends an experiment stop signal to the payload subsystems turning all of the instruments offline to conserve power. This closed loop interaction ensures that scientific experiments are conducted efficiently and that payload operates only when required, saving power and conserving the instrument’s operational lifetime.

The outputs that the payload subsystems receive from TCS is in the form of active heating and cooling. Each instrument in the payload has its own nominal operating temperature range and going above or below it would compromise on the effectiveness of data collection and instrument redundancy. To counteract this, the TCS provides heating through the means of a heat pipe or cooling through cryogenic cooling systems, depending on the time of the day and solar loads the structure receives.

Furthermore, it also receives an output in the form of electrical power from the power subsystem as all of the instrumentation will require power to function and start experimenting.

The Command and Data Handling (CDH) subsystem serves as the central data repository for all of the scientific data that is transmitted to and from the instrumentation to the onboard computer. This subsystem is responsible for smooth data flow throughout the duration of the mission. The CDH subsystem interacts with each of the subsystems in a certain order, first interacting with the payload subsystem where it interacts in a closed loop, with inputs from the payload and output from the CDH subsystem back into the payload.

This subsystem also inputs an autonomous event log and an overall system health report to the communications subsystem which then relays this information to the

MRO that relays that same scientific data back to the earth ground station.

The CDH subsystem also inputs different signals and commands into the navigation, TCS and power subsystem. The inputs into the navigation include path and mobility data based on the surface terrain data that it receives from the communications subsystem as well as the navigation command to direct the rover on where to find the next science research point of interest. It also transmits a thermal data report to the TCS subsystem that includes the temperature at the surface of the mars so that the TCS can heat or cool all of the subsystems accordingly. Finally, it inputs commands and signal feeds into the power subsystem for how much power is required for the system at the moment.

This is all done simultaneously as the CDH subsystem receives outputs from the communications, TCS and power subsystems. The outputs it receives from communications include terrain mapping data information. TCS sends a thermal status update to the CDH subsystem to ensure it is operating as required and is allocating the heat based on the thermal data report of the environment and lastly, it receives electrical power from the power subsystem as the onboard computer does need power to function.

The comm subsystem is a very important interface as it is responsible for sending and receiving important data from and to the MRO. This subsystem outputs data and commands received from MRO back to the onboard computer that is part of the CDH subsystem and also sends terrain and surface mapping data back into CDH so the onboard computer can come up with various efficient pathfinding routes and nearest research points for the rover to reach.

It also receives outputs from the TCS as it includes electronics that must be kept under operating temperatures as well as electrical power to operate.

The TCS subsystem is a critical subsystem that will guarantee success of the mission given the extreme thermal environment on Mars. Every subsystem requires either active heating or cooling. For instance, the payload would need both active heating and cooling, this is because the instruments operate nominally under specific operating temperature ranges and hence the instrument would either need cooling or heating.

This subsystem gets inputs from the CDH subsystem and outputs from the power as the TCS does require electrical power to operate.

Finally, the power subsystem lays all the groundwork to ensure all of the other subsystems and components operate and have the required voltage to function. Considering the fact that the rover will be semi-autonomous, everything will be

connected to the onboard computer through spacewire that will then be connected to the power distribution unit which will be connected throughout the rover’s main chassis to transfer power to each component.

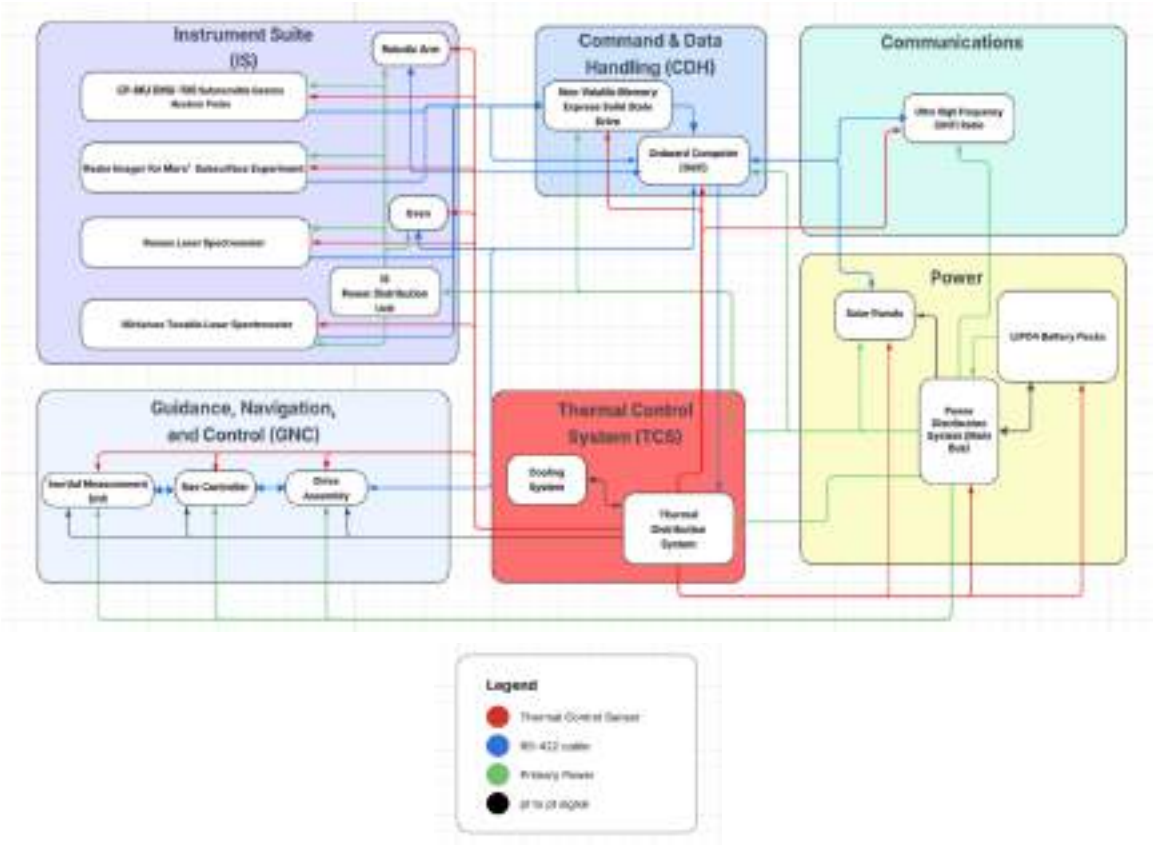

Figure 2.2.1: System Block Diagram

The block diagram is a more detailed version of the N^2 chart as it gives a better understanding of how each subsystem is interfacing with each other and what sort of connections they have with each other. At the top left, the instrument suite (IS) is located which contains all of the scientific instruments such as a spectrometer, a neutron probe, a robotic arm, an oven and a power distribution unit. The function of the robotic arm is to collect rock samples from the martian surface which will then be heated up in the oven to collect gas that will then be measured by the spectrophotometer to gather valuable scientific information. These instruments, however, receive primary power from the power distribution unit that is located in the instrument suite. The IS power distribution unit receives primary power from the main power distribution System that receives electrical power from the LiPO4 battery packs which it then sends to the solar panels and every single subsystem component in the system. The power distribution system is also connected to both the solar panels and the LiPO4 battery packs through a pt to pt signal connection, this connection is bi-directional to the battery packs as the signals ensure the PDS knows the status of the battery pack and it then feeds the amount of power available to the solar panels. The TCS subsystem includes a cooling system and a TDS, the TDS is connected to every single subsystem component through thermal sensors that ensure all of the components in the spacecraft are operating nominally. The cooling system is responsible for decreasing the temperature of the spacecraft components, in the case that it gets extremely hot, especially during the daylight hours and that’s where the radiators dissipate the heat and cool the systems down. The Cooling system interfaces with the TDS through a pt to pt signal which sends each other the status of both systems ensuring they are maintaining their operational integrity and so that in the case of a failure, one of the systems could be shut down or backup heaters/coolers can take over.

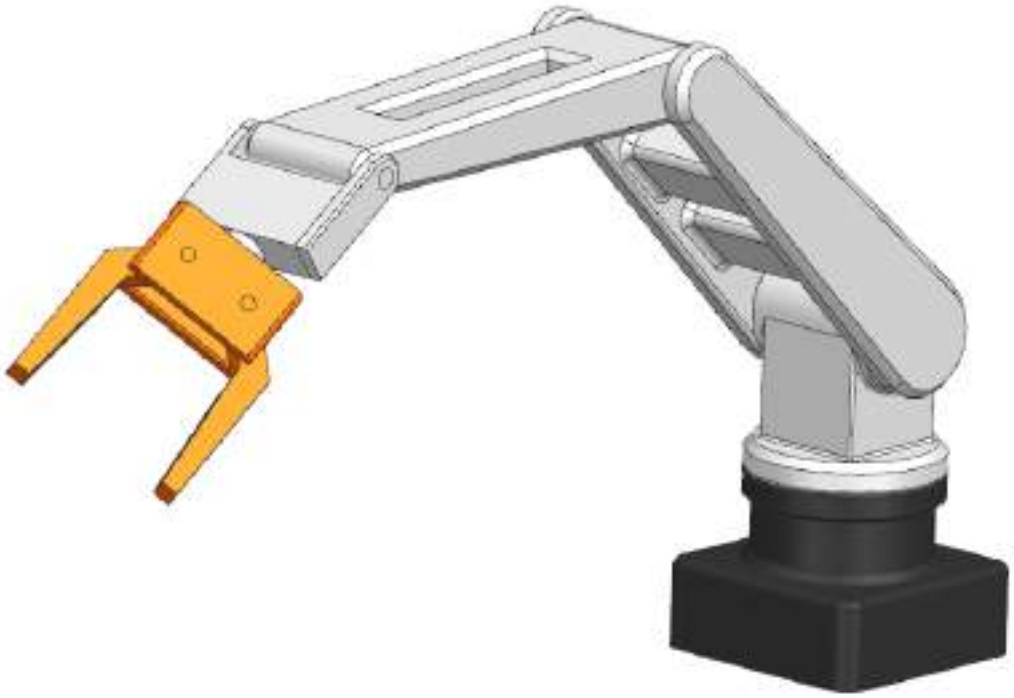

Figure 2.2.2: Robotic Arm Design

The GNC subsystem houses all of the mechanical subsystems and these consist of the inertial measurement unit, a navigation controller and a drive assembly. All of these subsystems receive their primary power from the PDS and have thermal control sensors on them to ensure they are under nominal temperature and do not excessively heat up to a point where they lose their navigation capability. They are also connected to the TCS through pt to pt signals, sending status and health reports to ensure each of the subsystems are operating properly. They are also connected with each other through RS-422 cables to ensure streamlined data and command execution with each other.

The navigation controller determines and executes the rover’s pathfinding capability. It processes navigation commands, plans routes between waypoints, and calculates the necessary steering and speed adjustments to follow the calculated path. The controller uses algorithms to ensure the rover avoids any obstacles, follows smooth

paths and maintains stability; it does that by generating target velocities and steering angles that are then sent to the drive system. In autonomous mode, it can also adapt to changing terrain to update the route in real time.

The drive assembly is the mechanical and electrical subsystem that physically moves the rover. It includes motors, wheels, gearboxes and any associated control components. The way this subsystem works is it receives commands from the navigation controller through the RS-422 cable connection on how fast the rover should move and in what direction and then translates these into actual movements the rover performs on the surface. It allows the rover to perform complex maneuvers on challenging terrain for which the boogie rover system was integrated.

The IMU is a sensor package that measures the rover’s orientation, acceleration and orientation. This system contains a gyroscope, an accelerometer and a magnetometer. The IMU consists of an accelerometer and gyroscope, which provide real time data on the rover’s lateral accelerations and angular velocities. This data is essential for navigation and stability, This allows the rover to utilize dead reckoning techniques and localization algorithms to track its position and orientation even when GNSS systems are unavailable.

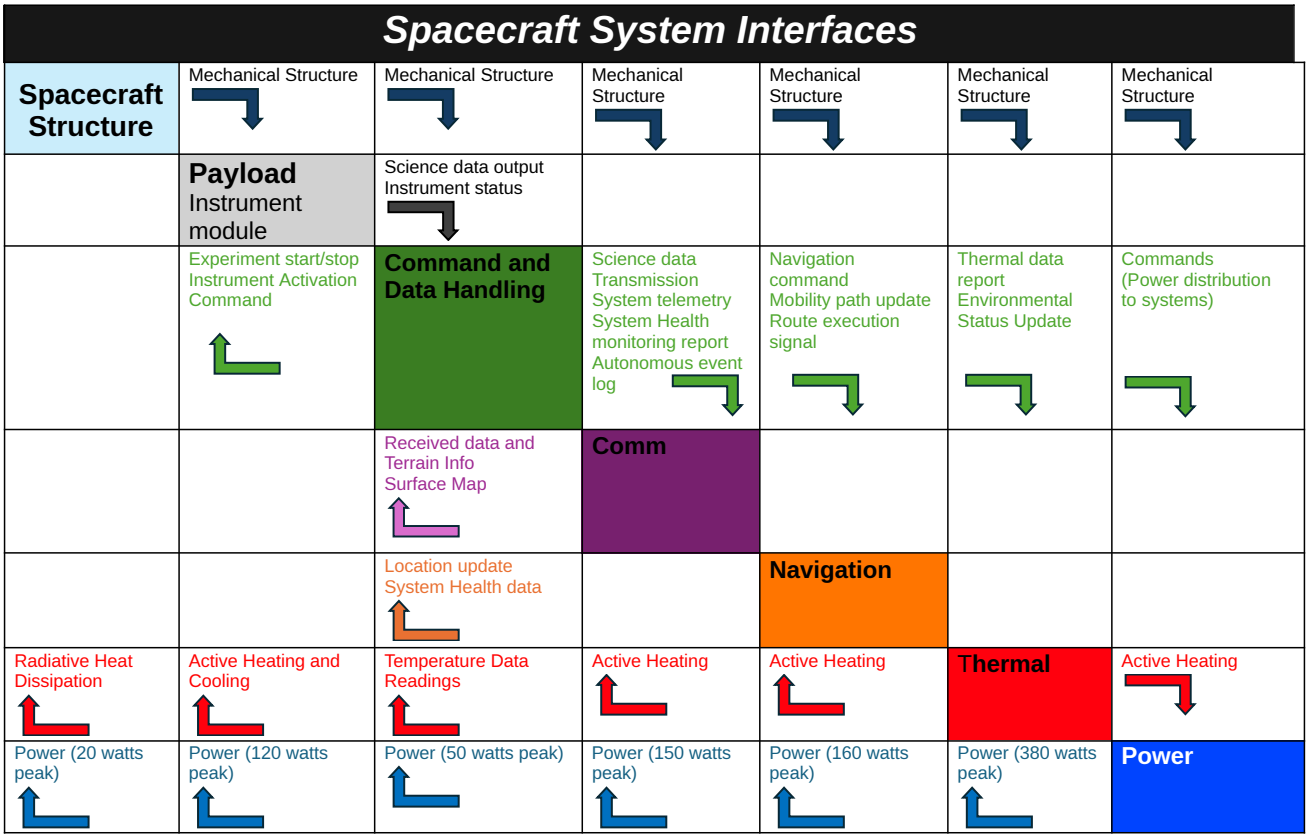

Figure 2.2.3: N^2 System Interfaces Chart

3.0 Science Mission Plan

3.1 Science Objectives

The P.H.O.E.N.I.X Mars rover will investigate the subsurface ice deposits in the planet's northern mid-latitudes to assess their potential for future human exploration. The mission will investigate the distribution of water ice, evaluate the interactions with the radiation environment, trace the history of Martian water, and analyze mineralogical evidence of past geologic and hydrologic processes. This research will help scientists determine the best locations for astronauts to land in the future, figure out how to use local resources on Mars, and advance our understanding of Mars' habitability. The acquired data will characterize the depth and purity of subsurface ice, identify the mineralogical composition of the regolith, and quantify surface radiation levels. Together, these results will help better understand the environmental factors that influence the potential habitability on Mars. Our chosen location, Erebus Montes, is an ideal future landing site because it lies within the northern mid-latitudes, where shallow ice has been located that provides water, oxygen, and fuel for astronauts [93]. With water-ice also existing on Mars, this keeps track of the depth and accessibility to understand Mars' past climate while also determining preferred landing zones [33]. However, it is important to first investigate the interactions with the radiation on the Martian surface due to the dangers it poses for astronauts, which will help future Mars exploration missions in designing safe shelters to protect astronauts [121]. Mars once had more water but overtime, it gradually depleted as the atmosphere thinned. Tracing the history of water on Mars reveals its climate change, past habitability, and where to search for signs of life [7]. When water and rocks interact with each other, minerals such as clay form, which can help point to past environments that might have supported life [93, 57]. Looking back at the STM, the mission goals rely on measurements from the chosen scientific instruments. For example, the Mini-TLS measures surface temperature and topography, helping determine ice distribution; the CP-MU DMU-100 Submersible Gamma Neutron Probe measures environmental gamma radiation dosage to contribute to material science innovation and protect mission-critical fluids; the RLS measures mineral composition, helping identify past water activity and geologic processes; and the RIMFAX measures subsurface layers using radar, helping map the depth, thickness, and structure of ice and rock beneath the surface. The Raman Laser Spectrometer identifies mineral crystal structures, revealing endogenic and exogenic processes that have influenced the water distribution over geological time on the Martian surface. These science instruments form a complementary payload and also generate a cohesive dataset capable of guiding future crewed missions and advancing our understanding of Mars' habitability potential.

3.2 Experimental Logic, Approach, and Method of Investigation

The rover's Radar Imager for Mars' Subsurface Experiment (RIMFAX) is mounted beneath the chassis and couples a flight-qualified electronics unit with a mission-tuned antenna to interrogate the Martian subsurface using frequency-modulated continuous-wave (FMCW) radar. By transmitting radio-frequency energy and recording echoes from dielectric contrasts, the system maps stratigraphy and flags potential ice-rich horizons with penetration to ≥10 m under nominal conditions [31]. Continuous, stable operation is enabled by tightly integrated subsystems: the power system supplies ~10 W average for steady profiling; thermal control holds the payload within −40 °C to +50 °C to preserve timing stability and gain linearity [78]; the command and data handling chain uses a RAD5545 radiation-hardened onboard computer (multi-core, ~1 GHz class, >2 GB memory) for real-time filtering and stacking, with an NVMe solid-state drive and RS-422 links provide noise-resilient, deterministic command and telemetry between RIMFAX and the CDH [77]. After onboard processing, data is forwarded over the rover's UHF relay, which hands the stream to Mars Reconnaissance Orbiter (MRO) for return to Earth [37]. Operations open with landing in a low-dust sector on the northwestern margin of the Erebus Montes region of interest. Immediately after touchdown, RIMFAX executes health checks and a calibration sweep to lock in baseline timing, bandwidth, noise figures, and depth-conversion references. As the rover drives toward concentric-crater-fill (CCF) and lobate debris apron (LDA) targets, the radar collects along-track soundings at roughly 10-cm intervals, building radargrams that resolve layer geometries, unconformities, and potential ice accumulations [31]. At prioritized stations on CCF and LDA units, the rover pauses for higher-density acquisitions (~5-cm sampling), boosting signal-to-noise and sharpening estimates of relative permittivity, electromagnetic wave velocity, and dust-layer thickness, key indicators of subsurface ice and hydrated volcanic materials [31]. Each raw acquisition is staged to the NVMe drive and pipelined by the RAD5545 through filtering, coherent stacking, and compression; the resulting data products are then routed through the UHF link to MRO and on to Earth, where the science team merges the radargrams into stratigraphic frameworks and identifies candidate zones for ISRU follow-up. Tight coordination with other rover assets improves interpretation and safety: navigation and hazard avoidance use rover state estimation and JMARS-derived geologic mapping to select low-risk, science-rich routes and waypoints; co-located spectrometer measurements constrain mineralogy and hydration to reduce ambiguity in radar signatures; and the mobility system's precise positioning and attitude control improve georeferencing and continuity across radar swaths. The plan itself is grounded in JMARS imagery and mapping, which guided the choice of a low-dust landing ellipse and a route network that samples glacial - volcanic contacts and morphologies linked to ice emplacement and preservation, thereby maximizing scientific return and strengthening contextual confidence in the radar-derived subsurface model.

The Raman Laser Spectrometer analyzes the minerals within rock and soil samples on the Martian surface. It works by shining a laser through a special window made of fused quartz onto the sample. When the laser hits the sample, it causes the molecules to scatter light at certain wavelengths unique to each mineral. The spectrometer then detects scattered light where it is analyzed to determine which minerals are in the sample as well as their chemical structures. The RLS connects to the rover's robotic arm which allows it to aim at different parts of the samples. The data collected by the RLS is sent to the rover's computer, which processes the information where it is then sent back to Earth for future studies.

The experimental logic behind the Mini-TLS instrument is to successfully detect and classify gases that may be released from gathered samples of volcanic rock, with the goal of identifying possible traces of water life on the Red Planet. This instrument has been selected to achieve the scientific goal of understanding the dynamic controls that have altered the presence of water, which contributes to the greater purpose of the P.H.O.E.N.I.X mission of research and discovery. The Mini-TLS will function with the use of a robotic arm to collect volcanic rock to then be transported into the embedded oven of the rover to dehydrate the rock by heating it up. The released gases from this are transported through sealed tubing into the gas cell of the Mini-TLS, where they are exposed to the tuned wavelengths to absorb light. The Mini-TLS is to be tuned and set at a wavelength between 2.6 μm to 2.8 μm to detect H_2O and HDO gas absorption patterns that are recorded to be sent back to Earth for analysis through the OBC. The integration of other subsystems' devices enables this instrument to successfully collect rock samples, facilitated by the implementation of a robotic arm, oven, and sealed tubes. With the use of thermal equipment, this instrument is also able to operate as intended in a range of temperatures that accommodate the unstable conditions on the red planet, such as through heat pipes that control excess heat. It is understood that this instrument is prone to overheating easily, so its placement within the rover has also been considered to be away from the other instruments that operate at similar higher temperatures.

The CP-MU DMU-100 Submersible Gamma Neutron Probe is mounted within the Fluid Protection System (FPS) on top of the rover to monitor Martian gamma radiation over the course of a one-year minimum mission. The FPS provides pressure stabilization and temperature control, maintaining the probe within its operating range of 30°C to +57°C using internal pressurization and CHD controlled electric fans that activate based upon the region's temperature sensed. The probe itself is a passive ionization chamber, where gamma rays entering the gas-filled chamber ionize the molecules, and an applied high voltage drives ions and electrons toward electrodes, producing a measurable current within the range of 1 μSv/h–10 Sv/h with a 12-second response time, ensuring precise, stable readings from subtle to extreme levels. Collected data will be stored on

the rover’s RAD5545 computer with NVMe SSD and transmitted via UHF through the Mars Reconnaissance Orbiter and back to earth. The probe will track a protected Earth pressurized fluid sample at weekly intervals for at least one year to evaluate the influence of Martian radiation and environmental conditions. The collected data will support advances in materials science by identifying potential risks to critical fluids, revealing previously unknown hazards, and guiding the design of improved storage systems. These results will directly contribute to technologies needed to protect astronaut health and the success of long duration missions on Mars.

3.3 Payload Success Criteria

RIMFAX will map subsurface stratigraphy and ice-bearing horizons by collecting continuous FMCW radargrams along the rover traverse, resolving near-surface layers at ≤0.15 m vertical resolution and achieving ≥8 m penetration in low-loss terrain; targeted stationary scans at key waypoints refine relative permittivity and EM-velocity estimates to ≤10% uncertainty. Potential failure modes include antenna degradation, timing/gain drift outside calibration bounds, electromagnetic interference from rover subsystems, thermal conditions beyond the −40 to +50 °C operating range, or data-link faults that mess with geo-registration. The results in depth, thickness, and lateral continuation of candidate ice layers across CCF and LDA units directly advance mission goals by prioritizing sites for ISRU prospecting and science drilling, while integrated 3-D stratigraphic models, fused with co-located spectroscopy and navigation data, reduce traverse risk and improve resource assessments

The RLS will identify the mineralogical composition of at least 80% of collected subsurface and surface samples within the mission, including hydrated minerals, carbonates, sulfates, and silicates that could indicate past water activity or habitability. Potential failure modes include laser misalignment, degradation or contamination of the fused quartz window, detector malfunction, or robotic arm positioning errors preventing proper targeting. The RLS results will address the mission goal by revealing the past mineralogical records on the Martian surface. These findings will help human exploration by identifying sites with potential resource availability and offering clues about habitability.

The success criteria selected for the Mini-TLS demonstrate how the instrument and its supporting subsystems achieve the mission’s scientific goals, ranging from basic functionality to ambitious outcomes. The minimum success criteria for the Miniature Tunable Laser spectrometer prove that the instrument functions properly and does what it is intended to do within the mission. By collecting a single sample, placing it into the oven, and successfully having the gases be analyzed for water confirms that the instrument and set systems for it are operating to create feasible scientific data. The optimum success criteria reach the scientific goal of the instrument by analyzing multiple samples of volcanic rock for the D/H ratio, demonstrating that the Mini-TLS, along with the subsystems, is capable of collecting multiple sets of data accurately and efficiently. The ability to collect multiple ratios of rock samples allows for more precise conclusions to be made about the volcanic rock at the mission location of Erebus Montes. As a stretch goal, the Mini-TLS is to collect data from samples of rock that deviate from the mission's location to gather more information about the possible past and present existence of water on the red planet. By straying away from the main selected site, a broader set of information is obtained while also verifying the ability of

the other subsystems that follow to function beyond one location.

The Gamma Neutron Probe has specific criteria that it shall meet in order to be qualified for flight and support the overarching science goals. At the mission minimum level, the probe must be able to perform measurements of Gamma radiation within a range of 1 µSv/h–10 Sv/h within a ten percent range of accuracy. This period of minimum success is defined to be under a calendar year. Under optimal conditions, the probe shall measure Gamma radiation within a 5 percent range of accuracy for a period of up to a Martian year. If this were to occur, the mission goal would stretch, and the measurement of µSv/h–10 Sv/h would occur for a period longer than one year, until such an event that the rover becomes inoperable and the mission shall end.

Category	Minimum Success	Optimum Success	Stretch Goal
Identification of RLS mineralogical composition	Identify 40% of hydrated minerals in the samples	Identify 80% of hydrated minerals in the samples	Identify 100% of hydrated minerals in the samples
Payload / Mini-TLS	Collection of 1 sample of volcanic rock is analyzed	More than 1 sample of volcanic rock D/H ratio is analyzed	Martian rocks are collected and analyzed from different locations other than mission location
RIMFAX- Subsurface stratigraphy and ice horizon detection	Traverse coverage ≥40%; vertical resolution ≤0.20 m (top 2 m); penetration ≥5 m on ≥50% of lines; ≥2 stationary scans resolving ≥1 continuous interface.	Coverage ≥80%; resolution ≤0.15 m (top 3 m); penetration ≥8 m on ≥70% of lines; ≥4 stationary scans; εr/EM-velocity uncertainty ≤10%; ≥2 candidate ice horizons.	100% coverage; resolution ≤0.12 m (top 3 m); penetration ~10 m on ≥80% of lines
CP-MU DMU-100 Submersible Gamma Neutron Probe/ environmental measurement	Measure Gamma radiation range of 1 µSv/h–10 Sv/h within ±10% accuracy for less than one year duration	Measure Gamma radiation range of 1 µSv/h–10 Sv/h within ±5% accuracy for one year duration	Measure Gamma radiation range of 1 µSv/h–10 Sv/h within ±5% accuracy for more than one year duration

Figure 3.3.1: Instrument Success Criteria

3.4 Testing and Calibration Measurements

RIMFAX:

RIMFAX runs a short, in-situ checkout tailored to local conditions. It starts with internal loopback and terminator tests to confirm chirp linearity, transmitter power, and receiver noise stability, then takes “sky” and “ground” references to lock the time-zero and amplitude scales. The rover parks over a flat patch for stationary sweeps; repeating the sweep at two antenna heights lets us solve for near-surface permittivity and velocity, which we use to convert two-way travel time to depth. We toggle likely EMI sources (UHF relay, mobility drives, high-speed links) to verify spectral cleanliness and schedule or notch any offenders. Control variables include chirp bandwidth and repetition rate, transmit power, antenna standoff/tilt, rover speed (sets along-track spacing), temperature, and bus voltage. Data quality is judged by a stable air ground bounce, physically plausible εr (≈2–4), repeatable reflectors on out-and-back passes, and SNR gains from coherent stacking; with those checks in family, the instrument transitions to traverse profiling and targeted scans with the mode and gating settings that best fit the site’s loss and layering. [31]

Raman Laser Spectrometer (RLS):

When the rover lands, the RLS will check its functionality by targeting a calibration target containing reference minerals stored in a sealed compartment on the rover. This verification process allows scientists to check if the laser alignment, focus, and detector sensitivity are functioning within expected parameters. The control variables for this process will be the known Raman spectral peaks of the calibration minerals and will be compared to the measured values to detect any instrument error. When confirmed, the RLS does a test scan of nearby rocks to verify its performance while under the Martian environment. The accuracy of RLS data will be determined by the match between calibration spectra and the known standards, as well as by comparing early readings to expected Martian mineral spectra based on orbital data. Any deviations will trigger in-situ recalibration using the onboard reference materials.

Mini-TLS:

Once at the landing site of Erebus Montes, the Mini-TLS instrument will undergo testing and calibration to ensure it functions properly. This step is essential to guarantee that data collected from gases released by volcanic rock are accurate and reliable.

The instrument will first be powered on and its settings adjusted to begin calibration tests. Following a method similar to the TLS on the SAM suite of the Curiosity rover, a reference sample of a known gas will be analyzed before any real rock samples are tested [115]. This calibration will be repeated three times at different

temperatures to mimic the environmental changes within the planet that could possibly impact measurements. If any results differ from the known properties of the reference gas, the instrument settings will be adjusted to repeat testing until the data readings are consistent.

Control variables for these tests include the composition of the reference gas, the pressure and temperature inside the gas cell, the instrument settings, and the oven temperature, which are to be monitored to be stable, as these will directly impact readings. Calibration is considered successful when the measured data align with the known properties of the reference sample, demonstrating that the Mini-TLS is functioning correctly and is ready to analyze Martian rock samples for water and D/H ratios.

CP-MU DMU-100 Submersible Gamma Neutron Probe:

Once the rover lands on Mars, the CP-MU DMU-100 Submersible Gamma Neutron probe will first perform a short series of in-situ calibration checks to ensure accurate radiation monitoring. First, it will measure background electronic noise, which is unwanted electrical signals generated by the detector’s electronics when no radiation is present. This “zero offset” must be subtracted so that only true radiation counts are recorded. Next, the probe may expose an internal reference source to confirm its sensitivity and apply temperature-based corrections to account for Martian environmental conditions. The probe will then record a baseline radiation profile for over 24 - 48 hours to establish normal background levels before beginning long-term monitoring of the fluid protection system. Periodic weekly checks-repeating zero and span calibrations, will confirm stability, while passive dosimeters, which are small passive devices such as thermoluminescent dosimeters (TLDs), will be placed alongside the probe. These dosimeters absorb radiation and later release measurable signals when heated or stimulated by light that will serve as an independent validation of cumulative radiation exposure. This process ensures the probe delivers reliable, traceable data throughout the mission.

3.5 Precision and Accuracy of Instrumentation

For the RIMFAX, near-surface vertical resolution is set by bandwidth ($\Delta z \approx c/[2B\sqrt{\varepsilon_r}]$) and, for our configuration, falls in the 0.12-0.20 m range. Depth accuracy is driven by the dielectric we assume, so we solve for ε_r in situ using a two-height sweep and an air/ground Fresnel reference; when ε_r is constrained to ±10%, depth error is ~±5%, and at ±20% it grows to ~±10% (stated assumption where specs are silent). After coherent stacking, amplitude repeatability is ≤±3% per sol, which keeps inter-sol reflectivity comparisons meaningful, and along-track geolocation on stationary or short retrace segments stays within ±0.1–0.2 m using odometry plus IMU. These bounds define the thinnest layers we can separate, the confidence on horizon depths, and how aggressively we need to stack in dusty versus low-loss units. They also justify bracketing key traverses with short calibration runs to catch drift before it leaks into depth maps.

The Raman Laser Spectrometer has an approximate spectral resolution of 0.2 nm or ∼4 cm^{-1} and an associated accuracy in Raman shift of ±0.4 cm^{-1}. This level of precision limits the ability to differentiate minerals whose spectral peaks are closer than about 4 cm^{-1}, so accurate calibration is essential, especially for temperature dependent shifts.

Accuracy and precision play a crucial role in the performance of the Mini-TLS, as they determine the isotopic ratios of present gases on Mars. The Mini-TLS instrument is designed to collect data with an accuracy in gas concentration and D/H ratio similar to that of the TLS on Curiosity’s SAM suite [125]. As a reasonable assumption, the Mini-TLS is to have an accuracy of ±1-2% for D/H ratios that can allow scientists to identify the history and presence of water on Mars, if any. Accuracy is also expected to be at ±5 ppm for gas concentration, along with the D/H ratios because this makes for reliable and precise measurements of each gas. Considering gas concentration accuracy is valuable because precise measurements of each gas ensure that the calculated D/H ratios are true based on their changes and not environmental fluctuations, allowing scientists to confidently interpret variations in water content and understand Mars’ water history.

As the gamma neutron probe instrument will achieve the human exploration goal, accuracy is a crucial aspect in making sure that happens. The instrument performance requirements indicate an accuracy of ±5%, though the predicted instrument performance achieves only ±10%. This means that if the actual radiation level is, for instance, 100 µSv/h, the instrument may report a value anywhere between 90 µSv/h and 110 µSv/h. While this discrepancy may appear small, over long- term monitoring it can influence the interpretation of cumulative radiation exposure. In particular, small but consistent deviations in accuracy could cause underestimation or overestimation of

contamination risks for the fluid protection system. There may also be a delay of up to 12 seconds in measuring radiation fluctuation as mentioned in the requirements meaning radiation levels may not be captured in real time with pin point accuracy. Instruments like this often exhibit drift when approaching thermal limits meaning the gamma radiation readings may deviate from the true value. For a long term mission like this, it would be difficult to keep the instrument in the exact operating range of 30°C to 57°C, and eventually the thermal stress could lead to drift that could compound measurement uncertainties.

3.6 Expected Data & Analysis

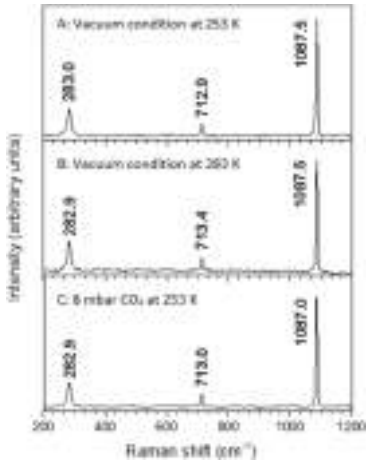

Figure 3.6.1: Raman spectra of a mineral under vacuum and CO_2 conditions

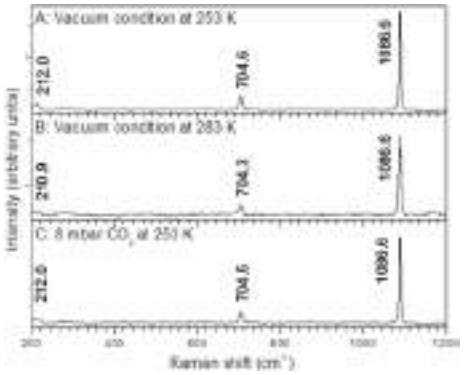

Figure 3.6.2: Raman spectra of a mineral showing shifts due to changes in temperature and pressure

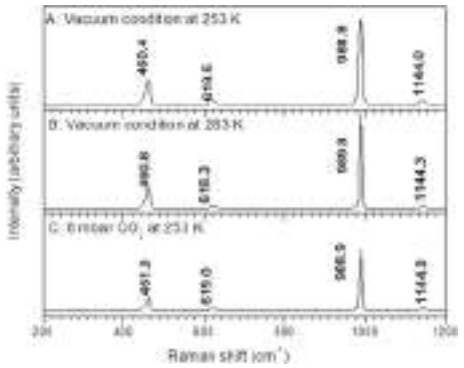

Figure 3.6.3: Raman spectra of minerals collected by a Mars rover in laboratory and simulated Martian conditions

The data collected on Mars by the RLS will go through several analysis steps. First, the rover collects the raw spectra, which are then cleaned to remove electronic noise and unwanted background signals. The instrument checks and adjusts the wavelength using built in reference lines to ensure Raman shift values stay accurate. Key Raman peaks are identified and measured with computational peak fitting. Their positions, widths, and intensities are then compared with reference samples from Earth. Computer analysis, including spectral preprocessing and library matching, is used to group minerals and identify errors or discrepancies. This process lets scientists identify minerals such as carbonates, sulfates, silicates, or serpentine. Researchers use their spectral features to look for signs of past water activity, hot fluid circulation, or heating events. By mapping these minerals in the Erebus Montes region of Arcadia Planitia, scientists can track the movement of liquids over time and how impacts or heat altered the rock. The RLS measured the main peaks of minerals like calcite, aragonite, and baryte. It measured them within 0.5–1 cm^{-1} in the lab and in simulated Martian conditions. When the same mineral was measured multiple times, the results stayed consistent. There were only small differences of about 0.5 cm^{-1} or 0.02 nm. The RLS gave reliable measurements during temperature changes or in the CO_2 atmosphere on Mars. This makes the RLS reliable for telling similar minerals apart. When comparing the example data to the expected data, both instruments can measure mineral peaks within about 1 cm^{-1} of where they appear in lab tests. For the example data, the temperature and pressure were changed to copy Mars conditions. The peaks mostly remained consistent. Some differences appeared: the expected data may not be as clean as the example data because dust, temperature changes, or background light can add extra noise. Unlike in a lab, the rover's movements and robotic arm positioning will also affect how samples are measured [60].

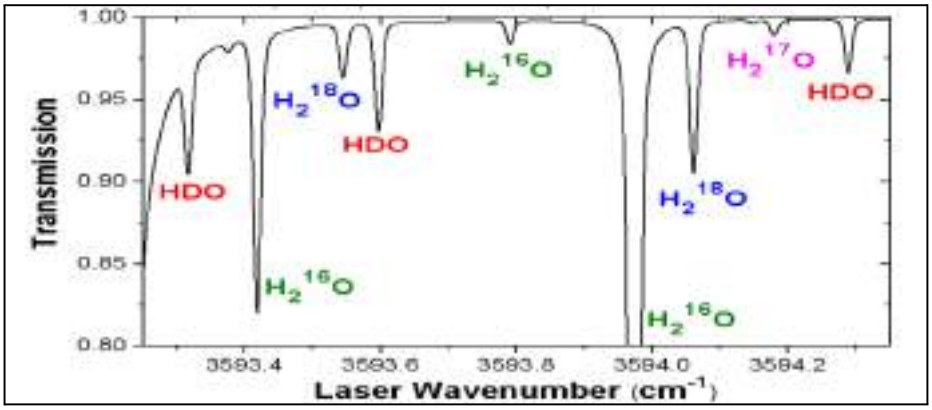

Figure 3.6.4: Transmission Data Graph Example

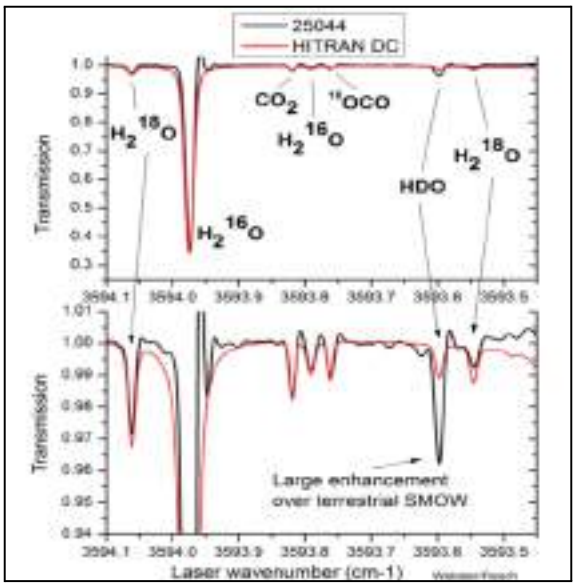

Figure 3.6.5: Comparative Transmission Spectra Example

The images above show example data similar to what the Mini-TLS is expected to produce when analyzing volcanic rock [118]. In these graphs, transmission refers to laser light passing through gases, which is absorbed at different wavelengths. Notable dips in the graphs signify the presence of water and other gases, as well as their amounts. The Mini-TLS will produce similar graphs as it measures gases released from Martian rocks, showing their types, amounts, and isotopic variations. This instrument will analyze these patterns by measuring the depth and area of each absorption dip. It will calculate gas concentrations in parts per million and determine isotopic ratios, such as D/H, allowing scientists to gain insight into Mars' past environmental conditions. The instrument is predicted to have an accuracy of approximately ±1-2% and a precision of ±5 ppm to be able to detect small variations reliably. Imperfections in heated samples of rock or ambient gases are potential sources of error. However, these can be reduced through repeated measurements and calibration of the instrument for accurate and precise data collection.

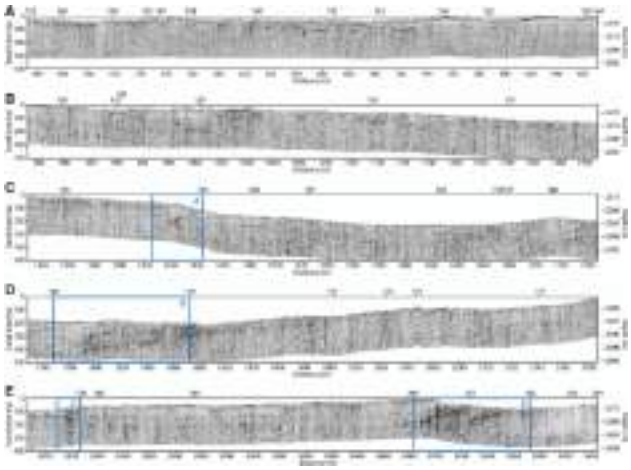

Figure 3.6.6: RIMFAX Example Data

The above picture is an example of the data returned by RIMFAX. These charts show reflected strength plotted as a function of linear distance (in meters) and depth (in meters) with vertical exaggeration by a factor of 3. This is done because Mars subsurface layers often change gradually or have shallow slopes, and this vertical exaggeration can help scientists detect and interpret subtle changes when looking at the data. Brighter areas in the diagram indicate stronger reflections, and this is the main focus of this mission as stronger reflections are caused by boundaries in different layers between dust, rock, and potential water ice. Patterns such as continuous layers, dipping reflectors, and abrupt signal changes help identify geological structures like sediment deposits or buried ice. As it traverses the surface, RIMFAX will produce similar data in the form of 2D cross-sectional images on the surface with roughly 10 centimeter lateral resolution and depth penetration up to 10 meters. These images will be analyzed by mission specialists and used to map layer thickness, detect dielectric contrasts, and learn more about the history of water on Mars by determining the presence of near-surface ice. The instrument can detect changes in material composition based on the strength and timing of signal returns, with depth estimates depending on assumptions about local dielectric properties. Sources of error may include surface roughness, rover tilt, and signal attenuation in highly dusty or homogeneous terrain. These effects will be minimized through topographic correction, calibration routines, and cross-validation with other rover instruments such as spectrometers and cameras [31].

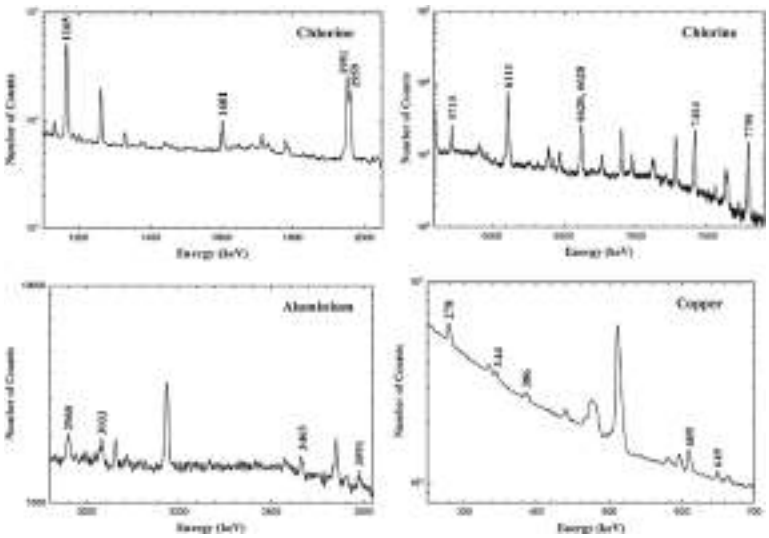

Figure 3.6.7: Gamma Neutron Example Data

The above figure shows the gamma neutron probe's data return as four plotted charts of linear functions of energy rates. This figure above would be familiar to the data returned by the CP-MU DMU-100 probe while it operates on the Martian surface, but the returned images would not be exactly the same for this mission's purposes. Instead of energy (keV) data logged, the graph would showcase the dosage rate (Sv/h) determined from the electric current read by the ionizing gas chamber. This data would present the rate of ionizing radiation that could cause biological damage to a person or object per unit of time. This data is useful for measuring gamma radiation spikes in the range of 1 µSv/h–10 Sv/h during changing Martian environmental factors such as region.

4.0 Mission Risk Management

4.1 Safety and Hazard Overview

With risks as a constant presence in all phases of the design and development of the rover, identifying and analyzing them has been a key objective of the team. Although there were various proposals for identification of risks that included, tracking risks after every deliverable and every month, the team decided on holding weekly meetings where every subteam responsible for the development and design of certain parts of the rover as well as scientists responsible for instrumentation think of risks that are justified. This was done every week and the risk matrix as well as the risk log was updated every time a status change of any risk occurred and it changed to one of the following: research, mitigate or accept, each with its own solid justification that was then explained in the meeting to ensure the risks were not guessed.

As shown in the risk log, certain risks were given priority over the others. The main criteria in deciding this was how critical is this subassembly and if the worst case scenario were to occur, to what extent would this affect the mission, would it entirely lead to mission failure due to no objectives being achieved, would it partially achieve the objectives or would it achieve one objective but not the other. For instance, picking from the advanced risk log, heat pipe failure would be critical as that would mean the rover will not be under nominal operating temperatures which would lead to electronics dying because of the cold martian night and may lead to inefficient data recorded by instrumentation. While the following sections go into much more detail, as an example, this risk was given more priority over other risks such as instrument calibration drift which is a major risk but it does not completely compromise the mission. Instances of one instrument being able to carry out the objectives of the other instrument if it were to fail was also considered. Inspiration for this risk management method was taken from the Lucy mission to Trojan asteroids that had various science instruments that would carry out multiple science objectives in the case of failure.

The spacecraft shall also be kept in a clean room during assembly and integration as well as 2-9 weeks leading up to launch and this is mainly due to planetary protection concerns and to ensure no microbial contamination reaches Mars as per NASA protocol.

4.1.1 Risk Analysis

Every space mission carries unique risks due to the complexity of spacecraft design and operations. The team is committed to identifying and mitigating these risks wherever possible using NASA-defined risk identification and mitigation strategies such as Risk-Informed Decision Making (RIDM) and Continuous Risk Management (CRM). RIDM enables structured, transparent decisions by explicitly weighing risks and uncertainties against mission goals and constraints, while CRM ensures that risks are continually identified, analyzed and managed throughout the project lifecycle.

By team consensus, the most effective methods for identifying risks included thorough Failure Modes and Effects Analysis (FMEA), in-depth Fault Tree Analysis (FTA), and regular expert reviews. To evaluate and prioritize risks, a risk matrix was developed that assesses each risk according to the likelihood of occurrence and the severity of its consequences. The matrix enabled the team to efficiently rank and allocate resources toward the most pressing risks.

The construction of this matrix followed NASA recommendations, customized with data from analogous missions such as the Mars Science Laboratory (Curiosity), the Mars Exploration Rovers (Spirit and Opportunity), and the Mars 2020 Perseverance rover, providing valuable insights from comparable operational environments.

Risk ranking in our project was the result of collaborative technical and non technical discussions among subteams and subteam leads. For each risk, likelihood and consequence ratings were justified using available data,technical analysis, and lessons learned from analogous missions.

The risk analysis approach for this mission is further strengthened by directly integrating RIDM and CRM within the team’s workflow. RIDM ensures that every major decision is weighed, maintaining alignment with overall mission drivers, while CRM ensures these risks are continuously managed and updated as the project moves forward in different phases.

Central to this process is the team’s ongoing development and use of a risk matrix. The risk matrix organizes all identified risks based on their likelihood and the severity of potential consequences. This tool not only drives prioritization for mitigation but is also actively referenced in decision making and design trade-offs. The team developed the matrix using the risks identified in the advanced risk log that is updated every other deliverable.

The information from the risk matrix is integral to mission design and operations, prompting targeted mitigations such as redundancies and contingency planning for high-priority risks. This matrix also frames weekly risk review meetings, where risk

status is tracked, new risks are identified.When certain risks are categorized as “Accepted,” the justification for this acceptance is thoroughly documented to ensure transparency, providing assurance to both internal teams and external stakeholders. In summary, the risk management strategy combines NASA’s RIDM and CRM approaches with proven identification and ranking tools such as FMEA and the risk matrix. At the moment, the team has not accepted any risks and have mainly moved forward with researching and mitigating risks as it pertains to the design of the rover as it is still in the design and development phase.

Subsystem-specific risks and mitigations include the following: due to the presence of sharp, embedded rocks on Mars, there is a risk of wheel skin puncture or grouser breakage, compromising wheel integrity and rover mobility. This risk is mitigated by using thicker wheel treads, adaptive driving algorithms, and regular wheel imaging to monitor and avoid hazardous terrain, as informed by experience from the Mars Exploration Rovers. The rover is also at risk of suspension fatigue, where high mass and frequent traverses could cause loss of shock absorption, increasing risk of failure to traverse rough terrain. Mitigation strategies include the use of robust suspension materials, periodic load analysis, and redundancy in suspension design, drawing on design lessons from the Curiosity rover [102].

Thermal Control Subsystem (TCS) failure, particularly in Mars’s harsh temperatures, could damage electronics. The team has decided to use multilayer insulation (MLI), redundant electric heaters, and real-time thermal monitoring, ensuring backup heaters are available if any were to fail which are approaches validated in previous missions such as Mars Pathfinder and InSight.

Instrumentation risks include dust infiltration addressed by seals, protective covers, and cleaning routines and possible mechanical misalignment or shock damage during landing, mitigated by shock-absorbing mounts and post landing calibration protocols similar to those employed on Mars 2020 Perseverance [102].

Power subsystem failure in the Martian environment could lead to electrical overloading of other subsystems, and ultimately to mission failure. To decrease the likelihood of this occurring, the team has integrated radiation-resistant materials into the design of our subsystem. Using deployable solar panels that are able to angle away from the sun, MLI panels that utilize bandgaps to absorb solar radiation, and engineering with redundancies allows the system to withstand the Martian environment for longer. Lessened radiation on the solar panels, batteries, and distribution units lessens the chances that the systems will degrade to critical levels.

Risk ranking is performed collaboratively across subteams, with each likelihood and consequence rating documented with clear rationale backed by technical analysis,

previous mission experience, and open dialogue between leads. These rankings are not stagnant; they are periodically revisited and updated as the mission evolves or new information is readily available.

In addition to technical risks, the team rigorously manages programmatic risks such as schedule delays, budget uncertainties, and resource constraints that could impact mission success. Drawing on lessons from NASA's Mars Pathfinder mission, a Discovery class mission that faced compressed timelines and strict budget limits, the mitigation plan the team decided on for programmatic risks are strategies like rapid prototyping, parallel subsystem development, and regular milestone reviews, enabling early problem detection and efficient resource reallocation [6]. Scheduling risks are proactively addressed with detailed planning, schedule reserves, and continuous progress monitoring, while budgeting risks are managed via ongoing cost tracking, contingency funding, and early identification of potential funding issues. Other programmatic factors, including supplier reliability and partner coordination, are incorporated into the risk matrix and reviewed regularly, ensuring these non-technical risks receive the same thorough attention and mitigation planning as technical challenges.

Planetary protection is ensured within the P.H.O.E.N.I.X mission as it is imperative to conserve the environment of the planet Mars from any form of external bacteria and microbes. Contamination may interfere with the Martian ecosystem and potentially mislead data collection for future scientific missions, rendering the data inaccurate to the original Martian domain. Furthermore, upholding ethical responsibility on Mars supports the sustainability of future exploration and ensures the protection of any potential life forms that may be present.

To explore responsibly and effectively, sterilization of spacecraft, instrumentation, and crew is carried out to minimize the risk of biological contamination to planetary environments and potential native organisms. Through the mission, contamination control is also guaranteed through various testing that may be conducted promptly, which upholds standards to meet expectations of scientific integrity.

Abiding by the Outer Space Treaty, this mission will respect the guidelines designed to protect celestial bodies for the preservation of their environments and the success of future exploration efforts [103].

With the addition of a self - contained atmospheric sampling instrument as a ride-along payload led to a descope leading to risk management focused solely on physical power and thermal management requirements. This enabled a more targeted identification and mitigation of risks that were strictly within the scope of rover accommodation and system integration.

Mechanically, requirements for the instrument's size, mass, and mounting options called for careful evaluation regarding impacts on the rover's structural integrity, center of mass, and internal volume distribution. This allowed the mechanical team to address potential risks associated with mounting stability, vibration tolerance, and changes to rover balance or mobility, ensuring safe and robust integration while also addressing the requirements for the new ride-along payload.

In terms of power, the new instrument's peak and idle power draws, as well as its sensitivity to voltage fluctuations, introduced electrical integration risks. Risk management efforts for this were centered around ensuring electrical isolation and a regulated power supply to this instrument to prevent voltage instability and interference with other onboard electronics.

The thermal requirements for this instrument presented further risk tied to its survival and operating temperature ranges, especially regarding vulnerability to rapid temperature swings. When externally mounted, the instrument required shielding or active heating, and since the contractor took responsibility for figuring out a thermal management solution, the team's risk management options were limited to verifying compatibility and readiness of the rover's mounting interface.

By clarifying the requirements and mitigating risks, the descope enhanced clarity and reduced liability for risks outside the team's control. This allowed for more robust risk tracking and allowed mitigation plans to remain practical and focused resulting in effective risk management practice.

For plans of decommissioning of the rover, the team identified several critical risks that extend beyond planetary protection and data handling. Additional concerns include potential release of hazardous materials or microplastics from the rover's components, accidental reactivation of hardware systems post mission and incomplete sterilization which will lead to biological contamination. The Martian dust could amplify the spread of this contaminant posing risks to both martian ecology as well as future scientific missions to mars.

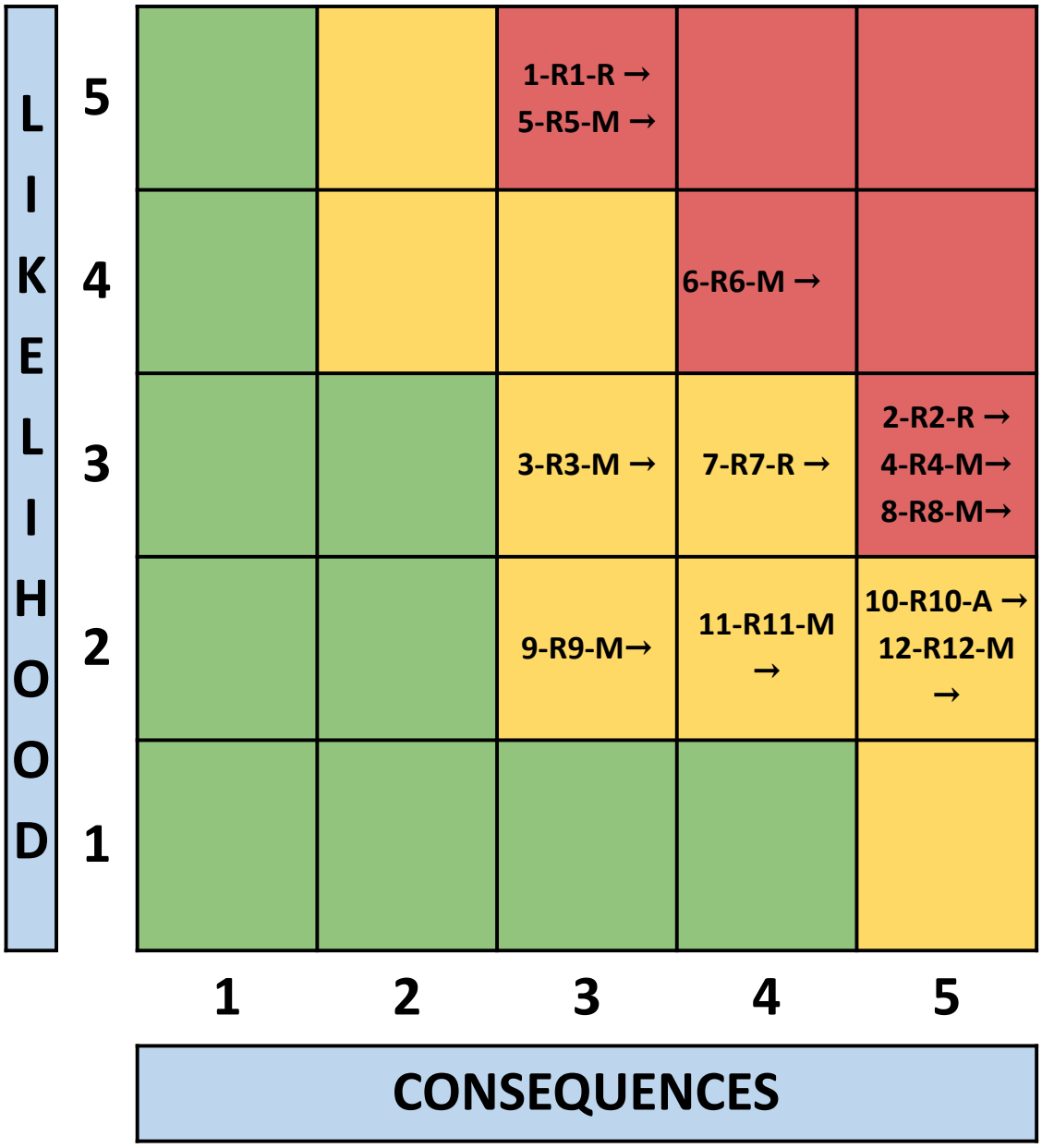

Fig 1.8.2.1 Risk Matrix

Rank	Risk ID #	WBS Element	Risk Owner	Category	Timeframe	Risk Title	Risk Statement	L	C	Rating	Approach	Trend	Mitigation Plans
1	R1	Thermal Payload	Flynn Mendoza	Cost/Scope	Medium Term	Electric heaters failure	Given that extremely low temperatures frequently occur on Mars, there is a possibility that the electric heaters on the rover may malfunction or cease to operate , resulting in an inability to maintain required temperatures for critical subsystems or instruments , thus risking the failure or degradation of performance of these key components of the rover.	5	3	High	Research (R)	→ Neutral	Make use of redundant heaters and seperate circuitry
2	R2	Thermal Payload	Andy Lien	Cost/Scope	Medium Term	Heat Pipe failure	Given that the rover will have to traverse through rough terrain, vibration and oscillation must be taken into account, there is a possibility that the heat pipes in the long-run will have its structural integrity deteriorated which can result in inadequate transfer of heat from one part of the rover to the other part which is critical when it comes to maintaining at required temperatures for other components and instrumentation. This failure can result in the mission being compromised completely if the damage is severe enough.	3	5	High	Research (R)	→ Neutral	Make use of redundant heat pipes.
3	R3	Electrical System	Audrey Sorenmann	Cost/Scope	Medium Term	Reduced power generation from solar panels due to Martian dust	Given that Martian dust can accumulate over time on exposed surfaces , there is a possibility of gradual build-up on the solar panels of the rover, reducing the amount of solar energy received by the power generation system, and consequently limiting the availability of electrical power for performing mission-critical activities.	3	3	Moderate	Mitigate (M)	→ Neutral	Make use of dust removal systems.

4	R4	Electrical System	Asherr Ralph	Cost/Scope	Medium Term	Battery degradation due to Martian temperature fluctuations	Given that Martian temperature fluctuates drastically between day and night, there is a possibility of accelerated battery wear adversely impacting energy storage capacity, which can result in limited rover operation during low-sunlight periods or high-power activities.	3	5	High	Mitigate (M)	→ Neutral	Battery enclosed in Phase Change Material (PCM) thermal enclosure to buffer temperature extremes, survival heaters supplement PCM during extended nights or dust events, and the Battery Management System monitors state-of-charge, temperature, and health.
5	R5	Payload System	Lucia Piedra	Cost/Scope	Short Term	Mini TLS overheating risk	Given that internal heat dissipation and external thermal conditions on Mars can cause localized temperature increases , there is a possibility that the Mini Tunable Laser Spectrometer (Mini TLS) may overheat during extended use or in sun-exposed environments , potentially impairing the instrument's measurement accuracy or causing component damage , thereby compromising atmospheric data collection and scientific mission	5	3	High	Mitigate (M)	→ Neutral	Only run instrument at temperature between -10 C up to 20 C

							objectives						
6	R6	Payload System	Anna Hulett	Cost/Scope	Short Term	RLS laser induced sample ignition	Given that the 785-nm laser used in the Raman Laser Spectrometer can deliver enough thermal damage or ignite certain materials, there is a possibility of initiating degradation of samples, triggering hazardous reactions with flammable, and explosive compounds adversely impacting the preservation of scientific evidence and the safety of the payload system, which can result in loss of data integrity, contamination of the instrument, and increased mission risk.	4	4	High	Mitigate (M)	→ Neutral	If applicable, use a lower power laser setting and avoid direct exposure of dark/unknown energetic materials
7	R7	Payload System	Anna Hulett	Cost/Scope	Medium Term	Window contamination from Martian Dust	Given that fine Martian dust particles are easily carried by wind and can settle on the RLS fused quartz optical window during operations, there is a possibility of reduced laser transmission and signal collection efficiency adversely impacting the instrument’s ability to obtain accurate Raman spectra, which can result in degraded data quality and the need for repeated measurements that consume mission resources.	3	4	High	Mitigate (M)	→ Neutral	Apply an durable, scratch resistant, anti-reflective coating to the fused quartz optical window to reduce reflection and abrasion by Martian dust.

Figure 4.1.1.1 Advanced Risk log

4.1.2 Failure Mode and Effect Analysis (FMEA)

FMEA is a structured risk assessment tool the team made use of to identify and evaluate potential failure modes within a system. It involves systematically examining components, subsystems or processes to predict how and where failures might occur, what their consequences could be and how severe their impacts could be. The goal of this analysis was to prioritize these potential failures based on their likelihood and seriousness, enabling the team to implement targeted actions to reduce or mitigate the most critical risks.

To help quantify risk, FMEA assigns three scores: severity (impact of the failure), occurrence (likelihood of happening), and detection (likelihood of the failure being discovered before it affects the mission). The product of these values yields a Risk Priority Number (RPN), which allows the team to rank risks and focus on these most critical to mission success.

THE FMEA not only highlights potential vulnerabilities but also directly informs our design and safety planning process. By ranking risks, the team can determine where redundancy is most needed, which subsystems require additional testing, and whether design modifications are justified before advancing to later phases. During operations, the FMEA further serves as a safety tool by identifying key failure points, ensuring contingency procedures are in place, and guiding mission operators in rapid anomaly response planning.

The Severity, Occurrence, and Detection values were determined through team discussions, drawing on lessons learned from prior missions such as Lucy mission to Trojan asteroids and Mars Perseverance [51],[67]. While some rankings are qualitative, they are grounded in aerospace industry risk assessment practices and aligned with NASA and SAE FMEA guidelines.

Should a loss of drive or steering capabilities occur, the mission would likely be compromised depending on the severity. In the worst case scenario significant mobility loss on the rover can lead to possibly getting stuck in one location. Most likely only one failure would occur, still compromising mobility, possibly limiting locations the rover could navigate to, and impact the speed with which the rover can navigate to new places. In such a case backups and manual steering would be implemented. Manual steering, if necessary, would require more man power and resources to perform this manual maneuvering, and introduces human error.

In regards to MLI degradation, the effects this would have on the mission should be minimal since the end of life conditions for the MLI will be taken into account in the calculations. As it degrades more power and resources will be required to maintain the

rover in its operational temperature, but that has been built into the design. In the worst scenario, debris could rip the MLI during a sandstorm, although unlikely, this will likely decrease the lifespan of the rover as the MLI would degrade to a less functional state than accounted for in the end of life calculations.

In the case of thermal sensor failure, this would compromise the science by compromising the ability to monitor the temperature of each instrument. Increasing the risk of failure for each of these instruments. Because of built in redundancies, failure of one should not compromise the thermal control system, since because of the redundant heat sensors the interior of the rover will be kept in the general operational range. On an instrument by instrument basis the risk is still minimal since there will be two sensors monitoring each instrument. Were multiple failures to occur at once though, likely from a power failure, to a degree where the redundancy does not help, the mission would likely be compromised as a whole. While the TCS could continue operating, without knowing exactly what temperatures P.H.O.E.N.I.X is operating at, the use of guesswork would exponentially increase the risk of overheating or getting too cold.

Regarding the CP-MU DMU-100 freeze risk, were this to occur despite the mitigation strategies, part of the science of the mission would be compromised and would be unable to be finished. P.H.O.E.N.I.X would have to return the data it collected before failure from that instrument.

Now considering loss of battery capacity, the effects on the mission would be catastrophic were multiple failures to occur. Power would be lost, rendering P.H.O.E.N.I.X inoperable. The rover would be kept operational as long as possible to collect and transmit as much data as possible, shutting down non critical systems to accomplish this. In the case of one battery failing to recharge or losing capacity power would begin using a second backup battery, at worst risking a reduced efficiency.

When considering the risk of electrical shortages in power distribution, it is important to consider in which subsystem the loss of power were to occur. Were it to stop providing power to the TCS during a cold night, there runs a risk of damage to the circuitry before system recovery can occur. Were the loss of power to happen to the science instruments, data would possibly be lost but recovery would be able restore the system later and recovery operability.

If the power generation from the solar panels were to be reduced from dust accumulation or something similar, that would result in the rover having to switch to a low power mode, reducing the efficiency of all systems, while dust removal measures are employed. At worst this would result in total power loss and the loss of the mission.

Were a process failure in the CDH subsystem to happen, communication abilities with the rover would be lost, rendering it inoperable. For this reason a redundant OBC is

implemented, so if failure in one happens the rover can switch to the backup system. Total mission loss would only occur if both failed.

ID	Function	Failure Mode	Effects	Sev	Cause	Occ	Prevention	Det	RPN	Actions	Approach
2	Mechanical Subsystem	Suspension fatigue	Loss of shock absorption, increased risk of mechanical failure	3	High mass and frequent traverses	2	Robust suspension materials, periodic load analysis, redundancy	7	42	Reducing speed and avoiding rough terrain can help slow further fatigue.	Research
3		Loss of drive or steering calculator	Reduced mobility, inability to steer or drive one or more wheels	7	Hardware or cable failure, wear over time.	3	Redundant actuators, regular actuator health checks.	4	84	Switching to backup or manual control is the most logical step.	Mitigate
4		Loss of shock absorption capability	Increased transmission of shocks to chassis and instruments	3	Material fatigue, extreme temperature cycling.	3	Use of advanced materials (e.g., shape memory alloys), regular health monitoring.	5	45	Rough terrain should be avoided if this failure persists	Mitigate
5	Thermal Subsystem	Heat Pipe failure	Loss of thermal regulation, risk of overheating or freezing	8	Faulty manufacturing, extreme pressure changes	1	Redundant heat pipes, redundant thermal control systems in the form of heaters	3	24	Rely on electric heaters, plan for alternate cooling systems	Mitigate
6		Multi-layer insulation (MLI) degrades over time.	Increased heat loss, reduced thermal protection.	7	Micrometeoroid impacts, material aging, radiation	3	Use of high-durability MLI, periodic thermal performance checks.	3	63	Operate rover primarily during warm periods away from areas of high radiation	Research
8		Thermal sensor Failure	Loss of thermal monitoring, risk a system failure is not reported	7	Material aging, overheating, electric	1	Redundant sensors, separate circuitry	6	42	Rely on redundant sensors, develop a software recovery plan	Mitigate

					failure						
9	Payload Subsystem	RIMFAX signal attenuation	reduce the depth it penetrates and degrade the signal-to-noise ratio	2	Materials like clays or ice-dust mixture which absorb and scatter radar energy	3	Running at its low end frequency of 150-1200 MHz band as low frequencies penetrate better	1	6	Reduce depth objective to 2 m - 4m for clear data and schedule multiple low frequency soundings	Research
10		RLS calibration drift	calibration change throughout image collection	3	temperature swings disrupt calibration due to temperature sensitivity	3	calibration verification before and after each science run	1	9	heating samples to 935 K and cooling them down to 120 K to reserve fully calibrated quantitative measurements for high temperature, and qualitative data for lower temperature	Mitigate
13	Power Subsystem	Loss of battery capacity or failure to recharge	Reduced operational time, possible mission loss.	9	Repeated charge/discharge cycles, extreme temperatures.	5	Battery health monitoring, thermal management, redundant batteries.	5	225	Utilize second battery. If second battery is also inoperable, begin powering down noncritical systems to reduce power load	Mitigate
14		Electrical short in power distribution	Loss of power to subsystems, reduced redundancy.	8	Dust, material degradation, component failure.	4	Robust insulation, regular voltage monitoring.	6	192	Shut down the system and reboot, if the issue persists then continue to monitor. Perform analysis on systems to ensure they remain within operational capacity.	Mitigate
15		Reduced power generation from solar	Insufficient power for operations	7	Dust accumulation, mechanical damage.	7	Dust removal systems.	3	147	Reduce subsystem power usage to redirect remaining power to critical systems. If transmission is impossible, store data for potential future collection	Mitigate

		panels									
16		Drift in transistors not allowing them to turn on/off	Loss of signals for power distribution	5	Radiation ionizing deposits within technological components	7	Shielding systems, radiation-hardened materials in manufacturing	3	105	Perform maneuvers to shield components from further damage, reduce operation of damaged systems, continue to monitor	Mitigate
17	CDH Subsystem	Processor failure	Loss of command/control, mission halt	10	Hardware defect, radiation, overheating	4	Use radiation-hardened processors, implement thermal control, redundant processors	8	320	Physical Redundancy by having two OBCs	Mitigate
18		Memory corruption	Loss of stored data, erratic behavior	2	Radiation, aging	8	Use ECC memory, regular memory scrubbing, software validation	3	48	Offboard system cleansing processes, rad-hard memory units	Research
19		Data uplink/downlink loss	Loss of communication with ground, inability to send/receive commands	2	Antenna failure, RF interference, ground station issue	8	Antenna redundancy, RF shielding, multiple ground stations	4	64	Autonomous sourcefinding recovery behavior	Research
20		Command errors	Incorrect commands executed, potential for unsafe actions	8	Software bug, memory corruption	4	Command validation, memory error detection, queue integrity checks	2	64	Increase detection using verification codes	Research

Figure 4.1.2.1: FMEA Table

4.1.3 Personnel Hazards and Mitigations

Notable hazards during the rover’s manufacturing process include injury from cutting, grinding, or drilling. Since components like the chassis and rocker-bogie mechanism are made from titanium and aluminum, machining is required. This poses risks such as lacerations, amputations, and injury from flying debris. To reduce this risk, all personnel will undergo safety training per NASA and OSHA standards [87, 88], use appropriate PPE including safety glasses, long pants, steel-toed shoes, respirators, gloves, and face shields. and operate machinery with proper guarding in designated areas.

Going along with the hazard of machining metals, a related personnel safety hazard is sharp edges on metal surfaces [20]. Machined parts typically have sharp edges, ridges, and burrs that can cause cuts or abrasions. This will be mitigated by making deburring tools readily available and using them immediately after any cutting, grinding, or drilling, as well as sectioning off working areas from walkways [89].

Another risk to personnel safety during the manufacturing process is crushing or pinching [93]. There are many heavy components of the rover that need to be manually lifted and integrated, for example the solar panels and battery systems. If not handled properly, the weight of these components could crush or pinch personnel and cause serious injuries. To mitigate this risk, personnel in contact with heavy components will complete proper heavy machinery training, utilize cranes whenever it is necessary to lift a heavy component, wear proper PPE when working with heavy components, and employ clear team communication and coordination to avoid any potential crushing or pinching [93].

In parallel with the risk of crushing and pinching is the risk of falling objects. Since heavy components are present in this design, they could fall and injure personnel if not secured properly [89]. To mitigate this risk, proper precautions will be taken while moving heavy objects, including but not limited to securing items with straps and supports, utilizing safety nets and protection when possible or applicable, and taking steps making sure components are always secure and before and during integration [80].

An additional risk associated with the heavy components of the rover is manual handling injuries. If proper technique is not used to lift heavy components, joint strain or muscle injuries could occur [91]. To mitigate this risk, personnel will complete training for and utilize cranes and hoists when applicable in addition to implementing manual lifting techniques [91].

In any high stakes work environment where personnel are tasked with large and meaningful responsibilities, the risk of psychological hazards (such as mental illness and fatigue/burnout) will be present [93]. To mitigate this risk, personnel will complete training in mental illness and suicide prevention, team leads and managers will create community through bimonthly team building events, and personnel will not be permitted to work more than 40 hours in one week or more than 4 hours consecutively without breaks [93].

Manufacturing risks and hazards are present in all phases of the design process. Another example applicable to the P.H.O.E.N.I.X rover is the risk of electrical shock. The rover's power system including the battery and electronics include many high voltage components, and improper handling during integration or testing could lead to electrical shock [90]. To mitigate this risk, personnel in contact with these hazards will complete the required training to interact with these components. Workers shall utilize proper PPE including rubber soled shoes, insulating gloves, and insulated tools, as well as ensure proper grounding and de-energize systems during assembly to follow safe electricity protocols such as LOTO [90].

Another electrical hazard that is present is the risk of arc flash. If the rover's power systems are incorrectly wired or short circuited, then it could release large amounts of light and heat in the form of arc flash [89]. To mitigate this risk, arc flash analysis will be conducted on the rover's power systems, personnel will wear PPE for arc flash scenarios when working on electrical systems including flame resistant clothing, safety goggles, and face shields, additionally fire extinguishers will be readily available, and safety protocols like LOTO shall be followed by performing routine checks of the system [89]. These mitigation techniques will accurately cover the potential hazard of a fire during manufacture.

One more type of hazard to be addressed is chemical hazards. When working with paints, adhesives, solvents, and batteries (composed of chemicals that could potentially lead to leaks), it's important to take the correct precautions to minimize risk to personnel [87]. To mitigate this risk, there will be proper ventilation in work areas, fume hoods will be used when dealing with toxic chemicals, PPE will be worn including respirators and chemical resistant gloves, additionally chemical emergency stations will be available throughout the lab slash manufacturing area including eye showers, chemical showers [87]

5.0 Activity Plan

5.1 Project Management Approach

For a NASA Discover-Class mission team sized between thirty and fifty personnel, the project's leadership and organizational structure is critical for team efficiency and mission effectiveness. At the top of the organizational chart, the Project Manager (PM) assumes responsibility for overall mission execution. They also possess authority over technical, programmatic, and personnel decisions. The Deputy Project Manager of Resources (DPMR) serves as the PM's primary support, overseeing daily operations and acting as the PM when necessary. Resources and project controls, including budgeting, major scheduling milestones, and compliance, fall under the DPMR. The DPMR directly oversees the programmatic team, however works in close coordination with both technical subteams.

Figure 5.1.1: Teamwide Organizational Chart

The team has decided to move forward with ten engineers per subteam. These engineers will serve to draft technical documentation, oversee contractors during manufacturing, ensure proper integration and testing. Additionally, each subteam shall consist of five technicians, a quality assurance specialist. The team has also decided to move forward with a Verification and Validation (V&V) team that will consist of ten personnel responsible for verifying requirements across each Engineering subteam and

scientific instrumentation. The V&V team will ensure the system shall meet specifications and shall serve mission needs. Each scientific instrument shall also have its own subteam, after a detailed review with the Chief scientist, the team decided there will be five scientists per instrument each having its own technician and a quality assurance specialist. Figure 1.6.1 represents the team-wide organizational structure that includes every personnel responsible for the success of this mission.

All subsystem leads including those for mechanical, thermal, CDH, electrical and payload systems will report directly to the Lead Systems Engineer. This chain of command ensures successful integration and coordination across all engineering disciplines, reducing the risk of technical misalignment. The programmatic team encompasses finance, scheduling, and documentation roles, and reports to the DPMR. Specialized teams including Quality Assurance (QA), Verification & Validation (V&V), Integration & Test, and Risk Management report to each subteam lead.

The programmatic team’s responsibilities include scheduling and budgeting, to ensure the mission maintains its budget and schedule. One financial analyst shall manage real time budget tracking, allocation, and report generation. Scheduling is managed by a dedicated scheduler or scheduling team, which maintains the integrated gantt chart created by programmatics and coordinates all project milestones and deadlines. Documentation and configuration management are also vital, handled by at least one specialist who is responsible for maintaining design change logs, requirements traceability, and version control across all project documentation which ensures clarity and accountability.

Beyond the core and academy teams, technical and specialized subteams are essential. The main engineering disciplines such as systems, mechanical, thermal, electrical/avionics, power systems, and structures/mechanisms are each represented as teams supporting the Systems Engineering Lead. Dedicated teams within each discipline are responsible for handling Integration & Test, V&V, Quality Assurance, and Risk Management. In addition, a Database Management Team is in place to handle the large quantities of mission telemetry, design files, and test data which will consist of 3 personnel.

Outreach and engagement are critical both for public awareness and education. Those responsibilities are organized under an Outreach & Communications team, which may include roles such as Communications Specialist, STEM Education Lead, Outreach and Engagement Coordinator, and Social Media Specialist. This team manages the mission’s public profile, including website updates, press releases, social campaigns, and educational resources for the STEM community and broader public. This approach was inspired by the Lucy mission to the trojan asteroids where the mission concept academy (MCA) and NASA proposal Writing and Evaluation

Experience (NPWEE) both act as outreach for the Lucy Mission, each having their own outreach & communications team that post frequently on social media platforms such as Instagram and platforms such as Linkedin, making the public aware of the Lucy mission [33].

Within this framework, budgetary authority is carefully distributed. Subsystem and team leads receive dedicated budgets from the DPMR, with autonomy restricted to mission-related expenses such as design, build, testing, and training. Non-mission team expenses such as morale events, team meals, or family days may be authorized up to a pre-defined cap, typically ranging from five hundred to fifteen hundred dollars per team annually for the core academy team. Minor, routine purchases can proceed within this cap, while any single expense over a defined threshold (such as $250) requires secondary approval from the PM or DPMR. This structure maintains fiscal responsibility while supporting flexibility at the team level. Technical, process, and purchasing decisions are permitted within budgetary boundaries, but any changes impacting system performance, cross-team integration, or major requirements require higher-level approval from the PM or DPM.

Every subteam is explicitly represented as a distinct branch in the organizational chart. This mirrors the structure of successful missions such as the Mars Pathfinder and supports close coordination across technical and programmatic teams.

Finally, this management strategy draws directly on NASA Discovery-class precedent. Strong discipline leads, clear separation between technical and support teams, integration of QA and V&V, explicit configuration management, and defined budgetary oversight have been repeatedly validated as best practice by missions such as Mars Pathfinder and InSight. Adopting and adapting these structures ensures your mission is set up for technical, financial, and public success.

5.2 Mission Schedule

5.2.1 Schedule Basis of Estimate

This Basis of Estimate outlines the foundational rules, assumptions, and relevant scheduling factors that influence the P.H.O.E.N.I.X mission. This estimate was developed as a result of detailed analysis and collaborative schedule development. Following a typical NASA lifecycle project management framework, this Basis of Estimate encompasses mission phases C through F, and is structured to ensure successful execution of all required system developments. Additionally, this schedule allows for testing and subsystem integration development. This BoE establishes the basic and strategic rationale that serves as the backbone of the planning content, and the expectations provided to the team regarding the timing and progress expected.

The mission schedule is organized into standard NASA phases: Phase C (Final Design and Fabrication), Phase D (System Assembly, Integration and Test, and Launch), Phase E (Operations and Sustainment), and Phase F (Closeout) [78]. The duration of each phase is based on historical analogs including the Mars Pathfinder, Mars Exploration Rover (MER), and InSight missions [73]. These timelines, however, were not directly copied for P.H.O.E.N.I.X's needs, as adjustments were made to account for the unique science and payload requirements. The scope, and risks associated with our mission were also taken into account while creating this schedule. While InSight faced notable schedule delays and launch window shifts, P.H.O.E.N.I.X cannot afford the same leniency due to a more constrained mission profile, limited contingency funds, and increasing scrutiny over Class C and D mission performance. Thus, the team adopted a conservative approach to schedule allocation, including appropriate schedule margin of 3 months ahead of a 27 months mission, and streamlined system integration after 14 months.

The ground rules for this schedule assume uninterrupted funding profiles and adequate workforce availability throughout all phases of this mission. Furthermore, the project assumes timely delivery of all long-lead components, including the high-priority thermal and CDH hardware, which are pivotal to maintaining downstream integration timelines. These assumptions are made in concert with procurement timelines for commercial vendors such as AZUR Space, Boeing, Blue Origin, and projected government procurement cycles. The mission architecture is not reliant on novel launch vehicle technology, aiding the mission in avoiding potential schedule disruption.

Key underlying assumptions of this estimate also include baseline performance from suppliers, historical integration duration trends, and NASA-mandated milestone reviews. Phase C is estimated to last approximately 30 months and includes final subsystem-level design freeze, initial manufacturing, and Engineering Test Units

(ETUs). Phase D will span approximately 18 months, encompassing integration, system-level testing, environmental qualification, pre-ship reviews, and launch readiness verification. This includes a minimum 45-day Launch Campaign period at the launch site leading up to the fixed December 1, 2029 launch date. In Phase E, the team assumes a 12-month primary operations period post-launch, supported by an extended operations plan that does not impact the original budget or resource allocations. Phase F, the shortest, covers the demobilization of operations infrastructure and archiving of mission data, scheduled over four months.

Scheduling includes approximately 8–12 weeks of critical path margin embedded throughout the integration and test flow. This margin is intended to buffer high-risk activities such as integrated environmental testing, propulsion system leak checks, and end-to-end functional testing of the science payload. The incorporation of slack in non-critical paths such as testbed development or training timelines—further supports the project's ability to absorb minor technical delays without affecting the overall launch window.

As the mission progresses, key personnel will be required to travel to a number of sites. Travel prior to launch will largely consist of team leadership conducting on-site progress inspections during each phase along with flying to present at critical mission milestones before a standing review board (SRB). Milestones requiring travel can be seen in Table 1.8.3.1. Inspections are conducted twice a year at minimum but key personnel may be on-site longer. Any type of major travel is assumed to be no less than five days, with a two day buffer to account for any travel delays scheduled in around the event that necessitated the travel. This margin can be seen in Figure 5.2.2.1 where five days are allotted to leadership presenting the CDR. Aside from testing and oversight, a streamlined two-person outreach team is assumed to have an event requiring quarterly travel.

Further assumptions are made regarding the additional personnel needed for each stage. While the exact composition varies depending on the mission phase, all necessary personnel will be onboarded at the beginning of Phase C, the phase that requires the most extra staff. Onboarding is assumed to be completed within a month and is projected to begin following the satisfaction KDP C parameters on the first day of FY 26. Shifts are assumed to be single unless absolutely necessary. This scenario could arise in phases C or D where the high number of personnel may not allow for the mission to remain on schedule unless double shifts are implemented; however, this hypothetical is unlikely to occur given the number of personnel, reflected in Table 5.3.3.1. The schedule assumes no major furloughs throughout the mission, but the additional margin in phases C and D, where personnel are most needed, covers any short-term work stoppages from center closures, furloughs, or government shutdowns.

Outreach for the mission is assumed to largely be handled by the dedicated outreach personnel along with occasional leadership appearances. Personnel are responsible for the implementation and maintenance of a website dedicated to raising public awareness and support for the mission alongside being the primary coordinators and facilitators of major outreach activities. Leadership appearances are assumed if and only if no other testing or presenting obligations are present and are scheduled to be no closer than one week away from a milestone as to not detract from the overall mission's focus. Outreach efforts will increase prior to launch with dedicated time for leadership to host any priority or special on-site visits.

Schedule drivers for the mission are predominantly technical. The integration of the spacecraft's payload suite, which includes multiple high-instrumentation packages with varying heritage, imposes significant alignment and verification requirements. To mitigate the risk of schedule bottlenecks, early integration and testing of Engineering Development Units (EDUs) are planned. Another major driver is the thermal and power subsystem verification campaign. Because of its tailored architecture and compact design, this subsystem requires extensive functional and thermal vacuum testing under full system loads. Launch window constraints, tied to orbital mechanics and planetary alignment, further reinforce the inflexibility of the final launch readiness date.

5.2.2 Mission Schedule

Phase C of the mission, spanning 30 months starting at the beginning of FY 26, is responsible for the finalization of the design and fabrication [77]. The phase can largely be split into two subphases–pre and post CDR–based on the CDR acting as a gate for acquisitions.

Prior to presenting the CDR, the first subphase will focus on satisfying requirements for KDP C, onboarding additional personnel to assist with future tasks, and finalizing designs at the subsystem and system level [77]. Additionally, risks to the mission are continually monitored and plans regarding verification and validation are drafted. CDRs at a subsystem-level are performed leading up to the system wide CDR presented to the SRB [81]. As no copies of systems are needed, a Production Readiness Review (PRR) is not necessary [77]. A timeline of these events can be seen in Figure 5.2.2.1, the gantt chart snippet for the subphase which details the task, its duration, and who it is assigned to. A month of schedule margin allows for ample time to compensate for delays with potential subphase risks regarding onboarding or finalizing designs.

Following the CDR, the mission shifts into the second subphase, C2, which encompasses acquisitions, fabrication, and testing at a subsystem level [77]. Figure 5.2.2.2 shows the schedule for the subphase. Following acquisitions and the finalization of technical documentation, the remaining tasks are largely dominated by the remaining tasks needed to satisfy the SIR, such as subsystem fabrication and testing or plans for integration alongside verification and validation [81]. Due to the enhanced level of risk associated with fabrication, a larger schedule margin of two months prior to SIR presentation is in place to cover any mishaps that may occur.

The timeline for the larger phase is in line with previous missions such as Pathfinder which cleared KDP C in July of 1993, passed CDR in September 1994, and began system assembly in June of 1995 [2]. Similarly, InSight passed its CDR in mid-May 2014 before entering integration and testing at the end of May 2015 [39, 42]. Although differing in mission architecture and scope, both Pathfinder and InSight provide valuable baselines for establishing a timeline for phase C as a whole. Adjustments applied based on instrumentation lead time alongside differences in scope allow these historical analogs to be relevant to the mission. Schedule estimations can be seen in Appendix Figures A.32-A35 for each instrument. Based on these missions, there exists precedent for the timing of the subphases.

Transitioning into phase D, which begins with its respective KDP, the mission now focuses on full system assembly, integration and testing, and launch [77]. Phase D

for this mission is split into four subphases which align with their own respective deliverables across a total of 18 months beginning April 1, 2028.

Subphase 1 entails the integration of subsystems alongside the third party science payload added in a previous descope. Verification and validation of subsystems alongside testing under environmental conditions representative of the mission occur prior to the start of system-level assembly. Testing durations are derived from historical data and are scheduled as the upper bound to add margin in this crucial phase .System level assembly spans across subphases D1 and D2 due to complexity and lead times, meaning that it will not be completed by the deadline for the SAR. Four months is allotted for subsystem integration to ensure that enough time remains in the phase to conduct qualification testing to satisfy SAR criteria [77]. Risks remain tracked throughout the process leading up to the composition of the SAR documentation at the end of calendar year 2028. Should any issues occur, a schedule margin in line with protocol of a month, or a little over 13 percent of the total phase duration, exists to cover high risk obstacles posed by factors such as the third part science payload. Delays with a third-party instrument endangered the continuation of the InSight mission, and if a similar case would occur with P.H.O.E.N.I.X, it is likely the mission would be canceled [23] Further descriptions and durations can be seen in Figure 5.2.2.3, the gantt chart for the section.

Subphase 2 concerns system-wide testing alongside the verification and validation process once the system is fully assembled two months after the start of the phase [77]. In addition to resolving any outstanding issues with verification and validation, crucial tasks required for the ORR regarding the operations handbook are baselined [69]. Testing is scheduled to conclude at the end of March 2029, as seen in Figure 5.2.2.4, the subphase gantt chart. This duration allows for the rest of the phase to entirely be focused on troubleshooting alongside providing ample time for the ORR documentation to be ready prior to traveling to present in front of the SRB [77]. In the event of unresolved problems, a larger margin of a month leading into the beginning of travel for the ORR is in place. While larger than the typical 15% upper bound for margin, the possibility of delay or mishap in assembly or testing justifies this departure from the norm [81, 23].

Subphase 3 covers the final three months the team has before delivering the rover for integration with the launch vehicle and EDL on October 1, 2029 [81, 45]. Activities are largely centered on preparation to satisfy FRR requirements prior to hand off alongside outreach efforts prior to launch [81]. Outreach as a general task spans across subphases D3 and D4 as the mission proceeds towards launch. When transferred over, the rover should have proven interface functionality alongside established supporting elements [57]. A margin of one month, which can be seen in

Figure 5.2.2.5, ensures everything is proven functional and up to standards before transfer and ample time to correct any last minute issues.

Subphase 4 is the period of time following platform transfer for launch vehicle integration and ultimately culminates in launch [77]. Team efforts switch to composing the FRR alongside supporting broader integration efforts regarding the launch vehicle [99]. Upon successful completion of the FRR and passage of KDP E, the vehicle is cleared for mission launch [96]. The entirety of the core team will travel to the launch site in Florida to attend the launch, as reflected in Figure 5.2.2.6, the subphase's gantt chart. Of note is the lack of margin for the subphase. This is due to the travel time and outreach overlapping with the launch date [72].

Phase D margins and time estimations are derived from previous missions of Spirit and Opportunity alongside Pathfinder [73, 8]. Adjusting for lead time alongside accounting for integration challenges with the third party science payload justifies the larger proportional margin allotment for each subphase.

Phase E accounts for cruise alongside EDL, seen in detail in Figure 5.2.2.7, and surface operations up to end of mission, displayed in Figure 5.2.2.8. The phase lasts for approximately 21 months following the December 1, 2029 launch date. Assuming a Homann transfer is used, an average travel time is around 9 months which places EDL on September 1, 2030. [100]. During cruise, tasks focus on ensuring all necessary steps are taken to satisfy the CERR [9]. A PLAR is also conducted within a month after the launch date. Engineers and scientists will monitor the rover upon landing as it initializes instrumentation and surface operations before navigating to target sites. The science instrumentation used on the rover is slated to at a minimum deliver trustworthy data from the surface of Mars for at least a year based on analysis from the team's scientists and engineers. Per Figure CONOPS, all critical mission data will be acquired by T+135 days, and schedule margin exists from that date to the mission close at T+365. During this margin, the team can apply for mission extensions if warranted. Plans regarding decommission & archiving are finalized going into the end of the mission and a DR is submitted [77].

Phase F consists of mission closeout alongside archiving data and documenting lessons learned [96]. The phase begins on the first of September, 2031 and will be complete by the end of the calendar year. After satisfying KDP F, both engineering and science data is gathered in preparation for archiving seen in Figure 5.2.2.9. The DRR is drafted and submitted prior to assets either being disposed of or returned to their respective facilities. Final documentation regarding the mission, its data, and lessons learned is baselined. Once finished with final documentation, the mission holds a final debrief by the end of December of 2031, as reflected in Figure 5.2.2.10.

Figure 5.2.2.1: Gantt Chart for Phase C1

Figure 5.2.2.2: Gantt Chart for Phase C2

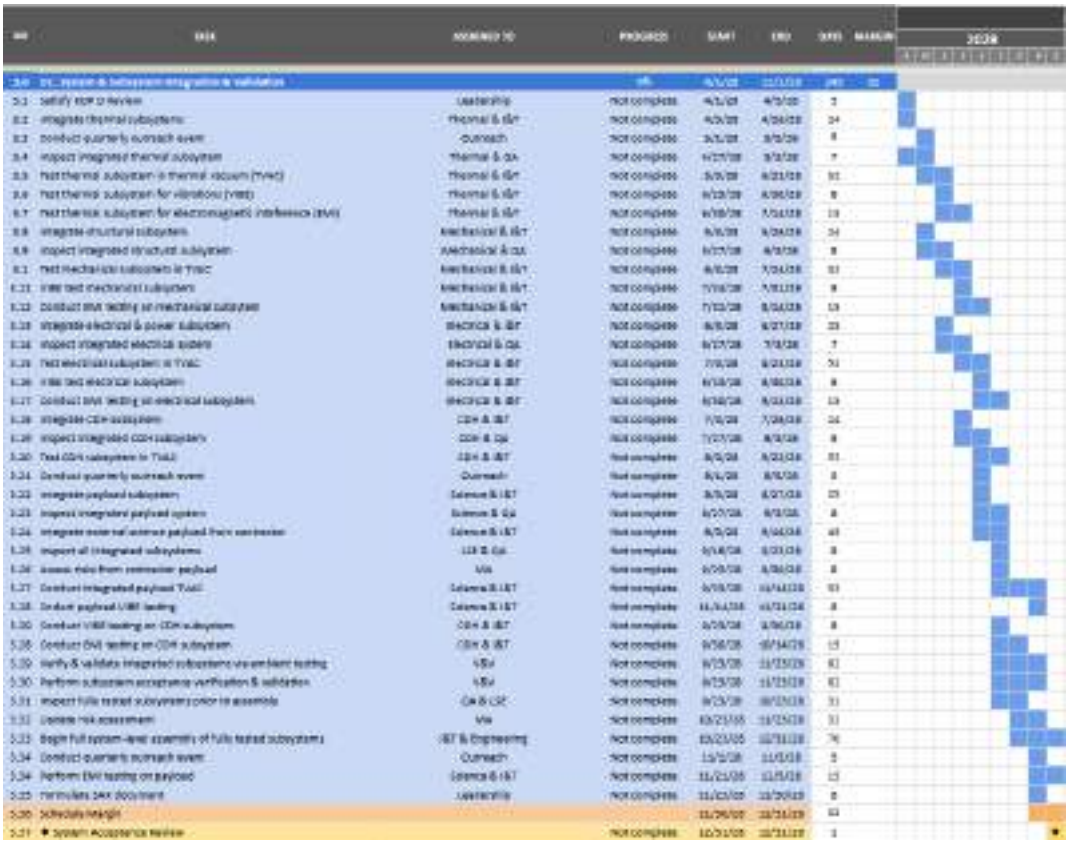

Figure 5.2.2.3: Gantt Chart for Phase D1

ID#	TASK	ASSIGNED TO	PROGRESS	START	END	DAYS	MARGIN
4.0	D2: System-Wide Testing & Validation & Verification		0%	1/1/29	6/30/29	181	32
4.1	Inspect all subsystems for QA post testing	QA	Not complete	1/1/29	1/15/29	15	
4.2	Assemble tested subsystems into system	Science, Engineering & I&T	Not complete	1/1/29	3/1/29	60	
4.3	Conduct quarterly outreach event	Outreach	Not complete	2/1/29	2/5/29	5	
4.4	Test software functionality across entire system	CDH	Not complete	3/1/29	3/15/29	15	
4.5	Update risks based on subsystem testing results	MA	Not complete	3/1/29	3/15/29	15	
4.6	Perform verification & validation tests for full system	Engineering V&V	Not complete	3/1/29	4/1/29	32	
4.7	Test assembled system in TVAC	Engineering & I&T	Not complete	3/1/29	4/22/29	53	
4.8	Assess verification & validation results	Science, Engineering, V&V	Not complete	4/1/29	4/15/29	15	
4.9	Conduct system-wide EMI test	Engineering & I&T	Not complete	4/22/29	5/6/29	15	
4.10	Perform WBE testing of system	Engineering & I&T	Not complete	5/6/29	5/13/29	8	
4.11	Inspect system after testing	QA	Not complete	5/13/29	5/20/29	8	
4.12	Resolve outstanding issues from testing	Engineering	Not complete	4/22/29	5/18/29	27	
4.13	Conduct quarterly outreach event	Outreach	Not complete	5/1/29	5/5/29		
4.14	Resolve outstanding verification & validation issues	Science, Engineering, V&V	Not complete	4/1/29	5/18/29	48	
4.15	Update mission risks post full system testing	MA	Not complete	5/13/29	5/20/29	8	
4.16	Archive verification & validation documentation	V&V & Database Management	Not complete	5/18/29	5/25/29	8	
4.17	Baseline operations handbook	All	Not complete	5/11/29	5/25/29	15	
4.18	Draft operation plans	All	Not complete	5/11/29	5/25/29	15	
4.19	Formulate ORR document	Leadership	Not complete	5/18/29	5/25/29	8	
4.20	Schedule Margin			5/25/29	6/25/29	32	
4.21	◆ Operational Readiness Review		Not complete	6/25/29	6/30/29	0	

Figure 5.2.2.4: Gantt Chart for Phase D2

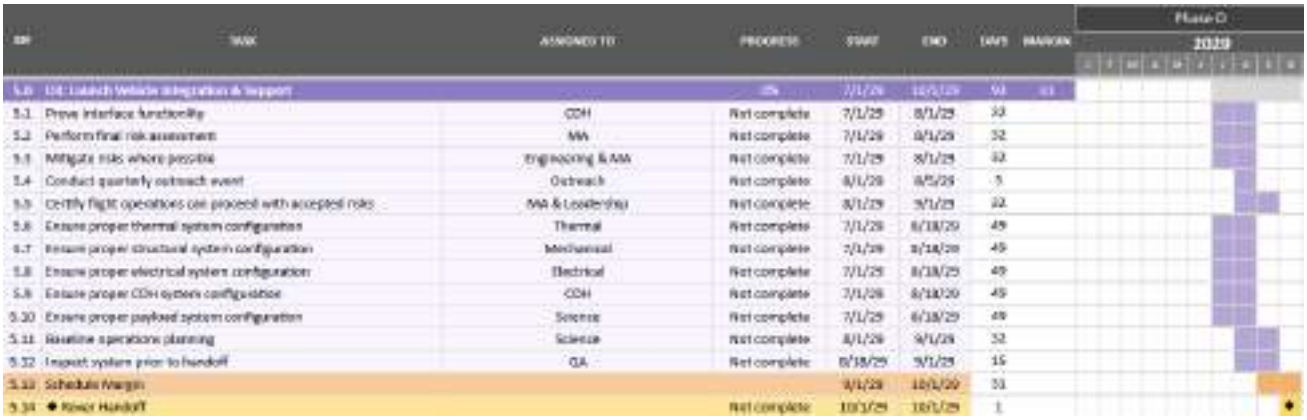

ID	Task	Assigned To	Progress	Start	End	Days	Margin
5.0	D4: Launch Vehicle Integration & Support		0%	7/1/29	10/1/29	93	11
5.1	Prove interface functionality	CDH	Not complete	7/1/29	8/1/29	33	
5.2	Perform final risk assessment	MA	Not complete	7/1/29	8/1/29	32	
5.3	Mitigate risks where possible	Engineering & MA	Not complete	7/1/29	8/1/29	32	
5.4	Conduct quarterly outreach event	Outreach	Not complete	8/1/29	8/5/29	5	
5.5	Certify flight operations can proceed with accepted risks	MA & Leadership	Not complete	8/1/29	9/1/29	32	
5.6	Ensure proper thermal system configuration	Thermal	Not complete	7/1/29	8/18/29	49	
5.7	Ensure proper structural system configuration	Mechanical	Not complete	7/1/29	8/18/29	49	
5.8	Ensure proper electrical system configuration	Electrical	Not complete	7/1/29	8/18/29	49	
5.9	Ensure proper CDH system configuration	CDH	Not complete	7/1/29	8/18/29	49	
5.10	Ensure proper payload system configuration	Science	Not complete	7/1/29	8/18/29	49	
5.11	Baseline operations planning	Science	Not complete	8/1/29	9/1/29	32	
5.12	Inspect system prior to handoff	QA	Not complete	8/18/29	9/1/29	15	
5.13	Schedule Margin			9/1/29	10/1/29	31	
5.14	◆ Flight Handoff		Not complete	10/1/29	10/1/29	1	

Figure 5.2.2.5: Gantt Chart for Phase D3

WP	TASK	ASSIGNED TO	PROGRESS	START	END	DAYS	MARGIN	Phase D 2029
6.0	D4: Flight Readiness & Launch		0%	10/2/29	12/1/29	61	1	
6.1	Draft documentation for FRR	Leadership	Not complete	10/2/29	10/15/29	14		
6.2	Train post-launch personnel on operational procedures	Science & Engineering	Not complete	10/2/29	10/15/29	14		
6.3	Support launch vehicle integration efforts	Engineering & QA	Not complete	10/2/29	11/30/29	60		
6.4	Finalize FRR document	Leadership	Not complete	10/4/29	10/18/29	15		
6.5	Satisfy KDP E requirements	Leadership	Not complete	10/19	10/19/29	1		
6.6	Conduct quarterly outreach event	Leadership & Outreach	Not complete	11/1/29	11/5/29	5		
6.7	Travel to Kennedy Space Center for Launch	All	Not complete	11/26/29	12/1/29	6		
6.8	Schedule Margin			11/30/29	11/30/29	1		
6.9	◆ Launch		Not complete	12/1/29	12/1/29	1		

Figure 5.2.2.6: Gantt Chart for Phase D4

WP	TASK	ASSIGNED TO	PROGRESS	START	END	DAYS	MARGIN	Phase E 2030
7.0	E1: Cruise & Entry, Descent, & Landing		0%	12/1/29	9/1/30	275	226	
7.1	Assess launch vehicle performance	Engineering	Not complete	12/1/29	1/2/30	32		
7.2	Document any anomalous flight behaviors	MA & Engineering	Not complete	12/1/29	1/2/30	32		
7.3	Update risks tracking	MA	Not complete	12/1/29	1/2/30	32		
7.4	Submit Post Launch Assessment Review (PLAR)	Leadership	Not complete	1/2/30	1/2/30	1		
7.5	Finalize critical activity operations plan	Science & Engineering	Not complete	12/1/29	1/2/30	32		
7.6	Implement fault protection strategy	Engineering	Not complete	12/1/29	1/2/30	32		
7.7	Draft decommissioning plans	All	Not complete	12/1/29	1/2/30	32		
7.8	Draft & submit Critical Event Readiness Review	Leadership	Not complete	1/2/30	1/16/30	15		
7.9	Conduct quarterly outreach event	Outreach	Not complete	2/1/30	2/5/30	5		
7.10	Conduct quarterly outreach event	Outreach	Not complete	5/1/30	5/5/30	5		
7.11	Conduct quarterly outreach event	Outreach	Not complete	8/1/30	8/5/30	5		
7.12	Monitor platform during cruise	Engineering	Not complete	12/1/29	9/1/30	274		
7.13	Schedule Margin			1/16/30	9/1/30	226		
7.14	◆ Entry, Descent, & Landing		Not complete	9/1/30	9/1/30	1		

Figure 5.2.2.7: Gantt Chart for Phase E1

Figure 5.2.2.8: Gantt Chart for Phase E2

ID	TASK	ASSIGNED TO	PROGRESS	START	END	DAYS	MARGIN	Phase F 2031
9.0	**F1: Data Recovery and Decomission**		0%	9/2/31	11/2/31	61	15	
9.1	Satisfy KDP F requirements	Leadership	Not complete	9/2/31	9/2/31	1		
9.2	Allocate storage for mission data archiving	Database Management	Not complete	9/2/31	9/16/31	15		
9.3	Gather relevant engineering telemetry data	Engineering	Not complete	9/2/31	10/2/31	31		
9.4	Collect science instrumentation data	Science	Not complete	9/2/31	10/2/31	31		
9.5	Ensure schedule, budget, & personnel resources are available	DPMR & Schedule & Budget	Not complete	9/2/31	9/16/31	15		
9.6	Draft & submit DRR	Leadership	Not complete	9/16/31	9/30/31	15		
9.7	Determine asset disposal or recovery	All	Not complete	9/2/31	9/16/31	15		
9.8	Recieve final data transmission from rover	Engineering	Not complete	10/1/31	10/15/31	15		
9.9	Collect remaining mission assets still in use	All	Not complete	9/16/31	10/11/31	26		
9.10	Begin drafting final documentation	Leadership	Not complete	10/11/31	10/18/31	8		
9.11	Schedule Margin			10/18/31	11/1/31	15		
9.12	◆ Rover Decomission and Asset Return		Not complete	11/1/31	11/1/31	1		

Figure 5.2.2.9: Gantt Chart for Phase F1

ID	TASK	ASSIGNED TO	PROGRESS	START	END	DAYS	MARGIN	Phase F 203
10	**F2: Final Reporting and Debriefing**		0%	11/1/31	12/31/31	61		
10.1	Finalize final mission report	All	Not complete	11/1/31	12/17/31	47		
10.2	Document & capture lessons learned	All	Not complete	11/1/31	12/3/31	33		
10.3	Archive mission data	Database Mangement & Leadership	Not complete	11/1/31	12/3/31	33		
10.4	Close outstanding archival and documentation tasks	All	Not complete	12/3/31	12/17/31	15		
10.5	Schedule Margin			12/24/31	12/31/31	8		
10.6	◆ Final mission debriefing		Not complete	12/31/31	12/31/31	1		

Figure 5.2.2.10: Gantt Chart for Phase F2

5.3 Budget

5.3.1 Budget Basis of Estimate

The Cost Basis of Estimate (BoE) for P.H.O.E.N.I.X defines the ground rules, assumptions, and cost drivers used to develop the preliminary cost estimate for phases C through F of the mission’s life cycle. The purpose of the BoE is to clearly define how cost estimates were developed from the rules, assumptions, and drivers.

Ground Rules

A $450M cost limit is established specifically for the Rover System, encompassing all expected mission costs including personnel, travel, outreach, hardware, testing, direct costs, as well as cost margins of safety. The BoE only targets Phase C through F. Costs will be estimated primarily using parametric models. It is assumed that these tools provide an accurate reflection of the anticipated cost. These estimates are then aggregated into a budget template that is derived and adjusted from the Lucy Mission Budget.

Assumptions

A constant 2.7% yearly compounding inflation rate is assumed to estimate the budget across the entire mission’s lifecycle [68], this annual inflation rate applied over the mission’s lifecycle is based on NASA's New Start Inflation Index (NNSI). It is assumed that personnel turnover will be minimal. In cases where turnover does occur, replacement costs are expected to be negligible and are covered by the total cost margin. Outreach costs relate to the team’s effort in increasing public awareness of P.H.O.E.N.I.X and the impact that it will have on the scientific community and the end science goals.To support outreach goals, four full time outreach personnel will be employed for the full duration of the mission. A graphic designer, a social media specialist, an event coordinator, and an education & curriculum specialist. These personnel will be responsible for creating content, organizing public events, and developing educational materials.

Personnel travel costs will be estimated through the City Pair Program for airfare. All mission flights are assumed to originate from Los Angeles International Airport (LAX) and arrive at Washington Dulles International Airport (MLB), using YCA Unrestricted Coach Class Contract Fares under the City Pair Program. In reality, flights will include trips to multiple NASA centers and outreach locations in the United States, with only a set of flights going to Washington D.C. for the Standing Review Board (SRB) meetings during KDPs. The LAX-IAD route was selected for cost modeling because it provided a high end estimate that builds in safety margins and reduces the likelihood of

underbudgeting. Lastly, FedRoom will be used for lodging, and per diem reimbursement for meals and rentals.

Tests are conducted at relevant NASA centers across the country, and launch takes place at Cape Canaveral, Florida. Key personnel will be flown in to oversee and conduct in-person testing of relevant components and subsystems with rental cars, lodging, and meals priced out using the aforementioned resources [63]. It is assumed that key subteam leads will travel to NASA testing centers twice per year during Phase C and D. It is also assumed that an outreach event will occur quarterly, with travel for 2 outreach team members. Every trip scheduled for the mission will be assumed to last 5 days with two days for margin. This assumption will hold for every trip including trips in front of the Standing Review Board unless specified otherwise.

Drivers

The primary cost drivers for P.H.O.E.N.I.X include items such as scope changes or descopes, which can shift the required designs and greatly impact system costs. External government policies such as changes in import tariffs may introduce some budget uncertainty, especially for foreign-sourced hardware. Lastly, any unforeseen engineering testing failures may lead to cost inflation due to vendor lead times and/or potential redesigns. The full budget will include breakdowns of costs for each phase of the mission as well as a per-item cost breakdown. To account for any delays, uncertainties, scope changes, and unexpected problems, a 30% total cost margin will be applied to the budget totals. This margin aligns with the standard 70% confidence level in lifecycle cost estimates at the PDR stage [65].

5.3.2 Total Mission Cost

The total estimated cost of P.H.O.E.N.I.X is $439 million, which is below the mission cost cap of $450 million. The estimate in Figure 5.3.2.1 includes all costs associated with Phases C through F of the mission and is broken down into four main categories: Personnel, Travel, Outreach, and Direct Costs.

P.H.O.E.N.I.X Budget							
Mission Phase	Phase C	Phase C	Phase C-D	Phase D	Phase E	Phase F	
Year	Year 1	Year 2	Year 3	Year 4	Year 5	Year 6	Cumulative Total
PERSONNEL							
Science Personnel	$ 1,200,000	$ 1,212,400	$ 843,200	$ 432,400	$ 2,127,280	$ 2,179,200	$ 8,014,560
Engineering Personnel	$ 3,840,000	$ 3,943,680	$ 2,529,600	$ 1,729,600	$ 880,400	$ 908,000	$ 13,837,280
Technicians	$ 2,100,000	$ 2,156,700	$ 2,213,400	$ 1,297,200	$ -	$ -	$ 7,767,300
Administration Personnel	$ 300,000	$ 308,100	$ 316,200	$ 324,300	$ 332,400	$ 140,500	$ 1,921,500
Project Management	$ 480,000	$ 492,960	$ 505,920	$ 518,880	$ 531,840	$ 544,800	$ 3,074,400
Total Salaries	$ 7,920,000	$ 8,133,840	$ 6,408,320	$ 4,302,380	$ 3,878,000	$ 3,972,500	$ 36,615,040
Total ERE	$ 2,210,472	$ 2,270,155	$ 1,788,562	$ 1,200,794	$ 1,082,350	$ 1,108,725	$ 9,661,058
Personnel Margin	$ 3,039,142	$ 3,121,198	$ 2,459,065	$ 1,650,952	$ 1,488,105	$ 1,524,367	$ 13,282,829
TOTAL PERSONNEL	$ 13,169,614	$ 13,890,373	$ 11,231,368	$ 7,733,611	$ 7,144,888	$ 7,497,347	$ 60,667,201
TRAVEL							
Total Flights Cost	$ 72,912	$ 114,104	$ 117,104	$ 210,181	$ 38,470	$ 39,407	$ 592,177
Total Hotel Cost	$ 29,165	$ 45,642	$ 46,841	$ 84,072	$ 15,388	$ 15,763	$ 236,871
Total Transportation Cost	$ 21,874	$ 34,231	$ 35,131	$ 63,054	$ 11,541	$ 11,822	$ 177,653
Total Per Diem Cost	$ 18,228	$ 28,526	$ 29,276	$ 52,545	$ 9,617	$ 9,852	$ 148,044
Travel Margin	$ 42,654	$ 66,751	$ 68,506	$ 122,956	$ 22,505	$ 23,053	$ 346,424
Total Travel Costs	$ 184,832	$ 297,063	$ 312,888	$ 575,066	$ 108,053	$ 113,383	$ 1,592,186
OUTREACH							
Total Outreach Materials	$ 70,000	$ 12,000	$ 15,000	$ 18,000	$ 20,000	$ 25,000	$ 160,000
Total Outreach Venue Costs	$ 20,000	$ 30,000	$ 40,000	$ 20,000	$ 20,000	$ 160,000	$ 290,000
Total Outreach Travel Costs	$ 17,500	$ 8,000	$ 10,000	$ 96,000	$ 15,000	$ 90,000	$ 236,500
Total Outreach Services Costs	$ 10,000	$ 12,000	$ 15,000	$ 100,000	$ 25,000	$ 30,000	$ 192,000
Total Outreach Personnel Costs	$ 514,198	$ 411,359	$ 411,359	$ 514,198	$ 411,359	$ 411,359	$ 2,673,831
Outreach Margin	$ 94,755	$ 142,008	$ 147,608	$ 224,459	$ 147,408	$ 214,908	$ 970,944
Total Outreach Costs	$ 726,453	$ 631,981	$ 673,259	$ 1,051,443	$ 707,253	$ 1,056,987	$ 4,847,876

DIRECT COSTS							
Mechanical Subsystem	$ 12,448,800	$ 12,448,800	$ 13,322,400	$ 14,196,000	$ 1,092,000	$ 1,092,000	$ 54,600,000
Power Subsystem	$ 4,765,200	$ 4,765,200	$ 3,099,600	$ 10,868,000	$ 418,000	$ 418,000	$ 26,534,000
Thermal Control Subsystem	$ 1,003,200	$ 1,003,200	$ 6,226,933	$ 1,144,000	$ 172,000	$ 172,000	$ 9,721,333
Comms & Data Handling Subsystem	$ 5,426,400	$ 5,426,400	$ 5,807,200	$ 6,188,000	$ 622,000	$ 622,000	$ 24,092,000
Guidance, Nav, & Control Subsystem	$ 5,449,200	$ 5,449,200	$ 5,831,600	$ 6,408,000	$ 622,000	$ 622,000	$ 24,380,000
Science Instrumentation	$ 7,843,200	$ 7,843,200	$ 8,303,600	$ 8,044,000	$ 688,000	$ 688,000	$ 34,400,000
Spacecraft Cost Margin	$ 11,080,800	$ 11,080,800	$ 13,404,400	$ 14,373,800	$ 1,084,200	$ 1,084,200	$ 62,058,200
Total Spacecraft Direct Costs	$ 48,016,800	$ 49,313,254	$ 61,222,363	$ 67,097,454	$ 5,205,606	$ 5,332,457	$ 236,187,933
Manufacturing Facility Cost	$ 1,115,000	$ 1,125,000	$ 1,300,000	$ 1,500,000	$ 250,000	$ 250,000	$ 5,540,000
Test Facility Cost	$ 26,493,600	$ 26,493,600	$ 18,641,800	$ 8,918,000	$ 846,000	$ 423,000	$ 81,816,000
Facility Cost Margin	$ 8,282,580	$ 8,285,580	$ 5,982,540	$ 3,125,400	$ 328,800	$ 201,900	$ 26,206,800
Total Facilities Costs	$ 35,891,180	$ 36,873,593	$ 27,324,254	$ 14,640,415	$ 1,578,678	$ 993,012	$ 117,301,133
Total Direct Costs	$ 83,907,980	$ 86,186,846	$ 88,546,617	$ 81,737,869	$ 6,784,284	$ 6,325,469	$ 353,489,065
Total MTDC	$ 48,016,800	$ 49,313,254	$ 61,222,363	$ 67,097,454	$ 5,205,606	$ 5,332,457	$ 236,187,933
FINAL COST CALCULATIONS							
Total F&A	$ 3,693,600	$ 3,823,245	$ 4,781,796	$ 5,277,365	$ 412,141	$ 424,826	$ 18,412,973
Total Projected Cost	$ 101,682,478	$ 104,829,509	$ 105,545,929	$ 96,376,255	$ 15,157,118	$ 15,418,012	$ 439,009,301
Total Cost Margin	$ 22,539,930	$ 22,696,337	$ 22,061,918	$ 19,447,568	$ 3,071,017	$ 3,048,428	$ 92,865,198
	22.2%	21.7%	20.9%	20.2%	20.3%	19.8%	
Total Project Cost	$ 101,682,478	$ 104,829,509	$ 105,545,929	$ 96,376,255	$ 15,157,118	$ 15,418,012	$ 439,009,301

Figure 5.3.2.1: P.H.O.E.N.I.X Full Budget Table

5.3.3 Personnel Budget

The personnel cost for P.H.O.E.N.I.X is derived from a combination of analogous space missions and expected personnel workload tailored for each mission phase. Personnel are allocated by mission phase based on expected demands, with peak staffing occurring during Phases C and D where the largest amount of critical design, integration, testing, and collaboration is required to ensure the rover is ready for launch.

The core mission team remains consistent throughout the mission lifecycle. The baseline P.H.O.E.N.I.X team consists of 3 teams; science, engineering, and programmatics (refer to Figure 1.8.2.1 Organizational Chart). Each subteam is led by a designated team leader, with oversight from the PM.

- Science: 4 Personnel & 1 Management
- Engineering: 8 Personnel & 1 Management
- Progammatics: 1 Personnel & 1 Management
- 1 Project Manager

This results in a baseline mission staff of 16 personnel.

On top of the baseline team, there will be an additional 104 support staff hired over the course of the mission to distribute the workload. The support staff includes 40 engineers, 24 technicians and the Quality & Validation team that consist of 8 quality assurance personnel and 10 V&V personnel, 20 scientists, 5 administration staff, and 4 outreach personnel. During peak design and fabrication activities in Phases C and D there will be an expected peak staffing of 111 personnel working on P.H.O.E.N.I.X

Although our projected peak staffing of 111 personnel during Phases C and D exceeds the recommended mission headcount of 30-50, this staffing level was intentionally chosen to ensure that all phases meet their scheduled deadlines and that P.H.O.E.N.I.X will meet its fixed launch window. An analogous mission of NASA’s Ingenuity Mars Helicopter, involved up to 150 personnel across JPL, AeroVironment, and other centers to achieve its quick development and milestones [49].To keep this amount of staff manageable, the mission uses a tiered management structure with the baseline team managers overseeing respective subteam leads.

Salaries for each role are assumed fixed except for inflation rates with a 28% benefits rate applied [82]. In Figure 1.10.3.1, technicians and the Quality & Validation(Q&V) team are grouped together as they receive the same base pay. Salaries are all derived from the Bureau of Labor Statistics and rounded up to the nearest thousand for buffer. It is assumed that all personnel are employed full time and that any turnover will be minimal or covered within the Total Cost Margin.

Personnel Phase Allotment Table						
	Phase C	**Phase C**	**Phase C-D**	**Phase D**	**Phase E**	**Phase F**
# People on Team	FY 1	FY 2	FY 3	FY 4	FY 5	FY 6
Science Personnel:	15	15	10	5	24	24
Engineering Personnel:	48	48	30	20	10	10
Technicians and Q&V:	35	35	35	20	0	0
Administration Personnel:	5	5	5	5	5	5
Outreach Personnel:	4	4	4	4	4	4
Management Personnel:	4	4	4	4	4	4
Total Personnel	111	111	88	58	47	47

Figure 5.3.3.1: Personnel Phase Allotment Table

Science:

The scientist staff count choice reflects a similar NASA mission, NASA's LROC mission which employed 22 science staff over its mission lifecycle [18]. In FY1 and 2, 15 science personnel are needed to collaborate with the team to set goals and validate that the appropriate instruments and devices are being integrated correctly and in accordance with the mission's science goals. Scientists are staffed at a peak of 24 in Phases E and F where the majority of data processing and scientific analysis are required.

Engineering:

As discussed in 5.1 Project Management Approach, there will be a need of 10 engineers per engineering subteam, with 4 engineering subteams resulting in 40 engineers being hired on top of the baseline team. For a peak total of 48 engineers. Engineers are allocated per phase based on workload. Phases C and D are where peak engineering work and fabrication is occurring, engineers are most needed then. Engineers for each subteam work closely with the Integration & Testing, QA, and Verification and Validation teams across both phases. Extensive testing at both the subsystem and full system level requiring additional personnel is conducted, which can be seen in Figures 5.2.2.1 to 5.2.2.4. Extra personnel are also utilized for assembly of the rover from the respective subsystems.

Technicians & Q&V:

Technicians are necessary for rover fabrication. Technicians contribute to mechanical, electrical, and general roles. A total of 35 technicians and Q&V personnel are needed during the critical phases of rover development and assembly. Technician

support is phased out following launch, with no staff assigned during Phases E and F.

Administrative, Outreach, and Management:

Administrative personnel are responsible for mission organization, project supervision, and ensuring the rover is delivered in time, in conjunction with management. Management is composed of personnel from the baseline team for a total of 4 managers. Outreach personnel are further detailed in section 1.10.5 Outreach Costs.

In total, the projected personnel cost for the mission is estimated at $60.7 million. These personnel costs reflect expected mission demands and accounts for direct and indirect labor expenses.

P.H.O.E.N.I.X Budget

Mission Phase	Phase C	Phase C	Phase C-D	Phase D	Phase E	Phase F	
Year	Year 1	Year 2	Year 3	Year 4	Year 5	Year 6	Cumulative Total
PERSONNEL							
Science Personnel	$ 1,200,000	$ 1,232,400	$ 843,200	$ 432,400	$ 2,127,360	$ 2,179,200	$ 8,014,560
Engineering Personnel	$ 3,860,000	$ 3,943,680	$ 2,529,600	$ 1,729,600	$ 886,400	$ 908,000	$ 13,857,280
Technicians	$ 2,100,000	$ 2,156,700	$ 2,213,400	$ 1,297,200	$ -	$ -	$ 7,767,300
Administration Personnel	$ 300,000	$ 308,100	$ 316,200	$ 324,300	$ 332,400	$ 340,500	$ 1,921,500
Project Management	$ 480,000	$ 492,960	$ 505,920	$ 518,880	$ 531,840	$ 544,800	$ 3,074,400
Total Salaries	$ 7,920,000	$ 8,133,840	$ 6,408,320	$ 4,302,380	$ 3,878,000	$ 3,972,500	**$ 34,615,040**
Total ERE	$ 2,210,472	$ 2,270,155	$ 1,788,562	$ 1,200,704	$ 1,082,550	$ 1,108,725	**$ 9,661,058**
Personnel Margin	$ 3,039,142	$ 3,121,198	$ 2,459,065	$ 1,650,952	$ 1,488,105	$ 1,524,367	**$ 13,282,829**
TOTAL PERSONNEL	$ 13,169,614	$ 13,890,373	$ 11,231,368	$ 7,735,031	$ 7,168,888	$ 7,497,167	$ 60,667,201

Figure 5.3.3.2: P.H.O.E.N.I.X Personnel Budget

5.3.4 Travel Budget

Personnel travel costs are estimated through the City Pair Program [119] for airfare, FedRoom [120] for lodging, and per diem rates [121] for meals and rentals These tools provide government negotiated rates, ensuring that cost estimates are accurate. For cost estimating purposes, all mission flights are assumed to originate from Los Angeles International Airport (LAX) and arrive at Washington Dulles International Airport (IAD), using YCA Unrestricted Coach Class Contract Fares under the City Pair Program. This approach to flight cost estimating proves peak-end estimating that builds in safety margins and reduces the likelihood of underbudgeting.

Tests are conducted at relevant NASA centers across the country, and launch takes place at Cape Canaveral, Florida. Key personnel will be flown in to oversee and conduct in-person testing of relevant components and subsystems with rental cars, lodging, and meals priced out using the aforementioned resources. It is assumed that key subteam leads will travel to NASA testing centers twice per year during Phase C and D. It is also assumed that an outreach event will occur quarterly, with travel for 2 outreach team members.

The Trip Estimate Breakdown figure below breaks down the trips that are allocated per fiscal year, the amount of personnel allocated, the trips allocated, and the total amount of individual trips in green. Furthermore, a trip margin of 10% has been applied to make up for last minute additions of trips or where specific staff may be needed to travel to accompany allocated staff for a trip.

Phase	FY	Purpose	Trips	Personnel	Personnel * Trips
C	FY1	CDR + Outreach + Testing Center	7	12	84
	FY2	PRR + SIR + Outreach + Testing Center	8	16	128
D	FY3	SAR + MRR + Outreach + Testing Center	8	16	128
	FY4	FRR + Launch + Outreach + Testing Center	8	28	224
E	FY5	EDL + Outreach	5	8	40
F	FY6	DRR + Outreach	5	8	40
				Trip Margin:	64
				Total Trips:	708

Figure 5.3.4.1: Trip Estimate Breakdown

Travel also occurs for presenting deliverables in front of SRBs when necessary per guidelines. Leadership will be flown in to deliver the presentation in person with trips lasting five days. Two travel days pad the presentation scheduled for day three of five, ensuring crucial presentations are not missed due to external factors beyond the team’s control.

A 30% cost margin is applied across all travel costs to account for unexpected scheduling changes, unforeseen delays, and or extra travel expenditures. Below is the budget formatted table for travel cost.

TRAVEL							
Mission Phase	**Phase C**	**Phase C**	**Phase C-D**	**Phase D**	**Phase E**	**Phase F**	
Year	**Year 1**	**Year 2**	**Year 3**	**Year 4**	**Year 5**	**Year 6**	**Total**
Total Flights Cost	$ 72,912	$ 114,104	$ 117,104	$ 210,181	$ 38,470	$ 39,407	**$ 592,177**
Total Hotel Cost	$ 29,165	$ 45,642	$ 46,841	$ 84,072	$ 15,388	$ 15,763	**$ 236,871**
Total Transportation Cost	$ 21,874	$ 34,231	$ 35,131	$ 63,054	$ 11,541	$ 11,822	**$ 177,653**
Total Per Diem Cost	$ 18,228	$ 28,526	$ 29,276	$ 52,545	$ 9,617	$ 9,852	**$ 148,044**
Travel Margin	$ 42,654	$ 66,751	$ 68,506	$ 122,956	$ 22,505	$ 23,053	**$ 346,424**
Total Travel Costs	$ 184,832	$ 297,063	$ 312,888	$ 575,966	$ 108,053	$ 113,383	**$ 1,592,186**

Figure 5.3.4.2: Travel Cost Breakdown Table

5.3.5 Outreach Budget

For social media, there is a highly unlikely chance of having financial expenses, due to the widespread use, availability, and accessibility of content creating applications. However, if the team is to hire graphic designers, social media specialists, education & curriculum specialists, and event planners, they will cost $65,000, $78,000, $65,000, and $60,000 annually, respectively [28]. However, most of the team members have advanced knowledge of content creation and editing, meaning there is a high chance that more professional outreach experts are not needed for promoting the mission.

For Lego NXT, each robot set will cost $400 [48]. The team will do a workshop in front of 30 students to educate them on the NASA mission with all of the robots for each student costing around $12,000. To rent an auditorium for the students, space is estimated at $1000 per session in a single day [122]. Overall, the process for hosting an informational session to 30 students with Lego NXT robots will take 1-2 weeks, depending on the response of the auditorium staff and the teachers. Two Lego workshops are scheduled per year.

For the RIMFAX geological presentation, the auditorium rental cost will be $1000 [122]. The event will be open to a large audience including high school students, college students, and workplace professionals seeking to learn more about space focused careers in science and engineering. The team will also make a one time purchase of a live radar subsurface imager which will be transported to each presentation. This radar imager will be used to demonstrate the key operating principles behind RIMFAX, and highlight how the technology is applied on the P.H.O.E.N.I.X rover, this will help promote the type of scientific research and technology development that occurs at NASA. The radar imager is estimated to cost around 23,000 dollars [31].

The Space Festival will occur yearly and will be heavily derived from the analogous Moon 2 Mars Festival [108]. It will take place at a NASA center. Tickets are estimated to cost around $60 per person [107], while children 12 years and under can enter for free to further promote STEM education for children. The tickets will allow the patrons to access as many events and attractions as possible that the space festival can provide. For the wages of the employees working the space festival, they will earn on average $25 an hour, with pay potentially increasing based on the position they are working. This includes catering staff, janitorial staff, event outreach workers and hosts. A separate budget of $40,000 per speaking instance will be set aside for paying industry professional speakers, professors or subject matter experts to speak at the festival. This speaker budget will account for travel, lodging, and associated fees for the speakers.

The outreach budget is further broken down in the table below:

OUTREACH							
Total Outreach Materials	$ 70,000	$ 12,000	$ 15,000	$ 18,000	$ 20,000	$ 25,000	$ **160,000**
Total Outreach Venue Costs	$ 20,000	$ 30,000	$ 40,000	$ 20,000	$ 20,000	$ 160,000	$ **290,000**
Total Outreach Travel Costs	$ 17,500	$ 8,000	$ 10,000	$ 96,000	$ 15,000	$ 90,000	$ **236,500**
Total Outreach Services Costs	$ 10,000	$ 12,000	$ 15,000	$ 100,000	$ 25,000	$ 30,000	$ **192,000**
Total Outreach Personnel Costs	$ 514,198	$ 411,359	$ 411,359	$ 514,198	$ 411,359	$ 411,359	$ **2,673,851**
Outreach Margin	$ 94,755	$ 142,008	$ 147,408	$ 224,459	$ 147,408	$ 214,308	$ **970,944**
Total Outreach Costs	$ 728,453	$ 831,981	$ 673,259	$ 1,051,443	$ 707,733	$ 1,058,387	$ **4,847,876**

Table 5.3.5.1: Outreach Budget Table

5.3.6 Direct Costs

Mechanical Subsystem Cost:

For the mechanical subsystem, cost estimates were derived using Xometry's automated manufacturing cost calculator. This tool provides a cost breakdown based on CAD geometry, material selection, and manufacturing process. Each of the tire treads have an estimated manufacturing cost of $232.03. Since there will be 6 wheels on the rover, this totals to an estimated $1392.18 for the tires. For the wheel spokes, each part had an estimated cost of $448.35. Given that there will be 6 wheel spokes for each wheel on the rover, this yields a total estimated cost of $2690.10. The rocker-bogie subsystem was split into 2 parts to allow for independent suspension. The front half of the rocker has an estimated price of $8,282.87 per piece. The back half of the rocker has an estimated manufacturing cost of $161,118.46. Since there are 2 of each parts of the rockers for either side of the rover drive, this yields a total estimated manufacturing cost of $322,236.92. The differential was split into 3 parts to allow for rotation in two planes. The two mounts have estimated manufacturing costs of $189.12 each, and the two rotating pegs have estimated manufacturing costs of $564.11 each. The bar connecting the pegs to the chassis has an estimated manufacturing cost of $592.26. The chassis, which has an estimated manufacturing cost of $1,435. This totals to a net manufacturing cost of $346,418.66. This figure will be rounded upwards to the nearest hundred thousand, yielding $400,000 for total cost margin considerations.

Power Subsystem Cost:

Utilizing the Mission Concept Cost Estimation Tool (MCCET) to aid in calculation of system components, the team was able to derive estimates of the cost for power subsystem components that had no readily available "shelf price". The planned battery, an EaglePicher SAr-10211 with a 4,380Wh rating, had an estimated cost of $37,869.36. Accounting for shipping, tax, testing costs, and integration costs, we estimated $40,000 for this component. As the mission cannot afford the weight of a second battery in the launch, this is the only estimate associated with the rechargeable battery.

The roll-out solar array is a custom component that allows the solar panels to utilize less mass, store for launch, and produce a larger margin of usable power when compared to other solar panel architectures. The deployment system for these panels, like those used on the International Space Station, will be provided by Redwire, while the panels will be manufactured by AZUR Space. The solar panels shall also utilize EDS to shield from dust and radiation risks. This is a custom technology, and will cost more to manufacture than a typical solar cell. The chosen panels weigh 17kg per 1.3 square meters (unrolled), and cost an estimated $120,337.62 per unit. Rounding to

include testing, shipping, and tax puts the estimated cost of this component at $150,000.

Providing isolated power to the external experiment requires the use of an isolated power distribution system. For the P.H.O.E.N.I.X mission, the WR62 4-Way Combining System Assembly produced by the Scientific Microwave Corporation. This bus shall provide adequate distribution and isolation for a resulting higher-efficiency architecture. For redundancy, the rover will carry two PDUs, for an estimated cost of $7,500 each, totalling $15,000 after integration, testing, shipping, and material handling costs.

For isolated thermal management of power components and batteries, the rover shall utilize variable heat pipes produced by Advanced Cooling Technologies, as well as the addition of a thermal buffer vapor chamber, which combined would cost an estimated $683,128.34, rounded to $700,000, due to the mass, complex architecture, and involved testing procedures.

In total, the estimated cost of the electrical power subsystem for this mission is $905,000.

Command and Data Handling (CDH) Subsystem Cost:

The Mission Concept Cost Estimate Tool (MCCET) provides the outline for cost estimates for various subsystems. For the costs related to CDH there are both electronics subsystem costs and software subsystems costs which must be incorporated. Both electronics and software cost estimates depend on the mass estimate of the electrical subsystem.

The RAD5545 OBC weighs 1.8 kg, and two shall be used on the rover. The SSDs weigh 620g and two will be used on the rover. The UHF transceiver weighs 2.0 kg. The data interface cable weighs ~3g/m, and at 150m of usage will weigh 0.45 kg. The UHF antenna weighs 0.6 kg. This puts the total CDH mass total at 8.25 kg. Using these mass estimates for the NICM, the output of the Cost Estimating Relationships (CERs), shall be found for the electronics and software subsystems. The electronics subsystem costs are 7,222.62, and the software development costs are 1,012.20, and therefore the estimated cost with inflation for electronic subsystems are $13,654,254.28, and software development costs are $1,912,754.34. Rounding to the nearest hundred thousand yields $13,700,000 for electronics, and $2,000,000 for software.

The Command and Data Handling (CDH) subsystem procurement costs are estimated to cost a total of $513,232. The RAD5545 onboard computer, sourced from BAE Systems, is priced at $250,000 per unit, with two units, totaling $500,000. Two Mercury RH3440 SSDs will be used for data storage at $18,000 each, totaling $36,000

[56]. The selected UHF transceiver, the L3Harris Electra-lite, is estimated at $250,000 based on past procurement of similar flight hardware. The RS-422 transceiver from Texas Instruments is estimated at $150 with 20 needed total [112]. The primary data interface cable, the WireMasters DXN2605 30 AWG twisted pair, will cost approximately $1,500 for 150 meters. The UC-3004-531R quadrifilar helix UHF antenna is priced at $600 [46]. The sum of all procurement costs is $791,10, and rounding to the nearest hundred thousand yields $800,000.

The total CDH costs are estimated at $16.5 million dollars.

Thermal Subsystem Cost:

The team utilized the NASA Instrument Cost Model (NICM) to calculate and estimate the cost of the thermal subsystem components. For Dwyeromega KHLVA-102/5 Electrical Heaters, the cost is provided on the Dwyeromega catalog page, with it being $115.87 per unit, and we would have around 30 electrical heaters. Thus, making the subtotal cost being $3,476.10; however, we must account for tax and delivery fees, thus it should be rounded to $4,000.00. The Sierra Space Thermal Louver radiator would cost around $1,283,750.26, which includes costs for thermal analysis, materials support, load definition, and instrument system thermal hardware, etc. These costs are derived via the utilization of the CER equations from NICM. However, this analysis shall be rounded up to $1,300,000.00 to account for any total cost margin [Figure A.1]. For NI Solution's thermistor, the cost for this specific thermal sensor is calculated to be around $351,940.55, like any other components of the subsystem, with consideration of thermal analysis, etc. This estimation also comes from the thermal portion of the CER of the NICM. This number shall be rounded to the nearest hundred thousand, which rounds to $400,000.00; therefore, it shall be put as the direct cost [Figure A.2]. For Advanced Cooling Technologies' Constant Conductance Heat Pipes (VCHP), the cost would be $571,808.15 with all considerations, using the same equation from CER, the team will utilize 5 of these specific heat pipes. This amount shall be rounded to $600,000.00 for total cost margin considerations as well [Figure A.3]. For the multilayer insulation (MLI), general information regarding the thickness of a particular layer is provided; however, the mass per unit square was not provided without the consultation of companies like Dunmore Aerospace and Sheldahl for quotes. This hindered the team's ability to calculate the cost for specific layers, for instance, double-sided mylar, goldized kapton. Without this, it also hindered operations on calculations for how much EPON 815C Epoxy Resin needs to be used, the amount of Kapton Tape, plus the amount of threads needed to stitch the MLI; thus, a total cost margin must be set in place for MLI-related components of this subsystem.

Instrumentation Subsystem Cost:

To calculate and determine costs within the instrumentation subsystem of P.H.O.E.N.I.X, each instrument was evaluated with the use of the Mission Concept Cost Estimate Tool (MCCET), which estimates the costs of wrap and testing facilities. Wrap costs include management, systems engineering, product assurance, integration, and test costs, which should be considerable because they ensure the instruments are properly supported and verified for flight readiness. Test facility costs include thermal vacuum, electromagnetic interference, vibration testing, and ambient testing, which all help confirm the quality and ability of the instruments to operate under the conditions the mission is bound to encounter. Costs are imperative to be valued properly to make informed decisions that allocate the given budget efficiently within the instrumentation subsystem.

Utilizing the Mission Concept Cost Estimation Tool (MCCET), an inflation rate of 188.97% was calculated to properly determine accurate inflation-adjusted costs for each of the four main instruments. This constant inflation rate impacts overall costs as it adjusts to the current economic conditions to prevent an inefficient use of the given budget for instrumentation that plays a major role in data collecting. With the use of the CER formula:

The CP-MU DMU-100 Submersible Gamma Neutron Probe (including its external box and probe) is approximately $1,104 based on its total values of 1.3 kg for mass and max power of 0.25 watts. The CER value calculates the final manufacturing cost per unit that includes manufacturing and wraps, approximating to a total of $2,700,000, and the final testing facility cost per unit that approximates to $800,000.

The RIMFAX instrument is made up of an externally mounted antenna at the back of the rover and an electronic unit inside the rover body. With a total mass of 3 kg and a max power of 10 watts, the CER formula calculated the cost to be $5843. This value created the total cost estimate for final manufacturing cost per unit to be approximately $14,600,000 and final testing facility cost per unit to $4,400,000.

The Miniature Tunable Laser Spectrometer (Mini-TLS) is approximately $2877 based on its total values of 1kg for mass and max power of 8 watts. The CER value calculates the final manufacturing cost per unit that includes manufacturing and wraps, approximating to a total of $7,200,000 and the final testing facility cost per unit that approximates to $2,200,000.The Raman Laser Spectrometer (RLS) is approximately $8153 based on its total values of 2.4 kg for mass and max power of 30 watts. The CER value calculates the final manufacturing cost per unit that includes manufacturing and wraps, approximating to a total of $7,200,000 and the final testing facility cost per unit that approximates to $2,200,000.

Total Direct Costs

The total direct costs for the mission can be seen in Table 5.3.6.1 which breaks down the direct cost of each respective subsystem. Cost is further divided by each phase and its respective calendar year. Total direct costs rounded to the nearest one hundred thousand dollars are 353.5 million dollars across all subsystems.

P.H.O.E.N.I.X Budget							
Mission Phase	Phase C	Phase C	Phase C-D	Phase D	Phase E	Phase F	
Year	2026	2027	2028	2029	2030	2031	Cumulative Total
DIRECT COSTS							
Mechanical Subsystem	$ 12,448,800	$ 12,448,800	$ 13,322,400	$ 14,196,000	$ 1,092,000	$ 1,092,000	$ 54,600,000
Power Subsystem	$ 4,765,200	$ 4,765,200	$ 5,099,600	$ 10,868,000	$ 418,000	$ 418,000	$ 26,334,000
Thermal Control Subsystem	$ 1,003,200	$ 1,003,200	$ 6,226,533	$ 1,144,000	$ 172,000	$ 172,000	$ 9,721,333
Comms & Data Handling Subsystem	$ 5,426,400	$ 5,426,400	$ 5,807,200	$ 6,188,000	$ 622,000	$ 622,000	$ 24,092,000
Guidance, Nav, & Control Subsystem	$ 5,449,200	$ 5,449,200	$ 5,831,600	$ 6,406,000	$ 622,000	$ 622,000	$ 24,380,000
Science Instrumentation	$ 7,843,200	$ 7,843,200	$ 8,393,600	$ 8,944,000	$ 688,000	$ 688,000	$ 34,400,000
Spacecraft Cost Margin	$ 11,080,800	$ 11,080,800	$ 13,404,400	$ 14,323,800	$ 1,084,200	$ 1,084,200	$ 52,058,200
Total Spacecraft Direct Costs	$ 48,016,800	$ 49,313,254	$ 61,222,363	$ 67,097,454	$ 5,205,606	$ 5,332,457	$ 236,187,933
Manufacturing Facility Cost	$ 1,115,000	$ 1,115,000	$ 1,300,000	$ 1,500,000	$ 250,000	$ 250,000	$ 5,540,000
Test Facility Cost	$ 26,493,600	$ 26,493,600	$ 18,641,800	$ 8,918,000	$ 846,000	$ 423,000	$ 81,816,000
Facility Cost Margin	$ 8,282,580	$ 8,280,580	$ 5,582,540	$ 3,125,400	$ 328,800	$ 201,900	$ 26,206,800
Total Facilities Costs	$ 35,891,180	$ 36,873,592	$ 27,324,254	$ 14,640,415	$ 1,578,678	$ 993,012	$ 117,301,133
Total Direct Costs	$ 83,907,980	$ 86,186,846	$ 88,546,617	$ 81,737,869	$ 6,784,284	$ 6,325,469	$ 353,489,065
Total MTDC	$ 48,016,800	$ 49,313,254	$ 61,222,363	$ 67,097,454	$ 5,205,606	$ 5,332,457	$ 236,187,933

Table 5.3.6.1: Direct Costs Table

5.4 Scope Management

5.4.1 Change Control Management

After a careful review on how to approach any significant changes to the design of the rover, the mission or the payload the team has decided to follow a standard protocol for any changes that occur throughout the life of the mission. This protocol will include a set of stages for each change from its introduction to its implementation into the system. A change log has been created to track these changes. Additionally, there is a process for addressing stakeholder feedback in the form of a request for action (RFA) or advisory (ADV) that will be important for understanding the depth of the change that is needed.

A change is anything that alters a previously baselined or not yet baselined plan for the mission. These changes may come in many forms including: design change, requirement change, objective change, programmatic changes, and stakeholder change (RFAs, ADVs, Scope). Design changes are those that change the physical configuration or functional behaviour of any system or subsystem. Requirement changes are modifications of mission requirements, low or high level. Objective changes are changes to the scientific objectives of the mission. If a change is needed to the timeline of the mission a schedule change will be implemented. Stakeholder changes include RFAs, ADVs, and scope changes from the customer, NASA. The process for scope change control is outlined in 1.11.2.

Changes can be brought up by any personnel whether it be technical or non technical. To request a change, the change log must be updated with all relevant information. Subsequently, the requestor will meet with their subteam lead and the team lead to explain the change. The leads discuss whether the change is necessary. To be approved to submit a change request the change must be supported by these two members.

If approved, a follow-up meeting with the leads and any personnel with affected subsystems will be conducted to discuss how the change impacts each subsystem and which personnel is responsible for its implementation. This information will be brought to the Change Control Board (CCB) by the identified relevant personnel through a change request if the plan was already baselined in a past deliverable. The change request is a L’SPACE required procedure to ensure the changes made are well justified and achievable. Once the change is approved, this personnel will implement it into the system.

Any RFA or ADV driven by stakeholder feedback will have its own process to change. They will follow the standard change process minus the necessity of a CCB or

change request form. RFAs and ADVs do not require that the team make any changes to past deliverables; however, they are a form of feedback for what should change in future deliverables. The tracking of this feedback has and will continue to help the team improve the overall clarity of the mission in each subsequent deliverable. Many of the sections stay the exact same but are improved by understanding this feedback. Scope changes will also be tracked on the change log but have a different process of management detailed in 5.4.2.

There are three layers of communication to ensure changes are completed. This communication will be through the change log as well as in threads in the team discord. All meetings conducted will also be through the discord. At these general team meetings, the change log will be displayed to ensure the whole team understands and has input into the changes. To track the completion of changes, any subteam lead with personnel working on a change will check in during subteam meetings.

Verification of tentatively completed changes will involve the same group of leads plus relevant personnel who implemented the change. They will discuss the changes that occurred, consider the risks, and ensure the full completion of the change. If it is not complete, it will continue to be worked on until it passes this board. Once completed, the change log will be updated to show the completed nature of the change. This includes the sign off of all four team leads.

The change log is a spreadsheet meant to track each change, the reason for a change, what will change, impacted subsystems, assigned individuals, and the changes current state.

Change Log										
ID	**Change**	**Type**	**Reasoning**	**Description of Change (If stakeholder state if RFA, ADV, Scope)**	**Assigned Individual**	**State**	**Chief Scientist Signoff**	**Lead System Engineer Signoff**	**DPMR Signoff**	**Project Manager Signoff**
0.1	Stakeholder Added Science Instrumentation	Stakeholder	The stakeholder has requested to add new scientific instrumentation to the vehicle with the option of external or internal mounting.	(Scope) A new scientific instrument will be externally mounted on the rover. Thermal - Increase in MLI and thermal coating to reduce power usage of active heaters. CDH - Antenna mounting must be moved 1m to protect the instrument from interference. Mobility systems and instruments cannot be used simultaneously to reduce risk of too much power draw.	Whole Team	Completed	Approved	Approved	Approved	Approved
0.2	Alteration of Science Objective 1 of HBS-1LM	Objective	Quantity of material to be collected for study was unquantified. The data transmission interval was too long.	One single sample will be collected and the new data transmission interval will be weekly.	Alanis and Matthew	Completed	Approved	Approved	Approved	Approved
0.3	MCR-RFA-2	Stakeholder	A thorough description of each region of interest and how they fulfill the team's science objectives must be provided.	The MCR will be changed to explain how the features of the Martian geography help fulfill the science objectives with the abundance of impact craters and lobate debris aprons which make asteroid rocks and hydrated volcanic rock abundant to study.	Conor	In Progress	Pending	Pending	Pending	Pending
0.4	MCR-ADV-1	Stakeholder	Provide more detail on the science data being collected for the Human Exploration Goal	(No change needed to MCR) In future deliverables ensure that there is a connection between data collected and the human exploration goal plus objectives.	Science Team	In Progress	Pending	Pending	Pending	Pending

Figure 5.4.1.1: Change Log

5.4.2 Scope Control Management

In the event that a scope change is needed, the team shall begin a process that ensures the change is implemented smoothly across the science, engineering, and programmatic teams. In both cases of descoping and upscoping, the first step should be defining mission impacts. The descope or upscope may cause science capabilities to be redefined, so the STM should be updated to reflect any necessary changes. Additionally, the requirements table and risk matrix should be updated if the descope or upscope poses new requirements or risks to the mission. All of these changes should be documented through the change control log, and all team members should be notified. Once the broader mission impacts have been identified, documented, and communicated, the descope or upscope shall go through its respective tiered process involving the management of potential engineering subsystem design changes, budget or schedule changes, and other scope change implications.

Downscoping Strategy:

The first tier of the descoping measures will be Tier 0: Redesign and Change Management. This will refer to instances where manufacturing times exceed the estimated baseline plus the 25% contingency margin (e.g., 11 business days extended to 14 days), or if manufacturing costs significantly surpass projections. In the case that machining lead times or costs exceed estimates, non-critical rocker-bogie elements or wheel tread geometry will be simplified to reduce machining complexity. This includes removing features such as edge blends on the rocker-bogie structure to simplify the machining process since they are not structurally necessary. This can reduce both material usage and production time without impacting the performance capabilities of the subsystems. Furthermore, the traverse route planning can be adjusted to reduce the wear and power consumption of the rover without compromising the primary science objectives by altering the traverse distance from 10 km to 8 km, focussing on sites with the highest subsurface ice potential.

The next tier of the descoping measures will be Tier 1: Design Simplification and Secondary Science Adjustments. This tier will involve minor alterations to the design of the mechanical subsystems such as the wheel diameter. The wheel diameter will be reduced slightly by at most, 5% if required to reduce the mass and machining costs. Additionally, the Raman Laser Spectrometer (RLS) sample count or spectral resolution for non-priority sites can be reduced by 15%, preserving critical D/H and ice data. Adjustments to the TLS measurement frequency from weekly to bi-weekly intervals can conserve energy and data bandwidth.

The Final tier of the descoping measures will be Tier 2: Instrument Reduction. This tier will involve the removal of the lowest-priority payload functions that have no

impact on the scientific objectives or their value to the scientific community. This includes removing non-essential RLS scans and limiting CP-MU Gamma Neutron Probe measurements to high-priority sites instead of full route coverage. Even with these changes, the P.H.E.O.N.I.X mission's core objectives of mapping accessible ice reservoirs, monitoring radiation hazards, and analyzing water source evolution, would remain fully achievable.

Upscoping Strategy:

The upscoping strategy will start with Tier 0: Redesign and Change Management. After engineering subteams are made aware of the upscope, the scope change will be accommodated for in subsystems. The scope change may involve added risks that must be managed or accepted, volume or mass reallocations, added instrumentation, or more. During this tier, engineering subteams will decide if their subsystem must be redesigned, or if the scope change can be accommodated with the subsystems as is. For the mechanical subsystem, this may look like this expanding the chassis volume, and for the thermal subsystem, this may involve recalculating the heat flow chart and incorporating extra electrical heaters. Engineering subteams have designed their subsystems with volume, weight, and power margins, so the upscope shall be integrated within those margins. All changes will be immediately documented in the change log.

The following tier of upscoping is Tier 1: Manufacturing and Procurement Readjustments. Each subteam has allotted error margins in lead time estimation, and this time shall be used to accommodate the upscope. If the manufacturing and procurement lead times exceed the projected times in addition to error margins, alternate machining or vendors will be considered. Alternate machining may involve simplifying component geometries or accepting decreased precision for quicker manufacturing times, and alternate vendors will involve searching for contractors with shorter lead times.

The final tier will be Tier 2: Reallocation of Resources. The programmatic subteam has left cost margins, and in the event of an upscope, additional budget shall be redistributed. To accommodate for increased material, manufacturing, or component costs, budget from facility, spacecraft, or total project margins should be transferred to more specific budgets such as the engineering subteam budgets. To accommodate for the possibility of needing additional engineers or technicians in order to stay on schedule, the personnel margin should be transferred to the engineering personnel or technician budgets. In the event of resource allocation, stakeholders will be notified, but the margins should cover any additional costs or schedule changes brought by the scope change.

5.5 Outreach Summary

An outreach plan will be initiated to raise awareness of the mission and inspire future generations to reach for the stars through STEM, non-STEM, and trade pathways into space exploration. Outreach will be initiated through multiple components such as:

1. **Social Media Content Creation** will be conducted on all popular social media platforms prior to the start of the mission and concluding once the mission has ended. This is performed with the goal of raising public awareness of the mission through social media posts, livestreams, Q&A with the NASA staff involved in the mission, and 3-D simulation videos discussing the rover's ongoing scientific experiments, and collected data. An emphasis will be placed on conveying non-technical information to provide an easy-to-understand and accessible education regardless of technical/related background that showcases how space contributes to life on earth and planetary science. Ways for students to participate, learn, and get involved with NASA will also be highlighted such as L'SPACE Mission Concept Academy, L'SPACE National Proposal Writing Evaluation Experience, NASA Community Aerospace Scholars program, challenges, internships, and activities for all ages. The below in-person events and future virtual events will be promoted on the social media platforms to encourage immersive engagement and in-person attendance.

2. **Lego NXT Robotics "Build-Your-Own-Rover" Challenge** for ages 8 - 17 years old at community center to encourage interest in space engineering. Participants will work in teams over the course of three days to build their rover, overcome Martian-inspired "terrain", utilize lego sensors (thermometers, infrared, Colour, Ultrasonic, Gyro, etc) to collect simulated Science data and return to "base". To remove financial barriers, the event will be free to the public with Lego NXT robotic sets provided with one per a team of 5 participants. This outreach component will bring together participants of all backgrounds, inspire a future workforce in engineering, raise awareness of rover navigation and science challenges embraced in mission: P.H.O.E.N.I.X, and provide educational opportunities for all. Participants will be awarded t-shirts, stickers, informational booklets, and posters to celebrate engagement with the challenge.

3. **RIMFAX Geological Presentation** of 2 hours in duration for students in high school through college and workforce professionals to raise awareness of space-related careers in Planetary Science, Biology, Geology, Geophysics, Engineering and more that may be unknown as an avenue to participants interested in space. A live radar imager demonstration along with a 3-D simulation will showcase how objects of interest are found through ground-penetrating waves, the engineering design of the instrument, physics of

the waves, and the low-environmental subsurface impact versus other intrusive methods (digging, scrapping, drilling, etc). From seeing inside Pyramids to locating ice beneath the surface of the Martian atmosphere, RIMFAX will inspire future curiosity that is out of this world. A 30 minute Q&A session will be held after to answer questions regarding the related career fields, how to get involved, where to learn more, and how to transition from another scientific field that may have overlap.

4. **Space Festival!** A fun, interactive all-day event oriented towards family fun for all ages. NASA scientists, engineers, interns, collaborative speakers and more will engage with the general public for Outreach regarding mission: P.H.O.E.N.I.X, which will include robotics engineering demonstrations of innovative technology used in the rover, Planetary Geology presentation talks on picking landing location and developing scientific objectives, challenges faced in the mission, and using real scientific data from the mission to educate how it will make meaningful contributions to both life on earth and future manned missions to Mars. Immersive and educational visual VR and short film entertainment will be available to watch and be immersed into the cosmos. Small children will be included in the fun with hands-on activities such as arts and crafts, face painting, and space games. Space-themed food vendors will be available for tasty eats during the day. As the day turns to night, a space-themed drone show will take place as a send-off and thank you to the attending participants and encourage returning for the next Space Festival.

6.0 Conclusion

Since the completion of the Mission Definition Review (MDR), the team has completed the outline for each subsystem for the mission timeline. The vehicle and payload subsystems have been identified and analyzed to the point where they are able to conduct their mission properly with the presence of other subsystems. The team resolved all TBD/TBRs in the Preliminary Design Review (PDR) by evaluating costs, times, needs, and risks. For the future, the team will need to present our findings and research to NASA to get feedback and later, approval for our mission to commence. The team will also need to collaborate on getting the necessary tools, funding, and workspace to conduct the spacecraft's development and any testing procedures.

The P.H.O.E.N.I.X mission will need to demonstrate our ability to prove that the technologies labelled in the Preliminary Design Review (PDR) are ready for testing and research in the Critical Design Review (CDR). This will prove essential for the team due to this being the first phase into the real-world application of materials, costs, and work. For the Critical Design Review (CDR), the team will present our manufacturing plans to NASA while working on our rover with the resources given. Overall, the mission still continues to meet NASA's science and exploration goals for Mars and gather useful science for planetary habitation.

Bibliography/References

1. “CP-MU Submersible Gamma Neutron Probe | Technical Assoc.” 2025. Tech-Associates.com. 2025. https://tech-associates.com/cp-mu-gn-submersible-gamma-neutron-probe/.
2. “Ion Chamber Design and Operation | Oncology Medical Physics.” n.d. https://oncologymedicalphysics.com/ionization-chamber-design-and-operation/.
3. “It’s Cold on Mars - NASA Science.” 2021. Nasa.gov. April 2, 2021. https://science.nasa.gov/blog/its-cold-on-mars/.
4. “Kapton Polyimide Flexible Heaters: Different Sizes and Wattages.” Kapton Polyimide flexible Heaters | Different sizes and wattages. https://sea.omega.com/th/pptst/KHRA-KHLVA-KHA-SERIES.html.
5. “Lead-Time Guide - Avnet Abacus.” 2025. Avnet.com. 2025. https://my.avnet.com/abacus/resources/lead-time-guide.
6. “McMaster-Carr.” 2025. Mcmaster.com. 2025. https://www.mcmaster.com/products/polyimide-heaters.
7. “Mineralogy of the Martian Surface.” 2021. Caltech.edu. 2021. https://authors.library.caltech.edu/records/635vw-7ga04.
8. “NASA Technical Reports Server (NTRS) Pathfinder.” Libraries. https://lib.ku.edu/database/nasa-technical-reports-server-ntrs.
9. “RLS – the Instrument | Raman Laser Spectrometer (RLS).” 2018. Inta-Csic.es. 2018. https://auditore.cab.inta-csic.es/rls/rls-the-instrument/.
10. “Space Technology | Sierra Space.” 2024. Sierra Space. September 18, 2024. https://www.sierraspace.com/space-technology/.

11. “Superior’s Military-Spec Threads | SuperiorThreads.com.” 2025. Superiorthreads.com. 2025. https://www.superiorthreads.com/mil-spec-threads.
12. Anywaves. Flight Heritage: Antennas for Space Missions. 2025. https://anywaves.com/references/flight-heritage/
13. ASM Aerospace Specification Metals Inc. *Titanium Ti-6Al-4V (Grade 5), ELI, Annealed*. MatWeb. Material data sheet.
14. Astronomy Magazine Staff. “MRO Eases into Working Orbit.” Astronomy, September 29, 2006. https://www.astronomy.com/science/mro-eases-into-working-orbit/
15. BAE Systems, RAD5545™ “SpaceVPX”, PDF, Version 1.2, 2025, BAE Systems. https://www.baesystems.com/en-us/dam/jcr:cd804739-19fa-43f6-b47a-c58eb18e3bba/17-c09-RAD5545-SpaceVPX-SBC-v1-2-Flight-ds-2025-web.pdf
16. BAE Systems. RAD5545 SpaceVPX SBC Datasheet. 2025. https://www.baesystems.com/en-us/dam/jcr:cd804739-19fa-43f6-b47a-c58eb18e3bba/17-c09-RAD5545-SpaceVPX-SBC-v1-2-Flight-ds-2025-web.pdf
17. BAE Systems. RAD750 Radiation-Hardened PowerPC Microprocessor Component Datasheet. 2025. https://www.baesystems.com/en-us/dam/jcr:c297f318-c618-4015-9399-adf76ac5cf55/16-f78-RAD750-Component-datasheet-2025-web.pdf
18. BAE Systems. RAD750 Radiation-Hardened PowerPC Microprocessor Component Datasheet. 2025. https://www.baesystems.com/en-us/dam/jcr:c297f318-c618-4015-9399-adf76ac5cf55/16-f78-RAD750-Component-datasheet-2025-web.pdf

19. Bowman, Abigail, ed. “Tunable Laser Spectrometer on NASA’s Curiosity Mars Rover.” NASA. https://www.nasa.gov/image-article/tunable-laser-spectrometer-nasas-curiosity-mars-rover/.
20. cdmc_admin. 2024. “Safety Practices at Work Should Include Deburring.” CDMC. January 14, 2024. https://cdmcmachine.com/safety-practices-at-work-should-include-deburring.
21. Chargex. CX48500 48V 500Ah Lithium Ion Battery Data Sheet. https://www.lithiumion-batteries.com/uploads/files/16456/CX48500-Data-Sheet.pdf
22. Chris Mellor, “Perseverance Rover Uses Space-Hardened SSD to Store Mars Data,” The Register, June 15, 2023. https://www.theregister.com/2023/06/15/mars_perseverance_rover_space_ssd
23. Clark, Stephen. “Fate of NASA’s Insight Mars Mission to Be Decided Soon.” Spaceflight Now, March 5, 2016. https://web.archive.org/web/20181116012749/https://spaceflightnow.com/2016/03/05/fate-of-nasas-insight-mars-mission-to-be-decided-soon/.
24. Consultative Committee for Space Data Systems (CCSDS). Proximity-1 Space Link Protocol. Blue Book 211.0-B-6. 2013. https://ccsds.org/Pubs/211x0b6e1.pdf
25. DwyerOmega. Self-Adhesive Polyimide Flexible Heaters 302°F Max – KHLVA Series. https://www.dwyeromega.com/en-us/self-adhesive-polyimide-flexible-heaters-302-f-max/KHRA-KHLVA-KHA-SERIES/p/KHLVA-102-5.

26. EaglePicher Technologies. SAR-10211 Aerospace Battery. EaglePicher Technologies. https://www.eaglepicher.com/sites/default/files/SAR-10211%201023.pdf
27. EEE-INST-002: Instructions for EEE Parts Selection, Screening, Qualification, and Derating (Incorporated Addendum 1). NASA/TP-2003-212242. Goddard Space Flight Center, Greenbelt, MD: NASA, April 2008. https://nepp.nasa.gov/docuploads/FFB52B88-36AE-4378-A05B2C084B5EE2CC/EEE-INST-002_add1.pdf
28. Finckenor, M. M., and D. Dooling. Multilayer Insulation Material Guidelines. https://ntrs.nasa.gov/api/citations/19990047691/downloads/19990047691.pdf.
29. GammaGuard. T007-T Thermal Neutron Detector. Accessed July 6, 2025. https://gammawatch.com/ct007-t-thermal-neutron-detector/
30. Gore. “DXN2605 Shielded Twisted Pair Cable Datasheet”. 2016. https://www.gore.com/sites/default/files/2016-04/dxn2605c.pdf
31. Hamran, S.-E., et al. 2020. “Radar Imager for Mars’ Subsurface Experiment—RIMFAX.” Space Science Reviews 216 (8): 128.
32. Hamran, Svein-Erik & Paige, David & Allwood, Abigail & Amundsen, Hans Erik Foss & Berger, Tor & Brovoll, Sverre & Carter, Lynn & Casademont, Titus & Damsgard, Leif & Dypvik, Henning & Eide, Sigurd & Fairén, Alberto & Ghent, Rebecca & Kohler, Jack & Mellon, Michael & Nunes, Daniel & Plettemeier, Dirk & Russell, Patrick & Siegler, Matt & Øyan, Mats. (2022). Ground penetrating radar observations of subsurface structures in the floor of Jezero crater, Mars. Science advances. 8. eabp8564. 10.1126/sciadv.abp8564.

33. Hassler, Donald M., John W. Norbury, and Günther Reitz. “Mars Science Laboratory Radiation Assessment Detector (MSL/RAD) Modeling Workshop Proceedings.” ADS, August 2017. https://ui.adsabs.harvard.edu/abs/2017LSSR...14....1H/abstract.
34. He, Fei, Zhaojin Rong, Zhaopeng Wu, Jiawei Gao, Kai Fan, Xu Zhou, Limei Yan, Yuqi Wang, and Yong Wei. “Martian Dust Storms: Reviews and Perspective for the Tianwen-3 Mars Sample Return Mission.” MDPI, July 17, 2024. https://www.mdpi.com/2072-4292/16/14/2613
35. Instar Engineering and Consulting, Inc. *Vibration Testing of Small Satellites—Part 5: Random Vibration Testing.* Rev B (July 24, 2017). PDF. Accessed August 18, 2025. https://www.instarengineering.com/pdf/resources/Instar_Vibration_Testing_of_Small_Satellites_Part_5.pdf
36. Isalamah, Ibrahim. “Lab 5: Watchdog Timers.” University of Texas at El Paso, 2017. https://www.cs.utep.edu/isalamah/courses/5372/labs/Lab5-Watchdog-Timers.pdf
37. Jean-Pierre Bibring, et al. Global Mineralogical and Aqueous Mars History Derived from OMEGA/Mars Express Data, February 10, 2010. https://www.woodsholediversity.org/wp-content/uploads/sites/14/2018/10/OMEGA_Bibring_Science_2006_58188.pdf.
38. Jet Propulsion Laboratory, California Institute of Technology (JPL). 2021. “Mars Reconnaissance Orbiter Communications System.”

39. Jet Propulsion Laboratory. “Construction to Begin on 2016 NASA Mars Lander.” https://www.jpl.nasa.gov/news/construction-to-begin-on-2016-nasa-mars-lander/.
40. Jet Propulsion Laboratory. “Deep Space Communications”, vol. 13, “Chapter 7,” Deep Space Communications and Navigation Systems Center of Excellence (DESCANSO). Pasadena, CA: Jet Propulsion Laboratory, California Institute of Technology, October 30, 2014. PDF. https://descanso.jpl.nasa.gov/monograph/series13/DeepCommo_Chapter7--141030.pdf.
41. Jet Propulsion Laboratory. "Mars Rovers Survive Dust Storms, Ready for Next Objectives." Passage of time, September 7, 2007. https://www.jpl.nasa.gov/news/mars-rovers-survive-dust-storms-ready-for-next-objectives/.
42. Jet Propulsion Laboratory. “NASA Begins Testing Mars Lander for Next Mission to Red Planet.” https://www.jpl.nasa.gov/news/nasa-begins-testing-mars-lander-for-next-mission-to-red-planet/.
43. Kelair Products, Inc. Louver Dampers. https://www.kelairdampers.com/products/louver-dampers.
44. Kounaves, S. P., Alyssa J. Barney, Steven W. Squyres, Christopher S. Edwards, Cary N. Craft, and David W. Langevin. 2014. “Evidence of Martian Perchlorate, Chlorate, and Nitrate in the Phoenix Lander Samples.” Journal of Geophysical Research: Planets 119 (2014): 1–10. https://doi.org/10.1016/j.jphs.2014.xx

45. L'Space Team 01 Summer 2025. Unpublished Mission Task Document. https://docs.google.com/document/d/1nnbnhPqEa0KyQb4esg_-8lgqv4nRSxk8Wdw3embVpIQ/edit?tab=t.0.
46. LambdaTek. “Exascend / Industry / NAND Flash / SSD / Radiation Hardened / PR4 / PCIe Gen4x4 / M.2 2242 / Standard[Streaming] / 480GB / 3D TLC / I-Temp.[-40~85] /.” https://www.lambda-tek.com/Exascend-EXPR4Q0480GB-sh/B50797748.
47. Lee, Sarah. 2025. “Ionization Chamber Calibration Essentials.” Numberanalytics.com. 2025. https://www.numberanalytics.com/blog/ionization-chamber-calibration-guide.
48. LEGO® Education. “Middle School STEAM Kits.” Shop – LEGO Education, The LEGO Group. https://education.lego.com/en-us/shop/middle/.
49. Lerner, Preston. “A Helicopter Dreams of Mars.” Air & Space Magazine, Smithsonian, April 2019. https://www.smithsonianmag.com/air-space-magazine/helicopter-dreams-of-mars-180971739/.
50. Lopez-Reyes, Guillermo. “Raman Laser Spectrometer (RLS) Calibration Target Design to Allow Onboard Combined Science between the RLS and MicrOmega Instruments on the ExoMars Rover.” Analytical Science Journals - Wiley Online Library, January 23, 2020.https://analyticalsciencejournals.onlinelibrary.wiley.com/doi/full/10.1002/jrs.462.

51. Lyons, John. SMEX-Lite Modular Solar Array Architecture. NASA Goddard Space Flight Center, January 1, 2002. https://ntrs.nasa.gov/citations/20020061277
52. NASA. n.d. “Lucy - NASA Science.” Science.nasa.gov. NASA. https://science.nasa.gov/mission/lucy/.
53. Marspedia. 2024. “Radiation.” Marspedia. October 7, 2024. https://marspedia.org/Radiation.
54. Martinez, G. M., C. N. Newman, A. De Vicente-Retortillo, E. Fischer, N. O. Renno, M. I. Richardson, A. G. Fairén, et al. “The Modern Near-Surface Martian Climate: A Review of in-Situ Meteorological Data from Viking to Curiosity - Space Science Reviews.” SpringerLink, April 25, 2017. https://link.springer.com/article/10.1007/s11214-017-0360-x.
55. Mengel, Aliyah. 2024. “Advanced Cooling Technologies Assisting in Lunar Rover Mission - Lancaster Chamber of Commerce.” Lancaster Chamber of Commerce. January 19, 2024. https://www.lancasterchamber.com/thermal-management-system-tms-designed-for-nasas-viper
56. Mercury Systems. “RH3440 3U VPX Solid-State Data Recorder Datasheet”. 2025. https://www.mrcy.com/application/files/5216/3001/4013/5008.22E_RH3440_3U_VPX_SRIO_SSDR.pdf
57. Mercury Systems. “Space Data Recorders.” https://www.mrcy.com/products/data-storage-and-transfer/space-data-recorders.

58. Military Aerospace. “BAE Systems Moves into Third Generation RAD-Hard Processors.” https://www.militaryaerospace.com/computers/article/16710930/bae-systems-moves-into-third-generation-rad-hard-processors.
59. Motamedi, K., AP Colin, JH Hooijschuur, O. Postma, R. Lootens, D. Pruijser, R. Stoevelaar, et al. “Design of a Mars Atmosphere Simulation Chamber and Testing A Raman Laser Spectrometer (RLS) under Conditions Pertinent to Mars Rover Missions - EPJ Techniques and Instrumentation.” SpringerOpen, September 22, 2015. https://epjtechniquesandinstrumentation.springeropen.com/articles/10.1140/epjti/s40485-015-0025-7?utm_source=chatgpt.com#Sec9.
60. Mouser Electronics. “SN65C1168EMPWSEP.” https://www.mouser.com/ProductDetail/Texas-Instruments/SN65C1168EMPWSEP?qs=XeJtXLiO41S%252BMj6J5XH9ug%3D%3D&srsltid=AfmBOorYEcBmBHVI5uPv4J6pYlfX4sMqyULc4rvleMsDNXUXagGqnLp3.
61. Mouser Electronics. “THVD9491DTSEP.” https://www.mouser.com/ProductDetail/Texas-Instruments/THVD9491DTSEP?qs=sGAEpiMZZMutXGli8Ay4kEO5oSXSnDEbcU5F2VWD%252B5U%3D.
62. Multilayer Insulation Material Guidelines. https://ntrs.nasa.gov/api/citations/19990047691/downloads/19990047691.pdf
63. NASA Goddard Space Flight Center. Texas Instruments Partnership Overview. 2025. https://partnerships.gsfc.nasa.gov/wp-content/uploads/Texas-instruments.pdf

64. NASA Jet Propulsion Laboratory. “Svc C++ API.” F´ Flight Software Framework. https://nasa.github.io/fprime/v3.1.0/UsersGuide/api/c%2B%2B/html/svc.html
65. NASA Jet Propulsion Laboratory. “Svc::Health.” F´ Flight Software Framework. https://fprime.jpl.nasa.gov/latest/Svc/Health/docs/sdd/
66. NASA Jet Propulsion Laboratory. F´ Documentation. https://fprime.jpl.nasa.gov/latest/docs/
67. NASA Langley Research Center. “Electra-Lite Transceiver Description.” 2004. https://discovery.larc.nasa.gov/PDF_FILES/29Electra_Description.pdf
68. NASA Science. “Mars 2020 Perseverance: Rover Components.” 2021. https://science.nasa.gov/mission/mars-2020-perseverance/rover-components/
69. NASA. “Appendix G. Life-Cycle and Technical Review Entrance and Success Criteria.” https://nodis3.gsfc.nasa.gov/displayDir.cfm?Internal_ID=N_PR_7123_001D_&page_name=AppendixG.
70. NASA. “Explore Item.” 2022. Nasa.gov. 2022. https://sma.nasa.gov/sma-disciplines/planetary-protection/explore/explore-item/how-to-build-a-clean-spacecraft
71. NASA. “Fault Management Handbook. Draft 2. NASA-HDBK-1002”. NASA, April 2, 2012. https://www.nasa.gov/wp-content/uploads/2015/04/636372main_NASA-HDBK-1002_Draft.pdf
72. NASA. “Insight Lander - NASA Science.” November 4, 2024. https://science.nasa.gov/mission/insight/.

73. NASA. “Mars Exploration Rovers: Spirit and Opportunity - NASA Science.” April 7, 2025. https://science.nasa.gov/mission/mars-exploration-rovers-spirit-and-opportunity/.
74. NASA. “Mars: Facts - NASA Science.” NASA, April 22, 2025. https://science.nasa.gov/mars/facts/.
75. NASA. “NASA Space Flight Program and Project Management Requirements w/Change 4.” August 3, 2021. https://nodis3.gsfc.nasa.gov/displayDir.cfm?t=NPR&c=7120&s=5E.
76. NASA. “Perseverance Science Instruments - NASA Science.” NASA, November 18, 2024. https://science.nasa.gov/mission/mars-2020-perseverance/science-instruments/.
77. NASA. “SEH 3.0 NASA Program/Project Life Cycle.” July 26, 2023. https://www.nasa.gov/reference/3-0-nasa-program-project-life-cycle/.
78. NASA. Earth Science Data Systems: Suppliers Map. 2025. https://www3.nasa.gov/specials/ESDSuppliersMap/
79. National Aeronautics and Space Administration (NASA). 2016. “Spacecraft Communication Standards: RS-422 Protocol.”
80. National Aeronautics and Space Administration (NASA). 2021. “Perseverance Rover Technical Specifications.” NASA Mars Exploration Program.
81. NodIS3 GSFC. “NASA Systems Engineering Processes and Requirements.” NASA Procedural Requirements. https://nodis3.gsfc.nasa.gov/OPD_docs/NID_7123_69_.pdf.

82. Office of Management and Budget. “Circular No. A-11: Preparation, Submission, and Execution of the Budget.” Executive Office of the President of the United States, 2016.
83. Office of the Chief Engineer. “NASA Systems Engineering Processes and Requirements.” NASA Procedural Requirements. https://nodis3.gsfc.nasa.gov/OPD_docs/NID_7123_69_.pdf.
84. Omega Engineering. 2025. “Kapton Polyimide Flexible Heaters (KHRA, KHLVA, KHA Series).” Omega Engineering. Accessed August 18, 2025. https://sea.omega.com/th/pptst/KHRA-KHLVA-KHA-SERIES.html.
85. OSHA Directorate of Training and Education. Construction focus four: Struck-by hazards, April 2011. https://www.osha.gov/sites/default/files/struckby_ig.pdf.
86. OSHA. “1926.759 - Falling Object Protection.” Occupational Safety and Health Administration. https://www.osha.gov/laws-regs/regulations/standardnumber/1926/1926.759.
87. OSHA. “Chemical Hazards and Toxic Substances - Overview.” Occupational Safety and Health Administration, n.d. https://www.osha.gov/chemical-hazards.
88. OSHA. “Control of Hazardous Energy (Lockout/Tagout) - Lockout/Tagout Program.” Occupational Safety and Health Administration, n.d. https://www.osha.gov/control-hazardous-energy/program.
89. OSHA. “Electrical - Electric-ARC Flash Hazards.” Occupational Safety and Health Administration, n.d. https://www.osha.gov/electrical/flash-hazards.
90. OSHA. “Electrical - Overview.” Occupational Safety and Health Administration. https://www.osha.gov/electrical.

91. OSHA. “ETools : Solutions for Electrical Contractors - Materials Handling - Heavy Lifting.” Construction Focus Four: Struck-By Hazards. https://www.osha.gov/etools/electrical-contractors/materials-handling/heavy.
92. OSHA. “Welding, Cutting, and Brazing - Standards.” Occupational Safety and Health Administration. https://www.osha.gov/welding-cutting-brazing/standards.
93. OSHA. “Workplace Stress - Overview.” Occupational Safety and Health Administration. https://www.osha.gov/workplace-stress.
94. Packet Digital. "MPPT-6SBB." Packet Digital. https://packetdigital.com/power-products/maximum-power-point-tracker/
95. Putzig, Nathaniel, Gareth Morgan, Hanna Sizemore, David Baker, Eric Petersen, Asmin Pathare, Colin Dundas, et al. “Mapping Ice Resources on Mars.” ADS, December 2021. https://ui.adsabs.harvard.edu/abs/2021AGUFM.P23B..07P/abstract.
96. Rhea, John. “BAE Systems Moves into Third Generation RAD-Hard Processors.” Military Aerospace, May 1, 2002. https://www.militaryaerospace.com/computers/article/16710930/bae-systems-moves-into-third-generation-rad-hard-processors.
97. Royal Meteorological Society. “Martian Meteorology.” MetMatters. https://www.rmets.org/metmatters/martian-meteorology
98. Samuel K. Moore, “How NASA Is Adapting Radios to a Noisier Mars,” IEEE Spectrum, August 5, 2012. https://spectrum.ieee.org/how-nasa-is-adapting-radios-to-a-noisier-mars

99. Sandilands, Steven. “Communications with Mars Curiosity.” 2012. https://sandilands.info/sgordon/communications-with-mars-curiosity#:~:text=X%2Dband:%208%20GHz,name%20are%20not%20clearly%20defined

100. SatCatalog. “Custom Thermal Insulation & MLI Blankets.” https://www.satcatalog.com/component/custom-thermal-insulation-mli-blankets/.

101. Schröder, Susanne, and Yuichiro Cho. Rax: The Raman Spectrometer for the MMX phobos rover. https://www.researchgate.net/publication/364196900_RAX_The_Raman_Spectrometer_for_the_MMX_Phobos_Rover.

102. Sierra Space Corporation. 2025. “Smallsat Solar Array System 780 W Articulated Array.” satsearch. Last updated February 24, 2025. https://satsearch.co/products/sierra-space-smallsat-solar-array-system-780-w-articulated-array.

103. Sierra Space. Sierra Space Product Catalog: October 2024, Rev. 1. https://www.sierraspace.com/wp-content/uploads/2024/11/SIERRA-SPACE-PRODUCT-CATALOG_OCT2024_R1.pdf.

104. Sinha, Rishitosh K., and Dwijesh Ray. “Extensive Glaciation in the Erebus Montes Region of Mars.” Icarus 367 (2021): 114557. https://doi.org/10.1016/j.icarus.2021.114557.

105. SkyGeek. Hexion EPON™ 815C Yellow Epoxy Resin – Gallon Jug. https://skygeek.com/momentive-epon-resin-815c-1-gallon.html.

106. Smith, Brett. “A Guide to Reading Raman Spectra.” AZoM, September 4, 2020.https://www.azom.com/article.aspx?ArticleID=18610#:~:text=Spectroscopy%20is%20a%20group%20of,as%20photons%20per%20time%20interval

107. Space Center Houston. “Membership.” Tickets – Space Center Houston. https://tickets.spacecenter.org/webstore/shop/viewItems.aspx?cg=membershipcg&c=membershipc.

108. Space Center Houston. “Moon 2 Mars Festival, Presented by Wellby Financial (March 9–22, 2025).” https://spacecenter.org/moon2marsfestival/

109. SPH Engineering. “RadSys Zond Aero 500 NG GPR Terrestrial System (IS-RS-ZOND-AERO-500-NG-TERR).” EngineerSupply.com. https://www.engineersupply.com/SPH-Engineering-RadSys-Zond-Aero-500-NG-GPR-Terrestrial-System-IS-RS-ZOND-AERO-500-NG-TERR.aspx.

110. Stephen Clark, “NASA Swaps Computers to Restore Curiosity Rover,” Spaceflight Now, March 20, 2013. https://spaceflightnow.com/mars/msl/120810computer

111. SwRI. “SwRI Delivers Innovative Instrument for NASA’s Europa Clipper Mission.” https://www.swri.org/newsroom/press-releases/swri-delivers-innovative-instrument-nasa-s-europa-clipper-mission.

112. Texas Instruments. “AN-1035: RS-422 and RS-485 Standards Overview.” 2016. https://www.ti.com/lit/an/snla044b/snla044b.pdf

113. Texas Instruments. “SN65C1168E-SEP Datasheet”. 2025. https://www.ti.com/lit/ds/symlink/sn65c1168e-sep.pdf?ts=1755459652159

114. Texas Instruments. “SN65C1168EMPWSEP.” Mouser Electronics. https://www.mouser.com/ProductDetail/Texas-Instruments/SN65C1168EMPWSEP?qs=XeJtXLiO41S%252BMj6J5XH9ug%3D%3D&srsltid=AfmBOorYEcBmBHVI5uPv4J6pYlfX4sMqyULc4rvleMsDNXUXagGqnLp3.

115. Texas Instruments. “THVD9491DTSEP.” Mouser Electronics. https://www.mouser.com/ProductDetail/Texas-Instruments/THVD9491DTSEP?qs=sGAEpiMZZMutXGli8Ay4kEO5oSXSnDEbcU5F2VWD%252B5U%3D

116. Tfaws ', and Eugene Ungar. 2002. “Modeling of Multi-Layer Insulation Layups with Transmissive Outer Layers.” https://tfaws.nasa.gov/TFAWS02/Data/Thermal/Ungar.pdf.

117. The sample analysis at Mars Investigation and instrument ... https://ntrs.nasa.gov/api/citations/20120002542/downloads/20120002542.pdf.

118. Toronto Metropolitan University. “VxWorks Watchdog Library.” EE8205 Data Sheets. https://www.ee.torontomu.ca/~courses/ee8205/Data-Sheets/Tornado-VxWorks/vxworks/ref/wdLib.html

119. U.S. General Services Administration. “City Pair Program (CPP).” Transportation (Airfare Rates, POV Rates, etc.), GSA. https://www.gsa.gov/travel/plan-a-trip/transportation-airfare-rates-pov-rates-etc/airfare-rates-city-pair-program

120. U.S. General Services Administration. “FedRooms.” Travel – Plan a Trip, Lodging, GSA. https://www.gsa.gov/travel/plan-a-trip/lodging/fedrooms

121. U.S. General Services Administration. “Per Diem Rates Results: Fiscal Year 2026, ZIP Code 32920, Florida.” Per Diem Rates, GSA. https://www.gsa.gov/travel/plan-book/per-diem-rates/per-diem-rates-results?action=perdiems_report&fiscal_year=2026&city=&state=FL&zip=32920.

122. University of Minnesota. “Space Rental.” Northrop: Theaters & Spaces. https://www.northrop.umn.edu/space-rental.

123. Villanueva, Geronimo L., Giuliano Liuzzi, Shohei Aoki, Shane W. Stone, Adrian Brines, Ian R. Thomas, Miguel Angel Lopez-Valverde, et al. “The Deuterium Isotopic Ratio of Water Released from the Martian Caps as Measured with TGO/Nomad.” ADS, June 6, 2022. https://ui.adsabs.harvard.edu/abs/2022GeoRL..4998161V.

124. Viola, Donna A. Expanded Craters on Mars: Implications for Shallow, Mid-Latitude Excess Ice. PhD diss., University of Arizona, 2017. https://repository.arizona.edu/handle/10150/625594.

125. Viola, Donna A., and R. E. Milliken. “Mid-Latitude Martian Ice as a Target for Human Exploration, Astrobiology, and In Situ Resource Utilization.” Paper presented at the 1st EZ Workshop for Human Missions to Mars, Houston, TX, June 8–10, 2015. https://www.hou.usra.edu/meetings/explorationzone2015/pdf/1011.pdf.

126. Warner, Nicholas H., Sukesh Gupta, Shih-Yuan Lin, Jung-Rack Kim, Jean-Pierre Müller, and Julie Morley. “Late Noachian to Hesperian Climate Change on Mars: Evidence of Episodic Warming from Transient Crater Lakes

Near Ares Vallis.” Journal of Geophysical Research: Planets 115, no. E6 (2010). https://doi.org/10.1029/2009JE003522.

127. Webster, Christopher, and Paul Mahaffy. ESA. https://sci.esa.int/documents/33745/35957/1567259793745-Methane2009_Session8_2_TLS_Webster.pdf.

128. Wind River Systems. VxWorks Datasheet. 2025. https://www.windriver.com/resource/vxworks-datasheet

129. WireMasters. “DXN2604.” https://www.wiremasters.com/dxn2604.

130. WireMasters. “DXN2605.” https://www.wiremasters.com/dxn2605.

Declaration of Generative AI Usage

During the preparation of this document, the team used OpenAI's ChatGPT as a search aid to find resources for various hardware. The tool was also used to ensure consistent information throughout the deliverable. During literature reviews, the team utilized Google's AI in Search to identify cited resources. The team identified key facts and figures and verified their technical correctness and references source materials. During the preparation of this document, the team utilized online translation tools including Google Translate to aid in writing and editing, specifically for bilingual or English-secondary-language team members.

After using various tools, the team reviewed and edited all content to ensure consistency, original contribution, and technical accuracy. Team 01 takes full responsibility for the content of this deliverable.

Appendices

TBD / TBR #	Plans and Timeline for Resolution
1	Rover speed of travel
2	Rate of heartbeat transmission from rover
3	Sol that the rover shall begin autonomous travel

Figure A.1: (TBD/TBR Table)

Changes	Description
MCR-RFA-1, Section 1.2	The measurement observables must directly relate to the physical parameters with which the STM was addressed and a CRF was filled due to changes in both our human exploration goal objectives to meet this RFA.
MCR-RFA-2, Section 1.3	A thorough description of each region of interest and how they fulfill the team's science objectives must be provided, and was also addressed by defining the region of interest.
CRF - Science objective 1# of HBS-1LM (waiting on approval)	Science objective 1# of HBS-1LM: The team is requesting a minor alteration to the science objective and add clarification within the STM from “various samples” (exact quantity was originally unspecified) to one single sample. Science objective 1# of HBS-1LM - STM observable: Change data transmission interval from “monthly” to “weekly”.
CRF - Science objective 2# of HBS-1LM (waiting on approval)	The second objective of HBS-1LM’s main purpose still remains the same, but the measurement approach to provide quantitative data had to change.

Figure A.2 (Mission Change Log)

Transfer Mode	Heat Transfer Equation	Thermal Resistance
Conduction	$\dot{Q} = \frac{dQ}{dt} = -kA\frac{dT}{dx} \approx -kA\frac{\Delta T}{L}$	$R_{\theta Cond} = \frac{L}{kA}$
Convection	$\dot{Q} = \frac{dQ}{dt} = -hA_S(T_S - T_f)$	$R_{\theta Conv} = \frac{1}{hA_S}$
Radiation	$\dot{Q} = \frac{dQ}{dt} = -\sigma\epsilon F A_S(T_S^4 - T_{SA}^4)$	$R_{\theta Rad} \approx \frac{\Delta T}{\sigma\epsilon F A_S(T_S^4 - T_{SA}^4)} = \frac{1}{h_{Rad}A_S}$

Figure A.3 (Heat Transfer Equations)

Figure A.4: (Submersible Gamma Neutron Probe with Rotary and Linear motion Sensors CAD)

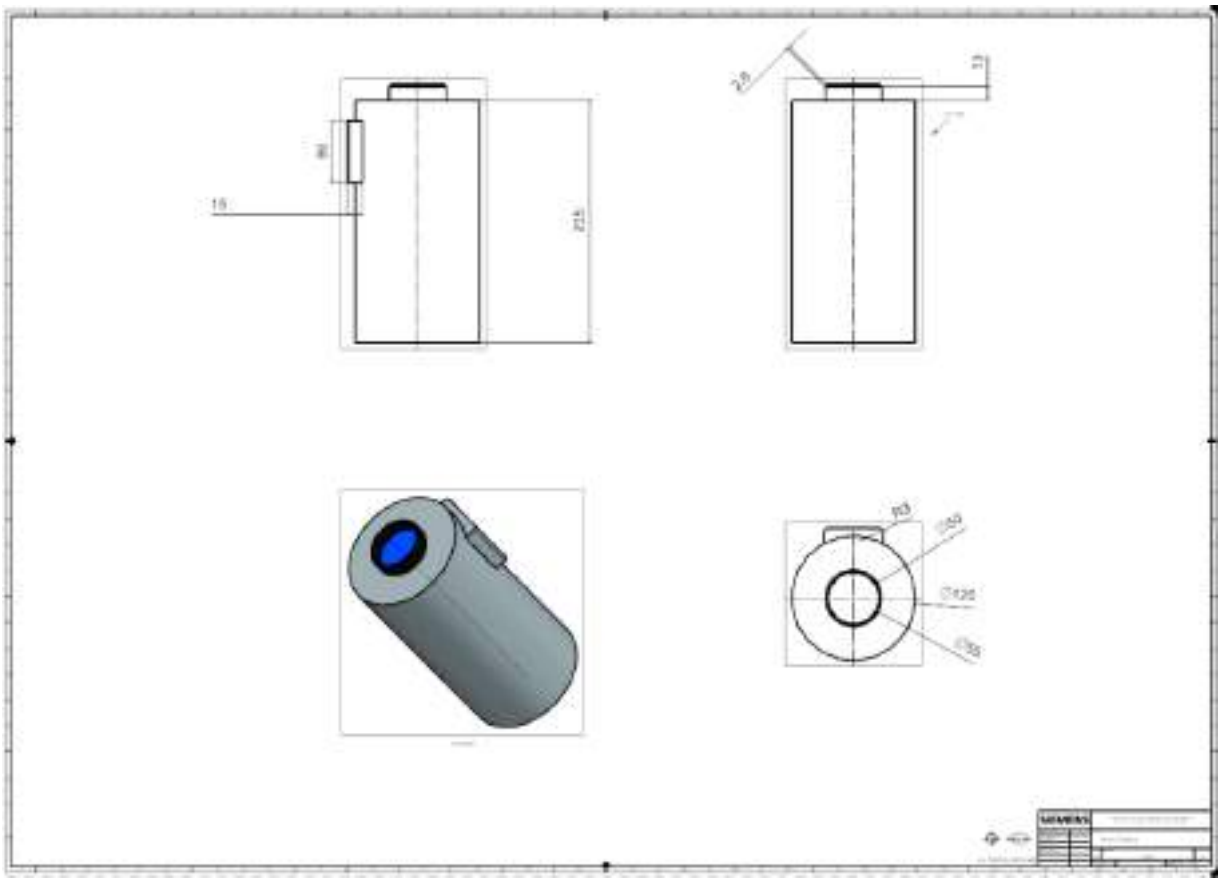

Figure A.5: (Submersible Gamma Neutron Probe with Rotary and Linear motion Sensors CAD Drawing)

Figure A.6: (Tire CAD)

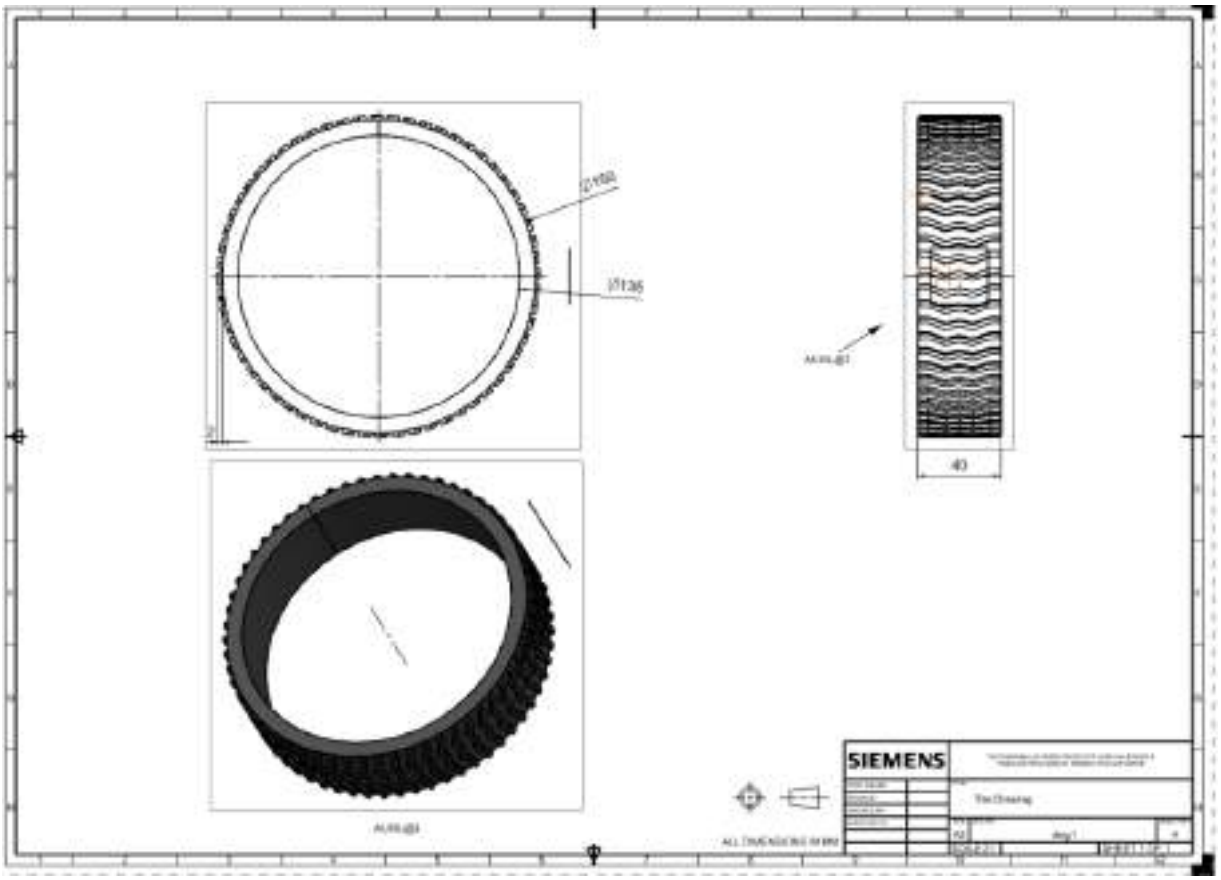

Figure A.7: (Tire CAD Drawing)

Figure A.8: (Spokes CAD)

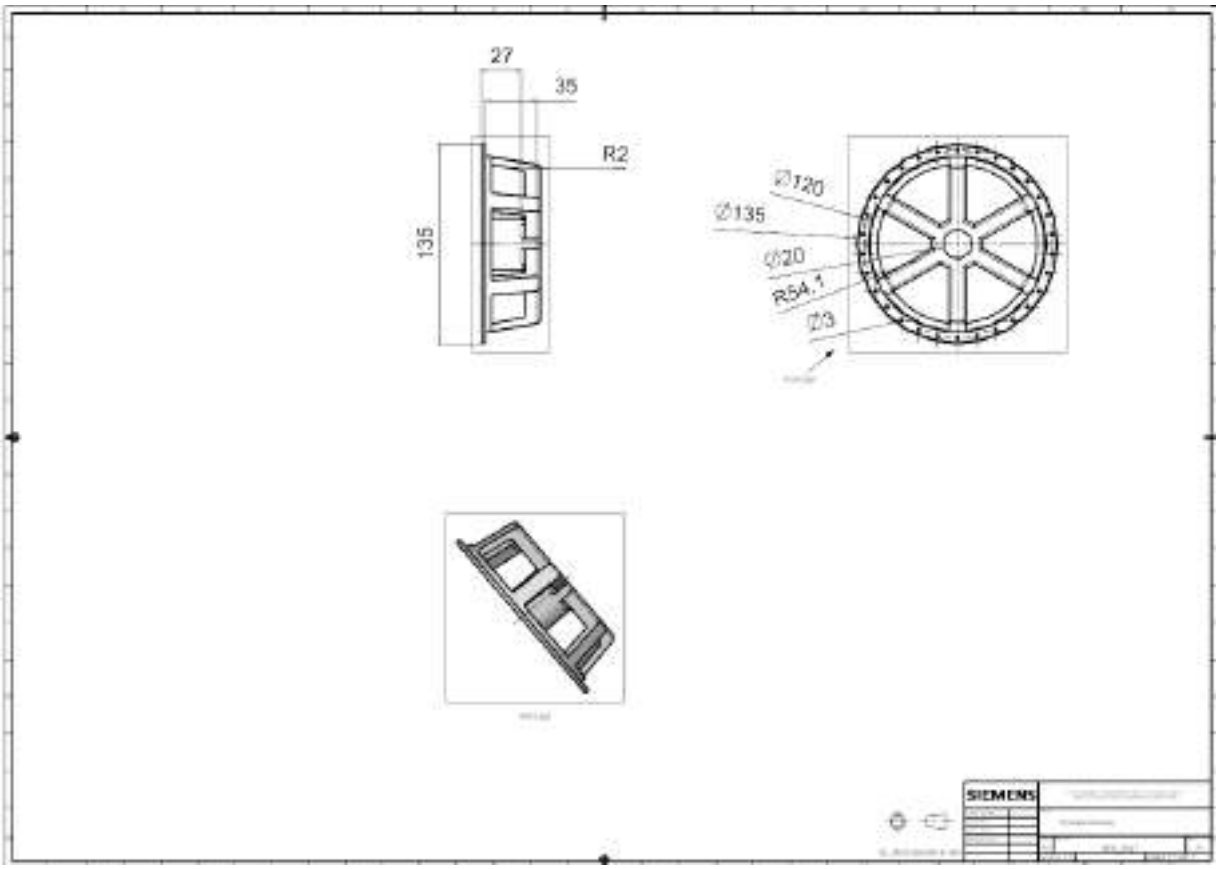

Figure A.9: (Spokes CAD Drawing)

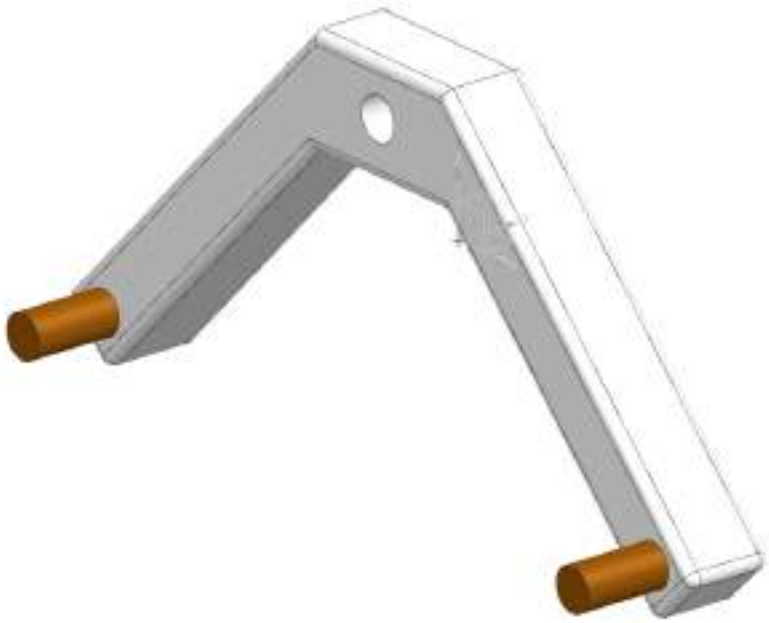

Figure A.10: (Front Rocker Bogie Arm CAD Drawing)

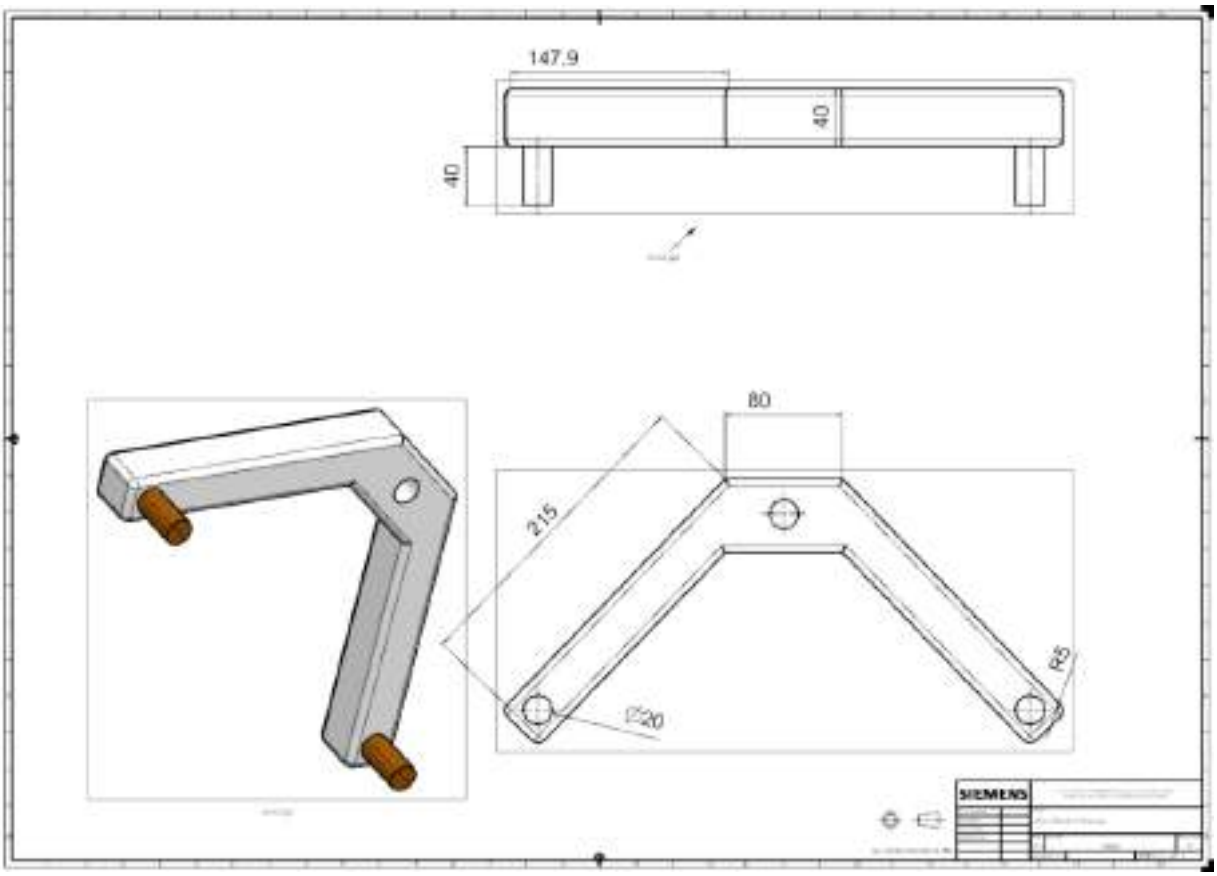

Figure A.11: (Front Rocker Bogie Arm CAD)

Figure A.12: (Back Rocker Bogie Arm CAD)

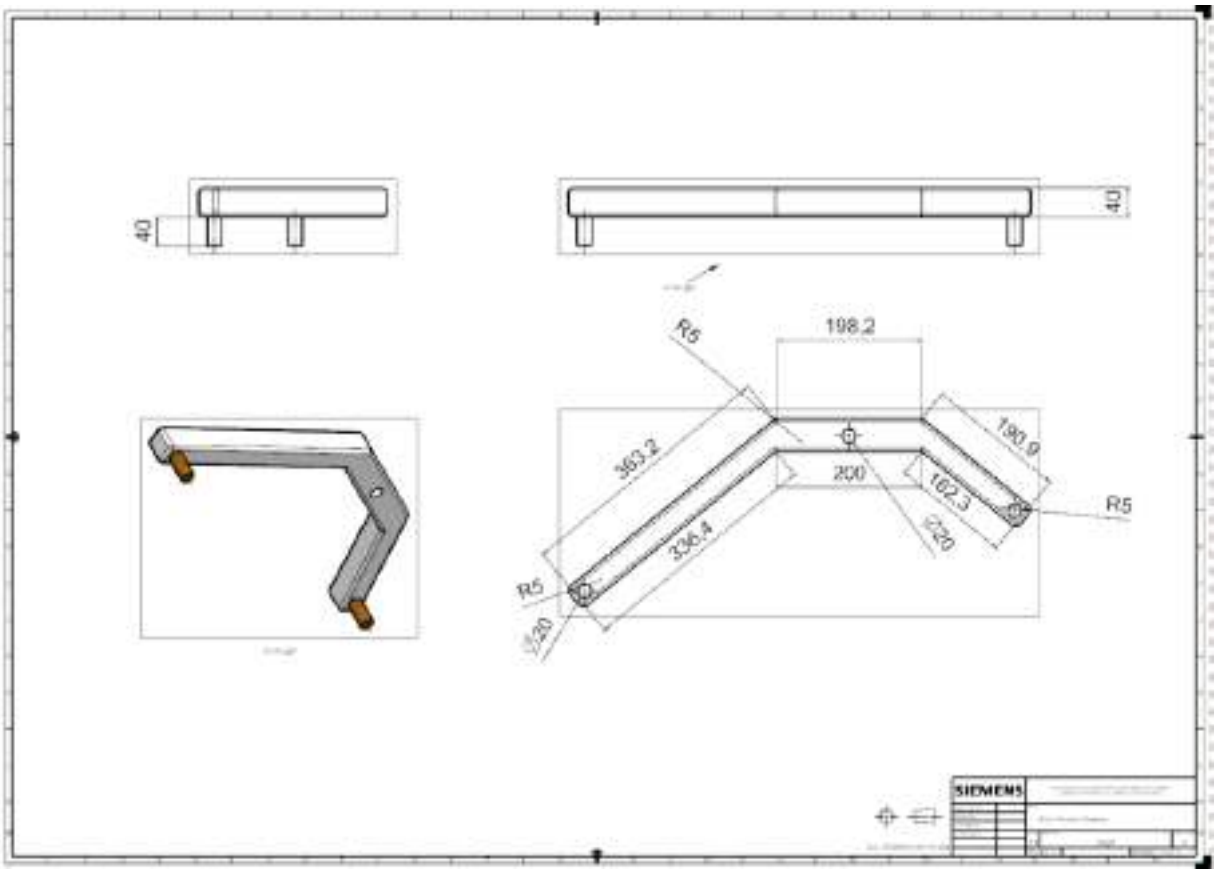

Figure A.13: (Back Rocker Bogie Arm CAD Drawing)

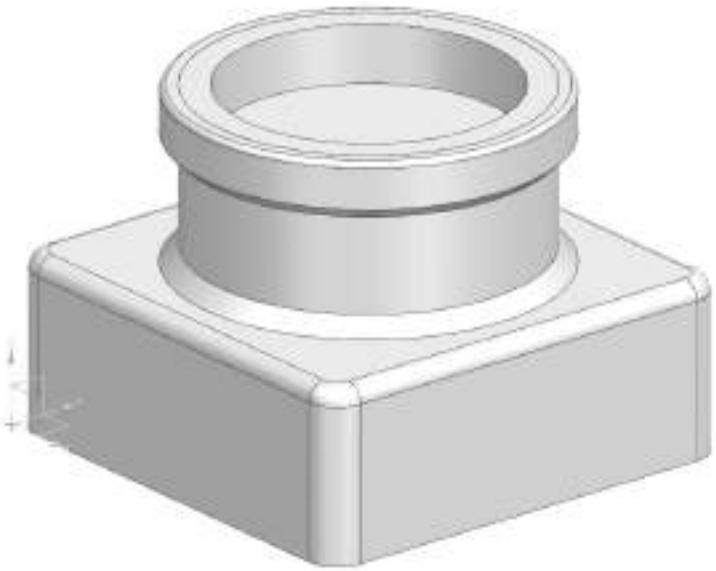

Figure A.14: (Robotic Arm Base CAD)

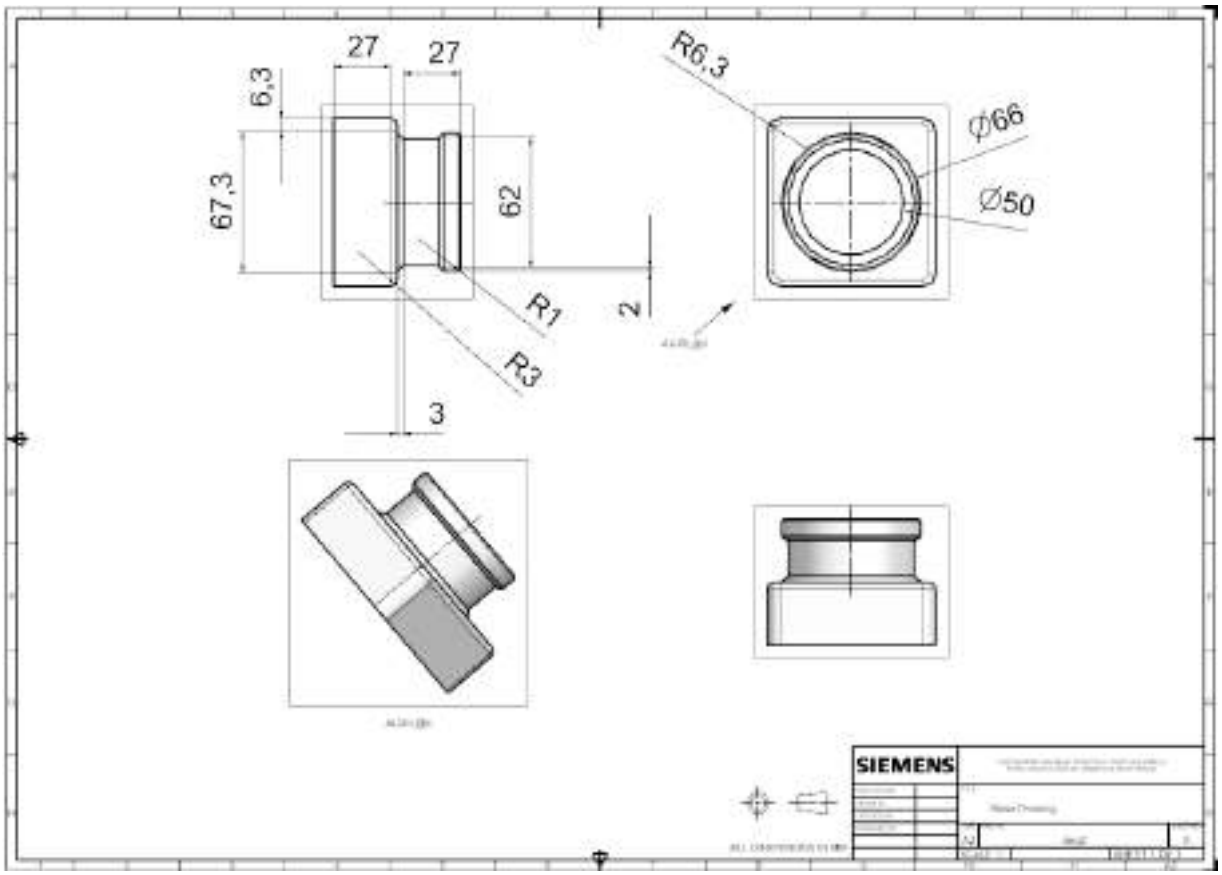

Figure A.15: (Robotic Arm Base CAD Drawing)

Figure A.16: (Robotic Arm Connector CAD)

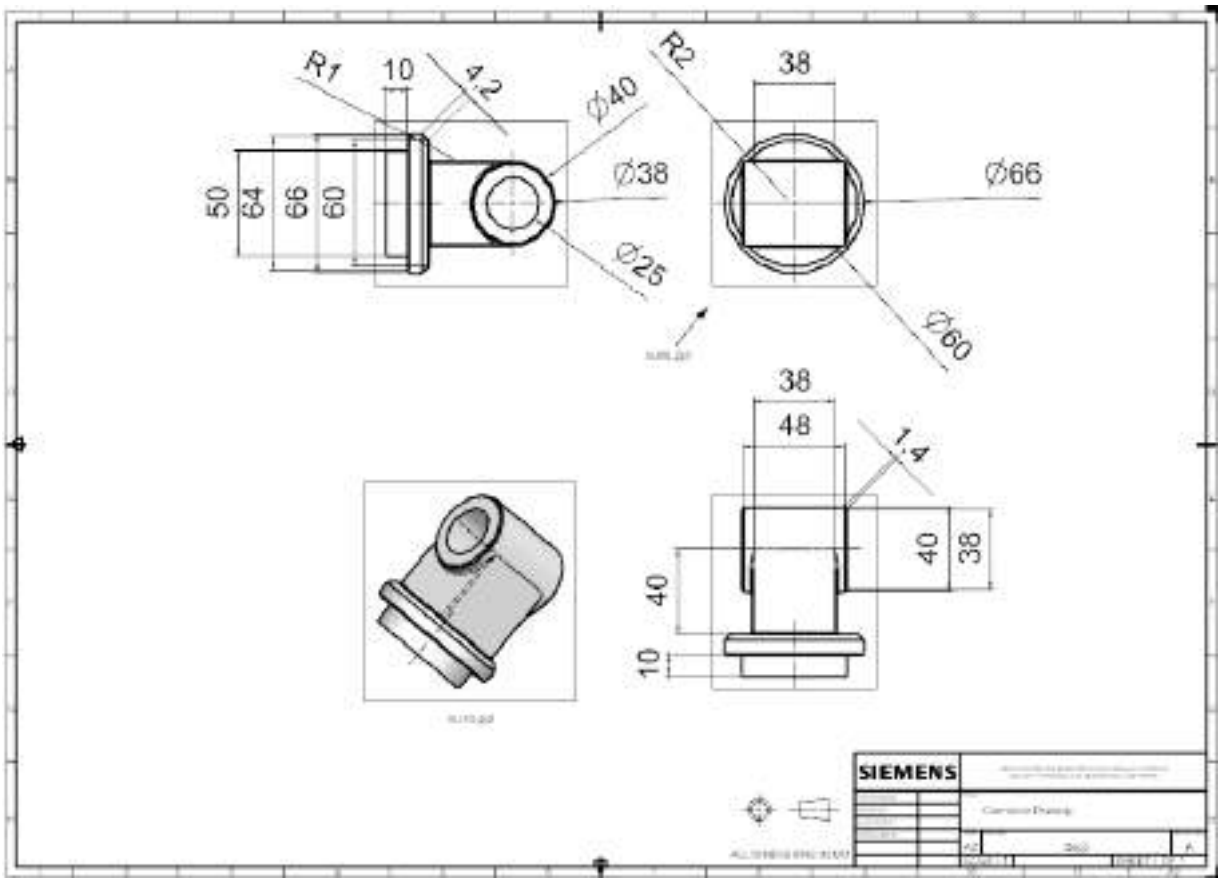

Figure A.17: (Robotic Arm Connector CAD Drawing)

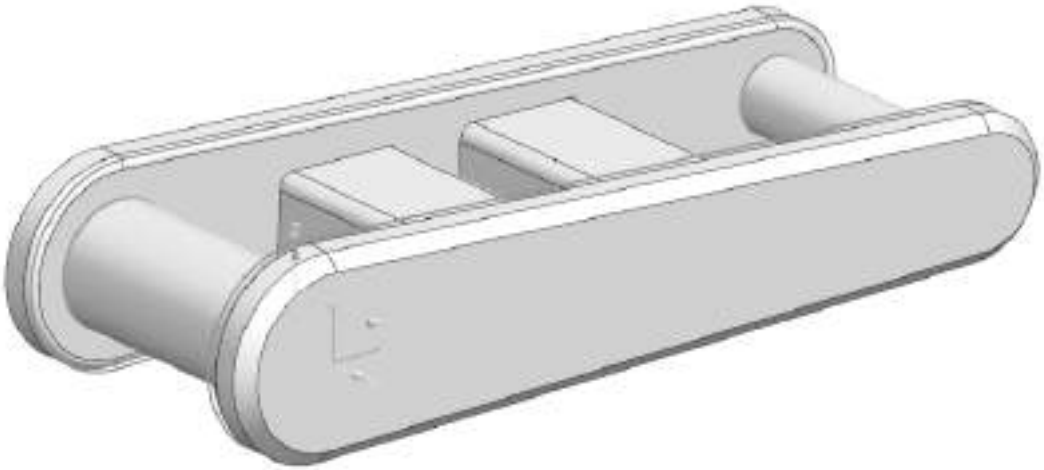

Figure A.18: (Robotic Arm Bottom Joint CAD)

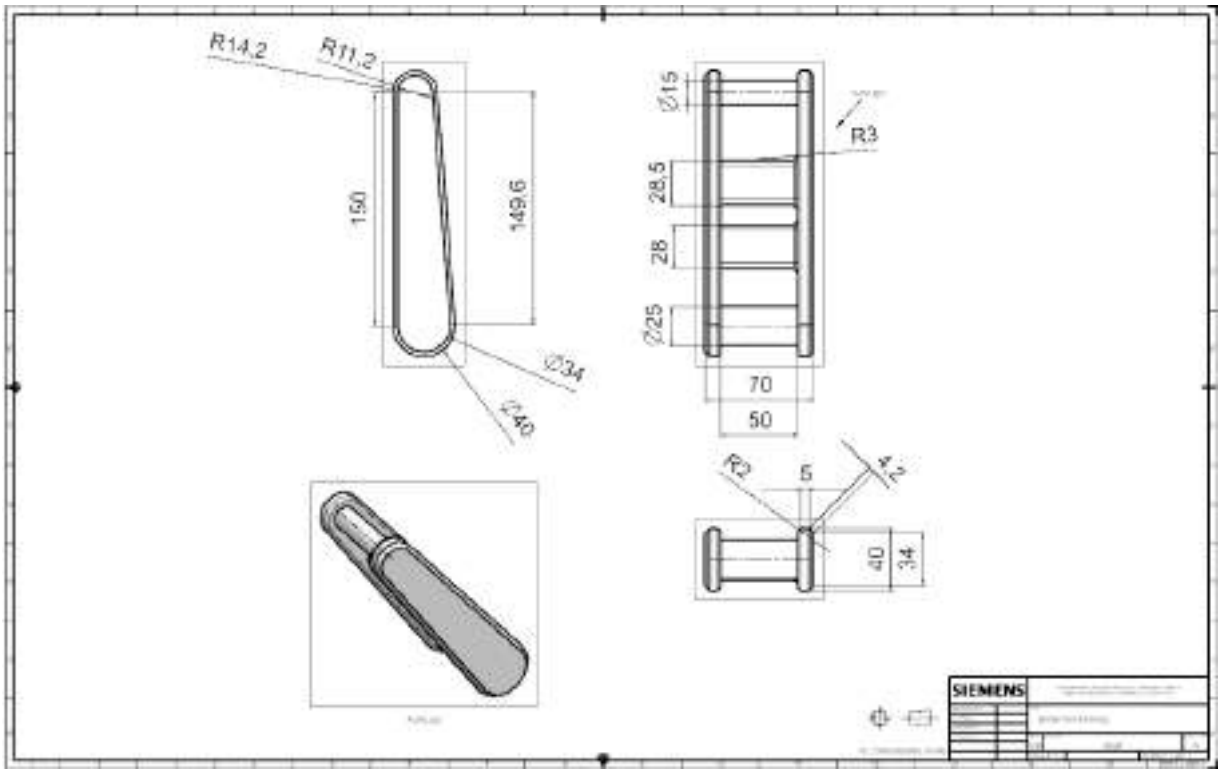

Figure A.19: (Robotic Arm Bottom Joint CAD Drawing)

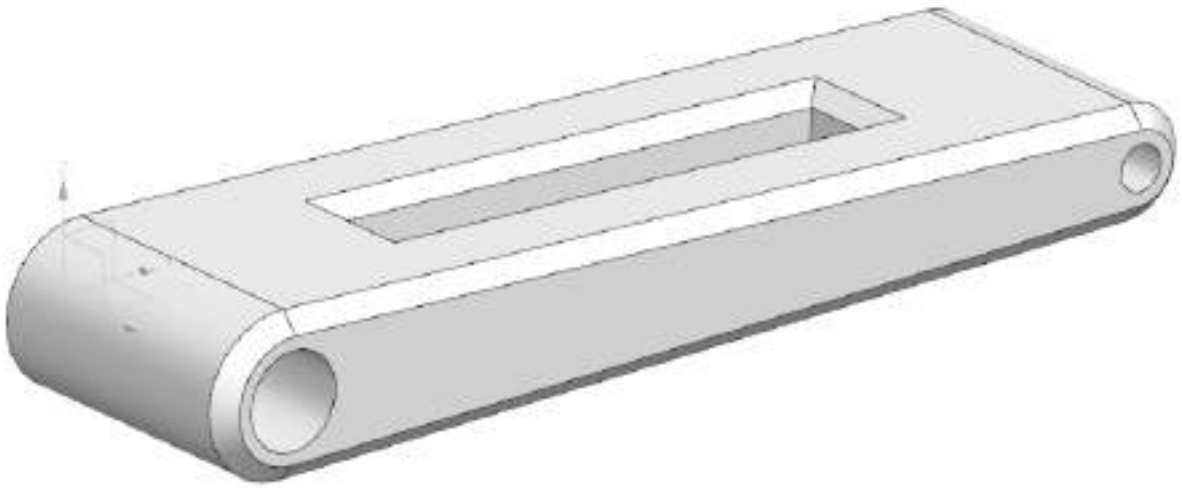

Figure A.18: (Robotic Arm Top Joint CAD)

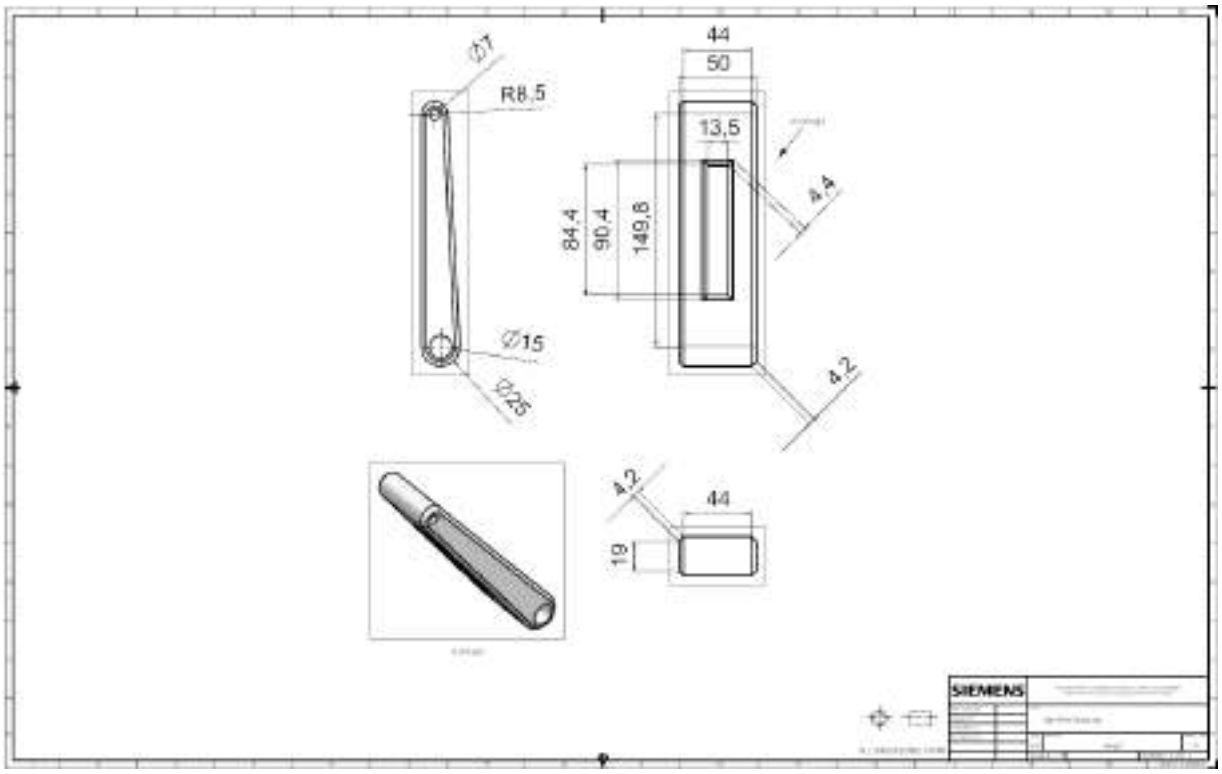

Figure A.20: (Robotic Arm Top Joint CAD Drawing)

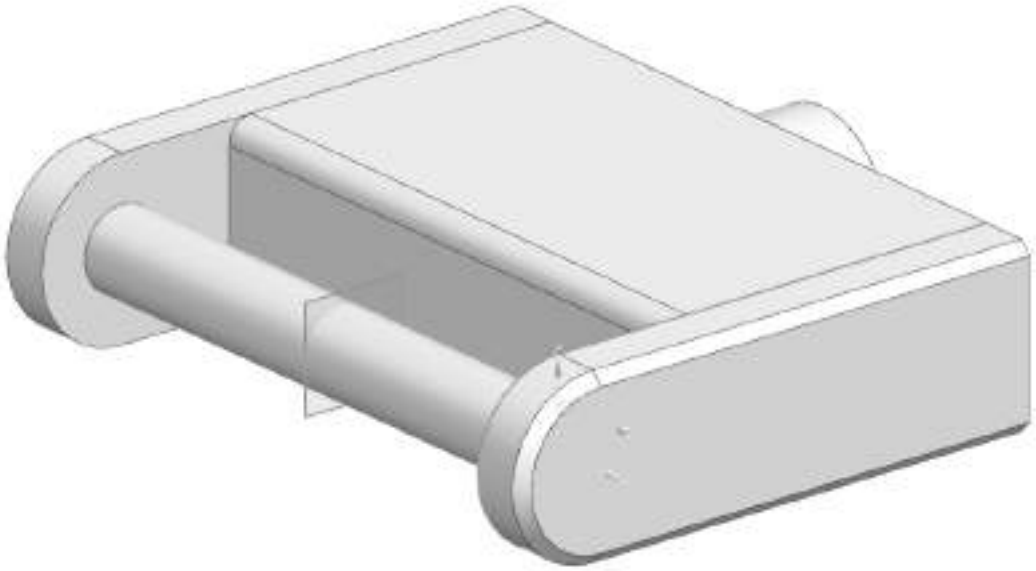

Figure A.21: (Robotic Arm Back Swivel CAD)

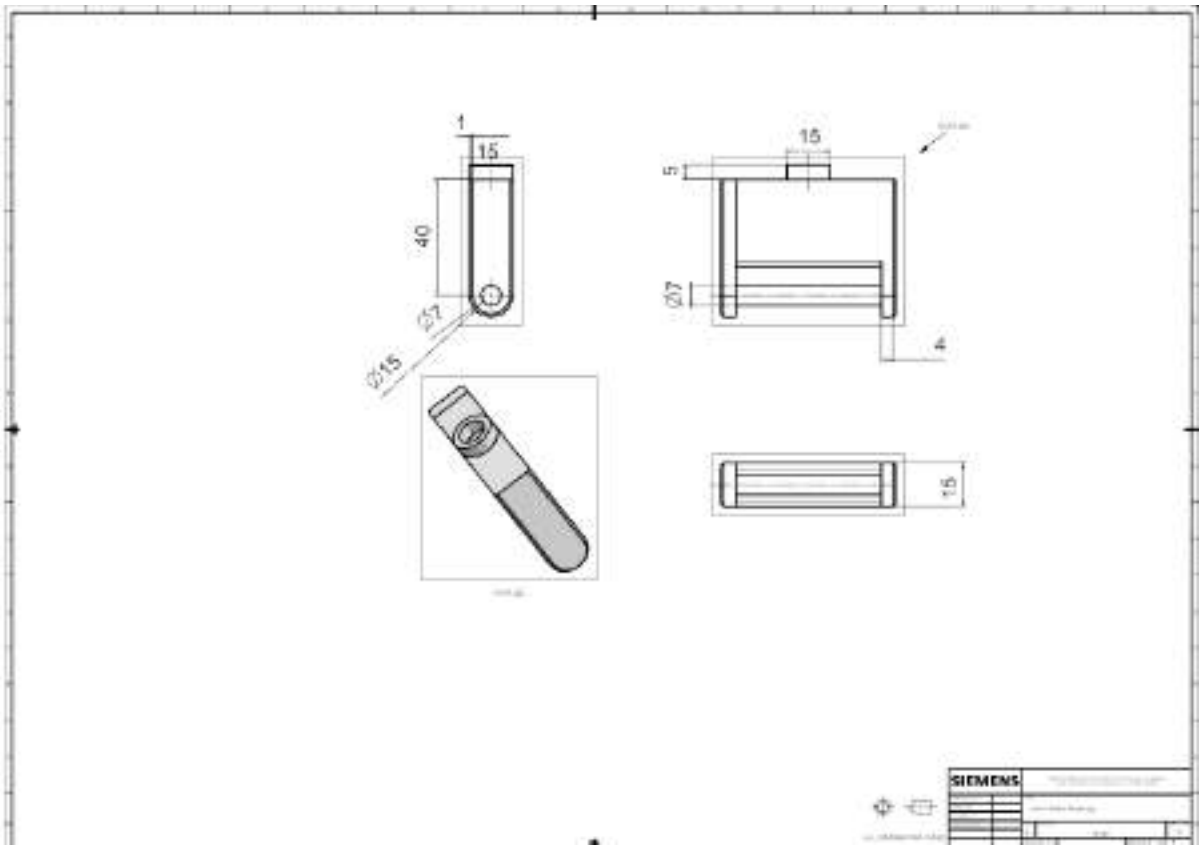

Figure A.22: (Robotic Arm Back Swivel CAD Drawing)

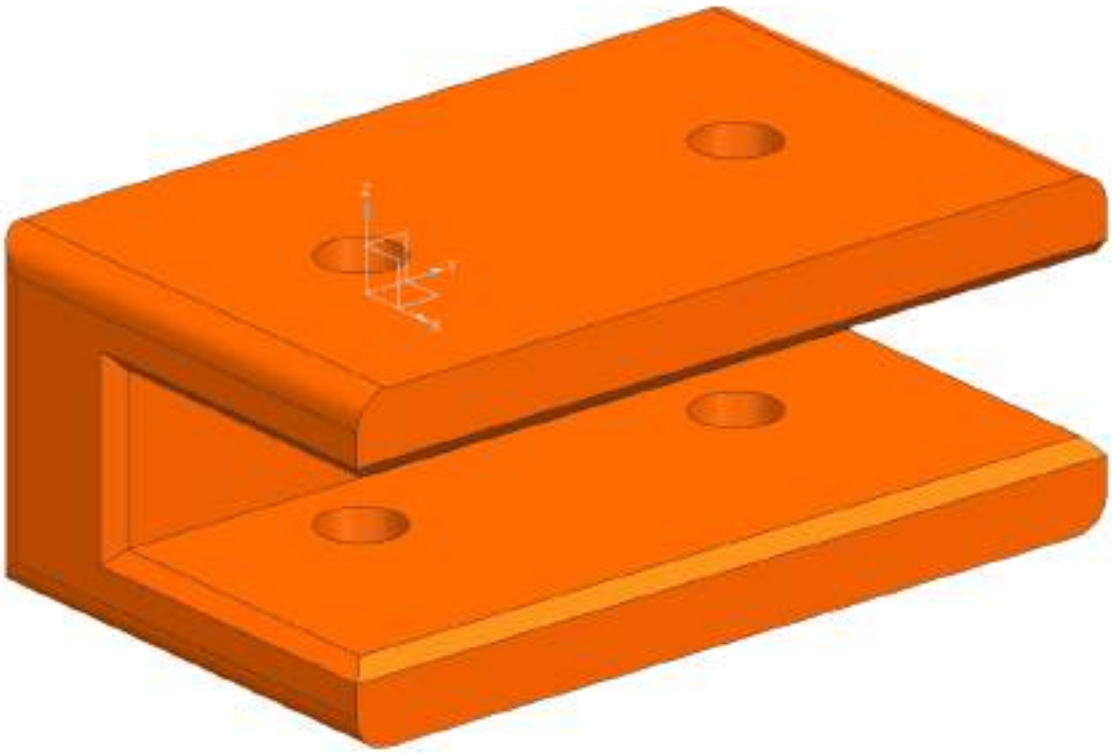

Figure A.23: (Robotic Arm Front Swivel CAD)

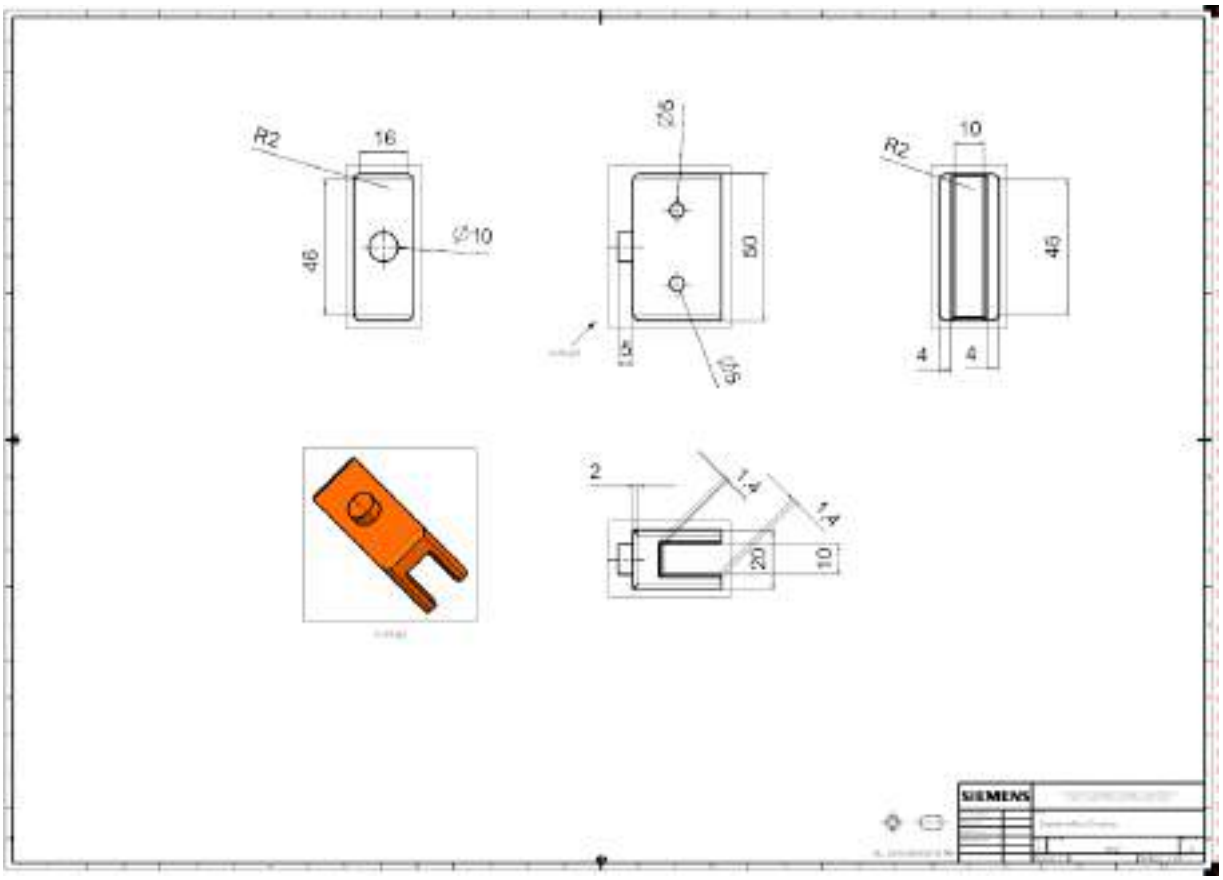

Figure A.24: (Robotic Arm Front Swivel CAD Drawing)

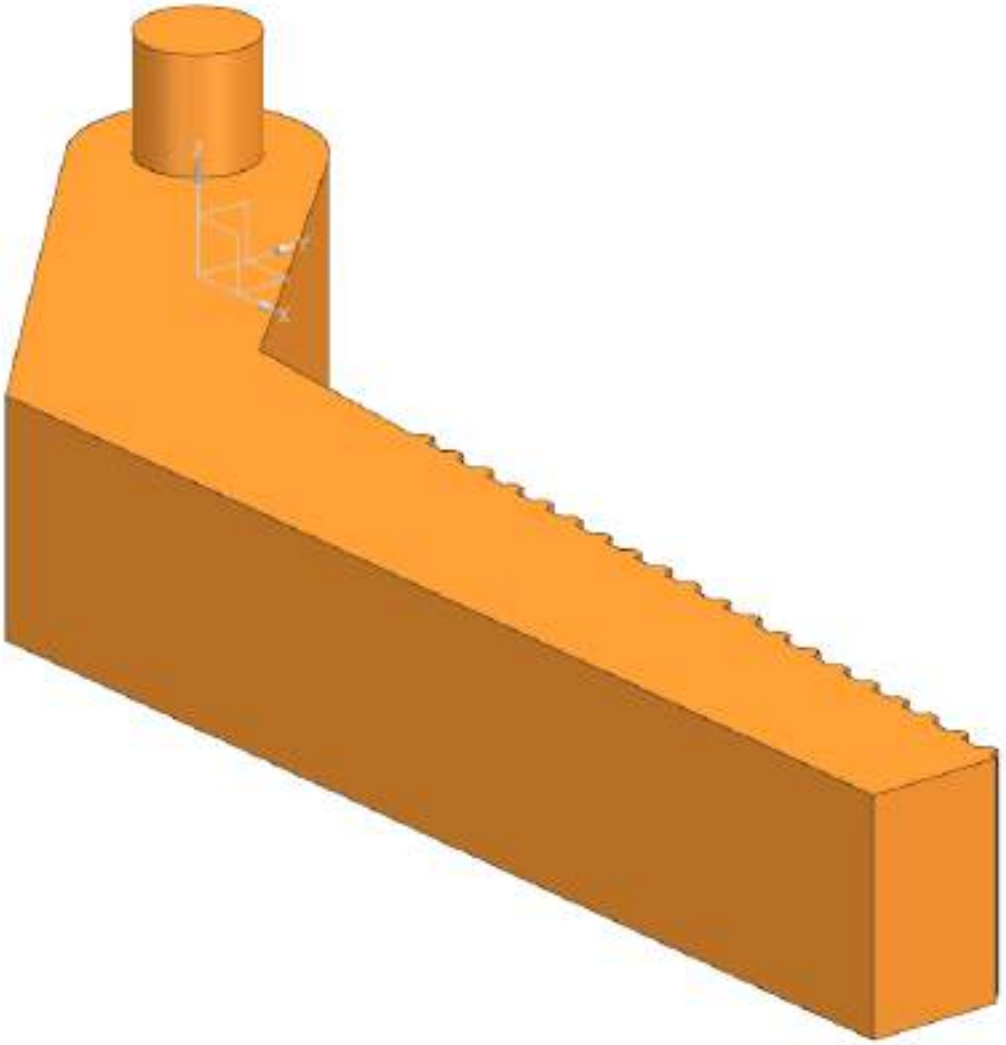

Figure A.25: (Robotic Arm Gripper CAD)

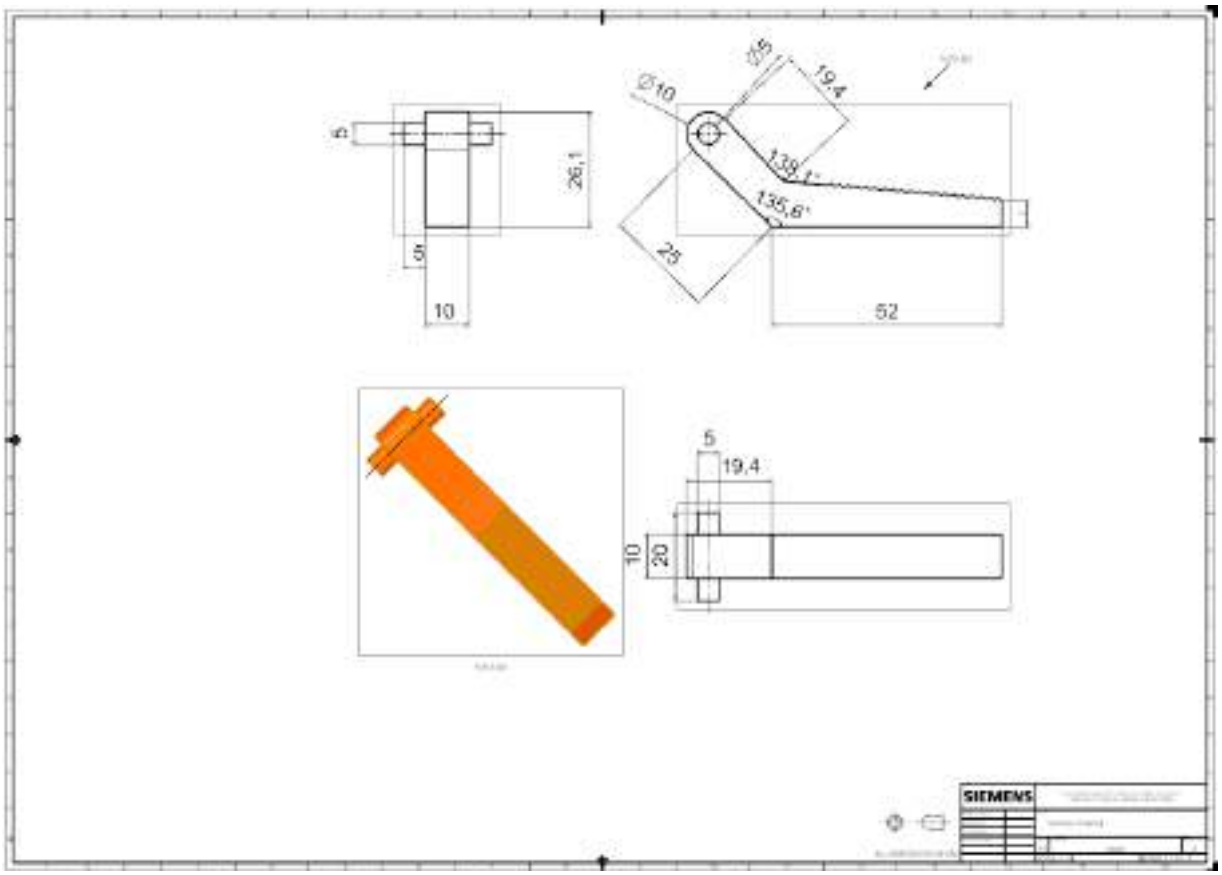

Figure A.26: (Robotic Arm Gripper CAD Drawing)

Figure A.27: (Chassis Differential CAD)

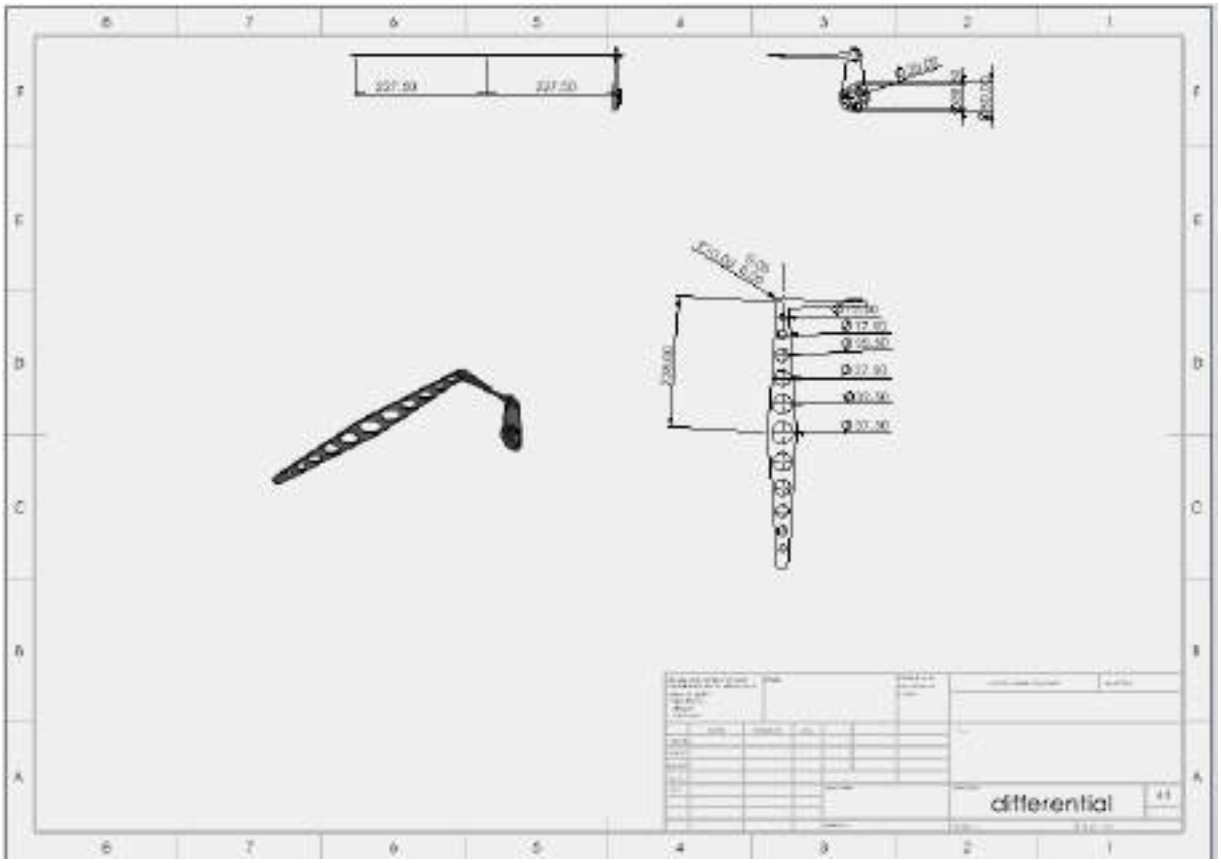

Figure A.28: (Chassis Differential CAD Drawing)

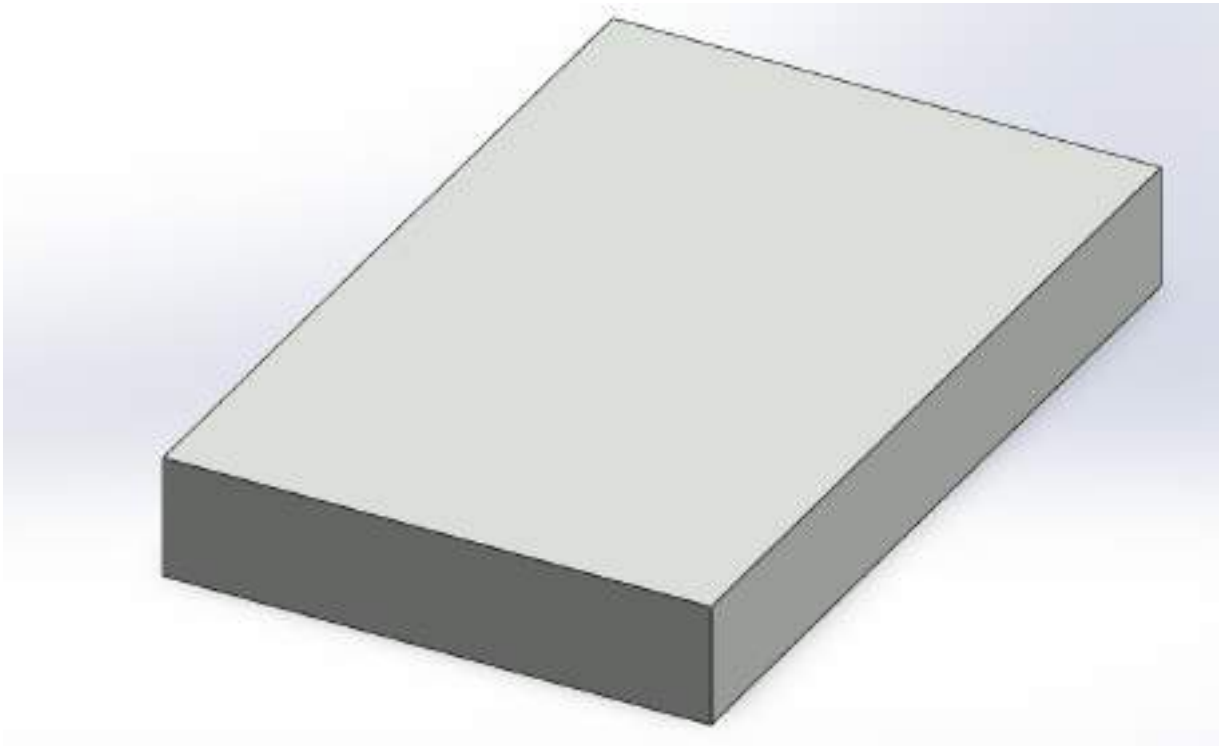

Figure A.29: (Chassis CAD)

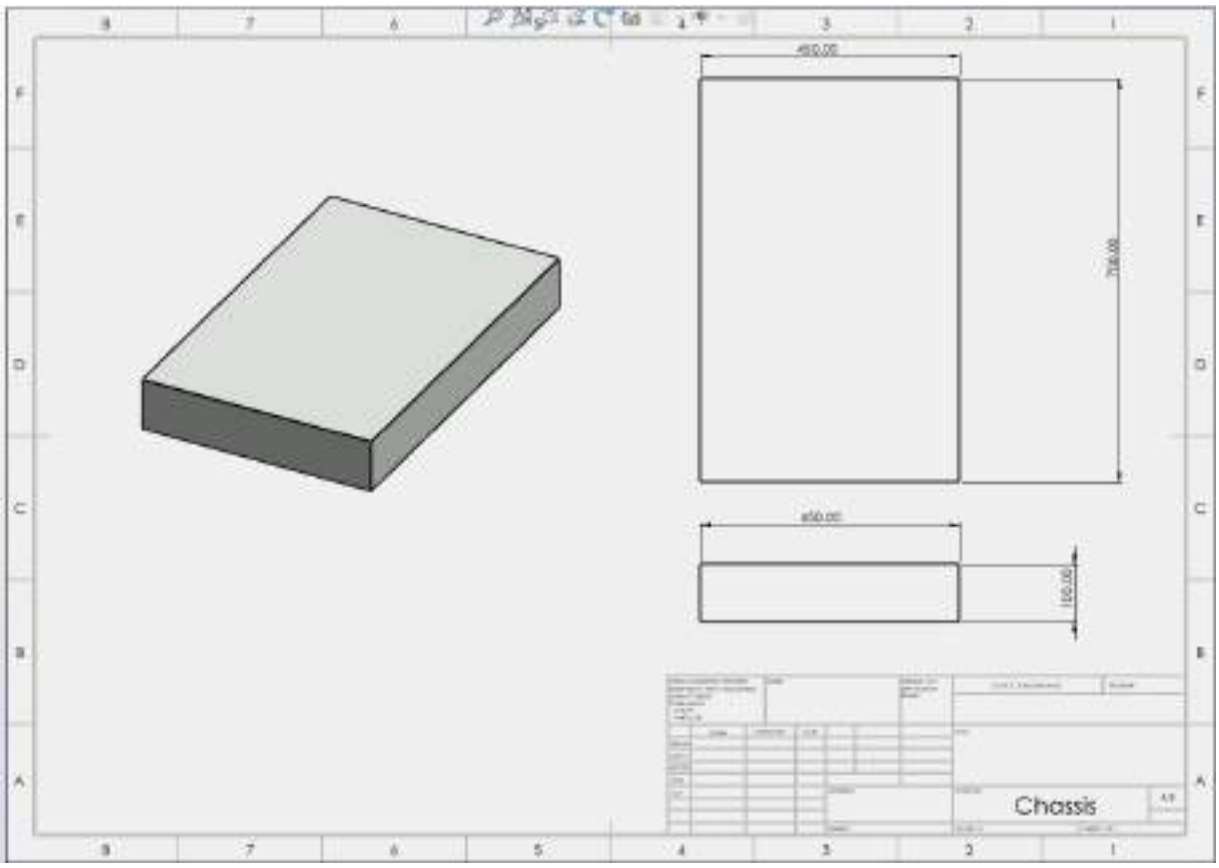

Figure A.30: (Chassis CAD Drawing)

Enter the number you recieved from the CER formula	21,487.90
Estimated cost with inflation (Without Wraps)	$40,613,983.90

Wrap Costs	Cost Estimate	Info
Management Costs	$1,860,000.00	?
Systems Engineering Costs	$1,420,000.00	?
Product Assurance Costs	$2,340,000.00	?
Integration & Test Costs	$8,370,000.00	?

Mechanical Subsystem

Final manufacturing cost per unit (manufacturing + wraps)	$54,000,000.00

Test Facility Cost	Cost Estimate	Info
TVAC	$8,190,000.00	?
EMI	$4,190,000.00	?
VIBE	$2,850,000.00	?
Ambient	$2,850,000.00	?

Final testing facility cost per unit	$35,880,000.00

Total cost breakdown per phase	Phase B (4% of total cost)	Phase C (57% of total cost)	Phase D (39% of total cost)
Manufacturing Costs	$2,164,000.00	$31,122,000.00	$21,294,000.00
Testing Costs	$658,000.00	$9,340,000.00	$6,390,000.00

Schedule Estimate Relation (SER)	Time in months
Planetary, Remote Sensing Instruments (Optical and Microwave)	47.5
Planetary, Remote Sensing Instruments (Fields and Particles)	52.4
Planetary, in situ Instruments	48.6

This information is only available for these hardware types

Figure A.31: (Mechanical Subsystem MCCET)

Schedule Estimate Relation (SER)	Time in months
Planetary, Remote Sensing Instruments (Optical and Microwave)	22.6
Planetary, Remote Sensing Instruments (Fields and Particles)	29.6
Planetary, in situ Instruments	29.3

Figure A.32: (SER for Mini-TLS)

Schedule Estimate Relation (SER)	Time in months
Planetary, Remote Sensing Instruments (Optical and Microwave)	27.8
Planetary, Remote Sensing Instruments (Fields and Particles)	36.5
Planetary, in situ Instruments	32.1

Figure A.33: (SER for Rimfax)

Schedule Estimate Relation (SER)	Time in months
Planetary, Remote Sensing Instruments (Optical and Microwave)	16.1
Planetary, Remote Sensing Instruments (Fields and Particles)	21.1
Planetary, in situ Instruments	25.2

Figure A.34: (SER for Gamma Neutron Probe)

Schedule Estimate Relation (SER)	Time in months
Planetary, Remote Sensing Instruments (Optical and Microwave)	30.9
Planetary, Remote Sensing Instruments (Fields and Particles)	40.5
Planetary, in situ Instruments	33.6

Figure A.35: (SER for Spectrometer)

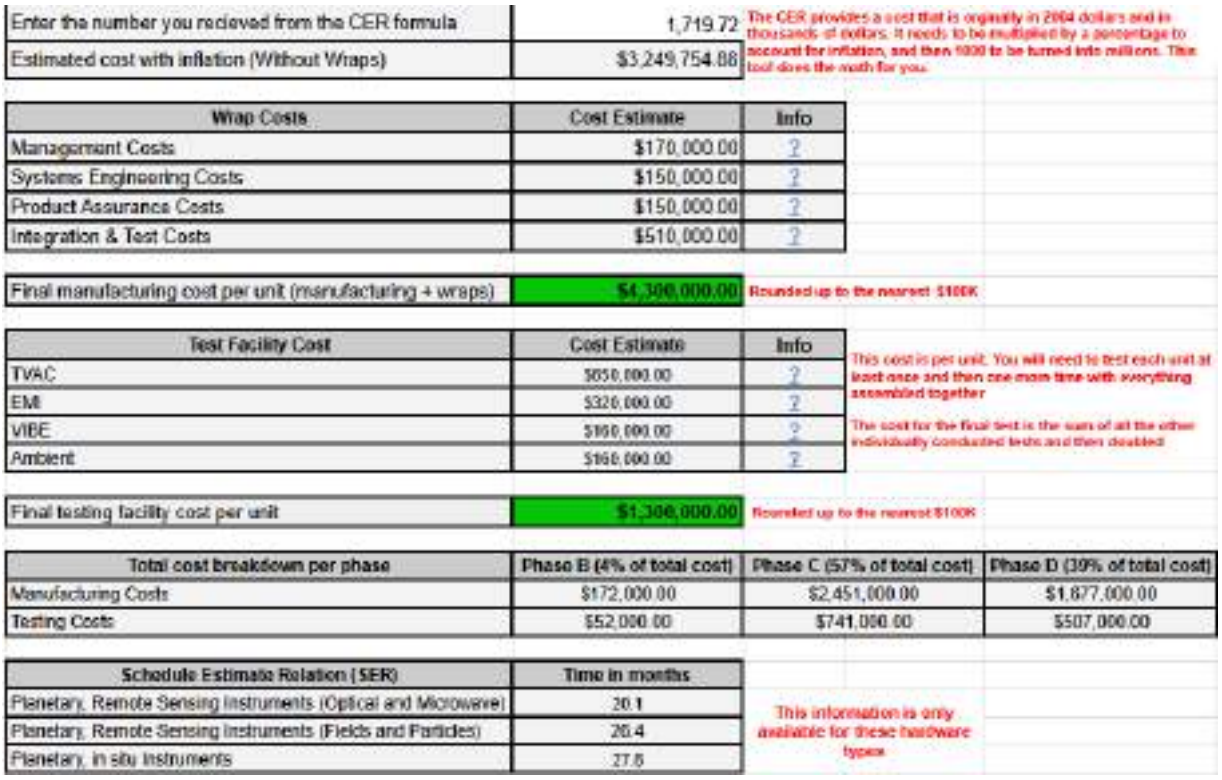

Enter the number you recieved from the CER formula	1,719.72	The CER provides a cost that is originally in 2004 dollars and in thousands of dollars. It needs to be multiplied by a percentage to account for inflation, and then 1000 to be turned into millions. This tool does the math for you.
Estimated cost with inflation (Without Wraps)	$3,249,754.88	

Wrap Costs	Cost Estimate	Info
Management Costs	$170,000.00	?
Systems Engineering Costs	$150,000.00	?
Product Assurance Costs	$150,000.00	?
Integration & Test Costs	$510,000.00	?

Final manufacturing cost per unit (manufacturing + wraps)	$4,300,000.00	Rounded up to the nearest $100K

Test Facility Cost	Cost Estimate	Info
TVAC	$650,000.00	?
EMI	$320,000.00	?
VIBE	$190,000.00	?
Ambient	$190,000.00	?

This cost is per unit. You will need to test each unit at least once and then one more time with everything assembled together

The cost for the final test is the sum of all the other individually conducted tests and then doubled

Final testing facility cost per unit	$1,300,000.00	Rounded up to the nearest $100K

Total cost breakdown per phase	Phase B (4% of total cost)	Phase C (57% of total cost)	Phase D (39% of total cost)
Manufacturing Costs	$172,000.00	$2,451,000.00	$1,677,000.00
Testing Costs	$52,000.00	$741,000.00	$507,000.00

Schedule Estimate Relation (SER)	Time in months
Planetary, Remote Sensing Instruments (Optical and Microwave)	20.1
Planetary, Remote Sensing Instruments (Fields and Particles)	20.4
Planetary, in situ Instruments	27.6

This information is only available for these hardware types

Figure A.36: (Thermal Subsystem MCCET)

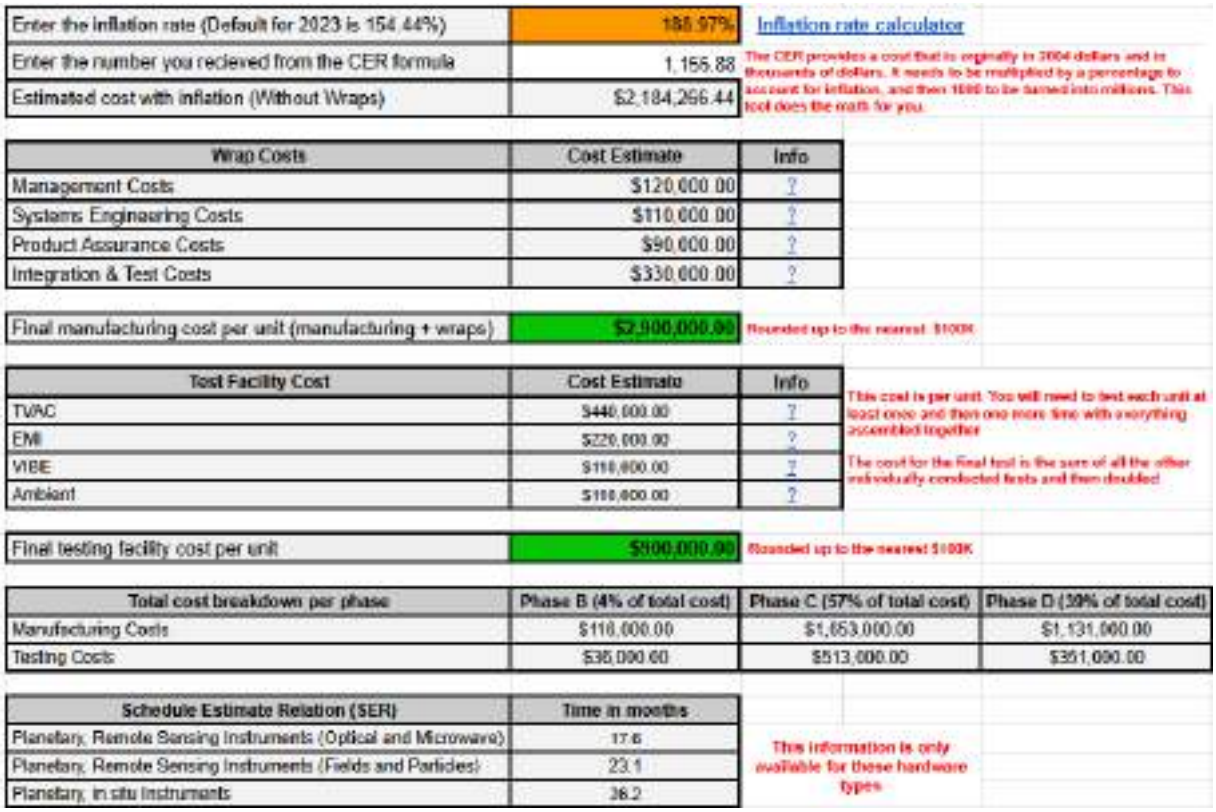

Enter the inflation rate (Default for 2023 is 154.44%)	188.97%	Inflation rate calculator
Enter the number you recieved from the CER formula	1,155.88	The CER provides a cost that is orginally in 2004 dollars and in thousands of dollars. It needs to be multiplied by a percentage to account for inflation, and then 1000 to be turned into millions. This tool does the math for you.
Estimated cost with inflation (Without Wraps)	$2,184,266.44	

Wrap Costs	Cost Estimate	Info
Management Costs	$120,000.00	?
Systems Engineering Costs	$110,000.00	?
Product Assurance Costs	$90,000.00	?
Integration & Test Costs	$330,000.00	?

Final manufacturing cost per unit (manufacturing + wraps)	$2,900,000.00	Rounded up to the nearest $100K

Test Facility Cost	Cost Estimate	Info
TVAC	$440,000.00	?
EMI	$220,000.00	?
VIBE	$110,000.00	?
Ambient	$110,000.00	?

This cost is per unit. You will need to test each unit at least once and then one more time with everything assembled together

The cost for the final test is the sum of all the other individually conducted tests and then doubled

Final testing facility cost per unit	$900,000.00	Rounded up to the nearest $100K

Total cost breakdown per phase	Phase B (4% of total cost)	Phase C (57% of total cost)	Phase D (39% of total cost)
Manufacturing Costs	$116,000.00	$1,653,000.00	$1,131,000.00
Testing Costs	$36,000.00	$513,000.00	$351,000.00

Schedule Estimate Relation (SER)	Time in months
Planetary, Remote Sensing Instruments (Optical and Microwave)	17.6
Planetary, Remote Sensing Instruments (Fields and Particles)	23.1
Planetary, In situ Instruments	36.2

This information is only available for these hardware types

Figure A.37: (Software MCCET)

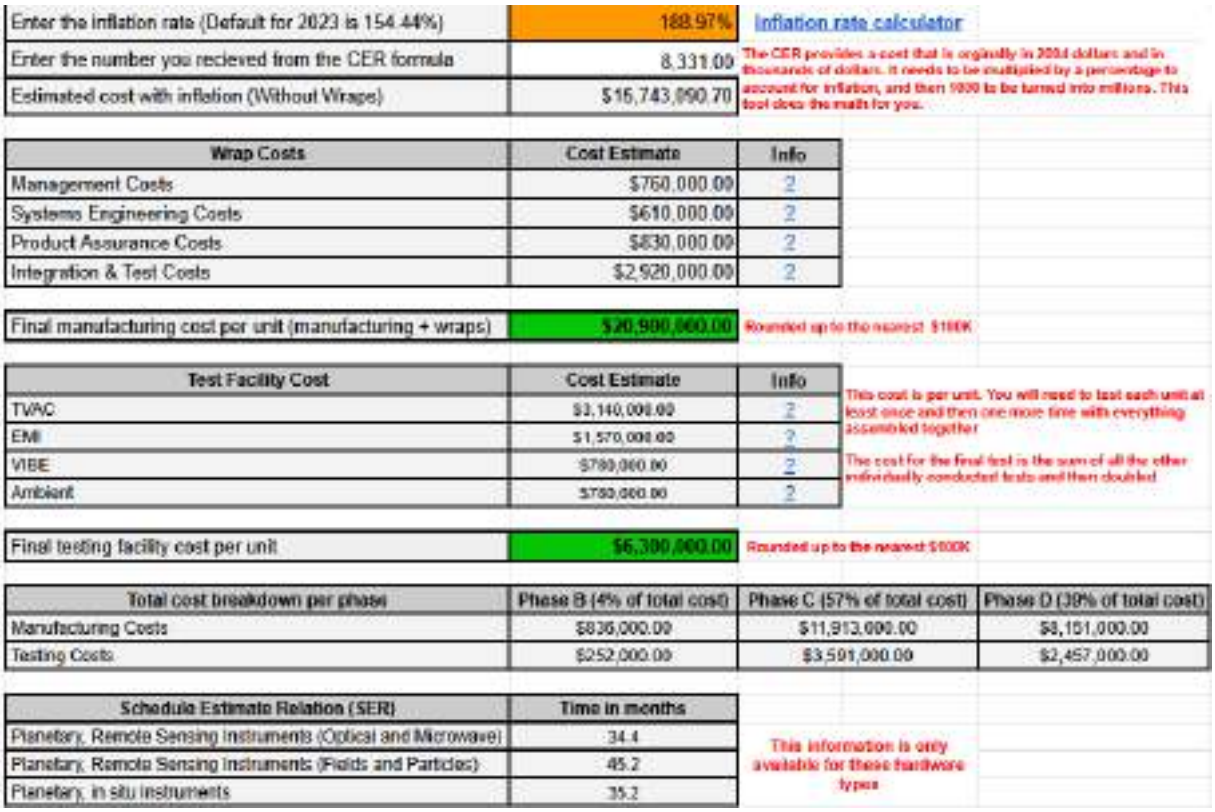

Enter the inflation rate (Default for 2023 is 154.44%)	188.97%	inflation rate calculator
Enter the number you recieved from the CER formula	8,331.00	The CER provides a cost that is orginally in 2004 dollars and in thousands of dollars. It needs to be multiplied by a percentage to account for inflation, and then 1000 to be turned into millions. This tool does the math for you.
Estimated cost with inflation (Without Wraps)	$16,743,090.70	

Wrap Costs	Cost Estimate	Info
Management Costs	$760,000.00	?
Systems Engineering Costs	$610,000.00	?
Product Assurance Costs	$830,000.00	?
Integration & Test Costs	$2,920,000.00	?

Final manufacturing cost per unit (manufacturing + wraps)	$20,900,000.00	Rounded up to the nearest $100K

Test Facility Cost	Cost Estimate	Info
TVAC	$3,140,000.00	?
EMI	$1,570,000.00	?
VIBE	$780,000.00	?
Ambient	$780,000.00	?

This cost is per unit. You will need to test each unit at least once and then one more time with everything assembled together

The cost for the final test is the sum of all the other individually conducted tests and then doubled

Final testing facility cost per unit	$6,300,000.00	Rounded up to the nearest $100K

Total cost breakdown per phase	Phase B (4% of total cost)	Phase C (57% of total cost)	Phase D (39% of total cost)
Manufacturing Costs	$836,000.00	$11,913,000.00	$8,151,000.00
Testing Costs	$252,000.00	$3,591,000.00	$2,457,000.00

Schedule Estimate Relation (SER)	Time in months
Planetary, Remote Sensing Instruments (Optical and Microwave)	34.4
Planetary, Remote Sensing Instruments (Fields and Particles)	45.2
Planetary, in situ instruments	35.2

This information is only available for these hardware types

Figure A.38: (Electronics MCCET)